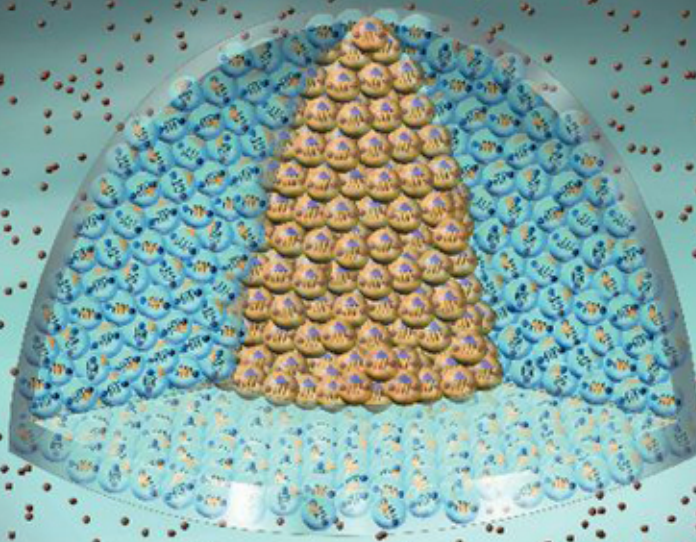


Philip Phillips

Advanced
**SOLID STATE
PHYSICS**

SECOND EDITION



CAMBRIDGE

more information - www.cambridge.org/9780521194907

Advanced Solid State Physics

Second Edition

Providing an up-to-date and lucid presentation of phenomena across modern advanced-level solid state physics, this new edition builds on an elementary understanding to introduce students to the key research topics with the minimum of mathematics. It covers cutting-edge topics, including electron transport and magnetism in solids. It is the first book to explain topological insulators and strongly correlated electrons.

Explaining solid state physics in a clear and detailed way, it also has over 50 exercises for students to test their knowledge. In addition to the extensive discussion of magnetic impurity problems, bosonization, quantum phase transitions, and disordered systems from the first edition, the new edition includes such topics as topological insulators, high-temperature superconductivity and Mott insulators, renormalization group for Fermi liquids, spontaneous symmetry breaking, zero and finite-temperature Green functions, and the Kubo formalism.

Philip Phillips is Professor of Physics at the University of Illinois. As a theoretical condensed matter physicist he has an international reputation for his work on transport in disordered and strongly correlated low-dimensional systems.

Cover illustration: phase diagram of the disordered quantum XY model. The arrows indicate the phase of the Cooper pairs (balls with springs). The yellow region represents a superconductor, the darker blue a glassy phase, and the lighter blue a phase-disordered insulator. The vertical axis represents the temperature while the in-plane axes represent the disorder and magnetic field strengths.

Advanced Solid State Physics

Second Edition

PHILIP PHILLIPS

University of Illinois at Urbana-Champaign



CAMBRIDGE UNIVERSITY PRESS
Cambridge, New York, Melbourne, Madrid, Cape Town,
Singapore, São Paulo, Delhi, Mexico City

Cambridge University Press
The Edinburgh Building, Cambridge CB2 8RU, UK

Published in the United States of America by Cambridge University Press, New York

www.cambridge.org
Information on this title: www.cambridge.org/9780521194907

© P. Phillips 2012

This publication is in copyright. Subject to statutory exception
and to the provisions of relevant collective licensing agreements,
no reproduction of any part may take place without the written
permission of Cambridge University Press.

First edition published by Westview Press, a member of the Perseus Books Group, 2002
Second edition published by Cambridge University Press 2012

Printed in the United Kingdom at the University Press, Cambridge

A catalog record for this publication is available from the British Library

Library of Congress Cataloging in Publication data
Phillips, Philip (Philip W.)

Advanced solid state physics / Philip Phillips. – 2nd ed.

p. cm.

Includes index.

ISBN 978-0-521-19490-7 (hardback)

1. Solid-state physics. I. Title.

QC176.P46 2012

530.4'1 – dc23 2011042607

ISBN 978-0-521-19490-7 Hardback

Additional resources for this publication at www.cambridge.org/solidstate

Cambridge University Press has no responsibility for the persistence or
accuracy of URLs for external or third-party internet websites referred to
in this publication, and does not guarantee that any content on such
websites is, or will remain, accurate or appropriate.

To Orestes and Angeliki

“The scientists of today think deeply instead of clearly. One must be sane to think clearly,
but one can think deeply and be quite insane.”

Nikola Tesla, July 1934.

Contents

<i>Preface</i>	<i>page</i> xi
1 Introduction	
1.1 Spontaneously broken symmetry	1
1.2 Tracking broken symmetry: order parameter	4
1.3 Beyond broken symmetry	7
References	9
2 Non-interacting electron gas	
Problems	15
3 Born–Oppenheimer approximation	
3.1 Basic Hamiltonian	16
3.2 Adiabatic approximation	17
3.3 Tight-binding approximation	20
Problem	22
References	23
4 Second quantization	
4.1 Bosons	24
4.2 Fermions	26
4.3 Fermion operators	27
Problems	30
References	30
5 Hartree–Fock approximation	
5.1 Non-interacting limit	31
5.2 Hartree–Fock approximation	33
5.3 Diagrams	35
Problem	36
References	36
6 Interacting electron gas	
6.1 Uniform electron gas	37
6.2 Hartree–Fock excitation spectrum	38
	40

6.3 Cohesive energy of metals	42
Summary	48
Problems	48
References	49
7 Local magnetic moments in metals	51
7.1 Local moments: phenomenology	51
7.2 Impurity density of states	54
7.3 Green functions	60
7.4 Friedel's sum rule and local moments	70
Summary	74
Appendix to Chapter 7: Luttinger's theorem	74
Problems	79
References	79
8 Quenching of local moments: the Kondo problem	80
8.1 The Kondo Hamiltonian	82
8.2 Why is J negative?	83
8.3 Scattering and the resistivity minimum	87
8.4 Electron–impurity scattering amplitudes	94
8.5 Kondo temperature	99
8.6 Poor Man's scaling	102
Summary	109
Appendix to Chapter 8: the Schrieffer–Wolff transformation	109
Problems	113
References	114
9 Screening and plasmons	115
9.1 Thomas–Fermi screening	115
9.2 Plasma oscillations and collective coordinates	117
9.3 Linear response theory	122
9.4 Dielectric response function	127
9.5 Kubo formula: electrical conductivity	137
9.6 Stopping power of a plasma	140
Summary	143
Problems	144
References	145
10 Bosonization	146
10.1 Luttinger liquid	146
10.2 Bosonization of Luttinger model	151
10.3 Pair binding: can electrons do it alone?	160
10.4 Excitation spectrum	162

Summary	167
Problems	167
References	168
11 Electron–lattice interactions	169
11.1 Harmonic chain	169
11.2 Acoustic phonons	171
11.3 Electron–phonon interaction	172
11.4 Ultrasonic attenuation	176
11.5 Electrical conduction	178
Summary	187
Problems	187
References	188
12 Superconductivity in metals	189
12.1 Superconductivity: phenomenology	189
12.2 Electron–phonon effective interaction	197
12.3 Model interaction	199
12.4 Cooper pairs	201
12.5 Fermi liquid theory	205
12.6 Pair amplitude	216
12.7 BCS ground state	221
12.8 Pair fluctuations	224
12.9 Ground state energy	226
12.10 Critical magnetic field	229
12.11 Energy gap	231
12.12 Quasi-particle excitations	233
12.13 Thermodynamics	237
12.14 Experimental applications	241
12.15 Josephson tunneling	253
Summary	255
Problems	255
References	257
13 Disorder: localization and exceptions	258
13.1 Primer on localization	259
13.2 Return probability: localization criterion	261
13.3 Weak localization	264
13.4 Scaling theory	269
13.5 Exceptions to localization	275
Summary	285
Problems	286
References	287

14 Quantum phase transitions	289
14.1 Quantum rotor model	291
14.2 Scaling	293
14.3 Mean-field solution	296
14.4 Landau–Ginsburg theory	302
14.5 Transport properties	306
14.6 Experiments	308
14.7 Scaling and T -linear resistivity	310
Problems	314
References	314
15 Quantum Hall and other topological states	317
15.1 What is the quantum Hall effect?	317
15.2 Landau levels	320
15.3 The role of disorder	324
15.4 Currents at the edge	326
15.5 Topological insulators	330
15.6 Laughlin liquid	343
Summary	349
Problems	349
References	350
16 Electrons at strong coupling: Mottness	353
16.1 Band insulator	354
16.2 Mott’s problem	357
16.3 Much ado about zeros: Luttinger surface	363
16.4 Beyond the atomic limit: Heisenberg versus Slater	368
16.5 Dynamical spectral weight transfer	380
16.6 Epilogue: $1 = 2 - 1$	396
Problems	397
References	398
<i>Index</i>	400

Preface

In writing the second edition of this text, I have tried to accomplish three things. First, correct all the typos in the first edition. This has turned out to be somewhat harder than I had anticipated. While I am certain my proofreaders and I corrected all mistakes we could find, that might not have been sufficient. As there will undoubtedly be a second printing, simply email me any errors you might find at dimer@illinois.edu. Second, include all the material that should have been in the first edition but that I had given up on writing. This includes Green functions, Luttinger's theorem, renormalization of short-range interactions for Fermi liquids, and symmetry. In keeping with this being a physics rather than a technique or mathematics tract, these subjects are interwoven wherever they are first needed. For example, the section on Green functions is in Chapter 7 where the Anderson impurity problem is treated. For completeness, Luttinger's theorem is also presented in the same chapter but in an appendix. Third, include new material that reflects the fast-moving pace of $\hbar = 1$ research in condensed matter physics. Here I made a judgement based on what I anticipate students would find most useful. Since there are no texts that present the pedagogy of topological insulators (though some excellent review articles exist) and Mott insulators, I chose to focus on those topics. In writing the topological insulator section, I have tried to stick to the formulations that require the fewest definitions and new concepts since the physics of these systems is inherently simple. Regarding the Mott problem, I present what I think is non-controversial but not written down anywhere in a single manuscript. Chapter 16 starts with the band insulator in which the rigid-band picture is valid and then demonstrates that the physics of the Mott problem stands apart because no such rigid-band picture applies. While tomes have been written about rigid-band models, no text deals with the breakdown of the rigid-band picture in strongly correlated electron problems. The cuprate problem is discussed in this context. I had also intended to write a chapter on quantum computing and extend the discussion in Chapter 14 to include the Bose–Hubbard model. However, including such topics would have pushed the page count well over 600 pages, thereby making the book unwieldy. Further, such topics are not, in my estimation, particularly suited to a core second-semester graduate class but rather to a more specialized course. Perhaps I will think differently in a few years.

I have benefitted from much input in the final editing of the current manuscript. Babak Seradjeh, Juan Jottar, and Taylor Hughes offered invaluable critiques of the topological insulator section. Wei-Cheng Lee, Mohammad Edalati, and Taylor Hughes also read the Mott chapter and caught several typos and inaccuracies. I also thank Mohammad for reading and correcting the chapter on symmetries and Robert Leigh for his characteristically level-headed and incisive remarks on strong coupling physics and symmetry. Wade deGottardi offered numerous suggestions on the bosonization chapter. While I received emails from

several students around the world detailing the typographical errors they have caught, I would especially like to thank Wei Han who found two key typos in two figures from the first edition. Many thanks to Taylor Hughes for redrawing these figures. The duty of proof-reading fell on my research group and other members of the ICMT group at Urbana whose arms are still recovering from the non-adiabatic distortions I applied to them. These include Wei-Cheng Lee, Mohammad Edalati, Seungmin Hong, Wade deGottardi, Rodrigo Garrido, and Kiaran Dave. In addition, at the proof stage, Kiaran Dave, Ka Wai Lo, and Huihuo Zheng read the entire manuscript and corrected it assiduously, in their relentless drive to eliminate all typographical errors. I would like to thank Matthew Feickert for converting the LaTeX files to the Cambridge style and for spotting several typographical errors along the way, and the Cambridge staff, Mike Nugent, Simon Capelin, Claire Poole, Abigail Jones and Frances Nex for their dedication to this project. Early influences without which this book might not have been possible include my high school English teacher, Duane Kusler, who encouraged me to write and my twin sisters Andi and Lyndi from whom I learned many math tricks. My endearing thanks go to my family for their support and calming presence.

Solid state physics grew out of applications of quantum mechanics to the problem of electron conduction in solids. This seemingly simple problem defied solution because the presence of an ion at each lattice site seemed to present an obvious impediment to conduction. How the electrons avoid the ions was thus the basic question. Although the answer to this question is well known, it does serve to illuminate the very essence of solid state physics: there is organization in the many. Each electron adjusts its wavelength to take advantage of the periodicity of the lattice. In the absence of impurities, conduction is perfect. Hence, by understanding this simple fact that periodicity implies perfect conduction, it became clear that the experimentally observed resistivity in a metal came not from electrons running into each of the ions but rather from dirt (disorder), thermal effects mediated by dynamical motion of the ions, or electron-electron interactions. This book examines each of these effects with an eye for identifying underlying organizing principles that simplify the physics of such interactions.

1.1 Spontaneously broken symmetry

The search for organizing principles that help simplify the physics of many-body systems is at the heart of modern solid state or, more generally, condensed matter physics. One such tool is symmetry. Consider the simple case of permutation symmetry typically taught in a first class in quantum mechanics. This symmetry was introduced into quantum mechanics by W. Heisenberg in the context of the indistinguishability of identical particles. The permutation group has a finite number of elements and hence is associated with a discrete symmetry. Permutation symmetry allows us to classify fundamental particles into two groups. Bosons are even with respect to interchange of two particles and fermions odd. This symmetry can be generalized to include a non-integer phase when two particles are interchanged, as we will see in the context of the fractional quantum Hall effect.

To a large extent, the symmetries that are most relevant in condensed matter systems are typically continuous, for example rotational symmetry. Spontaneously breaking a continuous symmetry has a fundamental consequence. For example, the existence of phonons in a solid or spin waves in a magnet follows from the spontaneous breaking of a continuous symmetry. By spontaneous, we mean without the application of an external field. A periodic arrangement of ions in a crystal breaks continuous translational and rotational symmetry. Such spontaneous breaking of a continuous symmetry by the very existence of the lattice is necessarily accompanied by a massless spinless bosonic excitation. That such massless

spinless bosons, known as Nambu–Goldstone bosons (G1961; N1960), necessarily accompany the breaking of a continuous symmetry can easily be deduced from the following considerations. We consider a system with a Lagrangian

$$\mathcal{L} = T - V(\phi), \quad (1.1)$$

consisting of a kinetic energy, T , and a potential energy, $V(\phi)$, where we are allowing for ϕ to be a complex function. The claim that such a system is invariant under a symmetry operation is captured by

$$V(\phi) = V(\phi + \epsilon\delta\phi), \quad (1.2)$$

where $\epsilon\delta\phi$ is the generator of the symmetry operation. Here ϵ is an infinitesimal. We have assumed for the moment that $\delta\phi$ is independent of space. To illustrate what is meant by this identity, consider a potential of the form $V(\phi) = \epsilon_0|\phi|^2$. This potential is invariant under transformations of the form $\phi \rightarrow \phi e^{i\theta}$. Let θ be a small quantity completely independent of space. Then we can expand the exponential and retain only the first-order term. Consequently, $\phi \rightarrow \phi(1 + i\theta)$ and we identify $\epsilon\delta\phi$ as $i\theta\phi$; that is, $\epsilon = \theta$ and $\delta\phi = i\phi$. This symmetry, known as U(1), is present in models that preserve charge conservation. Expansion of $V(\phi)$ to linear order in ϵ implies that

$$\delta\phi \frac{\delta V}{\delta\phi} = 0, \quad (1.3)$$

assuming that the symmetry is intact. Now assume explicitly that the symmetry is broken such that $V \rightarrow V(\phi_0 + \chi)$, where ϕ_0 minimizes the potential and χ cannot be written as a generator of a symmetry operation as in Eq. (1.2). Since the potential has a minimum, it makes sense to expand

$$V(\phi_0 + \chi) = V(\phi_0) + \frac{1}{2}\chi^2 \left. \frac{\partial^2 V}{\partial\phi^2} \right|_{\phi=\phi_0} = V(\phi_0) + \frac{1}{2}\chi^2 m^2, \quad (1.4)$$

truncating at the restoring term at second order. The second term, which can be used to define the mass (m) in a standard harmonic expansion, is inherently positive semi-definite since we have expanded about the minimum. With this equation in hand, we differentiate Eq. (1.3),

$$\frac{\partial\delta\phi}{\partial\phi} \frac{\delta V}{\delta\phi} + \delta\phi \frac{\partial^2 V}{\partial\phi^2} = 0, \quad (1.5)$$

with respect to ϕ . The first term vanishes when evaluated at the minimum, implying that

$$\delta\phi \left. \frac{\partial^2 V}{\partial\phi^2} \right|_{\phi=\phi_0} = 0 \quad (1.6)$$

must identically vanish for any variation of ϕ in the broken symmetry state. Since $\delta\phi$ is non-zero, Eq. (1.6) is satisfied only if the second-order-derivative term vanishes or equivalently if $m^2 = 0$. That is, the mass vanishes. This is Goldstone's theorem (G1961). A zero mode exists for each generator of a continuously broken symmetry. As a result of this theorem, symmetry occupies a central place in all areas of physics, in particular particle and condensed matter physics. Typically, the massless bosons that arise in condensed matter systems represent collective excitations of the entire many-body system. In fluids, phonons are purely longitudinal and arise from spontaneous breaking of Galilean invariance. In solids, phonons are both transverse and longitudinal, though with no simple correspondence with the spontaneous breaking of Galilean, translational, and rotational symmetry. In magnets, spin waves or magnons are the collective gapless excitations that emerge from the spontaneous breaking of rotational symmetry.

We can of course relax the constraint that θ be independent of space. In so doing, we can entertain what happens under local rather than global (θ independent of space) transformations. While our analysis on the potential energy remains the same, the kinetic energy,

$$T \rightarrow \frac{1}{2}(\partial_\mu\phi^*)(\partial^\mu\phi) + \frac{1}{2}|\phi|^2(\partial_\mu\theta(x))^2, \quad (1.7)$$

does acquire a new term describing the spatial variation of the phase. If the U(1) symmetry is not broken by this transformation, then the second term must vanish. Demanding that

$$\partial_\mu\theta = 0 \quad (1.8)$$

requires that θ be spatially homogeneous for the symmetry to be preserved. As a result, a consequence of breaking the continuous U(1) symmetry is that θ must be spatially non-uniform. This is the situation in a superconductor. In fact, the current inside a superconductor arises entirely from the spatial variation of the phase, as can be seen from the quantum mechanical equation for the current,

$$j_\mu = \frac{e\hbar}{m}\text{Im}\psi^\dagger\partial_\mu\psi = \frac{e^*\hbar}{m}|\Delta|^2\partial_\mu\theta, \quad (1.9)$$

if we interpret ψ as the wavefunction for the superconducting state; that is, $\psi = \Delta e^{i\theta}$. We will see in the chapter on superconductivity precisely how this state of affairs arises. We will interpret ψ as the order parameter of a superconducting state. While the Bardeen–Cooper–Schrieffer (BCS) theory of superconductivity was certainly not formulated as an example of a broken continuous symmetry, this is the basic principle that underlies this theory. In fact, the key ingredients of superconductivity, charge $2e$ carriers and a supercurrent, all follow from breaking U(1) symmetry.

Massless bosons that emerge from broken symmetry typically generate new unexpected physics. For example, phonons mediate pairing between electrons, thereby driving the onset of superconductivity in metals such as Hg and more complicated systems, for example MgB₂. However, strict rules determine how such Nambu–Goldstone bosons can affect

any system. As shown by Adler (A1965), the interactions induced by massless bosons arising from the breaking of a continuous symmetry must be proportional to the transferred momentum. More formally, interactions mediated by the exchange of a Nambu–Goldstone boson can only obtain through derivative couplings. Consequently, the interaction vanishes for zero exchanged momentum. This principle implies that the electron–phonon interaction which mediates pairing in elemental superconductors is inherently dynamical in nature. We will verify this important principle in the context of the electron–phonon coupling through an explicit derivation. Hence, entirely from the existence of a lattice, phonons and the kinds of interactions they mediate can be easily deduced.

1.2 Tracking broken symmetry: order parameter

The idea of an order parameter is another powerful concept in condensed matter physics. Order parameters track broken symmetry. That is, they are non-zero in the broken symmetry phase and zero otherwise. Consider a ferromagnet. Locally each spin can point along any direction. This is the case at high temperature in which no symmetry is broken. In a phase transition controlled by thermal fluctuations, typically it is the high-temperature phase that has the higher symmetry. To quantify the order in a collection of spins, we sum the z -component of each of the spin operators,

$$M = \frac{1}{N} \sum_i \langle S_i^z \rangle, \quad (1.10)$$

scaled by the number of spins, N . Here S_i^z is the z -component of the spin of the atom on site i and the angle brackets indicate a thermal average over the states of the system. M is the magnetization. At high temperature before any symmetry is broken, the magnetization is identically zero. At sufficiently low temperatures, the spins order and the magnetization acquires a non-zero value. Consider iron for which the Curie or ordering temperature is 1340 K. It turns out that most parts of a block of iron below the magnetization temperature have vanishing magnetization. This state of affairs obtains because the magnetization is in general a function of space. As a result, a block of iron does not break the symmetry uniformly. In fact, the actual magnetization in bulk magnets is not acquired spontaneously but rather by some external means to align all of the individual magnetic domains. At the boundary of a domain, the magnetization changes sign, creating a domain wall. Typical domain sizes in iron are roughly 300 ions. Placing a chunk of Fe in a magnetic field will orient all of the domains in the same direction, a state of affairs that will persist long after the field is turned off. This is important since the re-oriented domain state does not constitute a minimum energy state of the system. The domains lock into place by becoming pinned to defects. One would expect then that as the magnetizing field is varied, the magnetization would not change continuously but by discontinuous jumps as domain walls de-pin from defects. This is the essence of the Barkhausen effect, the tiny discontinuous jumps the magnetization makes in the presence of an external magnetic field and ultimately the reason why the magnetization curve in a ferromagnet exhibits hysteresis as depicted in Fig. 1.1.

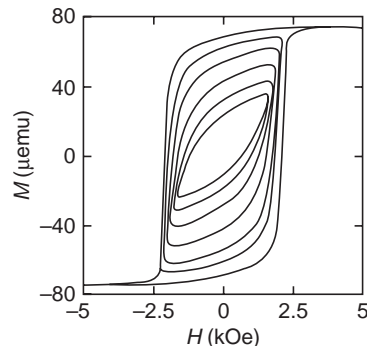


Fig. 1.1 Hysteresis curve of the magnetization as a function of the applied field for a CoPtCrB thin film. Multilayer Co/Pt is used in memory storage. Reprinted from Carpenter *et al.*, *Phys. Rev. B* **72**, 052410 (2005).

That is, ramping the field on and off is path dependent determined by which domains de-pin sequentially.

What is crucial in the magnetic system is that locally there are two degrees of freedom for each of the spins. At high temperature, both states are accessible. At sufficiently low temperature, one of the spin states is selected. Such state selectivity can be modeled with a double-well potential of the form

$$V(M) = -\frac{1}{2}\alpha M^2 + \frac{1}{4}\gamma M^4, \quad (1.11)$$

where M is the magnetization and α and γ are positive. The minima of this potential occur at

$$M_{\pm} = \pm \sqrt{\frac{\alpha}{\gamma}}. \quad (1.12)$$

Both of the minima are accessible at high temperature and no magnetization is possible. Our choice of $\alpha > 0$ ensures that deviations of M away from M_{\pm} cost energy. As a result, the minimum energy of V is not zero but rather the non-zero value of $V_0 = -\alpha^2/4\gamma$. As it stands, our theory is completely symmetrical with respect to the change $M \rightarrow -M$. Surely the physics cannot change if we were to recast our theory by shifting the scalar field M by a constant such that $M \rightarrow M_+ + \phi(x)$. The new potential

$$V' = V_0 + \left(-\frac{1}{2}\alpha + \frac{3}{2}\gamma M_+^2 \right) \phi^2 + \gamma M_+ \phi^3 + \frac{1}{4}\gamma \phi^4 \quad (1.13)$$

no longer looks symmetrical in terms of the new field ϕ . Why? What we have done by expanding around one of the minima of V is to hide the symmetry. Essentially we have broken the symmetry by setting the magnetization to M_+ . In the broken symmetry phase, up and down spins are no longer equivalent. The field M functions as the measure of the magnetic order. M is the order parameter. Unlike the old potential which was minimized by

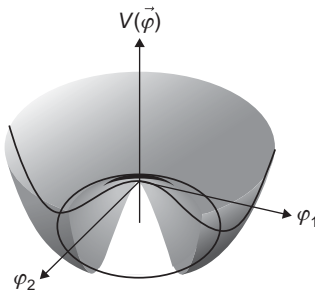


Fig. 1.2 Potential corresponding to the complex scalar field φ . The minima correspond to circles satisfying $\varphi_1^2 + \varphi_2^2 = \alpha/\gamma$.

a non-zero value of M , the minima of V' take place at $\phi(x) = 0$. This corresponds to a true vacuum. In classical models for ferromagnets, the magnetization turns on continuously,

$$M \propto |T - T_c|^\alpha, \quad (1.14)$$

at a non-zero temperature, T_c . It acquires its maximum value at $T = 0$. The exponent α is the critical exponent for the turn-on of the order parameter.

A slightly more complicated example of broken symmetry occurs when we modify our potential,

$$V(\varphi) = -\alpha\varphi^*\varphi + \gamma(\varphi^*\varphi)^2, \quad (1.15)$$

to allow for a complex scalar field $\varphi = \frac{1}{\sqrt{2}}(\varphi_1 + i\varphi_2)$. For $\alpha > 0$ and $\gamma > 0$, the potential is illustrated in Fig. 1.2. The corresponding Lagrangian takes the form

$$\mathcal{L} = \frac{1}{2}(\partial_\mu\varphi^*)(\partial^\mu\varphi) - (\alpha\varphi^*\varphi + \gamma(\varphi^*\varphi)^2). \quad (1.16)$$

Our Lagrangian has the global symmetry $\varphi \rightarrow \varphi e^{i\theta}$, where θ is a constant. As a result of this symmetry, the minima of V now take on a circle of values satisfying $\varphi_1^2 + \varphi_2^2 = \alpha/\gamma$, as illustrated in Fig. 1.2. That is, there are infinitely many saddle points as a result of the continuous global symmetry. As before with the single scalar field for the magnetization, we can expand about the circular minima by defining $\varphi = (\sqrt{\frac{\alpha}{\gamma}} + f(x) + ig(x))$. That is, we break the symmetry by hand. Because at the minima φ_1 and φ_2 are not independent, this transformation is not a simple translation of φ_1 and φ_2 separately. As a result, the quadratic term essentially has only one degree of freedom. We can interpret this as a vanishing of the mass for one of the scalar fields, in line with Goldstone's theorem that a massless mode must emerge upon the breaking of a continuous symmetry. Such a solution in which a complex field acquires a non-zero value is the heart of the superconducting transition. What the Bardeen–Cooper–Schrieffer solution laid plain is that the phenomenological Landau–Ginzburg treatment in terms of a complex order parameter acquiring a non-zero value in the superconducting state has a microscopic basis in the electron–phonon interaction. Such an interaction mediates pairing and the order parameter for the superconducting state is a product of an amplitude for pair formation times $e^{i\theta(r)}$, where θ is the phase of the pair field.

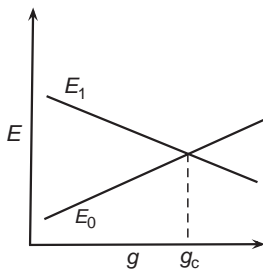


Fig. 1.3 Energy-level diagram for the ground state, E_0 , and first excited state, E_1 , as a function of a coupling constant, g . The crossing at g_c signals a phase transition between the ground and the first excited state.

Our statement that the low-temperature phase typically has lower symmetry is only true classically. There are many examples of symmetry breaking at $T = 0$ that have nothing to do with thermal fluctuations. Such phase transitions are governed by fluctuations of the vacuum, that is the uncertainty principle. In general, such phase transitions are governed by a transition among the quantum mechanical states of a many-body system simply by changing some system parameter. Consider a Hamiltonian $H(g)$, where g is a coupling constant. A typical energy-level diagram for this system as a function of g is depicted in Fig. 1.3. If, as a function of g , the first-excited and the ground states cross, a phase transition obtains to the first-excited state. For the transition to be continuous, we must have that $\partial E / \partial g = 0$. These types of situation are discussed explicitly in Chapter 14.

1.3 Beyond broken symmetry

Despite the utility of symmetry in classifying collective phenomena, physics is replete with examples of transitions between states of matter that share the same symmetry but are, nonetheless, distinct. An obvious example is the liquid–gas transition or the formation of the fractional quantum Hall state. However, the particular examples we focus on here, which typify the physics of strong coupling, are those in which the formation of some kind of bound state is the distinguishing feature. Consider, for example, the vulcanization or cross-linking transition in rubber. In the un-vulcanized state, rubber is a viscous liquid in which long-chain monomers move independently. Cross-linking between neighboring monomers, resulting in the formation of a highly entangled enmeshed amorphous state, defines the vulcanization transition. Although the monomers are localized in the vulcanized state, they are randomly located. Consequently, there are no Bragg peaks. Nonetheless, one can define an appropriate order parameter ([GCZ1996](#)) which reflects the fact that at $t = 0$ and $t = \infty$, the configuration of the monomer strands in the liquid changes while it is essentially static in the amorphous state. The resulting resilience and emergent static modulus of rubber both arise from the effective gluing together of the monomers. In high-energy physics, mesons or bound states of quarks are the propagating degrees of freedom at low energy in nuclei. They arise without the breaking of any continuous symmetry. In problems more

relevant for this text, a magnetic impurity in a non-magnetic host forms a bound state with all the conduction electrons below a characteristic temperature, once again without breaking any symmetry or even inducing a phase transition. The formation of such bound states is the essence of the Kondo problem which stands as one of the key triumphs of the renormalization group principle. As we will show from a systematic integration of the high-energy degrees of freedom, a bound state emerges because the coupling constant between the impurity and the host electrons diverges. Hence, at low temperatures it is not correct to think of the magnetic and conduction electron degrees of freedom separately. A new entity emerges at low energies that is not present in the starting ultraviolet (UV)-complete Lagrangian, a characteristic feature of strong-coupling systems. Although new degrees of freedom are present at strong coupling which are absent in the weakly coupled or high-temperature regime, the two states are still adiabatically connected in that by varying the system parameters, one can go smoothly from one phase to the other. Nonetheless, the phases are quite distinct. They possess different degrees of freedom, and no unified description exists of such systems in terms of a single entity. Bound-state formation is a standard paradigm in strong coupling physics and, as we will see, the Mott problem, an insulating state in a partially filled band, is no exception.

Another key example is Fermi liquid theory. The primary tenet of this theory is that the excited states of a metal stand in a one-to-one correspondence with those of a non-interacting electron gas. The interactions in a metal are of course non-zero. However, they are strongly screened and can be treated as essentially short-ranged. The Landau ([L1957](#)) assertion is that all such short-ranged repulsive interactions do not destroy the sharpness of the electron excitations in the non-interacting electron gas. That this state of affairs obtains is perhaps one of the most remarkable principles in nature. Why can the short-range interactions be ignored in a metal? The answer lies in a fundamental renormalization principle which we present in Chapter 12. The key to solving any many-body problem is to identify the propagating degrees of freedom. Identifying that the propagating degrees of freedom are single electrons with a dispersion relation given by $p^2/2m$ in an interacting electron gas is highly non-trivial. In fact, it cannot be deduced directly from the Hamiltonian. Some further fact is needed. That further fact is the existence of a Fermi surface. As we will see, the fundamental principle that makes Fermi liquid theory work is that a Fermi surface is remarkably resilient to short-range repulsive interactions. We will demonstrate explicitly that all renormalizations ([P1992](#); [SM1991](#); [BG1990](#)) arising from such interactions are towards the Fermi surface. As a result, such interactions can effectively be integrated out, leaving behind dressed electrons or quasi-particles, thereby justifying the key Landau tenet ([L1957](#)) that the low-energy electronic excitation spectrum of a metal is identical to that of a non-interacting Fermi gas. Consequently, breaking Fermi liquid theory in dimensions greater than or equal to two is notoriously difficult. In one spatial dimension, interactions are always relevant, as will be seen, and a new state of matter arises, termed a Luttinger liquid, in which spin and charge move but with different velocities. In higher dimensions, the problem is open and stands as the key outstanding problem in solid state physics.

As Fermi liquid theory made the BCS theory of the superconducting state possible in that it cleanly identified the propagating degrees of freedom, a similar identification of the propagating degrees of freedom in the normal state of the copper-oxide high-temperature

superconductors is necessary to know what pairs up to form the superconducting condensate. This problem is particularly difficult as the parent materials are all antiferromagnetic Mott insulators. Some of the agreed-upon physics of this remarkable problem and a forward-leaning perspective are discussed in the final chapter of this book.

References

- [A1965] S. L. Adler, *Phys. Rev. B* **137**, 1022 (1965); *Phys. Rev.* **139**, B 1638 (1965).
- [BG1990] G. Benfatto and G. Gallavotti, *J. Stat. Phys.* **59**, 541 (1990).
- [GCZ1996] P. M. Goldbart, H. E. Castillo, A. Zippelius, *Adv. Phys.* **45**, 393 (1996).
- [G1961] J. Goldstone, *Nuovo Cimento* **19**, 154 (1961).
- [N1960] Y. Nambu, *Phys. Rev.* **117**, 648 (1960).
- [L1957] L. D. Landau, *Sov. Phys. JETP* **3**, 920 (1957); **5**, 101 (1957); **8** 70 (1959).
- [P1992] J. Polchinski, arXiv:hep-th/9210046.
- [SM1991] R. Shankar, *Physica* **A177**, 530 (1991).

Non-interacting electron gas

At the close of the previous chapter, we noted that one can understand the elementary properties of metals in terms of non-interacting electrons and phonons. For example, the low-temperature specific heat of a metal is the sum of a term linear in the temperature, T , from the electrons and a term proportional to T^3 from the phonons. This result follows from a non-interacting particle picture. The electrical conductivity limited by non-magnetic impurity scattering is also well described by a non-interacting electron gas. In addition, from a knowledge of single-electron band theory, one can discern qualitatively the differences between metals, insulators, and semiconductors. The remarkable success of the non-interacting model is paradoxical because electrons and ions are strongly interacting both with themselves and with one another. Along with its successes, the non-interacting picture has colossal shortcomings, most notably its inability to describe old problems such as cohesive energies, superconductivity, magnetism, and newer phenomena such as doped Mott insulators, the Kondo problem, and the fractional quantum Hall effects. We first review the physics of the non-interacting electron gas. It is only after we develop methodology for dealing with electron interactions than we can lay plain the reasons why the non-interacting model works so well.

Electrons in metals are quantum mechanical particles with spin $\hbar/2$ obeying Fermi–Dirac statistics. The Hamiltonian of a single electron is $\hat{p}^2/2m$ where $\hat{\mathbf{p}}$ is the electron momentum (operator) and m the electron mass. Its eigenstates are plane waves of the form $e^{i\mathbf{p}\cdot\mathbf{r}/\hbar}/\sqrt{V}$ times a spinor which specifies the electron spin projection on a convenient axis (usually \hat{z}), $\hbar\sigma/2$ where $\sigma = \pm 1$; here V is the system volume. The Hamiltonian (operator) for N such non-interacting electrons,

$$\hat{H} = \sum_{i=1}^N \frac{\hat{p}_i^2}{2m}, \quad (2.1)$$

is simply the sum of the kinetic energies of the individual particles. In this case, the eigenstates are products of the occupied single-particle plane-wave states. Each plane-wave state can be occupied at most by one electron of a given spin. We label these eigenstates by the distribution function $f_{\mathbf{p}\sigma}$, which is 1 if the single-particle momentum-spin state is occupied and 0 otherwise. In the ground state, the lowest $N/2$ single-particle states are doubly occupied with electrons of opposite spin. Consequently, in the ground state (temperature $T = 0$), the distribution function is

$$f_{\mathbf{p}\sigma} = \Theta(\mu_0 - p^2/2m), \quad (2.2)$$

where $\Theta(x)$ is the Heaviside function, $\Theta(x > 0) = 1$, and 0 otherwise. Here μ_0 is the zero-temperature electron chemical potential, which in this case is simply the Fermi energy,

Table 2.1					
	Li	Na	K	Rb	Cs
r_s	3.25	3.93	4.86	5.2	5.62

the energy of the highest occupied state, $p_F^2/2m$, where p_F is the electron Fermi momentum. The Fermi temperature T_F equals μ_0/k_B .

In terms of $f_{\mathbf{p}\sigma}$, the total number of electrons is given by

$$N = \sum_{\mathbf{p},\sigma} f_{\mathbf{p}\sigma}. \quad (2.3)$$

In the ground state, we can replace the sum by an integral and find the electron density at $T = 0$:

$$n_e = \frac{N(T=0)}{V} = \frac{2}{V} \sum_{p < p_F} = 2 \int_0^{p_F} \frac{d\mathbf{p}}{(2\pi\hbar)^3} = \frac{p_F^3}{3\pi^2\hbar^3}. \quad (2.4)$$

The average interparticle spacing is essentially the radius, r_e , of a sphere containing a single electron,

$$\frac{4\pi r_e^3}{3} n_e = 1. \quad (2.5)$$

Thus, from Eq. (2.4), the scale for the interparticle separation is

$$r_e = \left(\frac{9\pi}{4} \right)^{1/3} \frac{\hbar}{p_F} = 1.92 \frac{\hbar}{p_F}, \quad (2.6)$$

which is on the order of the lattice spacing. For $r_e \approx 1 \text{ rA}$, we find that the Fermi velocity $v_F = p_F/m \approx \hbar/mr_e \approx 10^8 \text{ cm/s} \approx c/300$, where c is the speed of light. (Relativistic effects are generally not important for the motion of electrons in the ground state.) It is conventional to work with the dimensionless ratio $r_s = r_e/a_0$, where $a_0 = \hbar^2/me^2$ is the Bohr radius; this quantity provides a measure of the electron density. The dense limit corresponds to $r_s \ll 1$ and the dilute regime to $r_s \gg 1$. In metals, r_s varies between 2 and 6. Listed in Table 2.1 are values of r_s for the alkali metals. Cesium is, in fact, the most dilute of all metals. It is this large value of r_s that is responsible for the inhomogeneities in the density of Cs. In Chapter 5, we will discuss further physics associated with large r_s , such as the eventual formation of a Wigner crystal. We can also use Eq. (2.4) to solve for the zero-temperature chemical potential

$$\mu_0 = (3\pi^2)^{2/3} \frac{\hbar^2}{2m} n_e^{2/3}. \quad (2.7)$$

For Na, $\mu_0 = 3.1 \text{ eV}$; typically in a metal, μ_0 ranges between 1 and 5 eV.

The total energy of the system is the sum over the occupied states weighted by the single-particle energies, $\epsilon_{\mathbf{p}} = p^2/2m$:

$$E = \sum_{\mathbf{p},\sigma} \epsilon_{\mathbf{p}} f_{\mathbf{p}\sigma}. \quad (2.8)$$

At $T = 0$, the energy is given by

$$E_0 = \frac{p_F^5 V}{10m\pi^2 \hbar^3} = \frac{3}{5} N \mu_0. \quad (2.9)$$

From the thermodynamic relation, $P = -(\partial E / \partial V)_{T,N}$, we find the pressure in the ground state, $P_0 = 2\mu_0 n_e / 5$. This quantity is of order 10^6 atm and arises entirely from the exclusion principle between the particles.

At finite temperature, we define the distribution function which ranges between 0 and 1 and measures the average occupation of the single-particle states. For a system in equilibrium at chemical potential μ ,

$$f_{\mathbf{p}\sigma} = \frac{1}{e^{\beta(\epsilon_{\mathbf{p}} - \mu)} + 1} \quad (2.10)$$

is the Fermi–Dirac distribution, where $\beta = 1/k_B T$. The Fermi–Dirac distribution function maximizes the entropy at a given energy and electron number. In general, the entropy, S , is given by the log of the number of microscopic states W ,

$$S = k_B \ln W, \quad (2.11)$$

consistent with the macroscopic thermodynamic state of the system. For the electron problem, the microscopic states are indexed by a momentum \mathbf{p} with occupancy 0 or 1. The distribution function $f_{\mathbf{p}\sigma}$, however, is a smooth function over all the momentum states. To construct this function, we group the momentum states into cells, each cell containing g_i momentum states and n_i particles. Because each cell contains g_i states,

$$\sum_i g_i \cdots = \sum_{\mathbf{p},\sigma} \cdots. \quad (2.12)$$

For the i th cell, the number of distinct ways of distributing n_i particles in g_i states is given by the combinatoric factor $W_i = g_i! / n_i!(g_i - n_i)!$. Applying Stirling's approximation

$$\ln N! \approx N(\ln N - 1) \quad (2.13)$$

to W_i , we obtain

$$\ln W_i \approx -n_i \ln \frac{n_i}{g_i} - (g_i - n_i) \ln \frac{g_i - n_i}{g_i} \quad (2.14)$$

$$= -g_i \left[\frac{n_i}{g_i} \ln \frac{n_i}{g_i} + \left(1 - \frac{n_i}{g_i}\right) \ln \left(1 - \frac{n_i}{g_i}\right) \right], \quad (2.15)$$

where n_i/g_i is the fraction of states occupied in cell number i . In fact, $n_i/g_i = f_i$ is the smooth distribution function we seek. If we substitute this expression into the equation for

$\ln W_i$, we recover the familiar result for the entropy,

$$S = -k_B \sum_{\mathbf{p}, \sigma} [f_{\mathbf{p}\sigma} \ln f_{\mathbf{p}\sigma} + (1 - f_{\mathbf{p}\sigma}) \ln(1 - f_{\mathbf{p}\sigma})], \quad (2.16)$$

where we have converted the sum over cells to a sum over spin and momentum states by using Eq. (2.12). To obtain the distribution function, we maximize the entropy subject to the constraint that the particle number and energy are fixed. Extremizing $S - E/T + \mu N/T$ with respect to $f_{\mathbf{p}\sigma}$, we find

$$0 = \epsilon_{\mathbf{p}\sigma} - \mu - k_B T \ln(f_{\mathbf{p}\sigma}^{-1} - 1), \quad (2.17)$$

which implies that $f_{\mathbf{p}\sigma}$ is the Fermi distribution function in Eq. (2.10).

Let us now calculate the heat capacity from the thermodynamic relationship

$$C_V = T \left(\frac{\partial S}{\partial T} \right)_V. \quad (2.18)$$

To compute the temperature derivative of the entropy, we consider the general variation of the entropy,

$$\delta S = -2k_B \sum_{\mathbf{p}} \delta f_{\mathbf{p}} \ln \frac{f_{\mathbf{p}}}{1 - f_{\mathbf{p}}} = 2k_B \sum_{\mathbf{p}} \delta f_{\mathbf{p}} \frac{\epsilon_{\mathbf{p}} - \mu}{k_B T} \quad (2.19)$$

$$= 2V k_B \int \frac{d\mathbf{p}}{(2\pi\hbar)^3} \delta f_{\mathbf{p}} \frac{\epsilon_{\mathbf{p}} - \mu}{k_B T}, \quad (2.20)$$

with respect to the distribution function $f_{\mathbf{p}\sigma}$. We can simplify this expression further by introducing the single-particle density of states per unit volume

$$N(\epsilon) = 2 \int \frac{d\mathbf{p}}{(2\pi\hbar)^3} \delta(\epsilon - \epsilon_{\mathbf{p}}) \quad (2.21)$$

$$= \frac{1}{\pi^2 \hbar^3} \int p^2 \frac{dp}{d\epsilon_{\mathbf{p}}} \delta(\epsilon - \epsilon_{\mathbf{p}}) d\epsilon_{\mathbf{p}} \quad (2.22)$$

$$N(\epsilon_{\mathbf{p}}) = \frac{mp}{\pi^2 \hbar^3}. \quad (2.23)$$

The key point here is that the single-particle density of states is a linear function of momentum. An equivalent way of writing this quantity is $N(\epsilon_{\mathbf{p}}) = (dp/d\epsilon_{\mathbf{p}})(p^2/\pi^2 \hbar^3)$. If we rewrite δS in terms of the density of states,

$$\delta S = \frac{V}{T} \int d\epsilon_{\mathbf{p}} \delta f_{\mathbf{p}} N(\epsilon_{\mathbf{p}}) (\epsilon_{\mathbf{p}} - \mu), \quad (2.24)$$

we obtain a single integral that can be evaluated using the Sommerfeld expansion. While this expansion is standard, we will review it.

Sommerfeld expansion

Consider an integral of the form

$$I = \int_0^\infty d\epsilon f(\epsilon) h(\epsilon), \quad (2.25)$$

where $h(\epsilon)$ is any smooth function and $f(\epsilon) = 1/(e^{\beta(\epsilon-\mu)} + 1)$. We integrate I by parts:

$$I = \int_0^\infty f'(\epsilon)H(\epsilon) d\epsilon, \quad (2.26)$$

where

$$H = - \int_0^\epsilon h(x) dx. \quad (2.27)$$

Because $f'(\epsilon)$ is strongly peaked at the chemical potential, we can expand H in a Taylor series around $\epsilon = \mu$,

$$H(\mu) + (\epsilon - \mu) \left(\frac{\partial H}{\partial \epsilon} \right)_{\epsilon=\mu} + \frac{1}{2}(\epsilon - \mu)^2 \left(\frac{\partial^2 H}{\partial \epsilon^2} \right)_{\epsilon=\mu} + \dots, \quad (2.28)$$

which gives us a series of integrals of the form

$$L_j = - \int_0^\infty (\epsilon - \mu)^j f'(\epsilon) d\epsilon \quad (2.29)$$

to calculate. For $j = 0$, $L_0 = -f(\infty) + f(0) = 1$. In the remaining integrals, we can replace the lower limit with $-\infty$. Letting $x = \beta(\epsilon - \mu)$, we have

$$L_j = \frac{1}{\beta^j} \int_{-\infty}^\infty x^j \frac{e^x}{(e^x + 1)^2} dx. \quad (2.30)$$

Since the integrand is odd in x for j odd, only the even j 's survive. The first several values of L_j are

$$L_0 = 1, \quad (2.31)$$

$$L_2 = \frac{\pi^2}{3} (k_B T)^2, \quad (2.32)$$

$$L_4 = \frac{7\pi^4}{15} (k_B T)^4. \quad (2.33)$$

Consequently, we systematically obtain the series expansion for I :

$$I = \int_0^\mu h(\epsilon) d\epsilon + \frac{\pi^2}{6} (k_B T)^2 h'(\mu) + \frac{7\pi^4}{360} (k_B T)^4 h'''(\mu) + \dots. \quad (2.34)$$

For functions h independent of temperature, the first term in this expansion is independent of temperature and hence, at fixed μ ,

$$\int_0^\infty d\epsilon \delta f(\epsilon) h(\epsilon) = \frac{\pi^2}{3} h'(\epsilon = \mu) k_B^2 T \delta T \quad (2.35)$$

is the leading term when f_p is varied as a function of temperature.

Now let us return to the calculation of the low-temperature entropy. We want to calculate the temperature variation of the entropy at fixed particle number. We first calculate at fixed μ and then show that the change in chemical potential with temperature for fixed particle number can be neglected here. If we now substitute Eq. (2.35) into Eq. (2.24), we find that

the variation of the entropy per unit volume,

$$\delta s = \frac{\pi^2}{3} k_B^2 N(\epsilon_F) \delta T, \quad (2.36)$$

is a constant independent of temperature. The heat capacity per unit volume,

$$c_V = T \left(\frac{\delta s}{\delta T} \right)_V = \frac{\pi^2}{3} k_B^2 N(\epsilon_F) T, \quad (2.37)$$

scales as a linear function of temperature. This contribution arises entirely from the conduction electrons. The contribution per electron is

$$\frac{c_V}{n_e} = \frac{\pi^2 k_B^2 m T}{p_F^2} = \frac{\pi^2}{2} k_B \frac{T}{T_F}. \quad (2.38)$$

Comparing this result with the classical heat capacity, $3k_B/2$, we find that the quantum mechanical value is smaller by a factor of $\pi^2 T / 3T_F$. In a metal, only a fraction of the electrons are at the Fermi level. The ratio T/T_F defines this fraction of electrons within $k_B T$ of the Fermi energy. The further an electron is below the Fermi level, the smaller is its contribution to the heat capacity.

We may use the Sommerfeld expansion to show that the chemical potential as a function of density and temperature is given, at low T , by

$$\mu(n_e, T) = \mu(n_e, 0) \left(1 - \frac{\pi^2}{12} \left(\frac{T}{T_F} \right)^2 \right), \quad (2.39)$$

where $\mu(n_e, 0) = \epsilon_F$. The proof of this result is similar to that used to derive the entropy, and we leave the derivation as an exercise (Problem 2.2). From Eq. (2.39) we see that the first correction to the chemical potential at fixed n_e is of order T^2 , and hence this correction can be ignored in calculating the low-temperature entropy, Eq. (2.36).

Problems

2.1 Evaluate the integral

$$L_j = \int_{-\infty}^{\infty} x^j \frac{e^x}{(e^x + 1)^2} dx.$$

Show in particular that only the integrals for even j s survive.

- 2.2 Use the Sommerfeld expansion to compute the first temperature correction, Eq. (2.39), to the chemical potential of a Fermi gas as a function of the density.

In this chapter, we develop the basic framework to see how electron–electron (e–e), electron–ion (e–i), and ion–ion (i–i) interactions affect the properties of solids. We first show that the electron and ion degrees of freedom can be decoupled. Such a separation arises because ions and electrons have vastly different velocities in a solid; roughly, the electron velocity is 1000 times larger than the ion velocity. As a consequence, the electrons view the ions as providing a static background in which they move. This physical picture is at the heart of the Born–Oppenheimer approximation ([BO1927](#)).

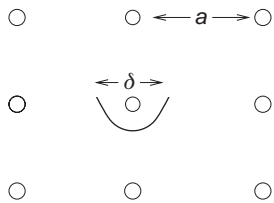
3.1 Basic Hamiltonian

It is useful at the outset to consider the total Hamiltonian to understand how to separate the electronic from the ionic motion. We denote the position and momentum of the i th ion by \mathbf{R}_i and \mathbf{P}_i , respectively, and that of the j th electron by \mathbf{r}_j and \mathbf{p}_j . We assume that all the ions have mass M and nuclear charge Ze . The total Hamiltonian is then

$$\begin{aligned} H = & \sum_i \frac{\mathbf{P}_i^2}{2M} + \sum_j \frac{\mathbf{p}_j^2}{2m} + \frac{(Ze)^2}{2} \sum_{i,i'} \frac{1}{|\mathbf{R}_i - \mathbf{R}_{i'}|} \\ & + \frac{e^2}{2} \sum_{j,j'} \frac{1}{|\mathbf{r}_j - \mathbf{r}_{j'}|} - Ze^2 \sum_{i,j} \frac{1}{|\mathbf{r}_j - \mathbf{R}_i|}. \end{aligned} \quad (3.1)$$

This Hamiltonian does not include external electric or magnetic fields or magnetic interactions among the constituents. The last three terms are the i–i, e–e, and e–i interactions, respectively. To progress with this Hamiltonian, we divide the electrons into two groups – the core and the valence or conduction electrons – depending on the degree to which they are bound. This separation is useful because core electrons move with the nuclei. Conduction or valence electrons transport throughout the solid. With this separation in mind, we obtain

$$\begin{aligned} H = & \sum_i \frac{\mathbf{P}_i^2}{2M} + \sum_{j=\text{cond.elec.}} \frac{\mathbf{p}_j^2}{2m} + \sum_{i,i'} V_{i,i'}(|\mathbf{R}_i - \mathbf{R}_{i'}|) \\ & + \frac{e^2}{2} \sum_{j,j'=\text{cond.elec.}} \frac{1}{|\mathbf{r}_j - \mathbf{r}_{j'}|} + \sum_{i,j} V_{ei}(|\mathbf{r}_j - \mathbf{R}_i|) + E_{\text{core}} \end{aligned} \quad (3.2)$$

**Fig. 3.1**

Ion lattice with spacing a . Each ion oscillates in a harmonic well with a deviation from its home position that is small relative to the ion spacing. The deviation is roughly $\delta \sim (m/M)^{1/4}a \sim 10^{-4}a$, where m is the electron mass and M the mass of the ions. It is for this reason that the ions can be treated essentially as fixed relative to the electronic degrees of freedom. That the ions comprise a fixed, almost rigid background for the electron motion is the essence of the Born–Oppenheimer approximation.

as the partitioned Hamiltonian. In Eq. (3.2), $V_{i,i'}$ and V_{ei} represent the effective potential between the ions and the valence electrons with the ions, respectively. The energy of the core electrons is E_{core} . In the example of Na, the total Z is 11, with the orbital filling $1s^2 2s^2 2p^6 3s$. There is only one unpaired valence electron. The effective charge of the ion in this representation is $Z = 1$.

3.2 Adiabatic approximation

To simplify Eq. (3.2), we separate the nuclear motion from that of the electrons, a separation that makes sense because the ions are much more massive than the electrons. Typically $m/M \sim 1/2000$ to $1/500\,000$. The small parameter characterizing the expansion is $(m/M)^{1/4}$. We now show that the ion velocity is related to the Fermi velocity by the ratio $(m/M)^{3/4}$. As a result, the ions can be treated as essentially static relative to the electrons. This allows us to solve for the electron motion assuming first that the ions are fixed at their equilibrium positions. The effects of the ion motion can be treated as a perturbation; that is, the electrons adjust adiabatically to the ion motion. From the perspective of the ions, the rapid motion of the electrons creates an overall average electron potential which they feel. This separation is the essence of the Born–Oppenheimer approximation.

To understand the relative orders of magnitude of the ionic and electron velocities and energies, we assume, for the sake of the argument, that ions individually move in harmonic wells (see Fig. 3.1) of the form $V_{\text{osc}} = M\omega^2 R^2 / 2$, where R measures the deviation of an ion from its home (or equilibrium) position. Consider displacing an ion by a lattice spacing, a . The energy required to do so, $\sim M\omega^2 a^2 / 2$, is essentially that required to distort the electron wavefunction, and thus the energy is of order $\hbar^2 / 2ma^2$, which in turn is of the order of the electron kinetic energy, $p_F^2 / 2m$. Thus $M\omega^2 a^2 / 2 \sim p_F^2 / 2m$. Solving for ω , we find that

$$\omega \sim (m/M)^{1/2} \frac{\hbar}{ma^2}. \quad (3.3)$$

However, for an ion in a harmonic well, $P^2/2M = \hbar\omega/2$, or equivalently, the square of the ion velocity is $\hbar\omega/M$. Combining this result with those for ω , we see that

$$v_{\text{ion}} \sim (m/M)^{3/4} v_F \sim (10^{-2} \text{ to } 10^{-3}) v_F. \quad (3.4)$$

Let us estimate how far the ions move from their equilibrium positions. For a displacement δ , $M\omega^2\delta^2/2 \sim \hbar\omega/2$. Substituting $\omega \sim (m/M)^{1/2}\hbar/m a^2$, we find an ion displacement,

$$\delta \sim a(m/M)^{1/4} \sim 10^{-4} a, \quad (3.5)$$

which is negligible, as illustrated in Fig. 3.1. As far as the electrons are concerned, the ions are static. We can calculate the role of the electronic degrees of freedom by developing a perturbation series in the small quantity δ/a or $(m/M)^{1/4}$. Note also that because $P^2/2M \sim \hbar\omega/2 \sim \epsilon_F(m/M)^{1/2} \ll \epsilon_F$, the ion kinetic energy is relatively small.

The formal development of the Born–Oppenheimer approximation begins with the assumption that the full wavefunction is a function of the many-electron positions $\mathbf{r} \equiv \{\mathbf{r}_j\}$ and ionic positions $\mathbf{R} \equiv \{\mathbf{R}_i\}$, and can be expanded as

$$\Psi(\mathbf{r}, \mathbf{R}) = \sum_n \Phi_n(\mathbf{R}) \Psi_{e,n}(\mathbf{r}, \mathbf{R}), \quad (3.6)$$

where the $\Psi_{e,n}(\mathbf{r}, \mathbf{R})$ (indexed by n) are the solutions to the electron–ion problem for a fixed set of ion positions \mathbf{R} . The ionic wavefunctions, $\Phi_n(\mathbf{R})$, on the one hand, describe the amplitude for the ions to be found at positions \mathbf{R} ; on the other hand they can be regarded as expansion coefficients of the electronic wavefunctions. The $\Psi_{e,n}$ form a complete orthonormal set. Consequently,

$$\int d\mathbf{r} \Psi_{e,n}^*(\mathbf{r}, \mathbf{R}) \Psi_{e,m}(\mathbf{r}, \mathbf{R}) = \langle en | em \rangle = \delta_{nm}. \quad (3.7)$$

Coupled with the orthogonality condition on the nuclear wavefunctions,

$$\int d\mathbf{R} \Phi_n^*(\mathbf{R}) \Phi_m(\mathbf{R}) = \delta_{nm}, \quad (3.8)$$

the complete electron–ion wavefunction is normalized,

$$\langle \Psi(\mathbf{r}, \mathbf{R}) | \Psi(\mathbf{r}, \mathbf{R}) \rangle = 1.$$

We determine each of the expansion coefficients from the equations of motion obeyed by Φ_n and $\Psi_{e,n}$. To proceed, we rewrite Eq. (3.2) as

$$H = T_i + T_e + V_{ii} + V_{ee} + V_{ei} + E_{\text{core}}, \quad (3.9)$$

where there is a one-to-one correspondence between the terms in (3.9) and those in (3.2). The eigenvalue equation for (3.9) is

$$(T_i + T_e + V_{ii} + V_{ee} + V_{ei} + E_{core}) \Psi = E\Psi \quad (3.10)$$

$$(T_i + V_{ii} + E_{core})\Psi + \sum_n \Phi_n(T_e + V_{ee} + V_{ei})\Psi_{e,n}(\mathbf{r}, \mathbf{R}) = E\Psi. \quad (3.11)$$

We simplify this equation by noting that $T_e + V_{ee} + V_{ei}$ only operates on the electron part of the product wavefunction. Let $E_{e,n}(\mathbf{R})$ be the energy of the electron system for a fixed set of nuclear coordinates. As a consequence, the nuclear and the electronic eigenvalue equations,

$$\sum_n (T_i + V_{ii} + E_{core} + E_{e,n} - E) \Phi_n \Psi_{e,n} = 0, \quad (3.12)$$

and

$$(T_e + V_{ee} + V_{ei})\Psi_{e,n}(\mathbf{r}, \mathbf{R}) = E_{e,n}(\mathbf{R})\Psi_{e,n}, \quad (3.13)$$

can be separated.

Let us multiply the nuclear eigenvalue equation by $\Psi_{em}^* = \langle em | \mathbf{r}, \mathbf{R} \rangle$ and integrate:

$$\sum_n \int d\mathbf{r} \Psi_{e,m}^*(\mathbf{r}, \mathbf{R}) T_i \Phi_n(\mathbf{R}) \Psi_{e,n}(\mathbf{r}, \mathbf{R}) + (V_{ii} + E_{core} + E_{e,m}(\mathbf{R}) - E) \Phi_m(\mathbf{R}) = 0. \quad (3.14)$$

Because the matrix element $\langle en | V_{ii}(\mathbf{R}) | em \rangle$ involves purely algebraic operators, it has only diagonal elements. The kinetic energy term, however, has off-diagonal elements; explicitly,

$$\begin{aligned} \sum_i \left\langle em \left| \frac{\mathbf{P}_i^2}{2M} \Phi_n(\mathbf{R}_i) \right| en \right\rangle &= -\frac{\hbar^2}{2M} \sum_i \int d\mathbf{r} \Psi_{e,m}^*(\mathbf{r}, \mathbf{R}) \left[(\nabla_{\mathbf{R}_i}^2 \Phi_n(\mathbf{R})) \right. \\ &\quad \left. + 2 (\nabla_{\mathbf{R}_i} \Phi_n(\mathbf{R})) \cdot \nabla_{\mathbf{R}_i} + \Phi_n(\mathbf{R}) \nabla_{\mathbf{R}_i}^2 \right] \Psi_{e,n}(\mathbf{r}, \mathbf{R}). \end{aligned} \quad (3.15)$$

Because $\nabla_{\mathbf{R}}^2$ acts exclusively on $\Phi_n(\mathbf{R})$ in the first term in the integral, the resultant matrix element is purely diagonal. For the moment, we ignore the last two terms in the kinetic energy matrix element and obtain

$$\sum_n (T_i + V_{ii} + E_{core} + E_{e,n}(\mathbf{R})) \Phi_n(\mathbf{R}) = \sum_n E_n \Phi_n(\mathbf{R}), \quad (3.16)$$

or, equivalently,

$$[T_i + V_{ii} + E_{core} + E_{e,n}(\mathbf{R})] \Phi_n(\mathbf{R}) = E_n \Phi_n(\mathbf{R}), \quad (3.17)$$

as the eigenvalue equation for the nuclear degrees of freedom. Equations (3.13) and (3.17) are the principal results in the Born–Oppenheimer method. In the nuclear eigenvalue equation, $E_{e,n}(\mathbf{R})$ serves as the effective nuclear potential that results when the electronic degrees of freedom are integrated out. The solutions to (3.17) will describe the phonon modes of the ions.

To justify this treatment of the ion kinetic energy term, we analyze the relative magnitude of the three contributions in Eq. (3.15). We first need a reasonably accurate form for the nuclear wavefunctions. For our purposes, the harmonic approximation we made in conjunction with the derivation of the ion velocity is adequate. In this case,

$$\Phi_n \sim e^{-M\omega(\mathbf{R}-\mathbf{R}^0)^2/2\hbar}, \quad (3.18)$$

where \mathbf{R}^0 is the equilibrium position of the ion. Consequently,

$$\frac{\hbar^2}{2M} \nabla_{\mathbf{R}_i}^2 \Phi_n \cdot \Psi_{e,n} \sim \frac{\hbar^2}{2M} \left(\frac{M\omega}{\hbar} \delta \right)^2 \Phi_n \Psi_{e,n} \sim \left(\frac{m}{M} \right)^{1/2} \epsilon_F \Phi_n \Psi_{e,n}. \quad (3.19)$$

Consider now the second term in Eq. (3.15). The inverse length scale on which the electron wavefunctions change is $\nabla_R \sim 1/a$. As a consequence,

$$\frac{\hbar^2}{2M} \nabla_{\mathbf{R}_i} \Phi_n \cdot \nabla_{\mathbf{R}_i} \Psi_{e,n} \sim \frac{\hbar^2}{2M} \frac{M\omega}{\hbar} \frac{\delta}{a} \Psi_{e,n} \Phi_n \sim \left(\frac{m}{M} \right)^{3/4} \epsilon_F \Phi_n \Psi_{e,n} \quad (3.20)$$

and

$$\frac{\hbar^2}{2M} \Phi_n \nabla_{\mathbf{R}_i}^2 \Psi_{e,n} \sim \frac{\hbar^2}{2M} \frac{1}{a^2} \Psi_{e,n} \Phi_n \sim \frac{m}{M} \epsilon_F \Phi_n \Psi_{e,n}. \quad (3.21)$$

As is evident, the largest contribution to the nuclear kinetic energy matrix element arises from $\nabla_{\mathbf{R}_i}^2 \Phi_n$. The primary reason why this is so is that gradients of Φ_n exceed those of $\Psi_{e,n}$ by a factor of $(M/m)^{1/4}$. Consequently, dropping the last two terms in Eq. (3.15) incurs a negligible error on the order of $(m/M)^{1/4}$.

To lowest order in m/M , we then neglect the ion kinetic energy and assume $\mathbf{R} = \mathbf{R}^0$. The ground electronic wavefunction is $\Psi_{e,n=0}(\mathbf{r}, \mathbf{R}^0)$; its corresponding energy, $E_{e,n=0}(\mathbf{R}^0)$, obeys the Schrödinger equation

$$[T_e + V_{ee} + V_{ei}(\mathbf{r} - \mathbf{R}^0)] \Psi_{e,n=0}(\mathbf{r}, \mathbf{R}^0) = E_{e,n=0}(\mathbf{R}^0) \Psi_{e,n=0}(\mathbf{r}, \mathbf{R}^0). \quad (3.22)$$

The subsequent ground-state nuclear wavefunctions and energies can be found with the effective potential $E_{e,n=0}(\mathbf{R}^0)$. If deviations about the equilibrium ion positions are considered within a simple harmonic oscillator model, the total energy of each low-energy state is given by

$$E_n = E_{e,n}(\mathbf{R}^0) + E_{\text{core}} + V_{ii}(\mathbf{R}^0) + \sum_q \hbar\omega_q \left(n_q + \frac{1}{2} \right) + \text{anharmonic terms.} \quad (3.23)$$

3.3 Tight-binding approximation

From our preceding discussion, the effective electron problem is

$$H_e = T_e + V_{ee} + V_{ion}(\mathbf{r}), \quad (3.24)$$

where

$$V_{ion}(\mathbf{r}) = \sum_{i,j} V_{ei}(\mathbf{r}_j - \mathbf{R}_i^0). \quad (3.25)$$

Here $V_{\text{ion}}(\mathbf{r})$ is the potential felt by the electrons produced by the ions in their equilibrium positions. To a good approximation, this potential is periodic. Let us group all the one-body terms together as $h_e(\mathbf{r}) = T_e + V_{\text{ion}}(\mathbf{r})$. The reduced electronic Hamiltonian is then

$$H_e = h_e + V_{ee}. \quad (3.26)$$

It is this Hamiltonian that we will primarily discuss in the remainder of this book.

A closer look at the one-body part of our Hamiltonian is warranted. In the previous chapter, we treated the electrons in a metal as if they were free particles not tethered to any ions. Of course this is wrong. Electrons know about the ions and interact strongly with them. Why then is it possible to regard the electrons as being free? It turns out that had we started with the localized picture advanced by Wannier, we would still end up with the same answer. The solution to the one-body part of the Hamiltonian is described by a set of periodic Bloch waves,

$$u_{n\mathbf{k}}(\mathbf{r}) = e^{i\mathbf{k}\cdot\mathbf{r}} c_{n\mathbf{k}}(\mathbf{r}), \quad (3.27)$$

for the n th band with momentum \mathbf{k} . Here $c_{n\mathbf{k}}(\mathbf{r})$ is a function that has the periodicity of the lattice. Since the Bloch functions are complete, we can form a state localized on a particular lattice site \mathbf{R} ,

$$w_n(\mathbf{R}, \mathbf{r}) = \frac{1}{\sqrt{N}} \sum_{\mathbf{k}} e^{-i\mathbf{k}\cdot\mathbf{R}} u_{n\mathbf{k}}(\mathbf{r}), \quad (3.28)$$

by expanding appropriately. Because the Bloch states are orthonormal, so are the Wannier ([W1937](#)) states,

$$\begin{aligned} \langle \mathbf{R}' | \mathbf{R} \rangle &\equiv \int d\mathbf{r} w_n(\mathbf{R}, \mathbf{r}) w_m^*(\mathbf{R}', \mathbf{r}) = \frac{1}{N} \sum_{\mathbf{k}, \mathbf{k}'} \int d\mathbf{r} e^{-i\mathbf{k}\cdot\mathbf{R} + i\mathbf{k}'\cdot\mathbf{R}'} u_{n\mathbf{k}}(\mathbf{r}) u_{m\mathbf{k}'}^*(\mathbf{r}) \\ &= \frac{1}{N} \sum_{\mathbf{k}, \mathbf{k}'} e^{-i\mathbf{k}\cdot\mathbf{R} + i\mathbf{k}'\cdot\mathbf{R}'} \delta_{m,n} \delta_{\mathbf{k}, \mathbf{k}'} \\ &= \delta_{\mathbf{R}, \mathbf{R}'} \delta_{m,n}, \end{aligned} \quad (3.29)$$

as can be seen from a direct calculation. The statement that Wannier states form an orthonormal basis is somewhat problematic. If we were to rewrite h_e in terms of the Wannier states,

$$h_e = \sum_{\mathbf{R}, \mathbf{R}'} |\mathbf{R}'\rangle \langle \mathbf{R}'| h_e | \mathbf{R} \rangle \langle \mathbf{R}|, \quad (3.30)$$

by using the completeness relationship on the state vectors associated with the Wannier states, $|\mathbf{R}\rangle$, we would have to conclude that there are no off-diagonal matrix elements of our Hamiltonian. That is, if the Wannier states on two neighboring sites do not have any overlap, any matrix element with the Hamiltonian should be zero. The statement that the Wannier basis forms an orthonormal basis in practice means that beyond nearest neighbors,

the wavefunctions have no appreciable amplitude. This is the tight-binding approximation and the Hamiltonian that results is termed the tight-binding (TB) Hamiltonian. Restricting ourselves to nearest neighbors, we define the parameters in our TB model as

$$\langle \mathbf{R} | h_e | \mathbf{R} \rangle \equiv E_0 \quad (3.31)$$

and the nearest-neighbor matrix element as

$$\langle \mathbf{R} | h_e | \mathbf{R} + \delta \rangle \equiv -t \quad (3.32)$$

where δ is a unit vector from site \mathbf{R} to the nearest neighbors. Our Hamiltonian simplifies to

$$H^{\text{TB}} = -t \sum_{\mathbf{R}, \delta} |\mathbf{R}\rangle \langle \mathbf{R} + \delta| + E_0 \sum_{\mathbf{R}} |\mathbf{R}\rangle \langle \mathbf{R}|. \quad (3.33)$$

Regardless of the form of the underlying lattice, the tight-binding model can be solved exactly by Fourier transforming,

$$|\mathbf{R}\rangle = \frac{1}{\sqrt{N}} \sum_{\mathbf{k}} e^{-i\mathbf{k}\cdot\mathbf{R}} |\mathbf{k}\rangle. \quad (3.34)$$

The resultant Hamiltonian,

$$H^{\text{TB}} = \sum_{\mathbf{k}} E(\mathbf{k}) |\mathbf{k}\rangle \langle \mathbf{k}|, \quad (3.35)$$

depends on a single parameter, namely the band structure

$$E(\mathbf{k}) = E_0 - t \sum_{\delta} e^{i\mathbf{k}\cdot\delta}. \quad (3.36)$$

The energy band, $E(\mathbf{k})$, defines the energy of a non-interacting particle with momentum \mathbf{k} and hence is the TB analog of the free-particle dispersion. The TB model can be viewed as the lattice analog of the free-particle problem.

Problem

- 3.1 This problem concerns the band structure of a single sheet of carbon, graphene (see Fig. 3.2). Nearest-neighbor atoms are connected by the set of vectors

$$\delta_1 = \frac{a}{2} (1, \sqrt{3}), \quad \delta_2 = \frac{a}{2} (1, -\sqrt{3}), \quad \delta_3 = -a (1, 0) \quad (3.37)$$

and the primitive lattice vectors are

$$\mathbf{a}_1 = \frac{a}{2} (3, \sqrt{3}), \quad \mathbf{a}_2 = \frac{a}{2} (3, -\sqrt{3}), \quad (3.38)$$

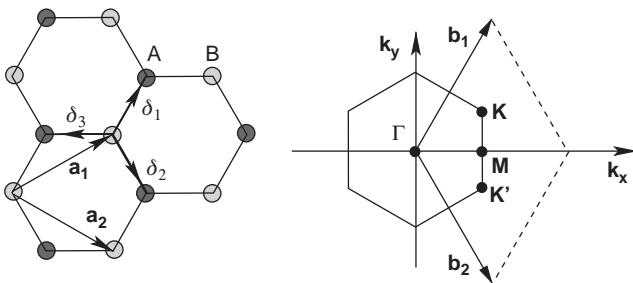


Fig. 3.2 Graphene lattice. The panel on the left shows the primitive lattice vectors, \mathbf{a}_i , and nearest-neighbor lattice vectors, δ_i . The labels A and B refer to the two kinds of carbon atoms in graphene. The panel on the right shows the first Brillouin zone spanned by the lattice vectors \mathbf{b}_i .

where $a = 1.42 \text{ \AA}$, the nearest-neighbor carbon–carbon spacing. The first Brillouin zone shown in Fig. 3.2 is spanned by the reciprocal vectors

$$\mathbf{b}_1 = \frac{2\pi}{3a} (1, \sqrt{3}), \quad \mathbf{b}_2 = \frac{2\pi}{3a} (1, -\sqrt{3}). \quad (3.39)$$

The corners of the first Brillouin zone are located at

$$\mathbf{K} = \frac{2\pi}{3a} \left(1, \frac{1}{\sqrt{3}} \right), \quad \mathbf{K}' = \frac{2\pi}{3a} \left(1, -\frac{1}{\sqrt{3}} \right). \quad (3.40)$$

You are to (a) write down the tight-binding Hamiltonian for this system and solve it for the energy bands, (b) determine the values (there are two) of \mathbf{k} for which the energy dispersion vanishes, (c) show that the dispersion can be written as

$$E(\mathbf{q}) = \pm \hbar v_F |\mathbf{q}|, \quad (3.41)$$

where $v_F = 3t/2\hbar a \approx 10^6 \text{ m/s}$ and q is the deviation from the value of the momentum at the zero crossing, and (d) show that the effective Hamiltonian near the zero crossings can be written as

$$H \equiv \hbar v_F \begin{pmatrix} 0 & q_x + iq_y \\ q_x - iq_y & 0 \end{pmatrix} = \hbar v_F \sigma \cdot \mathbf{q}$$

for the \mathbf{K}' point and

$$H \equiv \hbar v_F \begin{pmatrix} 0 & -q_x + iq_y \\ -q_x - iq_y & 0 \end{pmatrix} = \hbar v_F (-q_x \sigma_x + q_y \sigma_y)$$

for the \mathbf{K} point.

References

- [BO1927] M. Born and J. R. Oppenheimer, *Ann. d. Physik* **84**, 457 (1927).
 [W1937] G. H. Wannier, *Phys. Rev.* **52**, 191 (1937).

To solve many-particle problems, it is expedient to introduce the language of second quantization. This approach does not add new conceptual baggage to quantum mechanics. Rather, it provides a convenient book-keeping method for dealing with many-particle states. As a result, we will be brief in the formal development of this technique. For a more complete development, see, for example, Baym (B1969). We develop this approach for fermions, that is, particles that are antisymmetric with respect to interchange of any two of their coordinates, and for bosons, particles for which such interchanges do not incur any sign change in the many-particle wavefunction.

4.1 Bosons

Consider the many-body state of a boson system containing n identical particles:

$$\varphi_0(\mathbf{r}) = \langle \mathbf{r}_1, \mathbf{r}_2, \dots, \mathbf{r}_n | n \rangle. \quad (4.1)$$

For states containing different numbers of particles, the orthogonality condition

$$\langle n | m \rangle = \delta_{nm} \quad (4.2)$$

holds. As in the case of the harmonic oscillator, we define the operator a_0 such that

$$a_0 |n\rangle = \sqrt{n} |n-1\rangle. \quad (4.3)$$

That is, the operator a_0 annihilates a single particle from the state $|n\rangle$ and produces the corresponding $n-1$ particle state. The adjoint operation in Eq. (4.2) suggests that

$$\langle n | a_0^\dagger = \langle n-1 | \sqrt{n}. \quad (4.4)$$

As a consequence, the matrix element

$$\langle n | a_0^\dagger | n-1 \rangle = \sqrt{n} \langle n-1 | n-1 \rangle = \sqrt{n}. \quad (4.5)$$

An equivalent statement of the result in Eq. (4.5) is that

$$a_0^\dagger |n-1\rangle = \sqrt{n} |n\rangle. \quad (4.6)$$

The operator a_0^\dagger acts on the $|n-1\rangle$ particle state, producing the original state $|n\rangle$.

The choice of the factor of \sqrt{n} will now become clear when we consider the operator $\hat{N}_0 = a_0^\dagger a_0$. \hat{N}_0 is a Hermitian operator that, when acting on $|n\rangle$,

$$\hat{N}_0|n\rangle = a_0^\dagger a_0|n\rangle = a_0^\dagger \sqrt{n}|n-1\rangle = n|n\rangle, \quad (4.7)$$

counts the number of particles in state $|n\rangle$. Consequently, $\langle n|\hat{N}_0|n\rangle = n$, and \hat{N}_0 is called the number operator. Consider now the creation of the state $|n\rangle$ from the vacuum state $|0\rangle$. It follows from Eqs. (4.1) through (4.7) that

$$|n\rangle = \frac{(a_0^\dagger)^n}{\sqrt{n!}}|0\rangle. \quad (4.8)$$

We see then that the construction of an n -particle state of bosons is directly analogous to the rules for creating harmonic oscillator states. As such, the operators a_0 and a_0^\dagger must obey the commutation relation

$$[a_0, a_0^\dagger] = 1. \quad (4.9)$$

To see how this comes about, consider the operation $[a_0 a_0^\dagger - a_0^\dagger a_0]|n\rangle$. From Eqs. (4.1)–(4.7) we have found that

$$[a_0 a_0^\dagger - a_0^\dagger a_0]|n\rangle = (n+1-n)|n\rangle = |n\rangle, \quad (4.10)$$

which implies that $[a_0, a_0^\dagger] = 1$.

Let us now generalize to a boson state of the form $|n_0, n_1, n_2, \dots\rangle$, where n_i represents the occupation number for the boson state i . Application of the boson rules outlined previously yields

$$\begin{aligned} a_\ell |\dots, n_\ell, \dots\rangle &= \sqrt{n_\ell} |\dots, n_\ell - 1, \dots\rangle \\ a_\ell a_j |\dots, n_\ell, \dots, n_j, \dots\rangle &= \sqrt{n_\ell} \sqrt{n_j} |\dots, n_\ell - 1, \dots, n_j - 1, \dots\rangle. \end{aligned} \quad (4.11)$$

Analogous relationships hold for the creation operators. The generalized commutation relations are

$$\begin{aligned} [a_j, a_\ell^\dagger] &= \delta_{j\ell}, \\ [a_j, a_\ell] &= [a_j^\dagger, a_\ell^\dagger] = 0. \end{aligned} \quad (4.12)$$

A final note on the application of products of boson operators to the state $|n_0, \dots, n_j, \dots\rangle$ is in order. Because bosons commute, operations of the type $a_i^\dagger a_j^\dagger |\dots, n_i, \dots, n_j, \dots\rangle$ yield the same result, irrespective of the order of the operators a_i^\dagger and a_j^\dagger . As we will see, this is not the case with fermions.

4.2 Fermions

Let us assume now that the particles occupying the state $|n_0\rangle$ are fermions. We are restricted by the Pauli exclusion principle that $n_0 = 0, 1$. Analogously,

$$\begin{aligned} a_0|1\rangle &= |0\rangle, \\ a_0^\dagger|0\rangle &= |1\rangle. \end{aligned} \quad (4.13)$$

Note also that $a_0|0\rangle = a_1^\dagger|1\rangle = 0$, because no particle can be annihilated from the vacuum and each state can have at most one particle. To illustrate the inherent antisymmetry of fermions, consider the state $|n_0, n_1, \dots\rangle$. The sign convention for the application of creation and annihilation operators to this reference state is

$$a_j^\dagger| \dots, n_{j-1}, n_j, n_{j+1}, \dots \rangle = \begin{cases} (-1)^{\eta_j} | \dots, n_{j-1}, 1, n_{j+1}, \dots \rangle, & n_j = 0, \\ 0, & n_j = 1, \end{cases} \quad (4.14)$$

$$a_j| \dots, n_{j-1}, n_j, n_{j+1}, \dots \rangle = \begin{cases} (-1)^{\eta_j} | \dots, n_{j-1}, 0, n_{j+1}, \dots \rangle, & n_j = 1, \\ 0, & n_j = 0, \end{cases} \quad (4.15)$$

where η_j is the number of occupied states to the left of state j .

Let Ψ represent an occupation number wavefunction that contains the state j but not the state ℓ . Let's also assume $j > \ell$. Also let η_j and η_ℓ represent the number of occupied states immediately to the left of j and ℓ , respectively. By the rules in Eqs. (4.14) and (4.15), we have that

$$a_\ell^\dagger a_j \Psi = (-1)^{\eta_j + \eta_\ell} | \dots, n_{\ell-1}, 1, \dots, n_{j-1}, 0, \dots \rangle \quad (4.16)$$

$$a_j a_\ell^\dagger \Psi = (-1)^{\eta_\ell + \eta_j + 1} | \dots, n_{\ell-1}, 1, \dots, n_{j-1}, 0, \dots \rangle. \quad (4.17)$$

If we now add (4.16) and (4.17), we obtain

$$[a_\ell^\dagger a_j + a_j a_\ell^\dagger] \Psi = (-1)^{\eta_j + \eta_\ell} [1 - 1] | \dots, n_{\ell-1}, 1, \dots, n_{j-1}, 0, \dots \rangle, \quad (4.18)$$

or equivalently

$$\{a_\ell^\dagger, a_j\} = a_\ell^\dagger a_j + a_j a_\ell^\dagger = 0 \text{ for } j \neq \ell. \quad (4.19)$$

It is straightforward to show that if $j = \ell$ in Eq. (4.16), $a_j^\dagger a_j + a_j a_j^\dagger = 1$. The general anticommutation relation is

$$\{a_j^\dagger, a_\ell\} = \{a_j, a_\ell^\dagger\} = \delta_{j\ell}. \quad (4.20)$$

The remainder of the anticommutation relations, namely

$$\{a_j, a_\ell\} = \{a_j^\dagger, a_\ell^\dagger\} = 0, \quad (4.21)$$

can be derived in an analogous fashion. The final quantity we should define is the number operator,

$$\hat{N} = \sum_j a_j^\dagger a_j. \quad (4.22)$$

As in the boson case, $a_j^\dagger a_j$ counts the number of particles in state j .

4.3 Fermion operators

We now turn to the task of writing one- and two-body fermion operators in their second quantized form. A straightforward way of accomplishing this is to consider their action on a fully antisymmetrized many-particle state. Consider two single-particle states ϕ_1 and ϕ_2 . The normalized wavefunction that is antisymmetric with respect to particle interchange is

$$\langle \mathbf{r}_1, \mathbf{r}_2 | n_1, n_2 \rangle = \frac{1}{\sqrt{2}} [\phi_1(1)\phi_2(2) - \phi_1(2)\phi_2(1)]. \quad (4.23)$$

This state can be constructed from the determinant of ϕ_1 and ϕ_2 :

$$D_2 = \frac{1}{\sqrt{2!}} \begin{vmatrix} \phi_1(1) & \phi_2(1) \\ \phi_1(2) & \phi_2(2) \end{vmatrix}. \quad (4.24)$$

Dirac (D1929; D1958) and Slater (S1929) showed that the general rule for constructing an antisymmetric wavefunction out of n single-particle states is

$$D_n = \langle \mathbf{r}_1, \mathbf{r}_2, \dots | n_\alpha, n_\beta, \dots \rangle = \frac{1}{\sqrt{n!}} \| \phi_1 \cdots \phi_n \|, \quad (4.25)$$

where $\| \cdot \|$ represents the determinant. D_n contains all antisymmetrized permutations of the orbital set $\phi_1 \cdots \phi_n$ and hence may be written as

$$D_n = \langle \mathbf{r}_1, \mathbf{r}_2, \dots | n_1, n_2, \dots \rangle = \frac{1}{\sqrt{n!}} \sum_P (-1)^P P[\phi_1 \cdots \phi_n], \quad (4.26)$$

where P is the permutation operator. The inherent advantage in using second-quantized notation is that a general many-particle fermionic state can be written compactly as

$$|n_1, n_2, \dots \rangle = a_1^\dagger a_2^\dagger \cdots |0\rangle. \quad (4.27)$$

Complete antisymmetry under particle interchange is built into this many-body state as a result of the anticommuting property of the fermion operators. Note there is no $\sqrt{n!}$ normalization factor. In first quantization, however, an explicit $\sqrt{n!}$ factor appears, because particles are placed in particular single-particle states and all possible permutations are summed over. In second quantization, no labels are attached to the particles.

Let us now return to our initial goal. Consider the one-body operator \hat{H}_1 . The matrix element of a one-body operator between two many-particle states is non-zero only if the two

many-particle states do not differ by more than two single-particle states (see Problem 4.1). Consequently, the most \hat{H}_1 can do when it acts on a general many-body state is annihilate a particle from a particular single-particle state and fill the same or a previously vacant state. Hence, in second-quantized form, a general one-body operator is restricted to have a single creation–annihilation operator pair. Quite generally, then, we can write a one-body operator as

$$\hat{H}_1 = \sum_{v,\lambda} c_{\lambda v} a_{\lambda}^{\dagger} a_v. \quad (4.28)$$

To determine the coefficient $c_{\lambda v}$, we simply evaluate the matrix element $\langle \mu | \hat{H}_1 | \gamma \rangle$. Orthogonality of the single-particle states implies immediately that $\langle \mu | \hat{H}_1 | \gamma \rangle = c_{\mu \gamma}$. Consequently, the most general way of writing a one-body operator in second quantization is

$$\hat{H}_1 = \sum_{v,\lambda} \langle \lambda | \hat{H}_1 | v \rangle a_{\lambda}^{\dagger} a_v. \quad (4.29)$$

In the event that the single-particle states are eigenfunctions of \hat{H}_1 , then $\hat{H}_1 | v \rangle = \epsilon_v | v \rangle$, where ϵ_v is a c-number. Equation (4.29) then reduces to

$$\hat{H}_1 = \sum_{\lambda} \epsilon_{\lambda} a_{\lambda}^{\dagger} a_{\lambda} = \sum_{\lambda} n_{\lambda} \epsilon_{\lambda}. \quad (4.30)$$

Consequently, in the case that \hat{H}_1 is a one-body energy operator, the average of \hat{H}_1 determines the average energy of the system. The resultant expression is analogous to Eq. (2.8).

Consider now a general two-body operator

$$\hat{H}_2 = \frac{1}{2} \sum_{i,j} \hat{V}(i, j). \quad (4.31)$$

In the electron gas, $\hat{V}(i, j) = e^2 / |\hat{\mathbf{r}}_i - \hat{\mathbf{r}}_j|$, the Coulomb energy. A two-body operator can at most create two particle–hole excitations in a general many-body state. The general form of the operator that creates such excitations is $a_k^{\dagger} a_{\ell}^{\dagger} a_j a_i$. As a consequence, a general two-body operator in second-quantized form can be written as

$$\hat{H}_2 = \frac{1}{2} \sum_{i,j,k,\ell} V_{i,j,k,\ell} a_k^{\dagger} a_{\ell}^{\dagger} a_j a_i. \quad (4.32)$$

The interacting electron Hamiltonian containing both one- and two-body terms can be recast as

$$\hat{H}_e = \sum_{v,\lambda} \langle v | \hat{H}_1 | \lambda \rangle a_v^{\dagger} a_{\lambda} + \frac{1}{2} \sum_{i,j,k,\ell} \langle k | \langle \ell | \frac{e^2}{|\mathbf{r}_1 - \mathbf{r}_2|} | i \rangle | j \rangle a_k^{\dagger} a_{\ell}^{\dagger} a_j a_i. \quad (4.33)$$

To make contact with the electron gas, it is customary to transform to momentum space, in which the single-particle plane wave states,

$$\phi_p(\mathbf{r}) = \frac{e^{i\mathbf{p}\cdot\mathbf{r}/\hbar}}{\sqrt{V}}, \quad (4.34)$$

diagonalize exactly the electron kinetic energy. These states are defined in a box of volume V with periodic boundary conditions imposed. Particles with spin σ are added or removed from these states by the operators $a_{\mathbf{p}\sigma}^\dagger$ or $a_{\mathbf{p}\sigma}$ respectively. We introduce the *field operator*

$$\Psi_\sigma^\dagger(\mathbf{r}) = \sum_{\mathbf{p}} \frac{e^{-i\mathbf{p}\cdot\mathbf{r}/\hbar}}{\sqrt{V}} a_{\mathbf{p}\sigma}^\dagger, \quad (4.35)$$

which creates an electron at \mathbf{r} with spin σ . The Hermitian conjugate field, $\Psi_\sigma(\mathbf{r})$, annihilates a particle with spin σ at \mathbf{r} . Field operators create and annihilate particles at particular positions. In so doing, they do not add or remove particles from a particular momentum state. Rather, they add or subtract particles from a superposition of momentum states with amplitude $e^{\pm i\mathbf{p}\cdot\mathbf{r}/\hbar}/\sqrt{V}$. The product of the creation and annihilation field operators

$$\Psi_\sigma^\dagger(\mathbf{r})\Psi_\sigma(\mathbf{r}) = \frac{1}{V} \sum_{\mathbf{p}, \mathbf{p}'} e^{-i\mathbf{r}\cdot(\mathbf{p}-\mathbf{p}')/\hbar} a_{\mathbf{p}\sigma}^\dagger a_{\mathbf{p}'\sigma} \quad (4.36)$$

defines the particle density operator. Consequently, if we integrate Eq. (4.36) over \mathbf{r} ,

$$\begin{aligned} \hat{n}_\sigma &= \int d\mathbf{r} \Psi_\sigma^\dagger(\mathbf{r})\Psi_\sigma(\mathbf{r}) \\ &= \frac{1}{V} \int d\mathbf{r} \sum_{\mathbf{p}, \mathbf{p}'} e^{-i(\mathbf{p}-\mathbf{p}')\cdot\mathbf{r}/\hbar} a_{\mathbf{p}\sigma}^\dagger a_{\mathbf{p}'\sigma} \\ &= \sum_{\mathbf{p}} a_{\mathbf{p}\sigma}^\dagger a_{\mathbf{p}\sigma} = \sum_{\mathbf{p}} \hat{n}_{\mathbf{p}\sigma}, \end{aligned} \quad (4.37)$$

we obtain the total particle density for electrons with spin σ .

In analogy with Eq. (4.27), we can construct a general many-body state $|\mathbf{r}_{1\sigma_1} \cdots \mathbf{r}_{n\sigma_n}\rangle$,

$$|\mathbf{r}_{1\sigma_1} \cdots \mathbf{r}_{n\sigma_n}\rangle = \Psi_{\sigma_1}^\dagger(\mathbf{r}_1) \cdots \Psi_{\sigma_n}^\dagger(\mathbf{r}_n) |0\rangle, \quad (4.38)$$

from the vacuum state using the field operator $\Psi_{\sigma_i}^\dagger(\mathbf{r}_i)$. The rules for applying $\Psi_{\sigma_i}^\dagger$ and Ψ_{σ_i} to $|\mathbf{r}_{1\sigma_1} \cdots \mathbf{r}_{n\sigma_n}\rangle$ are

$$\Psi_{\sigma_{n+1}}^\dagger(\mathbf{r}_{n+1}) |\mathbf{r}_{1\sigma_1} \cdots \mathbf{r}_{n\sigma_n}\rangle = \sqrt{n+1} (-1)^{\eta_{n+1}} |\mathbf{r}_{1\sigma_1} \cdots \mathbf{r}_{n+1\sigma_{n+1}}\rangle \quad (4.39)$$

and

$$\Psi_\sigma(\mathbf{r}) |\mathbf{r}_{1\sigma_1} \cdots \mathbf{r}_{n\sigma_n}\rangle = \frac{1}{\sqrt{n}} \sum_{\alpha} \delta(\mathbf{r} - \mathbf{r}_\alpha) (-1)^{\eta_\alpha} |\mathbf{r}_1 \cdots \mathbf{r}_{\alpha-1}, \mathbf{r}_{\alpha+1} \cdots \mathbf{r}_n\rangle. \quad (4.40)$$

Here again, η_α is the number of occupied states to the left of \mathbf{r}_α .

Problems

- 4.1 Show that the matrix element of a one-body operator is non-zero between two many-particle states, provided the two many-body states do not differ by more than two single-particle states.
- 4.2 Prove explicitly that a general two-body operator can be written in the form

$$\hat{V}_2 = \sum_{\alpha\beta\gamma\delta} \langle \gamma | \langle \delta | V_2 | \alpha \rangle | \beta \rangle a_\gamma^\dagger a_\delta^\dagger a_\beta a_\alpha,$$

where $\langle \gamma\delta | V_2 | \alpha\beta \rangle$ is the matrix element of the two-body interaction between initial states ϕ_α and ϕ_β and final states ϕ_γ and ϕ_δ . Also, show that for fermions in a state of the form (4.27), one can factor the expectation value $\langle a_\gamma^\dagger a_\delta^\dagger a_\beta a_\alpha \rangle$ as

$$\langle a_\gamma^\dagger a_\delta^\dagger a_\beta a_\alpha \rangle = \langle a_\gamma^\dagger a_\alpha \rangle \langle a_\delta^\dagger a_\beta \rangle - \langle a_\gamma^\dagger a_\beta \rangle \langle a_\delta^\dagger a_\alpha \rangle.$$

- 4.3 Show that the field operators obey the commutation relations

$$\begin{aligned} [\Psi_\sigma^\dagger(\mathbf{r}), \Psi_\sigma(\mathbf{r}')]_\pm &= \delta(\mathbf{r} - \mathbf{r}'), \\ [\Psi_\sigma(\mathbf{r}), \Psi_\sigma(\mathbf{r}')]_\pm &= [\Psi_\sigma^\dagger(\mathbf{r}), \Psi_\sigma^\dagger(\mathbf{r}')]_\pm = 0, \end{aligned} \quad (4.41)$$

where \pm denotes the commutator for bosons and the anticommutator for fermions.

References

- [B1969] G. Baym, *Lectures on Quantum Mechanics* (W. A. Benjamin, Inc., New York, 1969; Perseus Books, Cambridge, MA, 1969).
- [D1929] P. A. M. Dirac, *Proc. Roy. Soc. Lond.* **A123**, 714 (1929).
- [D1958] P. A. M. Dirac, *The Principles of Quantum Mechanics*, 4th edn. (Oxford University Press, Oxford, 1958), p. 248.
- [S1929] J. C. Slater, *Phys. Rev.* **34**, 1293 (1929).

In the last chapter, we showed that the Hamiltonian for interacting electrons in a solid can be written in second-quantized form as

$$\hat{H}_e = \sum_{v\lambda} \langle v | \hat{h}(1) | \lambda \rangle a_v^\dagger a_\lambda + \frac{1}{2} \sum_{v\lambda\alpha\beta} \langle v\lambda | \frac{e^2}{|\mathbf{r}_1 - \mathbf{r}_2|} | \alpha\beta \rangle a_v^\dagger a_\lambda^\dagger a_\beta a_\alpha, \quad (5.1)$$

where $\hat{h}(1) = \hat{\mathbf{p}}_1^2/2m + \hat{V}_{\text{ion}}(\mathbf{r}_1)$ and the Greek letters denote single-particle orbitals. In this chapter, we introduce the Hartree–Fock approximation to the correlated electron problem. The basic assumption of this approximation is that the ground state is the same as that of the non-interacting system. The energy is taken to be the expectation value in this state.

5.1 Non-interacting limit

Let us first reformulate the non-interacting problem using second quantization. In the non-interacting electron problem at $T = 0$, all momentum states up to the Fermi level are doubly occupied. As a consequence, we represent the ground-state wavefunction for the filled Fermi sea as

$$|\psi_0\rangle = |\mathbf{p}_0\uparrow, \mathbf{p}_0\downarrow, \dots, \mathbf{p}_F\uparrow, \mathbf{p}_F\downarrow\rangle = a_{\mathbf{p}_0\uparrow}^\dagger a_{\mathbf{p}_0\downarrow}^\dagger \dots a_{\mathbf{p}_F\uparrow}^\dagger a_{\mathbf{p}_F\downarrow}^\dagger |0\rangle. \quad (5.2)$$

We compute the occupancy in the p th level by acting on the ground-state wavefunction with the number operator $\hat{n}_{\mathbf{p}\sigma}$ for a momentum state \mathbf{p} :

$$\hat{n}_{\mathbf{p}\sigma} |\psi_0\rangle = n_{\mathbf{p}\sigma} |\psi_0\rangle. \quad (5.3)$$

With this equality in hand, we simplify the expectation value of the kinetic energy,

$$\begin{aligned} \langle \hat{T} \rangle &= \langle \psi_0 | \sum_{\mathbf{p},\sigma} \frac{p^2}{2m} \hat{n}_{\mathbf{p}\sigma} | \psi_0 \rangle \\ &= 2 \sum_{p=0}^{p_F} \frac{p^2}{2m} \end{aligned} \quad (5.4)$$

to obtain the standard free-particle result,

$$\langle \hat{T} \rangle = \frac{3}{5} \frac{p_F^2}{2m} N. \quad (5.5)$$

In computing the expectation value of the ion term, we must evaluate an expression of the form $\langle \psi_0 | a_{\mathbf{p}\sigma}^\dagger a_{\mathbf{p}'\sigma} | \psi_0 \rangle$. Because all states with $p < p_F$ are full, $a_{\mathbf{p}\sigma}^\dagger | \psi_0 \rangle = 0$ for $p < p_F$. Similarly $a_{\mathbf{p}'\sigma} | \psi_0 \rangle = 0$ if $p' > p_F$. When $a_{\mathbf{p}\sigma}^\dagger a_{\mathbf{p}'\sigma}$ acts on $| \psi_0 \rangle$, a new state is created that differs from ψ_0 by at most two states. The overlap of this state with $| \psi_0 \rangle$ will be zero because of the orthogonality of the momentum eigenstates unless, of course, $\mathbf{p} = \mathbf{p}'$, $\sigma = \sigma'$:

$$\langle \psi_0 | a_{\mathbf{p}\sigma}^\dagger a_{\mathbf{p}'\sigma} | \psi_0 \rangle = \delta_{\mathbf{p}\mathbf{p}'} n_{\mathbf{p}\sigma}. \quad (5.6)$$

As a consequence,

$$\langle \hat{V}_{\text{ion}} \rangle = \sum_{\mathbf{p}, \sigma} n_{\mathbf{p}\sigma} V_{\text{ion}}(0), \quad (5.7)$$

where

$$V_{\text{ion}}(0) = \frac{1}{V} \int d\mathbf{r} V_{\text{ion}}(\mathbf{r}). \quad (5.8)$$

The final result is that

$$\langle \hat{H}_1 \rangle = 2 \sum_{p < p_F} \left(\frac{p^2}{2m} + V_{\text{ion}}(0) \right). \quad (5.9)$$

As a preliminary to the Hartree–Fock approximation, it is useful to write this result in position space. To reformulate our problem in position space, we undo the Fourier transform and write the momentum-creation operators as

$$a_{\mathbf{p}\sigma}^\dagger = \int d\mathbf{r} \frac{e^{i\mathbf{p}\cdot\mathbf{r}/\hbar}}{\sqrt{V}} \psi_\sigma^\dagger(\mathbf{r}). \quad (5.10)$$

Using Eq. (5.10) for the second-quantized operators in the Hamiltonian and doing the sum over p , we find that

$$\begin{aligned} \hat{H}_1 &= \sum_{\sigma} \int d\mathbf{r} \left[-\frac{\hbar^2}{2m} \psi_\sigma^\dagger(\mathbf{r}) \nabla^2 \psi_\sigma(\mathbf{r}) + \psi_\sigma(\mathbf{r}) V_{\text{ion}}(\mathbf{r}) \psi_\sigma(\mathbf{r}) \right] \\ &= \sum_{\sigma} \int d\mathbf{r} \left[\frac{\hbar^2}{2m} |\nabla \psi_\sigma|^2 + \hat{n}_\sigma(\mathbf{r}) V_{\text{ion}}(\mathbf{r}) \right]; \end{aligned} \quad (5.11)$$

the kinetic energy operator for a many-body system is proportional to the operator, $|\nabla \psi_\sigma|^2$. Likewise, the one-body potential term is weighted with the density operator $\psi_\sigma^\dagger(\mathbf{r}) \psi_\sigma(\mathbf{r})$.

It is instructive to connect the second-quantized expression (5.11) and the expectation value of \hat{H}_1 in the orbital basis defined in Eq. (5.1):

$$\begin{aligned} \langle \hat{H}_1 \rangle &= \sum_{\nu} \langle \nu | \hat{h}(1) | \nu \rangle n_\nu \\ &= \sum_{\nu \text{ (occ.)}} \int \left[\frac{\hbar^2}{2m} |\nabla \phi_\nu|^2 + \phi_\nu^*(\mathbf{r}) V_{\text{ion}}(\mathbf{r}) \phi_\nu(\mathbf{r}) \right] d\mathbf{r}. \end{aligned} \quad (5.12)$$

The gradient and orbital density terms directly correspond to those in Eq. (5.11). The only difference is that in the second-quantized expression (5.11), field operators $\psi_\sigma(\mathbf{r})$, which create or annihilate particles, replace the single-particle orbitals.

5.2 Hartree–Fock approximation

We now turn to the two-body part of H . The additional term we must evaluate is

$$\langle \hat{H}_2 \rangle = \langle \psi_0 | \hat{V}_{ee} | \psi_0 \rangle \quad (5.13)$$

$$= \frac{1}{2} \sum_{\alpha, \beta, \nu, \lambda} \langle \nu | \langle \lambda | \frac{e^2}{|\mathbf{r}_1 - \mathbf{r}_2|} | \alpha \rangle | \beta \rangle \langle a_\nu^\dagger a_\lambda^\dagger a_\beta a_\alpha \rangle, \quad (5.14)$$

where $\langle \dots \rangle = \langle \psi_0 | \dots | \psi_0 \rangle$ and $\langle r | \psi_0 \rangle$ is the ground state wavefunction in the orbital basis. We treat the spin indices as implicit in the α, β, \dots ; bear in mind, though, that the spin associated with the index ν is the same as that associated with α , while the spin associated with the index λ is the same as that associated with β .

To simplify Eq. (5.13), we must learn how to evaluate expectation values of strings of second-quantized operators in the orbital ground state $|\psi_0\rangle$. Consider first the expectation value in the state $|n_\alpha n_\beta\rangle$. Using the relation $a_\alpha |n_\alpha\rangle = \sqrt{n_\alpha} |n_\alpha - 1\rangle$, we have

$$\langle n_\alpha n_\beta | a_\nu^\dagger a_\lambda^\dagger a_\beta a_\alpha | n_\alpha n_\beta \rangle = \sqrt{n_\alpha n_\beta} \langle n_\alpha n_\beta | a_\nu^\dagger a_\lambda^\dagger | n_\alpha - 1, n_\beta - 1 \rangle. \quad (5.15)$$

Now this quantity is non-vanishing only if $\nu = \beta$ and $\lambda = \alpha$, or $\nu = \alpha$ and $\lambda = \beta$. Because of the anticommutation relations of the a s, these two cases will give contributions differing by a minus sign. We find then

$$\langle n_\alpha n_\beta | a_\nu^\dagger a_\lambda^\dagger a_\beta a_\alpha | n_\alpha n_\beta \rangle = (\delta_{\nu\alpha} \delta_{\lambda\beta} - \delta_{\nu\beta} \delta_{\lambda\alpha}) n_\alpha n_\beta, \quad (5.16)$$

or for the ground state given in Eq. (5.2),

$$\langle a_\nu^\dagger a_\lambda^\dagger a_\beta a_\alpha \rangle = (\delta_{\nu\alpha} \delta_{\lambda\beta} - \delta_{\nu\beta} \delta_{\lambda\alpha}) \langle \hat{n}_\alpha \rangle \langle \hat{n}_\beta \rangle. \quad (5.17)$$

The general rules for factoring such expectation values were laid down by Wick (W1950), who showed that $\langle a_\nu^\dagger a_\lambda^\dagger \dots a_\rho^\dagger a_\sigma a_\alpha \dots a_\gamma \rangle$ is given by the sum of all contractions, with the sign of each term determined by the number of particle interchanges necessary to line up side-by-side the contracted operators. Note when two operators are contracted, their indices become equal.

With this result in hand, we rewrite $\langle \hat{H}_2 \rangle$ as a sum of two integrals,

$$\begin{aligned} \langle \hat{H}_2 \rangle &= \frac{1}{2} \sum_{\lambda, \nu} \langle \nu | \langle \lambda | \frac{e^2}{|\mathbf{r}_1 - \mathbf{r}_2|} | \nu \rangle | \lambda \rangle n_\lambda n_\nu - \frac{1}{2} \sum_{\lambda, \nu} \langle \nu | \langle \lambda | \frac{e^2}{|\mathbf{r}_1 - \mathbf{r}_2|} | \lambda \rangle | \nu \rangle n_\lambda n_\nu \\ &= \frac{1}{2} \sum_{\lambda, \nu \text{ (occ.)}} (U_{\nu\lambda} - \delta_{\nu\lambda} J_{\nu\lambda}). \end{aligned} \quad (5.18)$$

The direct Coulomb interaction,

$$U_{\nu\lambda} = \int d\mathbf{r}_1 d\mathbf{r}_2 |\phi_\nu(\mathbf{r}_1)|^2 \frac{e^2}{|\mathbf{r}_1 - \mathbf{r}_2|} |\phi_\lambda(\mathbf{r}_2)|^2, \quad (5.19)$$

is a measure of the repulsion between two electrons at positions \mathbf{r}_1 and \mathbf{r}_2 ; the exchange interaction,

$$J_{\nu\lambda} = \int d\mathbf{r}_1 d\mathbf{r}_2 \phi_\nu^*(\mathbf{r}_1) \phi_\lambda^*(\mathbf{r}_2) \frac{e^2}{|\mathbf{r}_1 - \mathbf{r}_2|} \phi_\nu(\mathbf{r}_2) \phi_\lambda(\mathbf{r}_1), \quad (5.20)$$

arises solely when electrons of like spin exchange spatial coordinates. The negative sign accompanying the exchange term leads to an effective attraction between electrons of like spin. This attraction is the basis of Heisenberg's explanation of ferromagnetism. The Pauli exclusion principle, which results from the Fermi–Dirac statistics obeyed by electrons, leads to a depletion of electrons of the same spin in the neighborhood of an electron of given spin. The depletion is commonly called the “exchange hole” (P1953).

Equations (5.12) and (5.18) together comprise the exact expression for the expectation value of \hat{H}_e in the state $|\psi_0\rangle$. The total Hartree–Fock energy is

$$E_{HF} = \langle \hat{H}_1 \rangle + \frac{1}{2} \sum_{\lambda, \nu \text{ (occ.)}} [U_{\nu\lambda} - J_{\nu\lambda}]. \quad (5.21)$$

The only detail missing is the prescription for finding the orbitals ϕ_ν and ϕ_λ . To determine them, we minimize the ground state energy E_{HF} with respect to the ϕ s, subject to the condition that the ϕ s remain normalized. This latter condition can be imposed by introducing a Lagrange multiplier, ϵ_ν , in the minimization:

$$\frac{\delta E_{HF}}{\delta \phi_\nu^*(\mathbf{r})} = \epsilon_\nu \frac{\delta}{\delta \phi_\nu^*(\mathbf{r})} \int d\mathbf{r}' |\phi_\nu(\mathbf{r}')|^2. \quad (5.22)$$

We discuss below the physical significance of energies ϵ_ν . Performing the variation in Eq. (5.22) results in the celebrated Hartree–Fock equations

$$\begin{aligned} & \left[\frac{-\hbar^2}{2m} \nabla^2 + \hat{V}_{ion}(\mathbf{r}) + \sum_{\lambda} \int d\mathbf{r}' n_{\lambda}(\mathbf{r}') \frac{e^2}{|\mathbf{r} - \mathbf{r}'|} \right] \phi_{\nu}(\mathbf{r}) \\ & - \sum_{\lambda} \int d\mathbf{r}' \phi_{\lambda}^*(\mathbf{r}') \phi_{\nu}(\mathbf{r}') \frac{e^2}{|\mathbf{r} - \mathbf{r}'|} \phi_{\lambda}(\mathbf{r}) = \epsilon_{\nu} \phi_{\nu}(\mathbf{r}) \end{aligned} \quad (5.23)$$

for the single-particle orbitals $\phi_{\nu}(\mathbf{r})$. In the absence of translational invariance, these variational equations can be solved iteratively until a self-consistent set of orbitals with corresponding energies, ϵ_ν , are determined.

Multiplying Eq. (5.23) by $\phi_{\nu}^*(\mathbf{r})$ and integrating over \mathbf{r} , we derive the result for the single-particle energy, ϵ_ν ,

$$\epsilon_{\nu} = \langle \nu | h_1 | \nu \rangle + \sum_{\lambda \text{ (occ.)}} (U_{\nu\lambda} - J_{\nu\lambda}). \quad (5.24)$$

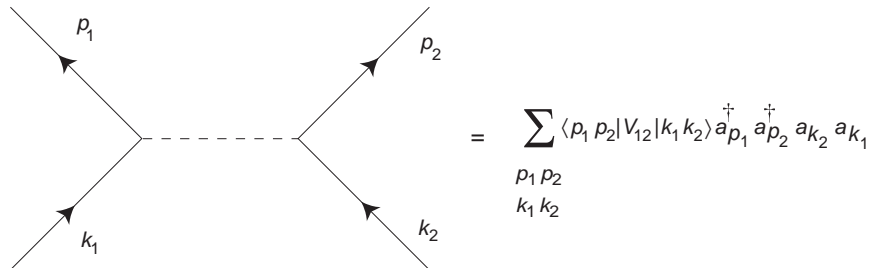


Fig. 5.1

General two-body interaction.

Because these energies involve the interaction with electrons in all other occupied orbitals, ϵ_v cannot be interpreted simply as the energy of the electron in orbital v . In fact, the total energy is not simply the sum of these single-particle energies, but, as follows from Eq. (5.21), is rather

$$E_{\text{HF}} = \sum_{v \text{ (occ.)}} \epsilon_v - \frac{1}{2} \sum_{\lambda, v \text{ (occ.)}} (U_{v\lambda} - J_{v\lambda}). \quad (5.25)$$

Koopmans (K1934) observed that the Hartree–Fock single-particle energy, ϵ_v , is the energy required to add a particle in the previously unoccupied orbital v . Consider adding an extra electron to a set of filled orbitals in a previously unoccupied orbital v . The change in the Hartree–Fock energy due to adding the particle is

$$\delta E_{\text{HF}} = E_{\text{HF}}^{\text{new}} - E_{\text{HF}} = \langle v | h(1) | v \rangle + \sum_{\alpha \neq v} (U_{v\alpha} - J_{v\alpha}) = \epsilon_v. \quad (5.26)$$

Likewise, had we removed an electron, the resultant Hartree–Fock energy would simply decrease by the energy of the orbital from which the electron was taken. Quite generally, in going from an N to an $N - 1$ particle system, $\delta E_{\text{HF}} = \epsilon_N = E_N^{\text{HF}} - E_{N-1}^{\text{HF}}$. Koopmans' theorem states that the negative of ϵ_N may be taken as a variational approximation to the system's first ionization potential. For atoms, the ionization potentials predicted by Koopmans' theorem are in reasonable agreement with experiment (W1964).

5.3 Diagrams

Throughout this book, we will use diagrams as a heuristic tool to represent processes involving interactions among particles. Fig. 5.1 illustrates the two-body interaction in Eq. (5.13). A forward-going arrow indicates the propagation of a particle of given momentum, and the dashed line represents the two-electron Coulomb interaction. Fig. 5.2 shows diagrammatically the terms in the interaction energy, Eq. (5.18). Here the backward-going line represents the propagation of a hole.

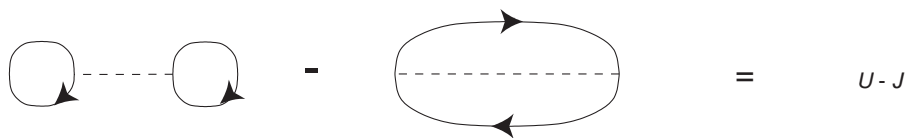


Fig. 5.2 Direct and exchange interactions.

Problem

5.1 Show that the Hartree–Fock energy can be written as

$$E_{\text{HF}} = \sum_{n=1}^N \epsilon_n, \quad (5.27)$$

where N is the number of single-particle orbitals and

$$\epsilon_n = \langle n | \hat{H}_1 | n \rangle + \sum_{\lambda=1}^n [U_{n\lambda} - J_{n\lambda}]. \quad (5.28)$$

Interpret this result in the light of the fact that the true Hartree–Fock energy cannot be written as a sum of the single-particle energies.

References

- [K1934] T. Koopmans, *Physica* **1**, 104 (1934). Interestingly, this theorem is Koopmans' only physics contribution. Immediately after publishing this work, he switched to economics, a field in which he later won the Nobel Prize.
- [P1953] D. Pines, *Phys. Rev.* **92**, 626 (1953).
- [W1964] See A. C. Wahl, *J. Chem. Phys.* **41**, 2600 (1964) for a failure of Koopmans' theorem in the molecule F_2 .
- [W1950] G.-C. Wick, *Phys. Rev.* **80**, 268 (1950).

We now turn to describing the properties of interacting electrons in metals. To a first approximation, we regard the ions as providing only a uniform background of positive charge to compensate the overall charge of the electrons. Such an approximation constitutes the Jellium model, first introduced by Herring and characterized extensively by Pines (P1955). For ions of charge Z and density n_i , the electron density n_e equals Zn_i . We start by considering the Hartree–Fock approximation to the uniform interacting electron system, which applies at high densities, and later introduce further approximations to treat the dilute regime of the interacting electron gas.

Typically, we associate the eigenstates

$$\phi_{\mathbf{p}}(\mathbf{r}) = \frac{e^{i\mathbf{p}\cdot\mathbf{r}/\hbar}}{\sqrt{V}} \quad (6.1)$$

with free electrons moving in a box of volume V with periodic boundary conditions. It turns out that such free-particle states also satisfy the Hartree–Fock equations for the Jellium model of an electron gas. However, as we derive below, the corresponding single-particle energies are no longer $p^2/2m$, but rather

$$\epsilon(\mathbf{p}) = \frac{p^2}{2m} - \frac{e^2 p_F}{\pi \hbar} \left(1 + \frac{p_F^2 - p^2}{2pp_F} \ln \left| \frac{p + p_F}{p - p_F} \right| \right). \quad (6.2)$$

The energies of the occupied energy levels are lowered below the free-particle result as a consequence of the exchange correlation among the electrons, which keeps particles of the same spin from lying atop one another. Hence, the Hartree–Fock approximation produces a dressed electronic excitation with a well-defined momentum. The fact that such excitations are described by plane-wave eigenstates suggests that the Hartree–Fock approximation is essentially a non-interacting treatment of the electron gas. Indeed this is true. Hartree–Fock produces a set of non-interacting quasi-particles which attempt to mimic the interacting system. We will see, however, that their imitation of the properties of the original system does not fare well. For example, the Hartree–Fock treatment fails to recover the linear temperature dependence of the heat capacity. It predicts instead a $\ln T$ divergence of the specific heat.

6.1 Uniform electron gas

The starting point for analyzing the interacting electron gas is the Hartree–Fock equation,

$$\begin{aligned}\epsilon_\nu \phi_\nu(\mathbf{r}) = & \left[\frac{-\hbar^2}{2m} \nabla_r^2 + V_{\text{ion}}(r) + e^2 \sum_\lambda \int d\mathbf{r}' n_{\phi_\lambda}(r') \frac{1}{|\mathbf{r} - \mathbf{r}'|} \right] \phi_\nu(\mathbf{r}) \\ & - e^2 \sum_\lambda \int d\mathbf{r}' \phi_\nu(\mathbf{r}') \phi_\lambda^*(\mathbf{r}') \phi_\lambda(\mathbf{r}) \frac{1}{|\mathbf{r} - \mathbf{r}'|}.\end{aligned}\quad (6.3)$$

Assuming at the outset that plane-wave states of the form of Eq. (6.1) satisfy the Hartree–Fock equations, converting sums over momentum to integrals and changing variables of integration in the exchange term to $\mathbf{x} = \mathbf{r}' - \mathbf{r}$, we obtain the eigenvalue equation,

$$\begin{aligned}\epsilon(\mathbf{p}) \phi_\mathbf{p}(\mathbf{r}) = & \left[\frac{p^2}{2m} + V_{\text{ion}}(r) + e^2 n_e \int d\mathbf{r}' \frac{1}{|\mathbf{r} - \mathbf{r}'|} \right] \phi_\mathbf{p}(\mathbf{r}) \\ & - e^2 \int \frac{d\mathbf{p}' d\mathbf{x}}{(2\pi\hbar)^3} \frac{e^{i(\mathbf{p}-\mathbf{p}') \cdot \mathbf{x}/\hbar}}{|\mathbf{x}|} \phi_\mathbf{p}(\mathbf{r}).\end{aligned}\quad (6.4)$$

In deriving this equation we first include the term with $\lambda = \nu$ in both the direct Coulomb and exchange terms in Eq. (6.3), and then let

$$\sum_\lambda n_{\phi_\lambda}(\mathbf{r}') = n_e(\mathbf{r}') \equiv n_e \quad (6.5)$$

in the direct term. While the direct Coulomb term explicitly excludes the interaction of an electron with itself, inclusion of the self-interaction in the exchange term as well cancels this overestimate of the Coulomb repulsion. As we see, plane-wave states do satisfy the Hartree–Fock equations for a uniform electron gas. As a consequence of the charge neutrality constraint,

$$V_{\text{ion}}(\mathbf{r}) = \sum_i \frac{-Ze^2}{|\mathbf{r} - \mathbf{R}_i^\rho|} \rightarrow -e^2 n_e \int \frac{d\mathbf{r}}{|\mathbf{r} - \mathbf{R}|}, \quad (6.6)$$

the second and third terms in the eigenvalue equation cancel. The energy of a particle in a momentum state \mathbf{p} is then

$$\epsilon(\mathbf{p}) = \frac{p^2}{2m} - e^2 \int_0^{p_F} \frac{d\mathbf{p}'}{(2\pi\hbar)^3} \int d\mathbf{x} \frac{e^{i(\mathbf{p}-\mathbf{p}') \cdot \mathbf{x}/\hbar}}{|\mathbf{x}|}. \quad (6.7)$$

The second term in Eq. (6.7) is the single-particle exchange energy,

$$\epsilon_{\text{exch}}(\mathbf{p}) = -e^2 \int \frac{d\mathbf{p}'}{(2\pi\hbar)^3} \int d\mathbf{x} \frac{e^{i(\mathbf{p}-\mathbf{p}') \cdot \mathbf{x}/\hbar}}{|\mathbf{x}|}. \quad (6.8)$$

Using the integral

$$\int d\mathbf{x} \frac{e^{i(\mathbf{p}-\mathbf{p}') \cdot \mathbf{x}/\hbar}}{|\mathbf{x}|} = \frac{4\pi\hbar^2}{|\mathbf{p} - \mathbf{p}'|^2}, \quad (6.9)$$

we find

$$\begin{aligned}\epsilon_{\text{exch}}(\mathbf{p}) &= -\frac{e^2}{\hbar} \int_0^{p_F} \frac{d\mathbf{p}'}{(2\pi)^3} \frac{4\pi}{|\mathbf{p} - \mathbf{p}'|^2} \\ &= -\frac{e^2}{\pi\hbar} \int_0^{p_F} \int_{-1}^1 \frac{p'^2 d\mathbf{p}' d\cos\theta}{p^2 + p'^2 - 2pp' \cos\theta} \\ &= \frac{e^2}{\pi p \hbar} \int_0^{p_F} p' d\mathbf{p}' [\ln|p - p'| - \ln|p + p'|].\end{aligned}\quad (6.10)$$

Then since

$$\int x \ln(x+a) dx = \frac{x^2 - a^2}{2} \ln(x+a) - \frac{1}{4}(x-a)^2,\quad (6.11)$$

we derive the result

$$\begin{aligned}\epsilon_{\text{exch}}(\mathbf{p}) &= \frac{e^2}{\pi p \hbar} \left[\frac{(p'^2 - p^2)}{2} \ln \left| \frac{p - p'}{p + p'} \right| - \frac{1}{4}(p + p')^2 + \frac{(p - p')^2}{4} \right]_0^{p_F} \\ &= -\frac{e^2 p_F}{\pi \hbar} \left(1 + \frac{(p_F^2 - p^2)}{2pp_F} \ln \left| \frac{p + p_F}{p - p_F} \right| \right).\end{aligned}\quad (6.12)$$

The single-particle energy is then as given in Eq. (6.2).

Note that the exchange energy is negative, since $p < p_F$ and $|\mathbf{p} - \mathbf{p}_F| < |\mathbf{p} + \mathbf{p}_F|$. The reason is the following. The exchange energy accounts for the fact that electrons of like spin avoid one another as a consequence of the exclusion principle, and hence the energy of the electron is lower than it would be were it moving in a uniform electron cloud of density n_e , as described by the direct term. Each electron develops an exchange cloud around it, in which the density of same-spin electrons is severely reduced. This space is the *exchange hole*. We will return to the energy spectrum after we evaluate the total energy.

The total Hartree–Fock energy is given as a sum over the single-particle energies of the occupied levels as

$$E_{\text{HF}} = 2V \int_0^{p_F} \frac{d\mathbf{p}'}{(2\pi\hbar)^3} \left(\frac{p^2}{2m} + \frac{1}{2}\epsilon_{\text{exch}}(\mathbf{p}) \right). \quad (6.13)$$

Note that the exchange energy enters with a factor 1/2 in the total energy. Simply (Problem 6.1),

$$\frac{1}{2} \int_0^{p_F} \frac{d\mathbf{p}}{(2\pi\hbar)^3} \epsilon_{\text{exch}}(\mathbf{p}) = -\frac{e^2 p_F^4}{4\pi^3 \hbar^4}. \quad (6.14)$$

Using this result, we may write the the total Hartree–Fock energy per particle,

$$\begin{aligned}\frac{E_{\text{HF}}}{N} &= \frac{e^2}{2a_0} \left[\frac{3}{5} \left(\frac{p_F a_0}{\hbar} \right)^2 - \frac{3}{2\pi} \left(\frac{p_F a_0}{\hbar} \right) \right] \\ &= \left(\frac{2.21}{r_s^2} - \frac{0.916}{r_s} \right) \text{Ry},\end{aligned}\quad (6.15)$$

in terms of $r_s = (9\pi/4)^{1/3} e^2 / \hbar v_F$, where Ry is the Rydberg constant, $e^2/2a_0 = 13.6 \text{ eV}$. The exchange energy lowers the total energy significantly, indicating that electron correlations

are important and that they must be treated correctly to describe the properties of real materials.

6.2 Hartree–Fock excitation spectrum

To delineate the limitations of the Hartree–Fock approximation, we focus on the excitation spectrum. We start by rewriting the single-particle exchange energy as $\epsilon_{\text{exch}} = \epsilon_F^0 F(x)$, where $x = p/p_F$,

$$F(x) = \frac{1}{2} + \frac{1-x^2}{4x} \ln \left| \frac{1+x}{1-x} \right|, \quad (6.16)$$

and ϵ_F^0 is the unperturbed Fermi energy $p_F^2/2m$. Then

$$\epsilon(\mathbf{p})/\epsilon_F^0 = [x^2 - 0.663r_s F(x)]; \quad (6.17)$$

$F(x)$ is plotted in Fig. 6.1 for $r_s = 3.0$. In a free-particle system, $\partial^2\epsilon/\partial p^2 = 1/m$. More generally, one defines the effective mass, m^* , of an electron at the Fermi surface by

$$\frac{1}{m^*} = \frac{1}{p_F} \left(\frac{\partial \epsilon(\mathbf{p})}{\partial \mathbf{p}} \right)_{p=p_F}. \quad (6.18)$$

The slope of $F(x)$ diverges logarithmically,

$$\frac{\partial F}{\partial x} \approx \frac{1}{2} \ln \left| \frac{1-x}{2} \right| \rightarrow -\infty, \quad (6.19)$$

as $x \rightarrow 1$. Thus, as one approaches the Fermi surface, the effective mass in the Hartree–Fock approximation from Eq. (6.18) behaves as

$$m^* \propto \frac{1}{\ln |1-x|}, \quad (6.20)$$

thereby vanishing at the Fermi surface. This result is not consistent with experiment.

As Bardeen showed (B1936), the vanishing in Hartree–Fock of the effective mass at the Fermi surface leads to an unphysical behavior of the low-temperature heat capacity. Quite generally, we may calculate the low-temperature heat capacity from Eq. (2.24). The density of states near $p = p_F$ is given in Hartree–Fock by

$$N(\epsilon) = \frac{p_F^2}{\pi^2 \hbar^3} \frac{\partial p}{\partial \epsilon} \approx \frac{mp_F/\pi^2 \hbar^3}{1 - (me^2/\pi \hbar p_F) \ln |(p - p_F)/2p_F|}. \quad (6.21)$$

The characteristic value of $p - p_F$ at low-temperature, T , is given by $|p^2/2m - p_F^2/2m| \sim |p - p_F|v_F \sim T$, where v_F is the bare Fermi velocity, p_F/m ; thus, carrying out the integral in Eq. (2.24) one eventually finds

$$C_V \sim \frac{T}{|\ln T|}, \quad (6.22)$$

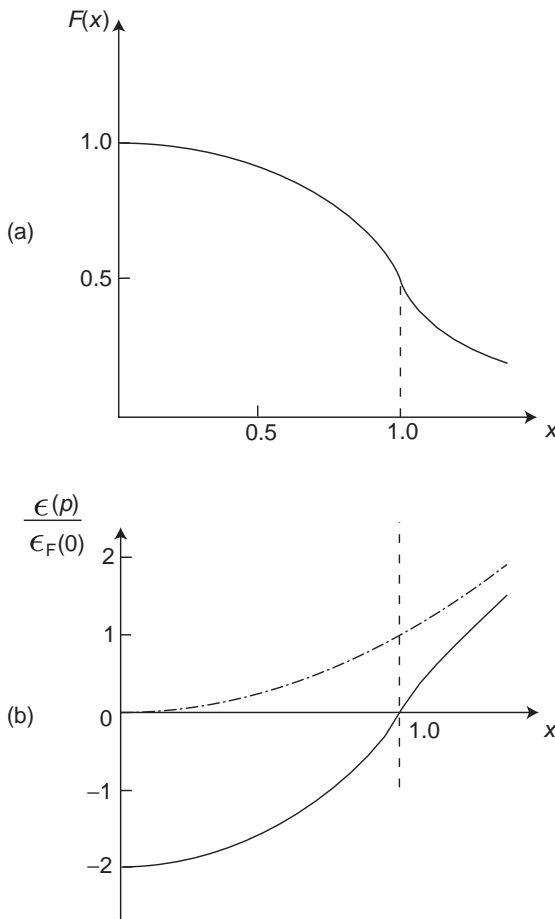


Fig. 6.1 (a) A plot of the function $F(x)$ defined by Eq. (6.16) for $r_s = 3.0$. The slope of $F(x)$ diverges as $x \rightarrow 1$, and $F(x = 1) = \frac{1}{2}$. For large x , $F(x)$ approaches $1/3x^2$. (b) The scaled Hartree–Fock single-particle energy dispersion (solid line) defined by Eq. (6.17). Hartree–Fock overestimates the bandwidth by the additive constant $0.331r_s\epsilon_F^0$. This increase in the bandwidth arises entirely from the exchange interaction. As a guide to the eye, the free-particle dispersion is plotted as a dash-dot line.

as T goes to zero. The unphysical logarithm arises from the long range of the Coulomb potential, which is reflected in the divergent behavior of the Fourier transform of $1/r \sim 1/k^2$ as $k \rightarrow 0$. This divergence is removed in fact by screening of the interaction between electrons, where the long-ranged e^2/r becomes modified to a short-range interaction, roughly of the form $e^2 \exp(-k_{TF}r)/r$, where k_{TF} is the inverse screening length. With screening, which we discuss at length in Chapter 9, the correct linear temperature dependence of the heat capacity, Eq. (2.37), is recovered.

Another difficulty with the Hartree–Fock approximation is that it overestimates the energy bandwidth, defined as $\Delta = \epsilon(x = 1) - \epsilon(x = 0)$. For a wide range of metals, the

non-interacting value of ϵ_F^0 well approximates the experimentally observed bandwidth. At the Hartree–Fock level, the bandwidth expands to

$$\Delta = \epsilon_F^0(1 + 0.331r_s). \quad (6.23)$$

The increase in the bandwidth, $\sim 0.331r_s$, is illustrated in Fig. 6.1(b).

6.3 Cohesive energy of metals

One of the key problems to which the Hartree–Fock approximation has been applied is the cohesive energy of a metal. When free atoms are brought together to form a metal, their energy decreases. The cohesive energy is defined as the difference

$$\epsilon_{\text{coh}} = (\epsilon/\text{atom})_{\text{metal}} - (\epsilon/\text{atom})_{\text{free atom}},$$

and it is negative in a bound metal. The measured cohesive energies in the alkalis are:

Table 6.1					
eV	Li	Na	K	Rb	Cs
$\epsilon_{\text{coh, expt}}$	-1.58	-1.13	-0.98	-0.82	-0.815

In order to calculate cohesive energies quantitatively, two improvements beyond Hartree–Fock need to be made. In addition to describing better the correlations among electrons, it is necessary to go beyond the approximation that the ions form a uniform background and take into account more precisely the interaction of the electrons with the ions and the average Coulomb energy of the ions. We follow here the strategy of Wigner and Seitz (WS1933) to calculate the cohesive energy of a metal, a scheme that enabled them to carry out the first quantitative application of quantum mechanics to calculating realistic properties of solids.

6.3.1 Wigner–Seitz method

The main idea of the Wigner–Seitz method is to divide the crystal into (Wigner–Seitz) cells, each containing a single ion and Z electrons, and to treat the interactions within each cell reasonably accurately. Since each cell is electrically neutral, the interaction energy between cells can be ignored to a first approximation. The cohesive energy is then given by

$$\epsilon_{\text{coh}} = \epsilon_0 - \epsilon_{\text{atom}} + \epsilon_{\text{kin}} + \epsilon_{\text{coul}}, \quad (6.24)$$

where ϵ_0 is the lowest energy of a conduction electron in the cell, physically the energy of the bottom of the conduction band, ϵ_{kin} is the average electron kinetic energy, and ϵ_{coul} is the average electron–electron Coulomb energy.

At this point, we restrict our attention to the alkali metals, in which a single conduction electron and an ion reside in each cell. One can initially ignore electron–electron interactions within each cell. Most simply, the Wigner–Seitz cell can be taken to be a sphere about the ion. To calculate ϵ_0 , we solve the Schrödinger equation

$$\left(\frac{\hat{p}^2}{2m} + V_{\text{ion}} \right) \varphi_0(\mathbf{r}) = \epsilon_0 \varphi_0(\mathbf{r}) \quad (6.25)$$

for the lowest conduction electron level in the presence of the ion potential. The boundary condition at the edge of each cell is that the normal derivative $\varphi'_0(\mathbf{r}) = 0$.

The resulting ϵ_0 s are shown in Table 6.2.

Table 6.2

eV	Li	Na	K	Rb	Cs
ϵ_{atom}	-5.37	-5.16	-4.34	-4.17	-3.89
ϵ_0	-9.15	-8.25	-6.58	-6.18	-5.85
$\epsilon_0 - \epsilon_{\text{atom}}$	-3.78	-3.09	-2.24	-2.01	-1.95

As is evident, $\epsilon_0 - \epsilon_{\text{atom}} < 0$, resulting from interactions between neighboring ions in a crystal that delocalize the electrons, an effect which ultimately lowers their energy.

The simplest estimate of ϵ_0 assumes that the ion provides a central $1/r$ potential and that, as a consequence of the exclusion principle with the core electrons, the electron cannot get closer than a_0 to the central potential. Consequently,

$$\epsilon_0 \simeq -n_e \int_{a_0}^{r_e} d\mathbf{r} \frac{e^2}{r} \quad (6.26)$$

$$= -\frac{3e^2}{2r_e^3} (r_e^2 - a_0^2) = -\frac{40.82 \text{ eV}}{r_s} \left(1 - \frac{1}{r_s^2} \right). \quad (6.27)$$

We next include the kinetic energy of the conduction electrons. The kinetic energy per electron in a free gas is given by

$$\epsilon_{\text{kin}}^0 = \frac{3}{5} \frac{p_F^2}{2m} = \frac{2.21}{r_s^2} \text{ Ry}. \quad (6.28)$$

Here is a list of r_s values and corresponding kinetic energies for the alkalis:

Table 6.3

eV	Li	Na	K	Rb	Cs
r_s	3.22	3.96	4.87	5.18	5.57
ϵ_{kin}	2.90	1.92	1.26	1.12	0.97

To set the scale, we ignore Coulomb interactions and compute the cohesive energy from just ϵ_0 , Eq. (6.27), and the kinetic energy as $\epsilon_{\text{coh}} \approx \epsilon_0 - \epsilon_{\text{atom}} + \epsilon_{\text{kin}}$, and find:

Table 6.4

eV	Li	Na	K	Rb	Cs
$\epsilon_{\text{coh,NI}}$	-0.89	-1.17	-0.97	-0.89	-0.98
$\epsilon_{\text{coh, expt}}$	-1.58	-1.13	-0.98	-0.82	-0.815

As is evident, our estimates of the cohesive energy at this level of theory are in fair to poor agreement with experiment.

We now include the direct Coulomb energy, treating the electron density as uniform and replacing each cell by a sphere of radius r_e . In such a sphere, the number of electrons enclosed in a sphere of radius $r < r_e$ is $n(r) = 4\pi r^3 n_e / 3$. The direct Coulomb energy is

$$\epsilon_{\text{direct}} = \int_0^{r_e} dr \frac{e^2}{r} n_e n(r). \quad (6.29)$$

Evaluating the integral, we obtain

$$\epsilon_{\text{direct}} = \frac{3}{5} \frac{e^2}{r_e} = \frac{6}{5r_s} \text{Ry}. \quad (6.30)$$

The interaction energy between neutral Wigner–Seitz cells is a higher order correction, which can be included in a more precise calculation.

We next include the exchange Coulomb energy at the Hartree–Fock level, assuming again that the electron density is uniform. From Eq. (6.15), the exchange energy is

$$\epsilon_{\text{exch}} = -\frac{0.916}{r_s} \text{Ry}. \quad (6.31)$$

The total electron–electron Coulomb energy is then

$$\epsilon_{\text{coul}} = \epsilon_{\text{exch}} + \epsilon_{\text{direct}} = \frac{0.284}{r_s} \text{Ry}, \quad (6.32)$$

and the cohesive energy becomes

$$\epsilon_{\text{coh,HF}} = \epsilon_0 - \epsilon_{\text{atom}} + \epsilon_{\text{kin}} + \epsilon_{\text{coul}}. \quad (6.33)$$

The Coulomb energy, together with a comparison of the new cohesive energies with the experimental values (P1955), is shown below:

Table 6.5

eV	Li	Na	K	Rb	Cs
ϵ_{coul}	1.24	1.01	0.82	0.77	0.72
$\epsilon_{\text{coh,HF}}$	0.32	-0.16	-0.15	-0.12	-0.26
$\epsilon_{\text{coh,expt}}$	-1.58	-1.13	-0.98	-0.82	-0.82

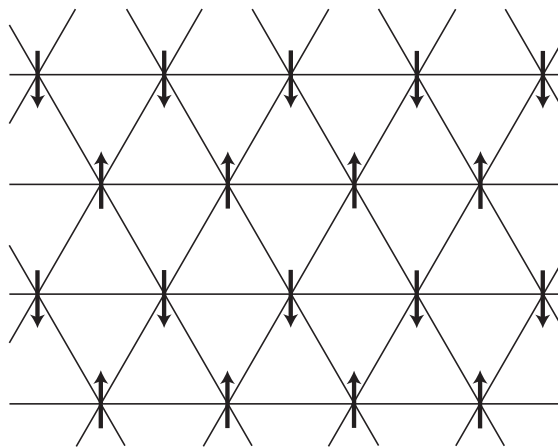


Fig. 6.2 A two-dimensional (2d) Wigner lattice of electrons. For $d = 2$, a triangular lattice minimizes the $1/r$ Coulomb repulsion between the electrons. The arrows on each lattice site reflect the orientation of the electron spin.

Because a triangular lattice is not bipartite, i.e., it cannot be split into two equivalent sublattices, it does not support long-range antiferromagnetic order. Monte Carlo calculations ([TC1989](#)) indicate that for $r_s > 37$, a transition to a Wigner solid occurs with the spin configuration shown here. Wigner solid formation has been observed for electrons on the surface of liquid helium ([G1979](#)), as well in a dilute hole gas ([Y1999](#)) confined to move at the interface between GaAs and AlGaAs. In the presence of an external magnetic field, the Wigner crystal should be stable at higher densities, since a magnetic field tends to freeze out the electron zero-point motion. Experiments on a dilute 2d electron gas in a large perpendicular magnetic field ([S1992](#)) also confirm the formation of a Wigner crystal.

As is evident, while the Hartree–Fock approximation predicts that atoms in a metal are bound, it does not give accurate quantitative predictions. In fact, the non-interacting picture, $\epsilon_{\text{coh},\text{NI}}$, did much better. To improve the theory, we need to include higher order electron–electron interactions, i.e., we need to determine more precisely the effect of correlations on the energy for a many-body system.

6.3.2 Wigner solid

Wigner's interpolation scheme ([W1934](#)), in which he treats the system at high densities ($r_s \rightarrow 0$) perturbatively and at low densities ($r_s \rightarrow \infty$) as a solid, is more directly applicable to calculating the effect of correlations on the energy of the electron gas. Wigner's crucial observation was that in a low-density electron gas in a uniform ion background, the electrons should form an ordered array. The 2d analog of a Wigner crystal is shown in Fig. 6.2. The basic idea is that, in this limit, the energy of the ground state, as a sum of kinetic and Coulombic terms, is dominated by the Coulomb repulsion, since $\epsilon_{\text{kin}} \sim 1/r_s^2$ while $\epsilon_{\text{coul}} \sim 1/r_s$, so that as $r_s \rightarrow \infty$, $\epsilon_{\text{kin}} < \epsilon_{\text{coul}}$. To minimize the Coulomb repulsion, the electrons find it energetically favorable to organize themselves in an ordered array. In three dimensions, the most favorable array is a body-centered cubic (bcc) lattice, although the face-centered array is quite close in energy; the simple cubic array is less favorable. An antiferromagnetic

bcc lattice is stable (CA1999) for $r_s > 93$. A transition to a ferromagnet (OHB1999) appears to occur around $r_s \approx 65$.

The energy of a Wigner solid is determined entirely by the Coulomb energy. To estimate the energy, we calculate the energy of a neutral Wigner–Seitz cell, this time containing an electron in its center with a uniform ion background. As earlier, the interaction energy between neutral Wigner–Seitz cells is a higher-order correction. In a spherical cell, the interaction energy between the uniform positive background and an electron localized at the center is given by

$$\epsilon_{ei} \approx -n_e e^2 \int_0^{r_e} \frac{d\mathbf{r}}{r} = -\frac{3}{2} \frac{e^2}{r_e}. \quad (6.34)$$

The compensating positive background provides a uniform electrostatic energy that is the analog of the direct Coulomb interaction determined in the earlier discussion of the Wigner–Seitz method, Eq. (6.30), $\epsilon_{\text{direct}} \simeq 3e^2/5r_e$. The energy of the Wigner solid is then

$$\epsilon_{ws} = \left(\frac{3}{5} - \frac{3}{2} \right) \frac{e^2}{r_e} = -\frac{9}{10} \frac{e^2}{r_e} = -\frac{1.8}{r_s} \text{Ry}. \quad (6.35)$$

The contribution to the energy of a Wigner crystal from zero-point fluctuations of the electrons around their equilibrium positions falls off as $1/r_s^{3/2}$ (Problem 6.5) and need not be included in extracting a first approximation to the correlation energy.

In order to identify the correlation energy in the Wigner solid, we write

$$\epsilon_{ws} = \epsilon_{\text{exch}} + \epsilon_{\text{corr}} = \left(\frac{-0.916}{r_s} - \frac{0.884}{r_s} \right) \text{Ry}. \quad (6.36)$$

For large r_s , the correlation energy is thus

$$\epsilon_{\text{corr}} \approx -\frac{0.884}{r_s} \text{Ry}, \quad r_s \rightarrow \infty. \quad (6.37)$$

In the high-density regime, one can resort to the perturbative treatment of Gell-Mann and Brueckner (GB1957). In perturbation theory, the second-order term in the electron–electron interaction is of the form

$$E_{\text{coul}}^{(2)} = \sum_{\mu \neq 0} \frac{\langle p | V_{ee} | \mu \rangle \langle \mu | V_{ee} | 0 \rangle}{E_0 - E_\mu}, \quad (6.38)$$

where $|\mu\rangle$ is an intermediate excited state. All terms in the perturbative expansion can be represented diagrammatically, as can be shown using Wick’s theorem. The second-order diagrams that enter are of the form shown in Fig. 6.3.

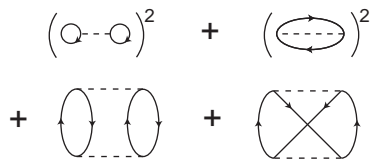


Fig. 6.3

Second-order correlation diagrams in a perturbation expansion for the ground state energy of the uniform electron gas. The solid lines indicate electrons, and the dashed lines represent the two-body Coulomb interaction.

The last diagram in Fig. 6.3, the exchange term involving just a single electron loop, is logarithmically divergent. Gell-Mann and Brueckner (GB1957) recognized that by clever resummation of a whole class of such divergent terms, they could get a finite but non-analytic result. Indeed, they found an expansion for the energy of the electron gas,

$$\epsilon_{\text{GB}} = \left(\frac{2.21}{r_s^2} - \frac{0.916}{r_s} + 0.062 \ln r_s - 0.096 + \dots \right) \text{Ry.} \quad (6.39)$$

Note the presence of the non-analytic term $\ln r_s$. This term reflects the fact that the energy of the system cannot be analytic in e^2 about $e^2 = 0$; indeed, the physics of a system of electrons with $e^2 < 0$ is that of a self-gravitating cloud, and is qualitatively different from that with $e^2 > 0$. The problem with applying perturbation theory, even in its resummed form, is that real metals lie in the region of $r_s > 1$, and hence one would have to sum the entire series to have quantitatively accurate results. It is customary to define the *correlation energy* by writing the energy of the electron system in the form

$$\epsilon = \epsilon_{\text{kin}} + \epsilon_{\text{exch}} + \epsilon_{\text{corr}}; \quad (6.40)$$

thus the Gell-Mann and Brueckner result for the correlation energy in the high-density limit is

$$\epsilon_{\text{corr}} \approx 0.062 \ln r_s - 0.096, \quad r_s \rightarrow 0. \quad (6.41)$$

Taking $\epsilon_{\text{corr}} = -0.096$ Ry at $r_s = 1$, we may write, in the spirit of Wigner, a simple approximate interpolation between the high- and low-density results:

$$\epsilon_{\text{corr}} = -\frac{0.884}{r_s + 8.21} \text{Ry} = -\frac{12.03}{r_s + 8.21} \text{eV.} \quad (6.42)$$

As Pines (P1955) has pointed out, the correlation energy at $r_s = 1$ is closer to -0.11 Ry. Nonetheless, we work within the perturbative scheme (GB1957) and use Eq. (6.42) as the interpolation formula for the correlation energy. With Eq. (6.42), we obtain the correlation and cohesive energies:

Table 6.6

eV	Li	Na	K	Rb	Cs
ϵ_{corr}	-0.7	-1.15	-1.07	-1.02	-1.17
$\epsilon_{\text{coh,W}}$	-1.64	-1.15	-1.02	-0.96	-0.92
$\epsilon_{\text{coh,expt}}$	-1.58	-1.13	-0.98	-0.82	-0.815

The improvement with the use of Wigner interpolation is marked.

However, while Eq. (6.42) is a useful interpolation formula for the cohesive energy, the Wigner scheme implicitly assumes that no new phases of the electron gas appear between the dense perturbative limit and the crystalline regime. There is really no basis for this assumption. In fact, one of the unsolved problems in solid state physics is what phase of matter arises when a Wigner crystal melts. As perturbation theory cannot be used at the Wigner melting boundary, this problem has no easy resolution. At the writing of this chapter, experiments on a dilute two-dimensional electron gas (K1999) indicate that this phase is exotic.

Summary

We have shown in this chapter how the Hartree–Fock procedure can be implemented in the context of the electron gas in a compensating positive background. The key result is that the eigenfunctions are plane waves, but the single-particle energy levels are lowered by the exchange interaction. The exchange interaction produces a diminished electron density around each electron. The Hartree–Fock description, however, does not describe accurately the bandwidth or the specific heat, leading to a $T/\ln T$ behavior in the latter quantity. In Chapter 9, we show how inclusion of electron screening remedies some of the failures of Hartree–Fock. To make accurate estimates of the cohesive energy of crystals, the Wigner interpolation scheme is quite successful. The underlying physics in this scheme is that at sufficiently low densities, an ordered electron lattice minimizes the energy of the electron gas. In $d = 3$, a bcc lattice is favored, while in $d = 2$, a triangular lattice of electrons forms.

Problems

6.1 Show that

$$\frac{1}{2} \int_0^{p_F} \epsilon_{\text{exch}}(\mathbf{p}) \frac{d\mathbf{p}}{(2\pi\hbar)^3} = -\frac{e^2 p_F^4}{4\pi^3 \hbar^4}.$$

6.2 Assuming the Hartree–Fock expression for the specific heat of an electron gas, $\sim T/|\ln T|$, determine the temperature for Na below which corrections to the linear specific heat would become significant (10% say).

- 6.3 Consider a uniform electron gas that interacts via a potential of the form $V(r) = V_0 e^{-r/a}/r$. (a) Solve the Hartree–Fock equations for this system for the eigenfunctions and excitation spectrum, $\epsilon(\mathbf{p})$. Evaluate the Fermi energy $\epsilon_F = \mu$. (b) At the Hartree–Fock level, show that the effective mass m^* is determined solely by the exchange contribution. Compute explicitly m^* in the limits $k_F a \ll 1$ and $k_F a \gg 1$. (c) Show that the exchange interaction contribution to ϵ_F is negligible when $k_F a \gg 1$ and that the direct and exchange terms are comparable for a short-range interaction with $k_F a \ll 1$.
- 6.4 Estimate the lowest energy ϵ_0 of an electron in a Wigner–Seitz cell by the following variational calculation. Assume that the potential due to the ion is Coulombic for $r > r_c$ and a repulsive hard core for $r \leq r_c$, where r_c is the radius of the outermost occupied Bohr orbit in the ionic core. Take as a trial wavefunction the correct ground state (boundary conditions and all) for an electron feeling the hard core repulsion but no Coulomb attraction. Express the result in eV and compare with more refined results.
- 6.5 Assuming a spherical cell, determine the potential felt by an electron in a Wigner lattice as it moves away from its equilibrium position. Calculate the zero point energy of the electron in this potential and show that the first correction to the energy of a low-density electron gas is $3/r_s^{3/2}$ Ry per electron.
- 6.6 A two-dimensional electron gas in a compensating background of positive charge exhibits a net magnetization, that is, a difference in the population between up and down spins. The electrons interact via a $1/r$ interaction. Define the relative magnetization in the electron gas as

$$\xi = \frac{n_\uparrow - n_\downarrow}{n_\uparrow + n_\downarrow}. \quad (6.43)$$

Show first that the Fermi momentum for up and down spins can be written as

$$p_{F\uparrow} = p_F \sqrt{1 + \xi}, \quad p_{F\downarrow} = p_F \sqrt{1 - \xi}. \quad (6.44)$$

Calculate the ground state energy, at the level of Hartree–Fock, of the electron gas as a function of ξ . For what values of ξ is the ground state stable? Estimate the value of r_s at which the ground state energy of the fully polarized (ferromagnetic) electron gas is lower in energy than the completely unpolarized ($\xi = 0$) gas.

References

- [B1936] J. Bardeen, *Phys. Rev.* **50**, 1098 (1936); see also E. P. Wohlfarth, *Phil. Mag.* **41**, 534 (1950).
- [CA1999] D. M. Ceperley and B. J. Alder, *Phys. Rev. Lett.* **45**, 566 (1980); see also D. Ceperley, *Nature (London)* **397**, 386 (1999).
- [GB1957] M. Gell-Mann and K. A. Brueckner, *Phys. Rev.* **106**, 364 (1957).
- [G1979] C. C. Grimes and G. Adams, *Phys. Rev. Lett.* **42**, 795 (1979).

- [K1999] S. V. Kravchenko, D. Simonian, M. P. Sarachik, W. Mason, and J. E. Furneaux, *Phys. Rev. Lett.* **77**, 4938 (1996).
- [OHB1999] G. Ortiz, M. Harris, and P. Ballone, *Phys. Rev. Lett.* **82**, 5317 (1999).
- [P1955] D. Pines, *Advances in Solid State Physics*, eds. F. Seitz and D. Turnbull (Academic Press, New York, 1955), Vol. I, p. 373.
- [S1992] M. B. Santos, Y. W. Suen, M. Shayegan, Y. P. Li, L. W. Engel, and D. C. Tsui, *Phys. Rev. Lett.* **68**, 1188 (1992). For a theoretical prediction for the onset of a Wigner crystal in the quantum Hall regime, see P. K. Lam and S. M. Girvin, *Phys. Rev. B* **30**, 473 (1984).
- [TC1989] B. Tanatar and D. M. Ceperley, *Phys. Rev. B* **39**, 5005 (1989).
- [W1934] E. Wigner, *Phys. Rev.* **46**, 1002 (1934).
- [WS1933] E. Wigner and F. Seitz, *Phys. Rev.* **43**, 804 (1933); **46**, 509 (1933).
- [Y1999] J. Yoon, C. C. Li, D. Shahar, D. C. Tsui, and M. Shayegan, *Phys. Rev. Lett.* **82**, 1748 (1999).

Matthias and co-workers, in a series of electron spin resonance (ESR) and nuclear magnetic resonance (NMR) experiments on non-magnetic metals – metals with no permanent magnetic moment – observed surprising evidence for long-lived local spin packets in the ESR lineshape ([M1960](#)). These data indicated the persistence of local magnetic moments. The magnetic moment was quickly traced to the presence of small amounts of magnetic impurities. While various systems were studied, such as Mn, Fe, and other iron group impurities in host materials such as Cu, Ag, and Au, the common ingredient shared by all the impurity ions is that they possessed one or more vacant inner-shell orbitals. In addition, the experiments demonstrated that varying the kind and amount of the magnetic impurities did not always result in the formation of local magnetic moments in non-magnetic metals. This finding added to the intrigue and established the question of the formation of local magnetic moments as central to understanding magnetism and transport in solids. In this chapter, we describe the origin of local moments, focusing primarily on Anderson's model ([A1961](#)), the model that rose to the fore as the standard microscopic view of local magnetic moment formation in metals.

7.1 Local moments: phenomenology

An impurity in a non-magnetic metal can give rise to a local moment if an electronic state on the impurity is singly occupied, at least on the time scale of the experiment. Friedel ([F1958](#)) was the first to introduce a phenomenological model to explain the onset of local moments. His model describes the effect of the impurity as generating a potential which is effectively a deep Coulombic core plus an angular momentum dependent centrifugal barrier $\sim \ell(\ell + 1)/r^2$, where the distance r is measured from the center of the impurity. Such a potential can support bound states. Those occurring well below the Fermi level will be doubly occupied, and have no need of a magnetic moment. A local magnetic moment can form, however, in a bound or resonant state of the impurity potential near the Fermi level if the levels corresponding to up and down spins are non-degenerate.

Anderson ([A1961](#)), adopting the basic ideas of Friedel, developed a one-band model of local moment formation, the essence of which is the following. The band in the non-magnetic metallic host, typically a transition metal such as titanium, is represented by a set of Bloch states. Measuring single-particle energies from the top of the Fermi sea, equivalent to choosing the Fermi energy $\epsilon_F = 0$, we take the band energies to be $\epsilon_{\mathbf{k}} = \hbar^2 k^2 / 2m - \hbar^2 k_F^2 / 2m$. The impurity is treated simply as a local site on which a single electronic orbital is placed.

Table 7.1

Symbol	Integral	Description	Magnitude
U	$\langle ii V_{ee} ii\rangle$	on-site	20 eV
V	$\langle ij V_{ee} ij\rangle$	nearest neighbor	2–3 eV
Y	$\langle ij V_{ee} ji\rangle$	exchange	1/40 eV

While this simplification does not capture the five-fold degeneracy of the d -orbitals of typical impurities such as Co, Fe, and Ni, this deficiency is not crucial. We denote the wavefunction of the orbital by $\phi_d(\mathbf{r})$. The energy required to place an electron on the impurity with spin either up or down is ϵ_d . The orbital can be either singly occupied or occupied by two electrons of opposite spin. The latter case costs an energy, U , which physically arises from the Coulomb repulsion between the electrons, and is thus given by

$$U = \langle dd|V_{ee}|dd\rangle = \int d\mathbf{r}_1 d\mathbf{r}_2 |\phi_d(\mathbf{r}_1)|^2 \frac{e^2}{|\mathbf{r}_1 - \mathbf{r}_2|} |\phi_d(\mathbf{r}_2)|^2. \quad (7.1)$$

The Coulomb repulsion has the effect of favoring single occupation of the impurity level. The final ingredient in the Anderson model is a spin-conserving coupling between the impurity level and the \mathbf{k} -states of the band in the metal, described by a matrix element V_{kd} . This interaction causes a hybridization of the band states and the impurity level. The basic Anderson Hamiltonian is then

$$H^A = \sum_{\mathbf{k}\sigma} \epsilon_{\mathbf{k}} a_{\mathbf{k}\sigma}^\dagger a_{\mathbf{k}\sigma} + \sum_{\sigma} \epsilon_d n_{d\sigma} + \sum_{\mathbf{k}\sigma} V_{kd} (a_{\mathbf{k}\sigma}^\dagger a_{d\sigma} + a_{d\sigma}^\dagger a_{\mathbf{k}\sigma}) + U n_{d\uparrow} n_{d\downarrow}, \quad (7.2)$$

where the $a_{\mathbf{k}\sigma}^\dagger$ create electrons in band states, $a_{d\sigma}^\dagger$ creates an electron with spin σ on the impurity, and $n_{d\sigma} = a_{d\sigma}^\dagger a_{d\sigma}$ is the number operator for a localized electron of spin σ .

The Anderson model includes only the on-site Coulomb repulsion between two localized electrons. In addition a localized electron interacts with localized electrons on other sites. These other terms are generally small, however. To estimate the size of these additional interactions, Hubbard (H1964) assumed a lattice model of 3d-electrons in transition metals, in which a localized state is placed at each lattice site, denoted by i, j, \dots , and calculated a series of matrix elements of the Coulomb potential of the form

$$\langle i | \langle j | V_{ee} | k \rangle | l \rangle = \int d\mathbf{r}_1 d\mathbf{r}_2 \phi_i^*(\mathbf{r}_1) \phi_j^*(\mathbf{r}_2) \frac{e^2}{|\mathbf{r}_1 - \mathbf{r}_2|} \phi_l(\mathbf{r}_2) \phi_k(\mathbf{r}_1). \quad (7.3)$$

The magnitudes of the various Coulomb matrix elements are listed in Table 7.1.

In this table i and j ($i \neq j$) denote nearest neighbor lattice sites. The nearest neighbor term is the direct Coulomb energy between densities of electrons at neighboring sites, and the “exchange” term is the corresponding exchange energy, as discussed in Chapter 5. As is evident, U is the largest contribution to the Coulomb interactions, and in many solid-state problems involving strongly correlated electrons, e.g., the Hubbard model (H1964), only the U term is retained. Generally, inclusion of U does not guarantee that all the relevant physics will be described. Polyacetylene is a famous case in point (BC1989), in which V as well as the other Coulomb matrix elements play a crucial role in the physics

of dimerization, as well as the optical properties. Here the additional density-bond matrix element, $X = \langle ii|V_{ee}|ij\rangle$, and the bond–bond matrix element, $\tilde{Y} = \langle ii|V_{ee}|jj\rangle$ – of respective order 1/2 eV and 1/40 eV in the transition metals – are significant. The notation “density” refers to the case $k = i$, where the corresponding wave functions give the electron density at site i ; the bond contributions are so-named because they are non-zero only if an electron has non-zero overlap in two neighboring localized states.

The Coulomb interaction favors the formation of local moments because it tends to inhibit double occupation of a site. On the other hand, the charge fluctuations on the impurity caused by strong hybridization of the impurity level with the band states tend to wash out local moments. The energy scale measuring this coupling is, as we shall see, essentially the rate at which the coupling causes transitions between electrons initially in the impurity state and a k -state in the band, and vice versa. From Fermi’s golden rule, the rate of hopping of an electron from the impurity to a state in the band of the metal with momentum \mathbf{k} is given by

$$\frac{1}{\tau} = 2\pi \frac{|V_{kd}|^2 N(\epsilon_d)}{\hbar} \equiv \frac{2\Delta}{\hbar}, \quad (7.4)$$

where $N(\epsilon_d)$ is the density of electron k -states of a particular spin at the impurity energy, ϵ_d . As a result of such virtual transitions, the energy levels on the impurity will be broadened; the width of the broadening is governed by the energy scale Δ . We refer to Δ as the hybridization energy as this energy arises solely from the overlap between the band and impurity states.

The physics of the Anderson model is governed by several parameters: the magnitude of the impurity energy, ϵ_d , and its location relative to the Fermi level, the on-site repulsion energy U , and the hybridization energy Δ . As illustrative cases, let us consider the limits of large and weak hybridization. In the case of weak hybridization, $U \gg \epsilon_d \gg \Delta$, that is, the cost of doubly occupying the d -level on the impurity far exceeds ϵ_d and the hybridization energy Δ . In this limit the system generally supports local moment formation. We assume generally that the impurity level lies below the Fermi sea, $\epsilon_d < 0$. In thermal equilibrium, the state with energy ϵ_d will be at least singly occupied. The cost of putting two electrons on the impurity is $2\epsilon_d + U$. Should $2\epsilon_d + U$ exceed the Fermi energy, that is $2\epsilon_d + U > 0$, the upper state of the impurity is unoccupied and the impurity is magnetic. The energy-level diagram for this case is shown in Fig. 7.1(a). However, in certain experimental situations, for example, rare earth compounds such as SmB₆ and heavy fermion systems, the impurity levels are close to the Fermi level. In these “mixed valence” situations, slight changes in the hybridization energy lead to a loss of the local moment. Consider the case in which $U \gg \Delta \gg \epsilon_d$, so that the upper level remains well above the Fermi level. Then the absolute energy of the lower impurity state is smaller than the width of the state. As a consequence, the occupation of this state undergoes rapid fluctuations, as illustrated in Fig. 7.1(b). This regime is non-magnetic.

Consider next the regime in which U is small compared with Δ . In this case, Δ determines the physics, not U . Because the broadening of each level exceeds the energy cost for double

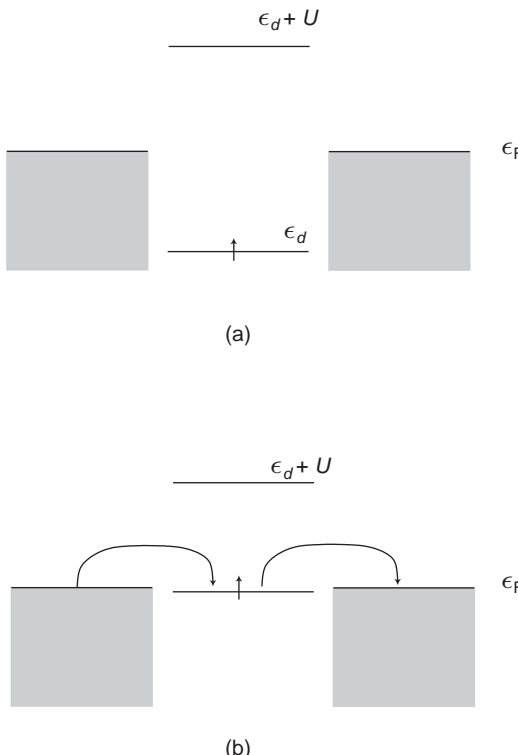


Fig. 7.1 Energy-level diagrams for the Anderson model in the local weakly-coupled regime, $U \gg \Delta$ (Δ is the hybridization energy). The left and right shaded regions show the same electronic states in the band of the host metal – as is customary in this problem to emphasize virtual second-order transitions from the continuum to the localized state to the continuum. The Fermi level is fixed at $\epsilon_F = 0$. The energies of the available single-particle states on the impurity are ϵ_d if the level is unoccupied and $\epsilon_d + U$ if the level is already singly occupied. (a) When ϵ_d is sufficiently below the Fermi surface, local moment formation is favored. (b) Energy-level diagram in the mixed valence regime for $U \gg \Delta \gg \epsilon_d$. The lower impurity level is very close to the Fermi surface. Charge fluctuations on the impurity are rapid and lead to a local spin fluctuation on the impurity. This case is not magnetic.

occupancy, the impurity is partially occupied with a spin up and a spin down electron with equal probability. This state is not magnetic, as the occupancy in the up and down spin levels is equal. This state of affairs is termed a *localized spin fluctuation*. By adjusting U and Δ , we can tune continuously from the magnetic to the localized spin fluctuation state; the model is thus a good starting point to discuss the physics of local moment formation.

7.2 Impurity density of states

The central quantity required to understand local moment formation is the occupancy of the states of the impurity. If the states have a greater probability of being occupied by electrons of one given spin than the other, then the site will have a local moment. The

occupancy of the impurity site is obtained by calculating the probability that an electron in a given occupied energy eigenstate of the system will be found on the impurity. If $|n\rangle$ is an eigenstate of the local moment Hamiltonian, H^A , with energy $\epsilon_{n\sigma}$, then $|\langle n\sigma|d\sigma\rangle|^2$ is the probability that the state $|n\sigma\rangle$ overlaps the impurity site, $|d\sigma\rangle$. This overlap is non-zero as a result of the hybridization coupling, V_{kd} . The net occupancy of an electron of spin σ on the impurity is then given by a sum over all occupied electron states with energy $\epsilon \leq \epsilon_F$:

$$\langle n_{d\sigma} \rangle = \sum_{n, \epsilon_{n\sigma} \leq \epsilon_F} |\langle n\sigma|d\sigma\rangle|^2 = \int_{-\infty}^{\epsilon_F} d\epsilon \rho_{d\sigma}(\epsilon), \quad (7.5)$$

where the density of states on the impurity is given by

$$\rho_{d\sigma}(\epsilon) = \sum_n \delta(\epsilon_{n\sigma} - \epsilon) |\langle n\sigma|d\sigma\rangle|^2. \quad (7.6)$$

The criterion for local moment formation is that $\langle n_{d\sigma} \rangle \neq \langle n_{d-\sigma} \rangle$.

The interaction term on the impurity makes constructing the single-particle energy levels and the impurity density of states non-trivial. To solve this problem, we adopt a mean-field or Hartree–Fock approximation to the interacting problem within which the single-particle energy levels are well defined. The criterion for local moment formation resulting from this procedure has in fact had spectacular success (GZ1974) in predicting the onset of local moment formation in magnetic alloys. In Hartree–Fock the ground state of the system has the form

$$|\Phi_0\rangle = \prod_{\epsilon_n < \epsilon_F} a_{n\sigma}^\dagger |0\rangle, \quad (7.7)$$

where

$$a_{n\sigma}^\dagger = \sum_{\mathbf{k}} \langle \mathbf{k}\sigma | n\sigma \rangle a_{\mathbf{k}\sigma}^\dagger + \langle d\sigma | n\sigma \rangle a_{d\sigma}^\dagger \quad (7.8)$$

is a linear combination of band and impurity states. In the Hartree–Fock approximation in terms of the new states (Eq. (7.8)), the one-body Hamiltonian is

$$H_{HF}^A = \sum_{n\sigma} \epsilon_{n\sigma} a_{n\sigma}^\dagger a_{n\sigma}. \quad (7.9)$$

The Hartree–Fock approximation to the Hamiltonian amounts to replacing the interaction term, $U n_{d\uparrow} n_{d\downarrow}$, by $U \langle n_{d\uparrow} \rangle n_{d\downarrow} + U \langle n_{d\downarrow} \rangle n_{d\uparrow} - U \langle n_{d\uparrow} \rangle \langle n_{d\downarrow} \rangle$, where the averages are in the state $|\Phi_0\rangle$. The last term provides an overall shift in the zero of energy; since it cannot affect the physics of the local moment we drop it. Redefining the defect site energies as

$$E_{d\sigma} = \epsilon_d + U \langle n_{d-\sigma} \rangle, \quad (7.10)$$

the Hartree–Fock approximation to the Anderson Hamiltonian is

$$H_{\text{HF}}^{\text{A}} = \sum_{\sigma} E_{d\sigma} n_{d\sigma} + \sum_{\mathbf{k}\sigma} \epsilon_{\mathbf{k}} n_{\mathbf{k}\sigma} + \sum_{\mathbf{k}\sigma} V_{\mathbf{k}d} (a_{\mathbf{k}\sigma}^\dagger a_{d\sigma} + a_{d\sigma}^\dagger a_{\mathbf{k}\sigma}). \quad (7.11)$$

As we see, the Hartree–Fock approximation of the Hamiltonian with on-site Coulomb repulsion amounts to a simple renormalization of the site energies; the quantity $E_{d\sigma}$ plays the crucial role in the mean field theory of local moment formation. The criterion for a local moment, that $\langle n_{d\sigma} \rangle \neq \langle n_{d-\sigma} \rangle$, is equivalent to the condition that $E_{d\sigma} \neq E_{d-\sigma}$. Once we define the single-particle levels, it is straightforward to show that Eqs. (7.9) and (7.11) are equivalent (Problem 7.3).

The single-particle energies $\epsilon_{n\sigma}$ are defined through the operator equations of motion,

$$[H_{\text{HF}}^{\text{A}}, a_{n\sigma}^\dagger] = \epsilon_{n\sigma} a_{n\sigma}^\dagger. \quad (7.12)$$

To evaluate the commutator in Eq. (7.12), we use the commutators

$$\begin{aligned} [H_{\text{HF}}^{\text{A}}, a_{\mathbf{k}\sigma}^\dagger] &= \sum_{\mathbf{k}'\sigma} \epsilon_{\mathbf{k}'} [a_{\mathbf{k}'\sigma}^\dagger a_{\mathbf{k}'\sigma}, a_{\mathbf{k}\sigma}^\dagger] + \sum_{\mathbf{k}'\sigma} V_{\mathbf{k}'d} [(a_{\mathbf{k}'\sigma}^\dagger a_{d\sigma} + a_{d\sigma}^\dagger a_{\mathbf{k}'\sigma}), a_{\mathbf{k}\sigma}^\dagger] \\ &= \epsilon_{\mathbf{k}} a_{\mathbf{k}\sigma}^\dagger + V_{\mathbf{k}d} a_{d\sigma}^\dagger \end{aligned} \quad (7.13)$$

and

$$[H_{\text{HF}}^{\text{A}}, a_{d\sigma}^\dagger] = E_{d\sigma} a_{d\sigma}^\dagger + \sum_{\mathbf{k}} V_{\mathbf{k}d} a_{\mathbf{k}\sigma}^\dagger, \quad (7.14)$$

and find

$$\begin{aligned} [H_{\text{HF}}^{\text{A}}, a_{n\sigma}^\dagger] &= \sum_{\mathbf{k}} \langle \mathbf{k}\sigma | n\sigma \rangle (\epsilon_{\mathbf{k}} a_{\mathbf{k}\sigma}^\dagger + V_{\mathbf{k}d} a_{d\sigma}^\dagger) + \langle d\sigma | n\sigma \rangle \left(E_{d\sigma} a_{d\sigma}^\dagger + \sum_{\mathbf{k}} V_{\mathbf{k}d} a_{\mathbf{k}\sigma}^\dagger \right) \\ &= \epsilon_{n\sigma} \sum_{\mathbf{k}} \langle \mathbf{k}\sigma | n\sigma \rangle a_{\mathbf{k}\sigma}^\dagger + \langle d\sigma | n\sigma \rangle a_{d\sigma}^\dagger. \end{aligned} \quad (7.15)$$

Thus

$$\epsilon_{n\sigma} \langle \mathbf{k}\sigma | n\sigma \rangle = \epsilon_{\mathbf{k}} \langle n\sigma | \mathbf{k}\sigma \rangle + V_{\mathbf{k}d} \langle d\sigma | n\sigma \rangle \quad (7.16)$$

and

$$\epsilon_{n\sigma} \langle n\sigma | d\sigma \rangle = E_{d\sigma} \langle d\sigma | n\sigma \rangle + \sum_{\mathbf{k}} \langle \mathbf{k}\sigma | n\sigma \rangle V_{\mathbf{k}d}. \quad (7.17)$$

Equations (7.16) and (7.17) define the single-particle levels, $\epsilon_{n\sigma}$. The explicit solution, which is left as a homework exercise (Problem 7.2), requires eliminating the states $\langle n\sigma | d\sigma \rangle$ and $\langle n\sigma | \mathbf{k}\sigma \rangle$ from Eqs. (7.16) and (7.17).

7.2.1 Impurity density of states

Now that we have shown how to obtain the single-particle energy levels that determine the density of states, we compute this quantity explicitly. We carry out the calculation in terms of resolvents or Green functions, which allow us to include directly the widths of the impurity levels. We begin by rewriting the density of states, making use of the relation

$$\begin{aligned}\delta(\epsilon - \epsilon_{n\sigma}) &= \frac{1}{\pi} \lim_{\Gamma \rightarrow 0} \frac{\Gamma}{(\epsilon - \epsilon_{n\sigma})^2 + \Gamma^2} \\ &= \frac{1}{2\pi i} \lim_{\Gamma \rightarrow 0} \left[\frac{1}{\epsilon - \epsilon_{n\sigma} - i\Gamma} - \frac{1}{\epsilon - \epsilon_{n\sigma} + i\Gamma} \right] \\ &= -\frac{1}{\pi} \lim_{\Gamma \rightarrow 0} \text{Im} \frac{1}{\epsilon - \epsilon_{n\sigma} + i\Gamma}.\end{aligned}\quad (7.18)$$

As a consequence,

$$\rho_{d\sigma}(\epsilon) = -\frac{1}{\pi} \lim_{\Gamma \rightarrow 0} \text{Im} \sum_n \frac{|\langle n\sigma | d\sigma \rangle|^2}{\epsilon - \epsilon_{n\sigma} + i\Gamma}. \quad (7.19)$$

The quantity $(\epsilon - \epsilon_{n\sigma} + i\Gamma)^{-1}$ is a resolvent related to the Green function for this problem. We define the Green (operator) function $G(E + i\Gamma)$ through

$$(E + i\Gamma - H)G = 1. \quad (7.20)$$

Dividing both sides of (7.20) by $(E - H + i\Gamma)$ and expanding in a complete set of eigenstates of H^A , we obtain

$$G(E + i\Gamma) = \sum_n \frac{|n\rangle \langle n|}{E + i\Gamma - E_n} \quad (7.21)$$

as the spectral resolution of the Green function, where $H|n\rangle = E_n|n\rangle$ and G is singular with poles at the eigenenergies E_n . The eigenfunctions of G are then $|n\rangle$.

For the single-particle Hamiltonian $H = H_{HF}^A$, we define the matrix elements of G through

$$\sum_\beta (E + i\Gamma - H)_{\alpha\beta} G_{\beta\mu} = \delta_{\alpha\mu}, \quad (7.22)$$

where the subscripts α , β , and μ label band or impurity states with a particular spin, that is, $|\mathbf{k}\sigma\rangle$ and $|d\sigma\rangle$, respectively. From the definition of G and Eq. (7.19), we can then rewrite $\rho_{d\sigma}(\epsilon)$ as

$$\begin{aligned}\rho_{d\sigma} &= -\frac{1}{\pi} \lim_{\Gamma \rightarrow 0} \text{Im} \sum_n \frac{|\langle n\sigma | d\sigma \rangle|^2}{\epsilon - \epsilon_{n\sigma} + i\Gamma} \\ &= -\frac{1}{\pi} \lim_{\Gamma \rightarrow 0} \text{Im} \langle d\sigma | G(\epsilon + i\Gamma) | d\sigma \rangle \\ &= -\frac{1}{\pi} \lim_{\Gamma \rightarrow 0} \text{Im} G_{dd}^\sigma\end{aligned}\quad (7.23)$$

if G is expressed in terms of the exact eigenstates of H . Equation (7.23), which relates the density of states to the diagonal matrix element of G , is the principal relationship we need

to formulate the local moment problem. From the equations for the Green function and the reduced Hamiltonian, we find that for $\alpha = \mu = d\sigma$

$$(\epsilon + i\Gamma - E_{d\sigma})G_{dd}^\sigma - \sum_{\mathbf{k}} V_{d\mathbf{k}} G_{\mathbf{k}d}^\sigma = 1, \quad (7.24)$$

and for $\alpha = k\sigma, \mu = d\sigma$,

$$(\epsilon + i\Gamma - \epsilon_{\mathbf{k}})G_{\mathbf{k}d}^\sigma - V_{\mathbf{k}d} G_{dd}^\sigma = 0. \quad (7.25)$$

If we eliminate $G_{d\mathbf{k}}^\sigma$ from Eq. (7.24) by using Eq. (7.25), we obtain

$$G_{dd}^\sigma(\epsilon + i\Gamma) = \left[\epsilon + i\Gamma - E_{d\sigma} - \sum_{\mathbf{k}} \frac{|V_{\mathbf{k}d}|^2}{\epsilon + i\Gamma - \epsilon_{\mathbf{k}}} \right]^{-1}. \quad (7.26)$$

[Note that the zeros of the denominator lie at the energies calculated in second-order perturbation Brillouin–Wigner theory, with the full ϵ in the energy denominator.] In the absence of the last term in the denominator of Eq. (7.26), the singularities of G_{dd}^σ lie at the renormalized site energy, $E_{d\sigma}$.

The transfer integral $V_{\mathbf{k}d}$ broadens the impurity level. To see the broadening, we rewrite the last term of $(G_{dd}^\sigma)^{-1}$ as

$$\sum_{\mathbf{k}} \frac{|V_{\mathbf{k}d}|^2}{\epsilon - \epsilon_{\mathbf{k}} + i\Gamma} = \sum_{\mathbf{k}} |V_{\mathbf{k}d}|^2 \frac{\epsilon - \epsilon_{\mathbf{k}} - i\Gamma}{(\epsilon - \epsilon_{\mathbf{k}})^2 + \Gamma^2}. \quad (7.27)$$

In the limit $\Gamma \rightarrow 0$, Eq. (7.27) reduces to

$$\begin{aligned} \lim_{\Gamma \rightarrow 0} \sum_{\mathbf{k}} \frac{|V_{\mathbf{k}d}|^2}{\epsilon - \epsilon_{\mathbf{k}} + i\Gamma} &= P \left(\sum_{\mathbf{k}} \frac{|V_{\mathbf{k}d}|^2}{\epsilon - \epsilon_{\mathbf{k}}} \right) - i\pi \sum_{\mathbf{k}} |V_{\mathbf{k}d}|^2 \delta(\epsilon - \epsilon_{\mathbf{k}}) \\ &= P \left(\sum_{\mathbf{k}} \frac{|V_{\mathbf{k}d}|^2}{\epsilon - \epsilon_{\mathbf{k}}} \right) - i\pi \langle |V_{\mathbf{k}d}|^2 \rangle N(\epsilon), \end{aligned} \quad (7.28)$$

where P indicates the principal value; we have used Eq. (7.18) to obtain the final result and replaced $|V_{\mathbf{k}d}|^2$ by its average value $\langle |V_{\mathbf{k}d}|^2 \rangle$. The first term in Eq. (7.27) is purely real and hence represents a shift of the d -impurity energy level. This term affects the physics only if it fluctuates wildly as a function of energy. The density of states of the host band, $N(\epsilon)$, is fairly constant, however, on the scale over which $E_{d\sigma}$ changes. Hence, the real part of (7.27) can be ignored and G becomes

$$G_{dd}^\sigma(\epsilon + i\Gamma) = \frac{1}{\epsilon + i\Gamma - E_{d\sigma} + i\Delta}, \quad (7.29)$$

where $2\Delta = 2\pi \langle |V_{\mathbf{k}d}|^2 \rangle N(\epsilon)$ is the effective transition rate between the impurity and the conduction electrons.

If we interpret $E_{d\sigma} - i\Delta$ as the new site energy, then as advertised, $2\hbar/\Delta$ is the lifetime of the impurity level. From Eqs. (7.23) and (7.29), we find that the density of states at the

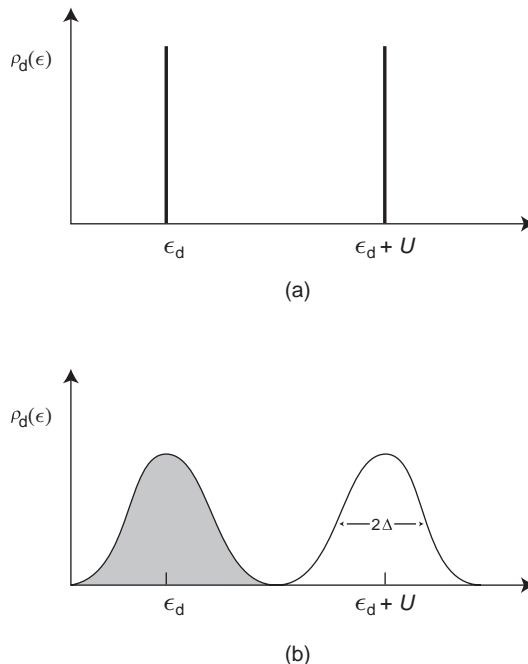


Fig. 7.2 (a) Single-particle density of states in the Anderson model when the hybridization between the d -level and the k -states vanishes. The sharp peak at single-particle energy ϵ_d corresponds to the situation in which the impurity level is vacant, while the sharp peak at $\epsilon_d + U$ corresponds to the situation in which the impurity level is already singly occupied by an electron of opposite spin. Including interactions at the Hartree–Fock level shifts these peaks to $E_{d\sigma} = \epsilon_d + U \langle n_{d-\sigma} \rangle$. (b) Density of states when the d and k -states are mixed. The width of each state is broadened by hybridization. As in (a) the lower level corresponds to the situation in which the impurity level is vacant, and the upper peak to the situation in which an electron of given spin already resides on the lower level. When the lower level is occupied and the upper vacant, as indicated by the unequal shading under the two peaks, the system has a localized moment.

d -impurity reduces to the Lorentzian form

$$\rho_{d\sigma}(\epsilon) = \frac{1}{\pi} \frac{\Delta}{(\epsilon - E_{d\sigma})^2 + \Delta^2} \quad (7.30)$$

in which, as expected, Δ appears as the half-width of the d -level.

The density of states approaches a delta function as the hybridization between the d -level and the conduction states vanishes. Why is this so? The density of states is determined by the imaginary part of the Green function. If as E approaches the real axis $G(E)$ is purely real, then the singularities of $G(E)$ are simple poles well-separated in energy. In this case, the density of states corresponds to a series of sharp (delta-function) peaks at the eigenenergies, $E_{d\sigma} = \epsilon_d + U \langle n_{d-\sigma} \rangle$. For single occupation of the level by an electron of given spin, the poles are separated by the on-site Coulomb repulsion, U , as illustrated in Fig. 7.2(a). This state of affairs persists if there is no mixing between the d -level and

the k -states in the conduction band. Once mixing is turned on, the poles move off the real axis, causing the pure d -levels to broaden. The resultant energy spectrum is no longer well separated in energy (see Fig. 7.2(b)).

7.3 Green functions

A digression on Green functions is in order. First, we refer to them as Green functions not Green's functions. The latter is ungrammatical. Consider the equally ungrammatical construction, the Bessel's function, which no one uses. Nonetheless, we will still refer to Green's theorem because that's whose theorem it is.

By inverting Eq. (7.20), we obtain that $G = (E - H + i\Gamma)^{-1}$ and hence G is an operator in the Hilbert space of the Hamiltonian. This allows us to spectrally resolve it,

$$G = \sum_n \frac{|n\rangle\langle n|}{E - E_n + i\Gamma}, \quad (7.31)$$

in terms of the eigenstates of the Hamiltonian, $H|n\rangle \equiv H|n\rangle = E_n|n\rangle$. Here Γ is a positive constant which lifts the poles of G off the real axis, placing them immediately below. As a consequence, G is analytic in the upper half-plane. Consequently, its Fourier transform,

$$G_{nn} = \int \frac{dE}{2\pi} \langle n | G | n \rangle e^{-iEt/\hbar} = \frac{1}{2\pi} \int dE \frac{e^{-iEt/\hbar}}{E - E_n + i\Gamma}, \quad (7.32)$$

is only non-zero if the contour is closed in the lower half-plane. This immediately leads to the causal nature of G . If $t < 0$, this integral must be completed by closing the contour in the upper half-plane to yield a finite result. Because G is analytic there, we find that $G = 0$ for $t < 0$. However, if $t > 0$, we can close in the lower half-plane encircling the poles and obtain the finite result

$$G_{nn} = -ie^{-iE_nt/\hbar}, \quad t > 0. \quad (7.33)$$

We have taken the limit $\Gamma = 0$ after we evaluated the contour. This dichotomous time behavior implies that G is a causal function. For the simple case of free particles, $E_n = p^2/2m$ and the Green function reduces to

$$G(p, E) = \frac{1}{E - p^2/2m + i\Gamma}. \quad (7.34)$$

7.3.1 Green function: general definition

Green functions have a long history. Their formal definition is the general solution,

$$(-i\hbar\partial_t + H) G(\mathbf{r}, t; \mathbf{r}', t') = -\hbar\delta(\mathbf{r} - \mathbf{r}')\delta(t - t'), \quad (7.35)$$

to a homogeneous differential equation with a unit discontinuity both in space and in time. The right-hand side makes it clear that whatever G is it preserves time and space translation

invariance. Consider the Fourier transform,

$$G(\mathbf{r}, t; \mathbf{r}', t') = \int_{-\infty}^{\infty} G(\mathbf{r}, \mathbf{r}'; \varepsilon) e^{-i\varepsilon(t-t')/\hbar} \frac{d\varepsilon}{2\pi}. \quad (7.36)$$

It is implicit in this definition that ε has an imaginary part subtracted from it. That is, $\varepsilon \rightarrow \varepsilon + i\Gamma$. If $t > t'$, we obtain a finite result. In the opposite regime, that is, $t < t'$, $G = 0$. The Green function that has this causal response is termed the retarded Green function.

We formulate the solution to Eq. (7.35) in terms of fermionic field operators,

$$\psi_\sigma^\dagger(\mathbf{r}, t) = \sum_{\mathbf{p}, \sigma} u_{\mathbf{p}}(\mathbf{r}) a_{\mathbf{p}, \sigma}^\dagger, \quad (7.37)$$

where $a_{\mathbf{p}, \sigma}^\dagger$ creates a particle with momentum \mathbf{p} and spin σ . We posit that

$$G_\sigma(\mathbf{r}, t; \mathbf{r}', t') = -iT \langle \psi_\sigma(\mathbf{r}, t) \psi_\sigma^\dagger(\mathbf{r}', t') \rangle \quad (7.38)$$

satisfies Eq. (7.35). Here $\langle \dots \rangle$ stands for the trace (Tr) over the quantum states of the system,

$$\langle \dots \rangle = \frac{\text{Tr} [e^{-\beta(H-\mu N)} \dots]}{\text{Tr} [e^{-\beta(H-\mu N)}]}, \quad (7.39)$$

not necessarily at $T = 0$. In addition, the symbol T denotes the time-ordered operator defined as

$$T(a(t_1)b(t_2)) = \begin{cases} a(t_1)b(t_2), & t_1 > t_2, \\ (-1)^P b(t_2)a(t_1), & t_2 > t_1, \end{cases} \quad (7.40)$$

with $P = 0$ for bosons and 1 for fermions. Given this definition, we can rewrite our posited solution as

$$G_\sigma(\mathbf{r}, t; \mathbf{r}', t') = -i\theta(t - t') \langle \psi_\sigma(\mathbf{r}, t) \psi_\sigma^\dagger(\mathbf{r}', t') \rangle + i\theta(t' - t) \langle \psi_\sigma^\dagger(\mathbf{r}', t') \psi_\sigma(\mathbf{r}, t) \rangle \quad (7.41)$$

with the Heaviside step function

$$\theta(x) = \begin{cases} 1, & x > 0, \\ 0, & x < 0 \end{cases} \quad (7.42)$$

replacing the time-ordering operator. The equations of motion for the Green function,

$$\begin{aligned} i\partial_t G_\sigma &= \delta(t - t') [\langle \psi_\sigma(\mathbf{r}, t) \psi_\sigma^\dagger(\mathbf{r}', t') \rangle + \langle \psi_\sigma^\dagger(\mathbf{r}', t) \psi_\sigma(\mathbf{r}, t) \rangle] \\ &\quad + \theta(t - t') \langle \dot{\psi}_\sigma(\mathbf{r}, t) \psi_\sigma^\dagger(\mathbf{r}', t') \rangle - \theta(t' - t) \langle \psi_\sigma^\dagger(\mathbf{r}', t') \dot{\psi}_\sigma(\mathbf{r}, t) \rangle, \end{aligned} \quad (7.43)$$

can be simplified by noting that, because of the δ -function, the first term reduces to the anticommutator

$$\{\psi_\sigma(\mathbf{r}, t), \psi_\sigma^\dagger(\mathbf{r}', t)\} = \delta(\mathbf{r} - \mathbf{r}'). \quad (7.44)$$

Hence, the first term reduces to the right-hand side of Eq. (7.35). In the remaining term, the Schrödinger equation can be used, leading to the term proportional to HG in Eq. (7.35). Consequently, Eq. (7.41) satisfies the most general equation of motion for a Green function. We can, however, define two other Green functions on the time interval $[t, t']$. The retarded Green function,

$$G_{\sigma}^R(\mathbf{r}, t; \mathbf{r}', t') = -i\theta(t - t') \langle \{\psi_{\sigma}(\mathbf{r}, t), \psi_{\sigma}^{\dagger}(\mathbf{r}', t')\} \rangle, \quad (7.45)$$

is non-zero only for $t > t'$, and the advanced Green function,

$$G_{\sigma}^A(\mathbf{r}, t; \mathbf{r}', t') = i\theta(t' - t) \langle \{\psi_{\sigma}(\mathbf{r}, t), \psi_{\sigma}^{\dagger}(\mathbf{r}', t')\} \rangle, \quad (7.46)$$

in the complementary domain $t < t'$. Both are constructed with a unit discontinuity built in as a result of the anticommutativity of ψ_{σ} and ψ_{σ}^{\dagger} . There are other functions that are typically defined at this time. For example, $G^> = -i\langle \psi_{\sigma}(\mathbf{r}, t)\psi_{\sigma}^{\dagger}(\mathbf{r}', t') \rangle$ and $G^< = i\langle \psi_{\sigma}^{\dagger}(\mathbf{r}', t')\psi_{\sigma}(\mathbf{r}, t) \rangle$. Although $G = G^>$ for $t > t'$ and $G = G^<$ for $t' > t$, the primary utility of these correlation functions is their relationship to the electron spectral function.

7.3.2 Properties of the Green function

The Green function is the work-horse of many-body theory as it contains all the information of the single-particle spectrum. We demonstrate here its relationship to (1) the particle density, (2) the spectral function and (3) its spectral representation.

Particle density

The Green function is fundamentally related to the particle density

$$\rho_{\sigma}(\mathbf{r}, t) = \langle \psi_{\sigma}^{\dagger}(\mathbf{r}, t)\psi_{\sigma}(\mathbf{r}, t) \rangle \quad (7.47)$$

at \mathbf{r} at time t . The limiting form,

$$G_{\sigma}(\mathbf{r}, t; \mathbf{r}' = \mathbf{r}, t = t + \delta t) = i\langle \psi_{\sigma}^{\dagger}(\mathbf{r}, t + \delta t)\psi_{\sigma}(\mathbf{r}, t) \rangle, \quad (7.48)$$

of the Green function suggests immediately that the particle density is given by

$$\rho(\mathbf{r}, t) = -iG_{\sigma}(\mathbf{r}, t; \mathbf{r}, t + \delta t). \quad (7.49)$$

Consequently, the average particle density is simply

$$\frac{N}{V} = -i \sum_{\sigma} \int d\mathbf{r} dt G_{\sigma}(\mathbf{r}, t; \mathbf{r}, t_+), \quad (7.50)$$

where t_+ implies the limiting procedure $t \rightarrow 0^+$.

Luttinger's sum rule relates the particle density to an integral in momentum space,

$$n = \int_{\text{Re } G(0, \mathbf{p}) > 0} \frac{d^d \mathbf{p}}{(2\pi)^d} \quad (7.51)$$

over which the real part of the Green function is positive. Stated in this fashion, it is not at all clear why such a connected surface in momentum space would be related to the particle density. To clarify this, we write the particle density,

$$n = -2i \int \frac{d^d \mathbf{p}}{(2\pi)^d} \lim_{t \rightarrow 0^+} \int \frac{d\omega}{2\pi} G(\omega, \mathbf{p}) e^{i\omega t}, \quad (7.52)$$

directly in terms of the frequency and momentum-dependent Green function. The factor of 2 arises from the sum over spin and $G(\omega, \mathbf{p})$ is the full Green function for either spin. Simplifying this expression begins by writing unity in a somewhat obscure way. In general, we can write a single-particle Green function,

$$G(\omega, \mathbf{p}) = (\omega - \epsilon(\mathbf{p}) - \Sigma(\omega, \mathbf{p}))^{-1}, \quad (7.53)$$

in terms of the self-energy $\Sigma(\omega, \mathbf{p})$. All of the information regarding the interactions between the particles is hidden in the self-energy. Taking the frequency-derivative of both sides of this expression, we write unity as

$$1 = \frac{\partial}{\partial \omega} G^{-1} + \frac{\partial}{\partial \omega} \Sigma(\omega, \mathbf{p}) \quad (7.54)$$

and hence the particle density as

$$\begin{aligned} n &= -2i \lim_{t \rightarrow 0^+} \int \frac{d^d \mathbf{p}}{(2\pi)^d} \int \frac{d\omega}{2\pi} \left(\frac{\partial}{\partial \omega} \ln G^{-1}(\omega, \mathbf{p}) + G(\omega, \mathbf{p}) \frac{\partial}{\partial \omega} \Sigma(\omega, \mathbf{p}) \right) e^{i\omega t} \\ &= I_1 - I_2. \end{aligned} \quad (7.55)$$

Evaluating these integrals is tricky and a bit tedious. It also involves an incursion into Matsubara or imaginary-time Green functions which are not used sparsely in the text. As a consequence, we evaluate them in the appendix to this chapter. We show there that the second integral vanishes and the first reduces explicitly to Eq. (7.51). The real part of the Green function acquires a positive value any time a pole is encountered. Poles count particle excitations. The number of such excitations corresponds to the particle number. Such cases in which the Green function consists entirely of poles corresponds to a Fermi liquid. In the last chapter, we consider the other case in which $\text{Re } G(0, \mathbf{p})$ becomes positive simply by passing through zero. While there is no general sum rule associated with the number of zeros of a Green function, they do have a physical significance. As we see in Chapter 16, they indicate the presence of a gap in the single-particle spectrum. That is, zeros indicate that one has isolated a quantity that does not propagate. Such is the case with electrons in a Mott insulator and quarks in the high-temperature phase of quantum-chromodynamics.

Spectral representation

We consider both $T = 0$ and finite temperature spectral representations of the Green function. It will be expedient to define $H' = H - \mu N$. At $T = 0$, the average,

$$\langle \cdots \rangle \equiv \langle 0 | \cdots | 0 \rangle, \quad (7.56)$$

is only over the ground state $|0\rangle$. Consequently, the Green function,

$$\begin{aligned} G_\sigma(\mathbf{r}, t; \mathbf{r}', t') = & -i\theta(t-t') \sum_m \langle 0 | \psi_\sigma(\mathbf{r}, t) | m \rangle \langle m | \psi_\sigma^\dagger(\mathbf{r}', t') | 0 \rangle \\ & + i\theta(t'-t) \sum_m \langle 0 | \psi_\sigma^\dagger(\mathbf{r}', t') | m \rangle \langle m | \psi_\sigma(\mathbf{r}, t) | 0 \rangle, \end{aligned} \quad (7.57)$$

simplifies. The explicit sum on $|m\rangle$ ranges over the excited states. The Heisenberg picture,

$$\hat{O} = S^{-1}OS, \quad (7.58)$$

where $S = \exp(-iH't/\hbar)$, permits a simplification of the time-dependence,

$$\begin{aligned} G_\sigma(\mathbf{r}, t; \mathbf{r}', t') = & -i\theta(t-t') \sum_m e^{i\omega_{0m}(t-t')} \langle 0 | \psi_\sigma(\mathbf{r}) | m \rangle \langle m | \psi_\sigma^\dagger(\mathbf{r}') | 0 \rangle \\ & + i\theta(t'-t) \sum_m e^{i\tilde{\omega}_{0m}(t'-t)} \langle 0 | \psi_\sigma^\dagger(\mathbf{r}') | m \rangle \langle m | \psi_\sigma(\mathbf{r}) | 0 \rangle, \end{aligned} \quad (7.59)$$

in the Green function. Since we are taking the overlap between $\langle 0 |$ and $\psi_\sigma(\mathbf{r}) | m \rangle$, the quantum states $|m\rangle$ and $|0\rangle$ must differ by a single particle, with $|m\rangle$ having $N+1$ particles. Hence, we define the frequencies as follows:

$$\begin{aligned} \omega_{0m} &= (E_0(N) - E_m(N+1) + \mu)/\hbar, \\ \tilde{\omega}_{0m} &= (E_0(N) - E_m(N-1) - \mu)/\hbar. \end{aligned} \quad (7.60)$$

Because $E_m(N+1) - E_0(N) > \mu$ and hence $E_0(N) - E_m(N-1) < \mu$, both ω_{0m} and $\tilde{\omega}_{0m}$ are negative. This fact will be important later when we separate $G_\sigma(\omega, \mathbf{p})$ into its real and imaginary parts. We are interested in the Fourier transform

$$G_\sigma(\omega, \mathbf{p}) = \int_{-\infty}^{\infty} d(t-t') \int \frac{d^3(\mathbf{r}-\mathbf{r}')}{(2\pi)^3} G_\sigma(\mathbf{r}, t; \mathbf{r}', t') e^{i\omega(t-t')} e^{-i\mathbf{p}\cdot(\mathbf{r}-\mathbf{r}')} \quad (7.61)$$

of the Green function. Substitution of Eq. (7.59) into Eq. (7.61) results in a sum of two terms. The time integration in the first is over the range $[0, \infty]$ and the second is over $[-\infty, 0]$. The time dependence in the exponentials is linear and hence the time integrations can be performed,

$$G_\sigma(\omega, \mathbf{p}) = \sum_m \int \frac{dx}{(2\pi)^3} \left[\frac{\langle 0 | \psi_\sigma(\mathbf{r}) | m \rangle \langle m | \psi_\sigma^\dagger(\mathbf{r}') | 0 \rangle}{\omega + \omega_{0m} + i0} + \frac{\langle 0 | \psi_\sigma^\dagger(\mathbf{r}') | m \rangle \langle m | \psi_\sigma(\mathbf{r}) | 0 \rangle}{\omega - \tilde{\omega}_{0m} - i0} \right] e^{-i\mathbf{p}\cdot\mathbf{x}}, \quad (7.62)$$

without delay. Here $\mathbf{x} = \mathbf{r} - \mathbf{r}'$. Note the factors of $\pm i0$ guarantee convergence of the integrals for $t > 0$ ($+i0$) and $t < 0$ ($-i0$). There are several simplifications that can be used at this time. First, we introduce $\hat{\mathbf{P}}$ as the total momentum operator and $T(r) = e^{-ir\cdot\hat{\mathbf{P}}}$ shifts a state by $-\mathbf{r}$. The invariance of matrix elements under such a shift by \mathbf{r} and then back is given by

$$\langle n | \psi_\sigma(0) | m \rangle = \langle n | e^{i\mathbf{r}\cdot\hat{\mathbf{P}}} \psi_\sigma(\mathbf{r}) e^{-i\mathbf{r}\cdot\hat{\mathbf{P}}} | m \rangle. \quad (7.63)$$

Note

$$e^{i\hat{\mathbf{P}} \cdot \mathbf{r}} |n\rangle = e^{i\mathbf{P}_n \cdot \mathbf{r}} |n\rangle \quad (7.64)$$

with \mathbf{P}_n the momentum of state $|n\rangle$. In the ground state $\mathbf{P}_0 = 0$. As a result,

$$\langle 0|\psi_\sigma(\mathbf{r})|m\rangle \langle m|\psi_\sigma^\dagger(\mathbf{r}')|0\rangle = e^{-i\mathbf{P}_{0m} \cdot (\mathbf{r}-\mathbf{r}')} |\langle 0|\psi|m\rangle|^2. \quad (7.65)$$

Using the fact that

$$\int d\mathbf{x} e^{-i\mathbf{p} \cdot \mathbf{x}} = \delta(\mathbf{p})(2\pi)^3, \quad (7.66)$$

we can perform the spatial integral in the Fourier transform in Eq. (7.62) to yield the spectral or Lehman representation,

$$G_\sigma(\omega, \mathbf{p}) = \sum_m \left(\frac{|\langle 0|\psi|m\rangle|^2 \delta(\mathbf{p} - \mathbf{P}_{0m})}{\omega + \omega_{0m} + i0} + \frac{|\langle m|\psi|0\rangle|^2 \delta(\mathbf{p} + \mathbf{P}_{0m})}{\omega - \tilde{\omega}_{0m} - i0} \right), \quad (7.67)$$

of the Green function. It explicitly shows that the Green function is a sum of particle addition (first term) and electron removal (second term) states. As a consequence, it is not an analytic function in either half-plane.

From the Lehman representation, we can write separate expressions for the real and imaginary parts of the Green function. To facilitate this, we define the residues for the electron addition,

$$A_m = |\langle 0|\psi|m\rangle|^2 \delta(\mathbf{p} - \mathbf{P}_{0m}), \quad (7.68)$$

and electron removal,

$$B_m = |\langle m|\psi|0\rangle|^2 \delta(\mathbf{p} + \mathbf{P}_{0m}), \quad (7.69)$$

parts of the spectrum. Noting that

$$\frac{1}{x \pm i0} = P\left(\frac{1}{x}\right) \mp i\pi \delta(x), \quad (7.70)$$

where P indicates the principal value, we write the real part of the Green function as

$$\text{Re } G_\sigma(\omega, \mathbf{p}) = \sum_m \left[\frac{A_m}{\omega + \omega_{0m}} + \frac{B_m}{\omega - \tilde{\omega}_{0m}} \right]. \quad (7.71)$$

Similarly, the imaginary part,

$$\text{Im } G_\sigma = \pi \sum_m (-A_m \delta(\omega + \omega_{0m}) + B_m \delta(\omega - \tilde{\omega}_{0m})), \quad (7.72)$$

is a sum of two terms as well. However, both terms do not contribute in the same energy range. This can be seen because both ω_{0m} and $\tilde{\omega}_{0m}$ are negative. As a consequence,

$$\text{Im } G_\sigma = \pi \sum_m \begin{cases} -A_m \delta(\omega + \omega_{0m}), & \omega > 0, \\ B_m \delta(\omega - \tilde{\omega}_{0m}), & \omega < 0. \end{cases} \quad (7.73)$$

Because A_m and B_m are both positive, we see clearly that $\text{Im } G_\sigma(\omega, \mathbf{p}) < 0$ for positive frequencies but is positive for $\omega < 0$. Consequently, it must vanish at $\omega = 0$. This behavior arises entirely from the causal nature of the Green function.

The procedure at finite temperature is identical with a few changes. The key difference is that the trace

$$\langle \dots \rangle = \sum_n e^{-\beta(E'_n - \Omega)} \langle n | \dots | n \rangle = \sum_n w_n \langle n | \dots | n \rangle \quad (7.74)$$

is over all the quantum states weighted with the Boltzmann factor w_n . In this expression $E'_n = \varepsilon_n - \mu N_n$. As in the $T = 0$ case, the Fourier transform of the Green function,

$$\begin{aligned} G_\sigma(\omega, \mathbf{p}) = & -i \int \frac{d\mathbf{x}}{(2\pi)^3} e^{i\mathbf{p}\cdot\mathbf{x}} \int_0^\infty dt \sum_{n,m} e^{i(\omega + \omega_{nm})t} w_n \langle n | \psi_\sigma(\mathbf{r}) | m \rangle \langle m | \psi_\sigma^\dagger(\mathbf{r}') | n \rangle \\ & + i \int \frac{d\mathbf{x}}{(2\pi)^3} e^{i\mathbf{p}\cdot\mathbf{x}} \int_{-\infty}^0 dt \sum_{n,m} e^{i(\omega - \tilde{\omega}_{nm})t} w_n \langle n | \psi_\sigma^\dagger(\mathbf{r}') | m \rangle \langle m | \psi_\sigma(\mathbf{r}) | n \rangle, \end{aligned} \quad (7.75)$$

consists of two terms from the retarded and advanced parts of the Green function with $\mathbf{x} = \mathbf{r} - \mathbf{r}'$. In the first term $N_m = N_n + 1$, whereas in the second $N_m = N_n - 1$. These terms can be combined by interchanging n and m in the second term. In this case $w_n \rightarrow w_m = w_n e^{\beta \hbar \omega_{nm}}$. The frequencies for particle addition, $\hbar \omega_{nm} = E'_n(N_n) - E'_m(N_n + 1)$, and removal, $\hbar \tilde{\omega}_{nm} = E'_n(N_n) - E'_m(N_n - 1)$, are related upon interchange of n and m through $\tilde{\omega}_{nm} = -\omega_{nm}$. As a result of interchanging n and m in the second term, when we perform the time and spatial integrations in the Fourier transform of the Green function, we are able to express the result,

$$\begin{aligned} G_\sigma(\omega, \mathbf{p}) &= \sum_{n,m} w_n \delta(\mathbf{p} - \mathbf{k}_{nm}) A_{nm} \left[\frac{1}{\omega + \omega_{nm} + i0} + \frac{e^{\beta \hbar \omega_{nm}}}{\omega + \omega_{nm} - i0} \right] \\ &= \sum_{n,m} w_n \delta(\mathbf{p} - \mathbf{k}_{nm}) A_{nm} \left[\frac{1 + e^{\beta \hbar \omega_{nm}}}{\omega + \omega_{nm}} - i\pi (1 - e^{\beta \hbar \omega_{nm}}) \delta(\omega + \omega_{nm}) \right], \end{aligned} \quad (7.76)$$

in terms of a single coefficient, $A_{nm} = |\langle n | \psi_\sigma | m \rangle|^2$.

Although the finite-temperature Green function is not an analytic function, its real and imaginary parts are related to analytic functions, namely the real and imaginary parts of G_σ^R and G_σ^A . To see how this works out, we write down explicitly the Fourier transform,

$$\begin{aligned} G_\sigma^R(\omega, \mathbf{p}) = & -i \int \frac{d\mathbf{x}}{(2\pi)^3} e^{i\mathbf{p}\cdot\mathbf{x}} \int_0^\infty dt \sum_{n,m} \left[e^{i(\omega + \omega_{nm})t} w_n \langle n | \psi_\sigma(\mathbf{r}) | m \rangle \langle m | \psi_\sigma^\dagger(\mathbf{r}') | n \rangle \right. \\ & \left. + e^{i(\omega - \tilde{\omega}_{nm})t} w_n \langle n | \psi_\sigma^\dagger(\mathbf{r}') | m \rangle \langle m | \psi_\sigma(\mathbf{r}) | n \rangle \right], \end{aligned} \quad (7.77)$$

of the retarded Green function. Once again, we simplify by interchanging n and m and perform the time and spatial integrals to obtain

$$G_\sigma^R(\omega, \mathbf{p}) = \sum_{n,m} \frac{w_n A_{nm} \delta(\mathbf{p} - \mathbf{k}_{nm})}{\omega + \omega_{nm} + i0} (1 + e^{\beta \hbar \omega_{nm}}) \quad (7.78)$$

as our working expression for the retarded finite T Green function. Comparing with Eq. (7.76), we find that

$$\text{Re } G_\sigma(\omega, \mathbf{p}) = \text{Re } G_\sigma^R(\omega, \mathbf{p}). \quad (7.79)$$

Because G^R is analytic in the upper half-plane, its real and imaginary parts,

$$\text{Re } G_\sigma^R(\omega, \mathbf{p}) = \frac{1}{\pi} P \int_{-\infty}^{\infty} \frac{\text{Im } G_\sigma^R(\omega', \mathbf{p})}{\omega' - \omega} d\omega', \quad (7.80)$$

are related via the Kramers–Kronig relationship. No such relationship is valid for the full Green function, $G_\sigma(\omega, \mathbf{p})$. A similar expression,

$$G_\sigma^A(\omega, \mathbf{p}) = \sum_{n,m} \frac{w_n A_{nm} \delta(\mathbf{p} - \mathbf{k}_{nm})}{\omega + \omega_{nm} - i0} (1 + e^{\beta \hbar \omega_{nm}}), \quad (7.81)$$

holds also for the advanced Green function. The only difference is that, since the contour is closed in the upper half-plane, the poles are shifted accordingly. Likewise, $\text{Re } G_\sigma^A(\omega, \mathbf{p}) = \text{Re } G_\sigma(\omega, \mathbf{p})$.

The imaginary parts are also related, though in a more complicated fashion. To proceed, we define

$$f_{nm}(\omega, \mathbf{p}) = w_n A_{nm} \delta(\omega + \omega_{nm}) \delta(\mathbf{p} - \mathbf{k}_{nm}). \quad (7.82)$$

Taking the imaginary part of Eq. (7.78), we find that

$$\text{Im } G_\sigma^R(\omega, \mathbf{p}) = -\pi (1 + e^{-\beta \hbar \omega}) \sum_{n,m} f_{nm}, \quad (7.83)$$

which is related to the imaginary part of the Green function,

$$\text{Im } G_\sigma(\omega, \mathbf{p}) = -\pi (1 - e^{-\beta \hbar \omega}) \sum_{n,m} f_{nm}, \quad (7.84)$$

through

$$\text{Im } G_\sigma^R(\omega, \mathbf{p}) = \coth \frac{\beta \hbar \omega}{2} \text{Im } G_\sigma(\omega, \mathbf{p}). \quad (7.85)$$

Likewise, for the advanced Green function, we have that

$$\text{Im } G_\sigma^A(\omega, \mathbf{p}) = -\coth \frac{\beta \hbar \omega}{2} \text{Im } G_\sigma(\omega, \mathbf{p}). \quad (7.86)$$

These are the key relationships among the various components of the Green functions. The key thing that these relationships reveal is that once one knows one of the Green functions, the other two can be constructed exactly. In fact, because of the Kramers–Kronig relationships only one of the components of either G^R or G^A is needed. Typically one works with the $\text{Im } G^R$. It is the special properties of this function that we now address.

Spectral function

The imaginary part of the retarded Green function occupies a special place in solid state physics. It is directly related to the spectral function

$$A_\sigma(\omega, \mathbf{p}) = -\frac{1}{\pi} \text{Im } G_\sigma^R(\omega, \mathbf{p}), \quad (7.87)$$

which contains all the information regarding the propagation of single-particle excitations. For example, the single-particle density of states per electron spin,

$$N_\sigma(\omega) = \sum_{\mathbf{p}} A_\sigma(\omega, \mathbf{p}), \quad (7.88)$$

is obtained by summing the spectral function over all momenta. The spectral function is also related to both $G_\sigma^>$ and $G_\sigma^<$. To see this, we rewrite $G_\sigma^>$,

$$G_\sigma^>(\omega, \mathbf{p}) = -i \int \frac{d\mathbf{x}}{(2\pi)^3} e^{i\mathbf{p}\cdot\mathbf{x}} \int_{-\infty}^{\infty} dt \sum_{n,m} e^{i(\omega+\omega_{nm})t} w_n \langle n | \psi_\sigma(\mathbf{r}) | m \rangle \langle m | \psi_\sigma^\dagger(\mathbf{r}') | n \rangle, \quad (7.89)$$

in terms of the Lehman representation. The form of the time integral,

$$\int_{-\infty}^{\infty} dt e^{i\omega t} = 2\pi \delta(\omega), \quad (7.90)$$

is at the heart of the difference between $G_\sigma^{>(<)}$ and the Green functions. In the Green functions, the time integrals always started or terminated at the origin. Consequently, the time integrations always yielded a function of the form, $1/(x \pm i0)$. Such a function has non-zero real and imaginary parts. Such is not the case in either $G_\sigma^>$ or $G_\sigma^<$. As a result,

$$G_\sigma^>(\omega, \mathbf{p}) = -i2\pi \sum_{n,m} f_{nm}. \quad (7.91)$$

From Eq. (7.84), we are able to relate the imaginary part of the retarded Green function,

$$\text{Im } G_\sigma^R(\omega, \mathbf{p}) = -\frac{i}{2} (1 + e^{-\beta\hbar\omega}) G_\sigma^>(\omega, \mathbf{p}), \quad (7.92)$$

directly to $G_\sigma^>(\omega, \mathbf{p})$ and, as a result, the spectral function:

$$A_\sigma(\omega, \mathbf{p}) = \frac{i}{2\pi} (1 + e^{-\beta\hbar\omega}) G_\sigma^>(\omega, \mathbf{p}). \quad (7.93)$$

The same steps allow us to recast

$$G_\sigma^<(\omega, \mathbf{p}) = 2\pi i e^{-\beta\hbar\omega} \sum_{n,m} f_{nm}, \quad (7.94)$$

which implies that

$$G_\sigma^<(\omega, \mathbf{p}) = -e^{-\beta\hbar\omega} G_\sigma^>(\omega, \mathbf{p}). \quad (7.95)$$

As a consequence,

$$\text{Im } G_\sigma^R(\omega, \mathbf{p}) = \frac{i}{2} (e^{\beta\hbar\omega} + 1) G_\sigma^<(\omega, \mathbf{p}). \quad (7.96)$$

Adding Eqs. (7.96) and (7.92), dividing by 2 and using Eq. (7.95) to simplify, we find that

$$A_\sigma(\omega, \mathbf{p}) = \frac{i}{2\pi} (G_\sigma^>(\omega, \mathbf{p}) - G_\sigma^<(\omega, \mathbf{p})). \quad (7.97)$$

We will use this expression in Chapter 16 where we derive the zero surface for the Green function in a Mott insulator.

The sum rule that gives the spectral function its extreme utility is

$$\int_{-\infty}^{\infty} A_\sigma(\omega, \mathbf{p}) d\omega = 1. \quad (7.98)$$

We prove this sum rule by performing the frequency integral

$$\begin{aligned} -i \int_{-\infty}^{\infty} d\omega \int \frac{d\mathbf{x}}{(2\pi)^3} e^{i\mathbf{p}\cdot\mathbf{x}} & \int_0^{\infty} dt \sum_{n,m} \left\{ e^{i(\omega+\omega_{nm})t} w_n \langle n | \psi_\sigma(\mathbf{r}) | m \rangle \langle m | \psi_\sigma^\dagger(\mathbf{r}') | m \rangle \right. \\ & \left. + e^{-i(\tilde{\omega}_{nm}-\omega)t} w_n \langle n | \psi_\sigma^\dagger(\mathbf{r}') | m \rangle \langle m | \psi_\sigma(\mathbf{r}) | n \rangle \right\} \end{aligned} \quad (7.99)$$

of $G_\sigma^R(\omega, \mathbf{p})$ explicitly. The ω integral yields $\pi\delta(t)$. Then the t integration is trivial, leaving

$$\begin{aligned} \int_{-\infty}^{\infty} d\omega G_\sigma^R(\omega, \mathbf{p}) &= -i\pi \int \frac{d\mathbf{x}}{(2\pi)^3} \sum_n w_n \langle n | \{ \psi_\sigma(\mathbf{r}), \psi_\sigma^\dagger(\mathbf{r}') \} | n \rangle \\ &= -i\pi \int \frac{d\mathbf{x}}{(2\pi)^3} \sum_n w_n \delta(x) \\ &= -i\pi, \end{aligned} \quad (7.100)$$

from which the sum rule, Eq. (7.98), immediately follows. Physically, this sum rule tells us that the probability of finding an electron in a particular momentum state is unity if all energies are considered. For a non-interacting system in which the quasi-particle concept applies, the sum rule is exhausted simply by integrating to the chemical potential. For Mott insulators, this is not the case as every state, regardless of its momentum, has non-zero spectral weight. This will be shown explicitly in the last chapter of this book.

7.4 Friedel's sum rule and local moments

Before we derive the condition for local moment formation, it is useful to see the structure of our results in terms of the phase shifts for the scattering of conduction electrons by the impurity. Using Eq. (7.22), we find that the Green function for the conduction electrons obeys

$$(\epsilon + i\Gamma - \epsilon_{\mathbf{k}})G_{\mathbf{kk}'}^{\sigma}(\epsilon + i\Gamma) = \delta_{\mathbf{kk}'} + V_{\mathbf{kd}}G_{d\mathbf{k}'}^{\sigma}(\epsilon + i\Gamma). \quad (7.101)$$

Eliminating $G_{\mathbf{kd}}^{\sigma}$ by using Eqs. (7.24) and (7.25), we obtain the closed expression

$$G_{\mathbf{kk}'}^{\sigma}(\epsilon + i\Gamma) = \frac{\delta_{\mathbf{kk}'}}{\epsilon + i\Gamma - \epsilon_{\mathbf{k}}} + \frac{V_{\mathbf{kd}}}{\epsilon + i\Gamma - \epsilon_{\mathbf{k}}}G_{dd}^{\sigma}(\epsilon + i\Gamma)\frac{V_{\mathbf{k}'d}^{*}}{\epsilon + i\Gamma - \epsilon_{\mathbf{k}'}}. \quad (7.102)$$

This expression for the Green function is of the form

$$G = G_0 + G_0 T G_0, \quad (7.103)$$

where T is the T -matrix,

$$T = V + V G_0 T. \quad (7.104)$$

Consequently, we identify the T -matrix for scattering of a conduction electron from momentum \mathbf{k} to momentum \mathbf{k}' as

$$T_{\mathbf{kk}'}^{\sigma}(\epsilon + i\Gamma) = V_{\mathbf{kd}}G_{dd}^{\sigma}(\epsilon + i\Gamma)V_{\mathbf{k}'d}^{*}. \quad (7.105)$$

Note that since the interaction $V_{\mathbf{kd}}$ is, by assumption, independent of the direction of \mathbf{k} , the scattering occurs only in s -waves. Substituting Eq. (7.29), we find that

$$T_{\mathbf{kk}'}^{\sigma}(\epsilon + i\Gamma) = \frac{|V_{\mathbf{kd}}|^2}{\epsilon + i\Gamma - E_{d\sigma} + i\pi N(\epsilon)V|\bar{V}_{\mathbf{kd}}|^2}, \quad (7.106)$$

and consequently, the imaginary part of the T -matrix,

$$\text{Im}T_{\mathbf{kk}'}^{\sigma}(\epsilon + i\Gamma) = -\pi|V_{\mathbf{kd}}|^2\rho_{d\sigma}(\epsilon), \quad (7.107)$$

is proportional to the density of states on the d -level.

From elementary scattering theory,

$$T_{\mathbf{kk}'}^{\sigma}(\epsilon + i\Gamma) \propto e^{2i\delta_{\sigma}} - 1 \propto \sin\delta_{\sigma}e^{i\delta_{\sigma}} = 1/(\cot\delta_{\sigma} - i). \quad (7.108)$$

Thus, we identify the s -wave phase shift as

$$\cot\delta_{\sigma}(\epsilon) = \frac{E_{d\sigma} - \epsilon}{\Delta}. \quad (7.109)$$

“On shell”, that is, for $\epsilon_{\mathbf{k}} = \epsilon_{\mathbf{k}'} = \epsilon$, the T -matrix element reduces to the standard form

$$T_{\mathbf{kk}'}^{\sigma}(\epsilon + i\Gamma) = -\frac{1}{\pi N(\epsilon)V}\sin\delta_{\sigma}e^{i\delta_{\sigma}}. \quad (7.110)$$

As discussed above, the average occupation, $\langle n_{d\sigma} \rangle$, of the d -level is given by the density of states integrated over the filled states,

$$\begin{aligned}\langle n_{d\sigma} \rangle &= \int_{-\infty}^{\epsilon_F=0} \rho_{d\sigma}(\epsilon) d\epsilon \\ &= \frac{\Delta}{\pi} \int_{-\infty}^0 \frac{d\epsilon}{(\epsilon - E_{d\sigma})^2 + \Delta^2} \\ &= \frac{1}{\pi} \cot^{-1} \left(\frac{E_{d\sigma}}{\Delta} \right).\end{aligned}\quad (7.111)$$

Using Eq. (7.109), we find

$$\langle n_{d\sigma} \rangle = \frac{\delta_\sigma(0)}{\pi}, \quad (7.112)$$

which is a simplified form of Friedel's sum rule between the occupancy of the impurity site and the phase shifts of conduction electrons at the Fermi energy scattering on the impurity. We emphasize that the phase shift calculated here arises entirely from non-spin-flip scattering at the d -level. The role of spin-flip scattering will be stressed in the next chapter when we consider explicitly the Kondo problem.

Substituting the expression $E_{d\sigma} = E_d + U \langle n_{d-\sigma} \rangle$ into Eq. (7.111), we obtain two coupled equations,

$$\langle n_{d\uparrow} \rangle = \frac{1}{\pi} \cot^{-1} \left(\frac{\epsilon_d + U \langle n_{d\downarrow} \rangle}{\Delta} \right) \quad (7.113)$$

and

$$\langle n_{d\downarrow} \rangle = \frac{1}{\pi} \cot^{-1} \left(\frac{\epsilon_d + U \langle n_{d\uparrow} \rangle}{\Delta} \right), \quad (7.114)$$

for the occupations of the \uparrow and \downarrow spin levels of the impurity. These are the central equations of the Hartree–Fock treatment of the Anderson Hamiltonian.

For local moment formation, we seek solutions in which $\langle n_{d\uparrow} \rangle \neq \langle n_{d\downarrow} \rangle$. Only in this case is the d -impurity magnetic. First, we see immediately that if $U = 0$, the only solution is $\langle n_{d\uparrow} \rangle = \langle n_{d\downarrow} \rangle$. Now in the limit in which $\Delta \rightarrow \infty$, we again find a non-magnetic solution, $\langle n_{d\uparrow} \rangle = \langle n_{d\downarrow} \rangle = 1/2$. A magnetic solution exists, however, in the intermediate parameter range, $\Delta/U \ll 1$. To simplify the notation we introduce the dimensionless parameters $x = -\epsilon_d/U$ and $y = U/\Delta$. The value $x = 0$ corresponds to the d -state energy ϵ_d lying right at the Fermi level. At $x = 1$, $\epsilon_d = -U$ and the upper d -state with energy $\epsilon_d + U$ is degenerate with the Fermi level. Hence, the energies 0 and $-U$ are symmetrically located around $x = 1/2$ or $\epsilon_d = -U/2$. As we will see, $x = 1/2$ is the most favorable case for a magnetic moment to form. In fact, magnetism persists only for $0 \leq x \leq 1$. When $\epsilon_d = -U/2$, the impurity terms in the Hamiltonian $\sum_\sigma (\epsilon_d n_{d\sigma} + V_{kd} a_{d\sigma}^\dagger a_{k\sigma}) + U n_{d\uparrow} n_{d\downarrow}$ are particle-hole symmetric under the transformation $a_d \leftrightarrow a_d^\dagger$ (see Problem 7.4).

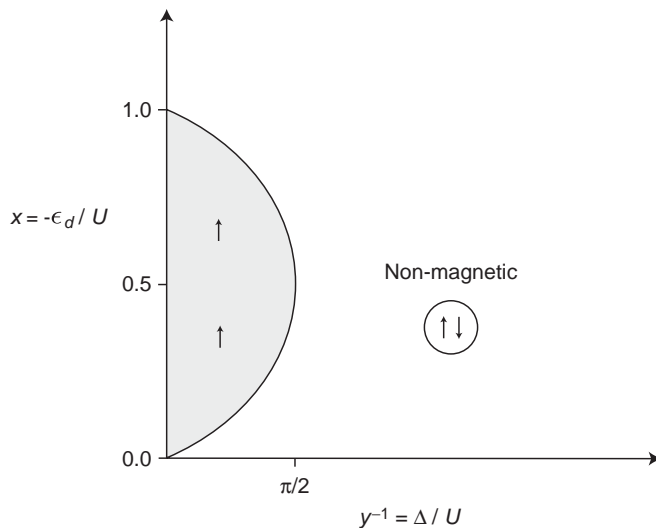


Fig. 7.3 Local moment phase diagram for the Anderson model. In the shaded region, local moments form stably. The solid curve separates the magnetic and non-magnetic regions.

In the limit $y \gg 1$ and $1 > x > 0$, Eqs. (7.113) and (7.114) predict a magnetic solution of the form

$$\pi \langle n_{d\uparrow} \rangle \simeq \pi + \frac{1}{y(\langle n_{d\downarrow} \rangle - x)} \quad (7.115)$$

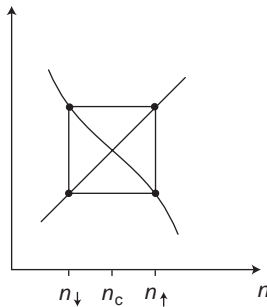
and

$$\pi \langle n_{d\downarrow} \rangle \simeq \frac{1}{y(\langle n_{d\uparrow} \rangle - x)}, \quad (7.116)$$

in which $\langle n_{d\uparrow} \rangle \sim 1$ and $\langle n_{d\downarrow} \rangle \sim 0$. In the limit of large y , the solution is

$$\begin{aligned} \langle n_{d\uparrow} \rangle &= 1 - \frac{1}{\pi xy} + \dots, \\ \langle n_{d\downarrow} \rangle &= x + \frac{1}{\pi xy} + \dots. \end{aligned} \quad (7.117)$$

The phase diagram for the complete range of magnetic parameters is shown in Fig. 7.3. On the transition curve and beyond, $\langle n_{d\uparrow} \rangle = \langle n_{d\downarrow} \rangle \equiv n_d$ or, equivalently, $\cot \pi n_d = (\epsilon_d + Un_d)/\Delta$. The mixed valence region corresponds to the lower left and upper left regions of the phase diagram in which either the lower or upper level is nearly degenerate with the Fermi level. In either of these regions, increasing Δ slightly results in a non-magnetic solution. As mentioned, many electronic systems, such as the heavy fermion materials, reside in this regime. At the boundary that defines the region of local moment formation, an infinitesimal perturbation of the equal occupation probability, $n_d = n_c$, thereby $\langle n_\sigma \rangle = n_c + \sigma \delta n$, leads to unequal occupancy of the impurity levels. Hence, from Eqs. (7.113) and

**Fig. 7.4**

A plot of the intersection of $y(n - x)$ and $\cot \pi n$. The vertices of the rectangle inscribing the intersection point correspond to magnetic solutions of Eqs. (7.113) and (7.114).

(7.114), we simply find that on the phase boundary, the occupation must also be a solution to the derivative of the local moment equations, so that

$$1 = \frac{U}{\Delta\pi} \frac{1}{1 + [(\epsilon_d + Un_c)/\Delta]^2}. \quad (7.118)$$

An equivalent way of deducing this form for the phase boundary is to consider solutions around the point at which the curves $\cot \pi n$ and $y(n - x)$ intersect, as shown in Fig. 7.4. A solution of Eqs. (7.113) and (7.114) is described by a rectangle of the type shown in Fig. 7.4 around such points, where for $\langle n_{d\uparrow} \rangle > \langle n_{d\downarrow} \rangle$, the vertical side on the right is at $\langle n_{d\uparrow} \rangle$, and on the left at $\langle n_{d\downarrow} \rangle$, as shown in the figure. Magnetic solutions will exist as long as the vertices of the rectangle touch the curves. An infinitesimal variation away from the intersection point where $\cot \pi n = y(n - x)$ leads to a magnetic solution, if the slopes of the two curves $\cot \pi n$ and $y(n - x)$ are equal in magnitude and opposite in sign. This is precisely the condition in Eq. (7.118).

Comparison of Eq. (7.118) with Eq. (7.30) reveals that the magnetic stability condition is equivalent to

$$U \rho_d(\epsilon = 0) = U \rho_d(\epsilon_F) = 1, \quad (7.119)$$

where $\rho_d(\epsilon) = \rho_{d\uparrow}(\epsilon)(\rho_{d\downarrow}(\epsilon))$ for equal occupancy. This equation is the principal result in Anderson's theory of local moments. Magnetic impurities with large densities of states at the Fermi level are expected to form local moments in non-magnetic metals. In fact, we can see the local moment criterion more intuitively by noticing that local moment formation is most favorable when the impurity levels are half-filled (see Fig. 7.3). At half-filling, the local moment criterion, Eq. (7.118), becomes $U/\pi\Delta > 1$. The hybridization energy is determined by the square of the hopping matrix element, through Δ . Hence, local

moment formation arises from a balancing of the on-site interaction with the hybridization energy.

A related result is Stoner's criterion for the onset of ferromagnetism in metals. Stoner ([S1938](#)) showed that within a simple model with a δ -function repulsion between electrons of the form $U\delta(\mathbf{r}_i - \mathbf{r}_j)$, the mean-field or Hartree–Fock criterion for the onset of ferromagnetism is $UN(\epsilon_F) \geq 1$, where $N(\epsilon_F)$ is the density of states per unit energy at the Fermi level of the metal. That ferromagnetism results from an interplay between the density of states and the Coulomb interaction can be understood as follows. Hopping processes which result in double occupancy of any lattice site with two electrons of the same spin are forbidden by the Pauli principle. However, when two neighboring lattice sites are occupied by electrons of opposite spin, the hopping process that doubly occupies one of the lattice sites has finite probability. Such antiferromagnetic double occupancy increases the energy of a lattice site as a result of the Coulomb repulsion. Nonetheless, hopping processes lower the kinetic energy of the electrons. Hence, whether the system of localized electrons becomes ferromagnetic and/or antiferromagnetic is ultimately determined by the competition between electron kinetic energy and the Coulomb repulsion; if Coulomb interactions dominate, the system is ferromagnetic. Effectively, at a given electron density, the density of states varies inversely with the electron kinetic energy, and the Stoner criterion reflects this competition between the Coulomb interaction and the kinetic energy.

Summary

We have seen that the Hartree–Fock solution to the Anderson model provides a simple criterion for local moment formation,

$$U\rho_d(\epsilon = 0) = U\rho_d(\epsilon_F) = 1. \quad (7.120)$$

Magnetic moments form when $U\rho_d(\epsilon_F) > 1$. Hence, an ion will have a tendency to be magnetic if either its density of d -states at the Fermi level or the on-site repulsion, U , is large. Ions with vanishing densities of states at the Fermi level will be non-magnetic. For a half-filled impurity, the local moment criterion can be written as $U/\pi\Delta > 1$. This criterion lays plain the competition between the local interaction energy and the hybridization that gives rise to local moment formation.

Appendix to Chapter 7: Luttinger's theorem

In this appendix, we evaluate the integrals that lead to Luttinger's sum rule. If it were not for the complex phase factor, $e^{i\omega t}$, the integrand in I_1 would reduce to a complete derivative and hence be straightforward to evaluate. But it isn't, unfortunately. Hence, we have to work a bit harder. The problem is that the full Green function is not an analytic function in either

half-plane. To this end, we define the Matsubara (M1955) “temperature Green function”,

$$\begin{aligned}\mathcal{G}_\sigma(\mathbf{r}_1, \tau_1; \mathbf{r}_2, \tau_2) = & -\theta(\tau_1 - \tau_2)\langle\psi_\sigma(\mathbf{r}_1, \tau_1)\psi_\sigma^\dagger(\mathbf{r}_2, \tau_2)\rangle \\ & + \theta(\tau_2 - \tau_1)\langle\psi_\sigma^\dagger(\mathbf{r}_2, \tau_2)\psi_\sigma(\mathbf{r}_1, \tau_1)\rangle.\end{aligned}\quad (7.121)$$

The difference between this and the other Green functions we have defined is that $\mathcal{G}(\mathbf{r}_1, \tau_1; \mathbf{r}_2, \tau_2)$ does not depend on t but rather imaginary time $\tau = it$. The interval of imaginary time is $[0, \beta\hbar]$. In units in which $\hbar = k_B = 1$, the upper limit is simply the inverse temperature. Explicitly, the thermal average in the Green function is a sum over diagonal elements of all possible states of the system regardless of their particle number. Because the factor of i is absent in the definition of the Matsubara Green function, the particle density becomes

$$n = \sum_\sigma \int d\mathbf{r} d\tau \mathcal{G}_\sigma(\mathbf{r}, \tau; \mathbf{r}, \tau_+). \quad (7.122)$$

All of the details leading to Luttinger's theorem are most conveniently done in Fourier space. The Matsubara Green function in frequency space is obtained from the standard Green functions by making the substitution $\omega \rightarrow i\omega_n$, where ω_n are the discrete frequencies, $2n\pi/(\beta\hbar)$ for bosons and $2\pi(n+1)/(\beta\hbar)$ for fermions. This can be shown in the following way. In so doing, one should replace the integral over real frequencies by a summation over the discrete frequencies:

$$\frac{1}{2\pi} \int d\omega \rightarrow i\frac{1}{\beta\hbar} \sum_{\omega_n}. \quad (7.123)$$

Formally, the Fourier transform of the imaginary-time Green function is defined as

$$\mathcal{G}_\sigma(\tau, \mathbf{p}) = \frac{1}{\beta\hbar} \sum_n e^{-i\omega_n \tau} \mathcal{G}(\omega, \mathbf{p}), \quad (7.124)$$

where τ measures the difference $\tau_1 - \tau_2$. Likewise,

$$\mathcal{G}_\sigma(\omega_n, \mathbf{p}) = \int_0^{\beta\hbar} e^{i\omega_n \tau} \mathcal{G}(\tau, \mathbf{p}) d\tau. \quad (7.125)$$

To show that the bosonic and fermionic cases correspond to even and odd Matsubara frequencies respectively, we rewrite the Fourier transform,

$$\begin{aligned}\mathcal{G}_\sigma(\omega_n, \mathbf{p}) &= \frac{1}{2} \int_{-\beta\hbar}^{\beta\hbar} e^{i\omega_n \tau} \mathcal{G}_\sigma(\tau, \mathbf{p}) d\tau \\ &= \frac{1}{2} \int_0^{\beta\hbar} e^{i\omega_n \tau} \mathcal{G}_\sigma(\tau, \mathbf{p}) d\tau + \frac{1}{2} \int_{-\beta\hbar}^0 e^{i\omega_n \tau} \mathcal{G}_\sigma(\tau, \mathbf{p}) d\tau,\end{aligned}\quad (7.126)$$

of the imaginary-time Green function. Consider the Matsubara Green function,

$$\mathcal{G}_\sigma(\mathbf{r}_1, \tau_1; \mathbf{r}_2, \tau_2) = \text{Tr}[e^{-\beta H} \psi_\sigma^\dagger(\mathbf{r}_2, \tau_2) e^{\beta H} e^{-\beta H} \psi_\sigma(\mathbf{r}_1, \tau_1)], \quad \tau_2 > \tau_1, \quad (7.127)$$

for negative values of $\tau = \tau_1 - \tau_2$. Using the cyclic permutation property of the trace, $\text{Tr}(ABC) = \text{Tr}(BCA) = \text{Tr}(CAB)$ and the Heisenberg representation, we find that

$$\mathcal{G}_\sigma(\mathbf{r}_1, \tau_1; \mathbf{r}_2, \tau_2) = \text{Tr} [e^{-\beta\hbar} \psi_\sigma(\mathbf{r}_1, \tau_1) \psi_\sigma^\dagger(\mathbf{r}_2, \tau_2 - \beta\hbar)], \quad \tau_2 > \tau_1. \quad (7.128)$$

Comparing with the definition of the Matsubara Green function (Eq. (7.121)), we arrive at the important conclusion

$$\mathcal{G}_\sigma(\tau, \mathbf{r}) = \mp \mathcal{G}_\sigma(\tau + \beta\hbar, \mathbf{r}), \quad (7.129)$$

where the lower sign applies to the bosonic case. For $\tau = \tau_1 - \tau_2 < 0$, $\tau + \beta\hbar \geq 0$. As a consequence, we have in Eq. (7.129) an expression relating the $\tau < 0$ to the $\tau > 0$ components of the Matsubara Green function. This results in an immediate simplification,

$$\begin{aligned} \mathcal{G}_\sigma(\omega_n, \mathbf{p}) &= \frac{1}{2} \int_0^{\beta\hbar} e^{i\omega_n\tau} \mathcal{G}_\sigma(\tau, \mathbf{p}) d\tau \mp \frac{1}{2} \int_{-\beta\hbar}^0 e^{i\omega_n\tau} \mathcal{G}_\sigma(\tau + \beta\hbar, \mathbf{p}) d\tau \\ &= \frac{1}{2} \int_0^{\beta\hbar} (1 \mp e^{-\beta\hbar\omega_n}) \mathcal{G}_\sigma(\tau, \mathbf{p}) d\tau, \end{aligned} \quad (7.130)$$

of the imaginary-time integral of the Matsubara Green function. This expression reduces to Eq. (7.125) only if

$$\omega_n = \begin{cases} \frac{(2n+1)\pi}{\beta\hbar} & \text{fermions,} \\ \frac{2n\pi}{\beta\hbar} & \text{bosons,} \end{cases}$$

thereby establishing a key claim at the outset of this appendix.

We need a second preliminary result. From Eq. (7.125), it follows that we need only consider $\mathcal{G}_\sigma(\tau > 0, \mathbf{p})$ when we compute explicitly the Fourier transform,

$$\mathcal{G}_\sigma(\omega_l, \mathbf{p}) = - \int \frac{d\mathbf{x}}{(2\pi)^d} e^{i\mathbf{p}\cdot\mathbf{x}} \int_0^{\beta\hbar} d\tau \sum_{n,m} e^{(\omega_l + i\omega_{nm})\tau} w_n \langle n | \psi_\sigma(\mathbf{r}) | m \rangle \langle m | \psi_\sigma^\dagger(\mathbf{r}') | n \rangle, \quad (7.131)$$

of the Matsubara Green function with $\mathbf{x} = \mathbf{r} - \mathbf{r}'$. The matrix elements can be simplified using the techniques we used to establish the Lehman representation of the real-time retarded and advanced Green functions. The result takes on the familiar form:

$$\mathcal{G}_\sigma(\omega_l, \mathbf{p}) = \sum_{n,m} w_n A_{nm} \delta(\mathbf{p} - \mathbf{k}_{nm}) \frac{1 + e^{\beta\hbar\omega_{nm}}}{\omega_{nm} + i\omega_l}. \quad (7.132)$$

Defining

$$Y_\sigma(\omega, \mathbf{p}) = \sum_{n,m} w_n A_{nm} \delta(\mathbf{p} - \mathbf{k}_{nm}) \delta(\omega - \omega_{nm}) (1 + e^{\beta\hbar\omega_{nm}}) \quad (7.133)$$

allows us to rewrite the Matsubara Green function,

$$\mathcal{G}_\sigma(\omega_n, \mathbf{p}) = \int_{-\infty}^{\infty} \frac{Y_\sigma(\alpha, \mathbf{p})}{\alpha + i\omega_n} d\alpha, \quad (7.134)$$

as an effective Hilbert transform. A consequence of this transform is that $\mathcal{G}_\sigma(\omega_n, \mathbf{p}) = \mathcal{G}_\sigma^*(-\omega_n, \mathbf{p})$. What is interesting is that the same function $Y_\sigma(\omega, \mathbf{p})$ enters the definition of the retarded Green function provided we make the substitution $\omega \rightarrow i\omega_n$. Such a continuation is only valid in the parameter space where $G_\sigma^R(\omega, \mathbf{p})$ is analytic. Comparing Eqs. (7.134) and Eq. (7.78), we find that

$$\mathcal{G}_\sigma(\omega_n, \mathbf{p}) = G_\sigma^R(i\omega_n, \mathbf{p}), \quad \omega_n > 0. \quad (7.135)$$

Similarly, in the lower half-plane, the advanced Green function is analytic, giving rise to the identity

$$\mathcal{G}_\sigma(\omega_n, \mathbf{p}) = G_\sigma^A(i\omega_n, \mathbf{p}), \quad \omega_n < 0. \quad (7.136)$$

We now have all the ingredients to proceed with our proof that I_1 simplifies as advertised. Our derivation mirrors Dzyaloshinskii's (D2003). Noting Eq. (7.5) and that the Matsubara Green function can be written as $\mathcal{G}_\sigma(\omega, \mathbf{p}) = 1/(i\omega - \epsilon(\mathbf{p}) - \Sigma(\omega, \mathbf{p}))$ or, equivalently,

$$i = \frac{\partial}{\partial \omega} \mathcal{G}^{-1} + \frac{\partial}{\partial \omega} \Sigma(\mathbf{p}, \omega), \quad (7.137)$$

allows us to recast the particle density as

$$\begin{aligned} n &= \frac{2}{(2\pi)^{d+1}} \lim_{\tau \rightarrow 0} \int_{-\infty}^{\infty} d\omega \int d^d \mathbf{p} e^{i\omega\tau} \mathcal{G}(\omega, \mathbf{p}) \\ &= \frac{2i}{(2\pi)^{d+1}} \lim_{\tau \rightarrow 0} \int_{-\infty}^{\infty} d\omega \int d^d \mathbf{p} e^{i\omega\tau} \mathcal{G}(\omega, \mathbf{p}) \left(\frac{\partial}{\partial \omega} \mathcal{G}^{-1} + \frac{\partial}{\partial \omega} \Sigma(\mathbf{p}, \omega) \right) \\ &= I_1 - I_2. \end{aligned} \quad (7.138)$$

In I_1 , we make the substitution $\xi = i\omega$ and integrate on a contour along the imaginary axis. The contours are shown in Fig. 7.5. Along the upper contour, C_+ , we can use the fact that \mathcal{G} can be represented by the analytical function, G^R , while in the lower contour, C_- , we use G^A . Consequently, we express I_1 naturally as a sum,

$$I_1 = \frac{2i}{(2\pi)^{d+1}} \lim_{\tau \rightarrow 0} \int d^d \mathbf{p} \left[\int_{C_+} e^{\xi\tau} d\xi \frac{\partial}{\partial \xi} \ln G^R(\xi, \mathbf{p}) + \int_{C_-} e^{\xi\tau} d\xi \frac{\partial}{\partial \xi} \ln G^A(\xi, \mathbf{p}) \right], \quad (7.139)$$

of two contour integrals. Here C_+ and C_- represent the upper and lower halves of the imaginary axis, as illustrated in Fig. 7.4. Because of the $e^{\xi\tau}$ factor and the analyticity of G^A and G^R in their respective half-planes, we can turn each of the contours to the left without any contribution from the boundary. Because the boundary contribution vanishes, we are

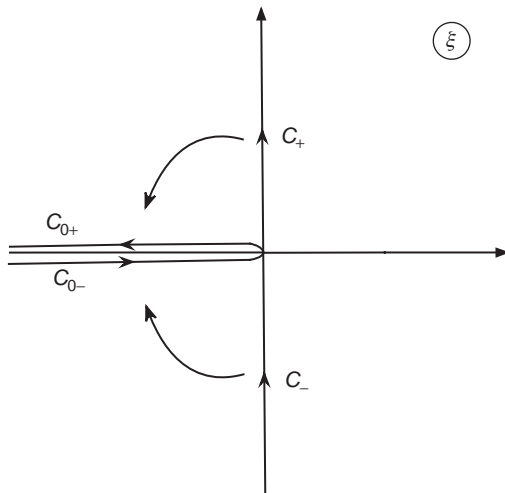


Fig. 7.5

Contours of integration in the complex ξ plane used in the evaluation of I_1 . C_+ is a contour along the real axis closed in the upper half-plane where G^R is analytic. Likewise, C_- is closed in the lower half-plane where G^A is analytic. C_{0-} and C_{0+} represent a 90° rotation of these and are closed entirely in the left half-plane relative to the imaginary axis.

allowed to take the $\tau \rightarrow 0$ limit before we do the integration over ξ . Using the fact that $\mathcal{G}(\omega, \mathbf{p}) = \mathcal{G}^*(-\omega, \mathbf{p})$, we have that

$$\begin{aligned} I_1 &= \frac{2i}{(2\pi)^{d+1}} \int d^d \mathbf{p} \int_{-\infty}^0 d\xi \frac{d}{d\xi} \ln \frac{G^R(\xi, \mathbf{p})}{G_R^*(\xi, \mathbf{p})} \\ &= -\frac{2}{\pi (2\pi)^d} \int d^d \mathbf{p} \int_{-\infty}^0 d\xi \frac{d}{d\xi} \phi_R \\ &= \frac{2}{(2\pi)^d} \int d^d \mathbf{p} \frac{1}{\pi} [\phi_R(-\infty) - \phi_R(0)] \end{aligned} \quad (7.140)$$

where ϕ_R is the phase of the retarded Green function. At $-\infty$, G^R is real and negative. Noting that the phase of the retarded propagator is π , we see immediately that I_1 reduces to Luttinger's theorem.

What about I_2 ? The integrand in I_2 can be integrated by parts provided that the self-energy is sublinear in ω . In many cases, this is true, and hence I_2 typically reduces to

$$I_2 = 2i \lim_{t \rightarrow 0^+} \int \frac{d^d \mathbf{p}}{(2\pi)^d} \int \frac{d\omega}{2\pi} \Sigma(\omega, \mathbf{p}) \frac{\partial}{\partial \omega} \mathcal{G}(\omega, \mathbf{p}) e^{i\omega t}. \quad (7.141)$$

This integral can be shown to vanish order-by-order in perturbation theory (L1960). The argument is quite simple. Each term involves higher powers of $1/\omega$ and hence vanishes when integrated from $-\infty$ to ∞ . As a result, we end up with the advertised result that the particle density is given by the integral over the region in momentum space where the Green function is positive. There are noted exceptions to Luttinger's theorem that we discuss in Chapter 16.

Problems

- 7.1 The matrix element V_{kd} takes into account the interaction between electrons on the impurity and the electrons in the band, which is omitted in the Hartree–Fock determination of the impurity states and the continuum states. The Coulomb matrix element, $\langle \mathbf{k}, \mathbf{k}' | V_{ee} | d, \mathbf{k}' \rangle$ summed over other band electrons k' moves an electron in the impurity level to a continuum level \mathbf{k} . Estimate the magnitude of V_{kd} from this residual Coulomb interaction.
- 7.2 Calculate explicitly the $\epsilon_{n\sigma}$ s in the Hartree–Fock approximation to the Anderson model.
- 7.3 Show explicitly that the Hartree–Fock approximation to the Anderson Hamiltonian can be written in the form of Eq. (7.9) with the $a_{n\sigma}^\dagger$ defined in Eq. (7.8).
- 7.4 Show that when $\epsilon_d = -U/2$ the impurity terms in the Anderson model, $\sum_\sigma (\epsilon_d n_{d\sigma} + U n_{d\uparrow} n_{d\downarrow})$, are invariant under the transformation $a_d^\dagger \leftrightarrow a_d$.
- 7.5 Consider the time-ordered bosonic Green function

$$G(\mathbf{r}, t; \mathbf{r}', t') = -i \langle T \psi(\mathbf{r}, t) \psi^\dagger(\mathbf{r}', t') \rangle, \quad (7.142)$$

and the advanced and retarded bosonic Green functions. Compute their Fourier transforms by repeating the analogous steps in the derivation of the fermionic Green function. Derive explicitly the relationships between the real and imaginary parts. In particular, you should prove that

$$G^R(\omega, \mathbf{p}) = \text{Re } G(\omega, \mathbf{p}) + i \tanh(\omega/2T) \text{Im } G(\omega, \mathbf{p}). \quad (7.143)$$

In the analogous expression for G^A , the second term enters with a minus sign.

References

- [A1961] P. W. Anderson, *Phys. Rev.* **124**, 41 (1961).
- [BC1989] D. Baeriswyl and D. K. Campbell, eds. *Interacting Electrons in Reduced Dimensions* (Plenum Press, New York, 1989).
- [D2003] I. Dzyaloshinskii, *Phys. Rev. B* **68**, 85113/1-6 (2003).
- [F1958] J. Friedel, *Nuovo Cimento Suppl.* **VII**, 287 (1958).
- [GZ1974] G. Grüner and A. Zawadowski, *Rep. Prog. Phys.* **37**, 1497 (1974).
- [H1964] J. Hubbard, *Proc. Roy. Soc. London A* **276**, 238 (1964).
- [L1960] J. M. Luttinger, *Phys. Rev.* **119**, 1153 (1960).
- [M1955] T. Matsubara, *Prog. Theor. Phys.* **14**, 351 (1955).
- [M1960] B. T. Matthias, M. Peter, H. J. Williams, A. M. Clogston, E. Corenzwit, and R. C. Sherwood, *Phys. Rev. Lett.* **5**, 542 (1960).
- [S1938] E. C. Stoner, *Proc. Roy. Soc. London A* **165**, 372 (1938).

8

Quenching of local moments: the Kondo problem

In the previous chapter we developed a mean-field criterion for local magnetic moment formation in a metal. As mean-field theory is valid typically at high temperatures, we anticipate that at low temperatures, significant departures from this treatment occur. The questions we focus on in this chapter are: (1) how does the presence of local magnetic moments affect the low-temperature transport and magnetic properties of the host metal, and (2) what is the fate of local magnetic moments at low temperatures in a metal? These questions are of extreme experimental importance because it has been known since the early 1930s that the resistivity of a host metal such as Cu with trace amounts of magnetic impurities, typically Fe, reaches a minimum and then increases as $-\ln T$ as the temperature subsequently decreases. This behavior is illustrated in Fig. 8.1 for various Mo and Nb alloys (SCL1964). A resistivity minimum and subsequent logarithmic temperature dependence are in stark contrast to the resistivity of the pure metal which tends to zero monotonically as the temperature decreases. An additional surprise is that the $-\ln T$ dependence of the resistivity does not continue indefinitely to low temperature, but rather below a characteristic temperature, the Kondo temperature, T_k , it phases out. Moreover, the spin properties of a magnetic impurity change fundamentally in the neighborhood of the Kondo temperature, as magnetic susceptibility measurements showed (H1969). Well above the Kondo temperature, the magnetic susceptibility of the impurity spins obeys the Curie $1/T$ law for free magnetic moments. Below T_k , however, the susceptibility tends to a constant (H1969). A constant susceptibility at $T = 0$ is characteristic of a singlet state polarized by a magnetic field (Problem 8.1). Hence, in addition to being the temperature at which the $-\ln T$ behavior of the resistivity ceases, T_k is the temperature at which the impurity and conduction electron spins begin to condense into singlet states. This condensation is complete at $T = 0$. The vanishing of the local moment below some characteristic temperature makes the Kondo problem fundamentally different from bulk ferromagnetism in which there is an onset of magnetism below some characteristic temperature, the Curie temperature. In the Kondo problem, just the opposite occurs; magnetism ceases at low temperatures.

Since the $-\ln T$ dependence of the resistivity vanishes once the impurities begin to condense into singlet states, the resistivity minimum must be due to the interaction of the impurity spin with those of the host metal. The inception of the first model that was capable of describing the interaction of a local spin with itinerant conduction electrons dates back to work in the 1940s and 1950s by Vosovskii (V1946), Zener (Z1951) and Kasuya (K1956). The essence of this model is that an exchange interaction, J , exists between a local impurity spin and the conduction electrons. This model, as we show, is related to the Anderson model in a certain parameter range.

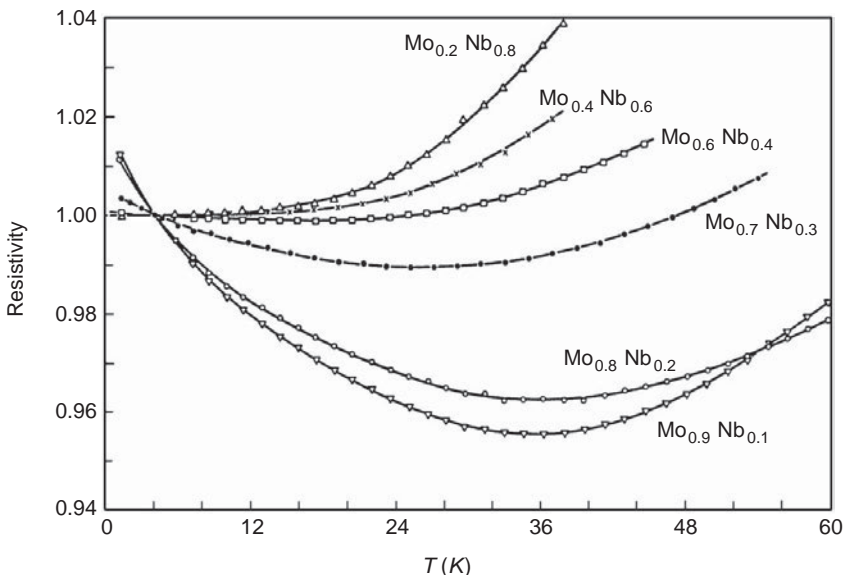


Fig. 8.1

Resistance minima for Fe in a series of Mo-Nb alloys (from Sarachik *et al.*, *Phys. Rev.* **135**, 1041 (1964)).

Kondo showed that a $-\ln T$ term appears in a perturbative theory to second order in J . Such scattering processes appear in addition to the scattering rate that arises between conduction electrons and phonons, which scales as T^5 at low temperatures. Because the resistivity is directly proportional to the total scattering probability, the logarithmic contribution from spin-flip scattering implies that a minimum occurs in the resistivity. Hence, Kondo's perturbative treatment offered a solution to the long-standing problem of the resistivity minimum in metal alloys.

However, all was not well with the Kondo solution. As $T \rightarrow 0$, the $\ln T$ terms diverge. The temperature at which the second-order term in the perturbative treatment of the scattering probability becomes comparable in magnitude to the first-order determines when the divergence occurs. This temperature is known as T_k , and it is the temperature around which the magnetic properties of the system change. The divergence implies that perturbation theory breaks down at low temperatures. As a consequence, Kondo's solution is valid only for $T \gg T_k$; other methods must be developed to understand the ultimate fate of a magnetic impurity near and below T_k . Experiments tell us, however, that ultimately the local moment does not survive at $T = 0$. The search for the theory that removes the divergence in Kondo's perturbative treatment and accounts for the formation of a bound singlet state at an impurity is known as the “Kondo problem”.

Anderson *et al.* (AYH1970) scaling hypothesis was the key concept that paved the way to the solution of this quite subtle problem. They showed within a perturbative scheme that the exchange interaction in the Kondo problem increases in magnitude as the effects of more and more high-energy excitations on the effective integration are included. Their scheme, while perturbative, was instrumental in pinpointing a physical mechanism by which the local moment vanishes and a ground state singlet ensues. The key breakthrough

in this problem, however, took place in the late 1970s when Wilson ([W1975](#)) developed a numerical renormalization group procedure to solve the Kondo problem. His solution confirmed the scaling hypothesis of Anderson and Yuval. The fact that the resolution of the Kondo problem required one of the key ideas in modern theoretical physics was certainly not anticipated. Indeed, the simplicity of the Kondo model belied the complexity of the physics it embodied. It is partly for this reason that the origin of the bound singlet state remained shrouded in divergent perturbation sums long after the resistivity minimum was satisfactorily explained.

In this chapter, we present the key ideas that led to the resolution of the resistivity minimum and Kondo problems. We first present the Kondo model and establish the origin of the antiferromagnetic interaction between the local moment and the conduction electrons. In so doing we will be able to establish the relationship between the Anderson and Kondo models. With the antiferromagnetic interaction in hand, we then perform the second-order perturbative analysis to uncloak the $\ln T$ dependence in the resistivity. It will become evident that a $\ln T$ dependence of the conductivity is anticipated anytime a local impurity has a degree of freedom, e.g., spin in the case of a local magnetic moment. We finally discuss the variational and scaling analyses of bound singlet state formation.

8.1 The Kondo Hamiltonian

The Kondo Hamiltonian describes the interaction of impurity spins, assumed to be spin-1/2, with those of the conduction electrons. We first introduce the two-component spinor operators that remove electrons from impurity and conduction states:

$$\Psi_{\mathbf{k}} = \begin{pmatrix} a_{\mathbf{k}\uparrow} \\ a_{\mathbf{k}\downarrow} \end{pmatrix}, \quad \Psi_d = \begin{pmatrix} a_d\uparrow \\ a_d\downarrow \end{pmatrix} \quad (8.1)$$

and spin matrix operators

$$\mathbf{S} = \frac{\hbar\sigma}{2}, \quad (8.2)$$

where the σ are the usual Pauli matrices,

$$\sigma_x = \begin{pmatrix} 0 & 1 \\ 1 & 0 \end{pmatrix}, \quad \sigma_y = \begin{pmatrix} 0 & -i \\ i & 0 \end{pmatrix}, \quad \sigma_z = \begin{pmatrix} 1 & 0 \\ 0 & -1 \end{pmatrix}. \quad (8.3)$$

We will also find useful the spin raising, $\frac{\hbar\sigma^+}{2} = S_x + iS_y = S^+$, and spin lowering, $\frac{\hbar\sigma^-}{2} = S_x - iS_y = S^-$, spin operators.

Kondo physics arises from the coupling of the spin of an impurity to that of a conduction electron. Hence, the simplest Hamiltonian that represents the interaction of a local spin

with a band of itinerant electrons is

$$H_K = \sum_{\mathbf{k}, \sigma} \epsilon_{\mathbf{k}} n_{\mathbf{k}\sigma} - \sum_{\mathbf{k}, \mathbf{k}'} \frac{J_{\mathbf{k}\mathbf{k}'}}{\hbar^2} (\Psi_{\mathbf{k}'}^\dagger \mathbf{S} \Psi_{\mathbf{k}}) \cdot (\Psi_d^\dagger \mathbf{S} \Psi_d). \quad (8.4)$$

The operator $\Psi_d^\dagger \mathbf{S} \Psi_d$ is the spin operator of electrons in impurity state d , while the spin operator $\Psi_{\mathbf{k}'}^\dagger \mathbf{S} \Psi_{\mathbf{k}}$ is the *transition* spin operator of electrons between conduction states \mathbf{k} and \mathbf{k}' . As the local impurity energy simply shifts the zero of the energy, we have dropped this term from the Hamiltonian. The interaction $J_{\mathbf{k}\mathbf{k}'}$, with units of energy, is the analog of the Heisenberg spin exchange interaction between the spin of a band electron and that of a localized electron. A positive $J_{\mathbf{k}\mathbf{k}'} > 0$ tends to favor spin alignment (see Eq. (5.18) in Chapter 5), and thus describes a ferromagnetic interaction, while $J_{\mathbf{k}\mathbf{k}'} < 0$ corresponds to an antiferromagnetic interaction.

8.2 Why is J negative?

We offer here a simple physical derivation of the exchange interaction in the Kondo Hamiltonian, appealing to the magnetic impurity model of Anderson. The complete derivation is detailed in the appendix. The interaction in the Kondo problem is non-zero when there is a net spin on the impurity – in the local moment phase for an impurity that can at most be doubly occupied. As we discussed in the previous chapter, the local moment phase in the Anderson model persists in the limit where the on-site Coulomb interaction, U , is much larger than the hybridization energy, Δ . It is precisely in the local moment limit that the Anderson and Kondo models describe the same physics. However, a fundamental difference between the Anderson and Kondo models is that the Anderson model includes charge fluctuations, which determine the hybridization energy, but they are absent in the Kondo model, which includes only spin–spin interactions. As we show now, the effect of charge fluctuations to second order in the hybridization matrix element, $V_{\mathbf{k}d}$, results in an antiferromagnetic interaction of the type in the Kondo model.

We focus on the processes, in the Anderson model, that lead to scattering of a conduction electron with a local moment and calculate to second order in the hybridization interaction, $\propto V_{\mathbf{k}d}$, which couples conduction electrons to the local moment. In perturbation theory, the amplitudes of such processes are of the form

$$V_{\mathbf{k}d} \frac{1}{E_i - E_{\text{int}}} V_{d\mathbf{k}}, \quad (8.5)$$

where E_i is the energy of the initial state and E_{int} is the energy of the intermediate state. Let us first consider the scattering of a conduction electron in state \mathbf{k} with spin down by a spin-up impurity, to a final electron state \mathbf{k}' of spin down with the impurity remaining with spin up. This process occurs by the electron \mathbf{k} hopping, via the hybridization interaction, to the impurity, as illustrated in Fig. 8.2(a); in this intermediate state, the impurity is doubly

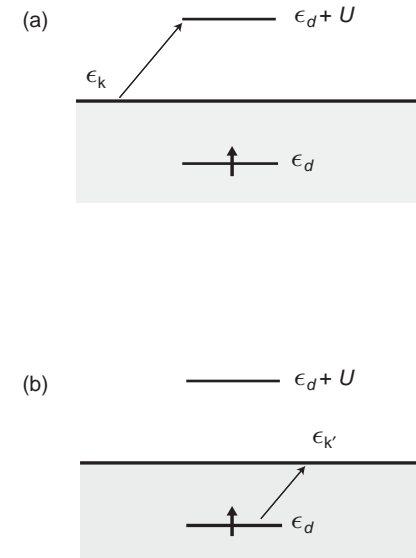


Fig. 8.2 Two processes that contribute to the second-order charge fluctuations on a singly-occupied d -level. The solid line denotes the initial conduction electron state, just below the Fermi surface. The energy levels are labeled as in Chapter 7.

occupied. The energy of the intermediate state is $2\epsilon_d + U$. Then the down-spin electron on the impurity hops to the final conduction electron state, \mathbf{k}' . The second-order matrix element for this process is

$$T_{(\mathbf{k}\sigma)+(d-\sigma)\rightarrow(\mathbf{k}'\sigma)+(d-\sigma)} = \frac{V_{kd}V_{d\mathbf{k}'}}{\epsilon_{\mathbf{k}} - \epsilon_d - U}. \quad (8.6)$$

On the other hand, the scattering of a conduction electron in state \mathbf{k} with spin up with a spin-up impurity, to a final electron state \mathbf{k}' of spin up with the impurity remaining with spin up, can only proceed by the electron on the impurity first hopping to \mathbf{k}' , as illustrated in Fig. 8.2(b). In the intermediate state, both electrons are in conduction states. The matrix element is then

$$T_{(\mathbf{k}\sigma)+(d\sigma)\rightarrow(\mathbf{k}'\sigma)+(d\sigma)} = -\frac{V_{kd}V_{d\mathbf{k}'}}{\epsilon_d - \epsilon_{\mathbf{k}'}}. \quad (8.7)$$

The minus sign arises from the exchange of the conduction and impurity electrons; the initial conduction electron ends on the impurity, while the initial electron on the impurity ends up in the conduction band. Similarly, the spin-flip scattering of a spin-up electron in state \mathbf{k} and a spin-down impurity to a final electron state $\mathbf{k}' \downarrow$ with the impurity ending with spin up proceeds either by this same process or as follows. A conduction electron first hops to the impurity, and then the down-spin electron on the impurity hops to the final state \mathbf{k}' . The amplitude is a linear superposition of those for the individual

processes,

$$T_{(\mathbf{k}\sigma)+(d-\sigma) \rightarrow (\mathbf{k}'-\sigma)+(d\sigma)} = -V_{\mathbf{kd}} V_{d\mathbf{k}'} \left(\frac{1}{\epsilon_{\mathbf{k}} - \epsilon_d - U} + \frac{1}{\epsilon_d - \epsilon_{\mathbf{k}'} } \right). \quad (8.8)$$

The minus sign again arises from exchange of the conduction and impurity electrons.

As shown in the appendix, the spin–spin interaction of the Kondo model, Eq. (8.4), yields the amplitude for the spin-flip process,

$$T_{(\mathbf{k}\sigma)+(d-\sigma) \rightarrow (\mathbf{k}'-\sigma)+(d\sigma)} = -\frac{1}{2} J_{\mathbf{kk}'} . \quad (8.9)$$

Consequently, we infer from Eqs. (8.8) and (8.9) that

$$J_{\mathbf{kk}'} = 2V_{\mathbf{kd}} V_{d\mathbf{k}'} \left(\frac{1}{\epsilon_{\mathbf{k}} - \epsilon_d - U} + \frac{1}{\epsilon_d - \epsilon_{\mathbf{k}'} } \right). \quad (8.10)$$

If we assume that the relevant \mathbf{k} -states of the host metal are close to the Fermi level, that is, $\epsilon_{\mathbf{k}} \approx \epsilon_{\mathbf{k}'} \approx 0$, then this expression reduces to

$$J_{\text{eff}} = -|V_{\mathbf{kd}}|^2 \frac{U}{|\epsilon_d|(U - |\epsilon_d|)} < 0. \quad (8.11)$$

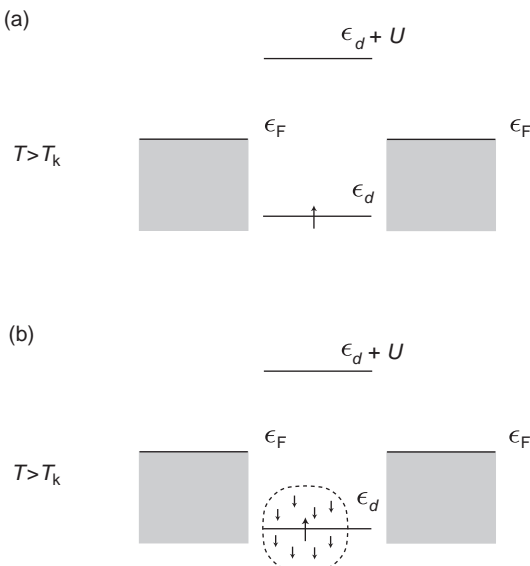
The effective coupling between the d -impurity and the band of electrons is indeed antiferromagnetic. To determine its magnitude, we consider the particle–hole symmetric point at which $\epsilon_d = -U/2$. In this limit, the exchange interaction,

$$J_{\text{eff}} = -4 \frac{|V_{\mathbf{kd}}|^2}{U}, \quad (8.12)$$

is inversely proportional to the on-site Coulomb repulsion. In the Anderson model, charge fluctuations between the conduction band and the impurity mediate the Kondo interaction. The coupling constant in the Kondo limit of the Anderson Hamiltonian scales as $\Delta/U \ll 1$. The interaction we derive here is the lowest term in a perturbation series in $V_{\mathbf{kd}}$. Why does taking charge fluctuations into account to second order lead to a spin dependence of the interaction? Physically the answer is the Pauli exclusion principle, which forbids intermediate states in which the impurity is occupied by two electrons of the same spin orientation.

In the appendix to this chapter we derive, via the Schrieffer–Wolff transformation, the full Hamiltonian to second order in $V_{\mathbf{kd}}$. The only difference for $J_{\mathbf{kk}'}$ from Eq. (8.10) is that the full answer Eq. (8.122) is symmetrized with respect to the two wavevectors \mathbf{k} and \mathbf{k}' . As the reader should verify, the full amplitude for the equal spin process in Eq. (8.7) arises from the direct interaction H_{dir} , Eq. (8.125), while the full amplitude for the opposite spin process in Eq. (8.6) arises from both the direct and spin–spin interactions.

The equivalence of the Kondo model to the Anderson model in the local moment phase suggests that the ground state of both models should be identical. Naively, one would associate the formation of a singlet state in the Anderson model with double occupancy of

**Fig. 8.3**

Schematic depiction of the energy levels in the Anderson model (a) above and (b) below the Kondo temperature. Even though the local moment begins to disappear as the temperature falls below T_k , the occupancy in the upper level remains unchanged from zero. This strange occurrence is the Kondo problem. Note that the Fermi sea does not develop a net magnetization below the Kondo temperature.

the impurity levels. This interpretation is problematic because, in the local moment phase of the Anderson model, the upper level is unoccupied. Further, the energy levels of the impurity remain fixed relative to the Fermi level when the temperature is lowered, the upper level (with energy $\epsilon_d + U$) remaining well above the Fermi level. Hence, it must be empty, as illustrated in Fig. 8.3.

Understanding the origin of the singlet ground state in the Anderson model at $T = 0$ is the essence of the Kondo problem. The singlet state emerges as a result of a new resonant level (GZ1972) that forms and remains pinned at the Fermi level. The change in the single-particle density of states in the Anderson model as a result of the formation of the resonant level is shown in Fig. 8.4. The peak grows logarithmically down (L1981) to the Kondo temperature; its width is proportional to T_k . Collectively, all the conduction electrons with energies within T_k of the Fermi surface contribute to the formation of the resonant level, as depicted in Fig. 8.3. For a spin-1/2 impurity, the resonant level is occupied on average by just a single conduction electron, which compensates the spin on the impurity. As we discuss at the end of Section 8.4, it is the logarithmic singularity in the electron–impurity scattering rate that gives rise to the sharp peak in the single-particle density of states at the Fermi level. The excess density of states at the Fermi level grows as the impurity loses its spin.

To summarize, at high temperatures the Hartree–Fock theory of local moment formation is valid, and the impurity density of states is well described by the two-peaked Lorentzian function derived in the last chapter. However, at low temperatures, new physics arises that is not described by the mean-field description of the Anderson model. At low temperatures, rapid spin-flip scattering occurs between the conduction electrons and the local moments. We now show how such processes underly the resistivity minimum in metallic alloys.

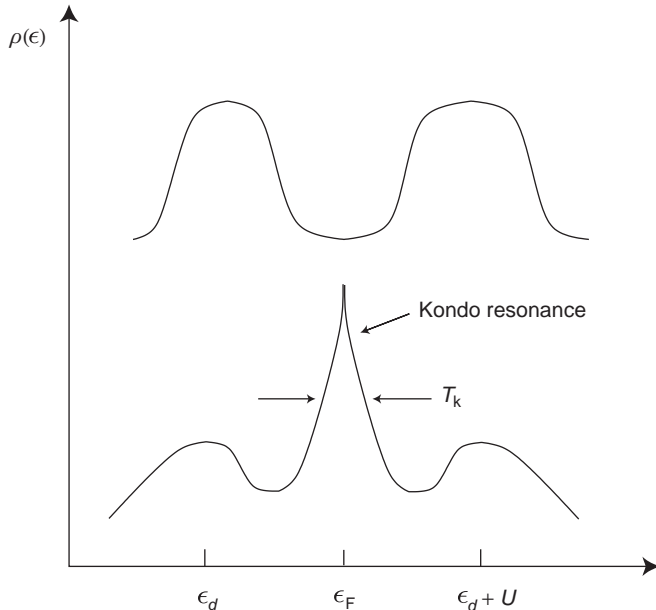


Fig. 8.4 Single-particle density of states in the Anderson model in the Kondo regime. The emergence of the sharp peak at the Fermi level is a many-body resonance effect. This peak increases logarithmically as the temperature is lowered.

8.3 Scattering and the resistivity minimum

The origin of the logarithmic contribution to the resistivity is the spin degree of freedom at the impurity. To see the role of the spin, we outline the key notions that underlie the structure of the scattering probability. As we will see, the scattering probability to lowest order in the exchange interaction is well behaved and temperature independent. Temperature dependence first arises in a calculation of the scattering amplitude to second order in the exchange interaction. Because the interaction depends on the spin degree of freedom, a second-order term can involve spin-flip processes on the impurity. However, the order in which the spins are flipped matters because, for example, $S^+S^- \neq S^-S^+$. This lack of commutativity combined with the restriction of the allowed occupancy of the intermediate states arising from the Pauli principle leads to a non-trivial temperature dependence of the scattering amplitudes. In second order, the contribution is of the form f/ϵ . This integral is logarithmically divergent, hence the origin of the Kondo logarithm. By contrast, if the impurity lacks any internal structure, the restriction on the filling of the intermediate states imposed by the Pauli principle cancels out entirely.

We now fill in the details of the derivation of the scattering amplitude to second order in the exchange interaction. Since the exchange interaction is a short-range point-like interaction, its Fourier transform should be constant in k -space. As a consequence, we make the approximation

$$J_{\mathbf{k}\mathbf{k}'} = J_0/V, \quad (8.13)$$

where J_0 is a negative constant, and V is the volume. The Kondo Hamiltonian is a sum of an unperturbed part

$$H_0 = \sum_{\mathbf{k},\sigma} \epsilon_{\mathbf{k}} n_{\mathbf{k}\sigma} \quad (8.14)$$

and the spin–spin interaction, which we treat perturbatively,

$$H' = -\frac{J_0}{2\hbar V} \sum_{\mathbf{k}',\mathbf{k}''} \left[S_d^z (a_{\mathbf{k}'\uparrow}^\dagger a_{\mathbf{k}''\uparrow} - a_{\mathbf{k}'\downarrow}^\dagger a_{\mathbf{k}''\downarrow}) + S_d^+ a_{\mathbf{k}'\downarrow}^\dagger a_{\mathbf{k}''\uparrow} + S_d^- a_{\mathbf{k}'\uparrow}^\dagger a_{\mathbf{k}''\downarrow} \right]. \quad (8.15)$$

Since we are interested only in the coupling to a single impurity, we write the interaction here in terms of the single impurity spin operator, S_d , rather than the second quantized description of the impurity in the Kondo Hamiltonian, Eq. (8.4). To get practice in spin algebra, we assume more generally that the impurity has total spin $S \equiv \hbar s$; the eigenstates of S_z are denoted by the eigenvalue $\hbar m_s$.

Let us first calculate in lowest order the total rate of scattering by an impurity of a conduction electron initially of momentum \mathbf{k} to momentum \mathbf{k}' ; we let the impurity have initial spin orientation m_s . The many-particle electron states are Slater determinants of single-particle states in the conduction band. Because H' involves one pair of creation and annihilation operators for the conduction band, it can only connect states that differ by a single orbital. Hence, the energy differences entering the calculation of scattering rates reduce to differences of single orbital energies.

The total scattering rate is the sum of the rates of two incoherent processes, the first in which the initial electron, which we take to be spin up, does not flip its spin and remains with spin up, and the second in which the electron goes from spin up to spin down, while the impurity goes from m_s to $m_s + 1$. Consider first the non-spin-flip process, for which the bare matrix element is

$$T_{\mathbf{k}\uparrow \rightarrow \mathbf{k}'\uparrow; m_s}^{(0)} = -\frac{J_0}{2V} m_s. \quad (8.16)$$

The lowest order rate of scattering is

$$\Gamma_{\mathbf{k} \rightarrow \mathbf{k}'}^0(m_s) = \frac{2\pi}{\hbar} \sum_{\mathbf{k}'} \delta(\epsilon_{\mathbf{k}} - \epsilon_{\mathbf{k}'}) \left(\frac{J_0}{2V} \right)^2 m_s^2, \quad (8.17)$$

where the sum is over a limited group of final states \mathbf{k}' . Note that the scattering is isotropic (s -wave). To compute the total rate of this process, we sum \mathbf{k}' over all final states, which gives a factor $N(0)V$ for \mathbf{k} close to the Fermi surface, where $N(0) = mk_F/2\pi^2\hbar^2 = 3n_e/4\epsilon_F$ is the single-spin electron density of states at the Fermi surface. The total scattering rate from a single impurity with no spin-flip is thus

$$\Gamma_{\text{non-flip}}^0(m_s) = \frac{\pi}{2\hbar V} N(0) J_0^2 m_s^2. \quad (8.18)$$

In the spin-flip process, the matrix element is

$$T_{\mathbf{k}\uparrow \rightarrow \mathbf{k}'\downarrow; m_s}^{(0)} = -\frac{J_0}{2\hbar V} \langle s, m_s + 1 | S_d^+ | s, m_s \rangle. \quad (8.19)$$

From the quantum theory of angular momentum,

$$\langle s, m_s \pm 1 | S^\pm | s, m_s \rangle = \hbar \sqrt{s(s+1) - m_s(m_s \pm 1)}, \quad (8.20)$$

so that

$$\Gamma_{\text{flip}}^0(m_s) = \frac{\pi}{2\hbar V} N(0) J_0^2(s(s+1) - m_s(m_s + 1)). \quad (8.21)$$

The total rate of scattering is the sum of (8.18) and (8.21),

$$\Gamma^0(m_s) = \frac{\pi}{2\hbar V} N(0) J_0^2(s(s+1) - m_s). \quad (8.22)$$

If we average over all initial spin orientations of the impurity, the m_s term vanishes. Summing over all impurities, we derive the spin-averaged scattering rate,

$$\Gamma^0 = \frac{\pi}{2\hbar} s(s+1) J_0^2 n_{\text{imp}} N(0) = \frac{2\pi}{3} \frac{\epsilon_F}{\hbar} s(s+1) c (N(0) J_0)^2, \quad (8.23)$$

where $c = n_{\text{imp}}/n_e$ is the fractional concentration and n_{imp} the density of impurities. The non-spin-flip contribution is 1/3 of the total, as one sees from the relation

$$\frac{1}{2s+1} \sum_{m_s} m_s^2 = \frac{1}{3} s(s+1). \quad (8.24)$$

The scattering rate (8.23) is well behaved and completely independent of temperature. All things being equal, each order of perturbation theory is smaller by a factor of $J_0 N(0)$. Hence, it might seem unnecessary to explore the second-order term. However, all things are not equal and a crucial divergence lurks at second order.

To determine the scattering rate to next order in H' , we calculate the scattering amplitude to second order. In general the second-order amplitude is given by

$$T_{a \rightarrow b}^{(2)} = \sum_{c \neq a} \frac{\langle b | H' | c \rangle \langle c | H' | a \rangle}{E_a - E_c}. \quad (8.25)$$

As in the lowest order, the scattering rate is a sum of processes in which the initial and final electron state have the same spin and in which the final electron spin is opposite to the initial spin. Figure 8.5 shows the second-order contributions to the amplitude in which the final electron has the same spin as the initial, and Fig. 8.6 shows the processes in which the final spin has flipped. In each of these processes, two types of contribution enter the intermediate states: non-spin-flip terms, in which the electron spin remains unchanged and which involve only S^z , and spin-flip terms involving the operators S^\pm .

Let us first consider the upper two processes in Fig. 8.5, in which an electron of initial momentum \mathbf{k} is scattered to final momentum \mathbf{k}' . On the one hand, the electron can scatter

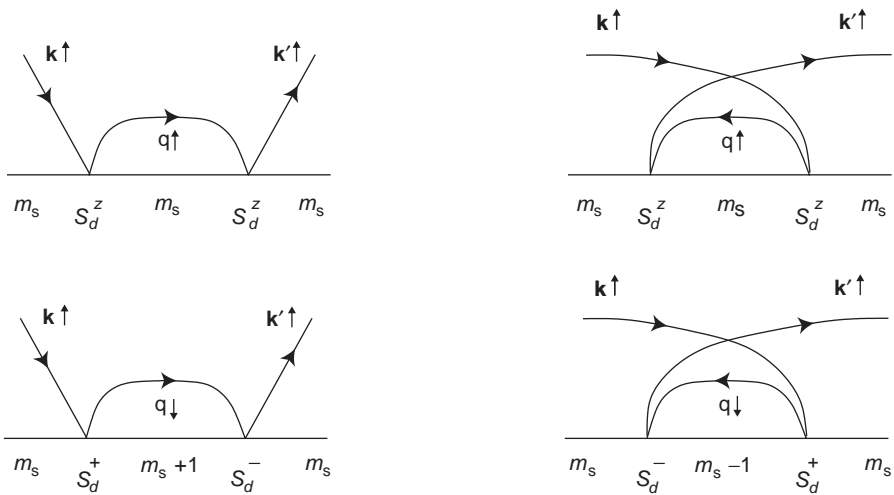


Fig. 8.5 Second-order processes between initial and final electron states $\mathbf{k} \uparrow$ and $\mathbf{k}' \uparrow$. The straight lines depict the spin of the impurity and the curved lines the electron. The line with a backwards arrow in the intermediate state represents a hole, that is, a particle that is present in the initial state and final state, but is absent in the intermediate state. The label on the hole is the momentum and spin of that electron in the initial state.

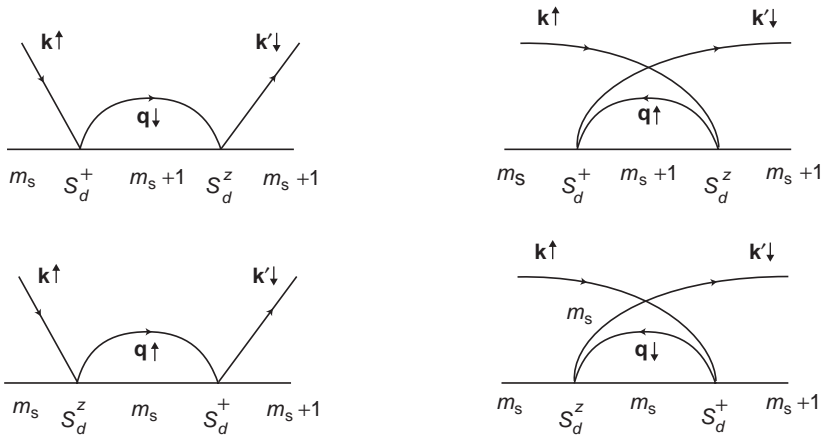


Fig. 8.6 Second-order spin-flip processes between initial and final electron states $\mathbf{k} \uparrow$ and $\mathbf{k}' \downarrow$.

from momentum \mathbf{k} to an unoccupied state with momentum \mathbf{q} and subsequently to the final state with momentum \mathbf{k}' , as shown in the upper left diagram. The contribution of this process to $T_{\text{non-flip}}^{(2)}(\mathbf{k} \rightarrow \mathbf{k}', m_s)$ is

$$\left(\frac{-J_0 m_s}{2}\right)^2 \frac{1}{V} \alpha, \quad (8.26)$$

where the sum over intermediate particle states is

$$\alpha = \frac{1}{V} \sum_{\mathbf{q}} \frac{1 - f_{\mathbf{q}}}{\epsilon_{\mathbf{k}} + i\eta - \epsilon_{\mathbf{q}}}. \quad (8.27)$$

The factor $1 - f_{\mathbf{q}}$, where $f_{\mathbf{q}}$ is the electron Fermi distribution function, guarantees that the state \mathbf{q} is empty. The positive infinitesimal imaginary number $i\eta$ guarantees that the scattering produces outgoing, rather than incoming, waves. Quantum mechanically coherent with this process is that shown in the upper right diagram (see Fig. 8.5) in which an electron in an occupied state \mathbf{q} scatters to the final state \mathbf{k}' , and another electron with momentum \mathbf{k} scatters into the vacated state \mathbf{q} , giving a contribution

$$\left(\frac{-J_0 m_s}{2V} \right)^2 \frac{1}{V} \gamma, \quad (8.28)$$

where

$$\gamma = -\frac{1}{V} \sum_{\mathbf{q}} \frac{f_{\mathbf{q}}}{\epsilon_{\mathbf{q}} + i\eta - \epsilon_{\mathbf{k}'}}. \quad (8.29)$$

In this latter process, the intermediate momentum state must be occupied; the rate is thus proportional to $f_{\mathbf{q}}$. The minus sign arises from the interchange of the operations of removing the initial electron and creating the final electron, $a_{\mathbf{k}} a_{\mathbf{k}'}^\dagger = -a_{\mathbf{k}'}^\dagger a_{\mathbf{k}}$ for $\mathbf{k} \neq \mathbf{k}'$. In an energy-conserving scattering ($\epsilon_k = \epsilon_{k'}$) process, the distribution functions cancel in the sum of the amplitudes for the two processes, and the amplitude for non-spin-flip processes is

$$T_{\text{non-flip}}^{(2)}(\mathbf{k} \uparrow \rightarrow \mathbf{k}' \uparrow; m_s) = \left(\frac{-J_0 m_s}{2V} \right)^2 \sum_{\mathbf{q}} \frac{1}{\epsilon_{\mathbf{k}} - \epsilon_{\mathbf{q}}}. \quad (8.30)$$

Because the f 's cancel, the non-spin-flip amplitudes are independent of temperature. The summation is formally divergent because we have ignored the momentum dependence of the matrix elements; once taken into consideration, this term is finite.

The lower two processes shown in Fig. 8.5 involve a single electron spin-flip in the intermediate state. The same two intermediate momentum states enter as in the non-spin-flip processes discussed above; however, they do not have the same weights. In the lower left diagram, the matrix elements give a factor $(-J_0/2\hbar V)^2 P_{+-}$ where

$$P_{+-} = \frac{1}{\hbar^2} |\langle s, m_s + 1 | S_d^+ | s, m_s \rangle|^2 = s(s+1) - m_s(m_s+1). \quad (8.31)$$

In the lower right diagram, where the intermediate state involves a filled state, the matrix elements give instead $(-J_0/2\hbar V)^2 P_{-+}$, where

$$P_{-+} = \frac{1}{\hbar^2} |\langle s, m_s - 1 | S_d^- | s, m_s \rangle|^2 = s(s+1) - m_s(m_s-1). \quad (8.32)$$

The sum of the matrix elements for these processes, for given m_s , is

$$\left(\frac{J_0}{2V}\right)^2 (P_{+-\alpha} + P_{-+\gamma}) = \left(\frac{J_0}{2V}\right)^2 (P_{+-}(\alpha + \gamma) + 2m_s\gamma). \quad (8.33)$$

Because $P_{+-} \neq P_{-+}$, the Fermi distributions do not cancel. The presence of the Fermi distribution function in the spin-flip transition amplitude, which introduces a temperature dependence into the transition rate, is the fundamental difference between the cases involving a spin-flip and a non-spin-flip in the intermediate states. The temperature dependence is intrinsically tied to the dynamics between the degenerate spin levels of the conduction electrons and the impurity. The sum over hole states γ is also generally dependent on the energy of the incoming particle. As in the non-spin-flip case, the part of the above expression proportional to $\alpha + \gamma$ is divergent because we have ignored the momentum dependence of the matrix elements. With such dependence, this term becomes finite, but remains independent of temperature.

The sum of the contributions of all four terms in Fig. 8.5 is

$$T^{(2)}(\mathbf{k} \uparrow \rightarrow \mathbf{k}' \uparrow; m_s) = \left(\frac{J_0}{2}\right)^2 \frac{1}{V} (2m_s\gamma + (s(s+1) - m_s)(\alpha + \gamma)). \quad (8.34)$$

The crucial temperature-dependent term in the second-order amplitude, which comes from the terms with an intermediate spin-flip, is the first on the right side of Eq. (8.34). We drop the second term, so that

$$T^{(2)}(\mathbf{k} \uparrow \rightarrow \mathbf{k}' \uparrow; m_s) \approx \frac{2m_s}{V} \left(\frac{J_0}{2}\right)^2 \gamma. \quad (8.35)$$

Converting the sum over \mathbf{q} in γ to an integral, and working in the $T = 0$ limit with the free-particle dispersion relation $\epsilon_{\mathbf{k}} = k^2/2m$, we have

$$\gamma = \frac{m}{\pi^2 \hbar^3} \int_0^{k_F} \frac{q^2 dq}{k^2 - q^2 - i\eta}. \quad (8.36)$$

The real part of the integral over momentum is of the type encountered in Chapter 6 in the context of the interacting electron gas:

$$\int_0^{k_F} \frac{q^2 dq}{k^2 - q^2} = -k_F - \frac{k}{2} \ln \left| \frac{k - k_F}{k + k_F} \right|. \quad (8.37)$$

For $T \neq 0$ but $\ll T_F$, the range of k for thermally excited electrons is given by $|k^2/2m - k_F^2/2m| \lesssim k_B T$; we thus approximate $|k - k_F|$ in the numerator of the logarithm by $mk_B T/k_F$, and let $k = k_F$ everywhere else. The leading $-k_F$ term on the right is a constant, which we drop. Thus

$$\gamma \approx N(0) \left(\ln \frac{T_F}{T} + \dots \right). \quad (8.38)$$

Substituting this expression into Eq. (8.35) and adding in the lowest-order scattering amplitude, we find the amplitude, to within constant terms, in second order,

$$T(\mathbf{k} \uparrow \rightarrow \mathbf{k}' \uparrow; m_s) = -\frac{J_0 m_s}{2V} \left(1 - J_0 N(0) \ln \frac{T_F}{T} + \dots \right). \quad (8.39)$$

Note that the second-order correction increases the magnitude of the scattering amplitude for $J_0 < 0$.

By a similar calculation, which is left as an exercise, one can derive the total amplitude for the four processes shown in Fig 8.6,

$$T^{(2)}(\mathbf{k} \uparrow \rightarrow \mathbf{k}' \downarrow; m_s) = -\left(\frac{J_0}{2}\right)^2 \frac{1}{\hbar V} \langle s, m_s + 1 | S_d^+ | s, m_s \rangle (\alpha - \gamma). \quad (8.40)$$

Adding in the lowest-order amplitude, we find the electron spin-flip amplitude, including the temperature-dependent part in second order,

$$T(\mathbf{k} \uparrow \rightarrow \mathbf{k}' \downarrow; m_s) \approx -\frac{J_0}{2\hbar V} \langle s, m_s + 1 | S_d^+ | s, m_s \rangle \left(1 - J_0 N(0) \ln \frac{T_F}{T} + \dots \right). \quad (8.41)$$

Note that both the non-spin-flip and spin-flip amplitudes are modified by the same temperature-dependent factor, $(1 - J_0 N(0) \ln(T_F/T))$.

To calculate the scattering rate to third order in J_0 , we need simply therefore to replace J_0 in Eq. (8.23) by $J_0(1 - J_0 N(0) \ln(T_F/T))$. The scattering rate to next order is thus

$$\Gamma = \Gamma^0 \left(1 - 2J_0 N(0) \ln \frac{T_F}{T} + \dots \right). \quad (8.42)$$

Note that the temperature-dependent correction to the scattering rate is independent of the total spin of the impurity. The logarithmic behavior in the scattering rate gives rise to the logarithmic rise in the resistivity. Resistance to electrical flow in a metal arises from electron scattering processes taking momentum from the electrons; the resistivity is inversely proportional to the time between scattering events. The transport equation that captures this result is the Boltzmann equation, as we discuss in Chapter 10. As we show there, the contribution from phonon scattering scales as T^5 . Note that, although the Kondo contribution to the scattering time is positive, it *decreases* with increasing temperature. Combining the electron–phonon scattering result with the logarithmic Kondo contribution, we see that the resistivity has the form

$$\rho(T) = aT^5 - bc \ln \frac{T}{T_F}, \quad (8.43)$$

where a and b are positive constants. The result (8.43) has a minimum at temperature

$$T_{\min} = \left(\frac{cb}{5a} \right)^{1/5}. \quad (8.44)$$

This expression for the temperature at the minimum, which depends only weakly on the concentration of magnetic impurities, is in excellent agreement with numerous Kondo alloys, most notably Fe in Au (K1964).

Although the scattering rate looks as if it can grow indefinitely as the temperature is lowered, the scattering amplitude is limited by unitarity. We will see this limit once we develop a little more technology to deal with the scattering amplitudes.

8.4 Electron–impurity scattering amplitudes

Since the overall spin of the impurity has little effect on the temperature-dependent terms in the scattering amplitude, we assume from here on that the impurity has spin-1/2. Since the interaction Hamiltonian is rotationally invariant, and thus conserves total angular momentum, it is often most convenient to analyze the scattering in terms of the total spin of the electron plus impurity. Two spin-1/2 particles can have total spin $S = \hbar$ or 0, i.e., be in a spin triplet or spin singlet. The spin eigenstates are:

$$\begin{aligned} |S = 1, M_S = 1\rangle &= |e_\uparrow d_\uparrow\rangle, \\ |S = 1, M_S = 0\rangle &= \frac{1}{\sqrt{2}} (|e_\uparrow d_\downarrow\rangle + |e_\downarrow d_\uparrow\rangle), \\ |S = 1, M_S = -1\rangle &= |e_\downarrow d_\downarrow\rangle, \\ |S = 0, M_S = 0\rangle &= \frac{1}{\sqrt{2}} (|e_\uparrow d_\downarrow\rangle - |e_\downarrow d_\uparrow\rangle). \end{aligned} \quad (8.45)$$

The two $S = 0$ terms can be written equivalently as

$$\begin{aligned} |e_\uparrow d_\downarrow\rangle &= \frac{1}{\sqrt{2}} (|S = 1, M_S = 0\rangle + |S = 0, M_S = 0\rangle), \\ |e_\downarrow d_\uparrow\rangle &= \frac{1}{\sqrt{2}} (|S = 1, M_S = 0\rangle - |S = 0, M_S = 0\rangle). \end{aligned} \quad (8.46)$$

Rotational invariance (for two spin-1/2 particles) has the lovely consequence that all scatterings are described by just two amplitudes, T_0 , the spin-singlet amplitude, and T_1 , the spin-triplet amplitude. The scattering amplitude from electron–impurity state $|a\rangle$ to $|b\rangle$ is

$$T_{a \rightarrow b} = \sum_{S, M_S} \langle a | S, M_S \rangle \langle S, M_S | b \rangle T_S. \quad (8.47)$$

The scattering $(\mathbf{k}\sigma) + (d\sigma) \rightarrow (\mathbf{k}'\sigma) + (d\sigma)$ is purely spin triplet, and thus

$$T_{(\mathbf{k}\sigma)+(d\sigma) \rightarrow (\mathbf{k}'\sigma)+(d\sigma)} = T_1. \quad (8.48)$$

On the other hand, the scattering $(\mathbf{k}\sigma) + (d - \sigma) \rightarrow (\mathbf{k}'\sigma) + (d - \sigma)$ proceeds through the singlet and triplet channels with equal weights. From Eqs. (8.46) and (8.47),

$$T_{(\mathbf{k}\sigma)+(d-\sigma) \rightarrow (\mathbf{k}'\sigma)+(d-\sigma)} = \frac{1}{2}(T_1 + T_0). \quad (8.49)$$

Similarly,

$$T_{(\mathbf{k}\sigma)+(d-\sigma) \rightarrow (\mathbf{k}'-\sigma)+(d\sigma)} = \frac{1}{2}(T_1 - T_0). \quad (8.50)$$

The minus sign on the right results from the opposite signs of the singlet state in the two parts of Eq. (8.46).

The results of the previous subsection for the scattering amplitudes to second order are (Eq. (8.16) added to Eq (8.34))

$$T(\mathbf{k} \uparrow \rightarrow \mathbf{k}' \uparrow; m_s) = -\frac{J_0}{2V} \left(m_s - \frac{J_0}{8} [3(\alpha + \gamma) - 4m_s(\alpha - \gamma)] \right) \quad (8.51)$$

and

$$T(\mathbf{k} \uparrow \rightarrow \mathbf{k}' \downarrow; m_s) = -\frac{J_0}{2V} \sqrt{s(s+1) - m_s(m_s+1)} \left(1 + \frac{J_0}{2} (\alpha - \gamma) \right), \quad (8.52)$$

which results from combining Eqs. (8.19) and (8.40). Thus, from Eqs. (8.49) and (8.50), we derive the results for the singlet

$$T_0 = \frac{3J_0}{4V} \left[1 + \frac{3J_0}{4} \left(\alpha - \frac{1}{3}\gamma \right) \right] \quad (8.53)$$

and triplet

$$T_1 = -\frac{J_0}{4V} \left[1 - \frac{J_0}{4} (\alpha + 5\gamma) \right] \quad (8.54)$$

amplitudes to second order. In deriving these amplitudes, we set $m_s = -1/2$.

The lowest-order amplitudes in these results can be readily understood by rewriting the interaction term, $-J_0/\hbar^2 V \mathbf{S}_e \cdot \mathbf{S}_d$, in terms of the total spin of the electron and the impurity. Using the identity for spin-1/2 particles,

$$\mathbf{S}^2 = (\mathbf{S}_e + \mathbf{S}_d)^2 = \frac{3\hbar^2}{2} + 2\mathbf{S}_e \cdot \mathbf{S}_d, \quad (8.55)$$

we see immediately that

$$\mathbf{S}_e \cdot \mathbf{S}_d = -\frac{3\hbar^2}{4} + \frac{1}{2}\mathbf{S}^2. \quad (8.56)$$

In a singlet state, $\mathbf{S}_e \cdot \mathbf{S}_d = -3\hbar^2/4$, and thus the bare interaction is $3J_0/4V$, as in Eq. (8.53); similarly, in a triplet state, $\mathbf{S}_e \cdot \mathbf{S}_d = \hbar^2/4$, so the bare interaction is $-J_0/4V$, as in Eq. (8.54).

At this stage, we can replace the bare interactions in the second-order terms in Eqs. (8.54) and (8.53) by the corresponding full scattering amplitudes, to derive the T -matrix equations,

$$\begin{aligned} T_1 &= -\frac{J_0}{4V} [1 + VT_1(\alpha + 5\gamma)], \\ T_0 &= \frac{3J_0}{4V} \left[1 + VT_0 \left(\alpha - \frac{1}{3}\gamma \right) \right], \end{aligned} \quad (8.57)$$

which give the total spin scattering amplitudes to all orders in the coupling. These equations are algebraic; we write their solutions in the form

$$T_1 = -\frac{J_0/4V}{1 + J_0\gamma + (J_0/4)(\alpha + \gamma)} \quad (8.58)$$

and

$$T_0 = \frac{3J_0/4V}{1 + J_0\gamma - (3J_0/4)(\alpha + \gamma)}. \quad (8.59)$$

We can now see how unitarity limits the total scattering amplitude, and prevents the logarithmic result, Eq. (8.39), from growing indefinitely. Let us consider \mathbf{k} just outside the Fermi surface. We use Dirac's identity to do integrals with a small imaginary part in the denominator,

$$\frac{1}{x + i\eta} = P \frac{1}{x} - i\pi\delta(x), \quad (8.60)$$

where P indicates that the principal value of the integral must be taken. Then

$$\alpha = P \int \frac{d\mathbf{q}}{(2\pi)^3} \frac{1 - f_{\mathbf{q}}}{\epsilon_{\mathbf{k}} - \epsilon_{\mathbf{q}}} - i\pi N(0). \quad (8.61)$$

On the other hand, since the denominator of the integral for γ does not vanish for \mathbf{k} outside the Fermi surface, γ has no imaginary part. By dropping the real part of the denominators in Eqs. (8.58) and (8.59), we readily derive the unitarity bound,

$$|T_S| \leq \frac{1}{\pi N(0)V}, \quad (8.62)$$

where $S = 0, 1$. Using the techniques of elementary scattering theory, one can write the singlet and triplet scattering amplitudes, in the case of isotropic scattering, in terms of the s -wave phase shifts δ_S as

$$T_S = -\frac{1}{\pi N(0)V} e^{i\delta_S} \sin \delta_S. \quad (8.63)$$

From this form we see that the unitary bound is realized for $\delta_S = (n + 1/2)\pi$, i.e., a scattering resonance.

The important terms in the Kondo problem are the temperature-dependent ones in the denominators of the scattering amplitudes, Eqs. (8.58) and (8.59). If we define the effective

coupling J_{eff} by

$$J_{\text{eff}} = \frac{J_0}{1 + J_0\gamma} \approx \frac{J_0}{1 + J_0N(0) \ln(T_F/T)}, \quad (8.64)$$

we see that the singlet and triplet amplitudes have the structure

$$T_0 = \frac{3J_{\text{eff}}/4V}{1 - (3J_{\text{eff}}/4)(\alpha + \gamma)} \approx \frac{3J_0/4V}{1 + J_0N(0) \ln(T_F/T)}, \quad (8.65)$$

and

$$T_1 = -\frac{J_{\text{eff}}/4V}{1 + (J_{\text{eff}}/4)(\alpha + \gamma)} \approx -\frac{J_0/4V}{1 + J_0N(0) \ln(T_F/T)}. \quad (8.66)$$

The amplitudes are those for lowest-order scattering, with the effective coupling J_{eff} replacing the bare coupling J_0 . Comparing with Eq. (8.63), we see that the singlet and triplet phase shifts are given by

$$\tan \delta_0 = -\frac{3\pi}{4} J_{\text{eff}} N(0), \quad \tan \delta_1 = \frac{\pi}{4} J_{\text{eff}} N(0). \quad (8.67)$$

Since $J_{\text{eff}} < 0$, the singlet phase shift is positive, and hence this channel is attractive, with a tendency towards formation of a bound state. The triplet phase shift is negative, indicating repulsion and no bound state formation. With increasing magnitude of J_{eff} , the singlet phase shift approaches the resonance point $\pi/2$.

This value of the singlet phase shift is particularly illuminating. From the simplified version of Friedel's sum-rule we derived in Chapter 7, Eq. (7.112), a value of $\pi/2$ for the singlet phase shift at the Fermi level implies that the occupancy on the impurity is 1/2. To put the Kondo singlet state in the context of the Anderson impurity, we focus on an impurity ion with ionic charge Z . Hence, Z is the total charge that must be screened by the conduction electrons. If the impurity is a transition metal ion with d -orbital symmetry, the condition for complete screening (the charge neutrality condition) is

$$Z = 5(\langle n_{d\sigma} \rangle + \langle n_{d\bar{\sigma}} \rangle) = \frac{5}{\pi} (\delta_{d\sigma} + \delta_{d\bar{\sigma}}). \quad (8.68)$$

In the absence of a magnetic field, the magnetic moment of the impurity spin can be oriented parallel or antiparallel to the conduction electron spin. Hence, there is no uniquely defined phase shift for the conduction electron scattering. We are free to choose $\delta_{d\sigma}$ or $\delta_{d\bar{\sigma}}$ but with equal probability. At $T = 0$, however, a well-defined single phase shift exists, $\delta = (\delta_{d\sigma} + \delta_{d\bar{\sigma}})/2$. Consequently, we can rewrite the charge neutrality condition as

$$\delta = \frac{\pi Z}{10}. \quad (8.69)$$

The resultant value for the T -matrix at the Fermi level,

$$T_{kk}(\epsilon = 0^+) = \frac{5}{\pi N(0)V} \left[\exp\left(i\frac{\pi Z}{10}\right) \sin\left(\frac{\pi Z}{10}\right) \right], \quad (8.70)$$

follows directly from Eq. (7.108). Taking the imaginary part of this expression results in the density of states,

$$\rho_{d\sigma}(0) = \frac{1}{\pi\Delta} \sin^2\left(\frac{\pi Z}{10}\right), \quad (8.71)$$

at the impurity (see Eq. (7.107)) at the Fermi level. This value of the density of states arises from the charge neutrality condition. Comparing this value with that arising from the Hartree–Fock approximation (Eq. (7.118)),

$$\rho_{d\sigma}^{\text{HF}}(0) = \frac{1}{\pi\Delta} \frac{1}{1 + [(\epsilon_d + Un_c)/\Delta]^2}, \quad (8.72)$$

we find complete disagreement. In fact, the density of states at the Fermi level arising from the charge-neutrality condition exceeds the Hartree–Fock value. To illustrate, for $Z = 5$, the charge neutrality condition leads to an impurity density of states at the Fermi level of $1/(\pi\Delta)$. In the Hartree–Fock approximation, the impurity density of states is always less than $1/(\pi\Delta)$ except at the impurity energy levels where it identically acquires this value. The discrepancy between Eqs. (8.71) and (8.72) arises because spin-flip scattering is absent in the Hartree–Fock procedure, and hence it is incapable of describing the formation of the singlet ground state at $T = 0$.

As Grüner and Zawadowski (GZ1972) have argued, there are two ways to resolve the large value of the density of states at the Fermi level arising from the charge neutrality condition. Either a single maximum occurs at the Fermi level, or at low temperatures an additional peak appears (superimposed on the Hartree–Fock density of states) as a result of the correlation effects arising from multiple scattering events. The first option would require a reorganization of the impurity levels on an energy scale of the order of the on-site Coulomb repulsion, U . As U is typically of order 1 eV, such a reorganization would occur at a temperature comparable to $10^4 K$. This option can be ruled out on experimental grounds; no reorganization of the impurity density of states occurs at such energy scales. The only option remaining is that a modification occurs at an energy scale on the order of T_k . Consequently, superimposed on the Hartree–Fock density of states is an additional resonance peak whose width must be of the order of T_k . As a result, the Kondo resonance causes a modification of the density of states at temperatures distinct from the Hartree–Fock energy scales. The precise form of the density of states in response to the formation of the Kondo resonance is shown in Fig. 8.3. The pinning of the Kondo resonance at the Fermi energy arises entirely from the fact that spin-flip scattering costs zero energy. It is for this reason that the Kondo resonance peak is sometimes called the zero-bias anomaly.

Extensive calculations (L1981) reveal that the Kondo resonance grows logarithmically down to the Kondo temperature. On average, for a spin-1/2 impurity, the Kondo resonance is occupied by a single electron of opposite spin to account for the spin singlet state at the impurity. However, the multiple powers of the density of states which appear in the T -matrices indicate that all the electrons within T_k of the Fermi energy contribute to the resonance.

The effective coupling J_{eff} sums the leading logarithms in all orders (A1957). Note that J_{eff} diverges at the temperature

$$T_k = T_F e^{1/N(0)J_0}. \quad (8.73)$$

As a consequence, the present treatment is valid only above T_k . To investigate the physical consequences of this singularity, we look first at a simple variational approach to the ground state of the Kondo problem.

8.5 Kondo temperature

In the presence of an antiferromagnetic interaction, a bound singlet state forms between the impurity spin and electrons in the conduction band. The simplest model of this phenomena, first suggested by Yosida (Y1966), is to assume that only a single conduction electron forms the total spin singlet state on the impurity, with the other electrons remaining in the Fermi sea, and to retain only the interactions between the impurity and this conduction electron. The role of the Fermi sea in the model is only to block states below the chemical potential to this electron.

A singlet, $\mathbf{S} = 0$, is given by the linear combination

$$|\mathbf{S} = 0\rangle = \frac{1}{\sqrt{2}} (|e_\uparrow, d_\downarrow\rangle - |e_\downarrow, d_\uparrow\rangle). \quad (8.74)$$

The interaction term between the spins is proportional to $\mathbf{S}_e \cdot \mathbf{S}_d$.

In a singlet state of the conduction electron and impurity spins, $\mathbf{S}_e \cdot \mathbf{S}_d = -3\hbar^2/4$, and the term in the interaction $\Psi_{\mathbf{k}}^\dagger \mathbf{S} \Psi_{\mathbf{k}} \cdot \Psi_d^\dagger \mathbf{S} \Psi_d$ simplifies to $-(3/4)\hbar^2 \Psi_{\mathbf{k}}^\dagger \Psi_{\mathbf{k}} \Psi_d^\dagger \Psi_d$; for a single impurity $\Psi_d^\dagger \Psi_d = 1$. The effective Hamiltonian for this problem is thus

$$H_K^{\text{eff}} = \sum_{\sigma} \left(\sum_{\mathbf{k}} \epsilon_{\mathbf{k}} a_{\mathbf{k}\sigma}^\dagger a_{\mathbf{k}\sigma} + \sum_{\mathbf{k}, \mathbf{k}'} \frac{3}{4} J_{\mathbf{k}\mathbf{k}'} a_{\mathbf{k}'\sigma}^\dagger a_{\mathbf{k}\sigma} \right), \quad (8.75)$$

where \mathbf{k} and \mathbf{k}' are restricted to be outside the Fermi sea. As a consequence of this restriction, the effective Hamiltonian does not contain the constant energy of the electrons in the Fermi sea, a term with no effect here.

To construct the full state of the system, we note that the operator

$$b_{\mathbf{k}}^{\dagger} = \frac{1}{\sqrt{2}}(a_{\mathbf{k}\uparrow}^{\dagger}\Psi_{d\downarrow}^{\dagger} - a_{\mathbf{k}\downarrow}^{\dagger}\Psi_{d\uparrow}^{\dagger}) \quad (8.76)$$

creates a spin-singlet state out of a conduction electron with momentum \mathbf{k} ($k > k_F$) and the impurity spin. The wavefunction of the singlet state plus the Fermi sea has the general form

$$|\Phi\rangle = \sum_{k>k_F} \alpha_{\mathbf{k}} b_{\mathbf{k}}^{\dagger} |F\rangle, \quad (8.77)$$

where $\alpha_{\mathbf{k}}$ is the amplitude for the conduction electron in the singlet state to have momentum \mathbf{k} , and the Fermi sea is given by $|F\rangle = \prod_{\mathbf{k} < k_F} a_{\mathbf{k}\uparrow}^{\dagger} a_{\mathbf{k}\downarrow}^{\dagger} |0\rangle$, where $|0\rangle$ is the vacuum. The amplitude for forming a singlet state is given by the overlap of the filled Fermi sea with the state $b_{\mathbf{k}}|\Phi\rangle$,

$$\langle F | b_{\mathbf{k}} | \Phi \rangle = \sum_{k'>k_F} \alpha_{\mathbf{k}'} \langle F | b_{\mathbf{k}} b_{\mathbf{k}'}^{\dagger} | F \rangle = \alpha_{\mathbf{k}}, \quad (8.78)$$

where $k > k_F$. The state $|\Phi\rangle$, while approximate, captures key features of the interaction of the spin moment with the conduction electrons.

To determine the energy eigenstates of this system, we construct the eigenvalue equation $H_K^{\text{eff}}|\Phi\rangle = E|\Phi\rangle$. From Eqs. (8.75) and (8.77) we have

$$H_K^{\text{eff}}|\Phi\rangle = \sum_{\mathbf{k}} \epsilon_{\mathbf{k}} \alpha_{\mathbf{k}} b_{\mathbf{k}}^{\dagger} |F\rangle + \sum_{\mathbf{k}, \mathbf{k}'} \frac{3}{4} J_{\mathbf{k}\mathbf{k}'} \alpha_{\mathbf{k}} b_{\mathbf{k}'}^{\dagger} |F\rangle = E|\Phi\rangle. \quad (8.79)$$

Using Eq. (8.78) we then obtain the eigenvalue equation

$$\epsilon_{\mathbf{k}} \alpha_{\mathbf{k}} + \frac{3}{4} \sum_{k'>k_F} J_{\mathbf{k}\mathbf{k}'} \alpha_{\mathbf{k}'} = E \alpha_{\mathbf{k}}, \quad (8.80)$$

where $k > k_F$.

As in the previous subsection, we write $J_{\mathbf{k}\mathbf{k}'} \approx J_0/V$. The eigenvalue equation now becomes separable. We find

$$\alpha_{\mathbf{k}} = \frac{3J_0}{4V} \frac{1}{E - \epsilon_{\mathbf{k}}} \sum_{\mathbf{k}'} \alpha_{\mathbf{k}'}. \quad (8.81)$$

We sum both sides of this expression over \mathbf{k} to obtain

$$1 = \frac{3J_0}{4V} \sum_{k>k_F} \frac{1}{E - \epsilon_{\mathbf{k}}}. \quad (8.82)$$

This type of equation is characteristic of the formation of a bound state. We will meet a similar equation in Chapter 12 in the Cooper pair problem, a prelude to understanding superconductivity. For $J_0 < 0$, the equation must admit a solution with $E < \epsilon_F$. To solve for E , we convert the sum to an integral,

$$\begin{aligned} 1 &= \frac{3J_0N(0)}{4} \int_{\epsilon_F}^D \frac{1}{E - \epsilon_k} d\epsilon_k \\ &= \frac{3J_0N(0)}{4} \ln\left(\frac{E - \epsilon_F}{E - D}\right), \end{aligned} \quad (8.83)$$

assuming that the density of states is a constant, $N(0)$, in an energy interval, $\epsilon_F < \epsilon < D$, where D is the upper energy in the conduction band. Then the energy of the singlet state is

$$E \approx \epsilon_F - De^{4/3J_0N(0)}. \quad (8.84)$$

Because E is less than the Fermi energy, we interpret

$$E_b = De^{4/3J_0N(0)} \quad (8.85)$$

as the binding energy of the singlet state. As we see, in the presence of a weak antiferromagnetic interaction, the Fermi sea is unstable to the formation of a singlet state with a localized impurity.

The singlet state breaks up for temperatures $T \gtrsim E_b/k_B$. The Kondo temperature in this picture emerges as the temperature scale

$$T_k = \frac{D}{k_B} e^{4/3J_0N(0)}, \quad (8.86)$$

below which the singlet state is stable. Although this derivation of T_k is not exact, Eq. (8.86) provides an excellent approximation to the experimentally observed Kondo temperature. In general, the Kondo temperature is only a function of the density of states of the host metal and the exchange interaction with the metal ion. For Fe impurities in Cu, the Kondo temperature is 6 K, considerably smaller than the bandwidth.

We can in fact understand the Yosida result directly in terms of the singlet channel scattering amplitude, Eq. (8.59), derived in the previous subsection. The assumption that the only function of the electron sea is to block states below the Fermi surface is equivalent to neglecting the term γ in the denominator of (8.59). For E below the Fermi sea, α has no imaginary part, and we see that the scattering amplitude has a pole when

$$\frac{3J_0}{4}\alpha = 1, \quad (8.87)$$

which is precisely Yosida's equation (8.82).

Experimentally, the Kondo effect is observed only for an antiferromagnetic interaction. The analogous triplet trial wavefunction in the ferromagnetic case corresponding to

Eq. (8.77) also leads to a bound state. This unphysical result is an indication that the simple variational approach is insufficient to describe the true ground state of the Kondo model. A key piece of physics that is missing is the collective many-body quenching of the local moment by all the electrons within T_k of the Fermi surface. This quenching can be thought of as the formation of a cloud of electrons around the impurity which screens out the spin moment. The existence of the low energy scale, T_k , implies that an exponentially large length scale, $\xi_k = \hbar v_F/k_B T_k$, should describe the screening cloud. For Fe in Cu, ξ_k is on the order of 2000 Å. The first correct attempt to include the many-body effects that lead to the ground state of the Kondo model is the “Poor Man’s scaling” approach of Anderson, to which we now turn.

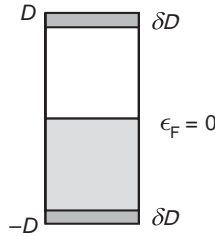
8.6 Poor Man’s scaling

The behavior of a many-body system at long wavelengths depends on interactions of the microscopic degrees of freedom on all length scales. In such a system the short-wavelength degrees of freedom determine the effective macroscopic parameters of the long-wavelength theory. A familiar example is hydrodynamics, which describes fluids on length and time scales that are large compared with particle mean free paths and scattering times, and in which only effective parameters such as the sound velocity and viscosities enter; these parameters are determined by the microscopic physics. The goal of a scaling analysis is to formulate a series of descriptions of a system valid on longer and longer wavelength scales with more and more of the higher momentum scales integrated over. Once integrated over, the degrees of freedom at higher momentum scales no longer appear explicitly in the problem. Thinning the degrees of freedom results in a simplified effective model from which the low-energy physics can be extracted. In this way, one formulates recursive equations for the physically relevant coupling constants as various degrees of freedom are integrated out.

The simplest scaling analysis of the Kondo problem successively eliminates high-energy excitations as intermediate states in perturbation theory. At each level, the spin–spin coupling constant, $J_{\mathbf{k},\mathbf{k}'}$, is modified. To see how this method works, we work only to second-order perturbation theory in the effective spin–spin coupling, whence the name “Poor Man’s scaling”. While higher-order terms in the perturbation theory do contribute to scaling, they do not lead to qualitatively new features (SZ1974).

Before presenting Anderson’s scaling analysis of the isotropic Kondo model, let us first quote its key result. As the temperature is varied, the number of states explored by the electrons increases, and the effective coupling, which we denote in this subsection as J , obeys the equation

$$\frac{dJ}{d \ln(T_F/T)} = -J^2 N(0), \quad (8.88)$$

**Fig. 8.7**

The particle and hole states to be eliminated in the “Poor Man’s” scaling approach. The width of states to be removed is δD .

with solution Eq. (8.64). This expression correctly predicts the essential physics of the Kondo problem, that smaller and smaller energy excitations (dominant at low temperatures) lead, through a bootstrapping process, to a divergence of the exchange interaction and the binding of an antiparallel electron at the local moment (A1978). Although Eq. (8.88) does not remove the divergence found earlier by Kondo, it does serve to illuminate how the exchange coupling increases in magnitude. A loose analogy can be made here between the process by which this increase occurs to the confinement of color degrees of freedom in quark physics (A1978). This analogy is loose because we do not know precisely how the latter obtains.

There are many ways to develop the scaling ideas, some simple and some complicated. We will present a streamlined version of the simple approach (H1993). We consider an electronic band with $-D < \epsilon_{\mathbf{k}} < D$. As illustrated in Fig. 8.7, we proceed by eliminating a narrow band of particle and hole states from the lower and upper regions of the band, respectively. The width of the states to be eliminated is δD . The basic idea will be to consider the scattering processes that enter the second-order transition amplitude and to determine how they change when the bandwidth is decreased by an infinitesimal amount, δD . Our hope is that as the bandwidth is reduced, we will be able to find a set of equations that relate the new exchange couplings to the original ones.

For simplicity, we will treat an $S = 1/2$ impurity but, for the sake of generality, we consider an anisotropic spin-flip Hamiltonian

$$H' = -\frac{1}{2\hbar V} \sum_{\mathbf{k}', \mathbf{k}'', \sigma} \left[J_z S_d^z (a_{\mathbf{k}'\uparrow}^\dagger a_{\mathbf{k}''\uparrow} - a_{\mathbf{k}'\downarrow}^\dagger a_{\mathbf{k}''\downarrow}) + J_+ S_d^+ a_{\mathbf{k}'\downarrow}^\dagger a_{\mathbf{k}''\uparrow} + J_- S_d^- a_{\mathbf{k}'\uparrow}^\dagger a_{\mathbf{k}''\downarrow} \right],$$

in which the spin-flip (J_{\pm}) and longitudinal (J_z) parts have different interaction strengths. Our goal is to simplify the second-order perturbative terms and show that they lead to a renormalization of the bare values of J_z and J_{\pm} . We consider first the two spin-flip events shown in Fig. 8.8. Because a two-spin-flip process leaves the impurity spin unchanged, we anticipate that the two-spin-flip terms will lead to a renormalization of the longitudinal coupling, J_z . The precise form of the correction to J_z can be obtained by performing the scaling analysis on each of the two-spin-flip diagrams. Consider the first diagram:

$$J_+ J_- \sum_{\mathbf{q}} \frac{S_d^-}{2\hbar V} a_{\mathbf{k}'\uparrow}^\dagger a_{\mathbf{q}\downarrow} (E - \hat{H}_0)^{-1} \sum_{\mathbf{q}'} \frac{S_d^+}{2\hbar V} a_{\mathbf{q}'\downarrow}^\dagger a_{\mathbf{k}\uparrow}. \quad (8.89)$$

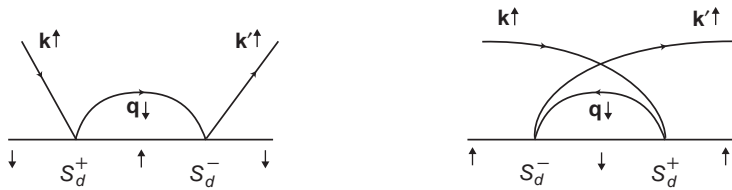


Fig. 8.8 Second-order two-spin-flip diagrams in which the intermediate state involves either a particle or a hole. The solid straight line indicates the spin of the impurity and the curved lines the electron.

To implement the scaling procedure, we restrict the sum on \mathbf{q}' to the states within δD from the top of the band. These states are created by $a_{\mathbf{q}'\downarrow}^\dagger$. Because the band-edge states are originally unoccupied, we must set $a_{\mathbf{q}} a_{\mathbf{q}'}^\dagger = \delta_{\mathbf{q},\mathbf{q}'}$.

In simplifying Eq. (8.89), we are not free to move the right-most creation and annihilation operators through the operator $1/(E - \hat{H}_0)$, because they do not commute with \hat{H}_0 . For any operator \hat{A} such that $[\hat{H}_0, \hat{A}] = b\hat{A}$, where b is a c-number, $\hat{H}_0^n \hat{A} = \hat{A}(b + \hat{H}_0)^n$. As a consequence,

$$\frac{1}{E - \hat{H}_0} \hat{A} = \frac{\hat{A}}{E} \sum_{n=0}^{\infty} \frac{(\hat{H}_0 + b)^n}{E^n} \quad (8.90)$$

$$= \hat{A} \frac{1}{E - b - \hat{H}_0}. \quad (8.91)$$

Using the fact that $[\hat{H}_0, a_{\mathbf{q}'\downarrow}^\dagger a_{\mathbf{k}\uparrow}] = a_{\mathbf{q}'\downarrow}^\dagger a_{\mathbf{k}\uparrow} (\epsilon_{\mathbf{q}'} - \epsilon_{\mathbf{k}})$, we simplify the matrix element in Eq. (8.89) to

$$J_+ J_- N(0) |\delta D| \frac{S_d^- S_d^+}{4V\hbar^2} a_{\mathbf{k}'\uparrow}^\dagger a_{\mathbf{k}\uparrow} (E - \epsilon_{\mathbf{q}} + \epsilon_{\mathbf{k}} - \hat{H}_0)^{-1}. \quad (8.92)$$

Because of the $a_{\mathbf{k}'\uparrow}^\dagger a_{\mathbf{k}\uparrow}$ dependence, we see clearly that the two-spin-flip term changes the value of the bare transverse exchange interaction. To extract the exact coefficient, we use $S_d^- S_d^+ = \hbar^2/2 - \hbar S_d^z$ and set $\epsilon_{\mathbf{q}} = D$. Further, if we measure E from the bottom of the band, then we can ignore the \hat{H}_0 dependence in the denominator of Eq. (8.92). The matrix element simplifies to

$$J_+ J_- N(0) \frac{|\delta D|}{4\hbar V} \left(\frac{\hbar}{2} - S_d^z \right) a_{\mathbf{k}'\uparrow}^\dagger a_{\mathbf{k}\uparrow} (E - D + \epsilon_{\mathbf{k}})^{-1}. \quad (8.93)$$

We can now evaluate the second diagram in Fig. 8.8 in the same way. Here, the intermediate states are particle states; hence, we set $\epsilon_{\mathbf{q}} = -D$ and obtain

$$J_+ J_- N(0) \frac{|\delta D|}{4\hbar V} \left(\frac{\hbar}{2} + S_d^z \right) a_{\mathbf{k}\uparrow} a_{\mathbf{k}'\uparrow}^\dagger (E - D - \epsilon_{\mathbf{k}'})^{-1}. \quad (8.94)$$

In deriving this result, we used the relationship $S_d^+ S_d^- = \hbar^2/2 + \hbar S_d^z$.

The remaining scaling equations involving two spin-flips we obtain by including the contribution from $\mathbf{k} \downarrow$ and $\mathbf{k}' \downarrow$. Scattering between down spin states will generate matrix elements proportional to $a_{\mathbf{k}\downarrow} a_{\mathbf{k}'\downarrow}^\dagger$. This term will contribute to the $m_s = -1$ spin component

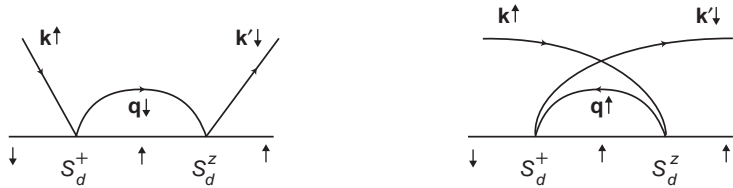


Fig. 8.9 Second-order one-spin-flip diagrams in which the intermediate state involves either a particle or a hole. The solid straight line indicates the spin of the impurity and the curved lines the electron.

of the S_z operator. We now define a new longitudinal interaction $J_z \rightarrow J_z + \delta J_z$. Noting that the coefficient of the bare interaction in Eq. (8.89) is $1/2\hbar V$, we find that Eqs. (8.93) and (8.94), combined with the down-spin equations, lead to

$$\delta J_z = \frac{1}{2} J_+ J_- N(0) |\delta D| \left[\frac{1}{E - D + \epsilon_{\mathbf{k}}} + \frac{1}{E - D - \epsilon_{\mathbf{k}'}} \right] \quad (8.95)$$

as the correction to J_z . The renormalization of J_z is energy dependent. Consider now excitations low in energy relative to D . We also evaluate $\epsilon_{\mathbf{k}}$ and $\epsilon_{\mathbf{k}'}$ at the Fermi level, $\epsilon_F = 0$. The J_z scaling equation simplifies to

$$\frac{dJ_z}{d \ln D} = N(0) J_{\pm}^2, \quad (8.96)$$

where we have taken δD to be negative and set $J_+ = J_- = J_{\pm}$.

Now consider the single-spin-flip terms shown in Fig. 8.9. The first diagram is of the form

$$-J_z J_+ \sum_{\mathbf{q}} \frac{S_d^z}{2\hbar V} a_{\mathbf{k}'\downarrow}^\dagger a_{\mathbf{q}\downarrow} (E - \hat{H}_0)^{-1} \sum_{\mathbf{q}'} \frac{S_d^+}{2\hbar V} a_{\mathbf{q}'\downarrow}^\dagger a_{\mathbf{k}'\uparrow}. \quad (8.97)$$

The minus sign in front of this equation arises from the minus sign that accompanies the down-spin component of S_d^z . Using the same techniques as in the two-spin-flip case, we reduce this matrix element to

$$\frac{-J_z J_+ N(0) |\delta D| S_d^+ a_{\mathbf{k}'\downarrow}^\dagger a_{\mathbf{k}'\uparrow}}{8\hbar V (E - D + \epsilon_{\mathbf{k}})}, \quad (8.98)$$

where we have used the fact that $S_d^z S_d^+ = \hbar S_d^+/2$. Hence, the renormalization of the spin-flip interaction involves the longitudinal component of J . Analogously, the other diagram in Fig. 8.9 has a value of

$$\frac{J_z J_+ N(0) |\delta D| S_d^+ a_{\mathbf{k}'\uparrow}^\dagger a_{\mathbf{k}'\downarrow}}{8\hbar V (E - D - \epsilon_{\mathbf{k}'})}. \quad (8.99)$$

Additional contributions of this form can be obtained by interchanging the order of S_d^z and S_d^+ . In this case, the identity $S_d^+ S_d^z = -\hbar S_d^+/2$ should be used. The contribution here will be identical to that in Eqs. (8.98) and (8.99).

Similarly, we combine the single-spin-flip results with those for scattering of a spin-down electron. Defining a new transverse interaction $J_\pm/2 \rightarrow (J_\pm + \delta J_\pm)/2$ and using the results of Eqs. (8.98) and (8.99) produces the scaling equation

$$\delta J_\pm = \frac{1}{2} J_\pm J_z N(0) |\delta D| \left[\frac{1}{E - D + \epsilon_{\mathbf{k}}} + \frac{1}{E - D - \epsilon_{\mathbf{k}'}} \right] \quad (8.100)$$

for the transverse components of the exchange interaction. Here again, the scaling of the transverse coupling constant is energy dependent. As in the longitudinal case, we consider excitations low in energy relative to D and evaluate $\epsilon_{\mathbf{k}}$ and $\epsilon_{\mathbf{k}'}$ at the Fermi level $\epsilon_F = 0$. The scaling equation simplifies to

$$\frac{dJ_\pm}{d \ln D} = N(0) J_z J_\pm. \quad (8.101)$$

Taking the ratio of Eqs. (8.96) and (8.101) and integrating, we see that the solutions are a family of hyperbolæ determined by

$$J_z^2 - J_\pm^2 = \kappa, \quad (8.102)$$

where κ is a constant. To extract the physical consequences of these scaling equations, it is advantageous to substitute Eq. (8.102) into the scaling equation for J_\pm . For the ferromagnetic and antiferromagnetic cases, we find that

$$\frac{dJ_\pm}{d \ln D} = \begin{cases} -N(0) J_\pm \sqrt{\kappa + J_\pm^2}, & J_z > 0, \text{ ferromagnetic}, \\ N(0) J_\pm \sqrt{\kappa + J_\pm^2}, & J_z < 0, \text{ antiferromagnetic}. \end{cases} \quad (8.103)$$

The physical consequences of the scaling analysis are now clear. Because the right-hand side of Eq. (8.103) is negative for $J_z > 0$, the scaling equations dictate that $J_\pm \rightarrow 0$ in this case. As a result, in the ferromagnetic case, the transverse exchange coupling becomes weaker and weaker as the bandwidth is reduced. However, in the antiferromagnetic case, the right-hand side of Eq. (8.103) is positive and the scaling equations dictate that $|J_\pm| \rightarrow \infty$. This is the strong coupling regime in which the Kondo effect occurs. The exchange coupling grows in magnitude upon a reduction in the bandwidth. It is this bootstrapping of the exchange interaction to larger values as the bandwidth decreases that leads to the formation of a singlet state at a Kondo impurity.

The flow diagrams shown in Fig. 8.10 lay plain the scaling analysis. The hyperbola is the result for anisotropic coupling, with $|J_+| > |J_z|$, and the straight lines are in the limit of isotropic coupling, when the solution collapses to $|J_+|^2 = J_z^2$. The arrows point in the direction of decreasing D . The curves for positive J_z (for a ferromagnetic coupling) show

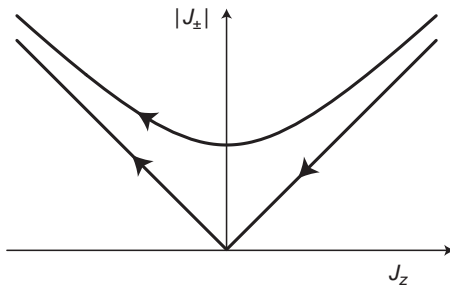


Fig. 8.10 Scaling trajectories for the Kondo model using Anderson's second-order perturbation theory argument. The hyperbola is for anisotropic coupling, and the straight lines for isotropic coupling. The region with $J_z > 0$ corresponds to ferromagnetic coupling, and the region where $J_z < 0$ to antiferromagnetic coupling.

that J_z and $|J_{\pm}|$ flow as D goes to zero, while the curves for negative J_z (for antiferromagnetic coupling) show that both couplings diverge as D goes to zero. Both the isotropic and anisotropic limits exhibit the same physics.

In the isotropic limit, $J_{\pm}(D) = J_z(D) = J(D)$, and the scaling equations reduce to the single equation

$$\frac{dJ}{d \ln D} = J^2 N(0), \quad (8.104)$$

which has the solution

$$J(D) = \frac{J(D_0)}{1 - J(D_0)N(0) \ln(D/D_0)}, \quad (8.105)$$

where D_0 is the initial bandwidth. Physically, we are interested in the situation that the effective bandwidth is in the range of states that are explored at finite temperature, of width $k_B T$ about the Fermi surface. Thus we may set, to logarithmic accuracy, $D/D_0 = k_B T/\epsilon_F = T/T_F$. With this identification, Eq. (8.105) is completely equivalent to Eq. (8.64).

Let us turn to extracting the Kondo temperature from the scaling equations. In doing so it is important to keep in mind that the Kondo temperature is a physical quantity and hence should not depend on the bandwidth D that we choose in our model description, i.e., T_k should be scale invariant,

$$D \frac{\partial T_k}{\partial D} = 0. \quad (8.106)$$

As a result, all physical quantities, such as the resistivity and the susceptibility, will depend on the ratio T/T_k (as well as having less singular behavior on T/T_F) but not on D .

If we define, in the isotropic case, the dimensionless coupling constant $g = N(0)J$, the scaling equation becomes

$$\frac{dg}{d \ln D} \equiv \beta(g) = g^2. \quad (8.107)$$

The logarithmic derivative of the coupling constant is generally referred to as the β -function after Gell-Mann and Low (GL1954); we will meet this concept again in Chapter 13 when we discuss localization. On dimensional grounds, the Kondo temperature must have the form $k_B T_k = Dy(g)$, where D sets the energy scale. To determine y , we substitute this form for T_k into the scale-invariant condition, Eq. (8.106), and obtain the linear differential equation

$$y(g) + \frac{\partial y}{\partial g} \frac{\partial g}{\partial \ln D} = 0. \quad (8.108)$$

The solution is simply

$$y(g) \sim e^{1/g}. \quad (8.109)$$

Hence, the Kondo temperature is given by $k_B T_k = D \exp(1/(N(0)J))$, consistent with the structure, (8.86), that we saw earlier. While it may seem contradictory that the Kondo temperature is independent of the bandwidth but an explicit factor D appears in front, it is not. The compensating dependence on D is in the coupling constant g such that Eq. (8.106) is satisfied.

The complete scaling structure of the Kondo problem was determined by Wilson in his key renormalization group analysis (W1975) of this problem. Wilson showed that as the energy scale goes to zero, the distribution of eigenstates becomes roughly equivalent to those of a system in which $J \rightarrow -\infty$. Hence, a system initially having a small exchange interaction crosses over smoothly, as the energy scale decreases, to one with a negatively diverging interaction. It is the divergence of the interaction that leads to the crossover to the singlet ground state in the Kondo problem. The divergence in the Wilson renormalization group approach occurs, however, at $T = 0$, not at a finite T_k . The divergence here at T_k is an artifact of the leading logarithm summation in perturbation theory.

This pretty much completes our story on the Kondo problem. However, more recent theoretical work includes: the Fermi liquid picture of Nozières (N1974) below T_k , the exact Bethe ansatz solution (TW1983; AFL1983) to the Anderson and Kondo models, and the conformal field-theoretic approach (AL1991; AZ1996). The inclusion of electron correlations (LT1992) leads to a Kondo temperature scaling algebraically with the exchange coupling as opposed to exponentially, as discussed here; the power is proportional to the strength of the interactions among the conduction electrons. In addition, a Kondo singlet state is predicted to be stable even for a ferromagnetic interaction (FN1994), a result established within the framework of the Luttinger liquid, which we discuss in Chapter 10.

Summary

The quenching of local moments in metals at low temperatures is the physics behind the Kondo problem. This effect arises from the many-body resonance that is pinned at the Fermi level. In this chapter we focused on extracting this picture from quite simple considerations. The Kondo temperature is a scale-invariant quantity given by $T_k = D \exp(1/g)$, where $g = N(0)J$ is the effective bare Kondo exchange interaction. Perturbatively, the Kondo temperature can be identified as the energy scale at which the second-order terms in the perturbation theory become of the order of the terms linear in J , a signature that perturbation theory is breaking down and higher-order terms are important as well. The resonance at the Fermi level is a true multiparticle effect; n th-order terms in perturbation theory contain the interactions of n electrons with the local moment. It is the summation of all such terms that creates the resonance.

Appendix to Chapter 8: the Schrieffer–Wolff transformation

In this appendix we present the complete derivation of the exchange interaction in the Kondo Hamiltonian from the Anderson Hamiltonian. Because the Anderson Hamiltonian contains empty as well as doubly occupied impurity states, a transformation that generates the Kondo Hamiltonian is equivalent to a diagonalization of the Anderson Hamiltonian in the subspace of the singly occupied impurity states. This diagonalization is carried out by the Schrieffer–Wolff transformation (SW1966).

We first separate the Anderson Hamiltonian into a zeroth-order part

$$H_0 = \sum_{\mathbf{k},\sigma} \epsilon_{\mathbf{k}} n_{\mathbf{k}\sigma} + \epsilon_d \sum_{\sigma} n_{d\sigma} + U n_{d\uparrow} n_{d\downarrow} \quad (8.110)$$

and a perturbed part

$$H_1 = \sum_{\mathbf{k}\sigma} V_{\mathbf{k}d} (a_{\mathbf{k}\sigma}^\dagger a_{d\sigma} + a_{d\sigma}^\dagger a_{\mathbf{k}\sigma}). \quad (8.111)$$

In this derivation, we will take $V_{\mathbf{k}d}$ to be real.

To proceed, we perform a canonical or similarity transformation, S , on the original Hamiltonian:

$$\begin{aligned} \tilde{H} &= e^S H e^{-S} \\ &= H + [S, H] + \frac{1}{2} [S, [S, H]] + \dots \end{aligned}$$

Note that since e^S is unitary, S must be antihermitian. If we choose S so as to cancel the linear dependence

$$H_1 + [S, H_0] = 0 \quad (8.112)$$

on the perturbation H_1 , the new Hamiltonian to lowest order becomes

$$\tilde{H} = H_0 + \frac{1}{2}[S, H_1], \quad (8.113)$$

and hence incorporates charge fluctuations to second order in $V_{\mathbf{k}d}$. The similarity transformation method is a general way of performing perturbative analyses once a small quantity has been identified.

The explicit form of S can be constructed by noting that because $[S, H_0] = -H_1$, the operator S must contain terms $\propto a_{\mathbf{k}\sigma}^\dagger a_{d\sigma}$; furthermore, its commutator with $U n_{d\uparrow} n_{d\downarrow}$ yields $\propto n_{d-\sigma} a_{\mathbf{k}\sigma}^\dagger a_{d\sigma}$. This suggests that we try a transformation of the form

$$S = \sum_{\mathbf{k}, \sigma} (A_{\mathbf{k}} + B_{\mathbf{k}} n_{d-\sigma}) a_{\mathbf{k}\sigma}^\dagger a_{d\sigma} - \text{h.c.}, \quad (8.114)$$

where $A_{\mathbf{k}}$ and $B_{\mathbf{k}}$ are c-numbers to be determined by Eq. (8.112).

Using the following commutators:

$$\begin{aligned} [n_{d\sigma}, a_{d\sigma'}] &= -\delta_{\sigma\sigma'} a_{d\sigma}, \\ [n_{d\sigma}, n_{d\sigma'}] &= 0, \\ [n_{d\sigma} n_{d-\sigma}, a_{d\sigma'}] &= -\delta_{\sigma\sigma'} n_{d-\sigma} a_{d\sigma} - \delta_{-\sigma\sigma'} n_{d\sigma} a_{d\sigma'}, \end{aligned} \quad (8.115)$$

together with the relation $[A, B^\dagger] = -[A, B]^\dagger$ provided $A = A^\dagger$, we straightforwardly evaluate the commutator of H_0 with S and find

$$\begin{aligned} [H_0, S] &= \sum_{\mathbf{k}, \sigma} \epsilon_{\mathbf{k}} (A_{\mathbf{k}} + B_{\mathbf{k}} n_{d-\sigma}) a_{\mathbf{k}\sigma}^\dagger a_{d\sigma} + \text{h.c.} + \sum_{\mathbf{k}, \sigma} \epsilon_d (-A_{\mathbf{k}} - B_{\mathbf{k}} n_{d-\sigma}) a_{\mathbf{k}\sigma}^\dagger a_{d\sigma} + \text{h.c.} \\ &\quad + U \sum_{\mathbf{k}, \sigma} (-A_{\mathbf{k}} n_{d-\sigma} - B_{\mathbf{k}} n_{d-\sigma}) a_{\mathbf{k}\sigma}^\dagger a_{d\sigma} + \text{h.c.} \\ &= \sum_{\mathbf{k}, \sigma} [(\epsilon_{\mathbf{k}} - \epsilon_d) A_{\mathbf{k}} + (\epsilon_{\mathbf{k}} - \epsilon_d - U) n_{d-\sigma} B_{\mathbf{k}} - A_{\mathbf{k}} U n_{d-\sigma}] a_{\mathbf{k}\sigma}^\dagger a_{d\sigma} + \text{h.c.}, \end{aligned} \quad (8.116)$$

where h.c. denotes the hermitian conjugate. In order to satisfy Eq. (8.112) we require that $(\epsilon_{\mathbf{k}} - \epsilon_d) A_{\mathbf{k}} = V_{\mathbf{k}d}$ and $(\epsilon_{\mathbf{k}} - \epsilon_d - U) B_{\mathbf{k}} - A_{\mathbf{k}} U = 0$, so that

$$A_{\mathbf{k}} = \frac{V_{\mathbf{k}d}}{\epsilon_{\mathbf{k}} - \epsilon_d}$$

and

$$B_{\mathbf{k}} = V_{\mathbf{k}d} \left[\frac{1}{\epsilon_{\mathbf{k}} - (\epsilon_d + U)} - \frac{1}{\epsilon_{\mathbf{k}} - \epsilon_d} \right].$$

Equation (8.114) coupled with the definitions of the constants $A_{\mathbf{k}}$ and $B_{\mathbf{k}}$ specifies the Schrieffer–Wolff transformation.

To find the new Hamiltonian, we need to evaluate the commutator $[S, H_1]$:

$$\begin{aligned} [S, H_1] = & \sum_{\mathbf{k}, \sigma, \mathbf{k}', \sigma'} \left\{ A_{\mathbf{k}} V_{\mathbf{k}'d} [\rho_{\mathbf{k}d\sigma}, (\rho_{\mathbf{k}'d\sigma'} + \rho_{\mathbf{k}'d\sigma'}^\dagger)] - B_{\mathbf{k}}^* V_{\mathbf{k}'d} [n_{d-\sigma} \rho_{\mathbf{k}d\sigma}^\dagger, (\rho_{\mathbf{k}'d\sigma'} + \rho_{\mathbf{k}'d\sigma'}^\dagger)] \right. \\ & \left. + B_{\mathbf{k}} V_{\mathbf{k}'d} [n_{d-\sigma} \rho_{\mathbf{k}d\sigma}, (\rho_{\mathbf{k}'d\sigma'} + \rho_{\mathbf{k}'d\sigma'}^\dagger)] - A_{\mathbf{k}}^* V_{\mathbf{k}'d} [\rho_{\mathbf{k}d\sigma}^\dagger, (\rho_{\mathbf{k}'d\sigma'} + \rho_{\mathbf{k}'d\sigma'}^\dagger)] \right\}, \end{aligned} \quad (8.117)$$

where we have simplified the notation by defining $\rho_{\mathbf{k}d\sigma} = a_{\mathbf{k}\sigma}^\dagger a_{\mathbf{k}\sigma}$. At this stage, the following commutators are useful:

$$\begin{aligned} [\rho_{\mathbf{k}d\sigma}, \rho_{\mathbf{k}'d\sigma'}] &= 0, \\ [\rho_{\mathbf{k}d\sigma}, \rho_{\mathbf{k}'d\sigma'}^\dagger] &= \delta_{\sigma\sigma'} [-\delta_{\mathbf{k}\mathbf{k}'} n_{d\sigma} + a_{\mathbf{k}\sigma}^\dagger a_{\mathbf{k}'\sigma}], \\ [n_{d-\sigma} \rho_{\mathbf{k}d\sigma}, \rho_{\mathbf{k}'d\sigma'}] &= -\delta_{\sigma'-\sigma} \rho_{\mathbf{k}d\sigma} \rho_{\mathbf{k}'d-\sigma}, \\ [n_{d-\sigma} \rho_{\mathbf{k}d\sigma}, \rho_{\mathbf{k}'d\sigma'}^\dagger] &= \delta_{-\sigma\sigma'} \rho_{\mathbf{k}d\sigma} \rho_{\mathbf{k}'d-\sigma}^\dagger + \delta_{\sigma\sigma'} (a_{\mathbf{k}\sigma}^\dagger a_{\mathbf{k}'\sigma} n_{d-\sigma} - \delta_{\mathbf{k}\mathbf{k}'} n_{d-\sigma} n_{d\sigma}). \end{aligned}$$

Substituting these relationships into (8.117), we find

$$\begin{aligned} [S, H_1] = & - \sum_{\mathbf{k}, \sigma} (A_{\mathbf{k}} V_{\mathbf{k}d} + B_{\mathbf{k}} V_{\mathbf{k}d} n_{d-\sigma}) n_{d\sigma} + \text{h.c.} + \sum_{\mathbf{k}, \mathbf{k}', \sigma} A_{\mathbf{k}} V_{\mathbf{k}'d} a_{\mathbf{k}\sigma}^\dagger a_{\mathbf{k}'\sigma} + \text{h.c.} \\ & - \sum_{\mathbf{k}, \mathbf{k}', \sigma} B_{\mathbf{k}} V_{\mathbf{k}'d} \rho_{\mathbf{k}\sigma} \rho_{\mathbf{k}'-\sigma} + \text{h.c.} + \sum_{\mathbf{k}, \mathbf{k}', \sigma} B_{\mathbf{k}} V_{\mathbf{k}'d} [a_{\mathbf{k}\sigma}^\dagger a_{\mathbf{k}'\sigma} n_{d-\sigma} + \rho_{\mathbf{k}\sigma} \rho_{\mathbf{k}'-\sigma}^\dagger] + \text{h.c.} \end{aligned} \quad (8.118)$$

Let us write the operators in the last term as

$$\begin{aligned} [a_{\mathbf{k}\sigma}^\dagger a_{\mathbf{k}'\sigma} n_{d-\sigma} + \rho_{\mathbf{k}d\sigma} \rho_{\mathbf{k}'d-\sigma}^\dagger] &= \frac{1}{2} (n_{d\sigma} + n_{d-\sigma}) a_{\mathbf{k}\sigma}^\dagger a_{\mathbf{k}'\sigma} \\ &\quad - \frac{1}{2} [(n_{d\sigma} - n_{d-\sigma}) a_{\mathbf{k}\sigma}^\dagger a_{\mathbf{k}'\sigma} - 2 \rho_{\mathbf{k}d\sigma} \rho_{\mathbf{k}'d-\sigma}^\dagger]. \end{aligned} \quad (8.119)$$

The second part of this term gives rise to the Kondo exchange interaction. To see how, we note that the product

$$\begin{aligned} \frac{4}{\hbar^2} (\Psi_{\mathbf{k}}^\dagger \mathbf{S} \Psi_{\mathbf{k}}) \cdot (\Psi_d^\dagger \mathbf{S} \Psi_d) &= (\Psi_{\mathbf{k}}^\dagger \sigma_z \Psi_{\mathbf{k}}) \cdot (\Psi_d^\dagger \sigma_z \Psi_d) + 2(\Psi_{\mathbf{k}}^\dagger \sigma^+ \Psi_{\mathbf{k}})(\Psi_d^\dagger \sigma^- \Psi_d) \\ &\quad + 2(\Psi_{\mathbf{k}}^\dagger \sigma^- \Psi_{\mathbf{k}})(\Psi_d^\dagger \sigma^+ \Psi_d) \\ &= \sum_{\sigma} [a_{\mathbf{k}'\sigma}^\dagger a_{\mathbf{k}\sigma} (n_{d\sigma} - n_{d-\sigma}) - 2 \rho_{\mathbf{k}'d\sigma} \rho_{\mathbf{k}d-\sigma}^\dagger] \end{aligned} \quad (8.120)$$

is precisely of the form of the last term in Eq. (8.119). The resulting contribution to \tilde{H} is

$$H_{\text{exch}} = -\frac{1}{\hbar^2} \sum_{\mathbf{k}, \mathbf{k}'} J_{\mathbf{k}\mathbf{k}'} (\Psi_{\mathbf{k}}^\dagger \mathbf{S} \Psi_{\mathbf{k}}) \cdot (\Psi_d^\dagger \mathbf{S} \Psi_d), \quad (8.121)$$

where

$$\begin{aligned} J_{\mathbf{k}\mathbf{k}'} &= (B_{\mathbf{k}} V_{\mathbf{k}d} + B_{\mathbf{k}}^* V_{\mathbf{k}'d}) \\ &= V_{\mathbf{k}'d} V_{\mathbf{k}d} \left[\frac{1}{\epsilon_{\mathbf{k}'} - (\epsilon_d + U)} + \frac{1}{\epsilon_{\mathbf{k}} - (\epsilon_d + U)} - \frac{1}{\epsilon_{\mathbf{k}} - \epsilon_d} - \frac{1}{\epsilon_{\mathbf{k}'} - \epsilon_d} \right]. \end{aligned} \quad (8.122)$$

This term, which arises from the last term in Eq. (8.119), is the Kondo interaction. Note that this result is the form (8.10), deduced from second-order perturbation theory, but symmetrized in \mathbf{k} and \mathbf{k}' . We see here a particular advantage of the similarity transformation method; it generates correctly the interaction matrix elements when the initial and final states do not have the same energy. By contrast, we can identify the second-order scattering amplitude with the interaction matrix element only when the initial and final states have the same energy, in which case Eqs. (8.10) and (8.122) agree. In the vicinity of the Fermi level, $k, k' \sim k_F$, the spin-exchange amplitude reduces to

$$J_{k_F k_F} \equiv J_o = -2V_{\mathbf{k}d}^2 \frac{U}{|\epsilon_d|(|\epsilon_d| - U)} < 0, \quad (8.123)$$

as advertised.

All together we can write \tilde{H} as

$$\begin{aligned} \tilde{H} &= H_0 + \frac{1}{2} [S, H_1] \\ &= H_0 + H'_0 + H''_0 + H_{\text{exch}} + H_{\text{dir}} + H_{\text{ch}}. \end{aligned} \quad (8.124)$$

The direct term

$$H_{\text{dir}} = \sum_{\mathbf{k}, \mathbf{k}'} \frac{1}{4} J_{\mathbf{k}\mathbf{k}'} (\Psi_d^\dagger \Psi_d)(\Psi_{\mathbf{k}'}^\dagger \Psi_{\mathbf{k}}) \quad (8.125)$$

results from the first term in Eq. (8.119). Here

$$\begin{aligned} W_{\mathbf{k}\mathbf{k}'} &= \frac{1}{2} (A_{\mathbf{k}'} V_{\mathbf{k}d} + A_{\mathbf{k}}^* V_{\mathbf{k}'d}) \\ &= \frac{1}{2} V_{\mathbf{k}'d} V_{\mathbf{k}d} \left[\frac{1}{\epsilon_{\mathbf{k}'} - \epsilon_d} + \frac{1}{\epsilon_{\mathbf{k}} - \epsilon_d} \right]. \end{aligned} \quad (8.126)$$

The energy denominators occurring in $W_{\mathbf{k}\mathbf{k}'}$ involve only the excitation process involving only the lowest state on the impurity, as shown in Fig. 8.2(b), while $J_{\mathbf{k}\mathbf{k}'}$ includes both processes in Fig. 8.2. Because $J_{\mathbf{k}\mathbf{k}'}$ and $W_{\mathbf{k}'\mathbf{k}}$ result from successive excitation and deexcitation processes, the impurity remains singly occupied in the process they describe.

The term

$$H'_0 = - \sum_{\mathbf{k}\sigma} \left(W_{\mathbf{k}\mathbf{k}'} + \frac{1}{2} J_{\mathbf{k}\mathbf{k}'} n_{d-\sigma} \right) n_{d\sigma}, \quad (8.127)$$

which emerges from the first term in Eq. (8.118). Similarly, the term

$$H''_0 = \sum_{\mathbf{k}, \mathbf{k}'} W_{\mathbf{k}\mathbf{k}'} \Psi_{\mathbf{k}}^\dagger \Psi_{\mathbf{k}'}, \quad (8.128)$$

which arises from the second term in Eq. (8.119), represents a renormalization of the potential felt by single electrons. Both H'_0 and H''_0 are important for understanding the

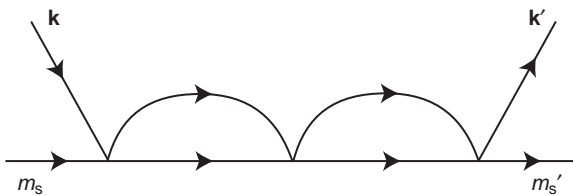


Fig. 8.11 Third-order Kondo diagram which contributes a linear correction to scaling (see Problem 8.4).

Kondo problem as they enter the non-spin-flip processes. The final term

$$H_{\text{ch}} = -\frac{1}{2} \sum_{\mathbf{k}, \mathbf{k}' \sigma} (B_{\mathbf{k}} V_{\mathbf{k}'d} \rho_{\mathbf{k}\sigma} \rho_{\mathbf{k}'-\sigma} + \text{h.c.}), \quad (8.129)$$

which arises from the third term in Eq. (8.118), changes the occupancy of the d -impurity by two, and thus is also not important for the Kondo problem. The two important terms in the interaction are the spin-exchange process and the direct impurity-electron scattering term.

Let us isolate the terms that correspond to single occupancy on the impurity. We note first that since H_{ch} eliminates both electrons on the d -impurity, it cannot connect to the one-electron states in the Hilbert space; we drop this term. In addition, in the one-electron subspace $\Psi_d^\dagger \Psi_d = 1$. As a consequence, H_{dir} is a one-electron term, as are H'_0 and H''_0 . In this subspace, H_{exch} is the only important term. To second order in $V_{\mathbf{k}d}$, the Anderson model yields the Kondo model with an antiferromagnetic exchange coupling. It is the antiferromagnetic nature of this interaction that leads to condensation into a singlet state at the d -impurity.

Problems

- 8.1 (a) The energy of a magnetic moment of fixed magnitude is linear in the magnetic field. Show that the high-temperature (Curie) magnetic susceptibility of a non-interacting collection of such moments is inversely proportional to T .
(b) On the other hand, the energy of a polarizable singlet state is quadratic in the magnetic field. Show that the magnetic susceptibility of a non-interacting collection of such moments becomes constant at low temperatures.
- 8.2 Repeat Yosida's single-electron variational calculation to derive a triplet bound state in the case of a ferromagnetic spin–spin interaction between an impurity and the conduction electrons. Solve the corresponding triplet stability equation and compute the triplet binding energy. Compared to the singlet, which is lower in energy for the same $|J_0|$?
- 8.3 Solve the anisotropic scaling equations (analytically or numerically) and verify that they satisfy the flow diagram shown in Fig. 8.10.
- 8.4 Consider the third-order Kondo diagram shown in Fig. 8.11. Explain how this diagram can give rise to a correction to scaling linear in δD . Assume that \mathbf{q} and \mathbf{q}' are independent. Evaluate the scaling coefficient explicitly.

- 8.5 Use the full Hamiltonian, Eq. (8.124), derived from the Schrieffer–Wolff transformation to evaluate the lowest-order scattering amplitudes: $T[(\mathbf{k}\sigma)+(d-\sigma) \rightarrow (\mathbf{k}'\sigma)+(d-\sigma)]$, $T[(\mathbf{k}\sigma)+(d\sigma) \rightarrow (\mathbf{k}'\sigma)+(d\sigma)]$ and $T[(\mathbf{k}\sigma)+(d-\sigma) \rightarrow (\mathbf{k}'-\sigma)+(d\sigma)]$. Compare with the results given in Section 8.2.

References

- [A1957] A. A. Abrikosov, *Physics* **2**, 5 (1965).
- [AL1991] I. Affleck and A. W. W. Ludwig, *Nucl. Phys. B* **352**, 849 (1991).
- [A1964] P. W. Anderson, *Phys. Rev.* **124**, 41 (1961).
- [AYH1970] P. W. Anderson, G. Yuval, and D. R. Hamann, *Phys. Rev. B* **1**, 4464 (1970).
- [A1978] P. W. Anderson, *Rev. Mod. Phys.* **50**, 191 (1978).
- [AFL1983] N. Andrei, K. Furuya, and J. H. Lowenstein, *Rev. Mod. Phys.* **55**, 331 (1983).
- [AZ1996] V. Barzykin and I. Affleck, *Phys. Rev. Lett.* **76**, 4959 (1996).
- [FN1994] A. Furusaki and N. Nagaosa, *Phys. Rev. Lett.* **72**, 892 (1994).
- [GL1954] M. Gell-Mann and F. Low, *Phys. Rev.* **111**, 582 (1954).
- [GZ1972] G. Grüner and A. Zawadowski, *Solid St. Comm.* **11**, 663 (1972).
- [H1969] A. J. Heeger, in *Solid State Physics*, eds. F. Seitz, D. Turnbull, and H. Ehrenreich (Academic Press, New York, 1969), p. 283.
- [H1993] A. C. Hewson, *The Kondo Problem to Heavy Fermions* (Cambridge University Press, New York, 1993).
- [K1956] T. Kasuya, *Prog. Theor. Phys.* **16**, 45 (1956).
- [K1964] J. Kondo, *Prog. Theor. Phys.* **32**, 37 (1964).
- [L1981] C. Lacroix, *J. Phys. F: Metal Phys.* **11**, 2389 (1981).
- [LT1992] D. H. Lee and J. Toner, *Phys. Rev. Lett.* **72**, 892 (1992).
- [N1974] P. Nozières, *J. Low Temp. Phys.* **17**, 31 (1974).
- [SCL1964] M. Sarachik, E. Corenzwit, and L. D. Longinotti, *Phys. Rev. A* **135**, 1041 (1964).
- [SW1966] J. R. Schrieffer and P. A. Wolff, *Phys. Rev.* **149**, 491 (1966).
- [SZ1974] J. Solyom and A. Zawadowski, *J. Phys. F: Metal Phys.* **4**, 80 (1974).
- [TW1983] A. M. Tsvelick and P. B. Wiegmann, *Adv. in Phys.* **32**, 453 (1983).
- [V1946] S. Vonskovskii, *Zh. Eksp. Teor. Fiz.* **16**, 981 (1946).
- [W1975] K. Wilson, *Rev. Mod. Phys.* **47**, 773 (1975).
- [Y1966] K. Yosida, *Phys. Rev.* **147**, 223 (1966).
- [Z1951] C. Zener, *Phys. Rev.* **81**, 440 (1951).

Screening of the local moment below T_k is the essence of the Kondo problem. A much less exotic example of screening takes place when a positive charge Q is introduced into an electron gas. To restore charge neutrality at the site of the positive charge, the electrons will screen the charge, thereby decreasing its net electric field. In fact, screening occurs regardless of the sign of the test charge. This state of affairs arises because as an electron moves through the electron gas, it does not have to push all the other electrons out of the way. The mutual repulsions among all the electrons in the electron gas help to clear a path for an electron to move. As a result, the effective interaction between the electrons is diminished from the long-range Coulomb $1/r$ to a much more short-ranged interaction. At the level of Thomas–Fermi, the new interaction falls off exponentially. While this interaction overestimates the effect of screening, it does illustrate how efficiently repulsive interactions screen electrons in an electron gas.

9.1 Thomas–Fermi screening

Let us assume a charge Q is at the origin. In the absence of the electron gas, an electron a distance r away from the origin feels a potential $\phi = Q/r$, such that the potential energy is given by

$$U = -e\phi = -e\frac{Q}{r}. \quad (9.1)$$

In the presence of the electron gas, the potential around the charge Q will be screened. Physically, the screening charge is determined by the difference between the charge density of the electron gas in the presence of the charge, Q , and the charge density in the absence of the external charge. Let $-e\delta n(\mathbf{r})$ represent this difference. Poisson's equation for the total charge distribution,

$$-\nabla^2\phi_{\text{eff}}(\mathbf{r}) = 4\pi[Q\delta(\mathbf{r}) - e\delta n(\mathbf{r})], \quad (9.2)$$

depends on both Q and the screening charge, $-e\delta n(\mathbf{r})$, with ϕ_{eff} , the true potential of the charge Q in the electron gas. The easiest way to solve Eq. (9.2) is by Fourier transform. We define

$$f(\mathbf{k}) = \int d\mathbf{r} e^{-i\mathbf{k}\cdot\mathbf{r}} f(\mathbf{r}). \quad (9.3)$$

As a consequence,

$$k^2 U_{\text{eff}}(\mathbf{k}) = -4\pi eQ + 4\pi e^2 \delta n(\mathbf{k}). \quad (9.4)$$

Solving this exact equation requires some ansatz for the screening charge. The simplest approximation is that of Thomas (T1927) and Fermi (F1928) in which the electron gas is assumed to respond to the charge Q as if it were locally a free electron gas. Physically, this assumption implies that the potential is a slowly varying function on a distance scale set by the Fermi wavelength. The net effect then is a shift in the chemical potential of the form, $\mu \rightarrow \mu + U_{\text{eff}}(\mathbf{r})$. Let us define a new single-particle energy level,

$$\epsilon_{\mathbf{k}}(\mathbf{r}) = \frac{\hbar^2 k^2}{2m} + U_{\text{eff}}(\mathbf{r}). \quad (9.5)$$

The effective Fermi–Dirac distribution function is

$$n_{\mathbf{k}}(\mathbf{r}) = \frac{1}{1 + e^{\beta(\epsilon_{\mathbf{k}}(\mathbf{r}) - \mu)}}, \quad (9.6)$$

so that the effective density at \mathbf{r} is

$$\begin{aligned} \langle n(\mathbf{r}) \rangle &= 2 \int \frac{d\mathbf{k}}{(2\pi)^3} n_{\mathbf{k}}(\mathbf{r}) \\ &= n_e - 2\beta \int \frac{d\mathbf{k}}{(2\pi)^3} U_{\text{eff}}(\mathbf{r}) \frac{e^{\beta(\epsilon_{\mathbf{k}} - \mu)}}{(1 + e^{\beta(\epsilon_{\mathbf{k}} - \mu)})^2} + \dots \\ &\simeq n_e - \frac{\partial n_e}{\partial \mu} U_{\text{eff}}(\mathbf{r}) + \dots, \end{aligned} \quad (9.7)$$

where we expanded the distribution function and retained only the linear term in U_{eff} . This expansion is valid only if $\epsilon_F \gg U_{\text{eff}}(\mathbf{r})$. We can now calculate $\delta n(\mathbf{r})$ because

$$\delta n(\mathbf{r}) = \langle n(\mathbf{r}) \rangle - n_e = -\frac{\partial n_e}{\partial \mu} U_{\text{eff}}(\mathbf{r}), \quad (9.8)$$

which implies that

$$k^2 U_{\text{eff}}(\mathbf{k}) = -4\pi e \left(Q + e \frac{\partial n_e}{\partial \mu} U_{\text{eff}}(k) \right) \quad (9.9)$$

or equivalently

$$U_{\text{eff}}(\mathbf{k}) = \frac{-4\pi e Q}{k^2 + 4\pi e^2 \partial n_e / \partial \mu}. \quad (9.10)$$

The inverse Fourier transform of $U_{\text{eff}}(\mathbf{k})$,

$$\begin{aligned} U_{\text{eff}}(\mathbf{r}) &= -\frac{4\pi e Q}{(2\pi)^3} \int \frac{e^{i\mathbf{k}\cdot\mathbf{r}} d\mathbf{k}}{k^2 + 4\pi e^2 \partial n_e / \partial \mu} \\ &= -2 \frac{e Q}{\pi r} \int_{-\infty}^{\infty} dk \frac{k \sin kr}{k^2 + 4\pi e^2 \partial n_e / \partial \mu} \\ &= -e Q \frac{e^{-kr}}{r}, \end{aligned} \quad (9.11)$$

demonstrates that the electrostatic potential arising from the electrons around the charge Q ,

$$\phi_{\text{eff}}(\mathbf{r}) = -e \frac{e^{-\kappa_{\text{TF}} r}}{r}, \quad (9.12)$$

decays exponentially. The electron gas attenuates the bare Coulomb field by screening the charge on a length scale determined by

$$\kappa_{\text{TF}}^2 = 4\pi e^2 \frac{\partial n_e}{\partial \mu}. \quad (9.13)$$

To reiterate, this result is valid in the limit of a slowly varying field induced by the electron gas. We estimate κ_{TF} by recalling from Chapter 2 that

$$n_e = \left(\frac{2m\mu_0}{\hbar^2} \right)^{3/2} \frac{1}{3\pi^2}. \quad (9.14)$$

As a consequence,

$$\frac{\partial n_e}{\partial \mu_0} = \frac{3}{2} \frac{n_e}{\mu_0} = \frac{3mn_e}{p_F^2}. \quad (9.15)$$

Recalling that $a_0 = \hbar^2/me^2$, $n_e = p_F^3/(3\pi^2\hbar^3)$, and $r_e = 1.92\hbar/p_F$ allows us to simplify,

$$\kappa_{\text{TF}}^2 = \frac{12\pi me^2 n_e}{p_F^2} = \frac{2.434}{a_0^2} \frac{1}{r_s}, \quad (9.16)$$

the inverse square of the Thomas–Fermi screening length. Recall that $r_s \sim 2$ to 6. Hence, $\kappa_{\text{TF}}^{-1} = 0.34\sqrt{r_s}\text{\AA}$, which is between 0.45 Å and 0.9 Å. While Thomas–Fermi theory predicts a screening length of electrons in metals generally shorter than the interparticle spacing, the result only describes the long-distance fall-off of the potential surrounding a given charge, as in Eq. (9.11). The theory does not correctly account for screening at distances comparable to the interparticle spacing. To see the behavior at short distances requires a more rigorous treatment, which we develop in a subsequent section.

9.2 Plasma oscillations and collective coordinates

We have developed a theory for the screening effects in an electron gas that assumes slow motion of the electrons. In general this is not true, especially at large wavevector comparable to the inverse interparticle spacing. In this limit, collective excitations of the electron gas become accessible. Such collective excitations are termed plasmons. Two formulations of plasmons will be developed. The first will be the more traditional equations of motion approach, while in the second we will go back to the original collective coordinate approach

of Bohm and Pines (BP1953). We will review this technique as it is now the standard procedure to describe collective phenomena.

The existence of plasma excitations can be established straightforwardly from the equations of motion for the electron density in momentum space. To proceed, we recall the form of the Coulomb interaction,

$$\sum_{\mathbf{k}} \frac{4\pi}{k^2} e^{i\mathbf{k}\cdot(\mathbf{r}_i - \mathbf{r}_j)} = \frac{1}{|\mathbf{r}_i - \mathbf{r}_j|}, \quad (9.17)$$

in momentum space, which implies that we can rewrite the Hamiltonian for our electron gas as

$$\begin{aligned} H &= \sum_i \frac{p_i^2}{2m} + \frac{1}{2} \sum_{i \neq j} \sum_{\mathbf{k}} \frac{4\pi e^2}{k^2} e^{i\mathbf{k}\cdot(\mathbf{r}_i - \mathbf{r}_j)} \\ &= \sum_i \frac{p_i^2}{2m} + \sum_{\mathbf{k}} \frac{V_{\mathbf{k}}}{2} (n_{\mathbf{k}} n_{-\mathbf{k}} - N) \end{aligned} \quad (9.18)$$

with $n_{\mathbf{k}} = \sum_i e^{i\mathbf{k}\cdot\mathbf{r}_i}$, N the number of electrons, and $V_{\mathbf{k}} = 4\pi e^2/k^2$. As we chose our box to be of unit volume, $n_{\mathbf{k}}$ appears without the V^{-1} normalization.

To determine the collective excitations, we need the time evolution of $n_{\mathbf{k}}$,

$$\begin{aligned} i\dot{n}_{\mathbf{k}} &= [n_{\mathbf{k}}, H]/\hbar \\ &= \frac{1}{\hbar} \sum_i \left[\frac{\hbar^2}{m} \nabla_{\mathbf{r}_i} e^{i\mathbf{k}\cdot\mathbf{r}_i} \cdot \nabla_{\mathbf{r}_i} + \frac{\hbar^2}{2m} \nabla_{\mathbf{r}_i}^2 e^{i\mathbf{k}\cdot\mathbf{r}_i} \right] \\ &= - \sum_i e^{i\mathbf{k}\cdot\mathbf{r}_i} \left(\frac{\mathbf{k} \cdot \mathbf{p}_i}{m} + \frac{\hbar k^2}{2m} \right). \end{aligned} \quad (9.19)$$

The second derivative is

$$\begin{aligned} \ddot{n}_{\mathbf{k}} &= \sum_i e^{i\mathbf{k}\cdot\mathbf{r}_i} \left(\frac{\mathbf{k} \cdot \mathbf{p}_i}{m} + \frac{\hbar k^2}{2m} \right)^2 + \frac{2\pi e^2}{\hbar} \sum_i \left[e^{i\mathbf{k}\cdot\mathbf{r}_i} \frac{\mathbf{k} \cdot \mathbf{p}_i}{m}, \sum_{\mathbf{q}} \left(\frac{n_{\mathbf{q}}^\dagger n_{\mathbf{q}} - N}{q^2} \right) \right] \\ &= \sum_i e^{i\mathbf{k}\cdot\mathbf{r}_i} \left(\frac{\mathbf{k} \cdot \mathbf{p}_i}{m} + \frac{\hbar k^2}{2m} \right)^2 - \frac{4\pi e^2}{m} \sum_{\mathbf{q}} \mathbf{k} \cdot \mathbf{q} \frac{n_{\mathbf{k}-\mathbf{q}} n_{\mathbf{q}}}{q^2}. \end{aligned} \quad (9.20)$$

We separate the $\mathbf{k} = \mathbf{q}$ interaction term, which can be written as

$$4\pi e^2 \frac{k^2}{mk^2} n_0 n_{\mathbf{k}} = \frac{4\pi e^2 n_e}{m} n_{\mathbf{k}} = \omega_p^2 n_{\mathbf{k}}. \quad (9.21)$$

That ω_p represents the frequency of the collective oscillations of the electron gas can be seen by rewriting $\ddot{n}_{\mathbf{k}}$ in the suggestive form

$$\ddot{n}_{\mathbf{k}} + \omega_p^2 n_{\mathbf{k}} = \sum_i e^{i\mathbf{k}\cdot\mathbf{r}_i} \left(\frac{\mathbf{k} \cdot \mathbf{p}_i}{m} + \frac{\hbar k^2}{2m} \right)^2 - \frac{4\pi e^2}{m} \sum_{\mathbf{q} \neq \mathbf{k}} \mathbf{k} \cdot \mathbf{q} \frac{n_{\mathbf{k}-\mathbf{q}} n_{\mathbf{q}}}{q^2}. \quad (9.22)$$

We see then that the density $n_{\mathbf{k}}$ oscillates at the frequency ω_p , the plasma frequency, if the terms on the right-hand side of Eq. (9.22) are small. The first term is of order $k^2 v_F^2 n_{\mathbf{k}}$. In

the next term, a product of $n_{\mathbf{q}}$ s appears. Because the density is a sum of exponential terms with randomly varying phases, one might expect that the contribution from the second term is minimal. The approximation that ignores this contribution is known as the random phase approximation (P1963). A well-defined plasma frequency exists at this level of theory if

$$\omega_p^2 \gg k^2 v_F^2. \quad (9.23)$$

For a density of $n_e \sim 10^{23} \text{ e}^-/\text{cm}^3$, $\omega_p \sim 10^{16} \text{ s}^{-1}$ or, equivalently, the energy in a plasma oscillation is

$$\hbar\omega_p \sim 12 \text{ eV}. \quad (9.24)$$

Such high-energy excitations cannot be created by thermal or phonon-like oscillations of the ions. They also cannot be excited by a single electron. Plasma oscillations or plasmons arise from a collective motion of all the electrons in a solid. As such, plasmons are long-wavelength oscillations. We estimate the maximum wavevector for which plasmons exist by considering the ratio $\omega_p/\kappa_{\text{TF}}$. Recall, $\kappa_{\text{TF}}^2 = 4me^2 p_F / \pi \hbar^3$. As a consequence,

$$\begin{aligned} \omega_p/\kappa_{\text{TF}} &= \left(\frac{4\pi e^2 n_e}{m} \frac{\pi \hbar^3}{4p_F m e^2} \right)^{1/2} \\ &= \frac{p_F}{\sqrt{3}m} = \frac{v_F}{\sqrt{3}}. \end{aligned} \quad (9.25)$$

We find that $\omega_p \propto v_F \kappa_{\text{TF}}$. Comparison with Eq. (9.23) reveals that well-defined plasma oscillations exist if $k \ll \kappa_{\text{TF}}$. For $k > \kappa_{\text{TF}}$, the electrons act individually. Note also that $\omega_p^2 \sim 1/m$. For an interacting system, we replace m by the effective mass, m^* . In insulators in which $m^* \rightarrow \infty$, the magnitude of ω_p is a sensitive measure of the insulator–metal transition in an interacting electron system.

The real analysis that showed that plasmons have the integrity of a well-defined excitation is due to the collective coordinate treatment of Bohm and Pines (BP1953). This is an extremely useful technique, as you will see again in our treatment of the Hubbard model in the last chapter on Mott insulators. The basic idea is to re-express the Hamiltonian in such a way that the long-range part of the Coulomb interactions between electrons is described in terms of collective fields (plasma mode) by enlarging the original Hilbert space. After we remove the unphysical states by a constraint, the resultant Hamiltonian will transform to an interacting electron gas with only short-range Coulomb interactions coupled to a plasma oscillating mode.

The starting point is the general interacting electron Hamiltonian,

$$H = \sum_i \frac{p_i^2}{2m} + 2\pi e^2 \sum_{\mathbf{k}, i, j} \frac{e^{i\mathbf{k} \cdot (\mathbf{x}_i - \mathbf{x}_j)}}{k^2} - 2\pi n_e^2 \sum_k \frac{1}{k^2},$$

where in the last term we have subtracted the self-interaction of the electrons. This term represents a uniform positive charge background. The key idea is to replace this Hamiltonian with an equivalent one expressed in terms of two real fields, a longitudinal vector potential,

$$\mathbf{A}(\mathbf{x}) = \sqrt{4\pi c^2} \sum_{\mathbf{k}} \theta_{\mathbf{k}} \epsilon_{\mathbf{k}} e^{i\mathbf{k} \cdot \mathbf{x}}, \quad (9.26)$$

with $\epsilon_{\mathbf{k}}$ a unit vector given by $\epsilon_{\mathbf{k}} = \mathbf{k}/|\mathbf{k}|$, and an electric field

$$\mathbf{E}(\mathbf{x}) = \sqrt{4\pi} \sum_{\mathbf{k}} \pi_{-\mathbf{k}} \epsilon_{\mathbf{k}} e^{i\mathbf{k}\cdot\mathbf{x}}, \quad (9.27)$$

such that our new Hamiltonian is essentially non-interacting,

$$H = \sum_i \frac{1}{2m} \left(p_i - \frac{e}{c} A(\mathbf{x}_i) \right)^2 + \int d\mathbf{x} \frac{\mathbf{E}(\mathbf{x})^2}{8\pi} - 2\pi n_e^2 \sum_k \frac{1}{k^2}, \quad (9.28)$$

except of course for the self-interaction. In so doing, we have had to expand the Hilbert space by introducing new canonical coordinates, $(\pi_{\mathbf{k}}, \theta_{\mathbf{k}})$, such that $[\theta_{\mathbf{k}}, \pi_{\mathbf{k}'}] = i\hbar\delta_{\mathbf{k},\mathbf{k}'}$. These are the natural variables to formulate plasmons. In general, when one is trying to isolate collective phenomena, there is no unique way to expand the Hilbert space. The hope is that the choice made captures the desired physics. Since we seek an essentially bosonic description of the interacting electron gas, canonical bosonic coordinates are appropriate. Substitution of the expressions for $E(\mathbf{x})$ and $A(\mathbf{x})$ into Eq. (9.28) results in

$$\begin{aligned} H = & \sum_i \frac{p_i^2}{2m} - 2\pi n_e^2 \sum_{\mathbf{k}} \left(\frac{1}{k^2} \right) - \frac{\sqrt{4\pi}e}{m} \sum_{i,\mathbf{k}} \epsilon_{\mathbf{k}} \cdot (\mathbf{p}_i - \hbar\mathbf{k}/2) \theta_{\mathbf{k}} e^{i\mathbf{k}\cdot\mathbf{x}_i} \\ & - \sum_{\mathbf{k}} \frac{1}{2} \pi_{\mathbf{k}} \pi_{-\mathbf{k}} + \frac{2\pi e^2}{m} \sum_{i,\mathbf{k},\mathbf{k}'} \epsilon_{\mathbf{k}} \cdot \epsilon_{\mathbf{k}'} \theta_{\mathbf{k}} \theta_{\mathbf{k}'} e^{i(\mathbf{k}+\mathbf{k}')\cdot\mathbf{x}_i} \end{aligned} \quad (9.29)$$

as our effective Hamiltonian. The negative sign on the second line of this equation comes from the fact that $\epsilon_{\mathbf{k}} \cdot \epsilon_{-\mathbf{k}} = -1$. While Eq. (9.29) and the interacting electron gas Hamiltonian might not seem identical, they are related via a canonical transformation

$$\tilde{S} = -\frac{1}{\hbar} \sum_{\mathbf{k},l} \left(\frac{4\pi e^2}{k^2} \right)^{1/2} \theta_{\mathbf{k}} e^{i\mathbf{k}\cdot\mathbf{x}_l}. \quad (9.30)$$

From the transformation rules,

$$e^{\tilde{S}} p_i e^{-\tilde{S}} = p_i + \sqrt{4\pi e^2} \sum_{\mathbf{k}} \theta_{\mathbf{k}} \epsilon_{\mathbf{k}} e^{i\mathbf{k}\cdot\mathbf{x}_i}, \quad (9.31)$$

$$e^{\tilde{S}} \pi_{\mathbf{k}} e^{-\tilde{S}} = \pi_{\mathbf{k}} - i\sqrt{4\pi e^2/k^2} \sum_l e^{i\mathbf{k}\cdot\mathbf{x}_l}, \quad (9.32)$$

we find that

$$\begin{aligned} \mathcal{H} = e^{\tilde{S}} H e^{-\tilde{S}} = & \sum_i \frac{p_i^2}{2m} + 2\pi e^2 \sum_{k,i,j} \frac{e^{i\mathbf{k}\cdot(\mathbf{x}_i-\mathbf{x}_j)}}{k^2} - 2\pi n_e^2 \sum_{\mathbf{k}} \frac{1}{k^2} \\ & - \sum_{\mathbf{k}} \frac{\pi_{\mathbf{k}} \pi_{-\mathbf{k}}}{2} + i \sum_{l,\mathbf{k}} \left(\frac{4\pi e^2}{k^2} \right)^{1/2} \pi_{\mathbf{k}} e^{-i\mathbf{k}\cdot\mathbf{x}_l}. \end{aligned} \quad (9.33)$$

However, to establish the equivalence, we have to impose two constraints:

$$\Omega_k = \pi_{-\mathbf{k}} + 2i \left(\frac{4\pi e^2}{k^2} \right)^{\frac{1}{2}} \sum_i e^{-i\mathbf{k} \cdot \mathbf{x}_i} = 0, \quad \forall \mathbf{k}, \quad (9.34)$$

so that all unphysical states are removed, and

$$\pi_{-\mathbf{k}} \psi = 0, \quad \forall \mathbf{k}, \quad (9.35)$$

where ψ is the ground state wavefunction. With these two constraints, all extra terms in Eq. (9.33) vanish and we recover exactly the electron gas Hamiltonian. The advantage of the model with the collective coordinates is that it is now possible to identify the plasmon modes directly without resorting to equations of motion. For the last term in Eq. (9.29), the dominant part comes from $\mathbf{k} = -\mathbf{k}'$. By defining the plasma frequency

$$\omega_p^2 = \frac{4\pi n_e^2}{m}, \quad (9.36)$$

we are able to simplify Eq. (9.29):

$$H = \sum_i \frac{p_i^2}{2m} - 2\pi n_e^2 \sum_{\mathbf{k}} \left(\frac{1}{k^2} \right) - \frac{\sqrt{4\pi}e}{m} \sum_{i,\mathbf{k}} \epsilon_{\mathbf{k}} \cdot (\mathbf{p}_i - \hbar\mathbf{k}/2) \theta_{\mathbf{k}} e^{i\mathbf{k} \cdot \mathbf{x}_i} - \frac{1}{2} \sum_{\mathbf{k}} (\pi_{\mathbf{k}} \pi_{-\mathbf{k}} + \omega_p^2 \theta_{\mathbf{k}} \theta_{-\mathbf{k}}), \quad (9.37)$$

which describes the non-interacting electron gas coupled to the plasma mode of frequency ω_p . Note, in our final Hamiltonian, the constraint $\pi_{-\mathbf{k}} \psi = 0$ is relaxed. The collective phenomena only emerges once the constraint is relaxed on the degrees of freedom that are introduced upon the expansion of the Hilbert space. Here, we have simplified the derivation by assuming the collective modes can oscillate with any frequency. In a realistic system, a maximum cutoff frequency, k_c , determined by the electron density, arises so that only the long-range electron-electron interaction can be transformed into the plasma mode, and the electron gas retains a short-range Coulomb interaction. The magnitude of k_c can be determined self-consistently by minimizing the total energy. To summarize, we have mapped the original electron-electron interacting Hamiltonian to a non-interacting electron gas coupled to the plasma mode. The key trick that made this happen was enlarging the original Hilbert space with an eye for isolating the underlying collective phenomena.

A final observation on plasmons is that their dispersion relationship is fundamentally tied to the dimensionality of space. If the electrons are confined to a plane ($d = 2$) but the electric field lines are allowed to live in three-dimensional space, thereby making the Coulomb interaction the standard $1/r$ potential (see Problem 9.3), there is no gap to excite plasmon excitations. In addition (see Problem 9.1), the screening length is independent of

density in 2d, at least at the level of Thomas–Fermi. Both of these effects illustrate how fundamentally different a 2d electron gas is from its 3d counterpart.

9.2.1 Dispersion of light

An application in which the plasma frequency naturally appears is the propagation of transverse electromagnetic radiation in metals. Consider the Maxwell equation for the magnetic induction in the presence of a current density:

$$\nabla \times \mathbf{B} - \frac{1}{c} \frac{\partial \mathbf{E}}{\partial t} = \frac{4\pi e \mathbf{j}}{c}. \quad (9.38)$$

The time derivative of this equation is

$$\frac{1}{c} \frac{\partial}{\partial t} \nabla \times \mathbf{B} = \frac{4\pi e}{c^2} \frac{\partial \mathbf{j}}{\partial t} + \frac{1}{c^2} \frac{\partial^2 \mathbf{E}}{\partial t^2}. \quad (9.39)$$

But $\partial \mathbf{B}/\partial ct = -\nabla \times \mathbf{E}$ and $\partial \mathbf{j}/\partial t = en_e \mathbf{E}/m$. For a transverse E-field $\nabla \cdot \mathbf{E} = 0$. As a consequence,

$$-\nabla \times (\nabla \times \mathbf{E}) = -\nabla(\nabla \cdot \mathbf{E}) + \nabla^2 \mathbf{E} = \nabla^2 \mathbf{E}. \quad (9.40)$$

The time derivative can now be written as

$$\left(-\frac{\partial^2}{\partial t^2} + c^2 \nabla^2 - \omega_p^2 \right) \mathbf{E} = 0. \quad (9.41)$$

The resultant dispersion relationship for light in a metal,

$$\omega^2 = c^2 k^2 + \omega_p^2, \quad (9.42)$$

illustrates clearly that transverse electromagnetic radiation cannot penetrate a metal for frequencies less than the plasma frequency.

9.3 Linear response theory

We now focus on formulating the screening problem in terms of the dielectric response function. To facilitate this derivation, we first introduce the general formalism of treating slowly varying time-dependent perturbations, namely linear response theory. Ultimately, we will apply this approach to calculate the density response of a homogeneous system perturbed by the electric field of an external charge.

Consider a Hamiltonian of the form $H = H_0 + W(t)$. In the presence of the perturbation, $W(t)$, the average value of any observable, Y , will acquire a non-trivial time-dependence through the time evolution of the density matrix. The average value of any dynamical observable, Y , at any time t is determined by

$$\langle Y(t) \rangle = \text{Tr}[\rho(t)Y], \quad (9.43)$$

where $\rho(t)$ is the density matrix appropriately normalized so that $\text{Tr}\rho = 1$. The time evolution of the density matrix

$$\begin{aligned}\dot{\rho} &= -\frac{i}{\hbar}[H, \rho] \\ &= -\frac{i}{\hbar}([H_0, \rho] + [W(t), \rho])\end{aligned}\quad (9.44)$$

is governed by the Liouville equation of motion. To solve this equation, it is easiest to work in the interaction representation. For any operator O , we define \widehat{O} to be the interaction representation,

$$\widehat{O}(t) = S^{-1}OS, \quad (9.45)$$

of O , where $S = e^{-iH_0 t/\hbar}$. To simplify notation, we have departed from the convention of using \widehat{O} to denote a generic operator, because \widehat{O} now indicates an operator in the interaction representation. Rewriting the original average of Y and the Liouville equation in the interaction representation, we obtain

$$\langle Y(t) \rangle = \text{Tr}[\widehat{\rho}(t)\widehat{Y}(t)] \quad (9.46)$$

and

$$\begin{aligned}i\hbar\dot{\widehat{\rho}} &= -H_0\widehat{\rho} + S^{-1}i\hbar\frac{\partial\rho}{\partial t}S + S^{-1}\rho H_0S \\ &= -[H_0, \widehat{\rho}] + S^{-1}[H_0 + W(t), \rho]S \\ &= [\widehat{W}(t), \widehat{\rho}(t)].\end{aligned}\quad (9.47)$$

Let ρ_0 be the density matrix before the perturbation is turned on. For a perturbation turned on at $t = -\infty$, the solution to the Liouville equation is the time-ordered product

$$\begin{aligned}\widehat{\rho}(t) &= T \exp\left(\frac{1}{i\hbar} \int_{-\infty}^t [\widehat{W}(t'), \widehat{\rho}] dt'\right) \\ &= \rho_0 - \frac{i}{\hbar} \int_{-\infty}^t [\widehat{W}(t_1), \rho_0] dt_1 - \frac{1}{\hbar^2} \int_{-\infty}^t dt_1 \int_{-\infty}^{t_1} dt_2 [\widehat{W}(t_1), [\widehat{W}(t_2), \rho_0]] + \dots\end{aligned}\quad (9.48)$$

Consequently, through first order in the perturbation, we find that

$$\langle Y(t) \rangle = \langle \widehat{Y}(t) \rangle_0 - \frac{i}{\hbar} \int_{-\infty}^t \text{Tr}(\widehat{Y}(t)[\widehat{W}(t'), \rho_0]) dt'. \quad (9.49)$$

Cyclically permuting under the trace leads to

$$\langle Y(t) \rangle = \langle \widehat{Y}(t) \rangle_0 - \frac{i}{\hbar} \int_{-\infty}^t \chi_{YW}(t, t') dt', \quad (9.50)$$

in which

$$\chi_{YW}(t, t') = \langle [\widehat{Y}(t), \widehat{W}(t')] \rangle_0 \quad (9.51)$$

is the two-time response function, and $\langle \dots \rangle_0$ signifies a trace with the equilibrium or initial density matrix, $\hat{\rho}_0$. The quantum susceptibility to linear order is $\chi_{YW}(t, t')$. This quantity governs the relaxation of a quantum system. For example, the crux of quantum linear response theory is that the fluctuation

$$\begin{aligned}\langle \delta Y(t) \rangle &= \langle Y(t) \rangle - \langle \hat{Y}(t) \rangle_0 \\ &= \frac{-i}{\hbar} \int_{-\infty}^t \chi_{YW}(t, t') dt'\end{aligned}\quad (9.52)$$

is determined by the time integral of the average value of the commutator of the observable at time t with the perturbation at time t' . A few useful properties of $\chi_{YW}(t, t')$ are

$$\chi_{YW}(t, t') = -\chi_{WY}(t', t) = -\chi_{YW}^*(t, t'). \quad (9.53)$$

These relationships follow because χ_{YW} is a commutator.

9.3.1 Fluctuation–dissipation theorem

Consider the general fluctuation

$$\begin{aligned}S_{YW}(t, t') &= \langle \delta \hat{Y}(t) \delta \hat{W}(t') \rangle_0 \\ &= \langle \hat{Y}(t) \hat{W}(t') \rangle_0 - \langle \hat{Y}(t) \rangle_0 \langle \hat{W}(t') \rangle_0.\end{aligned}\quad (9.54)$$

The fluctuation–dissipation theorem equates fundamentally the spontaneous fluctuations that occur in an equilibrium system with the relaxation of a non-equilibrium system displaced from equilibrium. The equilibrium density matrix is

$$\rho_0 = e^{-\beta H_0}. \quad (9.55)$$

The correlation function $S_{YW}(t, t')$ is a function of the time difference $t - t'$ rather than of t and t' separately. We want to show that $S_{YW}(t, t')$ is related to χ_{YW} . To do this, we first compute

$$\begin{aligned}\langle \hat{Y}(t) \hat{W}(t') \rangle_0 &= \text{Tr}[e^{-\beta H_0} \hat{Y}(t) \hat{W}(t')] \\ &= \text{Tr}[e^{-\beta H_0} \hat{W}(t') e^{-\beta H_0} \hat{Y}(t) e^{\beta H_0}] \\ &= \langle \hat{W}(t') \hat{Y}(t + i\beta\hbar) \rangle_0.\end{aligned}\quad (9.56)$$

Coupled with the identity

$$\begin{aligned}\langle \hat{Y}(t) \rangle_0 &= \text{Tr}[e^{-\beta H_0} \hat{Y}(t)] = \text{Tr}[e^{-\beta H_0} e^{-\beta H_0} \hat{Y}(t) e^{\beta H_0}] \\ &= \langle \hat{Y}(t + i\beta\hbar) \rangle_0,\end{aligned}\quad (9.57)$$

we arrive at the equality $S_{YW}(t, t') = S_{WY}(t', t + i\beta\hbar)$. In Fourier space, we have

$$\begin{aligned}S_{YW}(\omega) &= \int_{-\infty}^{\infty} d(t - t') S_{YW}(t, t') e^{i\omega(t-t')} \\ &= \int_{-\infty}^{\infty} d(t - t') S_{WY}(t', t + i\beta\hbar) e^{i\omega(t-t')}.\end{aligned}\quad (9.58)$$

Let $x = t' - t - i\beta\hbar$; $dx = d(t' - t)$. The Fourier transform of S_{YW} becomes

$$\begin{aligned} S_{YW}(\omega) &= e^{\beta\hbar\omega} \int_{-\infty}^{\infty} dx S_{YW}(x) e^{-i\omega x} \\ &= e^{\beta\hbar\omega} S_{YW}(-\omega). \end{aligned} \quad (9.59)$$

Combining these results to calculate $\chi_{YW}(\omega)$,

$$\begin{aligned} \chi_{YW}(\omega) &= \int_{-\infty}^{\infty} dt (t-t') e^{i\omega(t-t')} \langle [\widehat{Y}(t), \widehat{W}(t')] \rangle_0 \\ &= \int_{-\infty}^{\infty} dt (t-t') e^{i\omega(t-t')} [S_{YW}(t, t') - S_{YW}(t', t)] \\ &= (1 - e^{-\beta\hbar\omega}) S_{YW}(\omega). \end{aligned} \quad (9.60)$$

Consequently, spontaneous fluctuations in equilibrium are related to the linear response function $\chi_{YW}(\omega)$. This means that relaxation of fluctuations in a non-equilibrium system is determined by the same laws that govern the relaxation of spontaneous fluctuations in an equilibrium system. This is the fluctuation–dissipation theorem.

9.3.2 Density response

Let us apply linear response theory to density fluctuations. Consider a perturbation of the form

$$H'(t) = \int d\mathbf{r} n(\mathbf{r}, t) W(\mathbf{r}, t), \quad (9.61)$$

in which the electron density $n(\mathbf{r}, t)$ is changed by the application of an external field, $W(\mathbf{r}, t)$, which commutes with $n(\mathbf{r}, t)$ and H_0 . According to linear response theory,

$$\langle \delta n(\mathbf{r}, t) \rangle = \int_{-\infty}^t dt' d\mathbf{r}' \chi_{nn}(\mathbf{r}t, \mathbf{r}'t') W(\mathbf{r}', t'), \quad (9.62)$$

where

$$\chi_{nn}(\mathbf{r}t, \mathbf{r}'t') = -\frac{i}{\hbar} \langle [n(\mathbf{r}, t), n(\mathbf{r}', t')] \rangle. \quad (9.63)$$

As several response functions will be introduced, we stress that χ_{nn} represents the response of the system to the external (unscreened) field. We have subsumed the $-i/\hbar$ factor into the definition of the susceptibility. In Eq. (9.62), the time evolution of the density is determined entirely by H_0 .

For free electrons, we define χ_{nn}^0 to be the response function. We showed previously that

$$n(\mathbf{r}) = \frac{1}{V} \sum_{\mathbf{p}, \mathbf{p}', \sigma} e^{i(\mathbf{p}-\mathbf{p}') \cdot \mathbf{r}/\hbar} a_{\mathbf{p}'\sigma}^\dagger a_{\mathbf{p}\sigma} \quad (9.64)$$

is the time-independent operator for the electron density at \mathbf{r} . We remind the reader that we have dropped the ‘hat’ on an operator because this symbol is now reserved for the

interaction representation. To define $n(\mathbf{r}, t)$, we need the time dependence of $a_{\mathbf{p}\sigma}$. We obtain this through the Heisenberg equations of motion,

$$\begin{aligned} i\hbar \frac{\partial a_{\mathbf{p}\sigma}}{\partial t} &= [a_{\mathbf{p}\sigma}, H_0] \\ &= \sum_{\mathbf{p}', \sigma'} \epsilon_{\mathbf{p}'\sigma'} [a_{\mathbf{p}\sigma}, a_{\mathbf{p}'\sigma'}^\dagger a_{\mathbf{p}'\sigma'}] \\ &= \epsilon_{\mathbf{p}} a_{\mathbf{p}\sigma}, \end{aligned} \quad (9.65)$$

where H_0 is the Hamiltonian for free electrons. Integrating the above, we obtain that

$$a_{\mathbf{p}\sigma}(t) = e^{-i\epsilon_{\mathbf{p}}t/\hbar} a_{\mathbf{p}\sigma}(t=0). \quad (9.66)$$

Let us now evaluate χ_{nn} for a collection of free electrons. To simplify the notation, we define

$$q_{\mathbf{p}_{12}}(\mathbf{r}, t) = e^{i(\mathbf{p}_2 - \mathbf{p}_1) \cdot \mathbf{r}/\hbar} e^{i(\epsilon_{\mathbf{p}_1} - \epsilon_{\mathbf{p}_2})t/\hbar}, \quad (9.67)$$

$\delta_{\mathbf{p}_{ij}} = \delta_{\mathbf{p}_i \mathbf{p}_j}$, and $f_{\mathbf{p}_1 \mathbf{p}_2} = f_{\mathbf{p}_1}(1 - f_{\mathbf{p}_2})$, where $f_{\mathbf{p}}$ denotes the probability that the state \mathbf{p} is occupied. Combining our expression for $a_{\mathbf{p}\sigma}(t)$ together with Eq. (9.64), it follows that

$$\begin{aligned} \langle n(\mathbf{r}, t) n(\mathbf{r}', t') \rangle &= \frac{1}{V^2} \sum_{\substack{\mathbf{p}_1, \mathbf{p}_2, \mathbf{p}_3, \mathbf{p}_4 \\ \sigma_1, \sigma_2}} \langle a_{\mathbf{p}_1 \sigma_1}^\dagger a_{\mathbf{p}_2 \sigma_1} a_{\mathbf{p}_3 \sigma_2}^\dagger a_{\mathbf{p}_4 \sigma_2} \rangle q_{\mathbf{p}_{12}}(\mathbf{r}, t) q_{\mathbf{p}_{34}}(\mathbf{r}', t') \\ &= \langle n(\mathbf{r}, t) \rangle \langle n(\mathbf{r}', t') \rangle + \frac{1}{V^2} \sum_{\substack{\mathbf{p}_1, \mathbf{p}_2, \mathbf{p}_3, \mathbf{p}_4 \\ \sigma_1, \sigma_2}} \delta_{\sigma_1 \sigma_2} \delta_{\mathbf{p}_{14}} \delta_{\mathbf{p}_{23}} f_{\mathbf{p}_1 \mathbf{p}_2} q_{\mathbf{p}_{12}}(\mathbf{r}, t) q_{\mathbf{p}_{34}}(\mathbf{r}', t') \\ &= \langle n(\mathbf{r}, t) \rangle \langle n(\mathbf{r}', t') \rangle + \frac{1}{V^2} \sum_{\substack{\mathbf{p}_1, \mathbf{p}_2 \\ \sigma}} f_{\mathbf{p}_1 \mathbf{p}_2} q_{\mathbf{p}_{21}}(\mathbf{r}' - \mathbf{r}, t - t'). \end{aligned} \quad (9.68)$$

Substitution of Eq. (9.68) into Eq. (9.63) illustrates immediately that the response function,

$$\chi_{nn}^0(\mathbf{r}, t, \mathbf{r}', t') = \frac{1}{i\hbar V^2} \sum_{\mathbf{p}_1, \mathbf{p}_2, \sigma} (f_{\mathbf{p}_1 \sigma} - f_{\mathbf{p}_2 \sigma}) e^{i(\mathbf{p}_1 - \mathbf{p}_2) \cdot (\mathbf{r}' - \mathbf{r})/\hbar} e^{-i(\epsilon_{\mathbf{p}_1} - \epsilon_{\mathbf{p}_2})(t' - t)/\hbar}, \quad (9.69)$$

depends on the differences $\mathbf{r} - \mathbf{r}'$ and $t - t'$. Hence, this response function is independent of the particular choice of origin in space as well as in time. We will find it most useful to work with the Fourier transform of $\chi_{nn}^0(\mathbf{r}t, \mathbf{r}'t')$:

$$\begin{aligned} \chi_{nn}^0(\mathbf{k}, \omega) &= \int d\mathbf{x} dt e^{i\mathbf{k} \cdot \mathbf{x}} e^{-i\omega t} \chi_{nn}^0(x, t) \\ &= \frac{2}{i\hbar V} \sum_{\mathbf{p}_1, \mathbf{p}_2} \delta_{\hbar k, \mathbf{p}_2 - \mathbf{p}_1} (f_{\mathbf{p}_1} - f_{\mathbf{p}_2}) \int_{-\infty}^0 e^{-i(\hbar\omega + \epsilon_{\mathbf{p}_1} - \epsilon_{\mathbf{p}_2})t/\hbar} dt \\ &= \frac{2}{V} \sum_{\mathbf{p}_1} \frac{f_{\mathbf{p}_1} - f_{\mathbf{p}_1 + \hbar\mathbf{k}}}{\hbar\omega + \epsilon_{\mathbf{p}_1} - \epsilon_{\mathbf{p}_1 + \hbar\mathbf{k}}}. \end{aligned} \quad (9.70)$$

In Eq. (9.70), the factor of 2 comes from the spin summation, and the perturbation coupling to the density was assumed to be turned on at $t = -\infty$ and turned off at $t = 0$. It is this expression that will be used to formulate the Lindhard screening function.

Consider the zero-frequency limit of $\chi_{nn}^0(\mathbf{k}, \omega)$,

$$\begin{aligned}\chi_{nn}^0(\mathbf{k}, \omega = 0) &= 2 \int \frac{d\mathbf{p}}{(2\pi\hbar)^3} \frac{\partial f_{\mathbf{p}}}{\partial \epsilon_p} = -2 \int \frac{d\mathbf{p}}{(2\pi\hbar)^3} \frac{\partial f_{\mathbf{p}}}{\partial \mu} \\ &= -\frac{\partial n_e}{\partial \mu},\end{aligned}\quad (9.71)$$

which is precisely the Thomas–Fermi approximation to the screening function. This suggests that there is a fundamental connection between the density response function and screening. To establish the connection formally, we turn to the dielectric response function.

9.4 Dielectric response function

We reformulate the screening problem in terms of χ_{nn} by rewriting the perturbing field as

$$H' = \int d\mathbf{r} n(\mathbf{r}, t) U(\mathbf{r}, t), \quad (9.72)$$

where $U(\mathbf{r}, t)$ is the local electrostatic potential energy of the charge Q , which we take to be the Coulomb interaction. We must determine the net field felt by other electrons as a result of the test charge Q placed at the origin. We start by rewriting Eq. (9.4) as

$$U_{\text{eff}}(\mathbf{k}, \omega) = U(\mathbf{k}) + \frac{4\pi e^2}{k^2} \langle \delta n(\mathbf{k}, \omega) \rangle, \quad (9.73)$$

and using the linear response expression for the fluctuation (Eq. (9.63)),

$$\langle \delta n(\mathbf{k}, \omega) \rangle = \chi_{nn}(\mathbf{k}, \omega) U(\mathbf{k}), \quad (9.74)$$

we obtain

$$\begin{aligned}U_{\text{eff}}(\mathbf{k}, \omega) &= [1 + U(\mathbf{k}) \chi_{nn}(\mathbf{k}, \omega)] U(\mathbf{k}, \omega) \\ &= \varepsilon^{-1}(\mathbf{k}, \omega) U(\mathbf{k}),\end{aligned}\quad (9.75)$$

with $\varepsilon(\mathbf{k}, \omega)$ the dielectric function and $U(\mathbf{k}) = 4\pi e^2/k^2$. It is the dielectric function that contains the dynamics of the screening process described in the introduction to this chapter.

To make contact with our previous treatment of screening, we introduce a generalized screening function, χ_{sc} , through

$$\langle \delta n(\mathbf{r}, t) \rangle = \langle n(\mathbf{r}, t) \rangle - n_e = \int d\mathbf{r}' \chi_{\text{sc}}(\mathbf{r}, \mathbf{r}', t) U_{\text{eff}}(\mathbf{r}'). \quad (9.76)$$

The generalized screening function, χ_{sc} , describes the response of the system to the screened potential in contrast to χ_{nn} which is simply the response to the bare potential. From Eq. (9.7), we see that the Thomas–Fermi screening function is simply

$$\chi_{\text{sc}}(\mathbf{r}, \mathbf{r}', t) = -\frac{\partial n_e}{\partial \mu} \delta(\mathbf{r} - \mathbf{r}') \delta(t). \quad (9.77)$$

The Fourier transform of Eq. (9.76) yields

$$\langle \delta n(\mathbf{k}, \omega) \rangle = \chi_{\text{sc}}(\mathbf{k}, \omega) U_{\text{eff}}(\mathbf{k}, \omega), \quad (9.78)$$

which together with Eq. (9.73) implies that

$$U_{\text{eff}}(\mathbf{k}, \omega) = \left[1 - \frac{4\pi e^2}{k^2} \chi_{\text{sc}}(\mathbf{k}, \omega) \right]^{-1} U(\mathbf{k}) \quad (9.79)$$

is an equivalent expression for the total effective electrostatic potential in the presence of the test charge Q . Equating Eqs. (9.78) and (9.74), we see immediately that

$$\chi_{nn} = \varepsilon^{-1} \chi_{\text{sc}} = \frac{\chi_{\text{sc}}}{1 - \frac{4\pi e^2 \chi_{\text{sc}}}{k^2}}. \quad (9.80)$$

It is generally easier to construct a theory for χ_{sc} because it describes the response to the total field of the system. The lowest-order theory for χ_{sc} is the random phase approximation (RPA) in which it is assumed that

$$\chi_{\text{sc}}(\mathbf{k}, \omega) = \chi_{nn}^0(\mathbf{k}, \omega). \quad (9.81)$$

Alternatively, the effective interaction is given by the geometric series

$$\begin{aligned} U_{\text{eff}}(\mathbf{k}, \omega) &= U(\mathbf{k}) (1 + U(\mathbf{k}) \chi_{nn}^0(\mathbf{k}, \omega) + (U(\mathbf{k}) \chi_{nn}^0(\mathbf{k}, \omega))^2 + \dots) \\ &= \frac{U(\mathbf{k})}{1 - U(\mathbf{k}) \chi_{nn}^0(\mathbf{k}, \omega)}. \end{aligned} \quad (9.82)$$

This approximation, which is shown in Fig. 9.1, leaves out exchange effects and is essentially time-dependent Hartree–Fock. As shown in the previous section, the zero-frequency limit of χ_{nn}^0 is the Thomas–Fermi approximation.

To understand the role played by the frequency dependence, we expand the denominator in Eq. (9.70) for large ω . In this limit, we find that

$$\begin{aligned} \lim_{\omega \rightarrow \infty} \chi_{nn}^0(\mathbf{k}, \omega) &\rightarrow 2 \int \frac{d\mathbf{p}}{(2\pi\hbar)^3} (f_{\mathbf{p}} - f_{\mathbf{p}+\hbar\mathbf{k}}) \left[\frac{1}{\hbar\omega} - \frac{\epsilon_{\mathbf{p}} - \epsilon_{\mathbf{p}+\hbar\mathbf{k}}}{(\hbar\omega)^2} + \dots \right] \\ &= -\frac{2}{(\hbar\omega)^2} \int \frac{d\mathbf{p}}{(2\pi\hbar)^3} (f_{\mathbf{p}} - f_{\mathbf{p}+\hbar\mathbf{k}}) (\epsilon_{\mathbf{p}} - \epsilon_{\mathbf{p}+\hbar\mathbf{k}}) \\ &= \frac{2k^2}{m\omega^2} \int \frac{d\mathbf{p}}{(2\pi\hbar)^3} f_{\mathbf{p}} = \frac{k^2}{m\omega^2} n_e. \end{aligned} \quad (9.83)$$

The high-frequency limit of the dielectric function,

$$\begin{aligned} \varepsilon &= 1 - \frac{4\pi e^2 n_e}{mk^2} \frac{k^2}{\omega^2} \\ &= 1 - \left(\frac{\omega_p}{\omega} \right)^2, \end{aligned} \quad (9.84)$$

is fundamentally related to the plasma frequency. In fact, as we will see later, the plasma frequency is an exact zero of the dielectric function.

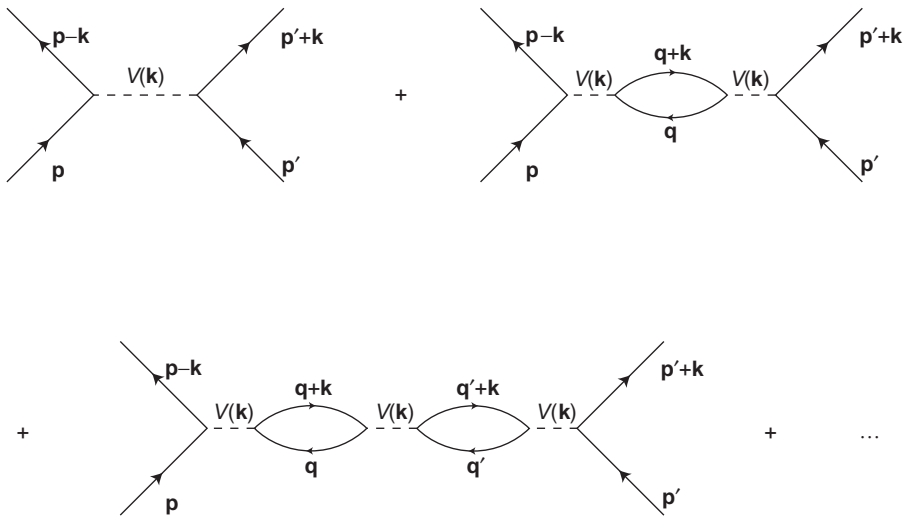


Fig. 9.1

Diagrammatic expansion in the RPA for the screened electron–electron interaction. Each bubble represents a particle–hole excitation. Mathematically, these excitations are described by the polarization function $\chi_{nn}^0(\mathbf{k}, \omega)$. The momentum exchanged between the particle and the hole is carried away by the Coulomb interaction at each dotted line as indicated. As a result, the argument of the Coulomb interaction is decoupled from the momentum summation in each bubble. Consequently, all such terms can be summed exactly. The result is Eq. (9.82).

9.4.1 Structure function

The time-dependent density response function defined in the previous section is a fundamental quantity in many-body theory. In addition to the screening function, the structure function, as well as the total energy of an interacting system, can all be written in terms of χ_{nn} . The principal reason for this is that the potential in most many-body systems is typically a sum of pair-wise interactions. In this section, we focus on calculating the structure function, as it will play a prominent role in later topics.

The structure function is defined as the autocorrelation function of the Fourier components

$$S(\mathbf{k}) = \frac{1}{N} \langle n_{\mathbf{k}} n_{-\mathbf{k}} \rangle \quad (9.85)$$

of the particle density. In equilibrium neutron scattering experiments, the central quantity that is measured is the structure function. As advertised, we can also write the total average energy of an interacting electron system in terms of $S(\mathbf{k}, \omega)$. This can be done trivially by computing the average value of the Hamiltonian for an interacting electron gas,

$$\langle H \rangle = E_0 = \epsilon_{\text{kin}} + N \sum_{\mathbf{k}} \frac{2\pi e^2}{k^2} [S(\mathbf{k}) - 1] \quad (9.86)$$

in momentum space (see Eq. (9.18)).

In the time domain, the structure function becomes

$$S(\mathbf{k}, t) = \frac{1}{N} \left\langle \sum_i e^{i\mathbf{k} \cdot \mathbf{r}_i(0)} \sum_j e^{-i\mathbf{k} \cdot \mathbf{r}_j(t)} \right\rangle. \quad (9.87)$$

By noting that

$$e^{i\mathbf{k} \cdot \mathbf{r}_i} = \int d\mathbf{r} e^{i\mathbf{k} \cdot \mathbf{r}} \delta(\mathbf{r} - \mathbf{r}_i) \quad (9.88)$$

and that the density at \mathbf{r} is

$$n(\mathbf{r}) = \sum_{i=1}^N \delta(\mathbf{r} - \mathbf{r}_i), \quad (9.89)$$

we rewrite Eq. (9.87) as

$$S(\mathbf{k}, t) = \frac{1}{N} \int d\mathbf{r} d\mathbf{r}' \langle n(\mathbf{r}, t=0) n(\mathbf{r}', t) \rangle e^{i\mathbf{k} \cdot (\mathbf{r} - \mathbf{r}')}. \quad (9.90)$$

As we have seen, $\langle n(\mathbf{r}, t) n(\mathbf{r}', t') \rangle$ depends only on $\mathbf{r} - \mathbf{r}'$ and $t - t'$. Hence, our choice of the time origin at $t = 0$ does not affect our results. The dynamic structure factor is the time Fourier transform,

$$S(\mathbf{k}, \omega) = \int_{-\infty}^{\infty} dt e^{-i\omega t} S(\mathbf{k}, t), \quad (9.91)$$

of $S(\mathbf{k}, t)$. It is $S(\mathbf{k}, \omega)$ that is measured in angle-resolved x-ray or neutron scattering experiments. The static and dynamic structure factors are related through the simple sum rule

$$S(\mathbf{k}) = \int_{-\infty}^{\infty} \frac{d\omega}{2\pi} S(\mathbf{k}, \omega). \quad (9.92)$$

For systems with inversion symmetry, such as most solids and all fluids, $S(\mathbf{k}, \omega)$ is invariant under a change of sign of \mathbf{k} : $S(\mathbf{k}, \omega) = S(-\mathbf{k}, \omega)$. From Eq. (9.59), it follows that $S(\mathbf{k}, \omega) = e^{\beta\hbar\omega} S(\mathbf{k}, -\omega)$. This relationship reflects the principle of detailed balance.

From Eq. (9.63), we have

$$\begin{aligned} i\hbar\chi_{nn}(\mathbf{k}, \omega) &= n_e \int_{-\infty}^0 dt e^{-i\omega t} \int_{-\infty}^{\infty} \frac{d\omega'}{2\pi} e^{i\omega' t} [S(\mathbf{k}, \omega') - S(\mathbf{k}, -\omega')] \\ &= n_e \int_{-\infty}^{\infty} \frac{d\omega'}{2\pi i} \frac{S(\mathbf{k}, \omega') - S(\mathbf{k}, -\omega')}{\omega' - \omega} \\ &= n_e \int_{-\infty}^{\infty} \frac{d\omega'}{2\pi i} (1 - e^{-\beta\hbar\omega'}) \frac{S(\mathbf{k}, \omega')}{\omega' - \omega}. \end{aligned} \quad (9.93)$$

We see then that the density response function, $\chi_{nn}(\mathbf{k}, \omega)$, can in principle be determined from experiment once $S(\mathbf{k}, \omega)$ is known.

9.4.2 Parameter differentiation of total energy

An expression identical to Eq. (9.86) can be derived using parameter differentiation. We consider a variation of the ground state energy with respect to e^2 :

$$\begin{aligned}\frac{\partial}{\partial e^2} E_0(e^2) &= \frac{\partial}{\partial e^2} \langle \psi(e^2) | H | \psi(e^2) \rangle \\ &= \left(\frac{\partial}{\partial e^2} \langle \psi(e^2) \right) | H | \psi(e^2) \rangle + \langle \psi(e^2) | H \left(\frac{\partial}{\partial e^2} | \psi(e^2) \rangle \right) + \langle \psi(e^2) | \frac{\partial H}{\partial e^2} | \psi(e^2) \rangle \\ &= E_0(e^2) \frac{\partial}{\partial e^2} \langle \psi(e^2) | \psi(e^2) \rangle + \left\langle \frac{\partial H}{\partial e^2} \right\rangle = \langle \psi | \frac{\partial H}{\partial e^2} | \psi \rangle.\end{aligned}\quad (9.94)$$

We have used the fact that $H| \psi(e^2) \rangle = E_0| \psi(e^2) \rangle$. Because the kinetic energy is independent of e^2 and $V \sim e^2$, we have that

$$\frac{\partial E_0}{\partial e^2} = \frac{1}{e^2} \langle \psi | V_e | \psi \rangle, \quad (9.95)$$

where V_e is the total potential for our interacting system:

$$\begin{aligned}V_e &= V_{ee} + V_{\text{ion-ion}} + V_{\text{e-ion}} \\ &= e^2 \left[\frac{1}{2} \sum_{j,j'} \frac{1}{|\mathbf{r}_j - \mathbf{r}_{j'}|} + \frac{1}{2} \int d\mathbf{r} d\mathbf{r}' \frac{n_e^2}{|\mathbf{r} - \mathbf{r}'|} - \sum_j \int d\mathbf{r} \frac{n_e}{|\mathbf{r} - \mathbf{r}_j|} \right].\end{aligned}\quad (9.96)$$

The second and third terms in the total potential represent the ion–ion and electron–ion interaction, respectively. The ions provide a homogeneous background of compensating positive charge for the electron gas. If we substitute the form for the density in Eq. (9.89), we can rewrite the total potential as

$$\begin{aligned}\frac{V_e}{e^2} &= \frac{1}{2} \int d\mathbf{r} d\mathbf{r}' \frac{n(\mathbf{r})n(\mathbf{r}')}{|\mathbf{r} - \mathbf{r}'|} + \frac{n_e^2}{2} \int d\mathbf{r} d\mathbf{r}' \frac{1}{|\mathbf{r} - \mathbf{r}'|} - n_e \int d\mathbf{r} d\mathbf{r}' \frac{n(\mathbf{r}')}{|\mathbf{r} - \mathbf{r}'|} \\ &= \frac{1}{2} \int d\mathbf{r} d\mathbf{r}' \frac{(n(\mathbf{r}) - n_e)(n(\mathbf{r}') - n_e)}{|\mathbf{r} - \mathbf{r}'|}.\end{aligned}\quad (9.97)$$

Consequently,

$$\begin{aligned}\frac{\partial E_0}{\partial e^2} &= \frac{1}{2} \int d\mathbf{r} d\mathbf{r}' \frac{\langle \delta n(\mathbf{r}) \delta n(\mathbf{r}') \rangle}{|\mathbf{r} - \mathbf{r}'|} \\ &= \frac{n_e}{2} \int d\mathbf{r} d\mathbf{r}' \int \frac{d\mathbf{k}}{(2\pi)^3} \frac{e^{i\mathbf{k} \cdot (\mathbf{r} - \mathbf{r}')}}{|\mathbf{r} - \mathbf{r}'|} \int_{-\infty}^{\infty} \frac{d\omega}{2\pi} \tilde{S}(k, \omega) \\ &= \frac{n_e V}{2} \int \frac{d\mathbf{k}}{(2\pi)^3} \frac{4\pi}{k^2} \int_{-\infty}^{\infty} \frac{d\omega}{2\pi} \tilde{S}(k, \omega),\end{aligned}\quad (9.98)$$

where we introduced a rescaled structure factor

$$n_e \tilde{S}(\mathbf{k}, \omega) = \int_{-\infty}^{\infty} dt e^{-i\omega t} e^{-i\mathbf{k} \cdot (\mathbf{r} - \mathbf{r}')} \langle \delta n(\mathbf{r}) \delta n(\mathbf{r}', t) \rangle d(\mathbf{r} - \mathbf{r}'). \quad (9.99)$$

The advantage of this definition of the structure factor is that it eliminates the n_e^2 term that would normally appear in the energy. This term simply shifts the zero of the potential

energy and hence is of no real consequence. Using the sum rule in Eq. (9.92) for $S(\mathbf{k}, \omega)$ yields

$$E_0(e^2) = E_0(e^2 = 0) + \frac{N}{2} \int_0^{e^2} de'^2 \int \frac{d\mathbf{k}}{(2\pi)^3} \frac{4\pi}{k^2} \tilde{S}(\mathbf{k}; e'^2), \quad (9.100)$$

where we have allowed for explicit e^2 dependence in the static structure factor. This is an exact expression. If the free particle form for $\tilde{S}(\mathbf{k})$ is used, Hartree–Fock theory results. Inclusion of the effects of screening allows us then to reduce $E_0(e^2)$ to the Gell-Mann–Brueckner perturbative expansion.

9.4.3 Evaluation of $\chi_{sc}(\mathbf{k}, \omega)$

Our goal now is to evaluate completely the effects of screening in the RPA. We start by rewriting the screening function as

$$\begin{aligned} \chi_{sc}(\mathbf{k}, \omega) &= \chi_{nn}^0(\mathbf{k}, \omega) = 2 \int \frac{d\mathbf{p}}{(2\pi\hbar)^3} \frac{(f_{\mathbf{p}} - f_{\mathbf{p}+\hbar\mathbf{k}})}{(\hbar\omega + \epsilon_{\mathbf{p}} - \epsilon_{\mathbf{p}+\hbar\mathbf{k}})} \\ &= 2 \lim_{\eta \rightarrow 0} \int_{-\infty}^{\infty} \frac{d\omega'}{\omega - \omega' + i\eta} \int \frac{d\mathbf{p}}{(2\pi\hbar)^3} (f_{\mathbf{p}} - f_{\mathbf{p}+\hbar\mathbf{k}}) \delta(\hbar\omega' - \epsilon_{\mathbf{p}+\hbar\mathbf{k}} + \epsilon_{\mathbf{p}}). \end{aligned} \quad (9.101)$$

Using Eq. (9.93), we rewrite the right side in terms of the structure factor. We find that

$$4\pi\hbar \int \frac{d\mathbf{p}}{(2\pi\hbar)^3} (f_{\mathbf{p}} - f_{\mathbf{p}+\hbar\mathbf{k}}) \delta(\hbar\omega' - \epsilon_{\mathbf{p}+\hbar\mathbf{k}} + \epsilon_{\mathbf{p}}) = n_e (1 - e^{-\beta\hbar\omega'}) S_0(k, \omega'),$$

where $S_0(\mathbf{k}, \omega')$ is the structure factor for the free system. We simplify the left side of this expression by noting that $f_{\mathbf{p}} - f_{\mathbf{p}+\hbar\mathbf{k}} = f_{\mathbf{p}}(1 - f_{\mathbf{p}+\hbar\mathbf{k}}) - f_{\mathbf{p}+\hbar\mathbf{k}}(1 - f_{\mathbf{p}})$ and $1 - f_{\mathbf{p}} = e^{\beta(\epsilon_{\mathbf{p}} - \mu)} f_{\mathbf{p}}$. Consequently,

$$f_{\mathbf{p}} - f_{\mathbf{p}+\hbar\mathbf{k}} = f_{\mathbf{p}}(1 - f_{\mathbf{p}+\hbar\mathbf{k}})(1 - e^{\beta(\epsilon_{\mathbf{p}} - \epsilon_{\mathbf{p}+\hbar\mathbf{k}})}), \quad (9.102)$$

and the explicit temperature-dependent factor multiplying the free particle structure function can be eliminated to yield

$$n_e S_0(\mathbf{k}, \omega) = 4\pi\hbar \int \frac{d\mathbf{p}}{(2\pi\hbar)^3} f_{\mathbf{p}}(1 - f_{\mathbf{p}+\hbar\mathbf{k}}) \delta(\hbar\omega - \epsilon_{\mathbf{p}+\hbar\mathbf{k}} + \epsilon_{\mathbf{p}}). \quad (9.103)$$

The factor $1 - f_{\mathbf{p}+\hbar\mathbf{k}}$ is the probability that the state with momentum $\mathbf{p} + \hbar\mathbf{k}$ is empty. Hence, $S_0(\mathbf{k}, \omega)$ is determined by the number of ways a particle can exchange energy with a hole with a total energy change $\hbar\omega = \epsilon_{\mathbf{p}} - \epsilon_{\mathbf{p}+\hbar\mathbf{k}}$. In this sense, $S_0(\mathbf{k}, \omega)$ can be thought of as the effective density of states for particle–hole excitations.

To evaluate the integral in Eq. (9.103) at $T = 0$, we shift the momentum in $f_{\mathbf{p}+\hbar\mathbf{k}}$ by $-\hbar\mathbf{k}$ so that the resultant integrand,

$$\begin{aligned} 2 \int \frac{d\mathbf{p}}{(2\pi\hbar)^2} (f_{\mathbf{p}} - f_{\mathbf{p}+\hbar\mathbf{k}}) \delta(\hbar\omega - \epsilon_{\mathbf{p}+\hbar\mathbf{k}} + \epsilon_{\mathbf{p}}) \\ = 2 \int \frac{d\mathbf{p}}{(2\pi\hbar)^2} f_{\mathbf{p}} [\delta(\hbar\omega - \epsilon_{\mathbf{p}+\hbar\mathbf{k}} + \epsilon_{\mathbf{p}}) - \delta(\hbar\omega - \epsilon_{\mathbf{p}} + \epsilon_{\mathbf{p}-\hbar\mathbf{k}})] \\ = 2 \int \frac{d\mathbf{p}}{(2\pi\hbar)^2} f_{\mathbf{p}} \left[\delta\left(\hbar\omega - \frac{(\hbar k)^2}{2m} - \frac{\mathbf{p} \cdot \hbar\mathbf{k}}{m}\right) - \delta\left(\hbar\omega + \frac{(\hbar k)^2}{2m} + \frac{\mathbf{p} \cdot \hbar\mathbf{k}}{m}\right) \right] \\ = I_{\omega} - I_{-\omega}, \end{aligned} \quad (9.104)$$

will contain a single Fermi distribution function. We now transform to spherical coordinates and obtain

$$\begin{aligned} I_{\omega} &= \frac{1}{\pi\hbar^2} \int_0^{p_F} p^2 dp \int_{-1}^1 d\mu \delta\left(\hbar\omega - \frac{(\hbar k)^2}{2m} - \frac{\hbar k p \mu}{m}\right) \\ &= \frac{m}{\pi k \hbar^3} \int_0^{p_F} p dp \Theta\left(1 - \left|\frac{m}{\hbar k p} \left(\hbar\omega - \frac{(\hbar k)^2}{2m}\right)\right|\right) \\ &= \frac{m}{\pi k \hbar^3} \int_{\frac{m}{\hbar k} \left|\hbar\omega - \frac{(\hbar k)^2}{2m}\right|}^{p_F} p dp \\ &= \frac{m}{2\pi k \hbar^3} \left[p_F^2 - \left(\frac{m}{\hbar k} \left(\hbar\omega - \frac{(\hbar k)^2}{2m}\right)\right)^2 \right] \Theta\left(p_F - \frac{m}{\hbar k} \left|\hbar\omega - \frac{(\hbar k)^2}{2m}\right|\right). \end{aligned} \quad (9.105)$$

Here $\Theta(x)$ is the Heaviside step function.

Subtracting the $\omega \rightarrow -\omega$ contribution, we find that

$$\begin{aligned} I_{\omega} - I_{-\omega} &= \frac{m}{2\pi k \hbar^3} \left[p_F^2 - \left(\frac{m}{\hbar k} \left(\hbar\omega - \frac{(\hbar k)^2}{2m}\right)\right)^2 \right] \Theta\left(p_F - \frac{m}{\hbar k} \left|\hbar\omega - \frac{(\hbar k)^2}{2m}\right|\right) \\ &\quad - \frac{m}{2\pi k \hbar^3} \left[p_F^2 - \left(\frac{m}{\hbar k} \left(\hbar\omega + \frac{(\hbar k)^2}{2m}\right)\right)^2 \right] \Theta\left(p_F - \frac{m}{\hbar k} \left|\hbar\omega + \frac{(\hbar k)^2}{2m}\right|\right) \end{aligned} \quad (9.106)$$

results. The Heaviside step function imposes the constraint

$$\frac{(\hbar k)^2}{2m} - \hbar k v_F < \hbar\omega < \frac{(\hbar k)^2}{2m} + \hbar k v_F \quad (9.107)$$

for the first term and

$$0 < \hbar\omega < \hbar k v_F - \frac{(\hbar k)^2}{2m} \quad (9.108)$$

for the second. For $\omega > 0$, the restrictions are represented graphically in Fig. 9.2 with $\omega_{\pm} = (\hbar k)^2/2m \pm \hbar k v_F$.

Because the range of ω for the first term in (9.106) exceeds that for the second, we consider three separate cases corresponding to (a) both terms contributing, (b) only the first, and (c) neither:

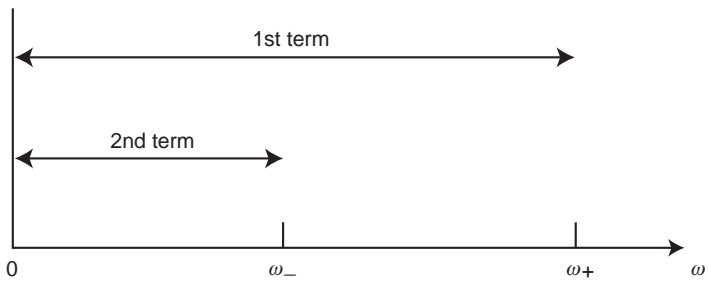


Fig. 9.2 Frequency range for the zero-temperature structure function.

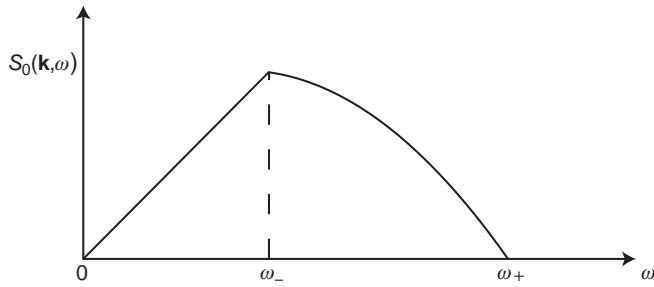


Fig. 9.3 Zero-temperature function as predicted from Eqs. (9.110–9.112).

Case (a) $0 < \hbar\omega < \hbar k v_F - (\hbar k)^2 / 2m$

$$I_\omega - I_{-\omega} = n_e S_0(\mathbf{k}, \omega) = \frac{m}{2\pi k \hbar^3} \left[p_F^2 - \left(\frac{m}{\hbar k} \left(\hbar\omega - \frac{(\hbar k)^2}{2m} \right) \right)^2 \right] - \left[p_F^2 - \left(\frac{m}{\hbar k} \left(\hbar\omega + \frac{(\hbar k)^2}{2m} \right) \right)^2 \right] \quad (9.109)$$

$$\Rightarrow n_e S_0(\mathbf{k}, \omega) = \frac{m^2 \omega}{\pi \hbar^2 k}; \quad (9.110)$$

Case (b) $\hbar k v_F - (\hbar k)^2 / 2m < \hbar\omega < \hbar k v_F + (\hbar k)^2 / 2m$

$$\Rightarrow n_e S_0(\mathbf{k}, \omega) = \frac{m}{2\pi k \hbar^3} \left[p_F^2 - \left(\frac{m}{\hbar k} \left(\hbar\omega - \frac{(\hbar k)^2}{2m} \right) \right)^2 \right]; \quad (9.111)$$

Case (c) $\hbar\omega > \frac{(\hbar k)^2}{2m} + \hbar k v_F$

$$\Rightarrow n_e S_0(\mathbf{k}, \omega) = 0. \quad (9.112)$$

Figure 9.3 contains the composite graph for all three cases.

At finite temperature, an explicit expression can also be obtained for $n_e S_0(\mathbf{k}, \omega)$. We simply need to compute I_ω and then let $\omega \rightarrow -\omega$. From Eq. (9.103) we have

that

$$\begin{aligned} I_\omega &= \frac{m}{\pi k \hbar^3} \int_{(1/2\hbar k)|2m\hbar\omega-k^2\hbar^2|}^{p_F} \frac{pd p}{e^{\beta(\epsilon_p-\mu)}+1} \\ &= \frac{m^2}{\beta\pi k \hbar^3} \int_a^{p_F} \left(\frac{\beta p}{m} \right) dp \frac{1}{e^{\beta(\epsilon_p-\mu)}+1} \\ &= \frac{m^2}{\beta\pi k \hbar^3} \int_{\beta a^2/2m}^{\beta p_F^2/2m} \frac{dx}{e^{x-\beta\mu}+1}. \end{aligned} \quad (9.113)$$

With the help of the integral

$$\int \frac{dx}{1+be^{cx}} = \frac{1}{c} [cx - \ln(1+be^{cx})], \quad (9.114)$$

which implies that

$$I_\omega = \frac{m^2}{\beta\pi \hbar^3 k} \left[x - \ln(1 + e^{x-\beta\mu}) \right]_{\beta a^2/2m}^{\beta p_F^2/2m}, \quad (9.115)$$

we obtain the final expression for the temperature-dependent structure:

$$\begin{aligned} (1 - e^{-\beta\hbar\omega})n_e S_0(\mathbf{k}, \omega) &= I_\omega - I_{-\omega} \\ &= \frac{m^2}{\beta\pi \hbar^3 k} \left[\beta\hbar\omega + \ln \left[\frac{1 + \exp \left(\beta \left(\frac{1}{2m} \left(\frac{m\omega}{k} - \frac{\hbar k}{2} \right)^2 - \mu \right) \right)}{1 + \exp \left(\beta \left(\frac{1}{2m} \left(\frac{m\omega}{k} + \frac{\hbar k}{2} \right)^2 - \mu \right) \right)} \right] \right]. \end{aligned}$$

In the limit of zero temperature, we obtain the expression previously derived at $T = 0$.

9.4.4 Dielectric function

We turn now to the calculation of the dielectric response function, $\varepsilon(\mathbf{k}, \omega) = 1 - 4\pi e^2 \chi_{sc}(\mathbf{k}, \omega)/k^2$, where the screening function at the RPA level,

$$\chi_{sc}(\mathbf{k}, \omega) = \lim_{\eta \rightarrow 0} \int_{-\infty}^{\infty} \frac{d\omega'}{2\pi\hbar} \frac{n_e S_0(\mathbf{k}, \omega')(1 - e^{-\beta\hbar\omega'})}{\omega - \omega' + i\eta}, \quad (9.116)$$

is a convolution of the structure function. In the limit that $\eta \rightarrow 0$, the screening function will acquire real and imaginary parts through

$$\lim_{\eta \rightarrow 0} \frac{1}{\omega - \omega' + i\eta} = P \frac{1}{\omega - \omega'} - i\pi \delta(\omega' - \omega). \quad (9.117)$$

The corresponding real and imaginary parts of the dielectric function are

$$\varepsilon_R(\mathbf{k}, \omega) = 1 - \frac{4\pi e^2}{k^2} P \int_{-\infty}^{\infty} \frac{d\omega'}{2\pi\hbar} \frac{n_e S_0(\mathbf{k}, \omega')(1 - e^{-\beta\hbar\omega'})}{(\omega - \omega')} \quad (9.118)$$

and

$$\varepsilon_I = \frac{2\pi e^2}{k^2 \hbar} n_e S_0(\mathbf{k}, \omega)(1 - e^{-\beta\hbar\omega}), \quad (9.119)$$

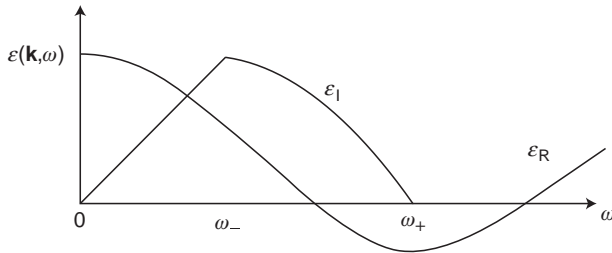


Fig. 9.4 Real (ε_R) and imaginary (ε_I) parts of the dielectric function at $T = 0$.

respectively. In the limit of zero temperature, $S_0(\mathbf{k}, \omega)$ is linear in frequency and hence ε_I is an odd function of frequency.

The real and imaginary parts of the dielectric function are related as a result of the causal nature of the response to the test charge. However, we have to be careful here. Only the part of the dielectric function that is directly related to χ_{sc} exhibits a causal response. That is, $\varepsilon_R - 1$,

$$\varepsilon_R - 1 = \frac{1}{\pi} P \int_{-\infty}^{\infty} \frac{d\omega' \varepsilon_I(\mathbf{k}, \omega')}{\omega' - \omega}, \quad (9.120)$$

and ε_I ,

$$\varepsilon_I = \frac{-P}{\pi} \int_{-\infty}^{\infty} \frac{d\omega' \varepsilon_R(\mathbf{k}, \omega') - 1}{\omega' - \omega}. \quad (9.121)$$

are related through the Kramers–Kronig relationships. Relationships of this sort are true in general for any complex function that is analytic in either the upper or lower half-planes as we saw in the Green function section of Chapter 7. In the context of linear response theory, they stem fundamentally from the causal nature of the response to the time-dependent perturbation.

Lindhard (L1954) has shown that at $T = 0$, ε_R is given by

$$\begin{aligned} \varepsilon_R = 1 + \frac{\kappa_{\text{TF}}^2}{k^2} & \left\{ \frac{1}{2} + \frac{k_F}{4k} \left[\left\{ 1 - \frac{(\omega - \hbar k^2/2m)^2}{k^2 v_F^2} \right\} \ln \left| \frac{\omega - kv_F - \hbar k^2/2m}{\omega + kv_F - \hbar k^2/2m} \right| \right. \right. \\ & \left. \left. + \left\{ 1 - \frac{(\omega + \hbar k^2/2m)^2}{k^2 v_F^2} \right\} \ln \left| \frac{\omega + kv_F + \hbar k^2/2m}{\omega - kv_F + \hbar k^2/2m} \right| \right] \right\}. \end{aligned} \quad (9.122)$$

Note first that this function is independent of the sign of ω . Hence, its parity is opposite that of ε_I . The general frequency dependence of the dielectric function is shown in Fig. 9.4. The large value of ε_R for $\omega \rightarrow 0$ indicates that the static screening is large. Another feature of the dielectric response function is that $\varepsilon(\mathbf{k}, \omega) = 0$ at the plasma frequency. The poles of $\varepsilon^{-1}(\mathbf{k}, \omega)$ occur at the excitation frequencies of the electron gas. Recall that this is precisely the result we derived previously in the context of a small k and large ω expansion for the dielectric function. When $\varepsilon(\mathbf{k}, \omega) = 0$, fluctuations in the electron density diverge as a result of the collective nature of plasma oscillations. At this point, the whole theory we have formulated breaks down, because we assumed that the electron density was a slowly varying function of the perturbing field. Let us investigate the behavior of $\varepsilon(\mathbf{k}, \omega)$

for small ω . Setting $\omega = 0$ in our expression for ε_R results in

$$\varepsilon(x, \omega = 0) = \varepsilon_R(x, \omega = 0) = 1 + \frac{\kappa_{\text{TF}}^2}{k^2} \left[\frac{1}{2} + \frac{1-x^2}{4x} \ln \left| \frac{1+x}{1-x} \right| \right], \quad (9.123)$$

the dielectric function in the static limit with $x = k/2k_F$. The $x = 0$ limit of $\varepsilon(x, \omega = 0) = 1 + \kappa_{\text{TF}}^2/k^2$ is exactly the Thomas–Fermi approximation to the screening of a positive charge at the origin.

As in the Thomas–Fermi case, we can construct the spatial potential that results from this kind of screening effect. To do so, we use the equation for the effective field $U_{\text{eff}}(k, \omega) = \varepsilon^{-1}(\mathbf{k}, \omega)U(\mathbf{k}, \omega)$. For an electron gas, $U(\mathbf{k}, \omega = 0) = 4\pi e^2/k^2$. If we use our expression for $\varepsilon(\mathbf{k}, \omega = 0)$, we find that

$$\phi_{\text{eff}}(\mathbf{r}) = 4\pi e \int \frac{d\mathbf{k}}{(2\pi)^3} \frac{e^{-i\mathbf{k}\cdot\mathbf{r}}}{k^2 + \kappa_{\text{TF}}^2 Q(\mathbf{k})} \quad (9.124)$$

is the spatial dependence of the effective potential, where $Q(\mathbf{k})$ denotes the Fourier transform of the bracketed term in Eq. (9.123). When $k = 2k_F$, $Q(\mathbf{k})$ is logarithmically divergent. This divergence yields a contribution to the electrostatic potential of the form

$$\phi_{\text{eff}} \sim \frac{\cos 2k_F r}{r^3} \quad (9.125)$$

as $r \rightarrow \infty$. This oscillatory behavior of the electrostatic potential is a consequence solely of screening and is known as a Friedel oscillation (F1954). At long distances, then, we find that the charge is not sufficiently screened to give rise to the $e^{-k_{\text{TF}}r}/r$ of Thomas–Fermi theory. Algebraic decay of the electrostatic potential signifies that a localized external charge affects the charge density everywhere in the electron gas. Kohn (K1959) was first to argue that this slow decay of the screened electrostatic potential arises from the sharpness of the Fermi surface. This effect shows up in the phonon spectrum of a metal for excitations with net momentum transfer $k > 2k_F$. He also pointed out with Luttinger (KL1965) that the negative contribution from ϕ_{eff} gives rise to a superconducting instability in an electron gas at $T = 0$. This observation is significant because it illustrates that, if left alone, an electron gas with bare repulsive interactions can become superconducting without the assistance of phonons.

9.5 Kubo formula: electrical conductivity

From the linear-response formalism, we can also derive the relationship developed by Kubo (K1957) which relates the conductivity tensor to the current. The general Hamiltonian for

the interaction of radiation with matter,

$$H = \frac{1}{2m} \sum_i \left(\mathbf{p}_i - \frac{e}{c} \mathbf{A}(\mathbf{r}_i, t) \right)^2 + H_{\text{other}}, \quad (9.126)$$

contains the vector potential $\mathbf{A}(\mathbf{r}_i, t)$ and H_{other} , which represents all the other terms that describe the many-body system. Assuming H_{other} is independent of the momentum of the particles, the velocity is given by

$$\mathbf{v}_i = \nabla_{\mathbf{p}_i} H = \frac{1}{m} \left(\mathbf{p}_i - \frac{e}{c} \mathbf{A}(\mathbf{r}_i) \right), \quad (9.127)$$

and as a consequence the total current,

$$\int d\mathbf{r} \mathbf{J}(\mathbf{r}, t) = \sum_i e \mathbf{v}_i = \sum_i \frac{e}{m} \left(\mathbf{p}_i - \frac{e}{c} \mathbf{A}(\mathbf{r}_i) \right), \quad (9.128)$$

has two distinct contributions. The paramagnetic term,

$$\mathbf{j}(\mathbf{r}, t) = \frac{e}{2m} \sum_i (\mathbf{p}_i \delta(\mathbf{r} - \mathbf{r}_i) + \delta(\mathbf{r} - \mathbf{r}_i) \mathbf{p}_i), \quad (9.129)$$

is typically written in symmetrized form, while the diamagnetic part,

$$\mathbf{j}_D(\mathbf{r}, t) = -\frac{e^2}{mcV} \sum_i \mathbf{A}(\mathbf{r}_i, t), \quad (9.130)$$

is directly proportional to the vector potential. We are ultimately interested in the thermal average of the current: $\langle \mathbf{J}(\mathbf{r}, t) \rangle_A$, where the subscript indicates the presence of the vector potential. Since we are only interested in linear response theory, we can approximate the diamagnetic term as

$$\mathbf{j}_D = -\frac{e^2 n_e}{mc} \mathbf{A}(\mathbf{r}, t) \quad (9.131)$$

and

$$\langle \mathbf{J}(\mathbf{r}, t) \rangle_A = \langle \mathbf{j}(\mathbf{r}, t) \rangle_A + \mathbf{j}_D. \quad (9.132)$$

To derive the conductivity in terms of the current, we note that all the terms involving the vector potential enter the Hamiltonian in the form

$$H' = -\frac{1}{c} \int d\mathbf{r} \mathbf{J}(\mathbf{r}, t) \cdot \mathbf{A}(\mathbf{r}, t) \quad (9.133)$$

In direct analogy with the density response, we apply Eq. (9.52) for the expectation value of the current to obtain

$$\langle J_\alpha(\mathbf{r}, t) \rangle_A = \frac{i}{\hbar} \int d\mathbf{r}' \int_{-\infty}^{\infty} dt' \theta(t - t') \langle [j_\beta(\mathbf{r}', t'), j_\alpha(\mathbf{r}, t)] \rangle A_\beta(\mathbf{r}', t') - \frac{n_e e^2}{m} A_\alpha(\mathbf{r}, t) \quad (9.134)$$

as our working expression for the average current. The current and the applied electric field obey a linear relationship,

$$\langle J_\alpha(\mathbf{r}, t) \rangle_A = \int d\mathbf{r}' \int_{-\infty}^{\infty} dt' \sigma_{\alpha\beta}(\mathbf{r} - \mathbf{r}', t - t') E_\beta(\mathbf{r}', t'), \quad (9.135)$$

the constant of proportionality being the conductivity tensor. Because $\mathbf{E}(\mathbf{r}, t) = -(1/c)\partial\mathbf{A}(\mathbf{r}, t)/\partial t$, the vector potential can be replaced with $c\mathbf{E}/i\omega$. Making this substitution into Eq. (9.134) allows us to identify

$$\begin{aligned} \sigma_{\alpha\beta}(\mathbf{q}, \omega) &= \frac{1}{\hbar\omega} \int_0^\infty dt e^{-i\omega t} \langle [j_\beta(-\mathbf{q}, 0), j_\alpha(\mathbf{q}, t)] \rangle - \frac{1}{i\omega} \frac{n_e e^2}{m} \delta_{\alpha\beta} \\ &= \frac{1}{i\hbar\omega} \chi_{j_\alpha j_\beta}(\mathbf{q}, \omega) - \frac{1}{i\omega} \frac{n_e e^2}{m} \delta_{\alpha\beta} \end{aligned} \quad (9.136)$$

as the electrical conductivity. Here $\chi_{j_\alpha j_\beta}(\mathbf{q}, \omega)$ is the current-current response function. The real part of the electrical conductivity is given by

$$\text{Re } \sigma_{\alpha\beta}(\mathbf{q}, \omega) = \frac{1}{\hbar\omega} \text{Im } \chi_{j_\alpha j_\beta}(\mathbf{q}, \omega). \quad (9.137)$$

Only in a superconductor does the diamagnetic term survive and the imaginary part of the conductivity diverges. Hence, in a metal, the first term on the right-hand side of Eq. (9.136) yields an imaginary contribution which cancels the diamagnetic response. The dc limit,

$$\sigma_{\alpha\beta}^{\text{dc}} = \lim_{\omega \rightarrow 0} \lim_{q \rightarrow 0} \left(\frac{1}{\hbar\omega} \text{Im } \chi_{j_\alpha j_\beta}(\mathbf{q}, \omega) \right), \quad (9.138)$$

is obtained by setting $q \rightarrow 0$ first so that a spatially uniform state results.

An alternative derivation of the conductivity can be formulated by writing the perturbation,

$$H' = -e \int \mathbf{r} \cdot \mathbf{E}(\mathbf{r}, t) d\mathbf{r}, \quad (9.139)$$

directly in terms of the applied electric field. With the help of Eq. (9.134) and the key result of linear response, Eq. (9.50), we identify

$$\sigma_{\alpha\beta}(t, t') = -\frac{e}{i\hbar} \langle [J_\alpha(t), r_\beta(t')] \rangle \quad (9.140)$$

as the conductivity. The current is simply,

$$\mathbf{J} = \frac{e}{m} \dot{\mathbf{r}}, \quad (9.141)$$

where $\dot{\mathbf{r}} = \mathbf{p} - e\mathbf{A}/c$. This form for the conductivity is particularly useful to derive what is known as the f-sum rule. We write first the Fourier transform,

$$\sigma_{\alpha\beta}(\omega) = \int_{-\infty}^{\infty} dt (t-t') e^{i\omega(t-t')} \sigma_{\alpha\beta}(t-t'), \quad (9.142)$$

of the conductivity. Consequently, the integrated weight of the conductivity

$$\begin{aligned} \frac{1}{2\pi} \int_{-\infty}^{\infty} \sigma_{\alpha\beta}(\omega) d\omega &= \frac{1}{2\pi} \int_{-\infty}^{\infty} d(t-t') 2\pi \delta(t-t') \sigma_{\alpha\beta}(t, t') \\ &= -\frac{1}{i\hbar} \frac{e^2}{m} \langle [r_\alpha, r_\beta] \rangle \\ &= \delta_{\alpha\beta} \frac{n_e e^2}{m} \end{aligned} \quad (9.143)$$

satisfies a sum rule. When we use this sum rule, we explicitly assume that the kinetic energy is given by the continuum form, $p^2/2m$, thereby giving rise to $\dot{\mathbf{r}} = \mathbf{p} - e\mathbf{A}/c$.

9.6 Stopping power of a plasma

When an electron is injected into a plasma with some incoming energy, it is expected to be slowed as a result of the Coulomb interactions with the electrons in the plasma. On these grounds, Bethe argued that the rate of energy loss of the injected electron should be proportional to $|V_{\text{int}}(\mathbf{p})|^2$, where V_{int} is the Coulomb interaction between the plasma and the electron. For a Coulomb potential, $V_{\text{int}} \sim p^{-2}$, as shown previously. Summing over all incoming momentum values, we find that the energy loss is given by

$$\frac{dE}{dt} \propto \int d\mathbf{p} p |V_{\text{int}}(\mathbf{p})|^2 \propto \int_0^{p_F} \frac{dp}{p}. \quad (9.144)$$

This integral is logarithmically divergent at the lower limit. As a result, this simple account produces a divergent energy loss, which is clearly incorrect. We see immediately that, for a screened interaction, the divergence at the lower limit would vanish, thereby making dE/dt finite. This is the primary failure of the Bethe approach. We will now formulate this problem in a rigorous way that gets around the Bethe divergence by including the effects of screening.

The physical problem at hand is that of a metal in some initial state $|i\rangle$ and an electron with initial momentum \mathbf{p} impinging on a metal. Upon interacting with the metal, the electron will have a new momentum, $\mathbf{p} - \hbar\mathbf{k}$, and the metal will be in some new state $|f\rangle$. We assume the states of the metal form a complete orthonormal set $\langle n|m \rangle = \delta_{nm}$. At the level of Fermi's golden rule, the transition rate between the initial and final states is

$$W_{\mathbf{p}, \mathbf{p}-\hbar\mathbf{k}} = \frac{2\pi}{\hbar} \sum_f |\langle f, \mathbf{p} - \hbar\mathbf{k} | V_{\text{int}} | i, \mathbf{p} \rangle|^2 \delta \left(\frac{\mathbf{p}^2}{2m} + E_i - \frac{(\mathbf{p} - \hbar\mathbf{k})^2}{2m} - E_f \right)$$

where E_i and E_f are the total energies of the states $|i\rangle$ and $|f\rangle$, respectively. The interaction energy,

$$V_{\text{int}}(\mathbf{r}) = \int d\mathbf{r}' [n(\mathbf{r}') - n_e] \frac{e^2}{|\mathbf{r}' - \mathbf{r}|}, \quad (9.145)$$

includes the ion as well as the electron Coulomb energy. The initial state of the electron is a plane wave of the form $|\mathbf{p}\rangle = e^{i\mathbf{p}\cdot\mathbf{r}/\hbar}/\sqrt{V}$ and the final electron state is $|\mathbf{p} - \hbar\mathbf{k}\rangle =$

$e^{i(\mathbf{p}-\hbar\mathbf{k})\cdot\mathbf{r}/\hbar}/\sqrt{V}$. With these states, we rewrite the matrix element in (9.145) as

$$\begin{aligned}\langle f, \mathbf{p} - \hbar\mathbf{k} | V_{\text{int}} | i, \mathbf{p} \rangle &= \int d\mathbf{r} d\mathbf{r}' \langle f | n(\mathbf{r}') - n_e | i \rangle \frac{e^{i\mathbf{k}\cdot\mathbf{r}}}{V} \frac{e^2}{|\mathbf{r} - \mathbf{r}'|} \\ &= \frac{4\pi e^2}{k^2} \int \frac{d\mathbf{r}}{V} e^{i\mathbf{k}\cdot\mathbf{r}} \langle f | n(\mathbf{r}) | i \rangle.\end{aligned}\quad (9.146)$$

Using the integral representation of the δ -function,

$$2\pi\hbar\delta(\hbar\omega + E_i - E_f) = \int_{-\infty}^{\infty} e^{i(\hbar\omega + E_i - E_f)t/\hbar} dt,$$

we recast the transition rate as

$$\begin{aligned}W_{\mathbf{p}, \mathbf{p}-\hbar\mathbf{k}} &= \left(\frac{4\pi e^2}{V\hbar k^2} \right)^2 \int_{-\infty}^{\infty} e^{i(\hbar\omega + E_i - E_f)t/\hbar} dt \sum_{f \neq i} |\langle f | \int d\mathbf{r} n(\mathbf{r}) e^{i\mathbf{k}\cdot\mathbf{r}} | i \rangle|^2 \\ &= \left(\frac{4\pi e^2}{V\hbar k^2} \right)^2 \int_{-\infty}^{\infty} dt e^{i\omega t} \sum_{f \neq i} \langle f | n(\mathbf{k}) | i \rangle \langle i | e^{iE_i \frac{t}{\hbar}} n(\mathbf{k}) e^{-iE_f \frac{t}{\hbar}} | f \rangle\end{aligned}\quad (9.147)$$

with $\hbar\omega = \epsilon_{\mathbf{p}} - \epsilon_{\mathbf{p}-\hbar\mathbf{k}}$. In the interaction representation,

$$\hat{n}(\mathbf{k}, t) = e^{iH_0 \frac{t}{\hbar}} n(\mathbf{k}) e^{-iH_0 \frac{t}{\hbar}}. \quad (9.148)$$

Consequently,

$$W_{\mathbf{p}, \mathbf{p}-\hbar\mathbf{k}} = \left(\frac{4\pi e^2}{V\hbar k^2} \right)^2 \int_{-\infty}^{\infty} e^{i\omega t} dt \sum_{f \neq i} \langle i | \hat{n}(\mathbf{k}, t) | f \rangle \langle f | n(\mathbf{k}) | i \rangle, \quad (9.149)$$

which can be simplified to

$$W_{\mathbf{p}, \mathbf{p}-\hbar\mathbf{k}} = \left(\frac{4\pi e^2}{\hbar k^2} \right)^2 \frac{n_e}{V} \left[S(\mathbf{k}, \omega) - \frac{1}{V} 2\pi \delta(\omega) n_e \right] \quad (9.150)$$

using the definition of the structure function and the completeness relation for the metal states, $\sum |f\rangle\langle f| = 1$. As expected, it is the dynamic structure factor that determines the response of our system to the incident electron. Screening effects are implicitly included in $S(\mathbf{k}, \omega)$. The Bethe result arises from the zero-frequency part of the transition rate.

We are primarily interested in the rate of energy loss to the plasma. This is determined by summing over all energy differences, $\epsilon_{\mathbf{p}} - \epsilon_{\mathbf{p}-\hbar\mathbf{k}}$, weighted by the transition rate, W :

$$\begin{aligned}\frac{dE}{dt} &= - \sum_{\mathbf{k}} (\epsilon_{\mathbf{p}} - \epsilon_{\mathbf{p}-\hbar\mathbf{k}}) W_{\mathbf{p}, \mathbf{p}-\hbar\mathbf{k}} \\ &= - \frac{\hbar n_e}{V} \sum_{\mathbf{k}} \omega \left(\frac{4\pi e^2}{\hbar k^2} \right)^2 S(\mathbf{k}, \omega) \\ &= -n_e \int \frac{d\mathbf{k}}{(2\pi)^3} \left(\frac{4\pi e^2}{\hbar k^2} \right)^2 \int_{-\infty}^{\infty} \omega d\omega S(\mathbf{k}, \omega) \delta(\hbar\omega - \epsilon_{\mathbf{p}} + \epsilon_{\mathbf{p}-\hbar\mathbf{k}}).\end{aligned}\quad (9.151)$$

To evaluate this quantity, we switch to polar coordinates and perform first the θ integral for the angle between \mathbf{p} and $\mathbf{p} - \hbar\mathbf{k}$:

$$\begin{aligned} 2\pi \int_0^\pi d\theta \sin \theta \delta(\hbar\omega - \epsilon_{\mathbf{p}} + \epsilon_{\mathbf{p}-\hbar\mathbf{k}}) &= 2\pi \int_{-1}^1 dx \delta\left(\hbar\omega + \frac{\hbar^2 k^2}{2m} - \frac{p\hbar k x}{m}\right) \\ &= \frac{2\pi m}{p\hbar k} \Theta(kv_p - |\omega + \hbar k^2/2m|). \end{aligned} \quad (9.152)$$

With this result, the rate of energy loss to the plasma simplifies to

$$\frac{1}{v_p} \frac{dE}{dt} = \frac{-4e^4 n_e}{\hbar^2 v_p^2} \int_0^\infty \frac{dk}{k^3} \int_{-kv_p - \frac{\hbar k^2}{2m}}^{kv_p - \frac{\hbar k^2}{2m}} d\omega \omega S(\mathbf{k}, \omega), \quad (9.153)$$

where v_p is the incoming velocity of the incident electron.

Complete stoppage of the electron by the plasma is most likely to occur if the electron gas acts collectively, that is, if plasma oscillations dominate. Thus, the electron gas obtains maximum stopping power if $|\omega| = \omega_p$, the plasma frequency. We seek then an expression for the structure function in the limit of high frequency. From the definition of the dielectric function (see Eqs. (9.75) and (9.93)), we express the imaginary part of $\varepsilon(\mathbf{k}, \omega)^{-1}$,

$$\text{Im } \varepsilon^{-1} = -\frac{2\pi e^2 n_e}{\hbar k^2} (1 - e^{-\beta \hbar \omega}) S(\mathbf{k}, \omega), \quad (9.154)$$

in terms of the structure function and use the high-frequency expansion for the dielectric function,

$$\varepsilon(\omega) \sim \lim_{\eta \rightarrow 0} \left(1 - \frac{\omega_p^2}{(\omega + i\eta)^2} \right). \quad (9.155)$$

In this limit, the imaginary part of ε^{-1} ,

$$\begin{aligned} \text{Im } \varepsilon^{-1}(\omega) &= \lim_{\eta \rightarrow 0} \text{Im} \left[\frac{\omega^2}{(\omega + i\eta)^2 - \omega_p^2} \right] \\ &= -\frac{\pi \omega_p}{2} [\delta(\omega - \omega_p) - \delta(\omega + \omega_p)], \end{aligned} \quad (9.156)$$

is a sum of two δ -functions at $\pm\omega_p$. With the aid of Eq. (9.154), we see immediately that in the $k \rightarrow 0$ limit,

$$S(\mathbf{k}, \omega) = \frac{\hbar\pi k^2}{m} \frac{[\delta(\omega - \omega_p) - \delta(\omega + \omega_p)]}{1 - e^{-\beta \hbar \omega}}. \quad (9.157)$$

The ω -integral in Eq. (9.153) is now straightforward:

$$\int_{\omega_\ell}^{\omega_u} d\omega \omega S(\mathbf{k}, \omega) = \frac{\hbar\pi k^2}{m} (1 + g_p) \Theta(\omega_\ell < \omega_p < \omega_u) - \hbar \frac{\pi k^2}{m} g_p \Theta(\omega_\ell < -\omega_p < \omega_u), \quad (9.158)$$

where $\omega_\ell = -kv_p - \hbar k^2/2m$ and $\omega_u = kv_p - \hbar k^2/2m$. In evaluating this integral, we introduced $g_p = (e^{\beta \hbar \omega_p} - 1)^{-1}$, which determines the number of plasmons thermally

excited at a temperature T . The energy loss is transformed to

$$\frac{1}{v_p} \frac{dE}{dt} = - \left(\frac{\omega_p e}{\hbar v_p} \right)^2 \int \frac{dk}{k} (1 + g_p) \Theta \left(\hbar k v_p - \frac{(\hbar k)^2}{2m} - \hbar \omega_p > 0 \right) - g_p \Theta \left(\frac{(\hbar k)^2}{2m} - \hbar k v_p < \hbar \omega_p < \frac{(\hbar k)^2}{2m} + \hbar k v_p \right). \quad (9.159)$$

The first term represents the energy loss upon the creation of a plasmon and the second the energy transferred to the electron by a plasmon thermally excited in the medium. As $T \rightarrow 0$, the probability that a plasmon will be thermally excited vanishes. As a result, plasmons can be excited only by an impinging electron. In this limit, the energy loss takes on the simple form:

$$\begin{aligned} \frac{1}{v_p} \frac{dE}{dt} &= - \left(\frac{\omega_p e}{\hbar v_p} \right)^2 \int \frac{dk}{k} \Theta \left(\hbar k v_p - \frac{\hbar^2 k^2}{2m} - \hbar \omega_p > 0 \right) \\ &= - \left(\frac{\omega_p e}{\hbar v_p} \right)^2 \ln \frac{k_+}{k_-}, \end{aligned} \quad (9.160)$$

where k_{\pm} are the solutions to

$$\hbar^2 k^2 - 2m\hbar k v_p + 2m\hbar \omega_p = 0, \quad (9.161)$$

or equivalently,

$$\hbar k_{\pm} = p \pm \sqrt{p^2 - 2m\hbar \omega_p}. \quad (9.162)$$

For the incident electron to excite a plasmon, $\frac{p^2}{2m} > \omega_p$. If we expand k_{\pm} in this limit, we find that

$$k_{\pm} = p \pm (p - m\hbar \omega_p/p) = \begin{cases} 2p - m\hbar \omega_p/p \\ m\hbar \omega_p/p \end{cases}. \quad (9.163)$$

We expect an absence of collective plasmon oscillations if $k \lesssim a^{-1}$, where a is the interparticle spacing. We should then cut off k_+ at $2p_F$. As a consequence,

$$\frac{dE}{dt} = - \frac{\omega_p^2 e^2}{v_p \hbar^2} \ln \frac{2p_F}{m\hbar \omega_p}, \quad (9.164)$$

which is completely well behaved and finite, unlike the Bethe result.

Summary

Electron gases exhibit a myriad of collective long-wavelength phenomena, such as plasma oscillations and screening, that alter significantly the independent electron picture of an electron gas. In the context of screening, an electron gas acts collectively to decrease the

bare interaction from $V_{\mathbf{q}}$ to

$$V_{\text{eff}} = \frac{V_{\mathbf{q}}}{\varepsilon(q, \omega)}, \quad (9.165)$$

where $\varepsilon(q, \omega)$ is the dielectric function. At metallic densities, the RPA is sufficient to describe the screening effects. In this approximation, uncorrelated particle–hole scattering to all orders of perturbation theory are summed to obtain the polarization function, or polarization bubble. Exchange effects are not included in the RPA. In sufficiently dilute electron systems, $r_s > 3$, where the Coulomb energy is comparable to or greater than the electron kinetic energy, a theory beyond the RPA is necessary. Methods such as the local-field approach (STLS1968), which attempt to model the correlation hole around each electron, have proven quite successful in this context (see Problem 9.5).

Problems

- 9.1 Redo the Thomas–Fermi screening problem for a $+Q$ charge located at the origin in dimensions $d = 1$ and $d = 2$. Assume the unscreened potential is Coulombic. Calculate explicitly the Thomas–Fermi screening length in $d = 1$ and $d = 2$. Show explicitly that in $d = 2$, the Thomas–Fermi screening length is independent of density and given by $1/\kappa_{\text{TF}} = a_0/2$.
- 9.2 In the Thomas–Fermi treatment of screening, evaluate explicitly the term proportional to U_{eff}^2 in Eq. (9.7). Under what condition can this term be ignored?
- 9.3 Use the method developed in the plasmon section to show that plasmons in $d = 2$ are described by a dispersion relationship that scales as $\omega_p \propto \sqrt{k}$.
- 9.4 Derive Eqs. (9.31) and use these results to derive Eq. (9.33).
- 9.5 Redo Bethe’s argument in $d = 1$ and $d = 2$ for the stopping power of a plasma. Why is the result finite?
- 9.6 In the limit of small wavevectors, the dielectric function takes on the form (N1964)

$$\lim_{q \rightarrow 0} \varepsilon(q, 0) = 1 + \frac{\kappa_{\text{TF}}^2}{q^2} \frac{\alpha}{\alpha_{\text{F}}}, \quad (9.166)$$

where α is the compressibility of the electron gas and κ_{F} is the compressibility of the free system. For the free system, $\alpha_{\text{F}} = 3/(n_e \epsilon_{\text{F}})$. Show that $\alpha/\alpha_{\text{F}} = 1$ in the RPA. Hubbard (H1957) showed that exchange hole effects can be included by introducing the factor $G(q) = q^2/2(q^2 + k_{\text{F}}^2)$ into the dielectric function as

$$\varepsilon(q, \omega) = 1 - \frac{v_{\mathbf{q}} \chi_{nn}^0}{1 + v_{\mathbf{q}} \chi_{nn}^0 G(q)}. \quad (9.167)$$

Using Eqs. (9.166) and (9.167), derive an expression for the compressibility in the Hubbard approximation. Plot α as a function of r_s . Determine the value of r_s at which α changes sign. Physically, what does a negative compressibility, $\alpha < 0$, mean?

References

- [BP1953] D. Bohm and D. Pines, *Phys. Rev.* **92**, 609 (1953).
- [F1928] E. Fermi, *Z. Phys.* **48**, 73 (1928).
- [F1954] H. Friedel, *Adv. Phys.* **3**, 446 (1954).
- [H1957] J. Hubbard, *Proc. R. Soc. London Ser. A* **243**, 336 (1957).
- [K1959] W. Kohn, *Phys. Rev. Lett.* **2**, 393 (1959).
- [KL1965] W. Kohn and J. H. Luttinger, *Phys. Rev. Lett.* **15**, 524 (1965).
- [K1957] R. Kubo, *J. Phys. Soc. Japan* **12**, 570 (1957).
- [L1954] J. Lindhard, *Kgl. Danske Videnskab. Selskab, Mat-fys. Medd.* **28**, 8 (1954).
- [N1964] P. Nozières, *Interacting Fermi Systems* (Benjamin, Reading, MA., 1964), p. 287.
- [P1963] D. Pines, *Elementary Excitations in Solids* (Benjamin, Reading, MA., 1963).
- [STLS1968] K. S. Singwi, M. P. Tosi, R. H. Rand, and A. Sjölander, *Phys. Rev. Lett.* **176**, 589 (1968).
- [T1927] L. H. Thomas, *Proc. Camb. Phil. Soc.* **23**, 542 (1927).

Let us look closely at the effective equations of motion for the Fourier components of the electron density in the limit where plasma oscillations occur. We showed in the previous chapter that, in the limit $\omega_p^2 \gg k^2 v_F^2$, the Fourier components obey the equations of motion

$$\ddot{\rho}_k + \omega_p^2 \rho_k = 0, \quad (10.1)$$

i.e. those of a harmonic oscillator. However, harmonic excitations obey Bose statistics. This suggests that plasma oscillations in some way represent bosonic excitations of the interacting electron gas. Equivalently, plasma oscillations can be thought of as harmonic excitations of the electrons in the gas. That this state of affairs holds profound consequences for the electron gas was pointed out initially by Tomonaga (T1950) who gave an explicit prescription for constructing the sound wave spectrum in a dense Fermi system. Three years later, Bohm and Pines (BP1953) showed that there is a natural connection between the sound wave (Bose) spectrum and the random phase approximation. Since then, the equivalence between long-wavelength excitations in a dense Fermi system and a collection of bosons has proven to be of fundamental importance in solid state physics as well as relativistic field theories. In this chapter, we focus on how a collection of interacting electrons in 1d obeying standard anticommutation relations can be described by an equivalent set of boson modes. The problem of constructing such a boson field theory for a collection of fermions is known as *bosonization*. In this context, we will first linearize the dispersion of the 1d Hubbard (H1964) model and, in so doing, obtain the Luttinger (L1960) liquid which we will then solve using bosonization. Luttinger liquids form the general basis for analyzing the properties of interacting electrons in 1d insofar as such systems are dominated by short-range Coulomb interactions. We will derive one of the most dramatic predictions of Luttinger liquid theory, *spin–charge separation* – the phenomenon that the spin and charge degrees of freedom of the electron decouple and propagate at different speeds.

10.1 Luttinger liquid

Before we introduce the Luttinger (L1960) model, let us review the form of the excitation spectra for non-interacting electrons. Electrons on a 1d lattice can be described by a

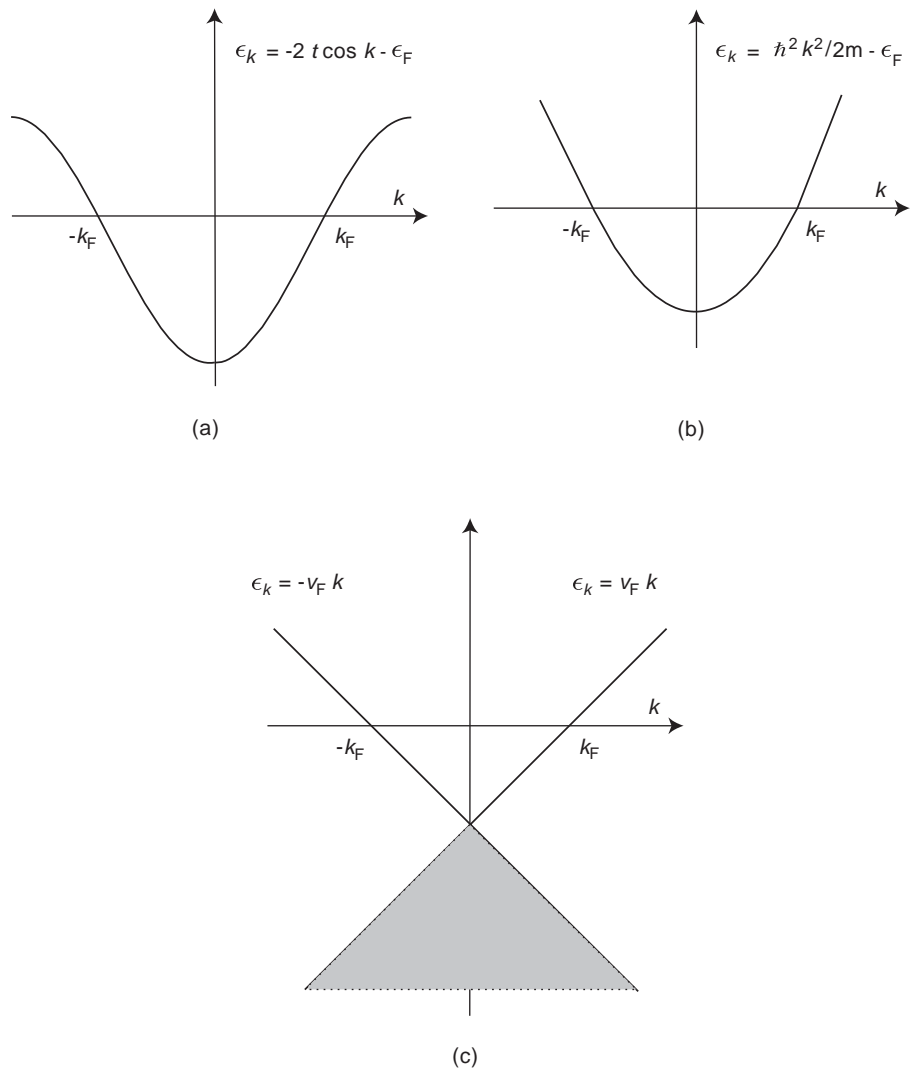


Fig. 10.1 (a) Energy bands in the lattice and (b) free-space models for non-interacting electrons in 1d ($\epsilon_F = -\mu$).
 (c) Linearized energy band in the vicinity of the Fermi level. The shaded region represents the filling of the negative energy states, the Dirac sea.

tight-binding model given by the Hamiltonian

$$H_F = -t \sum_{n\sigma} [\Psi_{n\sigma}^\dagger \Psi_{n+1\sigma} + \text{h.c.}] + \mu \sum_{n\sigma} \Psi_{n\sigma}^\dagger \Psi_{n\sigma}, \quad (10.2)$$

where t is the hopping integral between adjacent lattice sites with lattice constant a . The operator $\Psi_{n\sigma}$ annihilates an electron on site n with spin σ , μ is the chemical potential for the ordered system and $\rho_{n\sigma} = \Psi_{n\sigma}^\dagger \Psi_{n\sigma}$ is the electron density at the n th lattice site. The model described by H_F has a symmetric energy band, $\epsilon_k = -2t \cos ka + \mu$. Electrons in free space have a parabolic dispersion $\epsilon_k = \hbar^2 k^2 / 2m + \mu$. Both of these bands are plotted in Fig. 10.1.

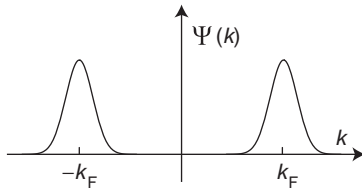


Fig. 10.2 Fourier components of the fermion fields. In the bosonization procedure, we retain only the momentum components of the fermion fields at $\pm k_F$.

In the ground state of the free system, all states with momentum $|k| \leq k_F$ are doubly occupied (e.g., $\mu = 0$ corresponds to $k_F = \frac{\pi}{2a}$). At any filling of the single-particle states, the dispersion relation in the vicinity of the Fermi level can be linearized, resulting in the spectrum shown in Fig. 10.1(c). The Luttinger liquid model $H_L = H_F + H_U$ can be derived from the 1d Hubbard model which includes an interaction term

$$H_U = U \sum_n \rho_{n\uparrow} \rho_{n\downarrow}, \quad (10.3)$$

which is the cost of doubly occupying any lattice site with electrons of opposite spin and U is the on-site Coulomb energy. In Chapter 7 on the Anderson impurity, we defined the on-site repulsion in terms of the on-site atomic orbitals. The goal is to recast H_L in an equivalent bosonic description in the linear approximation for the single-particle spectrum in the vicinity of the Fermi points, $\pm k_F$.

We now demonstrate how the dispersion relationship can be linearized for a 1d Fermi surface. We can accomplish this formally by writing the site amplitudes for each spin in the vicinity of $\pm k_F$ as a linear combination

$$\Psi_{n\sigma} = e^{ik_F n a} \Psi_{n\sigma+} + e^{-ik_F n a} \Psi_{n\sigma-} = R_\sigma(n) + L_\sigma(n) \quad (10.4)$$

of left-moving, $\Psi_{n\sigma-}$, and right-moving, $\Psi_{n\sigma+}$, fermion fields. The left- and right-moving fields are assumed to be slowly varying on the scale of the lattice constant. Further, they have mean momentum centered narrowly around $\pm k_F$. Consequently, we expand the fermion field for site $n + 1$ in terms of the amplitude for site $x = na$,

$$\Psi_{n+1\sigma\pm} = \Psi_{n\sigma\pm} + a\partial_x \Psi_{n\sigma\pm} + \dots, \quad (10.5)$$

and retain only the linear term. Substituting this expression along with Eq. (10.4) into the kinetic energy part of the Hamiltonian will result in cross-terms involving oscillating Fermi factors of the form $e^{\pm 2ik_F n a}$. The contribution of such terms is determined by the overlap of the left- and right-moving fields. However, this overlap is zero, because we are assuming the momentum spread of the \pm fields is narrow, as depicted in Fig. 10.2. Hence, the only

terms that survive in the linearized Hamiltonian,

$$H_F = -\hbar v_F \sum_{\sigma} \int_{-L/2}^{L/2} \left[\Psi_{\sigma+}^{\dagger}(x) (i\partial_x) \Psi_{\sigma+}(x) dx + \Psi_{\sigma-}^{\dagger}(x) (-i\partial_x) \Psi_{\sigma-}(x) dx \right], \quad (10.6)$$

are those involving products of fields with the same parity. The Fermi velocity is $\hbar v_F = 2at \sin k_F a$. In deriving Eq. (10.6), we transformed to the continuum representation. This limit is somewhat tricky. The continuum and lattice fields are related as follows: $\Psi_{n\sigma\pm} = \sqrt{a}\Psi_{\sigma\pm}(x)$. Hence, $\Psi_{\sigma\pm}(x)$ has units of $1/\sqrt{L}$. The second term in Eq. (10.6) is obtained by integrating by parts the Hermitian conjugate of the first term. To see that Eq. (10.6) is equivalent to a linearized fermion theory, substitute the momentum space representation of $\Psi_{\sigma\pm}(x)$,

$$\Psi_{\sigma\pm}(x) = \int_{-\infty}^{\infty} \frac{dk}{2\pi} e^{ikx} \Psi_{\sigma\pm}(k), \quad (10.7)$$

into Eq. (10.6). The resultant dispersion relationship is explicitly of the form $E_{\pm}(k) = \pm \hbar v_F k$, where the energy of left- and right-movers is distinct. Inclusion of negative energy states in the Luttinger model is the key difference between it and the Tomonaga model.

The negative energy states introduce, however, a subtle complexity into the Luttinger model. In the ground state, the negative momentum branch of the right-moving states and the positive momentum branch of the left-moving states are occupied. This is illustrated in Fig. 10.1(c) and can be thought of as the filling of the negative-energy Dirac sea. The analogy here is between the positron states in Dirac theory and the negative-energy single-particle states in the Luttinger model. However, the Hamiltonian, Eq. (10.6), is expressed in terms of creation operators for right- and left-moving fields $\Psi_{\sigma\pm}^{\dagger}$ that act on the space of zero-particle states. In this space, the interaction term between the electrons vanishes. Put another way, our Hamiltonian lacks a ground state energy. Luttinger (L1960) alleviated this problem by performing a canonical transformation of the form

$$\Psi_{\sigma+}(k) \rightarrow \begin{cases} b_{k\sigma}, & k \geq 0, \\ c_{k\sigma}^{\dagger}, & k < 0, \end{cases} \quad (10.8)$$

$$\Psi_{\sigma-}(k) \rightarrow \begin{cases} b_{k\sigma}, & k < 0, \\ c_{k\sigma}^{\dagger}, & k \geq 0, \end{cases} \quad (10.9)$$

to the left- and right-moving fields which effectively filled the negative-energy Dirac sea. The $b_{k\sigma}$ s and $c_{k\sigma}$ s obey the usual anticommutation relations. The action of the operator $\Psi_{\sigma+}(k)$ (which annihilates a right-moving electron of momentum k) on the filled Fermi sea corresponds to the annihilation of an electron for $k > 0$ or the creation of a hole for $k < 0$. A consequence of this transformation is that the elementary excitations in momentum state k are pair excitations consisting of a particle and a hole. Further, it is linear combinations of these excitations that now describe the collective or plasma excitations of the electron gas. Luttinger, however, was not aware that this canonical transformation affected also the value of commutators involving the electron density. This is the profound change that the canonical transformation introduces into the Luttinger model. Mattis and Lieb (ML1965) were the first to point this out and correctly solve the Luttinger model.

To illustrate the changes this switch of basis introduces, we rewrite the Hamiltonian in terms of the new particle-hole operators. The transformed free Hamiltonian,

$$H_F = \hbar v_F \int_{-\infty}^{\infty} |p| dp [b_p^\dagger b_p + c_p^\dagger c_p] + W, \quad (10.10)$$

contains the constant

$$W = -\hbar v_F \int_0^{\infty} p dp + \hbar v_F \int_{-\infty}^0 p dp, \quad (10.11)$$

which represents the infinite energy of the filled Dirac sea. This result could have been obtained by normal-ordering the operators in the original Hamiltonian. Consider an arbitrary reference state $|\Omega\rangle$ and an operator \hat{A} which can be written as a product of creation and annihilation operators. Normal-ordering the creation and annihilation operators in \hat{A} means moving all the creation operators to the left and the annihilation operators to the right. As a consequence, infinities arising from commutators are removed. We denote normal-ordering by the symbol $: \hat{A} :$. Consequently, $: \hat{A} : |\Omega\rangle = 0$ and any average of $: \hat{A} :$ with respect to the ground state $|\Omega\rangle$ identically vanishes, $\langle \Omega | : \hat{A} : |\Omega\rangle = 0$. Hence, the transformation in Eq. (10.8) is equivalent to normal-ordering the left-right moving field operators with respect to the filled Dirac sea. In so doing, one can extract the infinite energy of the filled negative energy states.

Let us look also at the momentum space representation of the density of right- and left-movers:

$$\begin{aligned} n_{\sigma\pm}(x) &= \Psi_{\sigma\pm}^\dagger(x) \Psi_{\sigma\pm}(x) \\ &= \int_{-\infty}^{\infty} \frac{dp}{2\pi} \frac{dq}{2\pi} \Psi_{\sigma\pm}^\dagger(p) \Psi_{\sigma\pm}(q) e^{i(q-p)x} \end{aligned} \quad (10.12)$$

with

$$n_{\sigma\pm}(q) = \int_{-\infty}^{\infty} dx e^{-iqx} n_{\sigma\pm}(x). \quad (10.13)$$

Substituting the transformed form for the left- and right-movers into Eq. (10.12) and taking the Fourier transform (according to Eq. (10.13)), we find that the form of $n_{\sigma\pm}(k)$,

$$\begin{aligned} n_{\sigma+}(k > 0) &= \int_0^{\infty} \frac{dq}{2\pi} [b_q^\dagger b_{k+q} + c_{-k-q} c_{-q}^\dagger + c_{-q} b_{k-q} \theta(k-q)], \\ n_{\sigma+}(k < 0) &= \int_0^{\infty} \frac{dq}{2\pi} [b_{k-q}^\dagger b_q + c_{-q} c_{k-q}^\dagger + b_q^\dagger c_{k+q}^\dagger \theta(-k-q)], \\ n_{\sigma-}(k > 0) &= \int_0^{\infty} \frac{dq}{2\pi} [b_{-k-q}^\dagger b_{-q} + c_q c_{k+q}^\dagger + b_{-q}^\dagger c_{k-q}^\dagger \theta(k-q)], \\ n_{\sigma-}(k < 0) &= \int_0^{\infty} \frac{dq}{2\pi} [b_{-q}^\dagger b_{k-q} + c_{q-k} c_q^\dagger + c_q b_{k+q} \theta(-k-q)], \end{aligned}$$

depends on the sign of the momentum. The form derived here for the momentum components of the density is equivalent to the form given by Mattis and Lieb (ML1965).

The difference arises in the definition of the Fourier transform of the density defined in Eq. (10.13). The dependence of the density on the sign of the momentum arises from the pair nature of the fundamental excitations.

It is also from this complexity that differences arise when certain commutators are calculated in the original left-right and the particle-hole basis. Consider the current operators for the total electron density

$$j_0^\sigma = \Psi_{\sigma+}^\dagger(x)\Psi_{\sigma+}(x) + \Psi_{\sigma-}^\dagger(x)\Psi_{\sigma-}(x) \quad (10.14)$$

and difference

$$j_1^\sigma = \hbar v_F (\Psi_{\sigma+}^\dagger(x)\Psi_{\sigma+}(x) - \Psi_{\sigma-}^\dagger(x)\Psi_{\sigma-}(x)) \quad (10.15)$$

of the electron densities. In the original left-right basis, commutators involving j_0^σ and j_1^σ identically vanish. However, if the new particle-hole basis is used, Eq. (10.8), we find that the equal-time commutation relations between the components of the current,

$$[j_0^\sigma(x), j_1^\sigma(y)] = -\frac{i\hbar v_F}{\pi} \partial_x \delta(x-y), \quad (10.16)$$

$$[j_0^\sigma(x), j_0^\sigma(y)] = [j_1^\sigma(x), j_1^\sigma(y)] = 0, \quad (10.17)$$

obey Bose statistics. The right-hand side of the first commutator is a c-number. This discrepancy is a bit surprising but not totally unexpected if we write the density in first quantized form,

$$n_{\sigma\pm}(k) = \int_{-\frac{L}{2}}^{\frac{L}{2}} dx e^{-ikx}. \quad (10.18)$$

These components commute trivially. However, this is not the physically relevant form for the density operators when the Dirac sea is filled. Schwinger (S1959) anticipated this apparent paradox that arises when the very existence of a ground state forces certain commutators to be non-zero, which would vanish trivially otherwise in the first quantized language. The full consequences for the Luttinger model were worked out by Mattis and Lieb (ML1965).

10.2 Bosonization of Luttinger model

Before solving the full Luttinger model, it is instructive to consider a simple example which epitomizes some of the features of the bosonization procedure. Consider a spinless version of H_F with fields Ψ_n . We also introduce standard Pauli spin operators $\sigma_n^{x,y,z}$ at every lattice site n ; these operators commute at different sites and are thus bosons. These

spins are not physically related to the electron spin; they simply provide a convenient representation of the bosonic operators. The bosonization of H_F can be performed by taking

$$\Psi_n = \frac{1}{2} \prod_{m < n} \sigma_m^z (\sigma_n^x + i\sigma_n^y). \quad (10.19)$$

The anticommutation relations obeyed by the Ψ_n s are enforced by the chain of bosonic operators (a so-called *Jordan–Wigner string*). The corresponding bosonic Hamiltonian can be obtained from Eq. (10.19) and H_F yielding

$$H_B = \sum_n -\frac{t}{2} (\sigma_n^x \sigma_{n+1}^x + \sigma_n^y \sigma_{n+1}^y) - \frac{\mu}{2} \sigma_n^z. \quad (10.20)$$

The equivalence between the fermionic and bosonic descriptions manifests itself in a number of ways and anticipates several analogous results for the Luttinger model. The equations of motion obeyed by Ψ_n and its bosonic counterpart are equivalent. Crucially, correlators obtained in either representation are the same (cf. Eq. (10.47) and Eqs. (10.51), (10.52)).

We turn now to the construction of an equivalent boson theory of the free part of the Luttinger model. To this end, we focus on the Heisenberg equations of motion,

$$-i\partial_t j_0^\sigma(x) = [H_F, j_0^\sigma(x)]. \quad (10.21)$$

It turns out that the value of the commutator in Eq. (10.21) is independent of the filling in the Dirac sea. That is, this commutator, unlike those involving the components of the density, is invariant to normal ordering. The commutators of the densities for left- and right-movers with the free Hamiltonian,

$$\begin{aligned} [H_F, n_{\sigma+}(\pm k)] &= \mp kn_{\sigma+}(\pm k), \\ [H_F, n_{\sigma-}(\pm k)] &= \pm kn_{\sigma-}(\pm k), \end{aligned} \quad (10.22)$$

depend on the sign of the momentum. Note the sign change relative to that of Mattis and Lieb. Here again, this difference arises from our definition of the Fourier transform, Eq. (10.13). Consequently,

$$\begin{aligned} \left[H_F, \int_{-\infty}^{\infty} dq e^{iqx} j_0^\sigma(q) \right] &= \hbar v_F \int_0^{\infty} dq e^{iqx} q (n_{\sigma-}(q) - n_{\sigma+}(q)) \\ &\quad + \hbar v_F \int_0^{\infty} dq e^{-iqx} q (n_{\sigma+}(-q) - n_{\sigma-}(-q)) \\ &= \hbar v_F \int_{-\infty}^{\infty} dq e^{iqx} q (n_{\sigma-}(q) - n_{\sigma+}(q)) \\ &= i\partial_x j_1^\sigma \end{aligned} \quad (10.23)$$

or, equivalently,

$$\partial_t j_0^\sigma = -\partial_x j_1^\sigma. \quad (10.24)$$

If we introduce the notation $t \rightarrow x_0$ and $x \rightarrow x_1$ with $x \equiv (x_0, x_1)$, we can rewrite the Heisenberg equation of motion as a conservation equation:

$$\partial_\mu j_\mu^\sigma = 0. \quad (10.25)$$

Hence, the total fermion current, normal-ordered with respect to the full Dirac sea, is conserved.

Conservation of the fermion current suggests that if we define a boson field $\Phi_\sigma(x)$ with conjugate momentum $\Pi_\sigma(x)$ such that

$$j_0^\sigma(x) = \frac{1}{\sqrt{\pi}} \partial_x \Phi_\sigma(x) \quad (10.26)$$

and

$$j_1^\sigma(x) = -\frac{1}{\sqrt{\pi}} \partial_t \Phi_\sigma(x) = -\frac{1}{\sqrt{\pi}} \Pi_\sigma(x), \quad (10.27)$$

the Heisenberg equation of motion,

$$\partial_t [\partial_x \Phi_\sigma(x)] = \partial_x \Pi_\sigma(x), \quad (10.28)$$

will resemble an equation of motion for two conjugate fields. To satisfy the Bose statistics of the currents,

$$[\Phi_\sigma(x), \Pi_{\sigma'}(y)] = i\delta_{\sigma\sigma'}\delta(x-y). \quad (10.29)$$

In the Bose basis, the free Hamiltonian density,

$$H_F = \frac{\hbar v_F}{2} \sum_\sigma \int dx [\Pi_\sigma^2(x) + (\partial_x \Phi_\sigma(x))^2], \quad (10.30)$$

yields an equation of motion that is equivalent to the Heisenberg evolution equation for the densities in the fermion basis. Hence, we have reformulated our fermion theory in terms of an equivalent boson theory. We emphasize that the boson theory has been constructed by an analogy based on the equations of motion. Hence, Eq. (10.30) is not a unique choice for the equivalent boson Hamiltonian density. By the construction of an equivalent boson theory, we imply no more than an equivalence between the equations of motion in the two accounts.

We can take the bosonization procedure a step further and construct explicitly the mapping between the fermion fields $\Psi_{\sigma\pm}(x)$ and the new boson field, $\Phi_\sigma(x)$. Such a mapping is problematic because the bosonic fields describe particle-hole excitations which involve two Fermi operators. Processes in which the electron number is changed are thus forbidden. For the moment, we set this problem aside and develop a mapping involving the boson

fields that preserves the anticommutation relations of the fermion fields. The key idea in bosonization is to associate (not equate) the left- and right-moving fermion fields with boson fields of the form

$$\begin{aligned}\Psi_{\sigma\pm}(x) &= \frac{1}{\sqrt{2\pi a}} e^{-i\sqrt{\pi}[\int_{-\infty}^x \Pi_\sigma(x') dx' \mp \Phi_\sigma(x)]} \\ &= \frac{1}{\sqrt{2\pi a}} e^{\pm i\sqrt{\pi}\Phi_{\sigma\pm}(x)},\end{aligned}\quad (10.31)$$

where

$$\Phi_{\sigma\pm}(x) = \Phi_\sigma(x) \mp \int_{-\infty}^x \Pi_\sigma(x') dx'. \quad (10.32)$$

It is crucial that the operator equivalence, Eq. (10.31), be understood strictly in the normal-ordered sense. For example, if Eq. (10.31) were naively substituted into the continuum version of the Hamiltonian, Eq. (10.6), the resultant boson Hamiltonian would correspond to twice Eq. (10.30). Such an equation would yield the incorrect equations of motion. This should underscore our disclaimer that the fermion fields should be associated, not equated, with the boson field, Eq. (10.31). True equalities arise in the two theories when average values of physical observables are computed. The physical motivation for Eq. (10.31) is as follows. The amplitude that a particle is at x is $\Psi_{\sigma\pm}(x)$. Classically, the translation of a particle from x to $x+a$ is effected by the displacement operator, $e^{a\hat{d}_x}$. Quantum mechanically, this quantity becomes the exponential of the momentum operator. Hence, $\Psi_{\sigma\pm}(x)$ must be proportional to the exponential of the momentum operator. We call this quantity $\Pi_\sigma(x)$. However, if this were the only dependence, then $\Psi_{\sigma\pm}(x)$ would commute with itself. The exponential is the simplest form that ensures the fermion anticommutation relations is Eq. (10.31).

To solve the problem that the bosonized form of the fermion fields cannot be used, in their current form, to connect electronic states that differ in particle number, we introduce ladder operators (KS1996; H1981) which change the particle number by integer values. Such ladder operators (traditionally known as “Klein factors”) must lie outside the space of the bosonic operators because bosons are necessarily composites of even numbers of fermions. No combination of bosonic operators can ever create a single electron. Let N_σ represent the deviation of the electron occupation number from the ground state value. Following the notation of Kotliar and Si (KS1996), we introduce the operator F_σ (F_σ^\dagger) which lowers (raises) N_σ by one. The F_σ s commute with all the boson fields in $\Psi_{\sigma\pm}$ for $q \neq 0$. Hence, F_σ and N_σ represent the zero-momentum modes of the electron gas. The $q \neq 0$ modes are particle-hole excitations. The additional commutation relations of the F_σ s are

$$\begin{aligned}F_\sigma^\dagger F_\sigma &= F_\sigma F_\sigma^\dagger = 1, \\ F_\sigma^\dagger F_{\sigma'} &= -F_{\sigma'} F_\sigma^\dagger, \\ F_\sigma F_{\sigma'} &= -F_{\sigma'} F_\sigma.\end{aligned}\quad (10.33)$$

The physical states of the electron are now captured by

$$\tilde{\Psi}_{\sigma\pm}^\dagger(x) = F_\sigma^\dagger e^{\frac{2\pi i x N_\sigma}{L}} \Psi_{\sigma\pm}^\dagger. \quad (10.34)$$

For processes which do not conserve particle number, “Klein factors” must be included ([KS1996](#); [H1981](#); [VDS1998](#)). However, as the problems on which we focus conserve particle number, we will omit the “Klein factors” as they cannot change the physics. Nonetheless, they are part of the complete story of bosonization.

We now turn to the bosonization of the interaction terms. In the continuum limit, the Hubbard interaction can be written as

$$H_U = aU \int_{-L/2}^{L/2} dx (R_\uparrow^\dagger(x) + L_\uparrow^\dagger(x))(R_\uparrow(x) + L_\uparrow(x))(R_\downarrow^\dagger(x) + L_\downarrow^\dagger(x))(R_\downarrow(x) + L_\downarrow(x)), \quad (10.35)$$

where $R_\sigma(x)(L_\sigma(x)) = \Psi_{n\sigma\pm} e^{\pm ik_F x} / \sqrt{a}$. To implement the bosonization scheme, we must normal-order the operators in the Hubbard interaction. As in the free system, normal-ordering of the operators in the Hubbard interaction,

$$H_U = : H_U : + Q, \quad (10.36)$$

will generate a constant term (Q) that is again infinite. In this case, the infinite term is associated with the infinite charge in the negative energy states. The important point here is that the infinite term is constant. Hence, it can be ignored.

If we now expand Eq. (10.35) keeping only the non-oscillatory terms, we find that the Hubbard interaction reduces to

$$\begin{aligned} H_U \rightarrow H_{\text{int}} = aU \int_{-L/2}^{L/2} dx & \left[(: \Psi_{\uparrow+}^\dagger \Psi_{\uparrow+} : + : \Psi_{\uparrow-}^\dagger \Psi_{\uparrow-} :) (: \Psi_{\downarrow+}^\dagger \Psi_{\downarrow+} : + : \Psi_{\downarrow-}^\dagger \Psi_{\downarrow-} :) \right. \\ & \left. + [: \Psi_{\uparrow+}^\dagger \Psi_{\uparrow-} : : \Psi_{\downarrow-}^\dagger \Psi_{\downarrow+} : + \text{h.c.}] \right]. \end{aligned} \quad (10.37)$$

Diagrams illustrating the two types of scattering processes retained in H_{int} are shown in Fig. 10.3. In Fig. 10.3(a), the net momentum transfer across each vertex is zero. Hence, the first term in Eq. (10.37) corresponds to forward scattering of the electrons. In the second term (see Fig. 10.3(b)), particles are converted from left (right) into right (left) movers. Hence, this term corresponds to a backscattering process. We have dropped the terms which have a prefactor of $e^{\pm i4k_F}$. At half-filling, $k_F = \pi/2$, and the exponential prefactor reduces to unity. The $4k_F$ term is referred to as an Umklapp process in which two right (left) movers are destroyed and two left (right) movers are created. We will come back to these terms later.

To complete the bosonization scheme, we need a rule for writing products of fermion operators in Eq. (10.37) in terms of the Bose fields. To proceed, we use the Baker–Hausdorff identity,

$$e^A e^B = e^{A+B} e^{\frac{1}{2}[A,B]}. \quad (10.38)$$

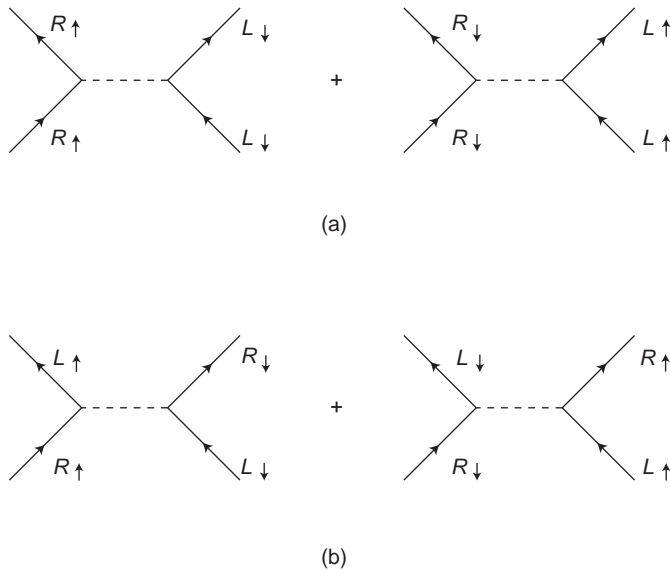


Fig. 10.3 (a) Forward scattering process corresponding to the first term in Eq. (10.37). $R(L)$ represent right- and left-moving fields. At each vertex of a forward scattering term the momentum change is zero. The dotted line indicates the Coulomb interaction aU . (b) Back scattering corresponds to the second term in Eq. (10.37). The magnitude of the momentum change at each vertex is $|2k_F|$.

Using the commutation relation, Eq. (10.29), we reduce the operator product

$$\Psi_{\sigma+}^\dagger \Psi_{\sigma-} = \frac{1}{2\pi a} e^{-i\sqrt{4\pi}\Phi_\sigma(x)} e^{-\pi i/2} = -i \frac{1}{2\pi a} e^{-i\sqrt{4\pi}\Phi_\sigma(x)} \quad (10.39)$$

in the backscattering terms to a simple exponential of the Bose field. The factor of $-i$ arises from the commutator

$$\begin{aligned} [\Phi_{\sigma+}(x), \Phi_{\sigma-}(y)] &= \left[\Phi_\sigma(x), \int_{-\infty}^y \Pi(x') dx' \right] + \left[\Phi_\sigma(y), \int_{-\infty}^x \Pi_\sigma(x') dx' \right] \\ &= i \int_{-\infty}^y dx' \delta(x-x') + i \int_{-\infty}^x dx' \delta(y-x') \\ &= i. \end{aligned} \quad (10.40)$$

Further simplification requires additional identities. The fermion field $\Psi_{\sigma\pm}$ is an exponential of two fields which obey Bose statistics. In analogy with the harmonic oscillator, we partition the exponential into a sum of creation and annihilation operator parts. Consequently, the $\Psi_{\sigma\pm}$ fields are of the form

$$\Psi_{\sigma\pm} = e^A = e^{A^+ + A^-}, \quad (10.41)$$

where $A^+(A^-)$ represents the creation (annihilation) operator part of A . Using the Baker-Hausdorff operator identity, Eq. (10.38), we find that

$$e^A = e^{A^+} e^{A^-} e^{-\frac{1}{2}[A^+, A^-]}. \quad (10.42)$$

Because the normal-ordering places all the creation operators to the left and the annihilation operators to the right,

$$: e^A : \equiv e^{A^+} e^{A^-} = e^A e^{\frac{1}{2}[A^+, A^-]} \quad (10.43)$$

is the corresponding normal-ordered form of the $\Psi_{\sigma\pm}$ fields. This expression is of utmost utility in the bosonization procedure. For example, it is common in the literature (M1975) to write the left-moving and right-moving fermion fields in the normal-ordered form. The normal-ordered form differs from Eq. (10.31) by the phase factor in Eq. (10.43). In the context of the backscattering terms, we can use Eq. (10.43) to evaluate a product of two normal-ordered operators. Upon using Eq. (10.43) twice, we find that

$$: e^A :: e^B := e^{[A^-, B^+]} : e^{A+B} :, \quad (10.44)$$

where $[A^\pm, B^\pm] = 0$. In general $[A^\pm, B^\mp]$ is a c-number. For the case that $\Phi_{\sigma+} = A$ and $\Phi_{\sigma-} = B$, the commutator in the exponential factor of Eq. (10.44) has been evaluated by Mattis (M1974) and Mandelstam (M1975). Its value is unity. As a consequence,

$$: \Psi_{\uparrow+}^\dagger \Psi_{\uparrow+} :: \Psi_{\downarrow-}^\dagger \Psi_{\downarrow+} : + \text{h.c.} = \frac{1}{2\pi^2 a^2} : \cos(\sqrt{4\pi}(\Phi_\uparrow(x) - \Phi_\downarrow(x))) : . \quad (10.45)$$

The forward scattering terms are slightly more difficult because operator products of the form $\Psi_{\uparrow+}^\dagger(x + \epsilon)\Psi_{\uparrow+}(x - \epsilon)$ are not well-defined in the limit that $\epsilon \rightarrow 0$. Naively, one might expect this quantity to equal unity. This is not so. We can evaluate this product by considering the fermion correlator,

$$\begin{aligned} \langle \Psi_{\sigma+}^\dagger(x) \Psi_{\sigma+}(0) \rangle &= \int_{-\infty}^{\infty} \frac{dk}{2\pi} \int_{-\infty}^{\infty} \frac{dq}{2\pi} e^{-iqx} \langle \Psi_{\sigma+}^\dagger(q) \Psi_{\sigma+}(k) \rangle \\ &= \int_0^{\infty} \frac{dk}{2\pi} e^{ikx}. \end{aligned} \quad (10.46)$$

That is, the double integrals contract to $2\pi\delta(k - q)$ with $k < 0$. The latter constraint arises because right-movers exist only in the negative momentum states in the ground state. Equation (10.46) is not well behaved for large momentum but it can be regularized by introducing the exponential factor e^{-ak} , where the lattice constant acts as a short-distance cutoff. We find then that

$$\langle \Psi_{\sigma+}^\dagger(x) \Psi_{\sigma+}(0) \rangle = \frac{1}{2\pi} \frac{1}{a - ix}. \quad (10.47)$$

For left-movers, the corresponding correlator is the complex conjugate of Eq. (10.47).

If we use the bosonized form of these field operators to evaluate the density correlator, we must obtain the same result. To proceed, we simplify a product of the form $e^A e^B$ using Eqs. (10.38) and (10.44),

$$e^A e^B = :e^{A+B} : e^{[A^-, B^+] + \frac{[A^-, A^+] + [B^-, B^+]}{2}}. \quad (10.48)$$

In general, the commutators appearing in Eq. (10.48) are c-numbers. Further, because $\langle (A^\pm)^2 \rangle = \langle A^+ A^- \rangle = 0$, it follows immediately that $\langle [A^-, A^+] \rangle = \langle A^2 \rangle$. Consequently,

$$\langle e^A e^B \rangle = \langle :e^{A+B} : \rangle e^{\langle AB + \frac{A^2 + B^2}{2} \rangle}. \quad (10.49)$$

The average value of the exponential of any normal-ordered operator is unity, $\langle :e^A : \rangle = 1$. Hence, we obtain the all-important rule for evaluating a correlation function,

$$\langle e^A e^B \rangle = e^{\langle AB + \frac{A^2 + B^2}{2} \rangle}, \quad (10.50)$$

from which it follows that

$$\langle \Psi_{\sigma+}^\dagger(x) \Psi_{\sigma+}(0) \rangle = \frac{1}{2\pi a} e^{\pi \langle \Phi_{\sigma+}(x) \Phi_{\sigma+}(0) - \Phi_{\sigma+}^2(0) \rangle}. \quad (10.51)$$

By analogy with Eq. (10.47), we find that

$$\begin{aligned} \langle \Psi_{\sigma+}^\dagger(x) \Psi_{\sigma+}(0) \rangle &= \frac{1}{2\pi a} e^{\pi G_+(x)} \\ &= \frac{1}{2\pi a} \frac{a}{a - ix} \end{aligned} \quad (10.52)$$

or, equivalently,

$$\langle e^{-i\eta\Phi_{\sigma\pm}} e^{i\eta\Phi_{\sigma\pm}} \rangle = \left(\frac{a}{a \mp ix} \right)^{\eta^2/\pi} \equiv e^{\eta^2 G_\pm}. \quad (10.53)$$

We now have the tools to evaluate the original fermion product:

$$\begin{aligned} : \Psi_{\sigma\pm}^\dagger(x) \Psi_{\sigma\pm}(x) : &= \lim_{\epsilon \rightarrow 0} \frac{1}{2\pi a} : e^{\mp i\sqrt{\pi}(\Phi_{\sigma\pm}(x+\epsilon) \pm \Phi_{\sigma\pm}(x-\epsilon))} : e^{\pi G_\pm} \\ &= \lim_{\epsilon \rightarrow 0} \frac{1}{2\pi a} : 1 \mp 2i\sqrt{\pi} \partial_x \Phi_{\sigma\pm} \epsilon + \dots : \left(\pm \frac{ia}{2\epsilon \pm ia} \right) \\ &= \lim_{\epsilon \rightarrow 0} \frac{\pm i}{2\pi(2\epsilon \pm ia)} + : \frac{1}{2\sqrt{\pi}} \partial_x \Phi_{\sigma\pm} + O(\epsilon) :. \end{aligned} \quad (10.54)$$

For arbitrarily small a , the first term in this expression is infinite, a reflection of the infinite number of right- and left-movers in the negative energy states. Normal-ordering the operators in the charge density results in the removal of the divergent charge density in

the ground state. As a consequence, the normal-ordered charge density

$$:\Psi_{\sigma\pm}^\dagger(x)\Psi_{\sigma\pm}(x):=\frac{1}{2\sqrt{\pi}}\partial_x\Phi_{\sigma\pm}(x) \quad (10.55)$$

has a well-defined interpretation in the boson basis. Noting that

$$:\Psi_{\sigma+}^\dagger(x)\Psi_{\sigma+}(x):+:\Psi_{\sigma-}^\dagger(x)\Psi_{\sigma-}(x):=\frac{1}{\sqrt{\pi}}:\partial_x\Phi_\sigma(x): \quad (10.56)$$

and using Eq. (10.45), we simplify the interaction terms to

$$H_{\text{int}}=aU\int dx\sum_\sigma\left[\frac{:\partial_x\Phi_\uparrow\partial_x\Phi_\downarrow:}{\pi}+\frac{1}{2\pi^2a^2}:\cos(\sqrt{4\pi}(\Phi_\uparrow(x)-\Phi_\downarrow(x))):\right]. \quad (10.57)$$

The utility of this expression and the bosonization procedure is made clear by introducing the charge, Φ_c , and spin, Φ_s , boson fields,

$$\Phi_c=\frac{\Phi_\uparrow+\Phi_\downarrow}{\sqrt{2}}, \quad \Phi_s=\frac{\Phi_\uparrow-\Phi_\downarrow}{\sqrt{2}}. \quad (10.58)$$

The new charge and spin fields obey the usual Bose commutation relations, as they are simply sums and differences of Bose fields. If we substitute these expressions into the bosonized pieces of the Hamiltonian, we obtain a Hamiltonian, $H_B=H_c+H_s$, in which the charge,

$$H_c=\frac{\hbar v_F}{2}\int dx\left[\Pi_c^2+g_c^2(\partial_x\Phi_c)^2\right], \quad (10.59)$$

and spin degrees of freedom,

$$H_s=\frac{\hbar v_F}{2}\int dx\left[\Pi_s^2+g_s^2(\partial_x\Phi_s)^2\right]+\frac{U}{2\pi^2a}\int dx:\cos\sqrt{8\pi}\Phi_s:, \quad (10.60)$$

are completely decoupled. The coupling constants

$$g_c^2=1+\frac{aU}{2\pi\hbar v_F} \quad (10.61)$$

and

$$g_s^2=1-\frac{aU}{2\pi\hbar v_F}, \quad (10.62)$$

which are now a function of the interactions, can be used to define new velocities for the spin and charge degrees of freedom. Let $v_F^c=v_F g_c$ and $v_F^s=v_F g_s$. To see that the spin and charge sectors are now moving with different velocities, we consider the transformation $\Phi_\nu\sqrt{g_\nu}\rightarrow\tilde{\Phi}_\nu$ and $\Pi_\nu 1/\sqrt{g_\nu}\rightarrow\tilde{\Pi}_\nu$, where $\nu=c, s$. This transformation leaves intact the

Bose commutation relations, Eq. (10.40). In terms of the rescaled fields, the charge degrees of freedom

$$H_c = \frac{\hbar v_F^c}{2} \int dx [\tilde{\Pi}_c^2 + (\partial_x \tilde{\Phi}_c)^2] \quad (10.63)$$

resemble a collection of non-interacting fermions but with a new Fermi velocity v_F^c that increases as the strength of the on-site repulsions increases. In the spin sector,

$$H_s = \frac{\hbar v_F^s}{2} \int dx [\tilde{\Pi}_s^2 + (\partial_x \tilde{\Phi}_s)^2] + \frac{U}{2\pi^2 a} \int dx : \cos \sqrt{8\pi/g_s} \tilde{\Phi}_s : \quad (10.64)$$

and the new velocity v_F^s of the spins lags behind that of the charge degrees of freedom for repulsive interactions between the electrons. Hence, the spin and charge degrees of freedom move with completely different velocities. Another difference between the spin and charge sectors is the $: \cos \tilde{\Phi}_s :$ term. In the bosonized language, this factor is equivalent to a mass term in the original fermion Hamiltonian. Physically, the mass term represents an energy gap. However, only in the case of attractive Coulomb interactions (S1990), in which case electrons form bound antiferromagnetic pairs, does a spin gap arise, thereby heightening the difference between the spin and charge sectors in 1d. As a result, for 1d interacting electron liquids, the electron falls apart into distinct spin and charge quasi-particles (see (Y2005) for claims of experimental observation). We can think of an electron then as a composite particle made out of two distinct entities. We will refer to the entity that carries the charge, the holon (or eon) and the spin part, the spinon. Holons (or eons) and spinons obey Bose statistics. The emergence of holon and spinon excitations in 1d represents a marked departure from Fermi liquid behavior. In Fermi liquid theory, there is a one-to-one correspondence between the excited states of the interacting and non-interacting systems. Spin and charge separation in 1d fundamentally destroy this correspondence because now the electron gives rise to two excitations rather than the single excitation indicative of Fermi liquid theory.

10.3 Pair binding: can electrons do it alone?

It is well known from the early argument of Kohn and Luttinger (see Chapter 9) that any Fermi system has a superconducting instability (albeit at an ultra-low temperature of the order of 10^{-5} K) when electronic vertex corrections are considered. Since their work, there have been numerous arguments presented for purely electronic mechanisms of superconductivity. Rather than present a specific mechanism, we focus instead on a general way of understanding pair binding from purely electronic considerations by appealing to the holon–spinon construct. Let Φ_n be the energy of an electronic system containing n extra electrons. The pair binding question is as follows: do two isolated systems each containing

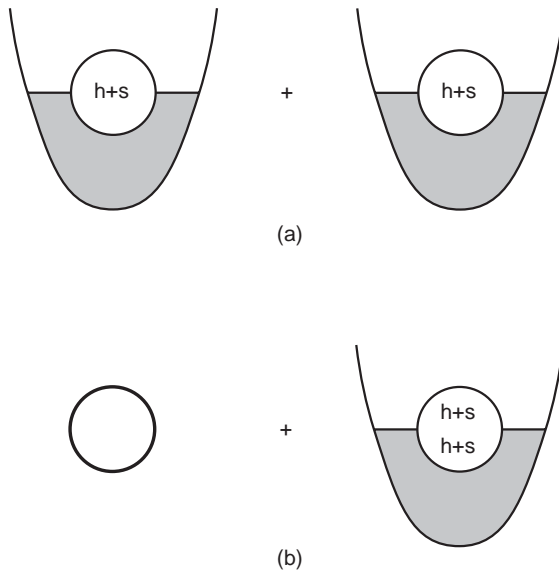


Fig. 10.4 The two electronic systems which are used to compute the pair-binding energy for $n = 1$. Pair binding occurs if the energy of (b) is lower than the energy of (a). Whether or not this state of affairs obtains for purely electronic reasons depends on the relative magnitudes of the holon–holon, spinon–spinon, and holon–spinon interaction strengths.

$n + 1$ and $n - 1$ extra electrons have lower total energy than two separate systems with n extra electrons? The energy difference

$$E_{\text{pair}}^{(n)} = 2\Phi_n - \Phi_{n+1} - \Phi_{n-1} \quad (10.65)$$

is the pair binding energy. If $E_{\text{pair}}^{(n)} > 0$, pairing is expected, as a net attraction favors disproportionation into $n + 1$ and $n - 1$ states. To illustrate that pair binding can result from repulsive interactions alone, we adopt the spin–charge dichotomy of the Luttinger liquid. For simplicity, we consider the case in which $n = 1$, as illustrated in Fig. 10.4. To compute the pair-binding energy, we must evaluate $2\Phi_1 - \Phi_2 - \Phi_0$. We set $\Phi_0 = 0$ and let E_h and E_s be the energy of the holon and spinon, respectively. Also, we define V_{hh} and V_{hs} to be the holon–holon and holon–spinon interaction. The relevant physical system is illustrated in Fig. 10.4. Within an additive constant, the energy of $2\Phi_1$,

$$2\Phi_1 = 2(E_h + E_s + V_{hs}), \quad (10.66)$$

is simply the sum of the energy of two independent electronic systems with an extra electron added, and that of the doubly-occupied state is

$$\Phi_2 = 2E_h + V_{hh} + 4V_{hs} + V_{ss} + 2E_s. \quad (10.67)$$

The factor of 4 arises from the two holon–spinon interactions for each electron and the cross-interaction between the two electrons. We have assumed that the spinon energy in the singlet is zero. The energy difference between these states is

$$E_{\text{pair}}^{(1)} = -(2V_{\text{hs}} + V_{\text{hh}} + V_{\text{ss}}). \quad (10.68)$$

Now, for an electron to be stable, $V_{\text{hs}} < 0$. Also Coulomb's law dictates that $V_{\text{hh}} > 0$. The spinon–spinon interaction energy then is the crucial quantity that determines whether or not $E_{\text{pair}}^{(1)} \leq 0$. In some situations, V_{ss} is of the right magnitude, such that $E_{\text{pair}}^{(1)} > 0$. In this case, pair binding can occur from purely repulsive electron interactions.

10.4 Excitation spectrum

If we compare Eq. (10.63) with the standard Hamiltonian for a harmonic oscillator, $H = P^2 + Q^2$, where P and Q are the canonical momentum and position, we find an equivalence between the bosonized charge sector and a collection of harmonic oscillators. As advertised, charge excitations in the Luttinger model are the usual bosonic modes, known more commonly as plasma excitations. What is the appropriate density of states for these excitations? It might be suspected that they are governed by the standard Bose–Einstein distribution. However, this is not the case. Charge excitations in a Luttinger liquid (L1960) have a vanishing density of states at the Fermi level of the form $|k - k_F|^\alpha$, which is due entirely to the correlations among the electrons. The power law is given by $\alpha = (g_c + g_c^{-1})/2 - 1$. Hence, rather than the smooth density of states indicative of Fermi liquids, Luttinger liquids develop a soft gap at the Fermi level for any $U \neq 0$. The source of this effect can be traced to the renormalization of v_F^c by g_c in the bosonized form of the electron gas.

We establish this result by calculating the total charge correlator

$$G(x) = \left\langle \sum_{\sigma} \left(\Psi_{\sigma+}(x) \Psi_{\sigma+}^{\dagger}(0) + \Psi_{\sigma-}(x) \Psi_{\sigma-}^{\dagger}(0) \right) \right\rangle. \quad (10.69)$$

To compact the notation, we define

$$\Theta_{\sigma}(x) = \int_{-\infty}^x \Pi_{\sigma}(x') dx'. \quad (10.70)$$

For each spin component, we make the substitution $\Phi_{\uparrow(\downarrow)} = (\Phi_c \pm \Phi_s)/\sqrt{2}$ and $\Theta_{\uparrow(\downarrow)} = (\Theta_c \pm \Theta_s)/\sqrt{2}$, where the upper sign applies to up spins and the lower sign to down spins. In the absence of a magnetic field, $n_{\uparrow}(x) = n_{\downarrow}(x)$. As a result, all averages linear in either Φ_s or Π_s vanish identically. We simplify the average in Eq. (10.69) even further by using the transformed fields $\tilde{\Phi}_v(x)$ and $\tilde{\Pi}_v(x)$. The average in Eq. (10.69) will now be over the

ground state of the non-interacting bosonized system characterized by the renormalized Fermi velocities, v_F^c and v_F^s . Consequently, we can use the standard rules for simplifying the average of a product of exponentials of boson operators. Using the third form for the Baker–Hausdorff identity (Eq. 10.48), we find that the correlator of the total electron density simplifies to

$$G(x) = \frac{1}{\pi a} e^{i \text{phase}} e^{\frac{\pi}{2} \sum_{v=c,s} (g_v^{-1} a_v + g_v b_v)}, \quad (10.71)$$

where

$$a_v = \langle \tilde{\Phi}_v(x) \tilde{\Phi}_v(0) - \tilde{\Phi}_v^2(0) \rangle \quad (10.72)$$

and

$$b_v = \langle \tilde{\Theta}_v(x) \tilde{\Theta}_v(0) - \tilde{\Theta}_v^2(0) \rangle. \quad (10.73)$$

The phase is determined by the cross-terms. For both charge and spin fields, the cross-terms are of the form $\langle \tilde{\Phi}_v(0) \tilde{\Theta}_v(0) + \tilde{\Theta}_v(0) \tilde{\Phi}_v(0) \rangle - \langle \tilde{\Phi}_v(x) \tilde{\Theta}_v(0) + \tilde{\Theta}_v(x) \tilde{\Phi}_v(0) \rangle$. This term is identically zero (see Problem 10.4).

The simplest way to evaluate the averages in $G(x)$ is to introduce the Fourier expansion for free boson fields:

$$\begin{aligned} \tilde{\Phi}_v(x) &= \int_{-\infty}^{\infty} \frac{dp}{2\pi\sqrt{2|p|}} e^{-a|p|/2} [\phi_v(x) e^{ipx} + \phi_v^\dagger(p) e^{-ipx}], \\ \tilde{\Pi}_v(x) &= \int_{-\infty}^{\infty} \frac{dp|p|}{2\pi\sqrt{2|p|}} e^{-a|p|/2} [-i\phi_v(x) e^{ipx} + i\phi_v^\dagger(p) e^{-ipx}], \end{aligned} \quad (10.74)$$

where

$$[\phi_v(p), \phi_v^\dagger(q)] = 2\pi\delta(q-p) \quad (10.75)$$

and $v = c, s$. From these expressions, it follows that

$$\langle \tilde{\Phi}_v(x) \tilde{\Phi}_v(0) - \tilde{\Phi}_v^2(0) \rangle = \frac{1}{4\pi} \ln \left(\frac{a^2}{a^2 + x^2} \right). \quad (10.76)$$

The derivation of the analogous result for the conjugate field is a bit more complicated, and hence we perform the calculation explicitly. From the definition of $\tilde{\Theta}(x)$, we reduce the correlator of $\tilde{\Theta}_v(x)$ to

$$\langle \tilde{\Theta}_v(x) \tilde{\Theta}_v(0) - \tilde{\Theta}_v^2(0) \rangle = \int_0^x dx' \int_{-\infty}^0 dx'' \langle \tilde{\Pi}_v(x') \tilde{\Pi}_v(x'') \rangle. \quad (10.77)$$

To simplify the average over the conjugate momentum fields, we note that $\langle \phi_v(p) \phi_v^\dagger(q) \rangle = 2\pi \delta(p - q)$. Consequently,

$$\begin{aligned}\langle \tilde{\Pi}_v(x') \tilde{\Pi}_v(x'') \rangle &= \int_{-\infty}^{\infty} \frac{dp|p|}{4\pi} e^{ip(x'-x'')} e^{-a|p|} \\ &= \frac{-1}{2\pi} \left[\frac{(x' - x'')^2 - a^2}{(a^2 + (x' - x'')^2)^2} \right].\end{aligned}\quad (10.78)$$

Substituting this expression into Eq. (10.77), we find that

$$\begin{aligned}\langle \tilde{\Theta}_v(x) \tilde{\Theta}_v(0) - \tilde{\Theta}_v^2(0) \rangle &= \frac{1}{2\pi} \int_0^x dx' \int_{-\infty}^{x'} dy \frac{y^2 - a^2}{(a^2 + y^2)^2} \\ &= \frac{-1}{2\pi} \int_0^x dx' \frac{y}{a^2 + y^2} \\ &= \frac{1}{4\pi} \ln \frac{a^2}{a^2 + x^2}\end{aligned}\quad (10.79)$$

and hence the correlator (Eq. (10.71)) of the total electron density

$$G(x) \propto |x|^{-\frac{g_c + g_c^{-1} + g_s + g_s^{-1}}{4}} \quad (10.80)$$

decays algebraically as a function of distance. Algebraic decay of the electron correlator is the key defining feature of 1d correlated electron systems. The momentum distribution function about k_F is defined through the Fourier transform

$$\begin{aligned}n(k) &= \int_{-\frac{L}{2}}^{\frac{L}{2}} dx e^{i(k-k_F)x} G(x) \\ &\propto \int_{-\frac{L}{2}}^{\frac{L}{2}} dx e^{i(k-k_F)x} |x|^{-\frac{g_c + g_c^{-1} + g_s + g_s^{-1}}{4}}.\end{aligned}\quad (10.81)$$

Changing variables to $y = (k - k_F)x$, we find that the momentum distribution function for electronic excitations,

$$n(k) \propto |k - k_F|^{\frac{g_c + g_c^{-1} + g_s + g_s^{-1}}{4} - 1}, \quad (10.82)$$

vanishes algebraically in the vicinity of the Fermi level, as depicted in Fig. 10.5. For spinless electrons, the factor of $1/\sqrt{2}$ that arises from the transformation to charge and spin fields does not appear. As a result, the factor of $\pi/2$ in the exponent of Eq. (10.71) is replaced by π . As a consequence, the corresponding exponent for spinless electrons is $(g_c + g_c^{-1})/2 - 1$. In both cases, however, we recover the Fermi liquid condition that the density of states is a non-zero constant at the Fermi level by setting $g_v = 1$. Algebraic vanishing of the distribution function at the Fermi level signifies that there are no well-defined quasi-particles in a Luttinger liquid, unlike the Fermi liquid case. The characteristic

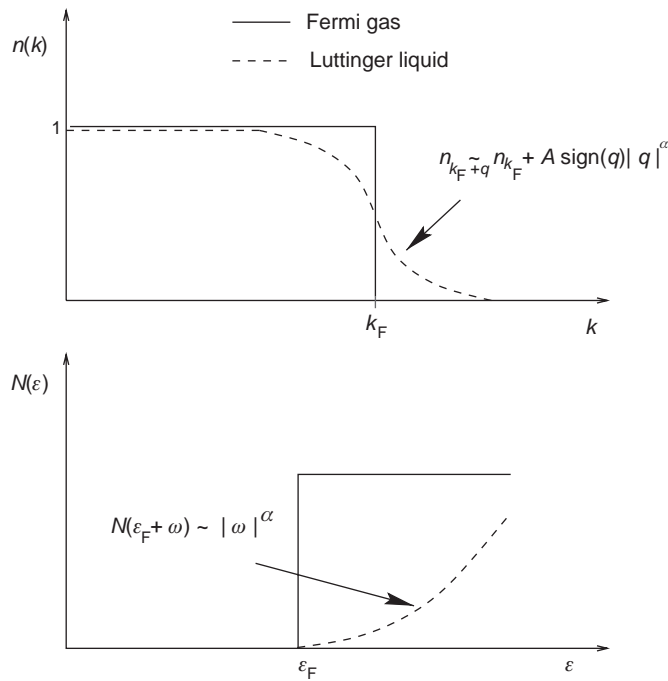


Fig. 10.5 Shown here are the momentum distribution (upper figure) and tunneling density of states (lower figure) for a Luttinger liquid (dashed line) and a Fermi gas (solid line). The characteristic algebraic dependence of the momentum distribution function in the vicinity of the Fermi energy is shown. In the Fermi gas limit, $\alpha = 0$ and the constant $A = -1/2$. The vanishing of the tunneling density of states at the Fermi level is responsible for the algebraic temperature dependence of the I - V characteristics shown in Fig. 10.6.

value of $k - k_F$ at low temperature is given by $|k^2/2m - k_F^2/2m| \sim |k - k_F|v_F \sim T$. Hence, algebraic vanishing of the momentum distribution function at the Fermi level translates into an algebraic temperature dependence of the form

$$n(T) \propto T^{\frac{g_c + g_c^{-1}}{2} - 1} \quad (10.83)$$

for the excitation spectrum. Such algebraic scaling is expected to have profound experimental consequences. Consider a tunneling experiment in which electrons traverse a barrier into a Luttinger liquid. Transport through any system is determined by the distribution of electronic states available to the charge carriers. Hence, one would expect a vanishing of the conductance (transmittance) as $T \rightarrow 0$ across a barrier that separates two Luttinger liquids. As a consequence, rather than increasing exponentially with a characteristic activation energy away from $T = 0$, the conductance should increase as a power law (KF1992). This power law should appear in measurements of the current–voltage (I - V) characteristics for transport in Luttinger liquids. Experiments illustrating the power-law dependence of

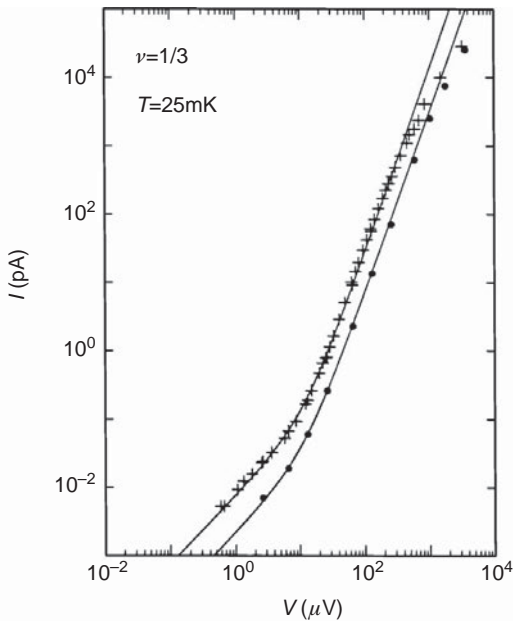


Fig. 10.6 Current–voltage (I - V) characteristics for tunneling from bulk-doped n -GaAs into the edge of the fractional quantum Hall effect state with a filling factor in the lowest Landau level of $\nu = 1/3$. The solid circles and crosses correspond to magnetic fields of $B = 10.8T$ and $B = 13.4T$, respectively. The edge states in the fractional quantum Hall state are Luttinger liquids. Algebraic dependence of I vs V is expected to occur for tunneling into a Luttinger liquid as a result of the algebraic dependence of the tunneling density of states (see Eq. (10.82)). The solid curves represent fits to the theoretical universal form, Eq. (10.84).

the I - V characteristics in a system exhibiting Luttinger liquid behavior were performed by Chang and co-workers (CPW1996). Their data are shown in Fig. 10.6. In these particular experiments, the Luttinger liquid was the edge of a fractional quantum Hall effect state. For these samples, Kane and Fisher (KF1992) showed that the current scales as

$$I \propto T^\alpha [x + x^\alpha] \quad (10.84)$$

with $\alpha = 3$ and $x = eV/2\pi k_F T$. Excellent agreement with theory was obtained for $\alpha = 2.7$ and the $1/2\pi$ scale factor between the voltage and the temperature. Similar results have also been obtained by Webb and co-workers (MUW1996) in quantum Hall systems and by Bockrath and colleagues (B1999) on carbon nanotubes. As a result, that electron correlations are at the heart of the power-law dependence of the current–voltage characteristics for 1d electronic systems is on firm experimental footing.

To close this chapter, we comment briefly on what happens when the Umklapp terms are retained at half-filling. In this case, a cosine term appears in the charge sector, which implies that there is a gap to excitations for repulsive interactions in the charge sector at half-filling. This signifies that the holons are not free to conduct without a huge energy cost. This situation arises because at half-filling there is exactly one electron per site. Hence, the energy cost to move an electron from site to site is U , the magnitude of the charge gap.

If U were negative, then the ground state at half-filling would correspond to two electrons tightly bound (with a binding energy of order U) per lattice site. Such an entity costs no energy to move. Hence, at half-filling, a charge gap exists only for repulsive interactions.

Summary

In 1d, it is possible to develop a bosonized view of the collective excitations of an electron gas in the presence of short-range interactions. This level of description enables a clear demonstration that spin and charge move with fundamentally different velocities in 1d. It is yet unknown how spin and charge separation can be formally established for $d > 1$. In addition, Coulomb interactions in 1d give rise to algebraic decay of the density of states at the Fermi level. Such characteristic decay of the density of states is the signature of Luttinger liquid behavior and is experimentally observable in tunneling experiments. Certain cases may require physics beyond the linear approximation, in which case the bosonization method presented here would have to be extended.

Problems

- 10.1 Show that if Eq. (10.31) were substituted into the continuum version of the Hamiltonian (Eq. (10.6)), the resultant boson Hamiltonian would correspond to twice Eq. (10.30).
- 10.2 Use Eq. (10.43) and the Baker–Hausdorff identity (Eq. (10.38)) to prove that

$$: e^A :: e^B := : e^{A+B} : e^{[A^-, B^+]}. \quad (10.85)$$

- 10.3 Prove that the equal-time commutation relations between the components of the current are given by

$$[j_0^\sigma(x), j_1^\sigma(y)] = -\frac{i\hbar v_F}{\pi} \partial_x \delta(x-y), \quad (10.86)$$

$$[j_0^\sigma(x), j_0^\sigma(y)] = [j_1^\sigma(x), j_1^\sigma(y)] = 0. \quad (10.87)$$

- 10.4 Show that the phase factor in Eq. (10.71) identically vanishes. You might find the following plan of attack helpful. Note first that Θ_ν and Φ_ν scale inversely with respect to g_ν . Hence, the cross-terms are independent of the rescaling factors. From the continuity equation $\partial_\tau \Phi = \partial_x \theta$, you can establish that

$$\theta(x, \tau) = \int_{-\infty}^x dx' \partial_\tau \phi(x', \tau) \quad (10.88)$$

and hence that

$$\begin{aligned} \langle \tilde{\Phi}_\nu(x, \tau) \tilde{\Theta}_\nu(0) - \tilde{\Theta}_\nu(0) \tilde{\Phi}_\nu(0) \rangle &= - \int_{-\infty}^x dx' \left\{ \partial_\tau G(x, x', \tau, 0) \Big|_{\tau=0} \right. \\ &\quad \left. - \partial_\tau G(0, x', \tau) \Big|_{x'=0, \tau=0} \right\}, \end{aligned} \quad (10.89)$$

- where $G(x, x', \tau, \tau') = \langle \Phi_\nu(x, 0) \Phi_\nu(x', \tau') \rangle$. You should then be able to show that the remaining contribution enters with the opposite sign, and hence the sum vanishes.
- 10.5 Calculate the partition function for a non-interacting Fermi gas with energy-level spacing ϵ (take the Fermi sea to be infinitely deep). One route to a solution is to demonstrate that the degeneracy of a state with energy $N\epsilon$ is equal to the number of partitions of N , $p(N)$ (e.g., $p(3) = 3$ since $3 = 3, 2 + 1$, and $1 + 1 + 1$). What is the bosonic system to which this partition function corresponds?
- 10.6 Derive Eq. (10.20).

References

- [B1999] M. Bockrath, D. H. Cobden, L. Jia, A. G. Rinzler, R. E. Smalley, L. Balents, and P. L. McEuen, *Nature (London)* **397**, 598 (1999).
- [BP1953] D. Bohm and D. Pines, *Phys. Rev.* **92**, 609 (1953).
- [CPW1996] A. Chang, L. Pfeiffer, and K. West, *Phys. Rev. Lett.* **77**, 2538 (1996).
- [H1981] F. D. M. Haldane, *J. Phys. C: Sol. State Phys.* **14**, 2585 (1981).
- [H1964] J. Hubbard, *Proc. Roy. Soc. A* **277**, 237 and 281 (1964).
- [KF1992] C. L. Kane and M. P. A. Fisher, *Phys. Rev. Lett.* **68**, 1220 (1992).
- [KS1996] G. Kotliar and Q. Si, *Phys. Rev. B* **53** (1996).
- [L1960] J. M. Luttinger, *Phys. Rev.* **119**, 1153 (1960).
- [M1975] S. Mandelstam, *Phys. Rev. D* **11**, 3026 (1975).
- [M1974] D. Mattis, *J. Math. Phys. (N.Y.)* **15**, 609 (1974).
- [ML1965] D. Mattis and E. Lieb, *J. Math. Phys.* **6**, 304 (1965).
- [MUW1996] F. P. Milliken, C. P. Umbach, and R. A. Webb, *Solid State Commun.* **97**, 309 (1996).
- [S1990] H. J. Schulz, *Phys. Rev. Lett.* **64**, 2831 (1990).
- [S1959] J. Schwinger, *Phys. Rev. Lett.* **3**, 296 (1959).
- [T1950] S. Tomonaga, *Prog. Theor. Phys. (Kyoto)* **5**, 544 (1950).
- [VDS1998] J. von Delft and H. Schoeller, *Annalen Phys.* **7**, 225 (1998).
- [Y2005] A. Yacoby, *Les Houches Summer School Proceedings* **81**, 605 (2005).

So far, we have focused on the electron problem, treating the ions as fixed in place at their equilibrium positions \mathbf{R}_i^0 . In the context of the electron gas, we adopted an even simpler view of the ions, namely that they provide a uniform background of compensating positive charge. To be able to describe the range of physics observed in a solid, we must invoke some realism into our treatment of ion motion. The coupling of electronic degrees of freedom with the motion of the ions is the electron–phonon problem. Phonons in a solid arise from collective motion of the ions. Such motion is quantized and fundamentally responsible for (1) polaron formation, (2) the electron attraction in superconductivity, and (3) the temperature dependence of the resistivity in metals. In this chapter, we focus on the general formulation of the electron–phonon problem and its subsequent application to the low-temperature resistivity in metals.

11.1 Harmonic chain

We begin with a brief review (M1981) of a 1d chain of N atoms joined by harmonic springs. Let x_i denote the deviation of each oscillator from its equilibrium position, ω , the frequency of oscillation of each spring, and M , the mass of each atom. The total Hamiltonian for this harmonic chain is

$$H = \sum_i \frac{P_i^2}{2M} + \frac{M\omega^2}{2} \sum_i (x_i - x_{i+1})^2. \quad (11.1)$$

We diagonalize this Hamiltonian by Fourier transforming the momentum

$$P_n = \frac{1}{\sqrt{N}} \sum_k e^{ikna} P_k \quad (11.2)$$

and the displacement operators

$$x_n = \frac{1}{\sqrt{N}} \sum_k e^{-ikna} x_k, \quad (11.3)$$

where a is the lattice constant. By noting that

$$\sum_n P_n^2 = \sum_k P_k P_{-k} \quad (11.4)$$

and

$$\sum_n x_n x_{n+m} = \sum_k x_k x_{-k} e^{-ikma}, \quad (11.5)$$

we rewrite the Hamiltonian in k -space:

$$H = \frac{1}{2M} \sum_k P_k P_{-k} + \frac{M}{2} \sum_k \omega_k^2 x_k x_{-k}, \quad (11.6)$$

where $\omega_k^2 = 2\omega^2(1 - \cos ka) = 4\omega^2 \sin^2 ka/2$. As a consequence, the $k = 0$ mode costs no energy to excite. This is a defining feature of acoustic phonons. The $k = 0$ mode corresponds to a uniform translation of the ions. By translational invariance, such a transformation cannot change the energy. Such long-wavelength bosonic excitations which cost no energy are called Goldstone modes (G1963) as discussed first in Chapter 1. In magnetic systems, such as ferromagnets and antiferromagnets, analogous long-wavelength excitations exist which at $k = 0$ cost no energy. Such excitations, known as spin waves or magnons, constitute the low-energy excitations in magnetic systems and hence determine the magnetic contribution to the specific heat, for example.

Let us define new operators

$$\tilde{Q}_k = x_k \left(\frac{M\omega_k}{2\hbar} \right)^{1/2} \quad (11.7)$$

and

$$\tilde{P}_k = \frac{P_k}{(2M\omega_k \hbar)^{1/2}}, \quad (11.8)$$

which allow us to re-cast H in the suggestive form

$$H = \sum_k \hbar\omega_k [\tilde{P}_k \tilde{P}_{-k} + \tilde{Q}_k \tilde{Q}_{-k}]. \quad (11.9)$$

We can factorize H once we define the creation

$$b_k^\dagger = (\tilde{Q}_{-k} - i\tilde{P}_{-k}) \quad (11.10)$$

and annihilation

$$b_k = (\tilde{Q}_k + i\tilde{P}_k) \quad (11.11)$$

operators. The commutation relations obeyed by b_k and b_k^\dagger ,

$$[b_k^\dagger, b_{k'}] = -\delta_{kk'}, \quad (11.12)$$

follow from the commutator

$$[\tilde{P}_k, \tilde{Q}_{-k}] = -\frac{i}{2} \delta_{kk'}. \quad (11.13)$$

The factorized Hamiltonian takes on the familiar oscillator form

$$H = \sum_k \hbar\omega_k \left(b_k^\dagger b_k + \frac{1}{2} \right), \quad (11.14)$$

which is indicative of a collection of bosons. The time dependence of the b_k s,

$$b_k(t) = b_k(t=0)e^{-i\omega_k t}, \quad (11.15)$$

is obtained by solving the Heisenberg equations of motion,

$$-i\hbar\dot{b}_k = [H, b_k] = -\hbar\omega_k b_k. \quad (11.16)$$

The operators $b_k^\dagger(t)$ create a collective lattice distortion with frequency ω_k at time t . The spatial resolution of this distortion is given by solving Eqs. (11.10) and (11.11) for x_k ,

$$\begin{aligned} x_k(t) &= \frac{1}{2} \left(\frac{2\hbar}{M\omega_k} \right)^{1/2} (b_k(t) + b_{-k}^\dagger(t)) \\ &= \left(\frac{\hbar}{2M\omega_k} \right)^{1/2} (b_k e^{-i\omega_k t} + b_{-k}^\dagger e^{i\omega_k t}), \end{aligned} \quad (11.17)$$

and then Fourier transforming,

$$x_\ell(t) = \sum_k \left(\frac{\hbar}{2MN\omega_k} \right)^{1/2} (b_k e^{-i\omega_k t} + b_{-k}^\dagger e^{i\omega_k t}) e^{ik\ell a}. \quad (11.18)$$

This expression for $x_\ell(t)$ tells us the amplitude of the lattice vibration on site ℓ at time t . The sum over k is restricted to the first Brillouin zone.

11.2 Acoustic phonons

To make more concrete contact with a solid, we consider a general pair-wise potential of interaction between ions:

$$V_{\text{ion}} = \sum_{i < j} V(\mathbf{R}_i - \mathbf{R}_j). \quad (11.19)$$

The equilibrium positions, $\{\mathbf{R}_i^0\}$, of the ions are determined by the condition that the net force on each ion vanishes:

$$\mathbf{F}_j = \sum_i \nabla V(\mathbf{R}_i^0 - \mathbf{R}_j^0) = 0. \quad (11.20)$$

Consequently, we represent the actual position of each ion,

$$\mathbf{R}_i = \mathbf{R}_i^0 + \mathbf{Q}_i, \quad (11.21)$$

by an expansion about the equilibrium positions. Here $\{\mathbf{Q}_i\}$ plays the role of $\{x_i\}$ in the linear chain as they represent the displacement of each ion from its home position. The vanishing

of the forces on each ion at the home positions guarantees that the Taylor expansion for the ion potential,

$$V_{\text{ion}} = \sum_{i < j} V(\mathbf{R}_i^0 - \mathbf{R}_j^0) + \frac{1}{2} \sum_{i < j} (\mathbf{Q}_i - \mathbf{Q}_j)_\mu (\mathbf{Q}_i - \mathbf{Q}_j)_\nu F_{\mu\nu}, \quad (11.22)$$

with

$$F_{\mu\nu} = \frac{\partial^2}{\partial R_\mu \partial R_\nu} V(\mathbf{R}_i^0 - \mathbf{R}_j^0), \quad (11.23)$$

is harmonic to lowest order in the fluctuation about the minimum, where repeated indices are summed over.

As in the 1d chain, we diagonalize this interaction by defining the collective coordinate

$$\mathbf{Q}_i(t) = \sum_{\mathbf{k}, \lambda} \left(\frac{\hbar}{2MN\omega_{\mathbf{k}, \lambda}} \right)^{1/2} (b_{\mathbf{k}, \lambda} \lambda_{\mathbf{k}} e^{-i\omega_{\mathbf{k}, \lambda} t} + b_{-\mathbf{k}, \lambda}^\dagger \lambda_{\mathbf{k}}^* e^{i\omega_{\mathbf{k}, \lambda} t}) e^{i\mathbf{k} \cdot \mathbf{R}_i^0},$$

where $\lambda_{\mathbf{k}}$ is a polarization vector of unit length which depends on the direction of propagation of the phonon. For a longitudinal phonon, $\lambda_{\mathbf{k}}$ is parallel to \mathbf{k} , while $\lambda_{\mathbf{k}}$ is perpendicular to \mathbf{k} for a transverse phonon. Because \mathbf{Q}_i is Hermitian, we choose the polarization vectors to be purely real. With this definition of $\mathbf{Q}_i(t)$, we rewrite the ion potential,

$$V_{\text{ion}} = \sum_{i < j} V(\mathbf{R}_i^0 - \mathbf{R}_j^0) + \frac{M}{2} \sum_{\mathbf{k}, \lambda} \omega_{\mathbf{k}, \lambda}^2 \mathbf{Q}_{\mathbf{k}, \lambda} \mathbf{Q}_{-\mathbf{k}, \lambda}, \quad (11.24)$$

in terms of the phonon or harmonic modes, $\mathbf{Q}_{\mathbf{k}, \lambda}$. For acoustic phonons, $\mathbf{Q}_{\mathbf{k}, \lambda}$ describes a distortion in which neighboring ions move in the same direction. These correspond to long-wavelength modes of the crystal. We will focus only on distortions of this sort. The conjugate momentum for a phonon mode is defined by computing $\mathbf{P}_i = M \dot{\mathbf{Q}}_i$, for example, in the site representation. \mathbf{P}_i and \mathbf{Q}_i obey the canonical commutation relations in Eq. (11.13).

11.3 Electron–phonon interaction

In our general many-body Hamiltonian, the interaction between each ion and the electrons is of the form

$$\begin{aligned} V_{\text{ei}} &= \sum_j V_{\text{ei}}(\mathbf{r}_j) \\ &= \sum_{i,j} V_{\text{ei}}(\mathbf{r}_j - \mathbf{R}_i). \end{aligned} \quad (11.25)$$

To make contact with the phonon expansion introduced in the previous section, we write the ion coordinate in terms of a deviation from the home position, $\mathbf{R}_i = \mathbf{R}_i^0 + \mathbf{Q}_i$ and Taylor series expand the electron–ion potential around \mathbf{R}_i^0 . To first order, we have that

$$V_{\text{ei}} = \sum_{i,j} V_{\text{ei}}(\mathbf{r}_j - \mathbf{R}_i^0) - \sum_{i,j} \mathbf{Q}_i \cdot \nabla_j V_{\text{ei}}(\mathbf{r}_j - \mathbf{R}_i^0) + O(Q^2) + \dots \quad (11.26)$$

The first term defines the periodic potential seen by a conduction electron and hence contains no new information regarding the coupling of the electrons to the lattice distortion. Such information is contained in the second term. To simplify this term, we introduce the Fourier transform of the electron–ion potential,

$$V_{ei}(\mathbf{r}) = \frac{1}{N} \sum_{\mathbf{k}} V_{ei}(\mathbf{k}) e^{i\mathbf{k}\cdot\mathbf{r}}. \quad (11.27)$$

With this definition in hand, we write the electron–ion potential as

$$V_{ei} = V_0 - \frac{i}{N} \sum_{\mathbf{k}, i, j} V_{ei}(\mathbf{k}) e^{i\mathbf{k}\cdot\mathbf{r}_j} \times \mathbf{k} \cdot \sum_{\mathbf{q}, \lambda} \left(\frac{\hbar}{2MN\omega_{\mathbf{q}, \lambda}} \right)^{1/2} \lambda_{\mathbf{q}} (b_{\mathbf{q}} + b_{-\mathbf{q}}^\dagger) e^{i(\mathbf{q}-\mathbf{k})\cdot\mathbf{R}_i^0}, \quad (11.28)$$

where we have set the first term in Eq. (11.26) equal to V_0 . We restrict the sums over \mathbf{q} and \mathbf{k} to the first Brillouin zone, such that

$$\frac{1}{N} \sum_i e^{i(\mathbf{q}-\mathbf{k})\cdot\mathbf{R}_i^0} = \sum_{\mathbf{L}} \delta_{\mathbf{k}, \mathbf{q}+\mathbf{L}}, \quad (11.29)$$

where the sum over L is over all reciprocal lattice vectors. We note also that the k th component of the electron density is

$$\rho_{\mathbf{k}} = \sum_j e^{i\mathbf{k}\cdot\mathbf{r}_j}. \quad (11.30)$$

We introduce the electron–phonon coupling constant

$$M_{\mathbf{q}, \mathbf{L}, \lambda} = -i \left(\frac{\hbar}{2MN\omega_{\mathbf{q}, \lambda}} \right)^{1/2} (\mathbf{q} + \mathbf{L}) \cdot \lambda_{\mathbf{q}} V_{ei}(\mathbf{q} + \mathbf{L}) \quad (11.31)$$

and recast the electron–phonon term as

$$V_{ei} = V_0 + \sum_{\mathbf{q}, \mathbf{L}, \lambda} M_{\mathbf{q}, \mathbf{L}, \lambda} (b_{\mathbf{q}} + b_{-\mathbf{q}}^\dagger) \rho_{\mathbf{q}+\mathbf{L}} = V_0 + H_{e-ph}. \quad (11.32)$$

The electron–phonon coupling constant contains the product $(\mathbf{q} + \mathbf{L}) \cdot \lambda_{\mathbf{q}}$. Two things follow from this. First, the electron–phonon interaction vanishes when no net momentum is transferred, as dictated by Adler’s theorem which was presented in Chapter 1. Second, when $\lambda_{\mathbf{q}}$ is perpendicular to $\mathbf{q} + \mathbf{L}$, $M_{\mathbf{q}+\mathbf{L}, \lambda} = 0$. That is, only the longitudinal acoustic phonon modes couple to the electrons. As a result, we can drop the λ subscript as there is only one longitudinal acoustic mode. This is an important result. However, there are certainly longitudinal optical phonons that couple to the electron motion. Such processes arise from a Coulombic rather than an elastic deformation coupling to the electron motion. In the optical phonon case, the linear q dependence of the coupling constant, $M_{\mathbf{q}}$, is replaced by a q^{-2} dependence. The inverse $1/q^2$ term arises from the Fourier transform of the Coulomb interaction. In polar crystals, optical phonons dominate over the acoustic modes. Because we are primarily interested in superconductivity, we limit our discussion solely to the acoustic case.

Let us now compute matrix elements of $H_{e\text{-ph}}$. To do this, we consider the composite electron–phonon state

$$|\psi_{e\text{-ph}}\rangle = |\{n_{\mathbf{k}}\}; \{N_{\mathbf{q},\lambda}\}\rangle. \quad (11.33)$$

Here, the electronic state $|\{n_{\mathbf{k}}\}\rangle$ represents a many-body state in which $n_{\mathbf{k}}$ electrons are in the single-particle Bloch state $\langle \mathbf{r} | \mathbf{k} \rangle \equiv e^{i\mathbf{k}\cdot\mathbf{r}} U_{\mathbf{k}}(\mathbf{r})$, and $|\{N_{\mathbf{q},\lambda}\}\rangle$ denotes a many-body phonon state in which $N_{\mathbf{q},\lambda}$ phonons are in the q th lattice mode of polarization $\lambda_{\mathbf{q}}$. The function $U_{\mathbf{q}}(\mathbf{r})$ has the same periodicity of the lattice as does the Fourier coefficient, $e^{i\mathbf{q}\cdot\mathbf{r}}$, namely $U_{\mathbf{k}}(\mathbf{r}) = U_{\mathbf{k}}(\mathbf{r} + \mathbf{R}_i^0)$. To evaluate matrix elements of the electron–phonon interaction, it is helpful to express $H_{e\text{-ph}}$ in second-quantized form. The only electron operator in $H_{e\text{-ph}}$ is the electron density, $\hat{\rho}_{\mathbf{k}}$. In second-quantized form, $\hat{\rho}_{\mathbf{k}}$ becomes

$$\hat{\rho}_{\mathbf{k}} = \sum_{\mathbf{k}_1, \mathbf{k}_2} \langle \mathbf{k}_1 | e^{i\mathbf{k}\cdot\mathbf{r}} | \mathbf{k}_2 \rangle a_{\mathbf{k}_1}^\dagger a_{\mathbf{k}_2}, \quad (11.34)$$

where the operator $a_{\mathbf{k}}^\dagger$ creates an electron in the momentum state \mathbf{k} . The electron–phonon interaction can now be written as

$$H_{e\text{-ph}} = \sum_{\mathbf{k}, \mathbf{L}, \mathbf{k}_1, \mathbf{k}_2, \mathbf{q}} M_{\mathbf{q}, \mathbf{L}} \langle \mathbf{k}_1 | e^{i(\mathbf{q}+\mathbf{L})\cdot\mathbf{r}} | \mathbf{k}_2 \rangle a_{\mathbf{k}_1}^\dagger a_{\mathbf{k}_2} (b_{\mathbf{q}} + b_{-\mathbf{q}}^\dagger). \quad (11.35)$$

Assuming the electron wavefunctions are simply plane waves, we find that the matrix element of the density operator is given exactly by

$$\langle \mathbf{k}_1 | e^{i\mathbf{k}\cdot\mathbf{r}} | \mathbf{k}_2 \rangle = \int \frac{d\mathbf{r}}{V} e^{i\mathbf{r}\cdot(\mathbf{k} + \mathbf{k}_2 - \mathbf{k}_1)} = \delta_{\mathbf{k}_1, \mathbf{k} + \mathbf{k}_2}. \quad (11.36)$$

In general, the electron wavefunctions need not be plane waves. We define

$$\alpha_{\mathbf{q}_1, \mathbf{q}_2} = \langle \mathbf{q}_1 | \mathbf{q}_2 \rangle \quad (11.37)$$

to be the general overlap between two electronic states. Because the $U_{\mathbf{k}}$ s have the periodicity of the lattice, the condition in Eq. (11.36) still holds, even when the electronic wavefunctions are more complicated than plane waves. Consequently, the full electron–phonon Hamiltonian reduces to

$$H_{e\text{-ph}} = \sum_{\mathbf{q}, \mathbf{k}, L} M_{\mathbf{q}, \mathbf{L}} \alpha_{\mathbf{k} + \mathbf{q} + \mathbf{L}, \mathbf{k}} a_{\mathbf{q} + \mathbf{L} + \mathbf{k}}^\dagger a_{\mathbf{k}} (b_{\mathbf{q}} + b_{-\mathbf{q}}^\dagger) \quad (11.38)$$

when Eqs. (11.35–11.37) are combined.

As is evident, this Hamiltonian contains a myriad of electron–phonon processes, some of which involve the electron’s moving from one Brillouin zone to another, $L \neq 0$. All such processes in which the electron wavevector is changed by $\mathbf{q} + \mathbf{L} + \mathbf{k}$ are called Umklapp processes. In German, *Umklapp* means “to flip over”. Normal processes refer to those in which momentum transfer does not result in an electron’s changing Brillouin zones. In such cases, a phonon of wavevector \mathbf{q} scatters an electron with momentum \mathbf{k} and yields an electron state with wavevector $\mathbf{q} + \mathbf{k}$. Diagrams illustrating the various kinds of scattering processes are shown in Fig. 11.1.

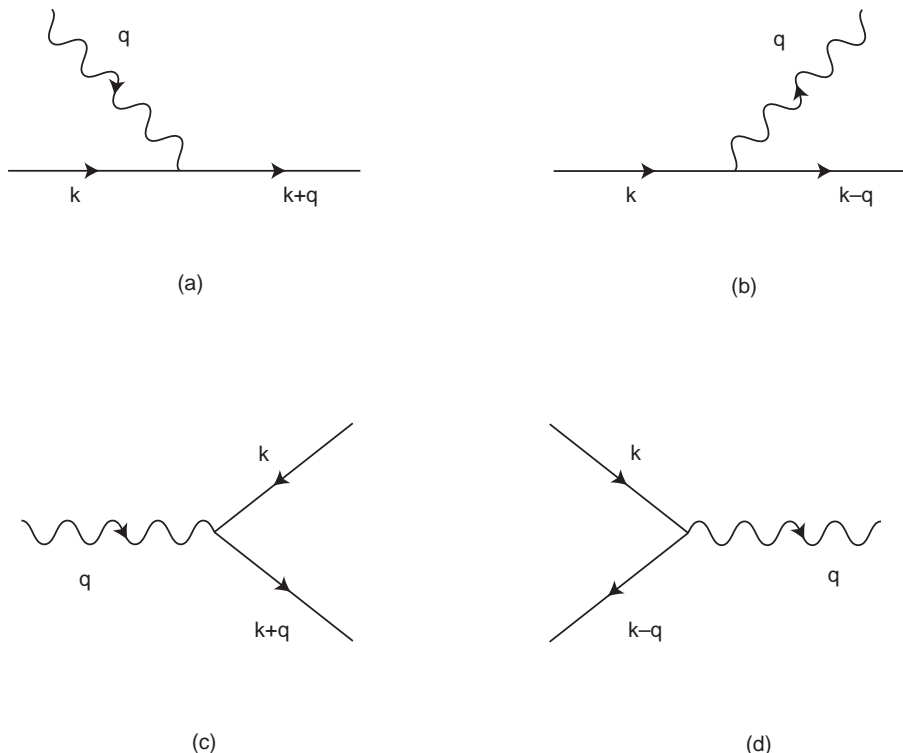


Fig. 11.1 Electron–phonon scattering. A wavy line represents a phonon, and incoming and outgoing arrows represent electrons and holes, respectively. (a) and (c) represent absorption, while (b) and (d) correspond to emission of a phonon.

We are interested primarily in the amplitude for emission and absorption. In emission, a phonon is created. Hence, only the $b_{-\mathbf{q}}^\dagger$ term contributes. Likewise in absorption, a phonon is annihilated. For an emission process, the initial and final states must be of the form

$$|\text{init}\rangle = |n_{\mathbf{k}+\mathbf{q}}, n_{\mathbf{k}}; N_{-\mathbf{q}}, N_{\mathbf{q}}\rangle \quad (11.39)$$

$$|\text{efin}\rangle = |n_{\mathbf{k}+\mathbf{q}} + 1, n_{\mathbf{k}} - 1; N_{-\mathbf{q}} + 1, N_{\mathbf{q}}\rangle. \quad (11.40)$$

The amplitude for emission involves the matrix elements

$$\langle \text{efin}|H_{\text{e-ph}}|\text{init}\rangle = M_{\mathbf{q}} \alpha_{\mathbf{k}+\mathbf{q}, \mathbf{k}} \langle \text{efin}|a_{\mathbf{q}+\mathbf{k}}^\dagger a_{\mathbf{k}} b_{-\mathbf{q}}^\dagger| \text{init}\rangle. \quad (11.41)$$

Because $n_{\mathbf{k}+\mathbf{q}}$ and $n_{\mathbf{k}}$ are restricted to be 1 or 0, $a_{\mathbf{k}}|\text{init}\rangle$ is non-zero only if $n_{\mathbf{k}} = 1$. Likewise, $a_{\mathbf{q}+\mathbf{k}}^\dagger|\text{init}\rangle$ will yield a non-zero result only if $1 - n_{\mathbf{q}+\mathbf{k}} = 1$. Consequently,

$$\langle \text{efin}|H_{\text{e-ph}}|\text{init}\rangle = M_{\mathbf{q}} \alpha_{\mathbf{k}+\mathbf{q}, \mathbf{k}} \sqrt{(1 - n_{\mathbf{q}+\mathbf{k}}) n_{\mathbf{k}} (N_{-\mathbf{q}} + 1)}. \quad (11.42)$$

In the event that $n_{\mathbf{k}} = 1$ and $n_{\mathbf{q}+\mathbf{k}} = 0$, the energy difference between the initial and final states is

$$\Delta E_{\text{emis}} = E_{\text{fin}} - E_{\text{init}} = E(\mathbf{q} + \mathbf{k}) - E(\mathbf{k}) + \hbar\omega_{\mathbf{q}}, \quad (11.43)$$

where $E(\mathbf{k})$ is the energy of an electron state with momentum \mathbf{k} .

In the absorption process, the final state in this case is

$$| \text{afin} \rangle = | n_{\mathbf{k}+\mathbf{q}} + 1, n_{\mathbf{k}} - 1; N_{-\mathbf{q}}, N_{\mathbf{q}} - 1 \rangle. \quad (11.44)$$

As a consequence,

$$\langle \text{afin} | H_{e-ph} | \text{init} \rangle = M_{\mathbf{q}} \alpha_{\mathbf{k}+\mathbf{q}, \mathbf{k}} \sqrt{(1 - n_{\mathbf{q}+\mathbf{k}}) n_{\mathbf{k}} N_{\mathbf{q}}}. \quad (11.45)$$

The energy difference here is

$$\Delta E_{\text{abs}} = E(\mathbf{k} + \mathbf{q}) - E(\mathbf{k}) - \hbar\omega_{\mathbf{q}}. \quad (11.46)$$

Applying Fermi's golden rule to the emission and absorption amplitudes yields

$$W_{\mathbf{k} \rightarrow \mathbf{k}+\mathbf{q}}^{\text{abs}} = \frac{2\pi}{\hbar} |M_{\mathbf{q}} \alpha_{\mathbf{k}+\mathbf{q}, \mathbf{k}}|^2 n_{\mathbf{k}} N_{\mathbf{q}} (1 - n_{\mathbf{q}+\mathbf{k}}) \delta(E(\mathbf{k} + \mathbf{q}) - E(\mathbf{k}) - \hbar\omega_{\mathbf{q}}) \quad (11.47)$$

and

$$W_{\mathbf{k} \rightarrow \mathbf{k}+\mathbf{q}}^{\text{emis}} = \frac{2\pi}{\hbar} |M_{\mathbf{q}} \alpha_{\mathbf{k}+\mathbf{q}, \mathbf{k}}|^2 n_{\mathbf{k}} (1 - n_{\mathbf{q}+\mathbf{k}}) (N_{-\mathbf{q}} + 1) \delta(E(\mathbf{k} + \mathbf{q}) - E(\mathbf{k}) + \hbar\omega_{\mathbf{q}}) \quad (11.48)$$

for the emission and absorption rates, respectively. The δ -functions ensure that energy is conserved. For the sake of generality, we have included explicitly the electron-occupation numbers, although $n_{\mathbf{k}} = 1$ and $n_{\mathbf{q}+\mathbf{k}} = 0$. It is customary at this stage of our calculation to replace the electron and phonon occupation numbers by their equilibrium Fermi–Dirac and Bose forms. This simplification is valid only if the electron–phonon system is in equilibrium before the transition occurs. We will find this simplification useful when we treat superconductivity.

11.4 Ultrasonic attenuation

Imagine that we send a beam of phonons into a metal. The total rate at which the phonons are absorbed is determined by the direct absorption into the metal and emission back into the beam. Consequently, the rate at which a beam loses $N_{\mathbf{q}, \lambda}$ phonons per unit time is given by a kinetic gain–loss equation:

$$\frac{dN_{\mathbf{q}, \lambda}}{dt} = - \sum_{\mathbf{p}} (W_{\mathbf{p} \rightarrow \mathbf{p}+\mathbf{q}}^{\text{abs}} - W_{\mathbf{p} \rightarrow \mathbf{p}-\mathbf{q}}^{\text{emis}}). \quad (11.49)$$

The first term represents the absorption of phonons from the beam and the second term the re-emission of phonons into the beam. Inclusion of the re-emission term is essential to describe the correct physics.

We can simplify our kinetic equation by recalling that the structure function for free electrons is given by

$$n_e S_0(\mathbf{p}, \omega) = \frac{2}{V} \sum_{\mathbf{p}'} f_{\mathbf{p}'} (1 - f_{\mathbf{p}+\mathbf{p}'}) 2\pi \hbar \delta(\hbar\omega - \epsilon_{\mathbf{p}+\mathbf{p}'} + \epsilon_{\mathbf{p}'}). \quad (11.50)$$

Physically, $S_0(\mathbf{p}, \omega)$ is the density of electron–hole excitations separated by an energy $\hbar\omega$. Inspection of the expressions for the phonon absorption and emission rates reveals that they are directly proportional to the right-hand side of the equation for the structure function. Let us assume that the electronic states are perfect plane waves with free-particle energies $\epsilon_{\mathbf{p}} = \mathbf{p}^2/2m$. As a result, the matrix element in Eq. (11.37) is equal to unity: $\alpha_{\mathbf{k}+\mathbf{q},\mathbf{q}} = 1$. Consequently, we rewrite the net absorption and emission rates as

$$\sum_{\mathbf{p}} W_{\mathbf{p} \rightarrow \mathbf{p} + \mathbf{q}}^{\text{abs}} = \frac{n_e V}{2\hbar^2} |M_{\mathbf{q}}|^2 N_{\mathbf{q},\lambda} S_0(\mathbf{q}, \hbar\omega_{\mathbf{q}}) \quad (11.51)$$

and

$$\sum_{\mathbf{p}} W_{\mathbf{p} \rightarrow \mathbf{p} - \mathbf{q}}^{\text{emis}} = \frac{n_e V}{2\hbar^2} |M_{\mathbf{q}}|^2 (N_{\mathbf{q},\lambda} + 1) S_0(-\mathbf{q}, -\hbar\omega_{\mathbf{q}}). \quad (11.52)$$

In the context of the fluctuation–dissipation theorem, we showed that

$$S_0(\mathbf{p}, \hbar\omega) = e^{\beta\hbar\omega} S_0(-\mathbf{p}, -\hbar\omega). \quad (11.53)$$

Substitution of this result into the equation of motion for $N_{\mathbf{q},\lambda}(t)$ yields

$$\dot{N}_{\mathbf{q},\lambda} = -\frac{n_e V}{2\hbar^2} |M_{\mathbf{q}}|^2 S_0(\mathbf{q}, \omega_{\mathbf{q}} \hbar) [N_{\mathbf{q},\lambda} - e^{-\beta\hbar\omega_{\mathbf{q}}} (N_{\mathbf{q},\lambda} + 1)]. \quad (11.54)$$

We define the net rate of phonons absorbed to be

$$\frac{1}{\tau_{\text{ph}}} = \frac{n_e V}{2\hbar^2} |M_{\mathbf{q}}|^2 (1 - e^{-\beta\hbar\omega_{\mathbf{q}}}) S_0(\mathbf{q}, \hbar\omega_{\mathbf{q}}) \quad (11.55)$$

and the equilibrium phonon distribution, $N_{\mathbf{q},\lambda}^{\text{eq}}$, to be the standard Bose–Einstein distribution function,

$$N_{\mathbf{q},\lambda}^{\text{eq}} = \frac{1}{e^{\beta\hbar\omega_{\mathbf{q}}} - 1}. \quad (11.56)$$

Consequently, our equations of motion become

$$\dot{N}_{\mathbf{q},\lambda} = \frac{-1}{\tau_{\text{ph}}} [N_{\mathbf{q},\lambda} - N_{\mathbf{q},\lambda}^{\text{eq}}], \quad (11.57)$$

and the solution to this linear differential equation has the characteristic

$$N_{\mathbf{q},\lambda}(t) = N_{\mathbf{q},\lambda}^{\text{eq}} + e^{-t/\tau_{\text{ph}}} (N_{\mathbf{q},\lambda}(t=0) - N_{\mathbf{q},\lambda}^{\text{eq}}) \quad (11.58)$$

exponential form. We find then that the number of phonons absorbed relaxes to an equilibrium value at long times with a rate $1/\tau_{\text{ph}}$. This effect is known as ultrasonic attenuation, the loss of phonons to a medium as a result of interactions with electrons. Because electrons in a superconductor are bound together in pairs, with a binding energy proportional to the gap,

they can absorb phonons only if the phonon frequency exceeds a critical value. As a consequence, ultrasound attenuation is used as a tool for measuring the gap in a superconductor. We will investigate this further in the next chapter.

A final observation is that the calculation we have performed here is valid only if electron interactions are negligible. That is, if τ_{ee} is the effective time scale for electron scattering, then our calculation is valid if $\omega_q \tau_{ee} \gg 1$. If this condition does not hold and $\tau_{ee} \omega_q < 1$, then sound waves are attenuated via electron scattering rather than by phonon-induced electron–hole pairs. For completeness, let us now evaluate τ_{ph} . At $T = 0$, we showed that at intermediate frequencies, $n_e S_0(\mathbf{k}, \omega) = m^2 \omega / \pi k \hbar^2$. Because $|M_q|^2 \sim q^2 / \omega_q |V_{ei}(q)|^2$, $1/\tau_{ph} \sim q |V_{ei}(q)|^2$. Focusing only on the zero-frequency part of the structure function, we find that $\epsilon_p = \epsilon_{p+k}$. For $p = p_F$, the transferred momentum is $k = 2p_F$. Hence, at low frequencies, τ_{ph} is determined by particle scattering across the Fermi surface.

11.5 Electrical conduction

The conductivity in a metal is measured by applying a voltage or an electric field to the material. The resultant current density

$$\mathbf{j} = \sigma \mathbf{E} \quad (11.59)$$

is directly proportional to the electric field through the conductivity, σ . The current density is in the direction of the carrier velocity, \mathbf{v} . The constant of proportionality is the net charge density, $-en_e$. Consequently,

$$\mathbf{j} = -n_e e \mathbf{v}. \quad (11.60)$$

Let us now express \mathbf{v} in terms of \mathbf{E} . In the absence of an electric field, $\langle \mathbf{v} \rangle = 0$ because \mathbf{v} is randomized. Let τ represent the collision time of the electron. That is, over a time period τ , an electron is moving with constant velocity which we estimate as follows. The force exerted on an electron by the electric field is simply $-e\mathbf{E}$. The acceleration of the electron is then $-e\mathbf{E}/m$. If the acceleration is constant over a time τ , then the average velocity is $\mathbf{v}_{avg} = -e\mathbf{E}\tau/m$ and the current density is

$$\mathbf{j} = \frac{e^2 n_e}{m} \mathbf{E} \tau = \sigma \mathbf{E} \quad (11.61)$$

or, equivalently,

$$\sigma = \frac{n_e e^2 \tau}{m}. \quad (11.62)$$

This is the Drude formula for the conductivity.

We have expressed the conductivity then in terms of a single unknown quantity, τ , the relaxation or collision time. Experimentally, once the conductivity is measured, τ can be extracted. Listed in Table 11.1 are a few relaxation times (AM1976) for the alkali earth

Table 11.1

Element	77 K	273 K
Li	7.3×10^{-14} s	8.8×10^{-15} s
Na	1.7×10^{-13} s	3.2×10^{-14} s
K	1.8×10^{-13} s	4.1×10^{-14} s
Rb	1.4×10^{-13} s	2.8×10^{-14} s
Cs	8.6×10^{-14} s	2.1×10^{-14} s

metals. We now want to develop a general theory that can account for the relaxation time and hence the conductivity. In a pure metal, the primary source of resistance is via interactions with lattice phonons. Any successful account of σ in a metal must explain the following: (1) σ is independent of E for moderate values of E ; (2) the wide variation of σ from metal to metal; (3) the Wiedemann–Franz law that the ratio of $\kappa/\sigma = T$, where κ is the thermal conductivity; (4) $\sigma \sim 1/T$ in most metals with a transition to $\sigma \sim T^{-5}$ at $T \rightarrow 0$. In this chapter, we focus entirely on the crossover from $1/T$ to T^{-5} behavior at low temperatures.

11.5.1 Boltzmann equation

To proceed, we develop the Boltzmann transport theory. We introduce the distribution function $f(\mathbf{r}, \mathbf{k}, t)$, which defines the probability that a quantum “state” is occupied with momentum \mathbf{k} and position \mathbf{r} at time t . Although we are interested only in one band, f can be generalized to include all bands in a solid. The distribution function f specifies both the position and momentum of an electron in a quantum state. Adopting such a distribution function is valid strictly at long wavelengths, that is, $\lambda \gg \hbar v_F / \kappa_B T$. Otherwise, the uncertainty principle is violated.

Consider the volume element $d\mathbf{k}d\mathbf{r}/(2\pi\hbar)^3 = d\Omega$. The product of this differential volume element with f , $f d\Omega$, defines the number of electrons in $d\Omega$. In the problem at hand, interactions with phonons alter the occupation in phase space. Let us refer to such processes as lattice collisions. Clearly, df/dt would be zero if no such collisions occurred. In fact, for a solid in equilibrium, f is simply the Fermi–Dirac distribution. For the non-equilibrium case, f must be determined from the general equations of motion. The total time derivative of f ,

$$\frac{df}{dt} = \frac{\partial f}{\partial t} + \dot{\mathbf{k}} \cdot \nabla_{\mathbf{k}} f + \dot{\mathbf{r}} \cdot \nabla_{\mathbf{r}} f = \left. \frac{\partial f}{\partial t} \right|_{\text{coll}}, \quad (11.63)$$

is determined by all the terms that either implicitly or explicitly depend on time. This is the Boltzmann equation. Because each volume element should be equivalent, the average number of electrons entering and leaving a volume element should be a constant. As a result, $\partial f / \partial t = 0$. In addition, our system is homogeneous even in the presence of an electric field. As a consequence, the spatial derivative of f vanishes and

$$\frac{\partial \mathbf{k}}{\partial t} \cdot \nabla_{\mathbf{k}} f = \left. \frac{\partial f}{\partial t} \right|_{\text{coll}}, \quad (11.64)$$

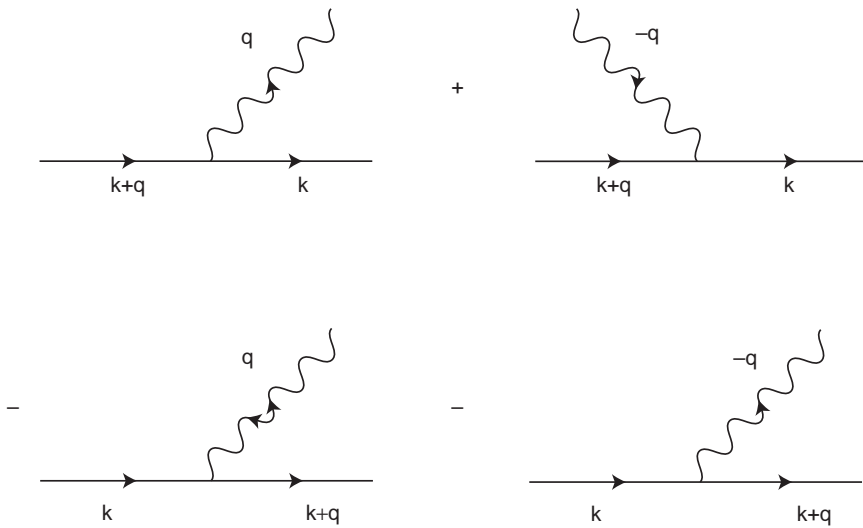


Fig. 11.2 Electron–phonon collision terms that enter the Boltzmann equation.

the steady-state Boltzmann equation, results. Physically $\partial\mathbf{k}/\partial t$ is the force on the electrons in the Fermi sea. In an electric field,

$$\frac{\partial \mathbf{k}}{\partial t} = -e\mathbf{E}, \quad (11.65)$$

and consequently all the electrons are accelerated equally by the field.

To apply this equation to an electron–lattice problem, we must include an analogous Boltzmann equation for the phonons. The appropriate Boltzmann equation is one in which the momentum term is absent, because in an unstrained crystal, there is no force on phonons. Let g be the phonon distribution function. It follows that

$$\left. \frac{\partial g}{\partial t} \right|_{\text{coll}} = \dot{\mathbf{r}} \cdot \nabla_{\mathbf{r}} g. \quad (11.66)$$

In all of our calculations to follow, we will replace g by its equilibrium value. Hence, we will not spend much time discussing g , though our treatment of f can be paralleled to solve for g . Because f is determined by electron–phonon exchanges, the most general expression we can write for the collisions is one in which all possible electron–phonon processes are summed over. Let W^{eq} represent an emission term and W^{aq} a phonon absorption process with wavevector \mathbf{q} . The general collision terms that enter the Boltzmann equation are shown in Fig. 11.2 and can be written as a gain–loss master equation,

$$\begin{aligned} \left. \frac{\partial f}{\partial t} \right|_{\text{coll}} &= \sum_{\mathbf{q}} (W_{\mathbf{k}+\mathbf{q} \rightarrow \mathbf{k}}^{eq} + W_{\mathbf{k}+\mathbf{q} \rightarrow \mathbf{k}}^{a-\mathbf{q}} - W_{\mathbf{k} \rightarrow \mathbf{k}+\mathbf{q}}^{a\mathbf{q}} - W_{\mathbf{k} \rightarrow \mathbf{k}+\mathbf{q}}^{e-\mathbf{q}}) \\ &= \sum_{\mathbf{q}} [\text{gain}(\mathbf{k}) - \text{loss}(\mathbf{k})], \end{aligned} \quad (11.67)$$

for electron states with momentum \mathbf{k} and $\mathbf{k} + \mathbf{q}$. From the exact expressions for W in Eqs. (11.47) and (11.48), it is convenient to define

$$W_{\mathbf{q}}^0 = \frac{2\pi}{\hbar} |M_{\mathbf{q}}|^2. \quad (11.68)$$

We have assumed that the electron states are plane waves. Hence, $\alpha_{\mathbf{k},\mathbf{q}} = 1$. The collision terms in Eq. (11.68) are easily computed if they are grouped as emission–absorption pairs:

$$\begin{aligned} \left. \frac{\partial f}{\partial t} \right|_{\text{coll}} &= \sum_{\mathbf{q}} (W_{\mathbf{k}+\mathbf{q} \rightarrow \mathbf{k}}^{\text{eq}} - W_{\mathbf{k} \rightarrow \mathbf{k}+\mathbf{q}}^{\text{aq}}) - (W_{\mathbf{k} \rightarrow \mathbf{k}+\mathbf{q}}^{\text{e-q}} - W_{\mathbf{k}+\mathbf{q} \rightarrow \mathbf{k}}^{\text{a-q}}) \\ &= \sum_{\mathbf{q}} W_{\mathbf{q}}^0 [(1 - f(\mathbf{k}))f(\mathbf{k} + \mathbf{q})(g(\mathbf{q}) + 1)\delta(\epsilon_{\mathbf{k}} - \epsilon_{\mathbf{k}+\mathbf{q}} + \hbar\omega_{\mathbf{q}}) \\ &\quad - (1 - f(\mathbf{k} + \mathbf{q}))f(\mathbf{k})g(\mathbf{q})\delta(\epsilon_{\mathbf{k}+\mathbf{q}} - \epsilon_{\mathbf{k}} - \hbar\omega_{\mathbf{q}})] \\ &\quad + W_{\mathbf{q}}^0 [(1 - f(\mathbf{k}))f(\mathbf{k} + \mathbf{q})g(-\mathbf{q})\delta(\epsilon_{\mathbf{k}} - \epsilon_{\mathbf{k}+\mathbf{q}} - \hbar\omega_{\mathbf{q}}) \\ &\quad - (1 - f(\mathbf{k} + \mathbf{q}))f(\mathbf{k})(g(-\mathbf{q}) + 1)\delta(\epsilon_{\mathbf{k}+\mathbf{q}} - \epsilon_{\mathbf{k}} + \hbar\omega_{\mathbf{q}})]. \end{aligned} \quad (11.69)$$

There are three common simplifications that are used to solve the Boltzmann equation for $f(\mathbf{k})$. The first is to assume that $g(\mathbf{q}) = g_{\text{equil}}$, which is known as the Bloch assumption. The Bose–Einstein distribution is just g_{equil} . Let $N_{\mathbf{q}} = g_{\text{equil}} = N_{-\mathbf{q}}$. We also define

$$W_{\mathbf{q}}(\mathbf{k}, \mathbf{k}') = W_{\mathbf{q}}^0 [\delta(\epsilon_{\mathbf{k}'} - \epsilon_{\mathbf{k}} + \hbar\omega_{\mathbf{q}})(N_{\mathbf{q}} + 1) + N_{\mathbf{q}}\delta(\epsilon_{\mathbf{k}'} - \epsilon_{\mathbf{k}} - \hbar\omega_{\mathbf{q}})].$$

The right-hand side of the Boltzmann equation now simplifies to

$$\left. \frac{\partial f}{\partial t} \right|_{\text{coll}} = \sum_{\mathbf{q}} [W_{\mathbf{q}}(\mathbf{k} + \mathbf{q}, \mathbf{k})f(\mathbf{k} + \mathbf{q})(1 - f(\mathbf{k})) - W_{\mathbf{q}}(\mathbf{k}, \mathbf{k} + \mathbf{q})f(\mathbf{k})(1 - f(\mathbf{k} + \mathbf{q}))]. \quad (11.70)$$

11.5.2 Relaxation-time approximation

In the next step, we assume that on average $f(\mathbf{k})$ is slowly varying when the field is applied. Collisions with phonons return the system to the equilibrium Fermi–Dirac distribution function, $f_0 = n_{\mathbf{k}}$. We write $f(\mathbf{k})$ as

$$f(\mathbf{k}) \simeq n_{\mathbf{k}} + \delta f_{\mathbf{k}}, \quad (11.71)$$

with $\delta f_{\mathbf{k}}$ the variation of $f(\mathbf{k})$ induced by the electric field. We suspect that $\delta f_{\mathbf{k}}$ is proportional to the acceleration, $\partial \mathbf{k} / \partial t$. To see how this comes about, we make the ansatz that collision-induced changes of $f(\mathbf{k})$ relax the system back to $n_{\mathbf{k}}$ with a mean relaxation time $\tau(\mathbf{k})$ such that

$$\left. \frac{\partial f}{\partial t} \right|_{\text{coll}} = -\frac{\delta f_{\mathbf{k}}}{\tau(\mathbf{k})}. \quad (11.72)$$

Note that introduction of a relaxation time at this stage can be done only at the expense of making τ \mathbf{k} -dependent. Using Eqs. (11.64) and (11.65) and linearizing with respect to the fluctuation $\delta f_{\mathbf{k}}$, we find that

$$\begin{aligned}\frac{\partial f}{\partial t} \Big|_{\text{coll}} &= -\frac{\delta f_{\mathbf{k}}}{\tau} = -e\mathbf{E} \cdot \nabla_{\mathbf{k}} f(\mathbf{k}) \\ &= -e\mathbf{E} \cdot \nabla_{\mathbf{k}} \epsilon_{\mathbf{k}} \frac{\partial n_{\mathbf{k}}}{\partial \epsilon_{\mathbf{k}}} \\ &= e \frac{\mathbf{E} \cdot \mathbf{k}}{m} n_{\mathbf{k}} (1 - n_{\mathbf{k}}) \beta,\end{aligned}\quad (11.73)$$

where we have used the free-particle dispersion relation, $\epsilon_{\mathbf{k}} = \mathbf{k}^2/2m$. Because $\delta f_{\mathbf{k}} = f(\mathbf{k}) - n_{\mathbf{k}}$, we obtain

$$f(\mathbf{k}) = n_{\mathbf{k}} + \beta \delta \Phi_{\mathbf{k}} n_{\mathbf{k}} (1 - n_{\mathbf{k}}), \quad (11.74)$$

with

$$\delta \Phi_{\mathbf{k}} = -e \frac{\mathbf{E} \cdot \mathbf{k}}{m} \tau(\mathbf{k}). \quad (11.75)$$

We see then that once $\tau(\mathbf{k})$ is determined, we can find the distribution function $f(\mathbf{k})$ immediately, and the conductivity can be obtained through the Drude formula.

11.5.3 Low-temperature resistivity

To simplify the Boltzmann equation, we observe that $W_{\mathbf{q}}(\mathbf{k}, \mathbf{k}')$ obeys the symmetry relationship

$$W_{\mathbf{q}}(\mathbf{k}, \mathbf{k}') e^{\beta \epsilon_{\mathbf{k}'}} = W_{\mathbf{q}}(\mathbf{k}', \mathbf{k}) e^{\beta \epsilon_{\mathbf{k}}}. \quad (11.76)$$

This statement is simply one of detailed balance. An equivalent, more useful way of writing Eq. (11.76) is

$$W_{\mathbf{q}}(\mathbf{k}, \mathbf{k}') = e^{\beta(\epsilon_{\mathbf{k}} - \epsilon_{\mathbf{k}'})} W_{\mathbf{q}}(\mathbf{k}', \mathbf{k}) \quad (11.77)$$

$$= \frac{n_{\mathbf{k}'}(1 - n_{\mathbf{k}})}{n_{\mathbf{k}}(1 - n_{\mathbf{k}'})} W_{\mathbf{q}}(\mathbf{k}', \mathbf{k}). \quad (11.78)$$

This identity implies that the quantity

$$Z_{\mathbf{q}}(\mathbf{k}, \mathbf{k}') = W_{\mathbf{q}}(\mathbf{k}, \mathbf{k}') n_{\mathbf{k}} (1 - n_{\mathbf{k}'}) \quad (11.79)$$

is symmetric with respect to interchange of its arguments. An immediate consequence of this identity is that the collision terms in the Boltzmann equation vanish identically when

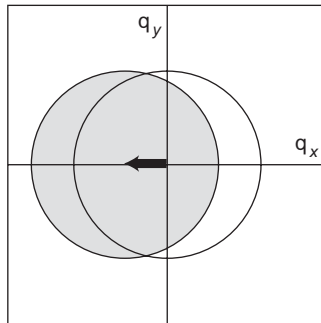


Fig. 11.3 Equilibrium Fermi surface and the Fermi surface in the presence of a uniform electric field. The drift velocity ansatz states that once the electric field is turned on, the new Fermi–Dirac distribution function is equivalent to the original one by simply translating $\mathbf{q} \rightarrow \mathbf{q} - m\mathbf{v}_d$.

$f(\mathbf{k}) = n_{\mathbf{k}}$:

$$\begin{aligned} W_{\mathbf{q}}(\mathbf{k}', \mathbf{k})(1 - n_{\mathbf{k}})n_{\mathbf{k}'} - W_{\mathbf{q}}(\mathbf{k}, \mathbf{k}')(1 - n_{\mathbf{k}'})n_{\mathbf{k}} &= Z_{\mathbf{q}}(\mathbf{k}', \mathbf{k}) - Z_{\mathbf{q}}(\mathbf{k}, \mathbf{k}') \\ &= 0. \end{aligned} \quad (11.80)$$

The consequences of this identity are immediate. Recall that we have approximated $f(\mathbf{k})$ as $f(\mathbf{k}) \simeq n_{\mathbf{k}} + \beta n_{\mathbf{k}}(1 - n_{\mathbf{k}})\delta\Phi_{\mathbf{k}}$. Hence, only the terms with at least a linear variation of δf survive in the Boltzmann equation:

$$\begin{aligned} \frac{\partial f}{\partial t} \Big|_{\text{coll}} &= \sum_{\mathbf{q}} W_{\mathbf{q}}(\mathbf{k}', \mathbf{k}) (\delta f_{\mathbf{k}'}(1 - n_{\mathbf{k}}) - n_{\mathbf{k}'}\delta f_{\mathbf{k}}) - (\mathbf{k} \leftrightarrow \mathbf{k}') \\ &= \beta \sum_{\mathbf{q}} Z_{\mathbf{q}}(\mathbf{k}', \mathbf{k}) [\delta\Phi_{\mathbf{k}'}(1 - n_{\mathbf{k}'}) - \delta\Phi_{\mathbf{k}}n_{\mathbf{k}} - (\mathbf{k} \leftrightarrow \mathbf{k}')] \\ &= \beta \sum_{\mathbf{q}} Z_{\mathbf{q}}(\mathbf{k}', \mathbf{k}) [\delta\Phi_{\mathbf{k}'} - \delta\Phi_{\mathbf{k}}]. \end{aligned} \quad (11.81)$$

In deriving Eq. (11.81), we dropped the $O(\delta\Phi^2)$ terms, thus obtaining the linearized Boltzmann equation.

As a result of the variation, $\delta\Phi_{\mathbf{k}} \sim \tau(\mathbf{k})$, the Boltzmann equation is in general an integral equation which must be solved self-consistently by some ansatz. As in all integral equations, a variational principle applies, and we are guaranteed that a trial solution for $\delta\Phi$ will result in a distribution function, f , that produces a higher energy than the true ground state energy. In the relaxation-time approximation, $\delta\Phi_{\mathbf{k}} = -e\mathbf{E} \cdot \mathbf{k}\tau(\mathbf{k})/m$. In an electric field, the drift velocity is $\mathbf{v}_d = -e\mathbf{E}\tau/m$. As a consequence, $\delta\Phi_{\mathbf{k}} \equiv \mathbf{v}_d \cdot \mathbf{k}$ is known as the drift velocity ansatz. Physically, this ansatz signifies that the electrons are in equilibrium with a drifting distribution. The drifting distribution is equivalent to the equilibrium Fermi–Dirac distribution with $\mathbf{q} \rightarrow \mathbf{q} - m\mathbf{v}_d$. As depicted in Fig. 11.3, the drift velocity ansatz amounts to an overall translation of the Fermi surface by an amount proportional (in linear order) to $m\mathbf{v}_d$. We close the Boltzmann equation by averaging the collision terms over the electron

momentum:

$$\begin{aligned} \frac{\partial}{\partial t} \langle \mathbf{k} \rangle \Big|_{\text{coll}} &= 2 \int \mathbf{k} \frac{\partial f}{\partial t} \Big|_{\text{coll}} \frac{d\mathbf{k}}{(2\pi\hbar)^3} \\ &= -2 \int \mathbf{k} \frac{d\mathbf{k}}{(2\pi\hbar)^3} \frac{f - f_0}{\tau} \\ &= -2 \int \mathbf{k} \frac{d\mathbf{k}}{(2\pi\hbar)^3} \frac{f_0(\mathbf{k} - m\mathbf{v}_d)}{\tau} \\ &= -\frac{m\mathbf{v}_d n_e}{\tau}. \end{aligned} \quad (11.82)$$

In deriving Eq. (11.82), we used the fact that $\langle \mathbf{k} \rangle$ in equilibrium vanishes.

Noting that the collision terms are antisymmetric with respect to interchange of \mathbf{k} and \mathbf{k}' , we find upon substituting Eq. (11.82) into the Boltzmann equation that

$$\begin{aligned} \frac{-m\mathbf{v}_d n_e}{\tau} &= \frac{\beta}{V} \sum_{\mathbf{k}} \mathbf{k} \sum_{\mathbf{k}'} W_{\mathbf{q}}(\mathbf{k}, \mathbf{k}') n_{\mathbf{k}} (1 - n_{\mathbf{k}'}) [\mathbf{v}_d \cdot \mathbf{k}' - \mathbf{v}_d \cdot \mathbf{k}] \\ &= \frac{\beta}{2V} \sum_{\mathbf{k}} \sum_{\mathbf{k}'} (\mathbf{k} - \mathbf{k}') W_{\mathbf{q}}(\mathbf{k}, \mathbf{k}') n_{\mathbf{k}} (1 - n_{\mathbf{k}'}) [\mathbf{v}_d \cdot \mathbf{k}' - \mathbf{v}_d \cdot \mathbf{k}] \\ &= -\frac{\beta}{2V} \sum_{\mathbf{k}} \sum_{\mathbf{q}} \mathbf{q} (\mathbf{v}_d \cdot \mathbf{q}) W_{\mathbf{q}}^0 n_{\mathbf{k}} (1 - n_{\mathbf{k}+\mathbf{q}}) [\delta(\epsilon_{\mathbf{k}+\mathbf{q}} - \epsilon_{\mathbf{k}} + \hbar\omega_{\mathbf{q}}) \\ &\quad \times (N_{\mathbf{q}} + 1) + N_{\mathbf{q}} \delta(\epsilon_{\mathbf{k}+\mathbf{q}} - \epsilon_{\mathbf{k}} - \hbar\omega_{\mathbf{q}})], \end{aligned} \quad (11.83)$$

with $\mathbf{k}' = \mathbf{k} + \mathbf{q}$. Recalling the definition of the free-particle structure function (see Eq. (11.50)), we reduce the linearized Boltzmann equation to

$$\begin{aligned} \frac{m\mathbf{v}_d n_e}{\tau} &= \frac{n_e \beta}{8\pi\hbar} \sum_q \mathbf{q} (\mathbf{v}_d \cdot \mathbf{q}) W_{\mathbf{q}}^0 [S_0(\mathbf{q}, \hbar\omega_{\mathbf{q}}) N_{\mathbf{q}} + (N_{\mathbf{q}} + 1) S_0(\mathbf{q}, -\hbar\omega_{\mathbf{q}})] \\ &= \frac{n_e \beta}{4\pi\hbar} \sum_q \mathbf{q} (\mathbf{v}_d \cdot \mathbf{q}) W_{\mathbf{q}}^0 N_{\mathbf{q}} S_0(\mathbf{q}, \hbar\omega_{\mathbf{q}}). \end{aligned} \quad (11.84)$$

To simplify Eq. (11.84) further, we replace $\mathbf{q} (\mathbf{v}_d \cdot \mathbf{q})$ with its angular average

$$\langle \mathbf{q} (\mathbf{q} \cdot \mathbf{v}_d) \rangle = \frac{1}{3} q^2 \mathbf{v}_d. \quad (11.85)$$

Substitution of Eq. (11.85) into Eq. (11.84) results in the general expression

$$\frac{1}{\tau} = \frac{\beta}{24\pi^2 M \hbar^3 m n_{\text{ion}}} \int_0^{q_D} \frac{q^6 dq}{\hbar\omega_{\mathbf{q}}} |V_{ei}(q)|^2 \frac{S_0(q, \hbar\omega_{\mathbf{q}})}{e^{\beta\hbar\omega_{\mathbf{q}}} - 1} \quad (11.86)$$

for the relaxation time. In Eq. (11.86), q_D is the momentum cut-off on the phonon spectrum.

We need an expression for S_0 that captures the essential physics at low temperatures. We showed in the previous chapter that at $T = 0$, $S_0 \propto 1/q$. Asymptotically, this expression vanishes as $q \rightarrow \infty$ and hence is expected to be valid as long as the phonon momentum is

cut-off. The Debye cut-off in the relaxation time justifies our use of the $T = 0$ limit. Away from $T = 0$ the explicit temperature dependence can be introduced by including the factor of $(1 - \exp(-\beta\hbar\omega_q))$, which appears in the original definition of $S_0(k, \omega)$. Consequently, we write

$$S_0(q, \hbar\omega_q) = \frac{m^2 \hbar\omega_q}{\pi n_e q \hbar^2 (1 - e^{-\beta\hbar\omega_q})}. \quad (11.87)$$

We also need an expression for $V_{ei}(q)$. In the Thomas–Fermi treatment of screening, we showed that

$$V_{ei}(q) = -\frac{4\pi Ze^2}{V(q^2 + \kappa_{TF}^2)}. \quad (11.88)$$

At low temperatures, we focus on the limit ($q \rightarrow 0$) of V_{ei} . Hence, we approximate $V_{ei}(q)$ with

$$\begin{aligned} V_{ei}(q) &= -\frac{4\pi Ze^2}{V\kappa_{TF}^2} \\ &= -\frac{\pi^2 Z \hbar^3}{V m p_F} = -\frac{Z}{N(\epsilon_F)}. \end{aligned} \quad (11.89)$$

The relaxation time can be written as

$$\frac{1}{\tau} = \frac{Z^2 \beta m}{24\pi^3 n_e \hbar^3 N^2(\epsilon_F) M n_{ion}} \int_0^{q_D} \frac{q^5 dq}{(1 - e^{-\beta\hbar\omega_q})(e^{\beta\hbar\omega_q} - 1)}. \quad (11.90)$$

For the phonon spectrum, we use the linear dispersion relationship, $w_q = sq/\hbar$, where s is a constant. Let $x = \beta\omega_q$. With the observation that

$$\frac{1}{(e^x - 1)(1 - e^{-x})} = -\frac{\partial}{\partial x} \frac{1}{e^x - 1}, \quad (11.91)$$

we rewrite the relaxation time as

$$\begin{aligned} \frac{1}{\tau} &= -\frac{Z^2 \beta m}{24\pi^3 \hbar^7 n_e M N^2(\epsilon_F) (\beta s)^6} \int_0^{q_D s \hbar / k_B T} x^5 \frac{\partial}{\partial x} \frac{dx}{(e^x - 1)} \\ &= \alpha_0 T^5 J_5(T_D/T), \end{aligned} \quad (11.92)$$

with

$$J_5(y) = - \int_0^y x^5 dx \frac{\partial}{\partial x} \frac{1}{e^x - 1}, \quad (11.93)$$

where $T_D = q_D s \hbar / k_B$ is the Debye temperature, and

$$\alpha_0 = \frac{m Z^2 k_B^5}{\hbar^7 24\pi^3 n_e n_{ion} M N^2(\epsilon_F) s^6}. \quad (11.94)$$

There are two cases of interest. At low temperatures $T_D/T \gg 1$, implying that the integral can be extended to infinity, leaving

$$\begin{aligned} J_5(\infty) &= - \int_0^\infty x^5 dx \frac{\partial}{\partial x} \frac{1}{e^x - 1} \\ &= 5! \zeta(5), \end{aligned} \quad (11.95)$$

where $\zeta(n)$ is the Riemann zeta-function. As a consequence

$$\frac{1}{\tau} = 5! \zeta(5) \alpha_0 T^5 \quad (11.96)$$

for $T \ll T_D$. From the Drude formula, we have that the resistivity $\rho \sim 1/\tau$. We see then that for $T \ll T_D$, the resistivity scales as $\rho \sim T^5$. The origin of the T^5 contribution is as follows. A factor of T^3 arises from the number of phonons present at $T = 0$. The remaining factors of T arise from momentum transfer and the fraction of electrons in the vicinity of ϵ_F that can scatter. Each of these processes scales as T . Note the factor α_0 correctly represents the scaling of the resistivity in terms of the ion mass M , the electron density n_e , and the density of states $N(\epsilon_F)$.

Consider now the high-temperature limit. In this case $T \gg T_D$, and the upper limit in Eq. (11.93) is $y \ll 1$. We can then series-expand the integrand to obtain

$$J_5(y) = - \int_0^y x^5 dx \frac{\partial}{\partial x} \left(\frac{1}{x} + \dots \right) = \int_0^y x^3 dx = \frac{y^4}{4}. \quad (11.97)$$

Because $y = T_D/T$, we find that at high temperatures,

$$\rho \sim \frac{1}{\tau} \propto T^5 \left(\frac{T_D}{T} \right)^4 \sim T. \quad (11.98)$$

Linear behavior sets in for $T/T_D > 0.2$. Of current interest is the linear- T resistivity in the normal state of the high-temperature copper oxide materials (GF1987). As this behavior persists until the onset of superconductivity, the linear- T resistivity is of fundamentally different (and currently unknown) origin than the high-temperature linear- T resistivity that results from phonon scattering.

Of course, normal non-magnetic impurities also contribute to the resistivity. When the concentration (n_{imp}) of non-magnetic impurities is small, the first-Born approximation can be used. In this limit, impurity scattering contributes a constant term to the relaxation rate, proportional to ϵ_F at $T = 0$. This is a reflection that scattering at normal impurities is governed by the electrons at the Fermi energy. For normal impurities of charge Z , the basic result for the impurity relaxation rate is

$$\frac{1}{\tau_{\text{imp}}} \propto \frac{2n_{\text{imp}}Z^2\epsilon_F}{\hbar n_e}. \quad (11.99)$$

Consequently, disorder in a metal is expected to lead to a non-zero resistance at $T = 0$, which is commonly referred to as the residual resistance in a metal. Of course, the situation changes dramatically in the strong-disorder regime. In this limit, perturbation theory breaks down. A transition to an Anderson localized state occurs when the strength of the disorder

exceeds a critical value for $d > 2$ (see Chapter 13). In the localized regime, the electronic states decay exponentially with distance. For $d \leq 2$, the transition is particularly striking as any amount of disorder leads to complete localization of all the electronic eigenstates. Localization of the eigenstates results in a vanishing of the dc conductivity and the onset of an insulating state. In three dimensions, the disorder must exceed a critical value before insulating behavior obtains. In an Anderson localized system, charge carriers must be thermally excited if they are to transport at all. Consequently, activated transport typically obtains in insulators above $T = 0$.

Summary

Two key results were derived in this chapter: (1) the form of the linear interaction between electrons and phonons and (2) the Boltzmann transport theory. Using the latter, we were able to derive the result we advertised initially in Chapter 8, namely that the resistivity vanishes as T^5 in a metal where collisions with phonons dominate all scattering processes. We derived this result using the relaxation-time approximation. An essential ingredient of the relaxation-time approximation is the drift-velocity ansatz. As illustrated in Fig. 11.3, in this approximation the Fermi surface is translated by an amount proportional to the drift velocity. Electrons in the translated Fermi surface are described by the original Fermi–Dirac distribution with the momentum shifted by $\mathbf{p} \rightarrow \mathbf{p} - m\mathbf{v}_d$.

Problems

- 11.1 Prove that $W_{\mathbf{q}}(\mathbf{k}, \mathbf{k}') = e^{\beta(\epsilon_{\mathbf{k}} - \epsilon_{\mathbf{k}'})} W_{\mathbf{q}}(\mathbf{k}', \mathbf{k})$.
- 11.2 Calculate explicitly the impurity contribution to the electrical relaxation rate $1/\tau$. Prove that the impurity contribution to the relaxation rate is proportional to the Fermi energy. A useful strategy is to (1) assume the electrons elastically scatter from the impurities from one plane-wave state to another; (2) average over the random position of the impurities using the random phase approximation in which an average of the form

$$\left\langle \sum_{i,j} e^{i(\mathbf{q}-\mathbf{q}') \cdot (\mathbf{R}_i - \mathbf{R}_j)} \right\rangle \quad (11.100)$$

is non-zero only when $\mathbf{R}_i = \mathbf{R}_j$ and reduces to $V n_{\text{imp}}$ where n_{imp} is the concentration of the impurities; (3) follow the same Boltzmann equation approach we used for the phonon problem invoking again the relaxation time approximation; (4) in the end, evaluate a structure factor of the form $S_0(\mathbf{k}, -\mathbf{k} \cdot \mathbf{v}_d)$. Solve this by a Taylor series expansion retaining only the linear $\mathbf{k} \cdot \mathbf{v}_d$ term. Be careful with the limits. It is from the structure factor that the ϵ_F dependence emerges. (5) Assume an impurity potential that is of the screened Coulomb form. Again take the small- k limit.

References

- [AM1976] N. W. Ashcroft and N. D. Mermin, *Solid State Physics* (Holt, Rinehart and Winston, New York, 1976).
- [G1963] J. Goldstone, *Nuovo Cimento* **19**, 155 (1963).
- [GF1987] M. Gurvitch and A. T. Fiory, *Phys. Rev. Lett.* **59**, 1337 (1987).
- [M1981] G. D. Mahan, *Many-Particle Physics* (Plenum Press, New York, 1981).

In this chapter we focus on the phenomenon of superconductivity and the Bardeen–Cooper–Schrieffer (BCS) ([BCS 1957](#)) theory behind it. Superconductivity obtains when a finite fraction of the conduction electrons in a metal condense into a quantum state characterized by a unique quantum-mechanical phase. The specific value of the quantum-mechanical phase varies from one superconductor to another. The locking in of the phase of a number of electrons on the order of Avogadro's number ensures the rigidity of the superconducting state. For example, electrons in the condensate find it impossible to move individually. Rather, the whole condensate moves from one end of the sample to the other as a single unit. Likewise, electron scattering events that tend to destroy the condensate must disrupt the phase of a macroscopic number of electrons for the superconducting state to be destroyed. Hence, phase rigidity implies collective motion as well as collective destruction of a superconducting condensate. The only other physical phenomenon that arises from a similar condensation of a macroscopic number of particles into a phase-locked state is that of Bose–Einstein condensation. There is a crucial difference between these effects, however. The particles that constitute the condensate in superconductivity are Cooper pairs, which do not obey Bose statistics. In fact, it is the Pauli principle acting on the electrons comprising a Cooper pair that prevents the complete mapping of the superconducting problem onto a simple one of Bose condensation. As we will see, it is the Pauli principle that makes BCS theory work so well. What do we mean by this? In BCS theory, it is assumed that electrons form Cooper pairs, and the pairs are strongly overlapping. Such a strong overlap would imply a strong correlation between pairs. In fact, it is the correlations between pairs that accounts for most of the observed properties of superconductors, for example the energy gap and the Meissner effect. In BCS theory, however, there is no explicit dynamical interaction between Cooper pairs. The only interaction, if it can be thought of in these terms, is that arising from the Pauli exclusion principle which precludes two Cooper pairs from occupying the same momentum state. That BCS theory works so well speaks volumes for the real nature of pair–pair correlations in metals. It would suggest that real pair–pair interactions in a metal arise primarily from the Pauli exclusion principle, rather than from some additional dynamical interaction. It is primarily for this reason that the simple pairing hypothesis of BCS has had such profound success.

12.1 Superconductivity: phenomenology

At the outset, we lay plain the experimental facts that any theory of superconductivity must explain.

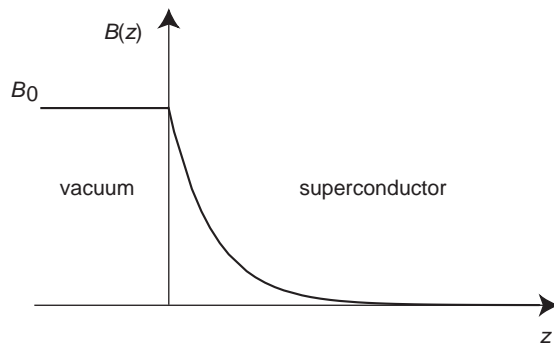


Fig. 12.1 Fall-off of the magnetic field in a Type I superconductor.

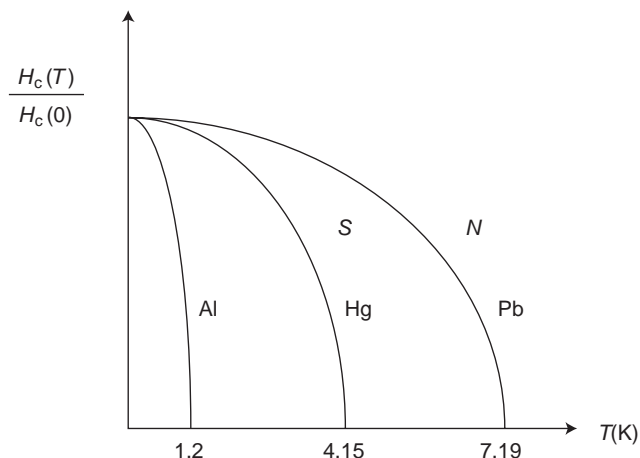


Fig. 12.2 The dependence of the critical field as a function of temperature. The temperatures indicated on the horizontal axis represent the superconducting transition temperatures for a series of metals.

- (a) **Zero resistance** The typical signature of superconductivity is the vanishing of the electrical resistance below some critical temperature T_c . The superconducting state is a thermodynamically distinct state of matter. Below T_c , a current flows without any loss. Until the high- T_c materials were made, Nb held the highest transition temperature at 9.26 K.
- (b) **Meissner effect** Another feature is the exclusion of magnetic fields, the Meissner effect. Materials in which the Meissner effect is complete are known as Type I superconductors. Consequently, the interior of a Type I superconductor is a perfect diamagnet. A magnetic field applied at the boundary of a Type I superconductor falls off exponentially with distance in the interior of the material, as illustrated in Fig. 12.1. The penetration depth, λ_L , is defined as the distance over which the magnetic field decreases by the factor $1/e$. Below T_c , the field needed to destroy superconductivity increases to some critical value $H_c(T)$, as illustrated in Fig. 12.2. Because the magnetic field inside a superconductor

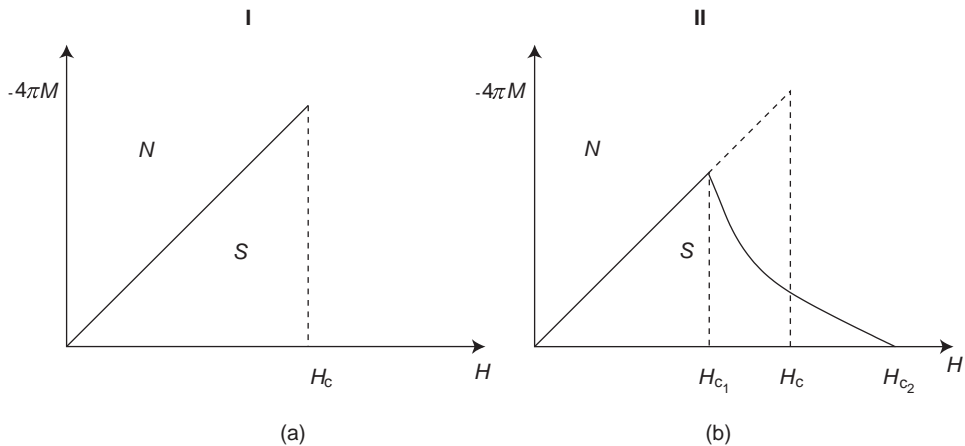


Fig. 12.3 (a) Magnetization vs applied field for a Type I superconductor. (b) Magnetization vs applied field for a Type II superconductor. Between H_{c_1} and H_c , magnetic field lines penetrate the superconductor but they do not destroy superconductivity. The field lines form a vortex lattice.

is zero,

$$B = 0 = H_{\text{appl}} + 4\pi M, \quad (12.1)$$

where H_{appl} is the applied field and M the magnetization. Solving this equation, we find that the magnetization is

$$M = -\frac{1}{4\pi}H_{\text{appl}}. \quad (12.2)$$

The negative value of M signals that the interior of a superconductor is diamagnetic. At any temperature less than T_c , the magnetization should be a linear function of the applied field. A material having a magnetization of this form is called a Type I superconductor. The normal state is indicated with an N and the superconducting state with an S . Above H_c , $B \neq 0$ and the magnetization no longer obeys Eq. (12.2).

In some materials, superconductivity is observed up to an upper critical field H_{c_2} , but an incomplete Meissner effect is seen between a lower critical field H_{c_1} and H_{c_2} . The resultant magnetization is shown in Fig. 12.3(b). Materials exhibiting a magnetization of this kind are known as Type II superconductors. Between H_{c_1} and H_{c_2} , the magnetic field penetrates the material but superconductivity is not destroyed. The field lines form a regular array known as the Abrikosov ([A1957](#)) vortex lattice. All high- T_c cuprate superconductors are Type II.

We are concerned primarily with Type I materials. To understand the penetration depth in a superconductor, we resort to the London equations. First, we need the Maxwell equation for the curl of an electric field: $-\partial \mathbf{B}/\partial t = c\nabla \times \mathbf{E} = c\rho \nabla \times \mathbf{J}$, where ρ is the resistivity. In a perfect conductor $\rho = 0$ and, as a consequence, $\partial \mathbf{B}/\partial t = 0$. In a superconductor, $\rho = 0$ as well. However, it is an experimental fact that $B = 0$

inside a superconductor. This result cannot be deduced from the Maxwell equations. It is the Meissner effect that sets superconductivity apart from materials that just display perfect conductivity. Inside a superconductor, expulsion of magnetic flux is mediated by the current that flows. London proposed in 1935 that everywhere in a superconductor

$$\mathbf{J} = -\text{const.}\mathbf{A}, \quad (12.3)$$

where \mathbf{A} is the vector potential and $\mathbf{B} = \nabla \times \mathbf{A}$. From this ansatz, London was able to show that a magnetic field decays exponentially inside a superconductor. Dimensionally, the constant has units of $1/(L \cdot \text{time})$. Let us write the constant as

$$\text{const.} = \frac{c}{4\pi\lambda_L^2}, \quad (12.4)$$

where c is the speed of light. If we take the curl of both sides of Eq. (12.3), we find that

$$\nabla \times \mathbf{J} = -\frac{c}{4\pi\lambda_L^2}\mathbf{B}. \quad (12.5)$$

From Ampère's law,

$$\nabla \times \mathbf{B} = \frac{4\pi}{c}\mathbf{j}, \quad (12.6)$$

we find that

$$\nabla \times (\nabla \times \mathbf{B}) = \frac{4\pi}{c}\nabla \times \mathbf{J}, \quad (12.7)$$

which implies that

$$\nabla^2\mathbf{B} = \frac{1}{\lambda_L^2}\mathbf{B}. \quad (12.8)$$

The solution to this equation,

$$B(r) = B(0)e^{-r/\lambda_L}, \quad (12.9)$$

is an exponentially decaying magnetic induction on a length scale λ_L . Exponential decay of the magnetic field into a superconductor is the Meissner effect. Let v_s , m^* , and e^* , respectively, be the velocity, mass, and charge of the current carriers in a superconductor. Then

$$m^*\dot{\mathbf{v}}_s = -e^*\mathbf{E}. \quad (12.10)$$

The current of these electrons is defined as $\mathbf{J} = -e^*\mathbf{v}_s n_s$, which, combined with Eq. (12.10), yields

$$\frac{\partial \mathbf{J}}{\partial t} = \frac{n_s e^{*2}}{m^*} E \quad (12.11)$$

for the time evolution of the current. Taking the curl of both sides, we find that

$$\begin{aligned} 0 &= \frac{\partial}{\partial t}(\nabla \times \mathbf{J}) - \frac{n_s e^2}{m^*} \nabla \times \mathbf{E} \\ &= \frac{\partial}{\partial t} \left(\nabla \times \mathbf{J} + \frac{n_s e^{*2}}{m^* c} \mathbf{B} \right). \end{aligned} \quad (12.12)$$

Comparing Eq. (12.12) with Eq. (12.5), we obtain that the penetration depth is

$$\lambda_L = \left(\frac{m^* c^2}{4\pi n_s e^{*2}} \right)^{1/2}. \quad (12.13)$$

We see then that as the superconducting density increases, λ_L decreases.

We can justify the main assumption in the London approach by appealing to the theory of Ginsburg and Landau (GL1950). The crucial ingredient in this phenomenological theory is that the difference in the free energy density between the superconducting and normal states can be written as a functional of an order parameter, $\psi(\mathbf{r})$, for the superconducting state. Physically, $|\psi(\mathbf{r})|^2$ is proportional to the charge density in the superconducting state, n_s . Consequently, we can interpret $\psi(\mathbf{r})$ as the wavefunction of the superconducting state. In BCS theory, $\psi(\mathbf{r})$ plays the role of the center-of-mass wavefunction for a Cooper pair. Near T_c , the superfluid density is small; hence $|\psi|^2 \ll n_e$. Consequently, Ginsburg and Landau expanded the free energy density for the superconducting state in the vicinity of T_c as a power series in $|\psi|^2$,

$$F = F_N + \int d\mathbf{r} \left(\frac{\hbar^2}{2m^*} |\nabla \psi|^2 + a(T) |\psi(\mathbf{r})|^2 + b(T) |\psi(\mathbf{r})|^4 \right), \quad (12.14)$$

retaining the kinetic energy term, $|\nabla \psi|^2$, to account explicitly for spatial variations of the field $\psi(\mathbf{r})$. The free energy of the normal state is F_N . The coefficients $a(T)$ and $b(T)$ are real and temperature-dependent and, for stability, $b(T) > 0$.

To find the ground state of the system, we minimize the free energy density with respect to $\psi^*(\mathbf{r})$:

$$-\frac{\hbar^2}{2m^*} \nabla^2 \psi(\mathbf{r}) + a(T) \psi(\mathbf{r}) + 2b(T) |\psi(\mathbf{r})|^2 \psi(\mathbf{r}) = 0. \quad (12.15)$$

Because the free energy density contains the term $|\nabla \psi|^2$, which is always positive, the free energy is minimized by demanding that $\nabla \psi(\mathbf{r}) = 0$ or, equivalently, that ψ be uniform in space. Consequently, the solution to the saddle point equation is either $\psi = 0$ or

$$|\psi_0|^2 = -\frac{a(T)}{2b(T)} = n_s, \quad (12.16)$$

which implies that $a(T) < 0$. Should $a(T)$ exceed zero, $\psi = 0$, and the system would be in the normal state. Since superconductivity vanishes at T_c , we must have that $a(T_c) = 0$. A Taylor expansion of $a(T)$ around T_c to first order leads to the result that

$$a(T) = a_1(T - T_c) \quad (12.17)$$

with $a_1 > 0$.

We obtain the London conjecture by recalling that the current density in the presence of a vector potential, \mathbf{A} , is

$$\mathbf{J} = \frac{e^* \hbar}{2im^*} (\psi^* \nabla \psi - \psi \nabla \psi^*) - \frac{e^{*2}}{m^* c} |\psi|^2 \mathbf{A}. \quad (12.18)$$

If we assume that the magnetic field is sufficiently small that the equilibrium value of ψ_0 is unchanged, then substitution of ψ_0 into Eq. (12.18) yields the London result

$$\mathbf{J} = -\frac{e^{*2} n_s}{m^* c} \mathbf{A}. \quad (12.19)$$

Using Eq. (12.13), we find that this result is consistent with Eq. (12.4). Hence, from this simple phenomenological approach, we are able to justify the London ansatz for the current density. Indeed, as we will see, the key intellectual content of the BCS theory of superconductivity is the existence of an order parameter describing a charge $2e$ condensate with a well-defined phase, as in the Ginzburg–Landau theory. Such a condensate breaks the $U(1)$ gauge symmetry, as discussed in Chapter 1. In fact, the very existence of the Meissner effect implies the breaking of a continuous symmetry. The fact that a magnetic field cannot penetrate a superconductor tells us immediately that in a superconductor, the photon is massive. Consequently, it can no longer be assumed that the electrons are the propagating degrees of freedom. In fact, in a superconductor they are not. The charge is quantized in units of $2e$, implying that $U(1)$ symmetry is broken.

- (c) **Heat capacity** In the superconducting state, the entropy decreases continuously but dramatically, signaling the formation of a highly ordered state. This is depicted in Fig. 12.4(a). As a result, the temperature derivative of the entropy must be steeper on the superconducting side than on the normal side of the transition. Consequently, the heat capacity is discontinuous at T_c , and superconductivity is a second-order phase transition. As shown in Fig. 12.4(b), in the superconducting state, the heat capacity, c_s , falls off as $c_s \propto \exp(-\Delta/k_B T)$, where Δ is an energy scale. A heat capacity of this form is indicative of an energy gap in the excitation spectrum, with $\epsilon_p > \mu$. Let us verify this with the simple calculation:

$$c_V = \frac{\partial}{\partial T} \int \frac{\epsilon_p d\epsilon_p}{(e^{\beta(\epsilon_p - \mu)} + 1)} \xrightarrow{T \rightarrow 0} \frac{\partial}{\partial T} \int \epsilon_p e^{-\beta(\epsilon_p - \mu)} d\epsilon_p. \quad (12.20)$$

If $(\epsilon_p - \mu) \approx \Delta$, then $c_V \sim \exp(-\Delta(T = 0)/k_B T)$. Consequently, in the superconducting state, we adopt the picture for the energy gap shown in Fig. 12.5.

The formation of a gap at the Fermi level in the superconducting state results in a lowering of the ground state energy of the system. The gap is actually 2Δ , not Δ . Hence, $\epsilon_p - \mu$ accounts for only half the gap. Experimentally, the gap can be measured by tunneling or ultrasound attenuation experiments. Thermodynamically, the gap gives rise to a discontinuity in the heat capacity. That is, $c_s(T_c^-) - c_N(T_c^+) \neq 0$. Across

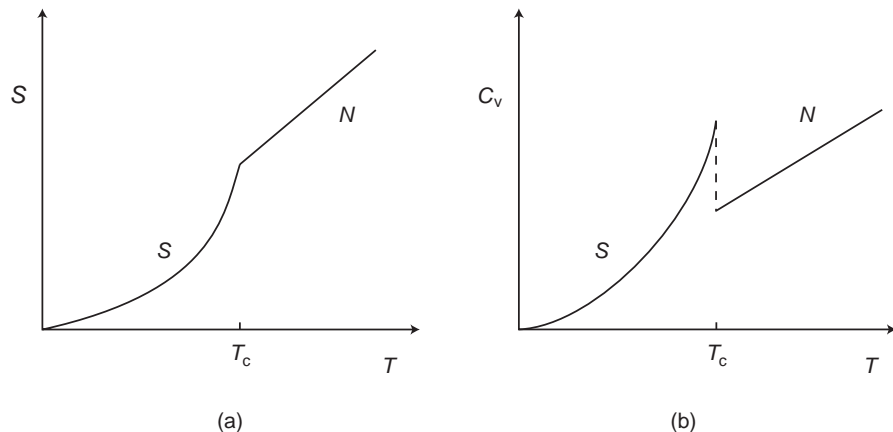


Fig. 12.4 (a) Behavior of the entropy across the superconducting transition. (b) Behavior of the heat capacity in the normal and superconducting states.

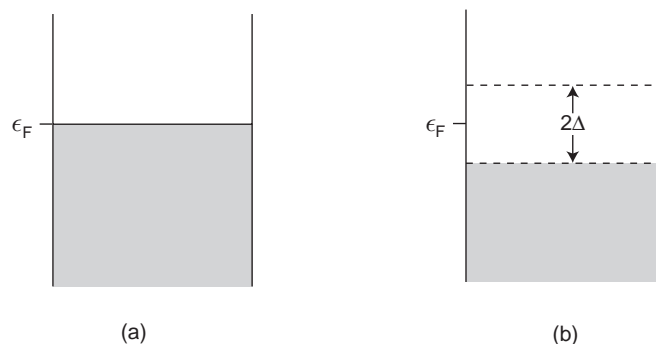


Fig. 12.5 (a) Filled energy levels in the normal state. (b) Formation of an energy gap in the superconducting state. The full gap is 2Δ , not Δ .

the superconducting transition, both first derivatives of the free energy vanish. Hence, no latent heat is associated with the superconducting transition. Above T_c , $\Delta = 0$, and at $T = 0$, Δ has its largest value. A typical plot of $\Delta(T)/\Delta(T = 0)$ is shown in Fig. 12.6. A weak-coupling superconductor has a ratio of $2\Delta(T = 0)/k_B T_c$ in the range 1 to 3. Strong coupling corresponds to $2\Delta(T = 0)/k_B T_c > 4$. The basic energy scale for the creation of an electron–hole pair in a superconductor is 2Δ .

- (d) **Microwave and infrared properties** As a result of the gap, photons possessing energies less than 2Δ are not absorbed: all such photons are reflected. Perfect reflection occurs for $\omega < 2\Delta(T = 0)/\hbar$. When this condition is true, photons see a completely resistanceless surface. As $\omega > 2\Delta(T = 0)/\hbar$ at absolute zero, the resistance begins to approach that of the normal state. We estimate this energy by assuming a weak-coupling description is valid for the superconductor. Then $\Delta \sim 2k_B T_c$, and $\omega \sim 4k_B T_c/\hbar$. For a T_c of 5 K, $\omega \sim 10^{12} \text{ s}^{-1}$. This frequency is in the infrared. Infrared radiation can then penetrate a superconductor and scatter the electrons.

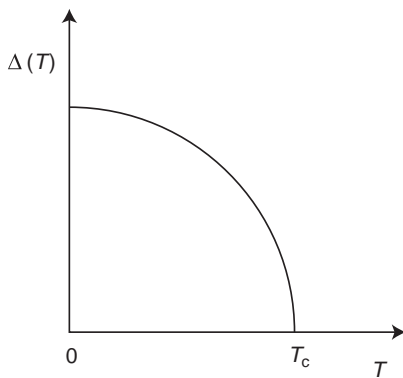


Fig. 12.6 The behavior of the superconducting gap, Δ , as $T \rightarrow T_c$.

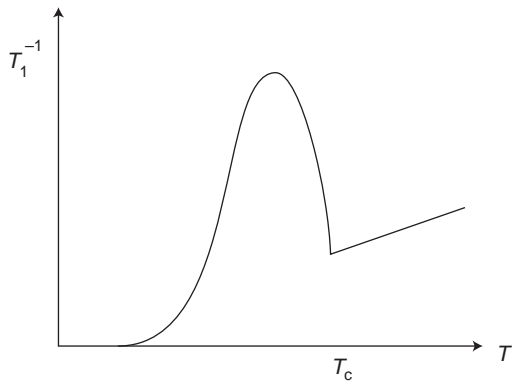


Fig. 12.7 Behavior of the spin-lattice relaxation time at and below T_c . The enhancement in $1/T_1$ is a signature that the spins in a superconductor are acting in consort.

- (e) **Ultrasonic attenuation** No damping of an impinging beam of phonons is observed if $\omega_q < 2\Delta/\hbar$. As in the microwave absorption case, ω_q must exceed the energy needed to create an electron–hole pair.
- (f) **Nuclear-spin relaxation** Consider a set of nuclei that have been forced to align with a magnetic field. The rate at which the equilibrium magnetization is recovered is the spin lattice relaxation rate, $1/T_1$. In a superconductor, $(1/T_1)_S > (1/T_1)_N$ just below T_c . That is, there is an enhancement in the relaxation rate that is brought on by the formation of the superconducting state. Hebel and Slichter ([HS1959](#)) were the first to see this effect experimentally. The peak in the relaxation rate just below T_c is known as the Hebel–Slichter peak.
- (g) **Isotope effect** Experimentally, it is observed that if the mass of the ions is changed isotopically, T_c changes accordingly:

$$T_c \propto \frac{1}{\sqrt{M}} \propto \omega_D. \quad (12.21)$$

This observation implies that electron–phonon coupling is at the heart of superconductivity (at least traditional superconductivity).

12.2 Electron–phonon effective interaction

The isotope dependence of T_c confirms that electron–phonon coupling is central to the mechanism of superconductivity. We show now how electron–phonon coupling can produce an attractive interaction between two electrons. The starting point for our analysis is an ordered band of electrons with kinetic energies $\epsilon_{\mathbf{k}}$ coupled to the quantized vibrational modes of the crystal. As a result, our Hamiltonian $H = H_o + H_{e-ph}$ is a sum of an ordered part,

$$H_o = \sum_{\mathbf{q}} \hbar \omega_{\mathbf{q}} b_{\mathbf{q}}^\dagger b_{\mathbf{q}} + \sum_{\mathbf{k}} \epsilon_{\mathbf{k}} a_{\mathbf{k}}^\dagger a_{\mathbf{k}}, \quad (12.22)$$

and the electron–lattice interaction

$$H_{e-ph} = \sum_{\mathbf{k}, \mathbf{q}} M_{\mathbf{q}} a_{\mathbf{k}+\mathbf{q}}^\dagger a_{\mathbf{k}} (b_{\mathbf{q}} + b_{-\mathbf{q}}^\dagger). \quad (12.23)$$

The electron–phonon coupling constant is defined in Section 11.3. We will assume that the electron–phonon interaction is weak and do perturbation theory to second order in this interaction. As a second-order perturbation, we anticipate that the electron–phonon interaction will provide a negative correction to the energy. While the final result can be established quite straightforwardly (see Problem 12.3) using second-order perturbation theory, we will use a similarity transformation, as this method has numerous applications in electron–phonon problems. Our analysis will mirror the Schrieffer–Wolff transformation. Eliminating the linear electron–phonon interaction will produce a second-order interaction, from which we will be able to deduce the conditions under which phonons effectively bind electrons.

We seek a transformation S , such that

$$[H_o, S] = -H_{e-ph}. \quad (12.24)$$

The transformed Hamiltonian will be

$$\begin{aligned} \tilde{H} &= e^{-S} H e^S \\ &= H_o + \frac{1}{2} [H_{e-ph}, S] + \dots \end{aligned} \quad (12.25)$$

We posit that S is of the form

$$S = \sum_{\mathbf{k}, \mathbf{q}} (A_{\mathbf{k}, \mathbf{q}} b_{-\mathbf{q}}^\dagger + B_{\mathbf{k}, \mathbf{q}} b_{\mathbf{q}}) M_{\mathbf{q}} a_{\mathbf{k}+\mathbf{q}}^\dagger a_{\mathbf{k}}, \quad (12.26)$$

where A and B are to be determined by the constraint in Eq. (12.24). To proceed, we need the commutators

$$\begin{aligned} \left[n_{\mathbf{k}}, a_{\mathbf{k}_1}^{\dagger} a_{\mathbf{k}_2} \right] &= a_{\mathbf{k}_1}^{\dagger} a_{\mathbf{k}_2} (\delta_{\mathbf{k}_1 \mathbf{k}} - \delta_{\mathbf{k}_2 \mathbf{k}}), \\ \left[b_{\mathbf{q}}^{\dagger}, b_{\mathbf{q}} \right] &= -1, \\ \left[b_{\mathbf{q}}^{\dagger} b_{\mathbf{q}}, b_{\mathbf{q}'} \right] &= -b_{\mathbf{q}} \delta_{\mathbf{q} \mathbf{q}'}. \end{aligned} \quad (12.27)$$

We find then that

$$\begin{aligned} [H_0, S] &= \sum_{\mathbf{q}', \mathbf{k}, \mathbf{q}} \hbar \omega_{\mathbf{q}'} \left[b_{\mathbf{q}'}^{\dagger} b_{\mathbf{q}'}, (A_{\mathbf{k}, \mathbf{q}} b_{-\mathbf{q}}^{\dagger} + B_{\mathbf{k}, \mathbf{q}} b_{\mathbf{q}}) a_{\mathbf{k}+\mathbf{q}}^{\dagger} a_{\mathbf{k}} \right] M_{\mathbf{q}} \\ &\quad + \sum_{\mathbf{k}', \mathbf{k}, \mathbf{q}} \epsilon_{\mathbf{k}'} M_{\mathbf{q}} \left[a_{\mathbf{k}'}^{\dagger} a_{\mathbf{k}'}, (A_{\mathbf{k}, \mathbf{q}} b_{-\mathbf{q}}^{\dagger} + B_{\mathbf{k}, \mathbf{q}} b_{\mathbf{q}}) a_{\mathbf{k}+\mathbf{q}}^{\dagger} a_{\mathbf{k}} \right] \\ &= \sum_{\mathbf{k}, \mathbf{q}} M_{\mathbf{q}} b_{-\mathbf{q}}^{\dagger} a_{\mathbf{k}+\mathbf{q}}^{\dagger} a_{\mathbf{k}} (\hbar \omega_{-\mathbf{q}} + \epsilon_{\mathbf{k}+\mathbf{q}} - \epsilon_{\mathbf{k}}) A_{\mathbf{k}, \mathbf{q}} \\ &\quad + \sum_{\mathbf{k}, \mathbf{q}} M_{\mathbf{q}} b_{\mathbf{q}} a_{\mathbf{k}+\mathbf{q}}^{\dagger} a_{\mathbf{k}} (\epsilon_{\mathbf{k}+\mathbf{q}} - \epsilon_{\mathbf{k}} - \hbar \omega_{\mathbf{q}}) B_{\mathbf{k}, \mathbf{q}}. \end{aligned} \quad (12.28)$$

This quantity must equal $-H_{e-ph}$. The $A_{\mathbf{k}, \mathbf{q}}$ and $B_{\mathbf{k}, \mathbf{q}}$ coefficients that satisfy this constraint are

$$A_{\mathbf{k}, \mathbf{q}} = -(\hbar \omega_{-\mathbf{q}} + \epsilon_{\mathbf{k}+\mathbf{q}} - \epsilon_{\mathbf{k}})^{-1} \quad (12.29)$$

and

$$B_{\mathbf{k}, \mathbf{q}} = -(\epsilon_{\mathbf{k}+\mathbf{q}} - \epsilon_{\mathbf{k}} - \hbar \omega_{\mathbf{q}})^{-1}. \quad (12.30)$$

Our unitary transformation is then

$$S = \sum_{\mathbf{k}, \mathbf{q}} \left[\frac{b_{-\mathbf{q}}^{\dagger}}{(\epsilon_{\mathbf{k}} - \epsilon_{\mathbf{k}+\mathbf{q}} - \hbar \omega_{-\mathbf{q}})} + \frac{b_{\mathbf{q}}}{(\epsilon_{\mathbf{k}} - \epsilon_{\mathbf{k}+\mathbf{q}} + \hbar \omega_{\mathbf{q}})} \right] M_{\mathbf{q}} a_{\mathbf{k}+\mathbf{q}}^{\dagger} a_{\mathbf{k}}. \quad (12.31)$$

Note the form of the energy denominators. The denominator of $b_{-\mathbf{q}}^{\dagger}$ corresponds to the energy difference for emission of a phonon of energy $\hbar \omega_{-\mathbf{q}}$ and the denominator of $b_{\mathbf{q}}$ to absorption. Let us define $\Delta_{\pm}(\mathbf{k}, \mathbf{q}) = \epsilon_{\mathbf{k}} - \epsilon_{\mathbf{k}+\mathbf{q}} \pm \hbar \omega_{\pm \mathbf{q}}$. The effective Hamiltonian is given by

$$\tilde{H} = H_0 + \frac{1}{2} \sum_{\mathbf{k}, \mathbf{q}, \mathbf{k}', \mathbf{q}'} \left[M_{\mathbf{q}} M_{\mathbf{q}'} (b_{-\mathbf{q}}^{\dagger} + b_{\mathbf{q}}) a_{\mathbf{k}+\mathbf{q}}^{\dagger} a_{\mathbf{k}}, \left(\frac{b_{-\mathbf{q}'}^{\dagger}}{\Delta_{-}(\mathbf{k}', \mathbf{q}')} + \frac{b_{\mathbf{q}'}^{\dagger}}{\Delta_{+}(\mathbf{k}', \mathbf{q}')} \right) a_{\mathbf{k}'+\mathbf{q}'}^{\dagger} a_{\mathbf{k}'} \right]. \quad (12.32)$$

We need to evaluate a commutator of the form

$$\left[(b_{-\mathbf{q}}^{\dagger} + b_{\mathbf{q}}) a_{\mathbf{k}+\mathbf{q}}^{\dagger} a_{\mathbf{k}}, b_{-\mathbf{q}'}^{\dagger} a_{\mathbf{k}'+\mathbf{q}'}^{\dagger} a_{\mathbf{k}'} \right]. \quad (12.33)$$

Specifically, we are interested in the two-electron terms that are produced from this commutator. If we were to evaluate the electron commutator part, we would obtain only a one-body potential. Such one-body potentials are not of interest here as they do not affect the interaction between two electrons. The commutator involving the phonon operators produces

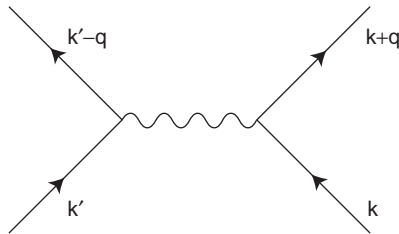


Fig. 12.8 Electron–phonon interaction giving rise to BCS pairing near the Fermi surface. The wavy line represents the interaction in Eq. (12.35).

an effective two-body potential that, interestingly enough, is negative in a narrow energy scale around the Fermi energy. To see this, we note that the phonon part of the commutator in Eq. (12.33) yields the constraint $\delta_{\mathbf{q}+\mathbf{q}'}$. Consequently, our effective Hamiltonian is

$$\begin{aligned}\tilde{H} &= H_0 + \frac{1}{2} \sum_{\mathbf{k}, \mathbf{k}', \mathbf{q}} M_{\mathbf{q}} M_{-\mathbf{q}} \left[\frac{a_{\mathbf{k}+\mathbf{q}}^\dagger a_{\mathbf{k}} a_{\mathbf{k}'-\mathbf{q}}^\dagger a_{\mathbf{k}'}^{} - a_{\mathbf{k}+\mathbf{q}}^\dagger a_{\mathbf{k}} a_{\mathbf{k}'-\mathbf{q}}^\dagger a_{\mathbf{k}'}^{} }{\Delta_{-}(\mathbf{k}', -\mathbf{q}) - \Delta_{+}(\mathbf{k}', -\mathbf{q})} \right] \\ &= H_0 + \sum_{\mathbf{k}, \mathbf{k}', \mathbf{q}} |M_{\mathbf{q}}|^2 a_{\mathbf{k}+\mathbf{q}}^\dagger a_{\mathbf{k}'-\mathbf{q}}^\dagger a_{\mathbf{k}'}^{} a_{\mathbf{k}}^{} \frac{\hbar\omega_{\mathbf{q}}}{(\Delta_{\mathbf{k}', \mathbf{q}})^2 - (\hbar\omega_{\mathbf{q}})^2}\end{aligned}\quad (12.34)$$

with $\Delta_{\mathbf{k}', \mathbf{q}} = \epsilon_{\mathbf{k}'} - \epsilon_{\mathbf{k}'-\mathbf{q}}$. In general, $\epsilon_{\mathbf{k}'}$ and $\epsilon_{\mathbf{k}'-\mathbf{q}}$ vastly exceed $\hbar\omega_{\mathbf{q}}$. However, if $|\epsilon_{\mathbf{k}'} - \epsilon_{\mathbf{k}'-\mathbf{q}}| < \hbar\omega_{\mathbf{q}}$, then the two-electron potential in Eq. (12.34) is negative, and the electrons experience a net attraction. Note that we have shown that a net attraction exists in k -space, not real-space. The k -space attraction allows two electrons to bind together so that they have a total energy that is lower than their non-interacting counterparts. This attraction is the basis for pairing in BCS superconductivity. Diagrammatically, this interaction is depicted in Fig. 12.8, where the wavy line represents the electron–phonon interaction,

$$V(\mathbf{k}', \mathbf{q}) = \frac{|M_{\mathbf{q}}|^2 \hbar\omega_{\mathbf{q}}}{(\epsilon_{\mathbf{k}'} - \epsilon_{\mathbf{k}'-\mathbf{q}})^2 - (\hbar\omega_{\mathbf{q}})^2}. \quad (12.35)$$

12.3 Model interaction

In a metal, of course, we must consider the electron–electron repulsion. We can represent this potential as

$$V_{ee}^o = \frac{V_e(\mathbf{q})}{\varepsilon(\mathbf{q}, \omega)}, \quad (12.36)$$

with $\varepsilon(q, \omega)$ the dynamic dielectric screening function. There is of course another source of electron–electron interaction, the attraction induced by phonons. The full interaction

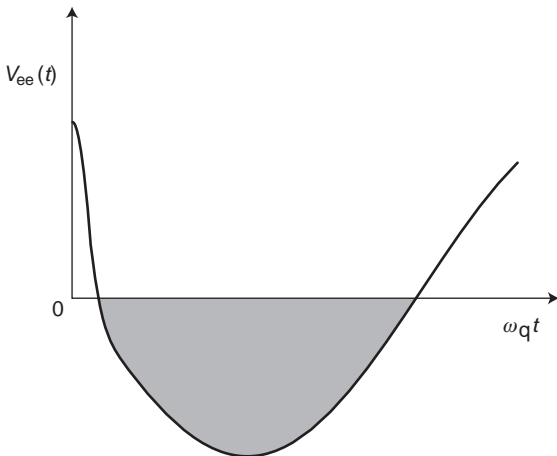


Fig. 12.9 Fourier transform of the full electron interaction including the contribution from phonons. The delta-function contribution from the electron repulsions has been smeared slightly in the vicinity of $t = 0$.

between electrons is of the form

$$V_{ee} = \frac{V_e(\mathbf{q})}{\varepsilon(\mathbf{q})} + \frac{\hbar\omega_{\mathbf{q}} |M_{\mathbf{q}}|^2}{(\Delta\epsilon_{\mathbf{k},\mathbf{q}})^2 - (\hbar\omega_{\mathbf{q}})^2}, \quad (12.37)$$

where we have taken the static limit of the screening function. Now $\varepsilon(\mathbf{q}) > 0$, unless the static compressibility is negative, as discussed in Chapter 9. We exclude this situation here as a negative compressibility occurs in the dilute regime where non-perturbative treatments of the Coulomb interaction are required. Typically, $V_e(\mathbf{q})$ is much greater than the phonon part of the potential. However, when $\Delta\epsilon_{\mathbf{k},\mathbf{q}} \simeq \hbar\omega_{\mathbf{q}}$, the phonon part dominates, and a net attraction is introduced. We see then that on different energy scales, either the phonon or the electron part can dominate. The largest phonon frequency that is relevant is $\hbar\omega_D$, the Debye energy. Hence, for $\Delta\epsilon_{\mathbf{k},\mathbf{q}} \leq \hbar\omega_D$, a net attraction is produced that dominates the electron repulsion. When both electrons have an energy close to the Fermi energy, then $\Delta\epsilon_{\mathbf{k},\mathbf{q}} \approx 0$, and an attractive interaction obtains. This is an essential feature of the BCS theory.

Before we leave this section, it is instructive to consider the time Fourier transform of the interaction potential, V_{ee} . Let $\hbar\omega = \Delta\epsilon_{\mathbf{k},\mathbf{q}}$. The Fourier transform of V_{ee} is

$$\begin{aligned} V_{ee}(t) &= \int_{-\infty}^{\infty} \frac{d\omega}{2\pi} e^{-i\omega t} \left[V_{ee}^0 + \frac{\hbar\omega_{\mathbf{q}} |M_{\mathbf{q}}|^2}{(\hbar\omega)^2 - (\hbar\omega_{\mathbf{q}})^2} \right] \\ &= V_{ee}^0 \delta(t) + |M_{\mathbf{q}}|^2 \frac{\hbar\omega_{\mathbf{q}}}{2\pi} \int_{-\infty}^{\infty} \frac{e^{-i\omega t}}{(\hbar\omega - \hbar\omega_{\mathbf{q}})(\hbar\omega + \hbar\omega_{\mathbf{q}})} d\omega \\ &= V_{ee}^0 \delta(t) - |M_{\mathbf{q}}|^2 \sin \omega_{\mathbf{q}} t. \end{aligned} \quad (12.38)$$

The repulsive part acts only at $t = 0$, while the attraction is an oscillatory function of time. The total potential is shown in Fig. 12.9. We find that the electron potential is attractive only over a time interval where the phonon attraction dominates. This is a key point; V_{ee}

in the time domain is not always attractive. Electron repulsions and the phonon-mediated attraction act on different time scales and hence pair-binding of electrons is possible.

Let us evaluate the two-body scattering amplitude,

$$A_s = \langle \mathbf{p}_{4\sigma_1} \mathbf{p}_{3\sigma_2} | V_{ee} | \mathbf{p}_{1\sigma_1} \mathbf{p}_{2\sigma_2} \rangle, \quad (12.39)$$

where

$$V_{ee} = \sum_{\mathbf{k}, \mathbf{k}', \mathbf{q}} V(\mathbf{k}, \mathbf{k}' - \mathbf{q}) a_{\mathbf{k}+\mathbf{q}}^\dagger a_{\mathbf{k}'-\mathbf{q}}^\dagger a_{\mathbf{k}'} a_{\mathbf{k}}. \quad (12.40)$$

As discussed in Chapter 5, any two-body amplitude of this form separates into a difference of direct and exchange Coulomb integrals. For a general momentum-dependent potential, the direct and exchange terms will enter with different combinations of the momenta and spin. For example, the exchange term will be of the form $V(\mathbf{p}_1, \mathbf{p}_3)$ with $\sigma_1 = \sigma_2$, whereas the direct term will enter with no restriction on the spins and will depend on $V(\mathbf{p}_1, \mathbf{p}_4)$. Let us assume that the net attractive potential is a constant of the form

$$V_{ee} = \begin{cases} -V_0, & |\Delta\epsilon_{\mathbf{k}_F, \mathbf{q}}| < \hbar\omega_D, \\ 0, & |\Delta\epsilon_{\mathbf{k}_F, \mathbf{q}}| > \hbar\omega_D. \end{cases} \quad (12.41)$$

Because the potential is momentum-independent, the direct and exchange integrals are equal, and the scattering amplitude vanishes when $\sigma_1 = \sigma_2$. The only non-zero contribution arises from $\sigma_1 \neq \sigma_2$. As a consequence, for a constant interaction, the scattering amplitude is non-zero only if the electrons are locked into a singlet state. In this case, phonons induce a net attraction between electrons of opposite spin. The corresponding matrix element is of the form

$$\langle \mathbf{p}_{4\uparrow} \mathbf{p}_{3\downarrow} | V_{ee} | \mathbf{p}_{1\uparrow} \mathbf{p}_{2\downarrow} \rangle = -V_0 \delta_{\mathbf{p}_1 + \mathbf{p}_2, \mathbf{p}_3 + \mathbf{p}_4} \quad (12.42)$$

for scattering in the vicinity of the Fermi surface. Two particles locked into a singlet state will give rise to a gap at the Fermi level.

12.4 Cooper pairs

Consider now the somewhat artificial problem of a full Fermi sea containing N non-interacting electrons with two additional interacting electrons outside the sea. As a result of the Pauli exclusion principle, the momentum of the electrons outside the Fermi sea must exceed p_F . We take the potential of interaction to be the constant singlet pair potential derived in the previous section, Eq. (12.42). The spin wavefunction is hence antisymmetric with respect to spin. The corresponding spatial part must be symmetric to satisfy the overall antisymmetry requirement. The eigenvalue equation for our subsystem of two particles is

$$\left[-\frac{\hbar^2}{2m} (\nabla_1^2 + \nabla_2^2) + V(\mathbf{r}_1 - \mathbf{r}_2) - E \right] \Psi(\mathbf{r}_1, \mathbf{r}_2; \uparrow_1, \downarrow_2) = 0. \quad (12.43)$$

In general, the two-body wavefunction is a composite state

$$\Psi(\mathbf{r}_1, \mathbf{r}_2; \uparrow_1, \downarrow_2) = \psi(\mathbf{r}_1, \mathbf{r}_2) \chi_S(\uparrow_1, \downarrow_2), \quad (12.44)$$

where $\chi_s(\uparrow_1, \downarrow_2)$ represents the singlet spin state and ψ contains the spatial dependence. For two particles, we can express the spatial wavefunction in terms of the relative coordinate, $\mathbf{r} = \mathbf{r}_1 - \mathbf{r}_2$, and a center of mass, $\mathbf{R} = (\mathbf{r}_1 + \mathbf{r}_2)/2$, as

$$\psi(\mathbf{r}_1, \mathbf{r}_2) = \varphi(\mathbf{r}) e^{i\mathbf{Q}\cdot\mathbf{R}/\hbar}. \quad (12.45)$$

Likewise, the momenta of interest are the center of mass, $\mathbf{Q} = \mathbf{p}_1 + \mathbf{p}_2$, and the relative momentum, $\mathbf{q} = (\mathbf{p}_1 - \mathbf{p}_2)/2$. We expand $\varphi(\mathbf{r})$ in a Fourier series as

$$\varphi(\mathbf{r}) = \sum'_{\mathbf{k}} \frac{e^{i\mathbf{k}\cdot\mathbf{r}/\hbar}}{\sqrt{V}} \alpha_{\mathbf{k}}, \quad (12.46)$$

in which the prime indicates that the restriction $\mathbf{k} > \mathbf{k}_F$ is restricted to all states whose energy exceeds ϵ_F . Because $\mathbf{k} \cdot \mathbf{r} = \mathbf{k} \cdot \mathbf{r}_1 - \mathbf{k} \cdot \mathbf{r}_2$, we see that the pair state has momenta $(\mathbf{k}, -\mathbf{k})$. Note, if $\mathbf{k}_1 + \mathbf{k}_2 = 0$, then the center-of-mass motion drops out of the problem.

We focus first on the $\mathbf{Q} = 0$ solution. To this end, we define the Fourier components of the interaction potential,

$$V_{\mathbf{kk}'} = \int \frac{d\mathbf{r}}{V} e^{-i(\mathbf{k}-\mathbf{k}')\cdot\mathbf{r}/\hbar} V(\mathbf{r}), \quad (12.47)$$

and introduce the center-of-mass Schrödinger equation

$$\left(-\frac{\hbar^2}{2\mu} \nabla^2 + V(\mathbf{r}) \right) \varphi(\mathbf{r}) = E \varphi(\mathbf{r}), \quad (12.48)$$

where μ is the reduced mass, $\mu = m/2$. Substituting the Fourier representation of $\varphi(\mathbf{r})$, multiplying by $\exp(-i\mathbf{k} \cdot \mathbf{r}/\hbar)$, and integrating, we obtain

$$(E - 2\epsilon_{\mathbf{k}}) \alpha_{\mathbf{k}} = \sum_{\mathbf{k}'} V_{\mathbf{kk}'} \alpha_{\mathbf{k}'} \quad (12.49)$$

as our new eigenvalue equation. Here, $\epsilon_{\mathbf{k}} = k^2/2m$. The matrix element $V_{\mathbf{kk}'}$ is equivalent to

$$V_{\mathbf{kk}'} = \langle \mathbf{k}, -\mathbf{k} | V_{ee} | \mathbf{k}', -\mathbf{k}' \rangle. \quad (12.50)$$

A typical scattering process in $V_{\mathbf{kk}'}$ is shown in Fig. 12.10.

If we now introduce the approximation that

$$V_{\mathbf{kk}'} = \begin{cases} -V_0, & k, k' > p_F, \\ 0, & \text{otherwise,} \end{cases} \quad (12.51)$$

the eigenvalue equation can be recast as

$$\begin{aligned} 1 &= -V_0 \sum_{k>k_F} \frac{1}{E - 2\epsilon_{\mathbf{k}}} \\ &= -V_0 \phi(E). \end{aligned} \quad (12.52)$$

This equation is satisfied as long as $\phi(E) = -1/V_0$. The poles of $\phi(E)$ occur at $E = 2\epsilon_{\mathbf{k}}$, the total energy of the pair, which is bounded from below by $2\epsilon_F$. In a finite system, $\epsilon_{\mathbf{k}}$ takes on discrete values because \mathbf{k} is quantized. As E approaches $2\epsilon_{\mathbf{k}}$ from below, $\phi(E)$ approaches $-\infty$. Just above $2\epsilon_{\mathbf{k}}$, $\phi(E)$ is $\sim +\infty$. For all $E < 2\epsilon_F$, $\phi(E)$ is negative. Hence,

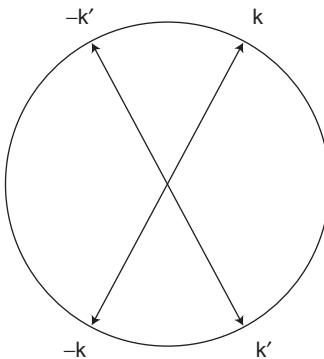


Fig. 12.10 Scattering between a pair of electron states across the Fermi surface.

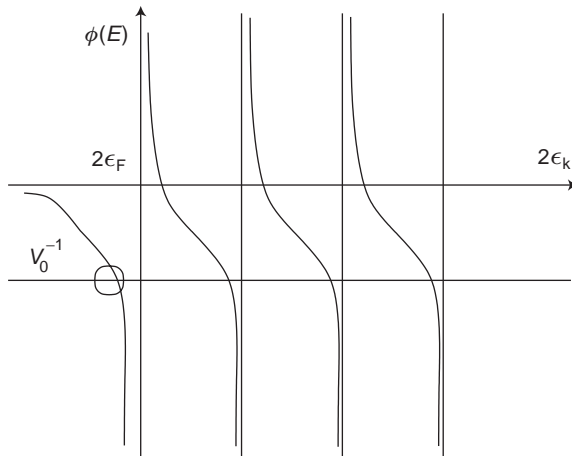


Fig. 12.11 A plot of $\phi(E)$ versus ϵ_k in the Cooper-pair problem. The intersection of $\phi(E)$ with the straight line $-V_0^{-1}$ determines the bound-state solutions for the pair.

a bound state forms when $\phi(E)$ crosses $-1/V_0$ for $E < 2\epsilon_F$. The intersection of $-1/V_0$ with $\phi(E)$ is illustrated graphically in Fig. 12.11. The existence of such a solution is the Cooper (C1956) pair problem. To find the precise energy of the bound state, we convert the sum in Eq. (12.52) to an integral,

$$1 = V_0 \sum'_{\epsilon(\mathbf{k})} \frac{1}{2\epsilon_{\mathbf{k}} - E} \rightarrow V_0 \int_{\epsilon_F}^{\epsilon_F + \hbar\omega_D} \frac{N(x)dx}{2x - E} \quad (12.53)$$

by introducing the density of states, $N(x)$. If we assume that $N(x)$ does not change significantly in the narrow range of integration, we can set $N(x) \approx N(\epsilon_F)$. Under these

assumptions, the integral yields

$$-\frac{2}{V_0 N(\epsilon_F)} = \ln \left[\frac{\epsilon_F - \frac{E}{2}}{\epsilon_F - \frac{E}{2} + \hbar\omega_D} \right], \quad (12.54)$$

which implies that

$$\left(\epsilon_F - \frac{E}{2} + \hbar\omega_D \right) \exp \left(-\frac{2}{V_0 N(\epsilon_F)} \right) = \epsilon_F - \frac{E}{2}. \quad (12.55)$$

This linear equation can be solved immediately for the eigenenergy E :

$$E = 2\epsilon_F - \frac{2\hbar\omega_D \exp(-2/V_0 N(\epsilon_F))}{1 - \exp(-2/V_0 N(\epsilon_F))}. \quad (12.56)$$

In the limit that $2 \gg V_0 N(\epsilon_F)$, the exponential in the denominator can be expanded. The pair-binding energy

$$E \simeq 2\epsilon_F - 2\hbar\omega_D \exp \left(-\frac{2}{V_0 N(\epsilon_F)} \right) \quad (12.57)$$

in the weak-coupling limit results. Either of these expressions indicates that the Cooper pair is bound with an energy $< 2\epsilon_F$ whenever V_0 is non-zero and positive. This is a profound result. It implies that two electrons directly below the Fermi surface can lower their energy by being excited into a Cooper pair with momentum $(\mathbf{k}, -\mathbf{k})$ just above the Fermi surface provided that an attractive interaction of the form in Eq. (12.51) exists. This is known as the Cooper instability.

Further, we can estimate how the pair-binding energy depends on the center of mass of the Cooper pair. At the onset, we suspect that this quantity might scale as Q^2 . We will show that this is not the case. To proceed, we extend the pair-binding criterion to the case in which $Q \neq 0$. For non-zero Q , the bare energy of the pair becomes $\epsilon_{\mathbf{q}+Q/2} + \epsilon_{-\mathbf{q}+Q/2}$. Consequently, the pair-binding condition becomes

$$1 = -V_0 \sum_{\mathbf{q}} \frac{1}{E - \epsilon_{\mathbf{q}+Q/2} - \epsilon_{-\mathbf{q}+Q/2}}. \quad (12.58)$$

For small Q , we can rewrite Eq. (12.58) as

$$1 = -V_0 \int_{\epsilon_F + v_F Q/2}^{\epsilon_F + v_F Q/2 + \hbar\omega_D} \frac{N(\epsilon_{\mathbf{q}}) d\epsilon_{\mathbf{q}}}{E - 2\epsilon_{\mathbf{q}}}, \quad (12.59)$$

dropping terms of $O(Q^2)$. The center-of-mass simply shifts the zero of the Fermi energy. The new pair-binding energy,

$$E = 2\epsilon_F + Qv_F - \frac{2\hbar\omega_D}{\exp(2/V_0 N(\epsilon_F)) - 1}, \quad (12.60)$$

is a linear function of the center-of-mass momentum. Translation of the center of mass strongly reduces the binding energy and could eventually break up the pair. To show this, we set $\epsilon_F = 0$ and evaluate the value of Q at which the Cooper pair loses most of its binding energy. We must then solve

$$\begin{aligned} Qv_F &= \frac{2\hbar\omega_D}{\exp(2/V_0N(\epsilon_F)) - 1} \\ &\approx k_B T_c. \end{aligned} \quad (12.61)$$

Equivalently, $Q/\hbar \sim k_B T_c / \hbar v_F \sim 10^4 \text{ cm}^{-1}$, which is roughly the reciprocal of the Pippard coherence length, $\xi \sim 10^{-4} \text{ cm}$. This is the effective radius of gyration of a Cooper pair, an enormous distance when compared to interatomic spacings. Such a large coherence length is a typical feature of phonon pairing mechanisms.

12.5 Fermi liquid theory

Of course, our problem is somewhat artificial in that we have ignored all interactions between the electrons save for the pair just above the Fermi surface. It is certainly reasonable to expect the simple picture of the Cooper instability to break down once we consider repulsive interactions among all of the electrons. That is, when electrons are interacting, we cannot *a priori* regard the non-interacting eigenstates as a valid description of our system (as we have done in the Cooper problem). We then are led to the question, is the instability real? We will answer this question by appealing to simple physical considerations arising from the scattering of electrons near the Fermi surface and a more formal argument involving the scaling of the full interacting Lagrangian. It is now well accepted that the normal state of a metal is described by Landau–Fermi liquid theory. In this account, it is claimed that the dominant effect of electron interactions in a metal is to renormalize the effective mass of the electron. The observed shift is on the order of 10 to 50 percent. Another essential claim of Fermi liquid theory is that there is a one-to-one correspondence between the excited states of the normal state of a metal and those of a non-interacting electron gas. The elementary excitations in Fermi liquid theory are called quasi-particles. A quasi-particle is a composite particle with a lifetime. The lifetime stems from collisions with other quasi-particles. When the lifetime (τ) of a quasi-particle is infinite, the state with such a particle is an eigenstate of the system. However, the minimum constraint that must hold for a quasi-particle state to be an eigenstate of a system is that $\hbar/\tau \ll \tilde{\epsilon}_p$, where $\tilde{\epsilon}_p$ is the energy of the quasi-particle. We will see below that as the energy of a quasi-particle approaches the Fermi level, its lifetime goes to infinity. The stability of quasi-particles at the Fermi level is a crucial tenet of Fermi liquid theory.

The vanishing of the scattering rate of electrons in the vicinity of the Fermi level can be shown as follows. Consider a near $T = 0$ distribution in which all but one of the electrons is below the Fermi surface. Let ϵ_1 be the energy of the electron above the Fermi surface. For an electron with this energy to scatter, it must interact with some electron with energy $\epsilon_2 < \epsilon_F$. The Pauli exclusion principle requires that after the scattering event, the electrons

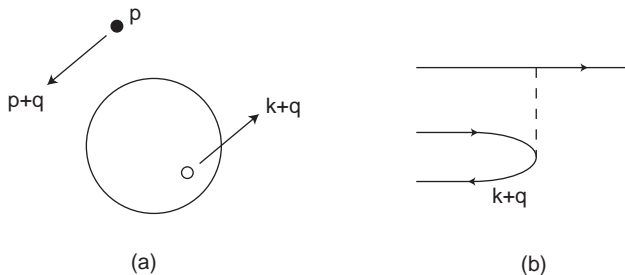


Fig. 12.12 (a) The scattering of an excited quasi-particle against particles in the ground state. (b) A diagrammatic representation of the momentum space scattering.

must occupy two states above the Fermi surface. Let the energy of these states be ϵ_3 and ϵ_4 . Energy conservation requires that $\epsilon_1 + \epsilon_2 = \epsilon_3 + \epsilon_4$. If $\epsilon_1 = \epsilon_F$, then all the other states must be at the Fermi level as well to satisfy energy conservation. As a consequence, for electrons at the Fermi level, the number of states into which they can be scattered is zero. Hence, the scattering rate, which is proportional to the density of scattering states, must vanish. As a result, the lifetime of electrons or quasi-particles at the Fermi level is infinite.

In the event that ϵ_1 moves away from the Fermi level, there is a window of states of width $\epsilon_1 - \epsilon_F$ from which we can choose the other three electronic states. Once we have chosen two of them from the narrow window $\epsilon_1 - \epsilon_F$, the energy of the last state cannot be chosen freely as a result of energy conservation. Consequently, there are $\epsilon_1 - \epsilon_F$ choices for ϵ_2 and $\epsilon_1 - \epsilon_F$ choices for ϵ_3 ; ϵ_4 is now fixed. As a result, the scattering rate should scale as $(\epsilon_1 - \epsilon_F)^2$.

To see this more rigorously, we calculate the scattering rate for two particles in momentum states $-\mathbf{k}$ and $-\mathbf{k} - \mathbf{q}$ scattering to states \mathbf{p} and $\mathbf{p} + \mathbf{q}$. A diagrammatic depiction of this interaction is shown in Fig. 12.12. The scattering rate for this process is

$$\frac{1}{\tau} = \frac{2\pi}{\hbar} \sum_{\mathbf{q}, \mathbf{k}, \sigma} |V(q)|^2 n_{\mathbf{k}\sigma} (1 - n_{\mathbf{k}-\mathbf{q}\sigma}) (1 - n_{\mathbf{p}+\mathbf{q}}) \delta(\hbar\omega_{\mathbf{pq}} + \hbar\omega_{\mathbf{kq}}), \quad (12.62)$$

where $V(q)$ is the Fourier transform of the Coulomb potential and $\hbar\omega_{\mathbf{pq}} = \epsilon_{\mathbf{p}+\mathbf{q}} - \epsilon_{\mathbf{p}}$. From energy conservation, it follows that $|\mathbf{p} + \mathbf{q}| < p$ and $|\mathbf{p} + \mathbf{q}| > p_F$. These conditions are summarized by the constraint $p_F^2 < |\mathbf{p} + \mathbf{q}|^2 < p^2$ or, equivalently,

$$p_F^2 - p^2 < 2pq \cos \theta + q^2 < 0. \quad (12.63)$$

As in our analysis of screening, we can simplify the sum over \mathbf{k} using the definition of the screening function (see Eq. (9.103)) for free particles. At $T = 0$, we obtain

$$\frac{1}{\tau} = \frac{n_e}{2\hbar^2} \sum_{\mathbf{q}} |V(q)|^2 S_0(q, \hbar\omega_{\mathbf{pq}}) (1 - n_{\mathbf{p}+\mathbf{q}}). \quad (12.64)$$

Because we are interested primarily in $p - p_F \approx 0$, we can take q to be small. We then take the $q \rightarrow 0$ limit of the screened Coulomb potential, $V(q \rightarrow 0) = 4\pi e^2/V\kappa_{TF}^2$, in the Thomas–Fermi approximation. Also, we take the $q \rightarrow 0$ form of the structure function derived in Chapter 9:

$$S(q, \omega_{pq}) \propto \frac{\omega_{pq}}{q}. \quad (12.65)$$

Consequently, the scattering rate simplifies to

$$\frac{1}{\tau} \propto \frac{1}{\epsilon_F} \int \sin \theta d\theta \int q \omega_{pq} dq. \quad (12.66)$$

We can replace the q -integral with one over ω_{pq} by solving $\hbar\omega_{pq} = (2pq \cos \theta + q^2)/2m$. The scattering rate is proportional to

$$\begin{aligned} \frac{1}{\tau} &\propto \frac{1}{\epsilon_F} \int_0^{\epsilon_p - \epsilon_F} d\omega \int_{-1}^1 \omega \left(1 - \frac{x p_F}{\sqrt{x^2 p_F^2 + \omega}} \right) dx \\ &\propto \frac{1}{\epsilon_F} \int_0^{\epsilon_p - \epsilon_F} \omega d\omega \propto \frac{(\epsilon_p - \epsilon_F)^2}{\epsilon_F}. \end{aligned} \quad (12.67)$$

We see clearly then that the scattering rate scales as $(\epsilon_p - \epsilon_F)^2$ and hence vanishes for states at the Fermi level. Setting $\epsilon_p - \epsilon_F \propto k_B T$, we find that the scattering rate is proportional to T^2 . As mentioned in the previous chapter, the resistivity (GF1987) in the normal state of the cuprate high- T_c materials is linear in temperature down to T_c . In light of the Fermi liquid result, this behavior strongly suggests that the normal state of these materials is a non-Fermi liquid.

The quadratic dependence of the quasi-particle scattering rate on temperature is a central prediction of Fermi liquid theory. At room temperature, $(k_B T)^2/\epsilon_F$ is of the order of 10^{-4} eV. This gives rise to a scattering lifetime that is of the order of 10^{-10} s at room temperature. A typical relaxation time in a metal is four orders of magnitude shorter (see Chapter 11). Hence, electron–electron interactions are not the dominant scattering mechanism for electrons in the vicinity of the Fermi level. It is for this reason that the non-interacting picture works so well and is a good approximation for the normal-state properties of a metal, at least at room temperature. Of course, at sufficiently low temperatures, the importance of electron–electron interactions increases tremendously, superconductivity being a case in point.

The ultimate statement (P1992; SM1991; BG1990) of Fermi liquid theory is that short-range repulsive interactions are irrelevant at a Fermi surface. This statement can be proven from a scaling analysis of the Lagrangian for the interacting system once we establish a few preliminary results on fermionic coherent states. Fermionic coherent states and a fermionic operator Ψ are conjoined by the eigenvalue equation

$$\Psi|\psi\rangle = \psi|\psi\rangle, \quad (12.68)$$

where $|\psi\rangle$ is the fermionic coherent state. The eigenvalue ψ is not an ordinary number, however. Its square, ψ^2 , vanishes, thereby implying the series of equalities

$$\Psi^2|\psi\rangle = \psi^2|\psi\rangle = 0|\psi\rangle \quad (12.69)$$

holds. ψ is a Grassmann variable, that is an anticommuting number. While this may seem weird, the vanishing of the square of a Grassmann is precisely what we need to engineer the Pauli principle into a fermionic path integral formulation.

So what are the states $|\psi\rangle$ that make Eq. (12.68) possible? We make an ansatz

$$|\psi\rangle = |0\rangle - \psi|1\rangle \quad (12.70)$$

that fits the bill for a fermionic coherent state. Here $\Psi|0\rangle = 0 = \Psi^\dagger|1\rangle = 0$ and $\Psi|1\rangle = |0\rangle$. We perform the check on our ansatz by first noting that

$$\Psi|\psi\rangle = -\Psi\psi|1\rangle = \psi\Psi|1\rangle = \psi|0\rangle. \quad (12.71)$$

However, $|0\rangle = |\psi\rangle + \psi|1\rangle$. Substituting, we obtain

$$\Psi|\psi\rangle = \Psi[|\psi\rangle + \psi|1\rangle] = \psi|\psi\rangle, \quad (12.72)$$

our desired result. Hence, $|\psi\rangle$ constitutes a fermionic coherent state. Consider now the adjoint $\langle\bar{\psi}|\Psi^\dagger$. The standard rules of quantum mechanics can be applied to the adjoint. For example,

$$\langle\bar{\psi}|\Psi^\dagger \equiv \langle\bar{\psi}|\bar{\psi}. \quad (12.73)$$

Using the fact that $\bar{\psi}|1\rangle = -(1|\bar{\psi}$, we obtain that

$$\begin{aligned} \langle\bar{\psi}|\psi\rangle &= \langle 0|0\rangle + \bar{\psi}\psi\langle 1|1\rangle \\ &= 1 + \bar{\psi}\psi = e^{\bar{\psi}\psi}. \end{aligned} \quad (12.74)$$

This expression might seem a bit strange since in no sense does the truncation follow from the smallness of $\bar{\psi}\psi$. This quantity is neither big nor small. Rather, the truncation follows because the square of a Grassmann variable is zero.

In proceeding, we will need a few integrals:

$$\int \psi d\psi = 1, \quad (12.75)$$

$$\int d\psi = \int d\bar{\psi} = 0, \quad (12.76)$$

$$\int \bar{\psi}\psi d\bar{\psi}d\psi = -1, \quad (12.77)$$

$$\int e^{-a\bar{\psi}\psi} d\bar{\psi}d\psi = \int (1 - a\bar{\psi}\psi) d\bar{\psi}d\psi = a, \quad (12.78)$$

$$\int e^{-\bar{\psi}M\psi} d\bar{\psi}d\psi = \text{Det}M. \quad (12.79)$$

These integrals allow us to establish several identities. First, the resolution of the identity,

$$\int |\psi\rangle\langle\bar{\psi}|e^{-\bar{\psi}\psi} d\bar{\psi}d\psi = |0\rangle\langle 0| + |1\rangle\langle 1| = I, \quad (12.80)$$

takes on a particularly simple form in terms of fermionic coherent states. In writing the path integral in terms of fermionic coherent states, we will need an expression for the trace of a bosonic operator. By bosonic we simply mean an operator that is made up of an even number of fermionic operators. Consider the quantity

$$\begin{aligned}\langle -\bar{\psi} | \psi \rangle &= [\langle 0 | -\bar{\psi} \langle 1 |] [\langle 0 | -\psi | 1 \rangle] \\ &= \langle 0 | 0 \rangle - \bar{\psi} \psi \langle 1 | 1 \rangle.\end{aligned}\quad (12.81)$$

To obtain just the sum of the diagonal elements, we perform the integral

$$\int [\langle 0 | 0 \rangle - \bar{\psi} \psi \langle 1 | 1 \rangle] e^{-\bar{\psi} \psi} d\bar{\psi} d\psi = \langle 0 | 0 \rangle + \langle 1 | 1 \rangle. \quad (12.82)$$

Consequently, the trace formula is given by

$$\text{Tr} \Omega = \int \langle -\bar{\psi} | \Omega | \psi \rangle e^{-\bar{\psi} \psi} d\bar{\psi} d\psi. \quad (12.83)$$

With these relationships, we proceed to express the partition function,

$$Z = \text{Tr} e^{-\beta H}, \quad (12.84)$$

in terms of coherent states. Making contact with the standard Schrödinger propagator, we identify β as an imaginary time. We subdivide this “time” interval by defining $\epsilon = \beta/N$ and raise our Boltzmann weight,

$$Z = \lim_{N \rightarrow \infty} \text{Tr} [e^{-\epsilon H}]^N, \quad (12.85)$$

to the N th power. In the large N -limit, we can truncate the exponential factor at the first term. For compactness, we define $\hat{D}_\epsilon \equiv \hat{D}_\epsilon(\psi^\dagger, \psi) = 1 - \epsilon H$. We then use the spectral resolution of the identity, Eq. (12.80), to obtain

$$\begin{aligned}Z &= \int \langle -\bar{\psi}_0 | \hat{D}_\epsilon | \psi_{N-1} \rangle e^{-\bar{\psi}_{N-1} \psi_{N-1}} \langle \bar{\psi}_{N-1} | \hat{D}_\epsilon | \psi_{N-2} \rangle e^{\bar{\psi}_{N-2} \psi_{N-2}} \\ &\quad \times \langle \bar{\psi}_{N-2} | \cdots | \psi_1 \rangle e^{-\bar{\psi}_1 \psi_1} \langle \bar{\psi}_1 | \hat{D}_\epsilon | \psi_0 \rangle e^{-\bar{\psi}_0 \psi_0} \prod_{i=0}^{N-1} d\bar{\psi}_i d\psi_i\end{aligned}\quad (12.86)$$

as our working expression for the partition function. Assume all operators in H are normal-ordered so that $H|0\rangle = 0$. As a consequence,

$$\langle \bar{\psi}_{i+1} | \hat{D}_\epsilon | \psi_i \rangle = \langle \bar{\psi}_{i+1} | D_\epsilon(\psi_{i+1}^\dagger, \psi_i) | \psi_i \rangle = e^{\bar{\psi}_{i+1} \psi_i} e^{-\epsilon H(\psi_{i+1}^\dagger, \psi_i)}. \quad (12.87)$$

We are almost done. We simply insert Eq. (12.87) into Eq. (12.86) N times,

$$Z = \lim_{N \rightarrow \infty} \int \prod_{i=0}^{N-1} e^{\left[\left(\frac{(\bar{\psi}_{i+1} - \bar{\psi}_i)}{\epsilon} \psi_i - H \right) \epsilon \right]} d\bar{\psi}_i d\psi_i, \quad (12.88)$$

where we have defined $\bar{\psi}_N = -\bar{\psi}_0$ and $\psi_N = -\psi_0$, and ψ_N and $\bar{\psi}_N$ are explicitly not integrated over. In the $N \rightarrow \infty$ limit, we can convert the sum in the exponential to an integral. Upon integrating the time-derivative term by parts with the boundary condition that $\psi(0) = \psi(\beta) = 0$, we reduce the partition function to the standard form

$$Z = \int \mathcal{D}\bar{\psi} \mathcal{D}\psi e^{-S_E}, \quad (12.89)$$

where S_E ,

$$S_E = \int (\bar{\psi} \partial_\tau \psi + H) d^d x d\tau, \quad (12.90)$$

is the Euclidean action with the τ integration performed on the interval $[0, \beta]$. This is the starting point for all fermionic quantum field theories.

Consider the case of non-interacting electrons. The Hamiltonian,

$$H = \sum_{\mathbf{p}, \sigma} (\epsilon_{\mathbf{p}} - \epsilon_F) \psi_\sigma^\dagger(\mathbf{p}) \psi_\sigma(\mathbf{p}), \quad (12.91)$$

is conveniently written in terms of creation and annihilation operators in momentum space with $\epsilon(\mathbf{p})$ the free particle dispersion and ϵ_F the Fermi energy. The corresponding action is

$$S = \int dt d^3 \mathbf{p} (i \psi_\sigma^\dagger(\mathbf{p}) \partial_t \psi_\sigma(\mathbf{p}) - \psi_\sigma^\dagger(\mathbf{p}) (\epsilon_{\mathbf{p}} - \epsilon_F) \psi_\sigma(\mathbf{p})), \quad (12.92)$$

where we have switched to real time. Technically we should have written the action in terms of fermionic coherent states rather than the fermionic creation and annihilation operators. While this distinction will not be crucial for the application we consider here, it is crucial in the fermionic path integral that the fermionic coherent states be used. Nonetheless, it is understood that path integrals written in terms of creation and annihilation operators actually imply coherent states as the operative basis.

We want to consider scalings towards the Fermi surface. We first need to introduce the concept of a scaling dimension. Consider the simple function $f(x) = x^2$. As a consequence of the scaling $x \rightarrow sx$, $f(x) \rightarrow s^2 x^2$, where s is assumed to be positive. If $s \rightarrow 0$, the function, f , vanishes. We define the scaling dimension of the parameter x as the power to which the scale factor, s , must be raised to obtain the scaling transformation of x . Operationally,

$$\text{Dim}[x] = \frac{df}{ds} \frac{s}{f} = \frac{d \ln f}{d \ln s} = 2. \quad (12.93)$$

In the context of a field theory, the scaling dimension plays a fundamental role. Let us partition our action as

$$S = S_0 + S_{\text{int}}, \quad (12.94)$$

where all the interactions are contained in

$$S_{\text{int}} = \int dt d^d \mathbf{k} \mathcal{O}(\mathbf{k}, t). \quad (12.95)$$

Here \mathcal{O} is some operator (of course a composite operator made out of the elemental fields) that determines the interactions. We choose the scaling of time and momenta and the bare fields such that $S_0 \rightarrow s^0 S_0 = S_0$. Under such a choice for the scaling, the interaction term will transform as $s^b S_{\text{int}}$. If $b > 0$, then the interactions generated by \mathcal{O} are irrelevant as they vanish in the scaling limit. In this case, we call \mathcal{O} an irrelevant operator. If $b < 0$, then \mathcal{O} is relevant. The marginal case arises when $b = 0$. Since we are considering scalings towards the Fermi surface, we want to scale all of the fields and spatial and time coordinates so that the associated free particle action has a scaling dimension of zero. We will then show that when the same scalings are applied to any repulsive short-range four-fermion interaction, the scaling dimension will be positive provided that $d \geq 2$. Following Polchinski (P1992), we write the momentum of an electron,

$$\mathbf{p} = \mathbf{k} + \ell, \quad (12.96)$$

as a sum of two momenta, one on the Fermi surface, \mathbf{k} , and one perpendicular to it, ℓ , which will represent the deviations from the Fermi surface. As a result, we expand the dispersion relationship of an electron around the Fermi surface,

$$\epsilon(\mathbf{p}) = \epsilon_F + \ell \frac{\partial \epsilon}{\partial \mathbf{p}} + O(\ell^2), \quad (12.97)$$

retaining only the linear term. Since the zero of energy is set to be the Fermi surface, the relevant scale changes which preserve the Fermi surface are $\mathbf{k} \rightarrow \mathbf{k}$, $\ell \rightarrow s\ell$ and $E \rightarrow sE$. As a result of the latter scaling for the energy,

$$\frac{\partial}{\partial t} \rightarrow s \frac{\partial}{\partial t}, \quad (12.98)$$

implying that $t \rightarrow s^{-1}t$. Likewise, $d^d \mathbf{p} \rightarrow d^{d-1} \mathbf{k} d(s\ell)$. Under these scale changes, the action,

$$s \int dt d^{d-1} \mathbf{k} d\ell \left(i\psi_\sigma^\dagger(\mathbf{p}) \partial_t \psi_\sigma(\mathbf{p}) - \ell v_F \psi_\sigma^\dagger(\mathbf{p}) \psi_\sigma(\mathbf{p}) \right), \quad (12.99)$$

scales linearly with s times the scaling dimension of the product $\psi_\sigma^\dagger(\mathbf{p}) \psi_\sigma(\mathbf{p})$. Our goal of obtaining a scale dimension of zero for the action requires that we scale the fields in the manner

$$\psi_\sigma(\mathbf{p}) \rightarrow s^{-1/2} \psi_\sigma(\mathbf{p}), \quad (12.100)$$

to absorb the overall factor of s arising from the scaling of ℓ and the energy. From our definition of the scaling dimension, it follows that

$$\text{Dim}[\psi_\sigma(\mathbf{p})] = -\frac{1}{2}. \quad (12.101)$$

Our theory on the Fermi surface then has scale dimension zero. However, we have not yet specified the chemical potential. Such a term,

$$\int dt d^{d-1}\mathbf{k} d\ell \mu(\mathbf{k}) \psi_\sigma^\dagger(\mathbf{p}) \psi_\sigma(\mathbf{p}), \quad (12.102)$$

takes the form of a mass term in our effective low-energy theory. This term scales as $s^{-1+1-2/2} = s^{-1}$. Hence, this term is always relevant. Nonetheless, this term can be absorbed into the kinetic energy term, implying that the sense in which we expand around the Fermi surface is with respect to the completely filled state, not one with a vacuum we can (conveniently) consider to be empty.

A theory is natural if there are no relevant perturbations. Consider the short-range four-fermion interaction term,

$$\int dt \prod_{i=1}^4 d^{d-1}\mathbf{k}_i d\ell_i V(\mathbf{k}_1, \dots, \mathbf{k}_4) \psi_\sigma^\dagger(\mathbf{p}_1) \psi_\sigma(\mathbf{p}_3) \psi_{\sigma'}^\dagger(\mathbf{p}_2) \psi_{\sigma'}(\mathbf{p}_4) \delta^d(\mathbf{p}_1 + \mathbf{p}_2 - \mathbf{p}_3 - \mathbf{p}_4). \quad (12.103)$$

At this point, the sign of V is arbitrary. Our focus on short-ranged interactions is warranted since we have shown that, at metallic densities, the interactions in metals are well screened. Under the scalings used for the free part of the action, we find that the interaction term scales as $s^{4-1-4/2} = s$ times the scaling of the delta-function. The s^4 term arises from the four factors of $d\ell$, s^{-1} from the time integration and s^{-2} from the four factors of the fields, $\psi_\sigma(\mathbf{p})$. What about the scaling of the δ -function? If we simply substitute Eq. (12.96) into the argument of the δ -function, we find that

$$\begin{aligned} \delta^d(\mathbf{p}_1 + \mathbf{p}_2 - \mathbf{p}_3 - \mathbf{p}_4) &= \delta^d(\mathbf{k}_1 + \mathbf{k}_2 - \mathbf{k}_3 - \mathbf{k}_4 + \mathbf{l}_1 + \mathbf{l}_2 - \mathbf{l}_3 - \mathbf{l}_4) \\ &\approx \delta^d(\mathbf{k}_1 + \mathbf{k}_2 - \mathbf{k}_3 - \mathbf{k}_4). \end{aligned} \quad (12.104)$$

Hence, the δ -function does not scale and we arrive at the conclusion that short-range interactions are irrelevant on the Fermi surface as they scale linearly with s .

However, this argument concedes too much to the Fermi surface. Superconductivity can be understood after all as an instability of the Fermi surface with respect to attractive contact interactions. Hence, the argument above is too broad. We fine-tune the argument by considering scattering processes that are connected by large momenta as a precursor to the superconducting problem where the scattering involves electrons on opposite sides of the Fermi surface depicted in Fig. 12.13. Specifically, consider a pair of electrons with momenta \mathbf{p}_1 and \mathbf{p}_2 that scatter to a state with momentum \mathbf{p}_3 and \mathbf{p}_4 . At the outset, we consider a generic case in which the momenta \mathbf{p}_1 and \mathbf{p}_2 share no special relationship, as depicted in Fig. 12.13. We write the scattered momenta as $\mathbf{p}_3 = \mathbf{p}_1 + \delta\mathbf{k}_3 + \delta\ell_3$ and $\mathbf{p}_4 = \mathbf{p}_2 + \delta\mathbf{k}_4 + \delta\ell_4$. The momentum conservation condition now becomes

$$\delta^d(\delta\mathbf{k}_3 + \delta\mathbf{k}_4 + \delta\ell_3 + \delta\ell_4). \quad (12.105)$$

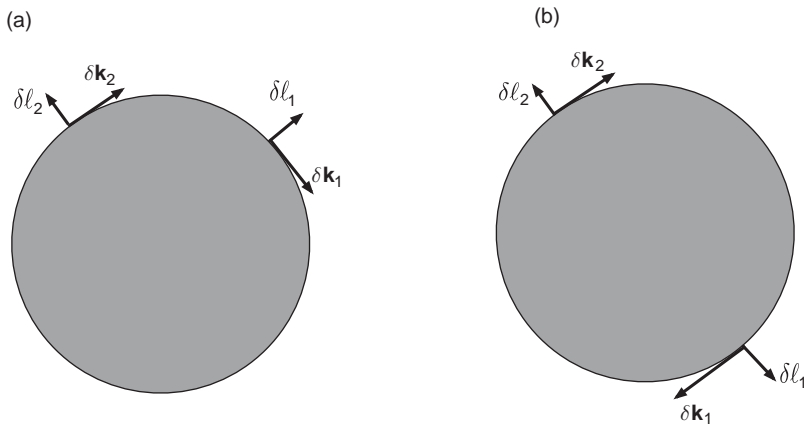


Fig. 12.13 (a) Momenta for two electrons generically located on the Fermi surface. (b) Here the momenta are opposite; that is, $\mathbf{p}_1 = -\mathbf{p}_2$. In this case, $\delta\mathbf{k}_1$ is parallel to $\delta\mathbf{k}_2$ and $\delta\ell_1$ and $\delta\ell_2$ point in exactly opposite directions.

When the $\delta\mathbf{k}$ s are linearly independent, the δ -function can be treated as before. Specifically, it has no scaling and our previous conclusion holds that four-fermion interactions are irrelevant. Consider the case shown in Fig. 12.13b, in which $\mathbf{p}_1 = -\mathbf{p}_2$ and hence $\delta\mathbf{k}_3$ and $\delta\mathbf{k}_4$ are parallel to one another. In this case, the δ -function that maintains momentum conservation,

$$\delta^d(\delta\mathbf{k}_3 + \delta\mathbf{k}_4)\delta^d(\delta\ell_3 + \delta\ell_4), \quad (12.106)$$

factorizes because both $\delta\ell_3$ and $\delta\ell_4$ are perpendicular to the $\delta\mathbf{k}_3$ and $\delta\mathbf{k}_4$. Under the scaling $\ell \rightarrow s\ell$, the second of the two δ -functions scales as s^{-1} . This factor cancels the linear s factor derived earlier. Consequently, we find quite generally that the four-fermion interaction when the pair of electrons has zero net momentum is neither relevant nor irrelevant. Rather, it scales as s^0 and hence is marginal.

So where does this leave us? We need to work harder to determine the fate of our Fermi surface when the electrons scatter to parity-symmetric momentum states. To this end, we evaluate the first correction in the hope of constructing a recursion relationship similar to those derived for the exchange coupling in the Kondo problem. Through order V^2 the relevant diagrams are shown in Fig. 12.14. The first diagram is just the bare electron-electron interaction vertex. The second diagram is the vertex through second-order in the interaction. We associate with each internal fermion line (that is the lines of the bubble) with a propagator of the form $1/(E - v_F\ell)$, where E is the energy of the internal fermion line. The second-order vertex takes the form

$$V^2 \int \frac{dE' d^2\mathbf{k} d\ell'}{2\pi^4} \frac{1}{[(1+i\epsilon)(E+E') - v_F(\mathbf{k}')\ell'][[(1+i\epsilon)(E-E') - v_F(\mathbf{k}')\ell']} \cdot \quad (12.107)$$

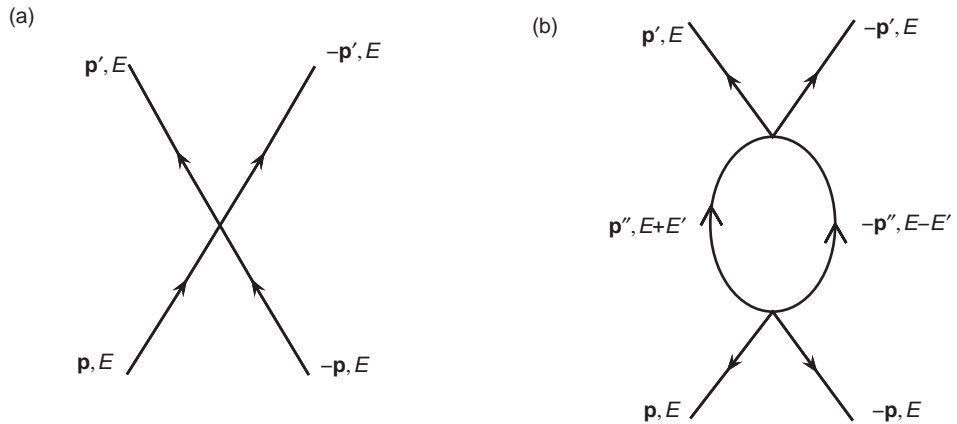


Fig. 12.14 (a) Bare interaction vertex for electrons in state (\mathbf{p}, E) and $(-\mathbf{p}, E)$ scattering to $(-\mathbf{p}', E)$ and $(-\mathbf{p}', E)$, and (b) $O(V^2)$ vertex. The integral corresponding to this vertex is evaluated in Eq. (12.107).

The $(1 + i\epsilon)$ factors serve to regularize the integral. In the end, we will take the limit of $\epsilon \rightarrow 0$. In performing the integrals in the bubble vertex, it is helpful to rewrite the denominator as

$$\frac{-1}{(1 + 2i\epsilon)[E' + E - (1 - i\epsilon)v_F(\mathbf{k}')\ell'][E' - E + (1 - i\epsilon)v_F(\mathbf{k}')\ell']}, \quad (12.108)$$

where we have explicitly approximated $(1 + i\epsilon)^2 \approx (1 + 2i\epsilon)$ since ϵ is strictly of $O(0)$. To evaluate this integral, we close in the upper half-plane. There are two poles of interest which are located at

$$E' = \pm E \mp v_F(\mathbf{k}')\ell' \pm i\epsilon v_F(\mathbf{k}')\ell', \quad (12.109)$$

where the upper sign corresponds to $\ell' > 0$ and the lower sign to $\ell' < 0$ so that both poles reside in the upper half-plane. Using the fact that the residue at each of these poles is

$$\frac{2\pi i}{\pm 2E \mp 2v_F(\mathbf{k}')\ell' \pm 2i\epsilon v_F(\mathbf{k}')\ell'}, \quad (12.110)$$

we reduce the second-order vertex to

$$\frac{-iV^2}{2}N \left[\int_0^{E_0} \frac{db}{E - b + i\epsilon} + \int_{-E_0}^0 \frac{db}{b - E - i\epsilon} \right], \quad (12.111)$$

where we have changed variables to $b = v_F(\mathbf{k}')\ell'$, defined

$$N = \int \frac{d^2\mathbf{k}'}{(2\pi)^3} \frac{1}{v_F(\mathbf{k}')}, \quad (12.112)$$

and ignored any prefactor on the terms proportional to the infinitesimal, ϵ . Each integral yields a logarithm:

$$iV^2 N \ln\left(\frac{E_0}{|E|}\right). \quad (12.113)$$

Noting that the bare four-fermion vertex is proportional to $-iV$, the effective interaction to second order becomes

$$V(E) = V - V^2 N \left(\ln\left(\frac{E_0}{|E|}\right) + O(1) \right) + O(V^3). \quad (12.114)$$

We differentiate both sides of this equation,

$$\frac{dV(E)}{dE} = NV(E)^2/E, \quad (12.115)$$

to obtain the scaling equation for the interaction vertex. This equation is identical to the scaling equation derived previously for the growth of the exchange interaction in the Kondo problem in Chapter 8. The solution to this equation is simply

$$V(E) = \frac{V}{1 + NV \ln(E_0/E)}. \quad (12.116)$$

We see clearly that for a positive bare value of the interaction, $V > 0$, the effective interaction decreases at low energy, that is, $E < E_0$. However, for $V < 0$, the interaction increases. This is the BCS instability and the fundamental statement that, except for short-range attractions, all renormalizations are towards the Fermi surface. Note that the bare interaction V is truly marginal. Consequently, superconductivity arising within BCS theory is an example of a marginal coupling becoming large and generating new degrees of freedom, namely a condensate of electron pairs, at strong coupling.

It is a crucial assumption of the BCS pairing theory of superconductivity that the normal-state properties are described by non-interacting quasi-particles with infinite lifetimes (L1964; L1965) which stand in a one-to-one correspondence with the bare electrons. This assumption is borne out by the scaling analysis just presented and experimentally in the normal state of a wide range of Type I, as well as Type II, materials. Since the normal state is essentially non-interacting, the energy of a particular quasi-particle is the energy required to add or subtract that particle from a state in the system. To illustrate this concept, we consider an interacting system described by some distribution function, $n_{p\sigma}^0$, generally taken to be the Fermi–Dirac distribution. Suppose a particle is added or subtracted from the system ever so slowly, so that the system remains in the ground state. This process represents an adiabatic change in the particle number. Nonetheless, this process will change the particle distribution to some new quantity, $n_{p\sigma}$, and in turn the ground state energy will change. Let $\delta n_{p\sigma}$ represent the resultant change in the particle distribution function. We

can calculate the change in the ground state energy,

$$\delta E = \frac{1}{V} \sum_{\mathbf{p}\sigma} \epsilon_{\mathbf{p}\sigma} \delta n_{\mathbf{p}\sigma} + \frac{1}{2V^2} \sum_{\mathbf{p}\sigma, \mathbf{p}'\sigma'} f_{\mathbf{p}\sigma, \mathbf{p}'\sigma'} \delta n_{\mathbf{p}\sigma} \delta n_{\mathbf{p}'\sigma'} + \dots, \quad (12.117)$$

by expanding in powers of the fluctuation, $\delta n_{\mathbf{p}\sigma}$. The Landau (L1956) parameter $f_{\mathbf{p}\sigma, \mathbf{p}'\sigma'}$ describes how quasi-particles interact. This quantity is invariant with respect to interchange of \mathbf{p} and \mathbf{p}' . We identify the energy of a quasi-particle,

$$\tilde{\epsilon}_{\mathbf{p}\sigma} = \epsilon_{\mathbf{p}\sigma} + \frac{1}{V} \sum_{\mathbf{p}'\sigma'} f_{\mathbf{p}\sigma, \mathbf{p}'\sigma'} \delta n_{\mathbf{p}'\sigma'} + \dots, \quad (12.118)$$

by taking the variation of the new ground state energy with respect to $\delta n_{\mathbf{p}\sigma}$. We see clearly then that the quasi-particle energy is itself a function of the distribution function. More explicitly, quasi-particles obey a Fermi–Dirac distribution function with $\epsilon_{\mathbf{p}} - \mu$ replaced with $\tilde{\epsilon}_{\mathbf{p}\sigma} - \mu$. At the Fermi surface, quasi-particles move with a velocity

$$v_F = \left(\frac{\partial \epsilon_{\mathbf{p}\sigma}}{\partial \mathbf{p}} \right)_{p=p_F} \quad (12.119)$$

that is equal to the Fermi velocity. Because $v_F = p_F/m^*$, the formal definition of the *effective mass* of a quasi-particle is

$$\frac{1}{m^*} = \frac{1}{p_F} \left(\frac{\partial \epsilon_{\mathbf{p}\sigma}}{\partial \mathbf{p}} \right)_{p=p_F}. \quad (12.120)$$

Consequently, in the vicinity of the Fermi surface, the quasi-particle energy

$$\epsilon_{\mathbf{p}\sigma} = \epsilon_F + v_F(p - p_F) \quad (12.121)$$

is linear in the displacement momentum $p - p_F$. As most of our focus will be on processes in the vicinity of the Fermi surface, this expression should suffice to describe the energy of a quasi-particle.

12.6 Pair amplitude

At this point it is customary to write down the BCS wavefunction and go on our merry way to elucidate the superconducting transition. However, we want to take a step back and explore the expectation value of the pairing amplitude for a Cooper pair. In so doing, we will be able to swindle BCS theory. Thus far, we have established that two electrons above the Fermi surface can lower their energy by forming a bound singlet Cooper pair just below ϵ_F , if the temperature is sufficiently low. This tells us that we should be able to define an order parameter whose expectation value should discern if the Cooper instability has occurred. The appropriate pairing operator for a $(\mathbf{p} \uparrow, -\mathbf{p} \downarrow)$ pair is

$$b_{\mathbf{p}}^\dagger = a_{\mathbf{p}\uparrow}^\dagger a_{-\mathbf{p}\downarrow}^\dagger, \quad (12.122)$$

while

$$b_{\mathbf{p}} = a_{-\mathbf{p}\downarrow} a_{\mathbf{p}\uparrow} \quad (12.123)$$

is the corresponding pair annihilation operator. Let $|N\rangle$ represent the ground state of an N -particle system. The Cooper instability suggests that $\langle N - 2 | b_{\mathbf{p}} | N \rangle \neq 0$ in the superconducting state. Let us define

$$\alpha_{\mathbf{p}} = \langle N - 2 | b_{\mathbf{p}} | N \rangle, \quad (12.124)$$

which is generally referred to as the pair amplitude. What we will show is that below a certain temperature, $\alpha_{\mathbf{p}}$ grows exponentially. In the normal state, $\alpha_{\mathbf{p}}$ equals 1 or 0. In BCS theory, $\alpha_{\mathbf{p}}$ is closely related to the order parameter.

We start by showing that $\alpha_{\mathbf{p}}$ is the general expansion coefficient for a pair state. To proceed, we write the general singlet pair state as

$$|\psi\rangle = \sum_{\mathbf{p} > \mathbf{p}_F} \eta_{\mathbf{p}} b_{\mathbf{p}}^\dagger |0\rangle = \sum_{\mathbf{p} > \mathbf{p}_F} \eta_{\mathbf{p}} |\mathbf{p}\uparrow - \mathbf{p}\downarrow\rangle, \quad (12.125)$$

where $\eta_{\mathbf{p}}$ is an expansion coefficient. To determine $\eta_{\mathbf{p}}$, we note that

$$\begin{aligned} \langle 0 | b_{\mathbf{p}} | \psi \rangle &= \sum_{\mathbf{p}'} \eta_{\mathbf{p}'} \langle 0 | b_{\mathbf{p}} b_{\mathbf{p}'}^\dagger | 0 \rangle \\ &= \sum_{\mathbf{p}'} \eta_{\mathbf{p}'} \delta_{\mathbf{p}\mathbf{p}'} = \eta_{\mathbf{p}}. \end{aligned} \quad (12.126)$$

Because $|\psi\rangle$ simply differs from $|0\rangle$ by two particles, $\eta_{\mathbf{p}} = \alpha_{\mathbf{p}}$.

The pair amplitude is the expansion coefficient for the general pairing state. Let us calculate the time evolution of $\alpha_{\mathbf{p}}$. To do this, we write the BCS Hamiltonian as

$$H = H_0 + H_{\text{int}}, \quad (12.127)$$

where

$$\begin{aligned} H_0 &= \sum_{\mathbf{p}, \sigma} \epsilon_{\mathbf{p}} a_{\mathbf{p}\sigma}^\dagger a_{\mathbf{p}\sigma} \\ H_{\text{int}} &= \sum_{\mathbf{p}\mathbf{p}'} V_{\mathbf{p}\mathbf{p}'} b_{\mathbf{p}}^\dagger b_{\mathbf{p}'}. \end{aligned} \quad (12.128)$$

In the Schrödinger picture, the time dependence of $\alpha_{\mathbf{p}}$ is carried in the wavefunctions. As a consequence,

$$\begin{aligned} i\hbar \frac{\partial}{\partial t} \alpha_{\mathbf{p}}(t) &= i\hbar \frac{\partial}{\partial t} \langle 0(t) | b_{\mathbf{p}} | \psi(t) \rangle \\ &= \langle 0(t) | [b_{\mathbf{p}}, H] | \psi(t) \rangle. \end{aligned} \quad (12.129)$$

To evaluate $[b_{\mathbf{p}}, H]$, we will find the commutators useful:

$$\begin{aligned} [b_{\mathbf{p}}, n_{\mathbf{p}'\sigma}] &= b_{\mathbf{p}} (\delta_{\mathbf{p}\mathbf{p}'} \delta_{\sigma\uparrow} + \delta_{\mathbf{p}-\mathbf{p}'} \delta_{\sigma\downarrow}), \\ [b_{\mathbf{p}}, b_{\mathbf{p}'}^\dagger] &= \delta_{\mathbf{p}\mathbf{p}'} (1 - n_{\mathbf{p}\uparrow} - n_{-\mathbf{p}\downarrow}). \end{aligned} \quad (12.130)$$

We see explicitly that the occupancy factors, $n_{\mathbf{p}\uparrow} + n_{-\mathbf{p}\downarrow}$, render the pair-creation operators non-commuting. These terms preserve the Pauli principle between electrons forming the pair. We can now evaluate $[b_{\mathbf{p}}, H]$:

$$\begin{aligned}[b_{\mathbf{p}}, H] &= \sum_{\mathbf{p}'\sigma} [b_{\mathbf{p}}, \epsilon_{\mathbf{p}'} n_{\mathbf{p}'\sigma}] + \sum'_{\mathbf{p}'\mathbf{p}''} \left[b_{\mathbf{p}}, b_{\mathbf{p}'}^\dagger b_{\mathbf{p}''} \right] \\ &= 2\epsilon_{\mathbf{p}} b_{\mathbf{p}} + \sum'_{\mathbf{p}'} V_{\mathbf{p}\mathbf{p}'} (1 - n_{-\mathbf{p}\downarrow} - n_{\mathbf{p}\uparrow}) b_{\mathbf{p}'}.\end{aligned}\quad (12.131)$$

The prime on the sum indicates a restricted sum over the thin momentum shell of width $2\hbar\omega_D$ around ϵ_F . We can gain physical insight into this result by noting that $(1 - n_{-\mathbf{p}\downarrow} - n_{\mathbf{p}\uparrow}) = (1 - n_{\mathbf{p}\uparrow})(1 - n_{-\mathbf{p}\downarrow}) - n_{\mathbf{p}\uparrow}n_{-\mathbf{p}\downarrow}$. If we use this result with Eq. (12.131), we obtain

$$\left(i\hbar \frac{\partial}{\partial t} - 2\epsilon_{\mathbf{p}} \right) \alpha_{\mathbf{p}}(t) = [(1 - n_{\mathbf{p}\uparrow})(1 - n_{-\mathbf{p}\downarrow}) - n_{\mathbf{p}\uparrow}n_{-\mathbf{p}\downarrow}] \sum'_{\mathbf{p}'} V_{\mathbf{p}\mathbf{p}'} \alpha_{\mathbf{p}'}(t) \quad (12.132)$$

as the time evolution of the pair amplitude. The probability that the particles forming the pair lie outside the Fermi surface is determined by the product $(1 - n_{\mathbf{p}\uparrow})(1 - n_{-\mathbf{p}\downarrow})$, while $n_{\mathbf{p}\uparrow}n_{-\mathbf{p}\downarrow}$ is the probability that they lie inside. This term can be ignored if we are interested strictly in pair formation between two momentum states just outside the Fermi surface, as in the Cooper problem. Our effective equation of motion is

$$\left(i\hbar \frac{\partial}{\partial t} - 2\epsilon_{\mathbf{p}} \right) \alpha_{\mathbf{p}}(t) = (1 - n_{\mathbf{p}\uparrow})(1 - n_{-\mathbf{p}\downarrow}) \sum'_{\mathbf{p}'} V_{\mathbf{p}\mathbf{p}'} \alpha_{\mathbf{p}'}(t) \quad (12.133)$$

in this limit. Because $i\hbar\partial/\partial t \rightarrow E$, the above expression is precisely the Schrödinger equation we solved previously to determine the Cooper bound state energy. However, the general pair amplitude equation, Eq. (12.132), dictates that all particles be involved in the pairing process whether they lie inside or outside the Fermi surface. This is the essence of BCS theory. Cooper included only the particles outside ϵ_F . BCS simply included the $n_{\mathbf{p}\uparrow}n_{-\mathbf{p}\downarrow}$ term in addition. This simple change made all the difference.

12.6.1 Instability: superconducting state

We turn to the evaluation of the pair amplitude. We want to show that below some characteristic temperature, T_c , the pair amplitude grows exponentially. We seek a solution of the form

$$\alpha_{\mathbf{p}}(t) = e^{-i\frac{z}{\hbar}t} \alpha_{\mathbf{p}}(t=0). \quad (12.134)$$

Substituting this expression into the pairing equation, we obtain

$$(z - 2\epsilon_{\mathbf{p}}) \alpha_{\mathbf{p}}(0) = (1 - n_{\mathbf{p}\uparrow} - n_{-\mathbf{p}\downarrow}) \sum'_{\mathbf{p}'} V_{\mathbf{p}\mathbf{p}'} \alpha_{\mathbf{p}'}(0) \quad (12.135)$$

as the Fourier transform of the pair amplitude equation.

For the model attractive potential in Eq. (12.51), the pair amplitude evolution equation becomes

$$(z - 2\epsilon_{\mathbf{p}}) \alpha_{\mathbf{p}}(0) = -V_0 (1 - n_{\mathbf{p}\uparrow} - n_{-\mathbf{p}\downarrow}) \sum'_{\mathbf{p}'} \alpha_{\mathbf{p}'}(0). \quad (12.136)$$

As before, we sum both sides of this expression to obtain

$$\sum'_{\mathbf{p}} \alpha_{\mathbf{p}}(0) = -V_0 \sum'_{\mathbf{p}} \frac{(1 - n_{\mathbf{p}\uparrow} - n_{-\mathbf{p}\downarrow})}{z - 2\epsilon_{\mathbf{p}}} \sum'_{\mathbf{p}'} \alpha_{\mathbf{p}'}(0), \quad (12.137)$$

which implies that

$$1 = -V_0 \sum'_{\mathbf{p}} \frac{(1 - n_{\mathbf{p}\uparrow} - n_{-\mathbf{p}\downarrow})}{z - 2\epsilon_{\mathbf{p}}}. \quad (12.138)$$

This is almost the expression we had previously except we are now including pairing between all particles. To obtain a solution, we plot the intersection of the left- and right-hand sides of the above equation. As before, we plot the RHS in the vicinity of the discrete energies $\epsilon_{\mathbf{p}}$.

As is evident, a solution exists only if $2\epsilon_F - 2\hbar\omega_D \leq \text{Re } z \leq 2\epsilon_F + 2\hbar\omega_D$. To solve our pair condition, we convert the sum to an integral and note that $n_{\mathbf{p}} = n_{-\mathbf{p}}$ for free particles. Also, because $\epsilon_{\mathbf{p}\uparrow} = \epsilon_{\mathbf{p}\downarrow}$, we have immediately that

$$n_{\mathbf{p}\uparrow} = n_{-\mathbf{p}\downarrow} = (e^{\beta(\epsilon_{\mathbf{p}} - \mu)} + 1)^{-1} \quad (12.139)$$

and

$$1 = -V_0 N(\epsilon_F) \int_{-\hbar\omega_D}^{\hbar\omega_D} d\epsilon \frac{\tanh \beta\epsilon/2}{z - 2\mu - 2\epsilon}, \quad (12.140)$$

where $N(\epsilon_F)$ is the density of states at the Fermi level. Exponential growth of the pairing amplitude will occur if z has a positive imaginary part. Let $z = 2\mu + x + iy$, where x and y are real. Consider first the case in which $y = 0$. We obtain in this limit that

$$1 = -V_0 N(\epsilon_F) \int_{-\hbar\omega_D}^{\hbar\omega_D} d\epsilon \tanh \frac{\beta\epsilon}{2} \left[P\left(\frac{1}{x - 2\epsilon}\right) - i\pi \delta(x - 2\epsilon) \right]. \quad (12.141)$$

To satisfy this equation, the imaginary part must vanish. This obtains only if $|x|/2 > \hbar\omega_D$ or, equivalently, $\text{Re } z > 2\epsilon_F + 2\hbar\omega_D$. As illustrated graphically in Fig. 12.15, the real part of the integrand is positive in this energy range. Consequently, $y = 0$ is not permissible.

For a solution to exist on the energy shell, $y \neq 0$. We write our pair constraint as

$$1 = -V_0 N(\epsilon_F) \int_{-\hbar\omega_D}^{\hbar\omega_D} \frac{(x - 2\epsilon - iy)}{(x - 2\epsilon)^2 + y^2} \tanh \frac{\beta\epsilon}{2} d\epsilon, \quad (12.142)$$

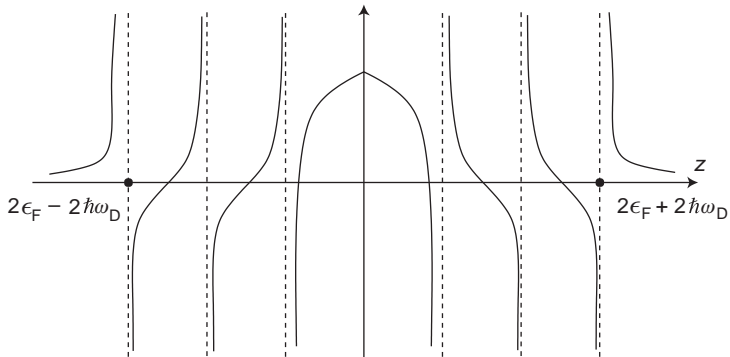


Fig. 12.15 The right-hand side of the pair amplitude equation as a function of the complex energy, z .

which is only true if the imaginary part,

$$\int_{-\hbar\omega_D}^{\hbar\omega_D} \frac{\tanh \beta\epsilon/2d\epsilon}{(x-2\epsilon)^2+y^2}, \quad (12.143)$$

vanishes. Because $\tanh(x) = -\tanh(-x)$, we rewrite this integrand as

$$\begin{aligned} 0 &= \frac{1}{2} \int_{-\hbar\omega_D}^{\hbar\omega_D} d\epsilon \tanh \frac{\beta\epsilon}{2} \left[\frac{1}{(x-2\epsilon)^2+y^2} - \frac{1}{(x+2\epsilon)^2+y^2} \right] \\ &= \frac{1}{2} \int_{-\hbar\omega_D}^{\hbar\omega_D} d\epsilon \tanh \frac{\beta\epsilon}{2} \left[\frac{8\epsilon x}{((x-2\epsilon)^2+y^2)((x+2\epsilon)^2+y^2)} \right]. \end{aligned} \quad (12.144)$$

It is now clear that $x = 0$ because $\epsilon \tanh \beta\epsilon/2$ is positive everywhere. Consequently, our solution must be of the form $z = 2\mu + iy$. We must solve then

$$1 = -N(\epsilon_F) V_0 \int_{-\hbar\omega_D}^{\hbar\omega_D} d\epsilon \frac{(-iy-2\epsilon) \tanh \beta\epsilon/2}{4\epsilon^2+y^2}. \quad (12.145)$$

The imaginary part of this integral is odd in ϵ and hence vanishes exactly. We are left with the single equation

$$1 = 4N(\epsilon_F) V_0 \int_0^{\hbar\omega_D} d\epsilon \frac{\epsilon \tanh \beta\epsilon/2}{4\epsilon^2+y^2}. \quad (12.146)$$

Here again the integrand is positive. As y increases, the integrand decreases. The same thing is true as T increases. Hence, for T greater than some temperature, no solution exists. This defines the critical temperature T_c . As $T \rightarrow 0$, we find that

$$\begin{aligned} 1 &= \frac{N(\epsilon_F) V_0}{2} \int_0^{(2\hbar\omega_D)^2} \frac{da}{a+y^2} \\ &= \frac{N(\epsilon_F) V_0}{2} \ln \left(\frac{(2\hbar\omega_D)^2+y^2}{y^2} \right). \end{aligned} \quad (12.147)$$

Exponentiation of both sides of this equation,

$$\begin{aligned} y^2 &= (2\hbar\omega_D)^2 \left(\exp\left(\frac{2}{N(\epsilon_F)V_0}\right) - 1 \right)^{-1} \\ &\approx (2\hbar\omega_D)^2 \exp\left(-\frac{2}{N(\epsilon_F)V_0}\right), \end{aligned} \quad (12.148)$$

results in the familiar equation for y , namely,

$$y = \pm 2\hbar\omega_D \exp\left(-\frac{1}{N(\epsilon_F)V_0}\right). \quad (12.149)$$

Choosing the positive solution, we conclude that as $T \rightarrow 0$, the pair amplitude grows as

$$\begin{aligned} \alpha_p(t) &\simeq e^{-izt} \\ &= e^{-2imt} e^{2\hbar\omega_D t \exp(-1/N(\epsilon_F)V_0)}. \end{aligned} \quad (12.150)$$

The existence of an exponentially growing pair amplitude is the signature of an instability in the N -particle ground state. We have essentially derived BCS theory by focusing solely on the pair amplitude, α_p . To obtain an exact expression for T_c , we consider our pair binding equation in the limit that $y = 0$. In this limit, the temperature that satisfies Eq. (12.146) is maximized. Hence, the $y = 0$ solution can be used to estimate T_c . Let us define $\beta_c = 1/k_B T_c$. We find that

$$1 = N(\epsilon_F)V_0 \int_0^{\hbar\omega_D\beta_c/2} \frac{\tanh x}{x} dx. \quad (12.151)$$

This integral must be done numerically. The transition temperature consistent with Eq. (12.151) is

$$k_B T_c = 1.14\hbar\omega_D \exp\left(-\frac{1}{N(\epsilon_F)V_0}\right). \quad (12.152)$$

We will show that the parameter y plays the role of the energy gap in BCS theory.

12.7 BCS ground state

Thus far, we have shown how the pairing hypothesis leads to an instability in the ground state for $T < T_c$. Our focus now is on the many-particle wavefunction describing this state. The starting point for our analysis is the many-body state for N non-interacting electrons:

$$|\Psi^0(N)\rangle = \prod_{\mathbf{p} < \mathbf{p}_F} b_{\mathbf{p}}^\dagger |0\rangle. \quad (12.153)$$

Because each momentum state is doubly occupied, we can construct such a state by successively operating on the vacuum with the pairing operator $b_{\mathbf{p}}^\dagger$. Relaxing the restriction $\mathbf{p} < \mathbf{p}_F$, we recast $|\Psi^0(N)\rangle$ in the form

$$|\Psi^0(N)\rangle = \prod_{\mathbf{p}} \left(u_{\mathbf{p}}^0 + v_{\mathbf{p}}^0 b_{\mathbf{p}}^\dagger \right) |0\rangle, \quad (12.154)$$

where

$$u_{\mathbf{p}}^0 = \begin{cases} 0, & \mathbf{p} < \mathbf{p}_F, \\ 1, & \mathbf{p} > \mathbf{p}_F, \end{cases} \quad (12.155)$$

$$v_{\mathbf{p}}^0 = \begin{cases} 1, & \mathbf{p} < \mathbf{p}_F, \\ 0, & \mathbf{p} > \mathbf{p}_F, \end{cases} \quad (12.156)$$

This representation of $|\Psi^0\rangle$ is identical to Eq. (12.153). Note also that because the $a_{\mathbf{p}}^\dagger$ anticommute, $|\Psi^0(N)\rangle$ is properly antisymmetrized.

BCS postulated that the general electron superconducting ground state can be written as

$$|\Psi_{\text{BCS}}\rangle = \prod_{\mathbf{p}} \left(u_{\mathbf{p}} + v_{\mathbf{p}} b_{\mathbf{p}}^\dagger \right) |0\rangle, \quad (12.157)$$

where the coefficients $u_{\mathbf{p}}$ and $v_{\mathbf{p}}$ are to be determined variationally and are referred to as *coherence factors*. The normalization condition $\langle \Psi_{\text{BCS}} | \Psi_{\text{BCS}} \rangle = 1$ imposes the constraint

$$1 = \langle 0 | \prod_{\mathbf{p}, \mathbf{p}'} \left(u_{\mathbf{p}}^* + v_{\mathbf{p}}^* b_{\mathbf{p}} \right) \left(u_{\mathbf{p}'} + v_{\mathbf{p}'} b_{\mathbf{p}'}^\dagger \right) |0\rangle. \quad (12.158)$$

Products of the form appearing in Eq. (12.158) can be simplified using the commutation relation in Eq. (12.130) and by noting that $b_{\mathbf{p}} b_{\mathbf{p}}^\dagger |0\rangle = 1$. We find that only the diagonal ($p = p'$) survives:

$$\langle \Psi_{\text{BCS}} | \Psi_{\text{BCS}} \rangle = \prod_{\mathbf{p}} \left(|u_{\mathbf{p}}|^2 + |v_{\mathbf{p}}|^2 \right), \quad (12.159)$$

implying that

$$|u_{\mathbf{p}}|^2 + |v_{\mathbf{p}}|^2 = 1. \quad (12.160)$$

If we expand the product in the BCS ground state, it becomes clear that $|\Psi_{\text{BCS}}\rangle$ is a sum of all $2m$ particle states,

$$|\Psi_{\text{BCS}}\rangle = \sum_m A_{2m} |\Psi_{2m}\rangle, \quad (12.161)$$

where m is an integer, A_{2m} is an expansion coefficient, and $|\Psi_{2m}\rangle$ is the ground state for $2m$ particles. We can relate $|\Psi_{2m}\rangle$ to $|\Psi_{\text{BCS}}\rangle$ by writing the expansion coefficients (S1964) as $A_{2m} = |A_{2m}|e^{2im\phi}$ so that

$$|\Psi_{\text{BCS}}^\phi\rangle = \sum_m e^{2im\phi} |A_{2m}| |\Psi_{2m}\rangle. \quad (12.162)$$

That is, we associate with each $2m$ -particle state an overall phase, $2m\phi$. To this end, we rewrite the BCS ground state

$$|\Psi_{\text{BCS}}^\phi\rangle = \prod_{\mathbf{p}} \left(u_{\mathbf{p}} + e^{2i\phi} v_{\mathbf{p}} b_{\mathbf{p}}^\dagger \right) |0\rangle \quad (12.163)$$

by multiplying each pair-creation operator by $\exp(2i\phi)$. Multiplying Eq. (12.162) by $\exp(-i2m\phi)$ and integrating over ϕ , we obtain a concise relation

$$|\Psi_{2m}\rangle = \frac{1}{2\pi |A_{2m}|} \int_0^{2\pi} d\phi e^{-i2m\phi} \prod_{\mathbf{p}} \left(u_{\mathbf{p}} + e^{2i\phi} v_{\mathbf{p}} b_{\mathbf{p}}^\dagger \right) |0\rangle \quad (12.164)$$

between each $2m$ -particle state and the BCS ground state. That only states with $2m$ particles survive on the right-hand side of Eq. (12.164) follows from the fact that

$$\frac{1}{2\pi} \int_0^{2\pi} e^{i\phi(N-N')} d\phi = \delta_{NN'}. \quad (12.165)$$

Because the $2m$ -particle states are mutually orthogonal, when we multiply Eq. (12.164) by $\langle \Psi_{2m} |$, the left-hand side becomes unity, allowing us to identify the square of the expansion coefficient as

$$\begin{aligned} |A_{2m}|^2 &= \int_0^{2\pi} \int_0^{2\pi} \frac{d\phi}{2\pi} \frac{d\phi'}{2\pi} e^{-i2m(\phi-\phi')} \langle 0 | \prod_{\mathbf{p}, \mathbf{p}'} \left(u_{\mathbf{p}}^* + e^{-2i\phi'} v_{\mathbf{p}}^* b_{\mathbf{p}} \right) \left(u_{\mathbf{p}'} + e^{2i\phi} v_{\mathbf{p}'} b_{\mathbf{p}'}^\dagger \right) |0\rangle \\ &= \frac{1}{2\pi} \int_0^{2\pi} d\phi e^{-2im\phi} \prod_{\mathbf{p}} \left(|u_{\mathbf{p}}|^2 + e^{2i\phi} |v_{\mathbf{p}}|^2 \right). \end{aligned} \quad (12.166)$$

Equation (12.166) should be construed as the probability distribution for $2m$ particles in the BCS state. This quantity is strongly peaked at the average number of particles in the BCS state and has a width proportional to the square root of the average number of particles in the system (see Problem 12.8).

Our rewriting of the BCS state as a linear superposition of all possible $2m$ -particle states, all with the same phase, ϕ , suggests that in a superconducting state, a conjugacy relationship exists between the phase and the particle number. Indeed, such a relationship exists. However, such a relationship cannot exist if one of the variables is bounded from below. Without loss of generality, we can treat the particle number as being a continuous variable from $-\infty < N < \infty$. We can establish the conjugacy relationship straightforwardly by

acting $-i\partial/\partial\phi$ on $|\psi_{\text{BCS}}^\phi\rangle$ in Eq. (12.164) and then integrating by parts. The result

$$\frac{1}{2\pi|A_{2m}|} \int_0^{2\pi} d\phi e^{-i2m\phi} \frac{-i\partial}{\partial\phi} \prod_{\mathbf{p}} \left(u_{\mathbf{p}} + e^{2i\phi} v_{\mathbf{p}} b_{\mathbf{p}}^\dagger \right) |0\rangle = 2m |\Psi_{2m}\rangle \quad (12.167)$$

implies that the particle number and the phase are related by

$$N \leftrightarrow -i \frac{\partial}{\partial\phi}, \quad (12.168)$$

as long as we regard the particle number as a continuous variable. Similarly, by applying $i\partial/\partial(2m)$ to Eq. (12.162), we establish analogously that

$$i \frac{\partial}{\partial N} \leftrightarrow \phi. \quad (12.169)$$

Hence, the phase and the particle number are conjugate dynamical variables as long as we consider the particle number to be a continuous variable. As such, the particle and phase must satisfy the Heisenberg uncertainty relationship $\Delta\phi\Delta N \geq 2\pi$ for two canonically conjugate variables. Consequently, complete certainty in the phase implies infinite uncertainty in the particle number, as is the case in a superconductor. In addition, the phase and the particle-number operators should also satisfy Hamilton's equations

$$\begin{aligned} i\hbar\dot{\hat{N}} &= [\hat{H}, \hat{N}] = i \frac{\partial\hat{H}}{\partial\hat{\phi}}, \\ i\hbar\dot{\hat{\phi}} &= [\hat{H}, \hat{\phi}] = -i \frac{\partial\hat{H}}{\partial\hat{N}} \end{aligned} \quad (12.170)$$

for two canonically conjugate variables. We will use these equations in the last section of this chapter where we formulate the Josephson effect.

12.8 Pair fluctuations

We focus now on computing $\langle b_{\mathbf{p}} \rangle$ for a BCS wavefunction. In the BCS ground state, the average of the pair operator

$$\begin{aligned} \langle b_{\mathbf{p}} \rangle_{\text{BCS}} &= \langle 0 | \prod_{\mathbf{p}', \mathbf{p}''} \left(u_{\mathbf{p}'}^* + v_{\mathbf{p}'}^* b_{\mathbf{p}'} \right) b_{\mathbf{p}} \left(u_{\mathbf{p}''} + v_{\mathbf{p}''} b_{\mathbf{p}''}^\dagger \right) |0\rangle \\ &= \langle 0 | u_{\mathbf{p}}^* v_{\mathbf{p}} b_{\mathbf{p}} b_{\mathbf{p}}^\dagger |0\rangle = u_{\mathbf{p}}^* v_{\mathbf{p}} \end{aligned} \quad (12.171)$$

is non-zero. However, for a normal state, $u_{\mathbf{p}}$ and $v_{\mathbf{p}}$ are never non-zero simultaneously (see Eqs. (12.155) and (12.156)). Hence, $\langle b_{\mathbf{p}} \rangle = 0$ in the normal state. Although $\langle b_{\mathbf{p}} \rangle$ is not

identical in form to the pair amplitude studied in the previous sections, it contains the same information. This state of affairs obtains because the BCS ground state is made up of states with different numbers of electrons. A non-zero value of $\langle b_p \rangle$ for a particular ground state indicates that that state favors pair formation.

It is reasonable then to define

$$\chi = \frac{1}{V} \sum_{\mathbf{p}} b_{\mathbf{p}} \quad (12.172)$$

as the effective order parameter for superconductivity. The average value of χ ,

$$\langle \chi \rangle_{\text{BCS}} = \frac{1}{V} \sum_{\mathbf{p}} u_{\mathbf{p}}^* v_{\mathbf{p}}, \quad (12.173)$$

has a definite value in the superconducting state. To prove this, it is sufficient to show that the second-order fluctuations of the order parameter vanish. We proceed by evaluating the second moment

$$\langle \chi^2 \rangle_{\text{BCS}} = \frac{1}{V^2} \left\langle \sum_{\mathbf{p}, \mathbf{p}'} b_{\mathbf{p}} b_{\mathbf{p}'} \right\rangle. \quad (12.174)$$

When we insert $|\Psi_{\text{BCS}}\rangle$, the only non-zero terms will come from the states whose momenta coincide with the indices in Eq. (12.174). Consequently, $\langle \chi^2 \rangle_{\text{BCS}}$ is a sum of

$$\frac{1}{V^2} \langle 0 | \sum_{\mathbf{p}, \mathbf{p}', \mathbf{p} \neq \mathbf{p}'} (u_{\mathbf{p}}^* + v_{\mathbf{p}}^* b_{\mathbf{p}}) (u_{\mathbf{p}'}^* + v_{\mathbf{p}'}^* b_{\mathbf{p}'}) b_{\mathbf{p}} b_{\mathbf{p}'} (u_{\mathbf{p}} + v_{\mathbf{p}} b_{\mathbf{p}}^\dagger) (u_{\mathbf{p}'} + v_{\mathbf{p}'} b_{\mathbf{p}'}^\dagger) | 0 \rangle \quad (12.175)$$

when $\mathbf{p} \neq \mathbf{p}'$ and

$$\frac{1}{V^2} \langle 0 | \sum_{\mathbf{p}} (u_{\mathbf{p}}^* + v_{\mathbf{p}}^* b_{\mathbf{p}}) b_{\mathbf{p}}^2 (u_{\mathbf{p}} + v_{\mathbf{p}} b_{\mathbf{p}}^\dagger) | 0 \rangle \quad (12.176)$$

for $\mathbf{p} = \mathbf{p}'$. The second expression vanishes because $\langle b_{\mathbf{p}}^2 \rangle = 0$. Hence, $\langle \chi^2 \rangle_{\text{BCS}}$ is off-diagonal in momentum space, and Eq. (12.175) reduces to

$$\begin{aligned} \langle \chi^2 \rangle_{\text{BCS}} &= \frac{1}{V^2} \sum_{\mathbf{p}, \mathbf{p}', \mathbf{p} \neq \mathbf{p}'} u_{\mathbf{p}}^* v_{\mathbf{p}} u_{\mathbf{p}'}^* v_{\mathbf{p}'} \\ &= \frac{1}{V^2} \sum_{\mathbf{p}, \mathbf{p}'} \langle b_{\mathbf{p}} \rangle \langle b_{\mathbf{p}'} \rangle (1 - \delta_{\mathbf{p}\mathbf{p}'}) \\ &= \langle \chi \rangle_{\text{BCS}}^2 - \frac{1}{V^2} \sum_{\mathbf{p}} \langle b_{\mathbf{p}} \rangle^2. \end{aligned} \quad (12.177)$$

The second-order fluctuation in the order parameter is

$$\langle \delta \chi^2 \rangle = \langle \chi^2 \rangle_{\text{BCS}} - \langle \chi \rangle_{\text{BCS}}^2 = -\frac{1}{V} \left[\frac{1}{V} \sum_{\mathbf{p}} \langle b_{\mathbf{p}} \rangle^2 \right]. \quad (12.178)$$

Once we determine the coefficients $u_{\mathbf{p}}$ and $v_{\mathbf{p}}$, we will be able to show that $\langle \delta \chi^2 \rangle \propto V^{-1}$ and hence vanishes in the thermodynamic limit. On this basis, we will argue that $\langle \chi \rangle$ takes on a definite value in the superconducting state and, as advertised, is the order parameter for the superconducting transition.

12.9 Ground state energy

We determine the coefficients $u_{\mathbf{p}}$ and $v_{\mathbf{p}}$ by minimizing the ground state energy subject to the normalization constraint (Eq. (12.160)) and a particle-number constraint on the ground-state energy. We impose that the average number of particles in the BCS ground state is the desired value (supposedly even) by introducing a Lagrange multiplier into the average value of the Hamiltonian:

$$E' = \langle H \rangle - \mu \langle N \rangle, \quad (12.179)$$

where μ is the chemical potential. To simplify this calculation, we rescale the single-particle energies such that $\epsilon_{\mathbf{p}} \equiv \mathbf{p}^2/2m - \mu$. The energy E' is now

$$E' = \sum_{\mathbf{p}, \sigma} \epsilon_{\mathbf{p}} \langle n_{\mathbf{p}\sigma} \rangle + \sum_{\mathbf{p}, \mathbf{p}'} V_{\mathbf{p}\mathbf{p}'} \langle b_{\mathbf{p}}^\dagger b_{\mathbf{p}'} \rangle. \quad (12.180)$$

Let us first compute $\langle n_{\mathbf{p}\sigma} \rangle$:

$$\begin{aligned} \langle n_{\mathbf{p}\sigma} \rangle &= \langle 0 | \prod_{\mathbf{p}' \mathbf{p}''} (u_{\mathbf{p}'}^* + v_{\mathbf{p}'}^* b_{\mathbf{p}'}) a_{\mathbf{p}\sigma}^\dagger a_{\mathbf{p}\sigma} (u_{\mathbf{p}''} + v_{\mathbf{p}''} b_{\mathbf{p}''}^\dagger) | 0 \rangle \\ &= \prod_{\mathbf{p}', \mathbf{p}''} |v_{\mathbf{p}'}|^2 \langle 0 | b_{\mathbf{p}'} n_{\mathbf{p}\sigma} b_{\mathbf{p}''}^\dagger | 0 \rangle (\delta_{\mathbf{p}, \mathbf{p}'} \delta_{\sigma, \uparrow} + \delta_{\mathbf{p}, -\mathbf{p}''} \delta_{\sigma, \downarrow}) \\ &= \begin{cases} |v_{\mathbf{p}}|^2, & \sigma = \uparrow, \\ |v_{-\mathbf{p}}|^2, & \sigma = \downarrow. \end{cases} \end{aligned} \quad (12.181)$$

Reflection symmetry requires that the expansion coefficients be invariant under $\mathbf{p} \rightarrow -\mathbf{p}$.

The dominant term in $\langle b_{\mathbf{p}}^\dagger b_{\mathbf{p}'} \rangle$ arises from $\mathbf{p} \neq \mathbf{p}'$ because $\langle b_{\mathbf{p}}^2 \rangle = 0$. In this case the average can be factorized: $\langle b_{\mathbf{p}}^\dagger b_{\mathbf{p}'} \rangle = \langle b_{\mathbf{p}}^\dagger \rangle \langle b_{\mathbf{p}'} \rangle = u_{\mathbf{p}} u_{\mathbf{p}'}^* v_{\mathbf{p}}^* v_{\mathbf{p}'}$. Consequently, the average value of the ground-state energy is

$$E' = 2 \sum_{\mathbf{p}} |v_{\mathbf{p}}|^2 \epsilon_{\mathbf{p}} + \sum_{\mathbf{p}, \mathbf{p}'} V_{\mathbf{p}\mathbf{p}'} u_{\mathbf{p}} u_{\mathbf{p}'}^* v_{\mathbf{p}}^* v_{\mathbf{p}'}. \quad (12.182)$$

We need to vary E' ,

$$\delta E' = 0 = 2 \sum_{\mathbf{p}} \epsilon_{\mathbf{p}} \delta v_{\mathbf{p}}^* v_{\mathbf{p}} + \sum_{\mathbf{p}, \mathbf{p}'} V_{\mathbf{p}\mathbf{p}'} \delta v_{\mathbf{p}}^* (u_{\mathbf{p}} u_{\mathbf{p}'}^* v_{\mathbf{p}'}) + \sum_{\mathbf{p}, \mathbf{p}'} V_{\mathbf{p}\mathbf{p}'} \delta u_{\mathbf{p}'}^* (u_{\mathbf{p}} v_{\mathbf{p}}^* v_{\mathbf{p}'}), \quad (12.183)$$

with respect to $v_{\mathbf{p}}^*$ and $u_{\mathbf{p}}^*$ to find the minimum energy. To eliminate $\delta u_{\mathbf{p}'}^*$, we note that the variation of the normalization constraint can be rewritten as

$$u_{\mathbf{p}} \delta u_{\mathbf{p}}^* + v_{\mathbf{p}} \delta v_{\mathbf{p}}^* = 0 \quad (12.184)$$

or, equivalently,

$$\delta u_{\mathbf{p}}^* = -\frac{v_{\mathbf{p}}}{u_{\mathbf{p}}} \delta v_{\mathbf{p}}^*. \quad (12.185)$$

Substitution of this expression into Eq. (12.183) yields

$$0 = \sum_{\mathbf{p}} \delta v_{\mathbf{p}}^* \left[2\epsilon_{\mathbf{p}} v_{\mathbf{p}} + \sum_{\mathbf{p}'} \left[V_{\mathbf{p}\mathbf{p}'} \left(u_{\mathbf{p}} u_{\mathbf{p}'}^* v_{\mathbf{p}'} \right) - V_{\mathbf{p}'\mathbf{p}} u_{\mathbf{p}'} v_{\mathbf{p}}^* \frac{v_{\mathbf{p}}^2}{u_{\mathbf{p}}} \right] \right], \quad (12.186)$$

which implies that

$$0 = 2\epsilon_{\mathbf{p}} v_{\mathbf{p}} - \Delta_{\mathbf{p}} u_{\mathbf{p}} + \Delta_{\mathbf{p}}^* \frac{v_{\mathbf{p}}^2}{u_{\mathbf{p}}}, \quad (12.187)$$

where we have defined

$$\Delta_{\mathbf{p}} = - \sum_{\mathbf{p}'} V_{\mathbf{p}\mathbf{p}'} u_{\mathbf{p}'}^* v_{\mathbf{p}'} . \quad (12.188)$$

As we will see, $\Delta_{\mathbf{p}}$ will play the role of the energy gap. In fact, we can see this immediately by dividing Eq. (12.187) by $u_{\mathbf{p}}$,

$$0 = 2\epsilon_{\mathbf{p}} \frac{v_{\mathbf{p}}}{u_{\mathbf{p}}} + \Delta_{\mathbf{p}}^* \left(\frac{v_{\mathbf{p}}}{u_{\mathbf{p}}} \right)^2 - \Delta_{\mathbf{p}}, \quad (12.189)$$

and solving this quadratic equation for $v_{\mathbf{p}}/u_{\mathbf{p}}$,

$$\frac{v_{\mathbf{p}}}{u_{\mathbf{p}}} = \frac{-\epsilon_{\mathbf{p}} \pm \sqrt{\epsilon_{\mathbf{p}}^2 + |\Delta_{\mathbf{p}}|^2}}{\Delta_{\mathbf{p}}^*}. \quad (12.190)$$

Let us define

$$\varepsilon_{\mathbf{p}} \equiv \sqrt{\epsilon_{\mathbf{p}}^2 + |\Delta_{\mathbf{p}}|^2}, \quad (12.191)$$

which will turn out to be the quasi-particle energy in the superconducting state. At this point we can see, at least heuristically, that $\Delta_{\mathbf{p}}$ does introduce a gap into the single-particle spectrum, $\epsilon_{\mathbf{p}}$. We can simplify Eq. (12.190) further by noting that

$$\begin{aligned} \frac{v_{\mathbf{p}}}{u_{\mathbf{p}}} &= \frac{\epsilon_{\mathbf{p}}^2 - \varepsilon_{\mathbf{p}}^2}{(-\epsilon_{\mathbf{p}} \mp \varepsilon_{\mathbf{p}}) \Delta_{\mathbf{p}}^*} \\ &= \frac{\Delta_{\mathbf{p}}}{\epsilon_{\mathbf{p}} \pm \varepsilon_{\mathbf{p}}}. \end{aligned} \quad (12.192)$$

We assess which sign is appropriate by noting that, in the free system, $v_p/u_p \rightarrow 0$ when $\epsilon_p > \epsilon_F$. Consequently, we should choose the + sign.

Coupled with the normalization constraint,

$$1 = |u_p|^2 + |u_p|^2 \frac{|\Delta_p|^2}{(\epsilon_p + \varepsilon_p)^2} = 2 |u_p|^2 \left[\frac{\epsilon_p (\epsilon_p + \varepsilon_p)}{(\epsilon_p + \varepsilon_p)^2} \right], \quad (12.193)$$

we determine the magnitude of u_p to be

$$|u_p|^2 = \frac{\epsilon_p + \varepsilon_p}{2\varepsilon_p}. \quad (12.194)$$

There is clearly a phase degree of freedom associated with the definition of u_p . To make life simple, we choose u_p to be positive and real. We find then that

$$u_p = \sqrt{\frac{\epsilon_p + \varepsilon_p}{2\varepsilon_p}} \quad (12.195)$$

and

$$v_p = \frac{\Delta_p}{\epsilon_p + \varepsilon_p} \sqrt{\frac{\epsilon_p + \varepsilon_p}{2\varepsilon_p}} = \sqrt{\frac{\Delta_p}{\Delta_p^*} \left(\frac{\varepsilon_p - \epsilon_p}{2\varepsilon_p} \right)}. \quad (12.196)$$

For the simple attractive interaction chosen, Δ_p is real if motion of the center-of-mass is ignored and v_p simplifies to

$$v_p = \sqrt{\frac{\varepsilon_p - \epsilon_p}{2\varepsilon_p}}. \quad (12.197)$$

Returning to our original problem of determining the ground state energy, we reduce the average energy

$$\begin{aligned} E'_s &= 2 \sum_p \epsilon_p |v_p|^2 + \sum_{p,p'} V_{pp'} u_{p'}^* v_{p'} u_p v_p^* \\ &= \sum_p \left(2\epsilon_p |v_p|^2 - \Delta_p u_p v_p^* \right) \\ &= - \sum_p \frac{(\varepsilon_p - \epsilon_p)^2}{2\varepsilon_p} \end{aligned} \quad (12.198)$$

to a single sum using the form of the coherence factors just derived. In the absence of the attractive interaction, we had that

$$E'_n = \sum_{\mathbf{p}} 2\epsilon_{\mathbf{p}} \theta(\mathbf{p}_F - \mathbf{p}) \quad (12.199)$$

with θ the Heaviside step function. Because we have redefined $\epsilon_{\mathbf{p}} \equiv \mathbf{p}^2/2m - \mu$, $\epsilon_{\mathbf{p}} < 0$ for $\mathbf{p} < \mathbf{p}_F$. Consequently, the energy difference between the superconducting and normal states is given by the integral

$$\begin{aligned} \delta E &= -N(\epsilon_F - \mu) \left[\int_{-\hbar\omega_D}^{\hbar\omega_D} \frac{(\epsilon_{\mathbf{p}} - \epsilon)^2}{2\epsilon_{\mathbf{p}}} d\epsilon + \int_{-\hbar\omega_D}^0 2\epsilon d\epsilon \right] \\ &= -N(\epsilon_F - \mu) \int_0^{\hbar\omega_D} \frac{(\epsilon_{\mathbf{p}} - \epsilon)^2}{\epsilon_{\mathbf{p}}} d\epsilon. \end{aligned} \quad (12.200)$$

To obtain the final result, we substitute the expression for $\epsilon_{\mathbf{p}}$ and perform the integral over ϵ . In obtaining the final result, it is expedient to introduce the new variable $\epsilon = \Delta \sinh y$. Consequently,

$$\begin{aligned} (\epsilon_{\mathbf{p}} - \epsilon)^2 &= \left(\Delta \sqrt{\sinh^2 y + 1} - \Delta \sinh y \right)^2 \\ &= (\Delta \cosh y - \Delta \sinh y)^2 = \Delta^2 e^{-2y}. \end{aligned} \quad (12.201)$$

As a result,

$$\delta E = -N(\epsilon_F - \mu) \Delta^2 \int_0^{\sinh^{-1}(\hbar\omega_D/\Delta)} e^{-2y} dy. \quad (12.202)$$

In general, $\hbar\omega_D/\Delta \gg 1$, and the upper limit can then be extended to ∞ . The y -integration yields $1/2$, and the energy difference is

$$\delta E = \frac{-N(\epsilon_F - \mu) \Delta^2}{2}. \quad (12.203)$$

That is, the ground state energy of the superconducting state is lower than that of the corresponding normal state. The condensation energy in a superconductor is δE .

12.10 Critical magnetic field

We showed in the previous section that the condensation energy in a superconductor is $2\delta E = -N(\epsilon_F - \mu) \Delta^2$. The negative sign ensures that the superconducting state is lower in energy than the normal state. The condensation energy is related to the critical field, H_c , as follows.

Consider placing a superconductor in a magnetic field with the cylindrical geometry shown in Fig. 12.16. The energy per unit volume produced by the magnetic field is $B^2/8\pi$.

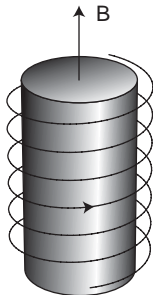


Fig. 12.16 Cylindrical piece of a superconductor surrounded by a magnetic coil.

The current in the magnetic coils is held constant by the field H . Hence, there must be a contribution from the interaction of the vector field, $\mathbf{A}(\mathbf{r})$, with the current produced by the magnetic field. Ampere's law states that

$$\nabla \times \mathbf{H} = \frac{4\pi}{c} \mathbf{J}, \quad (12.204)$$

where \mathbf{J} is the current in the coils that produce the magnetic field. The resultant contribution to the energy density is

$$\begin{aligned} W &= - \int \mathbf{A} \cdot \frac{\nabla \times \mathbf{H}}{4\pi} \frac{d\mathbf{r}}{V} \\ &= - \int \frac{\nabla \times \mathbf{A}}{4\pi} \cdot \mathbf{H} \frac{d\mathbf{r}}{V} \\ &= - \int \mathbf{B} \cdot \mathbf{H} \frac{d\mathbf{r}}{4\pi V}. \end{aligned} \quad (12.205)$$

In a uniform system, $\mathbf{B} = \mathbf{H}$, and the total internal energy due to the field is $H^2/8\pi - H^2/4\pi = -H^2/8\pi$. In the normal state, this energy must be included in the total ground state energy. As a consequence, the energy of the normal state in the presence of a magnetic field is given by $E_0^n = E_n' - H^2/8\pi$. Because the field does not penetrate a superconductor, the internal energy of the superconductor remains unchanged from E_s' . Superconductivity will persist until $E_n' - H^2/8\pi > E_s'$. Consequently,

$$\frac{H^2}{8\pi} > E_n' - E_s' = -\delta E \quad (12.206)$$

is the criterion for the critical value of the field. We find that the critical field,

$$H_c = \sqrt{-8\pi\delta E} = \sqrt{4\pi N (\epsilon_F - \mu)} \Delta, \quad (12.207)$$

is directly proportional to the gap parameter, Δ .

12.11 Energy gap

The physical motivation for introducing $\Delta_{\mathbf{p}}$,

$$\begin{aligned}\Delta_{\mathbf{p}} &= - \sum_{\mathbf{p}'} V_{\mathbf{p}\mathbf{p}'} u_{\mathbf{p}'}^* v_{\mathbf{p}'} \\ &= - \sum_{\mathbf{p}'} V_{\mathbf{p}\mathbf{p}'} \frac{\Delta_{\mathbf{p}'}}{2\varepsilon_{\mathbf{p}'}} ,\end{aligned}\quad (12.208)$$

as the gap is that this quantity breaks the continuous single-particle spectrum $\epsilon_{\mathbf{p}}$ into two branches. Specializing to the model potential which is non-zero only over a narrow momentum shell around the Fermi energy, we rewrite the gap equation as

$$\Delta_{\mathbf{p}} = V_0 \sum'_{\mathbf{p}'} \frac{\Delta_{\mathbf{p}'}}{2\sqrt{\varepsilon_{\mathbf{p}'}^2 + \Delta_{\mathbf{p}}^2}} .\quad (12.209)$$

The prime on the sum indicates the restriction $|\epsilon_{\mathbf{p}} - \epsilon_{\mathbf{p}_F}| < \hbar\omega_D$. Within the momentum shell, $\Delta_{\mathbf{p}}$ is relatively independent of \mathbf{p} only if the Fermi surface is isotropic. For *s*-wave pairing, the Fermi surface is entirely isotropic, and the gap can be taken to be independent of \mathbf{p} . For higher angular momentum pairing states such as *d*-wave, the Fermi surface has nodes, and the momentum dependence of the gap cannot be ignored. For our purposes, we will assume here that $\Delta_{\mathbf{p}}$ is independent of \mathbf{p} , at least within the thin momentum shell around the Fermi surface. An immediate solution to the gap equation is $\Delta = 0$. If $\Delta = 0$, then $\langle b_{\mathbf{p}} \rangle = 0$ and only the normal phase is possible.

To obtain a non-trivial solution to the gap equation, we convert the sum to an integral:

$$\begin{aligned}1 &= N(\epsilon_F - \mu) V_0 \int_{-\hbar\omega_D}^{\hbar\omega_D} \frac{d\epsilon}{2\sqrt{\epsilon^2 + \Delta^2}} \\ &= N(\epsilon_F - \mu) V_0 \int_0^{\hbar\omega_D/\Delta} \frac{d\epsilon}{\sqrt{\epsilon^2 + 1}} \\ &= N(\epsilon_F - \mu) V_0 \sinh^{-1} \frac{\hbar\omega_D}{\Delta}.\end{aligned}\quad (12.210)$$

Consequently, the gap is given by

$$\Delta = \frac{\hbar\omega_D}{\sinh(1/N(\epsilon_F - \mu)V_0)} .\quad (12.211)$$

Typically, $N(\epsilon_F - \mu)V_0 \ll 1$. In this limit, the gap takes on the familiar form

$$\Delta(T = 0) \simeq 2\hbar\omega_D \exp\left(-\frac{1}{N(0)V_0}\right) .\quad (12.212)$$

In the Cooper problem, we showed that the binding energy of a pair is identical to $\Delta(T = 0)$, except $1/(N(0)V_0) \rightarrow 2/(N(0)V_0)$. In the full theory, as remarked earlier, pairing of

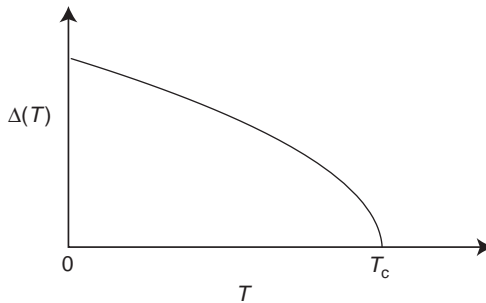


Fig. 12.17 Asymptotic behavior of the gap for the model BCS interaction. Asymptotically the gap scales as $\Delta(T) = \Delta(T = 0)(1 - \frac{T}{T_c})^{1/2}$.

particles below the Fermi energy is included as well. As a consequence, the exact exponent is $2/(2N(0)V_0) = 1/(N(0)V_0)$. In this sense, pairing of particles below the Fermi surface effectively doubles the density of states at the Fermi level. Comparing the gap with T_c (Eq. (12.152)), we find that

$$\frac{2\Delta}{k_B T_c} = \frac{4\hbar\omega_D}{1.14\hbar\omega_D} = 3.52, \quad (12.213)$$

which is the crucial ratio in BCS theory. It determines whether a superconductor is in the weak coupling (with respect to the phonon interaction) limit. Strong coupling corresponds to $2\Delta/k_B T_c > 3.5$.

To evaluate the gap at finite temperature, we include the Fermi distribution weight factor, $1 - n_{\mathbf{p}\uparrow} - n_{-\mathbf{p}\downarrow}$, which accounts for pairing among all the particles. Because $n_{\mathbf{p}\uparrow} = n_{-\mathbf{p}\downarrow}$, we can write the finite temperature gap equation as

$$\Delta_{\mathbf{p}} = - \sum_{\mathbf{p}'} V_{\mathbf{p}\mathbf{p}'} \frac{(1 - 2n_{\mathbf{p}'})}{2\varepsilon_{\mathbf{p}'}} \Delta_{\mathbf{p}'}. \quad (12.214)$$

For an isotropic system and the BCS model potential, we obtain

$$1 = V_0 N(0) \int_{-\hbar\omega_D}^{\hbar\omega_D} \frac{\tanh \beta \sqrt{\epsilon^2 + \Delta^2}/2}{2\sqrt{\epsilon^2 + \Delta^2}} d\epsilon \quad (12.215)$$

as the defining equation for the finite temperature gap in the excitation spectrum. This equation must be solved numerically. However, the approximate solution is $\Delta(T) = \Delta(T = 0)\sqrt{1 - T/T_c}$. This behavior is illustrated in Fig. 12.17.

Recalling that the second-order fluctuation in the order parameter,

$$\langle \delta\chi^2 \rangle = -\frac{1}{V^2} \sum_{\mathbf{p}} u_{\mathbf{p}}^{*2} v_{\mathbf{p}}^2, \quad (12.216)$$

is determined by the same combination of coherence factors as is the gap, we see immediately that if the gap is well behaved then $\langle \delta\chi^2 \rangle$ vanishes in the thermodynamic limit. Consequently, $\langle b_{\mathbf{p}} \rangle$ takes on a definite value in the superconducting state.

12.12 Quasi-particle excitations

To be able to determine the energy required to add an extra particle to a superconductor, we first determine the normalized creation operator for adding an extra electron to $|\Psi_{\text{BCS}}\rangle$. We note at the outset that

$$\begin{aligned} a_{\mathbf{p}'\uparrow}^\dagger |\Psi_{\text{BCS}}\rangle &= a_{\mathbf{p}'\uparrow}^\dagger \prod_{\mathbf{p}} (u_{\mathbf{p}} + v_{\mathbf{p}} b_{\mathbf{p}}^\dagger) |0\rangle \\ &= a_{\mathbf{p}'\uparrow}^\dagger u_{\mathbf{p}'} \prod_{\mathbf{p} \neq \mathbf{p}'} (u_{\mathbf{p}} + v_{\mathbf{p}} b_{\mathbf{p}}^\dagger) |0\rangle \\ &= u_{\mathbf{p}'} |\psi_{\mathbf{p}'\uparrow}\rangle \end{aligned} \quad (12.217)$$

and

$$\begin{aligned} a_{-\mathbf{p}'\downarrow} |\Psi_{\text{BCS}}\rangle &= a_{-\mathbf{p}'\downarrow} v_{\mathbf{p}'} a_{\mathbf{p}'\uparrow}^\dagger a_{-\mathbf{p}'\downarrow}^\dagger \prod_{\mathbf{p} \neq \mathbf{p}'} (u_{\mathbf{p}} + v_{\mathbf{p}} b_{\mathbf{p}}^\dagger) |0\rangle \\ &= -v_{\mathbf{p}'} |\psi_{\mathbf{p}'\uparrow}\rangle, \end{aligned} \quad (12.218)$$

where

$$|\psi_{\mathbf{p}'\uparrow}\rangle = a_{\mathbf{p}'\uparrow}^\dagger \prod_{\mathbf{p} \neq \mathbf{p}'} (u_{\mathbf{p}} + v_{\mathbf{p}} b_{\mathbf{p}}^\dagger) |0\rangle \quad (12.219)$$

is the normalized wavefunction when an extra electron with momentum \mathbf{p} and spin \uparrow is added to the BCS ground state. Consequently, $a_{\mathbf{p}'\uparrow}^\dagger$ and $a_{-\mathbf{p}'\downarrow}^\dagger$ are not the operators that should be used to construct the excited states because the resultant states are not normalized. However, the linear combination of the electron operators,

$$\gamma_{\mathbf{p}\uparrow}^\dagger = u_{\mathbf{p}}^* a_{\mathbf{p}\uparrow}^\dagger - v_{\mathbf{p}}^* a_{-\mathbf{p}\downarrow}^\dagger, \quad (12.220)$$

when acting on $|\Psi_{\text{BCS}}\rangle$,

$$\begin{aligned} \gamma_{\mathbf{p}\uparrow}^\dagger |\Psi_{\text{BCS}}\rangle &= (u_{\mathbf{p}}^* a_{\mathbf{p}\uparrow}^\dagger - v_{\mathbf{p}}^* a_{-\mathbf{p}\downarrow}^\dagger) \prod_{\mathbf{p}'} (u_{\mathbf{p}'} + v_{\mathbf{p}'} b_{\mathbf{p}'}^\dagger) |0\rangle \\ &= (|u_{\mathbf{p}}|^2 + |v_{\mathbf{p}}|^2) |\psi_{\mathbf{p}\uparrow}\rangle \\ &= |\psi_{\mathbf{p}\uparrow}\rangle \end{aligned} \quad (12.221)$$

does produce the normalized state $|\psi_{\mathbf{p}\uparrow}\rangle$. The corresponding creation operator for the state $|\psi_{-\mathbf{p}\downarrow}\rangle$ is

$$\gamma_{-\mathbf{p}\downarrow}^\dagger = u_{\mathbf{p}}^* a_{-\mathbf{p}\downarrow}^\dagger + v_{\mathbf{p}}^* a_{\mathbf{p}\uparrow}. \quad (12.222)$$

Because the $\gamma_{\mathbf{p}}$ s are linear combinations of the $a_{\mathbf{p}}$ s, they must obey the standard Fermi–Dirac anticommutation relationships, namely

$$\begin{aligned} [\gamma_{\mathbf{p}\sigma}, \gamma_{\mathbf{p}'\sigma'}^\dagger]_+ &= \delta_{\mathbf{p}\mathbf{p}'}\delta_{\sigma\sigma'}, \\ [\gamma_{\mathbf{p}\sigma}, \gamma_{\mathbf{p}'\sigma'}]_+ &= [\gamma_{\mathbf{p}\sigma}^\dagger, \gamma_{\mathbf{p}'\sigma'}^\dagger]_+ = 0. \end{aligned} \quad (12.223)$$

The anticommutation relationships guarantee that

$$\gamma_{\mathbf{p}\uparrow} |\Psi_{\text{BCS}}\rangle = \gamma_{-\mathbf{p}\downarrow} |\Psi_{\text{BCS}}\rangle = 0. \quad (12.224)$$

That is, no quasi-particles exist in the ground state of a superconductor.

Because the $\gamma_{\mathbf{p}}$ s are linear combinations of an electron and a hole operator with antiparallel spins, the excitations created by these operators do not carry a well-defined charge. That is, creation of a quasi-particle in a superconductor does not conserve charge. Quasi-particles have a well-defined spin, however, because adding an electron with spin $\hbar/2$ or a hole with spin $-\hbar/2$ creates an eigenstate of S_z with spin $\hbar/2$. Cooper pairs, on the other hand, carry charge $2e$ but are spinless in the singlet channel. Consequently, the quantities that carry well-defined spin and charge in a standard singlet BCS superconductor are distinct entities. It is in this sense that spin–charge separation obtains in singlet BCS superconductors. We show now that the energy dispersion relation for the spin carrier in a singlet superconductor is $\varepsilon_{\mathbf{p}}$. To prove this assertion, we start with the equations of motion for $a_{\mathbf{p}\uparrow}$,

$$\begin{aligned} i\hbar \dot{a}_{\mathbf{p}\uparrow} &= \epsilon_{\mathbf{p}} a_{\mathbf{p}\uparrow} - \sum_{\mathbf{p}_1, \mathbf{p}_2} V_{\mathbf{p}_1 \mathbf{p}_2} [a_{\mathbf{p}\uparrow}, b_{\mathbf{p}_1}^\dagger b_{\mathbf{p}_2}] \\ &= \epsilon_{\mathbf{p}} a_{\mathbf{p}\uparrow} + \sum_{\mathbf{p}_1} V_{\mathbf{p} \mathbf{p}_1} b_{\mathbf{p}_1} a_{-\mathbf{p}\downarrow}^\dagger, \end{aligned} \quad (12.225)$$

and for $a_{-\mathbf{p}\downarrow}^\dagger$,

$$i\hbar \dot{a}_{-\mathbf{p}\downarrow}^\dagger = -\epsilon_{\mathbf{p}} a_{-\mathbf{p}\downarrow}^\dagger + \sum_{\mathbf{p}_2} V_{\mathbf{p} \mathbf{p}_2} b_{\mathbf{p}_2}^\dagger a_{\mathbf{p}\uparrow}. \quad (12.226)$$

To simplify these equations of motion, we replace $\sum_{\mathbf{p}_1} V_{\mathbf{p} \mathbf{p}_1} b_{\mathbf{p}_1}$ by its average value: $-\Delta_{\mathbf{p}} = \sum_{\mathbf{p}_1} V_{\mathbf{p} \mathbf{p}_1} \langle b_{\mathbf{p}_1} \rangle$. As a consequence, the effective Hamiltonian

$$H_{\text{eff}} = \sum_{\mathbf{p}\sigma} \epsilon_{\mathbf{p}} n_{\mathbf{p}\sigma} - \sum_{\mathbf{p}} \Delta_{\mathbf{p}} (b_{\mathbf{p}}^\dagger + b_{\mathbf{p}}) \quad (12.227)$$

is linear in the pairing operator $b_{\mathbf{p}}^\dagger$, as opposed to quadratic as in the full Hamiltonian. As a result, particle number is not conserved in the reduced Hamiltonian. Nonetheless, the mean-field treatment of the BCS Hamiltonian provides an accurate description of the superconducting state. This state of affairs occurs partly because the BCS ground state does not have a fixed number of particles.

The mean-field closure leads to a coupled set of equations:

$$\begin{aligned} i\hbar \dot{a}_{\mathbf{p}\uparrow} &= \epsilon_{\mathbf{p}} a_{\mathbf{p}\uparrow} - \Delta_{\mathbf{p}} a_{-\mathbf{p}\downarrow}^\dagger, \\ i\hbar \dot{a}_{-\mathbf{p}\downarrow}^\dagger &= -\epsilon_{\mathbf{p}} a_{-\mathbf{p}\downarrow}^\dagger - \Delta_{\mathbf{p}} a_{\mathbf{p}\uparrow}, \end{aligned} \quad (12.228)$$

linear in the gap parameter, $\Delta_{\mathbf{p}}$. For economy of notation, we rewrite this set of equations in matrix form:

$$\begin{aligned} i\hbar \frac{\partial}{\partial t} \begin{pmatrix} a_{\mathbf{p}\uparrow} \\ a_{-\mathbf{p}\downarrow}^\dagger \end{pmatrix} &= \begin{pmatrix} \epsilon_{\mathbf{p}} & -\Delta_{\mathbf{p}} \\ -\Delta_{\mathbf{p}} & -\epsilon_{\mathbf{p}} \end{pmatrix} \begin{pmatrix} a_{\mathbf{p}\uparrow} \\ a_{-\mathbf{p}\downarrow}^\dagger \end{pmatrix} \\ &= \mathbf{H}_{\text{eff}} \begin{pmatrix} a_{\mathbf{p}\uparrow} \\ a_{-\mathbf{p}\downarrow}^\dagger \end{pmatrix}. \end{aligned} \quad (12.229)$$

To aid in diagonalizing the reduced Hamiltonian matrix, we introduce the angle $\theta_{\mathbf{p}}$, such that

$$\cos \theta_{\mathbf{p}} = \frac{\epsilon_{\mathbf{p}}}{\varepsilon_{\mathbf{p}}} \quad (12.230)$$

and

$$\sin \theta_{\mathbf{p}} = \frac{\Delta_{\mathbf{p}}}{\varepsilon_{\mathbf{p}}}. \quad (12.231)$$

The utility of this transformation is immediate because the BCS coefficients

$$u_{\mathbf{p}} = \frac{1}{\sqrt{2}} \left(1 + \frac{\epsilon_{\mathbf{p}}}{\varepsilon_{\mathbf{p}}} \right)^{1/2} = \frac{1}{\sqrt{2}} (1 + \cos \theta_{\mathbf{p}})^{1/2} \quad (12.232)$$

and

$$v_{\mathbf{p}} = \frac{1}{\sqrt{2}} \left(1 - \frac{\epsilon_{\mathbf{p}}}{\varepsilon_{\mathbf{p}}} \right)^{1/2} = \frac{1}{\sqrt{2}} (1 - \cos \theta_{\mathbf{p}})^{1/2} \quad (12.233)$$

form the eigenvector basis of the reduced Hamiltonian matrix,

$$\mathbf{H}_{\text{eff}} = \varepsilon_{\mathbf{p}} \begin{pmatrix} \cos \theta_{\mathbf{p}} & -\sin \theta_{\mathbf{p}} \\ -\sin \theta_{\mathbf{p}} & -\cos \theta_{\mathbf{p}} \end{pmatrix}. \quad (12.234)$$

The eigenvalues of this matrix are ± 1 . Consequently, the eigenvectors are of the form

$$\begin{pmatrix} \sin \theta_{\mathbf{p}} \\ \cos \theta_{\mathbf{p}} \pm 1 \end{pmatrix}. \quad (12.235)$$

The ratio of the coefficients in the eigenvectors is

$$\frac{\sin \theta_{\mathbf{p}}}{(\cos \theta_{\mathbf{p}} \pm 1)} = \pm \left(\tan \frac{\theta_{\mathbf{p}}}{2} \right)^{\pm 1}. \quad (12.236)$$

Because

$$\tan \frac{\theta_{\mathbf{p}}}{2} = \pm \left(\frac{\sqrt{1 - \cos \theta_{\mathbf{p}}}}{\sqrt{1 + \cos \theta_{\mathbf{p}}}} \right), \quad (12.237)$$

the eigenvectors of \mathbf{H}_{eff} can be written as

$$\mathbf{e}_1 = \begin{pmatrix} v_{\mathbf{p}} \\ u_{\mathbf{p}} \end{pmatrix} = \begin{pmatrix} \sin(\theta_{\mathbf{p}}/2) \\ \cos(\theta_{\mathbf{p}}/2) \end{pmatrix} \quad (12.238)$$

and

$$\mathbf{e}_2 = \begin{pmatrix} u_{\mathbf{p}} \\ -v_{\mathbf{p}} \end{pmatrix} = \begin{pmatrix} \cos(\theta_{\mathbf{p}}/2) \\ -\sin(\theta_{\mathbf{p}}/2) \end{pmatrix}. \quad (12.239)$$

It is now clear that $\mathbf{H}_{\text{eff}} \mathbf{e}_1 = -\varepsilon_{\mathbf{p}} \mathbf{e}_1$ and $\mathbf{H}_{\text{eff}} \mathbf{e}_2 = \varepsilon_{\mathbf{p}} \mathbf{e}_2$. Simply put, $\pm \varepsilon_{\mathbf{p}}$ are the two eigenenergies of \mathbf{H}_{eff} . To lay plain the utility of \mathbf{e}_1 and \mathbf{e}_2 , we multiply the equations of motion by \mathbf{e}_1 and \mathbf{e}_2 . The result for \mathbf{e}_2 ,

$$\begin{aligned} i\hbar \frac{\partial}{\partial t} (a_{\mathbf{p}\uparrow} u_{\mathbf{p}} - v_{\mathbf{p}} a_{-\mathbf{p}\downarrow}^{\dagger}) &= \mathbf{e}_2^T \mathbf{H}_{\text{eff}} \begin{pmatrix} a_{\mathbf{p}\uparrow} \\ a_{-\mathbf{p}\downarrow}^{\dagger} \end{pmatrix} \\ &= \varepsilon_{\mathbf{p}} \mathbf{e}_2^T \begin{pmatrix} a_{\mathbf{p}\uparrow} \\ a_{-\mathbf{p}\downarrow}^{\dagger} \end{pmatrix}, \end{aligned} \quad (12.240)$$

demonstrates that

$$i\hbar \dot{\gamma}_{\mathbf{p}\uparrow} = \varepsilon_{\mathbf{p}} \gamma_{\mathbf{p}\uparrow}. \quad (12.241)$$

Similarly, for \mathbf{e}_1 we have that

$$i\hbar \frac{\partial}{\partial t} (v_{\mathbf{p}}^* a_{\mathbf{p}\uparrow} + u_{\mathbf{p}}^* a_{-\mathbf{p}\downarrow}^{\dagger}) = -\varepsilon_{\mathbf{p}} \mathbf{e}_1^{\dagger} \begin{pmatrix} a_{\mathbf{p}\uparrow} \\ a_{-\mathbf{p}\downarrow}^{\dagger} \end{pmatrix} \quad (12.242)$$

and

$$i\hbar \dot{\gamma}_{-\mathbf{p}\downarrow}^{\dagger} = -\varepsilon_{\mathbf{p}} \gamma_{-\mathbf{p}\downarrow}^{\dagger}. \quad (12.243)$$

These equations of motion imply that the diagonalized form for the reduced Hamiltonian is

$$\mathbf{H}_{\text{eff}} = \sum_{\mathbf{p}} \varepsilon_{\mathbf{p}} (\gamma_{\mathbf{p}\uparrow}^{\dagger} \gamma_{\mathbf{p}\uparrow} + \gamma_{-\mathbf{p}\downarrow}^{\dagger} \gamma_{-\mathbf{p}\downarrow}). \quad (12.244)$$

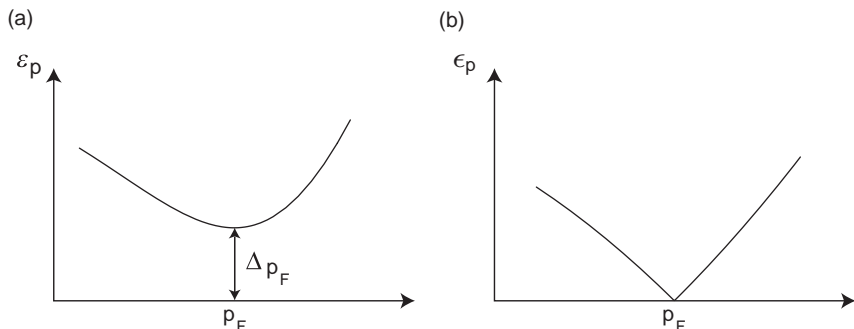


Fig. 12.18 Quasi-particle spectrum in the vicinity of the Fermi surface in the (a) superconducting and (b) normal states. The value of ϵ_p at the Fermi level is chosen to vanish. Consequently, the minimum excitation energy required at the Fermi surface is the gap energy.

Consequently, creating any quasi-particle, regardless of its spin and momentum, costs an energy ϵ_p . To reiterate, the quasi-particles of BCS theory are not electrons. Rather they are spinful entities with no well-defined charge, in contrast to singlet Cooper pairs, which have charge $2e$ but no spin. In this sense, spin-charge separation can be thought to obtain in a BCS superconductor. A plot of the quasi-particle energies is shown in Fig. 12.18. As is evident, adding or subtracting a particle costs at least the minimum energy Δ_p .

12.13 Thermodynamics

We are now in a position to calculate the thermodynamic properties of a superconductor. Of special interest are the heat capacity, C_v , and the Helmholtz free energy, the former of which has a discontinuity between the normal and superconducting states. To calculate these quantities, we need to express our equations of motion in a manner that is amenable to extracting finite temperature information. This is most easily done by rewriting the model Hamiltonian in terms of the quasi-particle operators. To proceed, we invert the quasi-particle operators and solve for the electron operators,

$$a_{\mathbf{p}\uparrow} = u_{\mathbf{p}}^* \gamma_{\mathbf{p}\uparrow} + v_{\mathbf{p}} \gamma_{-\mathbf{p}\downarrow}^\dagger \quad (12.245)$$

and

$$a_{-\mathbf{p}\downarrow} = -v_{\mathbf{p}} \gamma_{\mathbf{p}\uparrow}^\dagger + u_{\mathbf{p}}^* \gamma_{-\mathbf{p}\downarrow}. \quad (12.246)$$

We will show that the thermal average

$$\langle \gamma_{\mathbf{p}\sigma}^\dagger \gamma_{\mathbf{p}\sigma} \rangle = n_{\mathbf{p}\sigma}, \quad (12.247)$$

where $n_{\mathbf{p}\sigma}$ is the Fermi-Dirac distribution function evaluated at the quasi-particle energy, $\epsilon_{\mathbf{p}}$. We will assume that the entropy associated with such quasi-particle excitations is given

by the non-interacting form

$$S = -k_B \sum_{\mathbf{p}, \sigma} [n_{\mathbf{p}\sigma} \ln n_{\mathbf{p}\sigma} + (1 - n_{\mathbf{p}\sigma}) \ln (1 - n_{\mathbf{p}\sigma})] \quad (12.248)$$

presented in Chapter 2. Coupled with Eq. (12.244), the Fermi-Dirac distribution follows necessarily. Nonetheless we will establish the result explicitly.

We evaluate first the Helmholtz free energy, $F = E' - TS$, where $E' = \langle H - \mu N \rangle$. We need to express the internal energy at the mean-field level,

$$E' = \sum_{\mathbf{p}, \sigma} \epsilon_{\mathbf{p}} \langle a_{\mathbf{p}\sigma}^\dagger a_{\mathbf{p}\sigma} \rangle + \sum_{\mathbf{p}, \mathbf{p}'} V_{\mathbf{p}\mathbf{p}'} \langle b_{\mathbf{p}}^\dagger \rangle \langle b_{\mathbf{p}'} \rangle, \quad (12.249)$$

in terms of the $\gamma_{\mathbf{p}}$ s. The thermal average in these expressions is to be interpreted as a trace over all states of the system. An arbitrary excitation above the ground state is represented by

$$|\text{excited state}\rangle = \prod_i \gamma_{\mathbf{p}_i \sigma_i}^\dagger |\Psi_{\text{BCS}}\rangle \quad (12.250)$$

and hence contains a definite number of excited quasi-particles. As a consequence, any average of the form $\langle \gamma \gamma \rangle$ identically vanishes. From Eqs. (12.245) and (12.246), it follows that

$$\begin{aligned} \sum_{\mathbf{p}, \sigma} \langle a_{\mathbf{p}\sigma}^\dagger a_{\mathbf{p}\sigma} \rangle &= \sum_{\mathbf{p}} \langle (u_{\mathbf{p}} \gamma_{\mathbf{p}\uparrow}^\dagger + v_{\mathbf{p}}^* \gamma_{-\mathbf{p}\downarrow})(u_{\mathbf{p}}^* \gamma_{\mathbf{p}\uparrow} + v_{\mathbf{p}} \gamma_{-\mathbf{p}\downarrow}^\dagger) \rangle \\ &\quad + \sum_{\mathbf{p}} \langle (-v_{\mathbf{p}}^* \gamma_{\mathbf{p}\uparrow} + u_{\mathbf{p}} \gamma_{-\mathbf{p}\downarrow}^\dagger)(-v_{\mathbf{p}} \gamma_{\mathbf{p}\uparrow}^\dagger + u_{\mathbf{p}}^* \gamma_{-\mathbf{p}\downarrow}) \rangle \\ &= \sum_{\mathbf{p}} (|u_{\mathbf{p}}|^2 - |v_{\mathbf{p}}|^2) (n_{\mathbf{p}\uparrow} + n_{-\mathbf{p}\downarrow}) + 2 |v_{\mathbf{p}}|^2. \end{aligned} \quad (12.251)$$

In the ground state, we showed previously (see Eq. (12.171)) that $\langle b_{\mathbf{p}} \rangle = u_{\mathbf{p}}^* v_{\mathbf{p}}$. At finite temperature, the average of the pair operator

$$\begin{aligned} \langle b_{\mathbf{p}} \rangle &= \langle a_{-\mathbf{p}\downarrow} a_{\mathbf{p}\uparrow} \rangle = \langle (-v_{\mathbf{p}} \gamma_{\mathbf{p}\uparrow}^\dagger + u_{\mathbf{p}}^* \gamma_{-\mathbf{p}\downarrow})(u_{\mathbf{p}}^* \gamma_{\mathbf{p}\uparrow} + v_{\mathbf{p}} \gamma_{-\mathbf{p}\downarrow}^\dagger) \rangle \\ &= v_{\mathbf{p}} u_{\mathbf{p}}^* (1 - n_{-\mathbf{p}\downarrow} - n_{\mathbf{p}\uparrow}) \end{aligned} \quad (12.252)$$

contains the thermal factors that reflect the pairing of electrons above and below the Fermi level. Consequently,

$$\sum_{\mathbf{p}, \mathbf{p}'} V_{\mathbf{p}\mathbf{p}'} \langle b_{\mathbf{p}}^\dagger \rangle \langle b_{\mathbf{p}'} \rangle = \sum_{\mathbf{p}, \mathbf{p}'} V_{\mathbf{p}\mathbf{p}'} u_{\mathbf{p}} u_{\mathbf{p}'}^* v_{\mathbf{p}}^* v_{\mathbf{p}'} (1 - n_{\mathbf{p}\uparrow} - n_{-\mathbf{p}\downarrow}) (1 - n_{-\mathbf{p}'\downarrow} - n_{\mathbf{p}'\uparrow}), \quad (12.253)$$

and the total Helmholtz energy is

$$\begin{aligned} F' = & \sum_{\mathbf{p}} \epsilon_{\mathbf{p}} \left[\left(|u_{\mathbf{p}}|^2 - |v_{\mathbf{p}}|^2 \right) (n_{\mathbf{p}\uparrow} + n_{-\mathbf{p}\downarrow}) + 2 |v_{\mathbf{p}}|^2 \right] \\ & + \sum_{\mathbf{p}, \mathbf{p}'} V_{\mathbf{p}\mathbf{p}'} (1 - n_{-\mathbf{p}\downarrow} - n_{\mathbf{p}\uparrow}) (1 - n_{-\mathbf{p}'\downarrow} - n_{\mathbf{p}'\uparrow}) u_{\mathbf{p}} v_{\mathbf{p}}^* u_{\mathbf{p}'}^* v_{\mathbf{p}'} \\ & + k_B T \sum_{\mathbf{p}, \sigma} [n_{\mathbf{p}\sigma} \ln n_{\mathbf{p}\sigma} + (1 - n_{\mathbf{p}\sigma}) \ln (1 - n_{\mathbf{p}\sigma})]. \end{aligned} \quad (12.254)$$

Minimizing F' with respect to $u_{\mathbf{p}}$ and $v_{\mathbf{p}}$, we obtain the standard result that $u_{\mathbf{p}} = ((1 + \cos \theta_{\mathbf{p}})/2)^{1/2}$ and $v_{\mathbf{p}} = ((1 - \cos \theta_{\mathbf{p}})/2)^{1/2}$ with $\cos \theta_{\mathbf{p}} = \epsilon_{\mathbf{p}}/\varepsilon_{\mathbf{p}}$. In this case, however, the gap is temperature dependent through

$$\begin{aligned} \Delta_{\mathbf{p}} &= - \sum_{\mathbf{p}'} V_{\mathbf{p}\mathbf{p}'} \langle b_{\mathbf{p}'} \rangle \\ &= - \sum_{\mathbf{p}'} V_{\mathbf{p}\mathbf{p}'} (1 - n_{\mathbf{p}'\uparrow} - n_{-\mathbf{p}'\downarrow}) u_{\mathbf{p}'}^* v_{\mathbf{p}'}, \end{aligned} \quad (12.255)$$

where $\sin \theta_{\mathbf{p}} = \Delta_{\mathbf{p}}/\varepsilon_{\mathbf{p}}$. Varying F' with respect to $n_{\mathbf{p}\uparrow}$, we find that

$$\frac{\partial F'}{\partial n_{\mathbf{p}\uparrow}} = 0 = \epsilon_{\mathbf{p}} \left(|u_{\mathbf{p}}|^2 - |v_{\mathbf{p}}|^2 \right) + k_B T \ln \left(\frac{n_{\mathbf{p}\uparrow}}{1 - n_{\mathbf{p}\uparrow}} \right) + 2 \Delta_{\mathbf{p}} u_{\mathbf{p}} v_{\mathbf{p}}^*, \quad (12.256)$$

holding the coherence factors $u_{\mathbf{p}}$ and $v_{\mathbf{p}}$ fixed. The condition that is now imposed on $n_{\mathbf{p}\uparrow}$, namely

$$\begin{aligned} k_B T \ln \left(n_{\mathbf{p}\uparrow}^{-1} - 1 \right) &= \epsilon_{\mathbf{p}} \cos \theta_{\mathbf{p}} + 2 \Delta_{\mathbf{p}} u_{\mathbf{p}} v_{\mathbf{p}}^* \\ &= \epsilon_{\mathbf{p}} \cos \theta_{\mathbf{p}} + \Delta_{\mathbf{p}} \sin \theta_{\mathbf{p}} \\ &= \varepsilon_{\mathbf{p}}, \end{aligned} \quad (12.257)$$

is simply the requirement that $n_{\mathbf{p}\uparrow}$ is the Fermi–Dirac distribution evaluated at the quasi-energy $\varepsilon_{\mathbf{p}}$. The Fermi–Dirac distribution is the most likely distribution of the quasi-particle excitations at finite temperature.

The free-energy calculation is now straightforward if we use the mean-field value of the gap, Eq. (12.255):

$$\begin{aligned} E' &= \sum_{\mathbf{p}} \epsilon_{\mathbf{p}} \left[\left(|u_{\mathbf{p}}|^2 - |v_{\mathbf{p}}|^2 \right) (n_{\mathbf{p}\uparrow} + n_{\mathbf{p}\downarrow}) + 2 |v_{\mathbf{p}}|^2 \right] - \sum_{\mathbf{p}} \Delta_{\mathbf{p}} \frac{\sin \theta_{\mathbf{p}}}{2} (1 - 2n_{\mathbf{p}}) \\ &= \sum_{\mathbf{p}} \left[2\epsilon_{\mathbf{p}} \left(\cos \theta_{\mathbf{p}} n_{\mathbf{p}} + \sin^2 \frac{\theta_{\mathbf{p}}}{2} \right) - \Delta_{\mathbf{p}} \frac{\sin \theta_{\mathbf{p}}}{2} (1 - 2n_{\mathbf{p}}) \right]. \end{aligned} \quad (12.258)$$

Coupled with the fact that $\ln(1/n_{\mathbf{p}\sigma} - 1) = \varepsilon_{\mathbf{p}}/k_B T$, we simplify the entropy term to

$$TS = -2k_B T \sum_{\mathbf{p}} [\beta \varepsilon_{\mathbf{p}} n_{\mathbf{p}} + \ln(1 + e^{-\beta \varepsilon_{\mathbf{p}}})]. \quad (12.259)$$

The total free energy is then

$$\begin{aligned} F' = \sum_{\mathbf{p}} & \left[2\epsilon_{\mathbf{p}} \left(\cos \theta_{\mathbf{p}} n_{\mathbf{p}} + \sin^2 \frac{\theta_{\mathbf{p}}}{2} \right) - \Delta_{\mathbf{p}} \frac{\sin \theta_{\mathbf{p}}}{2} (1 - 2n_{\mathbf{p}}) \right] \\ & + 2k_B T \sum_{\mathbf{p}} [\beta \epsilon_{\mathbf{p}} n_{\mathbf{p}} + \ln(1 + e^{-\beta \epsilon_{\mathbf{p}}})]. \end{aligned} \quad (12.260)$$

The evaluation of this expression is left as a homework problem (see Problem 12.10).

The heat capacity,

$$\begin{aligned} C_v &= T \left(\frac{\partial S}{\partial T} \right)_V \\ &= -k_B T \sum_{\mathbf{p}, \sigma} \frac{\partial n_{\mathbf{p}\sigma}}{\partial T} \ln \left(\frac{n_{\mathbf{p}\sigma}}{1 - n_{\mathbf{p}\sigma}} \right) \\ &= \sum_{\mathbf{p}, \sigma} \epsilon_{\mathbf{p}} \frac{\partial n_{\mathbf{p}\sigma}}{\partial T}, \end{aligned} \quad (12.261)$$

contains the temperature derivative

$$\frac{\partial n_{\mathbf{p}}}{\partial T} = \frac{n_{\mathbf{p}}^2}{k_B T} \left[\frac{\epsilon_{\mathbf{p}}}{T} - \frac{\partial \epsilon_{\mathbf{p}}}{\partial T} \right] e^{\beta \epsilon_{\mathbf{p}}}, \quad (12.262)$$

which is compounded by the implicit temperature dependence of the gap, $\Delta_{\mathbf{p}}$. From the definition of $\epsilon_{\mathbf{p}}$, it follows that

$$\frac{\partial \epsilon_{\mathbf{p}}}{\partial T} = \frac{\partial \epsilon_{\mathbf{p}}}{\partial \Delta_{\mathbf{p}}} \frac{\partial \Delta_{\mathbf{p}}}{\partial T} = \frac{\Delta_{\mathbf{p}}}{\epsilon_{\mathbf{p}}} \frac{\partial \Delta_{\mathbf{p}}}{\partial T} = \frac{1}{2\epsilon_{\mathbf{p}}} \frac{\partial \Delta_{\mathbf{p}}^2}{\partial T}. \quad (12.263)$$

Because $\partial \epsilon_{\mathbf{p}}/\partial T$ vanishes in the normal state, we write the difference between the heat capacity in the superconducting and normal states at T_c as

$$\begin{aligned} (C_v^S - C_v^N)_{T=T_c} &= -\beta \sum_{\mathbf{p}} n_{\mathbf{p}}^2 \frac{\partial \Delta_{\mathbf{p}}^2}{\partial T} e^{\beta \epsilon_{\mathbf{p}}} \\ &= \sum_{\mathbf{p}} \frac{\partial n_{\mathbf{p}}}{\partial \epsilon_{\mathbf{p}}} \frac{\partial \Delta_{\mathbf{p}}^2}{\partial T} \Big|_{T=T_c}. \end{aligned} \quad (12.264)$$

In the vicinity of $T = T_c$, the gap is well-approximated by $\Delta^2 \sim |1 - T/T_c|$. We find then that $\partial \Delta^2/\partial T \sim 1/T_c$, and the discontinuity in the heat capacity is identically

$$C_v^S - C_v^N = \frac{N(\epsilon_F)}{T_c} \quad (12.265)$$

at $T = T_c$. The positive sign associated with this difference indicates that the heat capacity in the superconducting state just below T_c exceeds C_v^N .

The second result we seek is the exponential fall-off of C_v^S just below T_c . To obtain this behavior, we analyze Eq. (12.261) in the limit that $T \rightarrow 0$. In this limit, $\partial \Delta_{\mathbf{p}}^2/\partial T \rightarrow 0$,

$n_{\mathbf{p}} \rightarrow e^{-\beta \varepsilon_{\mathbf{p}}}$, and the heat capacity is dominated by

$$\begin{aligned} \lim_{T \rightarrow 0} C_v &= 2\beta^2 k_B \sum_{\mathbf{p}} \varepsilon_{\mathbf{p}}^2 n_{\mathbf{p}} (1 - n_{\mathbf{p}}) \\ &\simeq 2\beta^2 k_B N(\epsilon_F) \Delta^2(T=0) \int_0^\infty d\epsilon e^{-\beta \sqrt{\Delta^2(T=0) + \epsilon^2}} \\ &\simeq 2\beta^2 k_B N(\epsilon_F) \Delta_0^2 e^{-\beta \Delta_0} \int_0^\infty d\epsilon e^{-\beta \epsilon^2 / 2\Delta_0} \\ &= N(\epsilon_F) \sqrt{\frac{\pi}{2}} k_B \beta^{3/2} \Delta_0^{5/2} e^{-\beta \Delta_0}, \end{aligned} \quad (12.266)$$

which decays exponentially as advertised with $\Delta_0 = \Delta(T=0)$. The exponential fall-off is dominated by the gap at $T=0$. In simplifying the integrals leading to this result, we used the fact that the integrals are largest when $\Delta \gg \epsilon$.

12.14 Experimental applications

One of the key successes of the BCS theory is the ease with which physical observables, such as the phonon attenuation rate, can be calculated. In fact, it was the calculation of the spin-lattice relaxation time using the BCS theory and its subsequent experimental confirmation that led to the wide acceptance of BCS theory. In this section, we perform three of these calculations explicitly: (1) electromagnetic absorption, (2) ultrasonic attenuation, and (3) the spin-lattice relaxation rate. Appearing in each of these calculations are particular combinations of the coherence factors, $u_{\mathbf{p}}$ and $v_{\mathbf{p}}$. We will see that each combination of the coherence factors can generate completely different physics. That the physical properties are so intimately connected with the coherence factors is a hallmark of the BCS pairing hypothesis. In each of these calculations, we will treat the coherence factors as being real. As we have seen, for the simple model potential we have chosen, Eq. (12.41), the coherence factors are in fact real.

12.14.1 Electromagnetic absorption

In a BCS superconductor, absorption of electromagnetic radiation is suppressed for frequencies less than Δ/\hbar . We have now the machinery to derive this result explicitly. In the electromagnetic problem, the perturbation term is obtained by replacing the momentum with $\mathbf{p} - e\mathbf{A}(\mathbf{r}, t)/c$, where $\mathbf{A}(\mathbf{r}, t)$ is the vector potential. To lowest order in $\mathbf{A}(\mathbf{r}, t)$, the perturbation is of the form, $\mathbf{p} \cdot \mathbf{A} + \mathbf{A} \cdot \mathbf{p}$. We will require that the vector potential satisfy the transversality condition, $\nabla \cdot \mathbf{A} = 0$. As a consequence, the second-quantized form of the perturbation for absorption of an electromagnetic wave with frequency $\omega_{\mathbf{q}}$ is

$$H_{\text{abs}} = -\frac{e}{mcV} \sum_{\mathbf{p}, \sigma} \mathbf{A} \cdot \mathbf{p} a_{\mathbf{p}+\mathbf{q}\sigma}^\dagger a_{\mathbf{p}\sigma}. \quad (12.267)$$

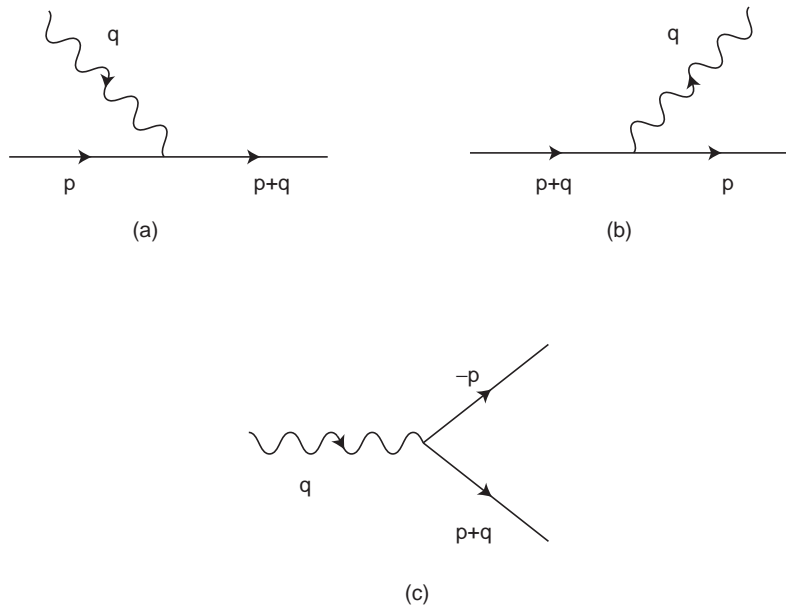


Fig. 12.19 Quasi-particle excitations arising from the matrix element for electromagnetic absorption: (a) $\gamma_{\mathbf{p}+\mathbf{q}}^\dagger \gamma_{\mathbf{p}}$, (b) $\gamma_{\mathbf{p}}^\dagger \gamma_{\mathbf{p}+\mathbf{q}}$, and (c) $\gamma_{\mathbf{p}+\mathbf{q}}^\dagger \gamma_{-\mathbf{p}}^\dagger$. The wavy line represents the photon interaction.

We must compute a matrix element of the form

$$\langle f | H_{\text{abs}} | i \rangle = -\frac{e}{Vmc} \sum_{\mathbf{p}\sigma} \mathbf{A} \cdot \mathbf{p} M_{\text{if}}^\sigma, \quad (12.268)$$

where

$$M_{\text{if}}^\sigma = \langle f | a_{\mathbf{p}+\mathbf{q}\sigma}^\dagger a_{\mathbf{p}\sigma} | i \rangle \quad (12.269)$$

and $|i\rangle$ and $|f\rangle$ are the initial and final quasi-particle states, respectively. As in the calculation of the heat capacity, we rewrite this matrix element,

$$\begin{aligned} \sum_\sigma M_{\text{if}}^\sigma &= \langle f | (u_{\mathbf{p}'} \gamma_{\mathbf{p}'\uparrow}^\dagger + v_{\mathbf{p}'} \gamma_{-\mathbf{p}'\downarrow}) (u_{\mathbf{p}} \gamma_{\mathbf{p}\uparrow} + v_{\mathbf{p}} \gamma_{-\mathbf{p}\downarrow}^\dagger) | i \rangle \\ &\quad + \langle f | (-v_{-\mathbf{p}'} \gamma_{-\mathbf{p}'\uparrow} + u_{-\mathbf{p}'} \gamma_{\mathbf{p}'\downarrow}^\dagger) (-v_{-\mathbf{p}} \gamma_{-\mathbf{p}\uparrow}^\dagger + u_{-\mathbf{p}} \gamma_{\mathbf{p}\downarrow}) | i \rangle, \end{aligned}$$

in terms of the quasi-particle operators. There are a number of distinct kinds of quasi-particle excitations that arise from the terms above. These are illustrated in Fig. 12.19.

At $T = 0$, there are no quasi-particles in the ground state. Hence, only the last process shown in Fig. 12.19, which creates two quasi-particles, survives at $T = 0$. We will specialize to $T = 0$, as in this case the essential physics is easily unearthed. We find that

$$M_{\text{if}}^\uparrow + M_{\text{if}}^\downarrow = u_{\mathbf{p}+\mathbf{q}} v_{\mathbf{p}} \langle f | \gamma_{\mathbf{p}+\mathbf{q}}^\dagger \gamma_{-\mathbf{p}\downarrow}^\dagger | i \rangle - u_{-(\mathbf{p}+\mathbf{q})} v_{-\mathbf{p}} \langle f | \gamma_{\mathbf{p}+\mathbf{q}\downarrow}^\dagger \gamma_{-\mathbf{p}\uparrow}^\dagger | i \rangle \quad (12.270)$$

and

$$\langle f | H_{\text{abs}} | i \rangle = -\frac{e}{mcV} \sum_{\mathbf{p}} (\mathbf{A} \cdot \mathbf{p}) \langle f | u_{\mathbf{p}+\mathbf{q}} v_{\mathbf{p}} \gamma_{\mathbf{p}+\mathbf{q}\uparrow}^{\dagger} \gamma_{-\mathbf{p}\downarrow}^{\dagger} - u_{-(\mathbf{p}+\mathbf{q})} v_{\mathbf{p}} \gamma_{\mathbf{p}+\mathbf{q}\downarrow}^{\dagger} \gamma_{-\mathbf{p}\uparrow}^{\dagger} | i \rangle. \quad (12.271)$$

To simplify this expression, we note that if we shift the momentum in the second term by $\mathbf{p} \rightarrow -(\mathbf{p} + \mathbf{q})$, then $\mathbf{p} \cdot \mathbf{A} \rightarrow -\mathbf{A} \cdot (\mathbf{p} + \mathbf{q}) = -\mathbf{A} \cdot \mathbf{p}$. The last equality follows because the vector potential is transverse to the electromagnetic field. We find that

$$\langle f | H_{\text{abs}} | i \rangle = -\frac{e}{mcV} \sum_{\mathbf{p}} (\mathbf{A} \cdot \mathbf{p}) (u_{\mathbf{p}+\mathbf{q}} v_{\mathbf{p}} - u_{\mathbf{p}} v_{\mathbf{p}+\mathbf{q}}) \langle f | \gamma_{\mathbf{p}+\mathbf{q}\uparrow}^{\dagger} \gamma_{-\mathbf{p}\downarrow}^{\dagger} | i \rangle. \quad (12.272)$$

In the matrix element in Eq. (12.272), we write the final state as $|f\rangle = |\mathbf{p}' \uparrow, \mathbf{p}'' \downarrow\rangle$.

The quasi-particle matrix element reduces to

$$\langle f | \gamma_{\mathbf{p}+\mathbf{q}\uparrow}^{\dagger} \gamma_{-\mathbf{p}\downarrow}^{\dagger} | i \rangle = \delta_{\mathbf{p}'', -\mathbf{p}} \delta_{\mathbf{p}', \mathbf{p}+\mathbf{q}}. \quad (12.273)$$

The total absorption rate per unit volume,

$$\Gamma_s = \frac{2\pi}{\hbar} \left(\frac{e}{mcV} \right)^2 \sum_{\mathbf{p}, \mathbf{p}'} (\mathbf{A} \cdot \mathbf{p})^2 \delta_{\mathbf{p}+\mathbf{p}', \mathbf{q}} (u_{\mathbf{p}'} v_{\mathbf{p}} - u_{\mathbf{p}} v_{\mathbf{p}'})^2 \delta(\varepsilon_{\mathbf{p}} + \varepsilon_{\mathbf{p}'} - \hbar\omega_{\mathbf{q}}), \quad (12.274)$$

involves the coherence factors

$$\begin{aligned} (u_{\mathbf{p}'} v_{\mathbf{p}} - u_{\mathbf{p}} v_{\mathbf{p}'})^2 &= \left[\sqrt{\frac{\varepsilon_{\mathbf{p}'} + \varepsilon_{\mathbf{p}'}}{2\varepsilon_{\mathbf{p}'}}} \sqrt{\frac{\varepsilon_{\mathbf{p}} - \varepsilon_{\mathbf{p}'}}{2\varepsilon_{\mathbf{p}}}} - \sqrt{\frac{\varepsilon_{\mathbf{p}'} - \varepsilon_{\mathbf{p}'}}{2\varepsilon_{\mathbf{p}'}}} \sqrt{\frac{\varepsilon_{\mathbf{p}} + \varepsilon_{\mathbf{p}'}}{2\varepsilon_{\mathbf{p}}}} \right]^2 \\ &= \frac{1}{2\varepsilon_{\mathbf{p}}\varepsilon_{\mathbf{p}'}} (\varepsilon_{\mathbf{p}}\varepsilon_{\mathbf{p}'} - \varepsilon_{\mathbf{p}}\varepsilon_{\mathbf{p}'} - \Delta^2). \end{aligned} \quad (12.275)$$

We convert the sums to integrals,

$$\frac{1}{V} \sum_{\mathbf{p}} \rightarrow N(\epsilon_F) \int d\epsilon_{\mathbf{p}} \int \frac{d\Omega_{\mathbf{p}}}{4\pi}, \quad (12.276)$$

where $d\Omega_{\mathbf{p}}$ represents an integral over the solid angle. The absorption rate is now

$$\begin{aligned} \Gamma_s &= N(\epsilon_F)^2 \frac{2\pi}{\hbar} \int d\epsilon d\epsilon' \delta(\varepsilon + \varepsilon' - \hbar\omega_{\mathbf{q}}) \frac{\varepsilon\varepsilon' - \epsilon\epsilon' - \Delta^2}{2\varepsilon\varepsilon'} \\ &\times \int \frac{d\Omega}{4\pi} \frac{d\Omega'}{4\pi} \delta(\mathbf{p} + \mathbf{p}' - \mathbf{q}) \left(\frac{e}{mc} \mathbf{p} \cdot \mathbf{A} \right)^2. \end{aligned} \quad (12.277)$$

We note first that symmetry about the Fermi surface dictates that we must obtain the same result under the transformation $\epsilon \leftrightarrow -\epsilon$. As a consequence, the $\epsilon\epsilon'$ terms vanish. If we are interested primarily in the contribution from the vicinity of the Fermi surface, then we can set $|\mathbf{p}| = |\mathbf{p}'| = p_F$. The angular terms are trivial and yield $(p_F A e)^2 / 3(mc)^2$. The remaining integration,

$$\Gamma_s = N(\epsilon_F)^2 \frac{8\pi}{3\hbar} \left(\frac{p_F A e}{mc} \right)^2 \int_0^\infty d\epsilon \int_0^\infty d\epsilon' \delta(\varepsilon + \varepsilon' - \hbar\omega_{\mathbf{q}}) \frac{\varepsilon\varepsilon' - \Delta^2}{2\varepsilon\varepsilon'}, \quad (12.278)$$

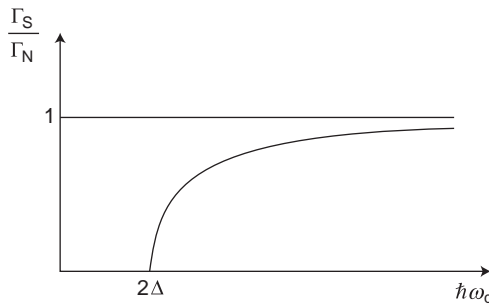


Fig. 12.20 The ratio of the electromagnetic absorption in the superconducting state to that in the normal state. The x -axis is the frequency and Δ is the gap energy.

is over the free particle energies. The factor of 4 arises from the conversion of the lower limit of integration from $-\infty$ to zero. Because $\Gamma_s > 0$, the integral must be positive for all ε and ε' . We see immediately that $\varepsilon\varepsilon' > \Delta^2$ or, equivalently, that $\hbar\omega_q > 2\Delta$. Thus, Γ_s must vanish for $\hbar\omega_q < 2\Delta$. This is the principal result of this section.

We can obtain a more quantitative prediction by changing variables and noting that because $\varepsilon = (\epsilon^2 + \Delta^2)^{1/2}$, $\varepsilon d\varepsilon = \epsilon d\epsilon$. This variable change introduces a lower limit cut-off

$$\Gamma_s = \text{const.} \int_{\Delta}^{\infty} d\varepsilon \int_{\Delta}^{\infty} d\varepsilon' \delta(\varepsilon + \varepsilon' - \hbar\omega_q) \frac{(\varepsilon\varepsilon' - \Delta^2)}{(\varepsilon'^2 - \Delta^2)^{1/2} (\varepsilon^2 - \Delta^2)^{1/2}} \quad (12.279)$$

on the range of integration on ε and ε' . The δ -function constraint, $\varepsilon' - \hbar\omega_q = -\varepsilon$, allows us to rewrite the ε -integral as

$$\Gamma_s = \text{const.} \int_{\Delta}^{\hbar\omega_q - \Delta} d\varepsilon \frac{\varepsilon (\hbar\omega_q - \varepsilon) - \Delta^2}{(\varepsilon^2 - \Delta^2)^{1/2} ((\hbar\omega_q - \varepsilon)^2 - \Delta^2)^{1/2}}, \quad (12.280)$$

where we approximated the upper limit by the lower bound $\hbar\omega_q - \Delta$. When $\Delta = 0$, the integrand reduces to a constant and $\Gamma_s \rightarrow \text{const.} \hbar\omega_q$. If we refer to the $\Delta = 0$ value of Γ_s as Γ_N and plot Γ_s/Γ_N , we obtain the result shown in Fig. 12.20. The form we have derived here for Γ_s agrees well with experiment.

12.14.2 Ultrasonic attenuation

Consider now the problem of a beam of phonons impinging on a superconductor. We have advertised that a superconductor should be transparent to phonon absorption unless the

energy of the impinging phonon beam exceeds 2Δ . To show this, we rewrite the electron–phonon Hamiltonian, Eq. (12.23), in terms of the quasi-particle operators,

$$H_{e-ph} = \sum' M_q (b_q + b_{-q}^\dagger) \left[(u_{p+q} \gamma_{p+q\uparrow}^\dagger + v_{p+q} \gamma_{-(p+q)\downarrow}) (u_p \gamma_{p\uparrow} + v_p \gamma_{-p\downarrow}^\dagger) \right. \\ \left. + (u_{-(p+q)} \gamma_{p+q\downarrow}^\dagger - v_{-(p+q)} \gamma_{-(p+q)\uparrow}) (u_{-p} \gamma_{p\downarrow} - v_{-p} \gamma_{-p\uparrow}^\dagger) \right], \quad (12.281)$$

using Eqs. (12.245) and (12.246). There are two distinct kinds of term that arise from the quasi-particle–phonon coupling: (1) single quasi-particle excitations and (2) quasi-particle pair creation and annihilation. The single-quasi-particle creation and annihilation processes,

$$H_{e-ph}^{qp} = \sum' M_q (b_q + b_{-q}^\dagger) \left[u_{p+q} u_p \gamma_{p+q\uparrow}^\dagger \gamma_{p\uparrow} + v_{p+q} v_p \gamma_{-(p+q)\downarrow} \gamma_{-p\downarrow}^\dagger \right. \\ \left. + u_{-(p+q)} u_{-p} \gamma_{p+q\downarrow}^\dagger \gamma_{p\downarrow} + v_{-(p+q)} v_{-p} \gamma_{-(p+q)\uparrow} \gamma_{-p\uparrow}^\dagger \right], \quad (12.282)$$

arise from a conjugate $\gamma_p, \gamma_{p'}^\dagger$ pair. The additional scattering channel,

$$H_{e-ph}^{\text{pair}} = \sum' M_q (b_q + b_{-q}^\dagger) \left[u_{p+q} v_p \gamma_{p+q\uparrow}^\dagger \gamma_{-p\downarrow}^\dagger - u_{-(p+q)} v_{-p} \gamma_{p+q\downarrow}^\dagger \gamma_{-p\uparrow}^\dagger \right. \\ \left. + v_{p+q} u_p \gamma_{-(p+q)\downarrow} \gamma_{p\uparrow} - v_{-(p+q)} u_{-p} \gamma_{-(p+q)\uparrow} \gamma_{p\downarrow} \right], \quad (12.283)$$

is mediated by quasi-particle pair creation and annihilation.

Both types of process are expected to occur when phonons are excited in a superconductor. However, as in the electromagnetic absorption problem, pair creation and annihilation is expected only when $\hbar\omega_q > 2\Delta$. Because our goal is to show that absorption of phonons is attenuated at frequencies less than 2Δ , we can ignore the pair scattering terms. We specialize then to the $\hbar\omega_q < \Delta$ case in which only single-particle scattering contributes to the transition amplitude. The two representative classes of emission and absorption terms are shown in Figs. 12.21(a) and 12.21(b). Each term contributes identically for \downarrow and \uparrow electron states. First, consider emission. The operator describing emission of a phonon in a single quasi-particle exchange is

$$V_{\text{emiss}}^{qp} = M_q b_{-q}^\dagger \left(u_{p+q} u_p \gamma_{p+q\sigma}^\dagger \gamma_{p\sigma} + v_{-(p+q)} v_{-p} \gamma_{p\sigma} \gamma_{p+q\sigma}^\dagger \right), \quad (12.284)$$

where we have set $-p \rightarrow p$ and $-p - q \rightarrow p$ in the second term in Eq. (12.282). From the anticommutation relation for the γ s, we can rewrite the emission term as

$$V_{\text{emiss}}^{qp} = M_q b_{-q}^\dagger \left[(u_{p+q} u_p - v_{-(p+q)} v_{-p}) \gamma_{p+q\sigma}^\dagger \gamma_{p\sigma} + v_{-(p+q)} v_{-p} \delta_{p,p+q} \right]. \quad (12.285)$$

The last term requires that $p = p + q$ or, equivalently, $q = 0$. However, M_q is linear in q and hence vanishes when $q = 0$. In the emission process, the final composite electron–phonon state must contain the phonon with momentum q and the quasi-particle with momentum $p + q$ and spin σ . The quasi-particle with momentum p is absent from this state. The initial

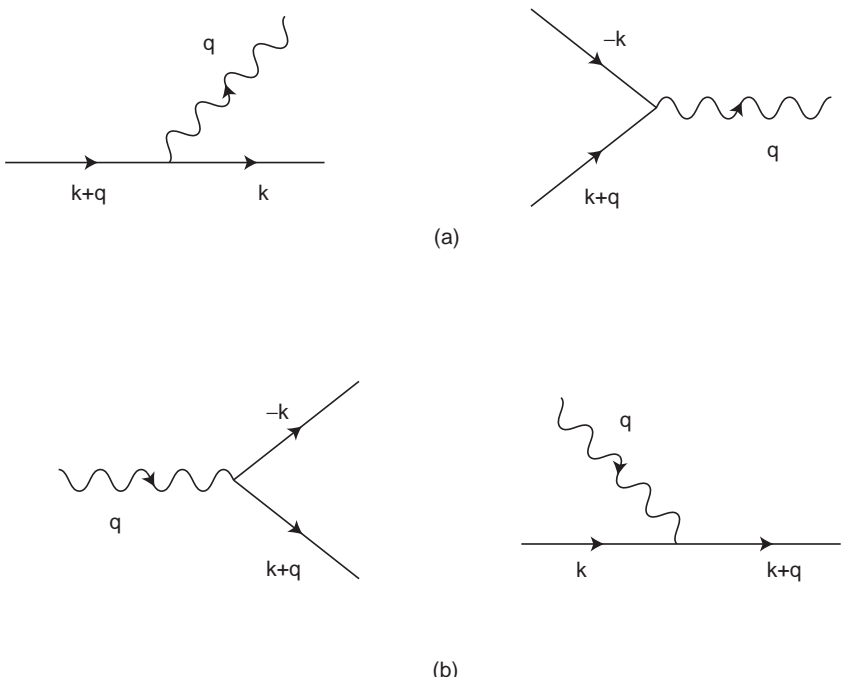


Fig. 12.21 (a) Emission and (b) absorption processes contributing to the ultrasonic attenuation. The wavy line represents the quasi-particle–phonon interaction.

state is in general some determinantal state containing any number of quasi-particles, but in particular the quasi-particle with momentum \mathbf{p} and spin σ . Let $|\mathbf{p} + \mathbf{q}\sigma, \mathbf{q}\rangle$ and $|\mathbf{p}\sigma\rangle$ be the final and initial states, respectively. The emission matrix element simplifies to

$$\langle \mathbf{p} + \mathbf{q}\sigma, \mathbf{q} | V_{\text{emiss}}^{\text{qp}} | \mathbf{p}\sigma \rangle = M_{\mathbf{q}} (u_{\mathbf{p}+\mathbf{q}} u_{\mathbf{p}} - v_{-(\mathbf{p}+\mathbf{q})} v_{-\mathbf{p}}) \sqrt{N_{\mathbf{q}} + 1} \sqrt{n_{\mathbf{p}} (1 - n_{\mathbf{p}+\mathbf{q}})}, \quad (12.286)$$

where $n_{\mathbf{p}}$ is the occupation of quasi-particles in momentum state \mathbf{p} . Consequently, when both \uparrow and \downarrow spins are included, the Fermi golden rule rate for emission is

$$\begin{aligned} \Gamma_{\text{emiss}}^{\text{qp}} &= \frac{2}{\hbar} \sum_{\mathbf{p}} (N_{\mathbf{q}} + 1) |M_{\mathbf{q}}|^2 (u_{\mathbf{p}+\mathbf{q}} u_{\mathbf{p}} - v_{\mathbf{p}+\mathbf{q}} v_{\mathbf{p}})^2 \\ &\times n_{\mathbf{p}} (1 - n_{\mathbf{p}+\mathbf{q}}) 2\pi \delta (\hbar\omega_{\mathbf{q}} + \varepsilon_{\mathbf{p}} - \varepsilon_{\mathbf{p}+\mathbf{q}}). \end{aligned} \quad (12.287)$$

Analogous arguments can be applied to absorption of a phonon. There are two principal differences in the form of the transition rate. First, the factors of $N_{\mathbf{q}} + 1$ are replaced by $N_{\mathbf{q}}$. This change arises because, in the case of absorption, the final state has one fewer phonon. Second, the initial state and final states are of the form $|\mathbf{p} + \mathbf{q}\sigma\rangle$ and $|\mathbf{p}\sigma, \mathbf{q}\rangle$, respectively. The rate of absorption between all such initial and final states,

$$\Gamma_{\text{abs}}^{\text{qp}} = \frac{2}{\hbar} \sum_{\mathbf{p}} N_{\mathbf{q}} |M_{\mathbf{q}}| (u_{\mathbf{p}+\mathbf{q}} u_{\mathbf{p}} - v_{\mathbf{p}+\mathbf{q}} v_{\mathbf{p}})^2 n_{\mathbf{p}+\mathbf{q}} (1 - n_{\mathbf{p}}) 2\pi \delta (\hbar\omega_{\mathbf{q}} + \varepsilon_{\mathbf{p}} - \varepsilon_{\mathbf{p}+\mathbf{q}}), \quad (12.288)$$

is a sum of the individual rates, which we treat at the level of the Fermi golden rule.

The difference between the emission and absorption rates,

$$\begin{aligned}\Gamma_{\mathbf{q}} &= \Gamma_{\text{abs}}^{\text{qp}} - \Gamma_{\text{emiss}}^{\text{qp}} \\ &= \frac{2}{\hbar} \sum'_{\mathbf{p}} |M_{\mathbf{q}}|^2 (u_{\mathbf{p}+\mathbf{q}} u_{\mathbf{p}} - v_{\mathbf{p}+\mathbf{q}} v_{\mathbf{p}})^2 2\pi \delta(\hbar\omega_{\mathbf{q}} + \varepsilon_{\mathbf{p}} - \varepsilon_{\mathbf{p}+\mathbf{q}}) \\ &\quad \times [N_{\mathbf{q}} (n_{\mathbf{p}+\mathbf{q}} - n_{\mathbf{p}}) - n_{\mathbf{p}} (1 - n_{\mathbf{p}+\mathbf{q}})],\end{aligned}\quad (12.289)$$

contains a part which depends on the phonon occupation (through $N_{\mathbf{q}}$) and a term that does not. In combining the absorption and emission terms, we used the time-reversal invariance of the coherence factors. The part independent of the phonon occupation defines the effective spontaneous emission rate, whereas the first term defines the total rate at which $N_{\mathbf{q}}$ phonons are absorbed. We define then

$$\begin{aligned}\frac{dN_{\mathbf{q}}}{dt} &= -\frac{2}{\hbar} \sum_{\mathbf{p}} |M_{\mathbf{q}}|^2 (u_{\mathbf{p}+\mathbf{q}} u_{\mathbf{p}} - v_{\mathbf{p}+\mathbf{q}} v_{\mathbf{p}})^2 2\pi \delta(\hbar\omega_{\mathbf{q}} + \varepsilon_{\mathbf{p}} - \varepsilon_{\mathbf{p}+\mathbf{q}}) N_{\mathbf{q}} (n_{\mathbf{p}+\mathbf{q}} - n_{\mathbf{p}}) \\ &= -\alpha_{\mathbf{q}} N_{\mathbf{q}}\end{aligned}\quad (12.290)$$

as the net acoustic attenuation rate.

To evaluate $\alpha_{\mathbf{q}}$, we convert the sum to an integral

$$\begin{aligned}\alpha_{\mathbf{q}} &= \frac{4\pi}{\hbar} |M_{\mathbf{q}}|^2 g^2(0) \int d\epsilon_{\mathbf{p}} d\epsilon_{\mathbf{p}'} (u_{\mathbf{p}} u_{\mathbf{p}'} - v_{\mathbf{p}} v_{\mathbf{p}'}) (n_{\mathbf{p}'} - n_{\mathbf{p}}) \\ &\quad \times \delta(\hbar\omega_{\mathbf{q}} + \varepsilon_{\mathbf{p}} - \varepsilon_{\mathbf{p}'}) \int \frac{d\Omega_{\mathbf{p}}}{4\pi} \frac{d\Omega_{\mathbf{p}'}}{4\pi} \delta(\mathbf{p} - \mathbf{p}' - \mathbf{q})\end{aligned}\quad (12.291)$$

in which momentum conservation is ensured by the angular factor $\delta(\mathbf{p} - \mathbf{p}' - \mathbf{q})$. To simplify Eq. (12.291), we note that the angular factors are identical in the normal and superconducting states. Because the gap is assumed to be isotropic, we can separate out the angular dependence. Let us call this factor A_{Ω} . We need now an expression for the coherence factors:

$$(u_{\mathbf{p}} u_{\mathbf{p}'} - v_{\mathbf{p}} v_{\mathbf{p}'})^2 = \frac{1}{2\varepsilon_{\mathbf{p}} \varepsilon_{\mathbf{p}'}} [\varepsilon_{\mathbf{p}} \varepsilon_{\mathbf{p}'} + \epsilon_{\mathbf{p}} \epsilon_{\mathbf{p}'} - \Delta^2], \quad (12.292)$$

where we have assumed that the gap is a constant, $\Delta = \Delta_{\mathbf{p}} = \Delta_{\mathbf{p}'}$. We note that $n_{\mathbf{p}}$ and $\varepsilon_{\mathbf{p}}$ are both even in $\epsilon_{\mathbf{p}}$. Hence, integration over the linear $\epsilon_{\mathbf{p}} \epsilon_{\mathbf{p}'}$ factors vanishes because the limits are even. As a further simplification, we change the variable of integration from $\epsilon_{\mathbf{p}}$ to $\varepsilon_{\mathbf{p}}$ by noting that $d\varepsilon_{\mathbf{p}}/d\epsilon_{\mathbf{p}} = \varepsilon_{\mathbf{p}}/\epsilon_{\mathbf{p}}$. We are left with

$$\begin{aligned}\alpha_{\mathbf{q}} &= \frac{8\pi}{\hbar} |M_{\mathbf{q}}|^2 g^2(0) A_{\Omega} \int_{\Delta}^{\infty} d\varepsilon_{\mathbf{p}} \int_{\Delta}^{\infty} d\varepsilon_{\mathbf{p}'} \frac{\varepsilon_{\mathbf{p}} \varepsilon_{\mathbf{p}'}}{\epsilon_{\mathbf{p}} \epsilon_{\mathbf{p}'}} \left(1 - \frac{\Delta^2}{\varepsilon_{\mathbf{p}} \varepsilon_{\mathbf{p}'}}\right) \\ &\quad \times (n_{\mathbf{p}'} - n_{\mathbf{p}}) \delta(\hbar\omega_{\mathbf{q}} + \varepsilon_{\mathbf{p}} - \varepsilon_{\mathbf{p}'})\end{aligned}\quad (12.293)$$

The quantity $N(0)d\epsilon_{\mathbf{p}}/d\varepsilon_{\mathbf{p}} = N(0)\varepsilon_{\mathbf{p}}/\epsilon_{\mathbf{p}}$ is roughly the density of quasi-particle excitations. At the Fermi surface, $\epsilon_{\mathbf{p}} \rightarrow 0$ and $d\epsilon_{\mathbf{p}}/d\varepsilon_{\mathbf{p}} \rightarrow \infty$. However, over the range of

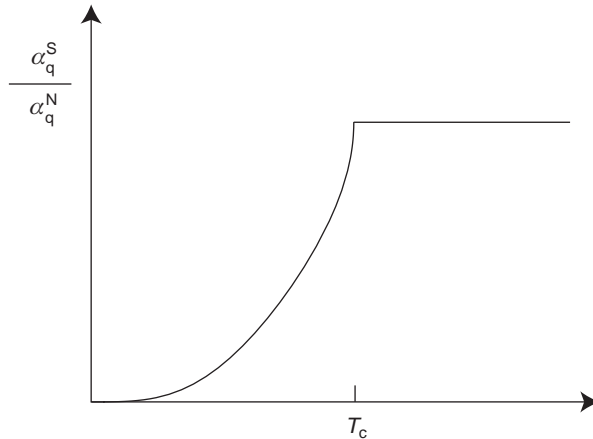


Fig. 12.22 Ratio of the ultrasound attenuation in the superconducting state to that in the normal state, as predicted by Eq. (12.297). The fall-off of this ratio in the superconducting state is a signature of Cooper pair formation.

integration, $\varepsilon_{\mathbf{p}}/\varepsilon_{\mathbf{p}'}$ is finite. In the limit that $\hbar\omega_{\mathbf{q}} \ll \Delta$, $\varepsilon_{\mathbf{p}'} \approx \varepsilon_{\mathbf{p}}$. Consequently,

$$\frac{\varepsilon_{\mathbf{p}}}{\varepsilon_{\mathbf{p}}} \frac{\varepsilon_{\mathbf{p}'}}{\varepsilon_{\mathbf{p}'}} \left(1 - \frac{\Delta^2}{\varepsilon_{\mathbf{p}} \varepsilon_{\mathbf{p}'}}\right) \rightarrow \frac{\varepsilon_{\mathbf{p}}^2}{\varepsilon_{\mathbf{p}}^2} \left(\frac{\varepsilon_{\mathbf{p}}^2 - \Delta^2}{\varepsilon_{\mathbf{p}}^2}\right) = 1. \quad (12.294)$$

It is certainly valid to work within this limit, because we are considering phonon absorption as a result of single-quasi-particle excitations only. Evaluating the remaining integrand at $\varepsilon_{\mathbf{p}'} = \varepsilon_{\mathbf{p}} + \hbar\omega_{\mathbf{q}}$, we find that

$$\begin{aligned} \alpha_{\mathbf{q}} &= \frac{8\pi}{\hbar} |M_{\mathbf{q}}|^2 g^2(0) A_{\Omega} \int_{\Delta}^{\infty} d\varepsilon_{\mathbf{p}} (n(\varepsilon_{\mathbf{p}} + \hbar\omega_{\mathbf{q}}) - n(\varepsilon_{\mathbf{p}})) \\ &\simeq -\frac{8\pi}{\hbar} |M_{\mathbf{q}}|^2 g^2(0) A_{\Omega} \hbar\omega_{\mathbf{q}} n(\Delta). \end{aligned} \quad (12.295)$$

In the normal state, $\Delta = 0$ and resultantly,

$$\alpha_{\mathbf{q}}^N = -\frac{8\pi}{\hbar} |M_{\mathbf{q}}|^2 g^2(0) A_{\Omega} \hbar\omega_{\mathbf{q}} n(0) = -\frac{4\pi}{\hbar} |M_{\mathbf{q}}|^2 g^2(0) A_{\Omega} \hbar\omega_{\mathbf{q}}. \quad (12.296)$$

The ratio of $\alpha_{\mathbf{q}}^S/\alpha_{\mathbf{q}}^N$ reduces to

$$\frac{\alpha_{\mathbf{q}}^S}{\alpha_{\mathbf{q}}^N} = \frac{2}{e^{\beta\Delta(T)} + 1}. \quad (12.297)$$

At $T = T_c$, $\Delta = 0$, and this ratio yields unity, as illustrated in Fig. 12.22. The calculation (S1964) of the ultrasonic attenuation rate is in excellent agreement with experimental results. Here again, we see that it is the gap that ultimately determines the absorption of sound waves in the superconducting states. This calculation is valid, of course, for longitudinal phonons only. Unlike the longitudinal case in which $M_{\mathbf{q}}$ is the same in the normal as well as in the superconducting state, $M_{\mathbf{q}}$ for transverse phonons changes drastically from

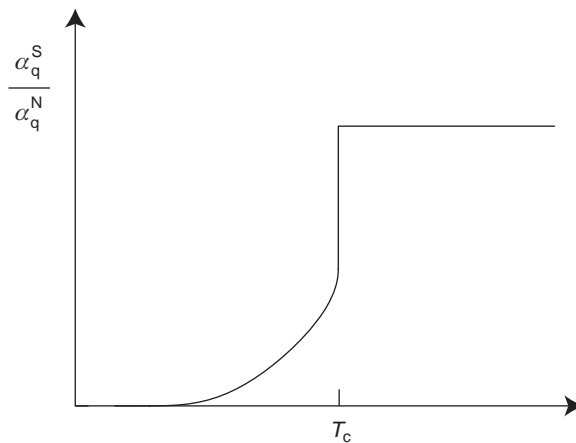


Fig. 12.23 Ratio of the superconducting and normal state ultrasound absorption rates for transverse phonons as a function of temperature T .

the normal to the superconducting state. In this case, the magnetic dependence of $M_{\mathbf{q}}$ leads to a discontinuous drop in the attenuation rate at $T = T_c$, as depicted in Fig. 12.23 (S1964).

12.14.3 Spin-lattice relaxation

The final calculation we present using the BCS coherence factors is that of the spin-lattice relaxation time, T_1 . For historical reasons, this is a key calculation because the prediction that a peak should occur in $1/T_1$ just below T_c predated the experiment by Hebel and Slichter (HS1959). In fact, experimental confirmation of the enhancement of $1/T_1$ just below T_c was the crowning evidence that led to the wide acceptance of the BCS theory. To define T_1 , we consider applying a magnetic field to a collection of nuclear spins. Once the field is turned off, the spins will relax back to achieve the equilibrium magnetization. The time for this process to occur is referred to as T_1 . In insulators, it is the coupling between the nuclei and electronic impurities that causes the nuclei to relax. Left alone, nuclei cannot achieve an equilibrium spin temperature. The lattice temperature must be communicated to the nuclei by some agent. In a metal, it is the conduction electrons that provide the coupling. Because the electrons in a superconductor are locked into a coherent state, we expect T_1 to be drastically altered. Consider a nucleus with magnetic moment \mathbf{S}_N located at the origin, $\mathbf{r} = 0$. The net electron spin at $\mathbf{r} = 0$ is given by the local electron spin density, $\mathbf{S} = \hbar \Psi^\dagger(0) \sigma \Psi(0)/2$, at the origin, where $\Psi(0)$ is the electron wavefunction at $\mathbf{r} = 0$ and σ are the Pauli spin matrices. The Fermi contact,

$$H_{\text{int}} = \frac{8\pi}{3} \mu_B \mathbf{S}_N \cdot \mathbf{S}, \quad (12.298)$$

defines the coupling between a nucleus and an electron at $\mathbf{r} = 0$. In Eq. (12.298), μ_B is the Bohr magneton.

To apply this coupling to a calculation of T_1 in a superconductor, we simply need to express \mathbf{S} in terms of the quasi-particle operators. To do this, we introduce the spinor field operators

$$\Psi(\mathbf{r}) = \frac{1}{\sqrt{V}} \sum_{\mathbf{p}} e^{i\mathbf{p}\cdot\mathbf{r}} \begin{pmatrix} a_{\mathbf{p}\uparrow} \\ a_{\mathbf{p}\downarrow} \end{pmatrix}. \quad (12.299)$$

In spinor notation, the local electron spin density at the origin becomes

$$\mathbf{S} = \frac{\hbar}{2V} \sum_{\mathbf{p}, \mathbf{p}'} \begin{pmatrix} a_{\mathbf{p}'\uparrow}^\dagger & a_{\mathbf{p}'\downarrow}^\dagger \end{pmatrix} \sigma \begin{pmatrix} a_{\mathbf{p}\uparrow} \\ a_{\mathbf{p}\downarrow} \end{pmatrix}. \quad (12.300)$$

We now express the Fermi contact interaction in terms of $\Psi(\mathbf{r})$. Because the product $\mathbf{S}_1 \cdot \mathbf{S}_2 = S_1^z S_2^z + 2(S_1^+ S_2^- + S_1^- S_2^+)$, we write the Fermi contact,

$$H_{\text{int}} = \frac{4\pi}{3V} \mathbf{S}'_B \sum_{\mathbf{p}, \mathbf{p}'} \mathbf{S}_N^z \left(a_{\mathbf{p}'\uparrow}^\dagger a_{\mathbf{p}\uparrow} - a_{\mathbf{p}'\downarrow}^\dagger a_{\mathbf{p}\downarrow} \right) + 2\mathbf{S}_N^+ a_{\mathbf{p}'\downarrow}^\dagger a_{\mathbf{p}\uparrow} + 2\mathbf{S}_N^- a_{\mathbf{p}'\uparrow}^\dagger a_{\mathbf{p}\downarrow}, \quad (12.301)$$

in the familiar Kondo form, where $\mu'_B = \mu_B/\hbar$.

We are particularly interested in those terms in which the nuclear spin is flipped. Hence, we can focus on either the \mathbf{S}_N^- or the \mathbf{S}_N^+ term. Consider \mathbf{S}_N^+ . Let H_{int}^+ be that part of the interaction in which the nuclear spin is flipped up. Here again, we introduce the quasi-particle representation of

$$a_{\mathbf{p}'\downarrow}^\dagger = u_{-\mathbf{p}'} \gamma_{\mathbf{p}'\downarrow}^\dagger - v_{-\mathbf{p}'} \gamma_{-\mathbf{p}'\uparrow}, \quad (12.302)$$

and

$$a_{\mathbf{p}\uparrow} = u_{\mathbf{p}} \gamma_{\mathbf{p}\uparrow} + v_{\mathbf{p}} \gamma_{-\mathbf{p}\downarrow}, \quad (12.303)$$

so that H_{int}^+ is transformed to

$$\begin{aligned} H_{\text{int}}^+ = \frac{4\pi}{3V} \mu'_B \mathbf{S}_N^+ \sum_{\mathbf{p}, \mathbf{p}'} & \left(u_{-\mathbf{p}'} u_{\mathbf{p}} \gamma_{\mathbf{p}'\downarrow}^\dagger \gamma_{\mathbf{p}\uparrow} - v_{-\mathbf{p}'} v_{\mathbf{p}} \gamma_{-\mathbf{p}'\uparrow} \gamma_{-\mathbf{p}\downarrow}^\dagger \right. \\ & \left. - u_{\mathbf{p}} v_{-\mathbf{p}'} \gamma_{-\mathbf{p}'\uparrow} \gamma_{\mathbf{p}\uparrow} + u_{-\mathbf{p}'} v_{\mathbf{p}} \gamma_{\mathbf{p}'\downarrow}^\dagger \gamma_{-\mathbf{p}\downarrow}^\dagger \right). \end{aligned} \quad (12.304)$$

The first two terms describe processes in which quasi-particles of opposite spin are created and annihilated, while the latter terms contain quasi-particle pair production or annihilation. Typically, nuclear Zeeman energies are small relative to the quasi-particle gap energy. Hence, if we focus on the frequency range $\hbar\omega \approx \mu_B H$, with H the external magnetic field, only the former terms are relevant. We have reduced our effective interaction to

$$H_{\text{int}}^+ \simeq \frac{4\pi}{3V} \mu'_B \mathbf{S}_N^+ \sum_{\mathbf{p}, \mathbf{p}'} \left(u_{-\mathbf{p}'} u_{\mathbf{p}} \gamma_{\mathbf{p}'\downarrow}^\dagger \gamma_{\mathbf{p}\uparrow} + v_{-\mathbf{p}'} v_{\mathbf{p}} \gamma_{-\mathbf{p}\downarrow}^\dagger \gamma_{-\mathbf{p}'\uparrow} \right). \quad (12.305)$$

Matrix elements of this quantity will be non-zero if the initial state is of the form $|\mathbf{p} \uparrow, \mathbf{S}_N^z\rangle$ and the final state is $|\mathbf{p} \downarrow, \mathbf{S}_N^z + 1\rangle$. Let $\alpha_N = \langle \mathbf{S}_N^z + 1 | \mathbf{S}_N^+ | \mathbf{S}_N^z \rangle$. The resultant matrix element

$$\begin{aligned}\Gamma_{\text{SLR}}^{\mathbf{pp}'} &= \frac{8\pi}{3} \mu'_B \alpha_N \left(u_{-\mathbf{p}'\downarrow} u_{\mathbf{p}\uparrow} \sqrt{(1 - n_{\mathbf{p}'\downarrow}) n_{\mathbf{p}\uparrow}} + v_{-\mathbf{p}'\downarrow} v_{\mathbf{p}\uparrow} \sqrt{(1 - n_{-\mathbf{p}'\downarrow}) n_{\mathbf{p}\uparrow}} \right) \\ &= \frac{4\pi}{3} \mu'_B \alpha_N (u_{-\mathbf{p}'\downarrow} u_{\mathbf{p}\uparrow} + v_{-\mathbf{p}'\downarrow} v_{\mathbf{p}\uparrow}) \sqrt{(1 - n_{\mathbf{p}'\downarrow}) n_{\mathbf{p}\uparrow}}\end{aligned}\quad (12.306)$$

leads to the nuclear-spin lattice relaxation rate

$$T_1^{-1} = \frac{32\pi^3}{9\hbar} \mathbf{S}_B^2 |\alpha_N|^2 \sum_{\mathbf{p}, \mathbf{p}'} (u_{-\mathbf{p}'\downarrow} u_{\mathbf{p}\uparrow} + v_{-\mathbf{p}'\downarrow} v_{\mathbf{p}\uparrow})^2 (1 - n_{\mathbf{p}'\downarrow}) n_{\mathbf{p}\uparrow} \delta(\varepsilon_{\mathbf{p}'} - \varepsilon_{\mathbf{p}}). \quad (12.307)$$

At this level of theory, we are ignoring, of course, the Kondo effect. The Kondo regime of a magnetic impurity in a superconductor is a subtle problem indeed, which we will not consider here.

The procedure from here on is now standard: (1) convert the sum to an integral by introducing the density of states, (2) evaluate the coherence factors, and (3) cancel all integrals linear in the bare energy, ϵ . From the ultrasonic attenuation calculation, we have that

$$(u_{\mathbf{p}'\downarrow} u_{\mathbf{p}\uparrow} + v_{\mathbf{p}'\downarrow} v_{\mathbf{p}\uparrow})^2 = \frac{1}{2\varepsilon_{\mathbf{p}}\varepsilon_{\mathbf{p}'}} (\varepsilon_{\mathbf{p}}\varepsilon_{\mathbf{p}'} + \epsilon_{\mathbf{p}}\epsilon_{\mathbf{p}'} + \Delta_{\mathbf{p}}\Delta_{\mathbf{p}'}) . \quad (12.308)$$

Here again, we assume that the gap is constant and the relaxation rate reduces to

$$\begin{aligned}T_1^{-1} &= \frac{64\pi^3}{9\hbar} \mu_B'^2 |\alpha_N|^2 g^2(0) \int_0^\infty d\varepsilon_{\mathbf{p}} \int_0^\infty d\varepsilon_{\mathbf{p}'} n_{\mathbf{p}} (1 - n_{\mathbf{p}'}) \left(\frac{\varepsilon_{\mathbf{p}}\varepsilon_{\mathbf{p}'} + \Delta^2}{\varepsilon_{\mathbf{p}}\varepsilon_{\mathbf{p}'}} \right) \delta(\varepsilon_{\mathbf{p}'} - \varepsilon_{\mathbf{p}}) \\ &= \frac{64\pi^3}{9\hbar} \mu_B'^2 |\alpha_N|^2 g^2(0) \int_\Delta^\infty d\varepsilon n(\varepsilon) (1 - n(\varepsilon)) \frac{\varepsilon^2 + \Delta^2}{\varepsilon^2 + \Delta^2}.\end{aligned}\quad (12.309)$$

At $T = 0$, the product $n(1 - n) = 0$ because $n = 1$ at $T = 0$.

At $T = 0$, there is a divergence when $\varepsilon = \pm\Delta$. In the vicinity of $\pm\Delta$, we write the integrand as

$$\begin{aligned}T_1^{-1} &\rightarrow \frac{64\pi^3}{9\hbar} \mu_B'^2 |\alpha_N|^2 g^2(0) \int_\Delta^\infty \frac{\varepsilon^2 + \Delta^2}{\varepsilon^2 - \Delta^2} n(\varepsilon) (1 - n(\varepsilon)) d\varepsilon \\ &\propto \int_\Delta^\infty \frac{\varepsilon + \Delta}{\varepsilon - \Delta} d\varepsilon,\end{aligned}\quad (12.310)$$

which is logarithmically divergent. The coefficient of the ln-divergence is proportional to the gap, Δ . This implies then that the ln-divergence starts at $T = T_c$ where the gap begins to arise. In experiments, the gap is anisotropic as a result of its momentum dependence. Consequently, the divergence of T_1 is smeared out slightly over a range comparable to the average value of Δ . Hebel and Slichter (HS 1959) were the first to observe this behavior, which is illustrated in Fig. 12.7.

The ln-divergence we have predicted at this low order in perturbation theory might be removed, or at least broadened, by the summation of all higher-order terms. Hence, it is worthwhile to investigate precisely how robust the ln-divergence is. The full series for the electron–nucleus interaction is

$$\Gamma_{\text{int}}^{\text{full}} = \langle f | H_{\text{int}}^+ | i \rangle + \sum_{\mathbf{p}} \frac{\langle f | H_{\text{int}}^+ | \mathbf{p} \rangle \langle \mathbf{p} | H_{\text{int}}^+ | i \rangle}{E - \varepsilon_{\mathbf{p}} + i\eta} + 0(H^3) + \dots . \quad (12.311)$$

In the context of the local-moment problem, we defined the Green function to be

$$G(E + i\eta) = \sum_{\mathbf{p}} \frac{|\mathbf{p}\rangle\langle\mathbf{p}|}{E - \varepsilon_{\mathbf{p}} + i\eta}. \quad (12.312)$$

Schematically, the perturbation series is of the form

$$\begin{aligned} \Gamma_{\text{int}}^{\text{full}} &= \langle f | H_{\text{int}}^+ | i \rangle + \langle f | H_{\text{int}}^+ G(E + i\eta) H_{\text{int}}^+ | i \rangle + \dots \\ &= \left\langle f \left| \frac{H_{\text{int}}^+}{1 - H_{\text{int}}^+ G(E + i\eta)} \right| i \right\rangle. \end{aligned} \quad (12.313)$$

To determine the divergent part of $\Gamma_{\text{int}}^{\text{full}}$, we convert the sum in the Green function to an integral,

$$\begin{aligned} G(E + i\eta) &= N(0) \int d\varepsilon_{\mathbf{p}} \frac{1}{E - \varepsilon_{\mathbf{p}} + i\eta} \\ &= N(0) \int_{\Delta}^{\infty} \left(\frac{d\varepsilon_{\mathbf{p}}}{d\varepsilon_{\mathbf{p}}} \right) \frac{d\varepsilon_{\mathbf{p}}}{E - \varepsilon_{\mathbf{p}} + i\eta}. \end{aligned} \quad (12.314)$$

We have shown previously that $N(0)d\varepsilon_{\mathbf{p}}/d\varepsilon_{\mathbf{p}}$ defines the density of states,

$$\rho(\varepsilon_{\mathbf{p}}) = \frac{N(0)\varepsilon_{\mathbf{p}}}{\sqrt{\varepsilon_{\mathbf{p}}^2 - \Delta_{\mathbf{p}}^2}} = N(0) \frac{\varepsilon_{\mathbf{p}}}{\epsilon_{\mathbf{p}}}, \quad (12.315)$$

which is divergent at $\varepsilon_{\mathbf{p}} = \Delta_{\mathbf{p}}$. Consequently,

$$\begin{aligned} \lim_{\eta \rightarrow 0} G(E + i\eta) &= \int_{\Delta}^{\infty} \rho(\varepsilon_{\mathbf{p}}) \left[P \left(\frac{1}{E - \varepsilon_{\mathbf{p}}} \right) - i\pi \delta(E - \varepsilon_{\mathbf{p}}) \right] d\varepsilon_{\mathbf{p}} \\ &= \text{Re}G - i\pi \rho(E), \end{aligned} \quad (12.316)$$

and the perturbation series becomes

$$\Gamma_{\text{int}}^{\text{full}} = \left\langle f \left| \frac{H_{\text{int}}^+}{(1 - H_{\text{int}}^+ \text{Re}G) + i\pi H_{\text{int}} \rho(E)} \right| i \right\rangle. \quad (12.317)$$

In the vicinity of $E = \Delta$, the denominator of Eq. (12.317) is dominated by the $\rho(E)$ term. In this limit, $\Gamma_{\text{int}}^{\text{full}} \rightarrow 1/(i\pi \rho(E))$. The square of this quantity exactly cancels the divergent term, $1/(\varepsilon_{\mathbf{p}}^2 - \Delta^2)$, in our previous expression for the relaxation rate.

To see this more clearly, we rewrite the relaxation rate as

$$T_1^{-1} = \frac{64\pi^3}{9\hbar} \mu_B^2 |\alpha_N|^2 g^2(0) \int_{\Delta}^{\infty} d\varepsilon n(\varepsilon) (1 - n(\varepsilon)) \left(\frac{\rho(\varepsilon)}{\varepsilon} \right)^2 \times \frac{(\varepsilon^2 + \Delta^2)}{(1 - H_{\text{int}}^+ \text{Re}G)^2 + \pi^2 |H_{\text{int}}^+|^2 \rho^2(\varepsilon)}, \quad (12.318)$$

which reduces to

$$T_1^{-1} \propto \int_{\Delta}^{\infty} d\varepsilon (1 - n(\varepsilon)) n(\varepsilon) \frac{\varepsilon^2 + \Delta^2}{(1 + \pi^2 |H_{\text{int}}^+|^2 g^2(0)) \varepsilon^2 - \Delta^2}. \quad (12.319)$$

In deriving Eq. (12.319), we ignored the real part of the Green function as it serves no relevant purpose as far as the convergence is concerned. This expression is completely convergent at $\varepsilon^2 = \Delta^2$. In fact, because $(1 + \pi^2 |H_{\text{int}}^+|^2 g^2(0)) > 1$, the integral does not diverge over the complete integration range. Consequently, summing high-order terms in the perturbation series results in a smearing of the peak in the relaxation rate immediately below T_c .

12.15 Josephson tunneling

Consider two superconductors separated from one another by a thin insulating barrier. Naively, we would expect no appreciable transport of charge between the two superconductors in the absence of an applied voltage, save possibly for single quasi-particle tunneling through the insulating barrier. Josephson (J1962) showed that this naive picture is not correct. In particular, he proved that in the absence of an applied voltage for a sufficiently thin barrier, Cooper pairs flow coherently between the two superconductors, thereby establishing a supercurrent through the barrier. Further, the transport of Cooper pairs across the barrier does not result in the creation of quasi-particles in either superconductor. When an applied voltage is present, the supercurrent oscillates with a well-defined period. The essence of both of these effects, dc and ac Josephson tunneling, rests in the phase coherence that obtains in the superconducting state.

We focus first on the dc Josephson effect. Consider two superconductors separated by a thin insulating barrier. Let H_T represent the Hamiltonian for single-particle tunneling across the thin barrier. The specific form of this term is not essential here. The only important feature is that H_T transfers only one electron at a time. We assume at the outset that there is no voltage difference between the two superconductors, and hence they are at the same chemical potential. We can derive the Josephson effect by making an analogy with electron transport in a 1d periodic chain in the tight-binding approximation. In this approximation, a single orbital is placed on each lattice site and a hopping term mediates transport among nearest-neighbor sites. In such a system, no energy is required to transport an electron

across m lattice sites. Likewise, it requires no energy to translate m Cooper pairs across the barrier in the absence of an external voltage differential between the two superconductors. Let $|\Phi_{2m}\rangle$ represent the many-body state when $2m$ Cooper pairs are transferred across the barrier. The degeneracy of these states is split by the single-electron tunneling term, H_T . Consequently, we expand the total state of our system as a linear combination

$$|\Psi_\phi\rangle \equiv |\phi\rangle = \sum_m e^{2im\phi} |\Phi_{2m}\rangle \quad (12.320)$$

over all such pair states. The phase ϕ plays the role of the wavevector k in the 1d periodic tight-binding model. As we have established earlier, the particle number, $2m$, and the phase, ϕ , are conjugate variables.

To compute the energy shift as a result of the tunneling processes, we employ perturbation theory. The first-order term, $\langle\phi|H_T|\phi\rangle$, vanishes identically because ϕ is a sum of all pair states and H_T is a one-body operator. Consequently, the first non-zero term appears in second order. Let

$$\hat{H}_T^{(2)} = \hat{H}_T \frac{|I\rangle\langle I|}{E - E_I} \hat{H}_T \quad (12.321)$$

represent the tunneling operator at second order with E_I the energy of the intermediate state, $|I\rangle$. The second-order correction to the energy,

$$\begin{aligned} E_\phi &= \langle\phi|\hat{H}_T^{(2)}|\phi\rangle \\ &= \sum_{m,m'} e^{2i\phi(m-m')} \langle 2m'|\hat{H}_T^{(2)}|2m\rangle \\ &= \sum_m \left(e^{2i\phi} \langle 2m|\hat{H}_T^{(2)}|2(m+1)\rangle + e^{-2i\phi} \langle 2m|\hat{H}_T^{(2)}|2(m-1)\rangle \right), \end{aligned} \quad (12.322)$$

is a sum of all matrix elements that differ by a single Cooper pair. We have assumed that $\langle\phi|\phi\rangle = 1$. To simplify this expression, we note that the energy of the intermediate state involves a particle-hole excitation, and hence E_I must exceed E by at least 2Δ . Consequently, $E - E_I < 0$. If we regard the tunneling term to be purely real, we simplify the energy shift to

$$E_\phi = -\frac{\hbar J_0}{2} \cos 2\phi, \quad (12.323)$$

with

$$\hbar J_0 = 4 \sum_m \left| \langle 2m|\hat{H}_T^{(2)}|2(m+1)\rangle \right|. \quad (12.324)$$

The minus sign in the energy shift arises from the sign of the excitation energy. From the Hamilton equation, Eq. (12.170), it is clear that if the energy shift depends on the phase,

then the pair number fluctuates on either side of the barrier. This fluctuation is due entirely to the tunneling processes. We calculate the pair current directly,

$$I = 2e \frac{d\langle 2m \rangle}{dt} = 2e \left\langle \frac{dE_\phi}{d\hbar\phi} \right\rangle = 2eJ_0 \sin 2\phi, \quad (12.325)$$

by differentiating the energy shift with respect to the phase. Consequently, in the absence of an applied voltage, a dc supercurrent flows across the barrier. The value of the current ranges from $-2eJ_0$ to $2eJ_0$. A supercurrent of this form was first observed by Anderson and Rowell (AR1963). If a potential difference V exists across the barrier, then a term of the form $2mV$ must be added to the Hamiltonian. Consequently, from Hamilton's equations, Eq. (12.170), the phase fluctuates in time according to

$$\frac{d(\hbar\phi)}{dt} = 2eV. \quad (12.326)$$

Together, these two equations, Eq. (12.325) and Eq. (12.326), completely determine the behavior of the supercurrent across the barrier. To illustrate, consider the simplest case in which the voltage V is a constant in time. In this case, the phase ϕ varies linearly with time and, as a consequence, the current oscillates as $\sin(2eVt/\hbar)$. Hence, an alternating current flows with a frequency of $2eV/\hbar$.

Summary

We have shown that the pairing hypothesis of BCS is sufficient to account for all relevant experimental observables of low-temperature superconductors. In fact the BCS pairing mechanism is the only account available currently to describe the transition to a superconducting state. In contrast to low- T_c materials, superconductivity in the cuprates originates from doping an insulator. Further, the insulator possesses a partially-filled band and hence falls into the class of Mott insulators in which an absence of transport originates from strong electron repulsions. Consequently, we know *a priori* that we are not justified in starting from Fermi liquid theory to describe even the normal state properties. Simply stated, the deep phenomenology of the cuprates lies in the physics of doped Mott insulators. Whether a theory as succinct and crystal clear as the BCS account can be formulated for such systems remains to be seen.

Problems

- 12.1 Within the Ginsburg–Landau phenomenological approach, determine the form of the free energy density when a magnetic field is present. Show that the free energy

difference between the superconducting and normal states is given by

$$F_S - F_N = -\frac{H_c^2(T)}{8\pi}. \quad (12.327)$$

- 12.2 Writing the Ginsburg–Landau wavefunction as $\psi(\mathbf{r}) = \sqrt{n(\mathbf{r})}e^{i\theta(\mathbf{r})}$, show that the current density in terms of the variables θ and $n(\mathbf{r})$ is given by

$$\mathbf{j} = \frac{e\hbar}{m} \left(\nabla\theta - \frac{e\mathbf{A}}{c\hbar} \right) n(\mathbf{r}). \quad (12.328)$$

Now assume that in the bulk of a material, the current density vanishes. As a consequence, $\hbar\nabla\theta = e\mathbf{A}$. Integrate both sides of this expression around a closed loop in a superconducting ring and show that the resultant magnetic flux enclosed is quantized. What is the correct value of e for a superconductor?

- 12.3 Use second-order perturbation theory directly to show that the electron–phonon interaction is negative and given by the second term in Eq. (12.34).
- 12.4 Redo the Cooper pair instability calculation for triplet pairing between the electrons.
- 12.5 Evaluate $\langle r^2 \rangle$ for a singlet Cooper pair.
- 12.6 In the problem of the instability of the superconducting state in the presence of the BCS pairing interaction, determine the form of the growth rate of the pair amplitude as $T \rightarrow T_c$.
- 12.7 Evaluate the commutator $[b_k, b_k^\dagger]$, where the b'_k s are the Cooper pair annihilation operators. What does the lack of commutativity of the Cooper pair creation and annihilation operators mean?
- 12.8 Calculate the average number of particles in a superconductor. Let $|\Psi\rangle$ represent the BCS pair state. Show that the average value of the number operator, N , is given by

$$\langle \Psi | N | \Psi \rangle = \langle \Psi | \sum_{k,\sigma} a_{k\sigma}^\dagger a_{k\sigma} | \Psi \rangle = 2 \sum_k |v_k|^2 \quad (12.329)$$

in the pair state. Also evaluate the fluctuation $\langle (N - \langle N \rangle)^2 \rangle$. You should obtain a simple result involving u_k and v_k only. For what special value of u_k and v_k is the fluctuation maximized? Interpret your result.

- 12.9 So far we have ignored any spatial inhomogeneities in the gap. Consider a gap of the form $\Delta_{\mathbf{q}} = \Delta_0 e^{2i\mathbf{q}\cdot\mathbf{r}}$, where $q \ll p_F$. Find the new self-consistent condition for Δ_0 . At $T = 0$, show that Δ is independent of q for $q < q_c \approx \Delta_0/\hbar v_F$. Near T_c , expand the gap equation to find that

$$\frac{\Delta(T)}{k_B T_c} \approx \frac{8\pi^2}{7\zeta(3)} (1 - T/T_c) - \frac{2}{3} \left(\frac{\hbar^2 p_F}{mk_B T_c} \right)^2 q^2. \quad (12.330)$$

Then determine the critical value of q that makes the gap vanish.

- 12.10 Evaluate the sums explicitly in Eq. (12.260) and show that for $T/T_c \ll 1$, $F_N - F_S \propto 1 - (T/T_c)^2$.
- 12.11 An Anderson-type impurity is placed in a superconductor. You are to formulate this problem and develop a criterion for local moment formation. There are a number of assumptions that can be applied. First, when you transform to the quasi-particle basis, ignore all terms that do not conserve spin and particle number. The problem

should now be straightforward. You should be able to redo the Anderson problem completely. Discuss clearly when the local moment exists and when it does not.

References

- [A1957] A. A. Abrikosov, *Sov. Phys. JETP* **5**, 1174 (1957).
- [AR1963] P. W. Anderson and J. M. Rowell, *Phys. Rev. Lett.* **10**, 230 (1963).
- [BCS1957] J. Bardeen, L. N. Cooper, and J. R. Schrieffer, *Phys. Rev.* **106**, 162 (1957); **108**, 1175 (1957).
- [BG1990] G. Benfatto and G. Gallavotti, *J. Stat. Phys.* **59**, 541 (1990).
- [C1956] L. N. Cooper, *Phys. Rev.* **104**, 1189 (1956).
- [GL1950] G. V. L. Ginsburg and L. D. Landau, *J. Exptl. Theor. Phys. (USSR)* **20**, 1064 (1950).
- [GF1987] M. Gurvitch and A. T. Fiory, *Phys. Rev. Lett.* **59**, 1337 (1987).
- [HS1959] L. C. Hebel and C. P. Slichter, *Phys. Rev.* **113**, 1504 (1959); L. C. Hebel, *Phys. Rev.* **116**, 79 (1959).
- [J1962] B. D. Josephson, *Phys. Lett.* **1**, 251 (1962).
- [L1956] L. D. Landau, *Sov. Phys. JETP* **3**, 920 (1956); **8**, 70 (1959).
- [L1964] A. I. Larkin, *Sov. Phys. JETP* **19**, 1478 (1964).
- [L1965] A. J. Leggett, *Phys. Rev. Ser. A* **140**, 1869 (1965).
- [P1992] J. Polchinski, arXiv:hep-th/9210046.
- [SM1991] R. Shankar, *Physica* **A177**, 530 (1991).
- [S1964] J. R. Schrieffer, *Theory of Superconductivity* (Benjamin, New York, 1964).

A problem that has always been central to solid state physics is the insulator–metal transition. The question to answer here is why some materials conduct and others do not. Metals are characterized by a non-zero dc conductivity $\sigma(0)$ at zero temperature, whereas $\sigma(0) = 0$ in an insulator. There are currently three standard models that describe a transition between these two extremes. Anderson ([A1958](#)) was first to point out that scattering from a static but random potential can disrupt metallic conduction and lead to an abrupt localization of the electronic eigenstates. Mott ([M1949](#)), on the other hand, proposed that an insulating state can obtain even in a material such as NiO which possesses a partially filled valence band. The insulating state arises from strong electron correlations which induce a gap at the Fermi energy. The closing of the gap, signaling the onset of a metallic state, results typically in the intermediate-coupling regime in which the kinetic energy effects can destroy the ordering tendencies of the potential energy. Finally, a structural transition in which the lattice periodicity doubles can also thwart metallic transport. While all of these mechanisms are of considerable interest in their own right, our focus in this chapter will be the disorder-driven insulator–metal or Anderson transition.

We start by reviewing the essential physics and some of the key controversies surrounding the disorder-induced localization transition. Two controversies we address are the role of perturbation theory and whether or not the conductivity is continuous in the vicinity of the Anderson transition. To address the latter question, we develop the scaling theory of localization. The two key predictions of this approach are that the localization transition is continuous and that an Anderson transition exists only for $d > 2$. That is, any amount of disorder localizes all the electronic states in $d = 1$ and $d = 2$. Finally, the weak-localization analysis makes it profoundly clear that the Anderson transition occurs precisely in the strong-disorder limit in which perturbation theory breaks down. Consequently, no amount of perturbation theory can be harnessed to describe the disorder-induced localization transition. Nonetheless, the essential physical process in weak localization, time-reversed back scattering, appears to be the mechanism behind the Anderson transition. However, even when time-reversal symmetry is intact, there are important exceptions to the standard localization scenario in $d \leq 2$. We close this chapter by considering all three known examples: (1) the general class of one-dimensional models which defeat both strong and weak localization, namely the random dimer model, (2) insulator–superconductor transitions in thin films, and (3) the newly discovered conducting state in a dilute 2d electron gas.

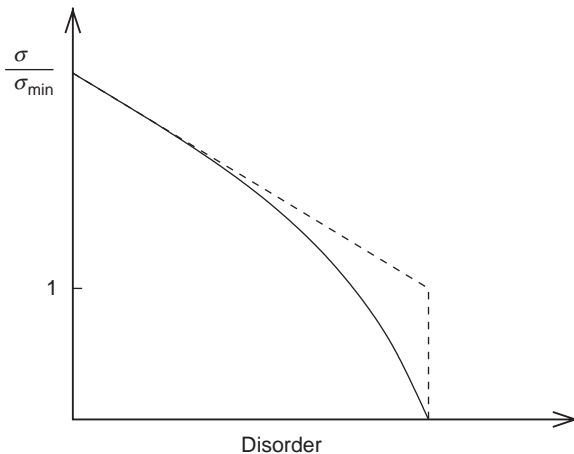
13.1 Primer on localization

Anderson's original model grew out of a series of electron spin resonance experiments by Feher and collaborators ([FFG1955](#)) on donor impurities such as P and As in Si. They noticed that the electron spin on each ^{31}P nucleus retained its characteristic frequency on a time scale ranging from seconds to minutes. A simple golden rule calculation (of the type performed in the context of the Kondo problem but in this case it is sufficient to retain only the $O(J^2)$ term), however, predicted that the expected lifetime as a result of interaction with the other impurities would range from 0.1 to 10^{-6} s ([A1958](#)). The persistence of localized spin packets in the Feher experiments indicated an absence of spin diffusion among the ^{31}P impurity spins. As the host Si was otherwise extremely pure, Anderson traced the absence of spin diffusion to disorder arising from the random distribution of the dopant impurities. To capture the essence of quantum mechanical transport in the presence of a random potential, Anderson proposed the tight-binding model

$$H = \sum_n \epsilon_n a_n^\dagger a_n + V \sum_{n,m} a_n^\dagger a_m \quad (13.1)$$

for conduction in an impurity band in which one orbital and a single site energy ϵ_n are assigned at random to the lattice sites. A constant nearest-neighbor matrix element V mediates transport between nearest-neighbor sites. In Eq. (13.1), $a_n^\dagger (a_n)$ creates (annihilates) an electron on site n . In general, V depends on distance, such as in the spin diffusion problem in which dipolar interactions give rise to a matrix element that decays as $V \propto 1/r^3$. However, including randomness in the matrix elements does not qualitatively change the nature of the transport problem.

The site-disordered tight-binding model in Eq. (13.1) describes a localization-delocalization transition, as can be seen by considering two simple limits. We assume initially that the site energies are chosen from a uniform distribution of width W . When $W = 0$, an ordered system obtains as all the sites have the same energy. The resultant eigenstates are delocalized Bloch states that remain unscattered over the size of the sample. Transport in this regime is ballistic. However, in the limit that $V = 0$, none of the sites are connected and transport ceases. That is, the resultant eigenstates are localized. Hence the Anderson model describes a localization-delocalization transition that is governed, at least partially, by the ratio V/W . On physical grounds, it is tempting to argue that in all cases, gradually increasing the ratio V/W will lead to a smooth interpolation between the limit of extreme localization, $V = 0$, and the ballistic regime, $V \gg W$. We know now from the scaling theory of localization, as well as from the early work of Mott and Twose ([MT1961](#)) and Borland ([B1963](#)), that this is not the case. For $d \leq 2$, it is now well-established (except in some special $d = 1$ cases ([DWP1990](#))) that an infinitesimal amount of disorder precludes the existence of extended states. That is, the smooth interpolation between the ballistic and localized regimes does not obtain for $d = 1, 2$. In three dimensions, extended states fail to

**Fig. 13.1**

Two possibilities for the behavior of the conductivity in the vicinity of the mobility edge of the Anderson transition. The dashed line represents the minimum-metallic conductivity hypothesis of Mott. The solid line, on the other hand, depicts the continuous decrease of the conductivity at the Anderson transition. The latter is observed experimentally and is predicted by the scaling theory of localization.

form when W/V exceeds some critical value, $(W/V)_c$. When $W/V < (W/V)_c$, extended and localized states coexist in the energy band but are separated at an energy now known as the mobility edge, E_c , such that if the energy E of a particle exceeds E_c , then the particle is extended. Localization obtains in the opposite regime, $E < E_c$.

A natural question that arises in the context of the localization transition is what happens to the conductivity in the vicinity of the mobility edge? There are two possibilities. Either the conductivity goes to zero continuously as the mobility edge is approached from the metallic side or, as Mott (M1972) proposed, σ decreases to some minimum value and then plummets to zero discontinuously. Both of these possibilities are shown in Fig. 13.1. The Mott minimal conductivity has proven to be one of the most controversial but wrong ideas proposed for the localization transition. The intuitive appeal of this idea is immediate, however, when one rewrites the Drude dc conductivity,

$$\sigma(0) = \frac{e^2 n_e \tau}{m} \approx \left(\frac{e^2}{\hbar}\right) \frac{a^{2-d}}{\pi} \frac{\ell}{a} = \sigma_0 \frac{\ell}{a}, \quad (13.2)$$

in terms of the mean-free path, $\ell = v_F \tau$. We have approximated the electron density of a d -dimensional system as $n_e = a^{-d}$, where a is the lattice spacing. Disorder enters through the ratio ℓ/a . Clearly, if ℓ has a minimum value, then so will $\sigma(0)$. Within Boltzmann transport theory, ℓ cannot be smaller than the lattice spacing. Consequently, Mott (M1949) postulated that a minimum-metallic conductivity of the form $\sigma_{\min} = b\sigma_0$ must exist. The constant σ_0 is universal, whereas b is generally taken to be between 0.08 and 0.3. The minimum-metallic conductivity hypothesis is that $\sigma(0)$ should decrease as ℓ and hence should plummet to zero once $\ell = a$, as depicted in Fig. 13.1. Experimentally, this prediction has not been borne out, as there are now numerous examples in which conductivities lower than σ_{\min} have been measured in the vicinity of the localization transition. Further, the scaling theory

of localization predicts a continuous transition. Both of these results completely invalidate the σ_{\min} hypothesis. As we will see, the Anderson transition cannot be described within Boltzmann transport theory. Hence, the minimum value that Boltzmann theory imposes on the mean-free path is not correct.

13.2 Return probability: localization criterion

The least a theory of Anderson localization should provide is an accurate method for distinguishing between localized and extended states. To do so, we focus on the return probability. Consider placing a particle at the origin of a site-disordered d -dimensional lattice at $t = 0$. As a result of the hopping term, the particle has a finite probability of moving away from the origin. We can ask the question then, does any probability remain at the origin as $t \rightarrow \infty$? If, as $t \rightarrow \infty$, the probability at the origin remains non-zero, then the particle has a finite probability of returning to the origin. Consequently, it is localized. On the other hand, if the probability at the origin decays to zero, the particle will be found throughout the lattice and hence will be delocalized. The site-return probability is the key quantity in the localization problem (A1958; AAT1973). In addition, it is the phase relationship between time-reversed closed paths that leads to weak localization.

In the context of the model in Eq. (13.1), we define $c_n(t)$ to be the probability amplitude that an electron is on site n at time t . The return probability at long times is determined by the square of the site probability amplitudes, $\lim_{t \rightarrow \infty} |c_n(t)|^2$. To obtain this quantity, we focus on the Heisenberg equations of motion,

$$i\hbar\dot{c}_n(t) = \epsilon_n c_n + \sum_m V_{nm} c_m, \quad (13.3)$$

for the probability amplitude $c_n(t)$, where V_{nm} is zero unless sites n and m are nearest neighbors in which case $V_{nm} = V$. From this equation, it is clear that, in the absence of the hopping term, the site probabilities do not evolve from their initial values. Hence, an initially localized distribution will remain localized. What is surprising is that localized solutions exist for the probability amplitudes even when the hopping term is non-zero. The criterion for localization can be established as follows. We first Laplace transform the equations of motion

$$c_n(E) = \frac{i\hbar c_n(t=0)}{iE - \epsilon_n} + \sum_{m \neq n} \frac{V_{nm} c_m(E)}{iE - \epsilon_n} \quad (13.4)$$

by defining

$$c_n(E) = \int_0^\infty e^{-Et/\hbar} c_n(t) dt, \quad (13.5)$$

with E a general complex variable with units of energy. We consider the localized initial condition, $c_n(t=0) = \delta_{n0}$. The Laplace-transformed equation is best solved by iteration,

leading to

$$c_0(E) = \frac{i\hbar}{(iE - \epsilon_0)} + \sum_{l \neq 0} \frac{V_{0l}V_{l0}}{(iE - \epsilon_0)(iE - \epsilon_l)} + \dots \quad (13.6)$$

as our equation for the site-probability amplitude at the origin. As a result of the localized initial condition, the linear term in V vanishes. Because of the restriction that $l \neq 0$, the n th term in this series represents a self-avoiding random walk of n steps that starts and ends at the origin. No site except the origin is visited twice. We sum the series in Eq. (13.6) by defining the self-energy, $S_n(E)$, for site n such that

$$c_n(E) = \frac{i\hbar}{iE - \epsilon_n - S_n(E)}. \quad (13.7)$$

Random walks of all lengths are summed into the site self-energy. The question of localization at long times ($E \rightarrow 0$) now rests on the self-energy.

There is a close connection between the site-probability amplitudes and the diagonal elements of the exact Green function for our original Hamiltonian. As a resolvent, the Green function, $G(E) = (E - H)^{-1}$, contains all information about the exact eigenstates of Eq. (13.1). The matrix elements of the single-particle Green function are

$$(E - \epsilon_n)G_{nm}(E) = \delta_{nm} + \sum_{n \neq l} V_{nl}G_{lm}(E). \quad (13.8)$$

The form of Eq. (13.8) is illuminating for two primary reasons. First, because the tight-binding states form the atomic basis, the m th eigenstate of the Green function can be written quite generally as a superposition

$$|\phi_m\rangle = \sum_n c_{nm}|n\rangle \quad (13.9)$$

of these states. The coefficients c_{mn} determine the amplitude that the m th eigenstate overlaps site n . Without the second term in Eq. (13.8), the singularities of the Green function are simple poles with energies $E = \epsilon_m$, and the exact eigenstates reduce to $|\phi_m\rangle = |m\rangle$. This corresponds to the strongly localized regime. When the hopping term is present, the most general statement that can be made about a localized state is that not all the c_{mn} s are non-zero. In fact, if a sufficiently large number of the site amplitudes vanish, the resulting eigenstate is characterized by an exponentially decaying envelope, $\phi_m \propto e^{-r/\xi_m}$, where ξ_m is the localization length (spatial extent) of the eigenstate. An example of an exponentially localized state in the one-dimensional random binary alloy is shown in Fig. 13.2.

Secondly, the expansion in powers of V for the diagonal elements of the Green function,

$$\begin{aligned} G_{nn}(E) &= \frac{1}{(E - \epsilon_n)} + \sum_{l \neq n} \frac{V_{nl}V_{l0}}{(E - \epsilon_n)(E - \epsilon_l)} + \dots \\ &= \frac{1}{E - E_n - S_n(E)}, \end{aligned} \quad (13.10)$$

is identical to that for the site-probability amplitudes. Hence, the analytical properties of the Green function are directly related to the fate of the return probability. In general, E can be complex. However, if as E approaches the real axis, $S_n(E)$ is purely real, then the

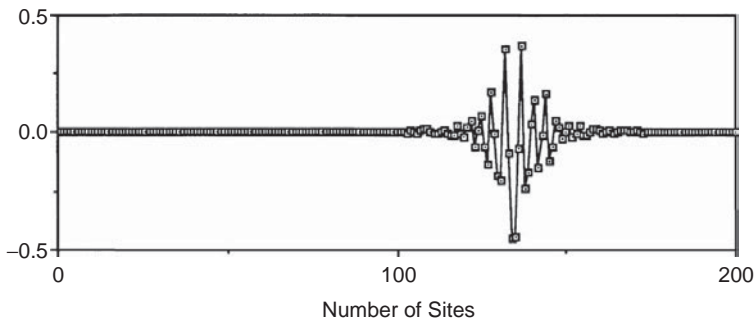


Fig. 13.2 The real part of a typical eigenstate in a random binary alloy.

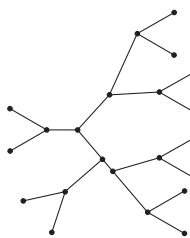


Fig. 13.3 A Cayley tree of connectivity $K = 3$.

singularities of $G_{nn}(E)$ are once again simple poles, and the eigenstates are localized states. Extended states form only when $G_{nn}(E)$ is complex or, equivalently, when $\text{Im } S_n(E)$ is non-vanishing as E approaches the $\text{Re } E$ axis. That is, the inverse of $\text{Im } S_n(E)$ determines the lifetime of the state at energy E . If the state with energy E has a finite lifetime, the return probability will vanish at long times. For the Anderson model, the self-energy, $S_n(E)$, is a function of the distribution of site energies. Hence, they are themselves random variables. For this reason, the precise quantity which is relevant to the localization problem is the probability distribution of the site self-energies (A1958). The signature of the absence of extended states is the vanishing of the probability distribution of the site self-energy for all energies along the real E -axis. The critical value $(W/V)_c$ determines the amount of disorder required to make the Anderson transition obtain.

The primary hurdle in the Green function analysis of the localization problem is the computation of the site self-energy. The self-energy requires the enumeration of all self-avoiding walks that return to a given site. Hence, on lattices lacking closed loops such as Cayley trees, the site self-energy can be calculated exactly. A typical Cayley tree is depicted in Fig. 13.3. A further simplification that is employed in the analysis of the probability distribution of the self-energy is to ignore the real part of the self-energy. As we showed in the context of the local moment model in Chapter 7, the contribution from the real part of the self-energy is significant only if the density of states fluctuates wildly. For the localization problem, inclusion of the real part of the self-energy suppresses the critical amount of disorder required for the localization transition. The analysis of

the Anderson transition (AAT1973) in which the real part of the self-energy is ignored yields

$$(W/2V)_c = 4K \ln(W/2V)_c \quad (13.11)$$

for the upper critical value of the disorder beyond which no state is extended. Attempts have certainly been made (EC1970; SE1984) to extend the self-energy analysis to hypercubic lattices. In such approaches, the self-energy is calculated through self-avoiding walks of M steps. Economou and Cohen (EC1970) argued that a stability analysis of the M th root of the term of order M in the self-energy can be used to distinguish between localized and extended states. If in the limit that $M \rightarrow \infty$, the M th root of the $O(M)$ term in the self-energy exceeds unity, then the perturbative expansion for $S_n(E)$ diverges, and the electronic state at energy E is extended. Although this criterion is not as precise as the vanishing of the probability distribution for the imaginary part of the self-energy, it does appear to provide reliable results for square lattices, as shown by Soukoulis and Economou (SE1984).

13.3 Weak localization

To understand the essential physics leading to a non-zero return probability, we focus on weak localization (A1980; B1982). The goal of weak localization is to perturbatively evaluate the role of scattering processes that are precursors to Anderson localization. Consider a collection of non-interacting quantum mechanical particles moving in a random uncorrelated distribution of point-like scatterers. In the weak disorder limit, the mean-free path, ℓ , of the particle is much larger than the average particle separation, $a \approx k_F^{-1}$. Hence, in weak localization, $k_F\ell \gg 1$, and we can define the small parameter

$$\gamma = \frac{1}{\pi k_F \ell} \ll 1 \quad (13.12)$$

as a measure of the strength of the disorder. The goal is to develop a perturbative theory for the conductivity in terms of γ . To this end, we write the conductivity

$$\sigma = \sigma_0 + \delta\sigma, \quad |\delta\sigma| \ll \sigma_0 \quad (13.13)$$

as a sum of a zeroth-order dc conductivity indicative of the metallic regime, σ_0 , and a correction $\delta\sigma$ which depends non-trivially on γ . We will treat σ_0 in the Boltzmann transport limit described in Chapter 11. In this limit, all scattering events, even if they involve visitations to the same site, are considered to be uncorrelated. This approximation is clearly inadequate if there is an inherent tendency for repetitive scattering from the same site. Hence, the average scattering rate (or relaxation rate in the linearized Boltzmann equation) with the random impurities, τ^{-1} , is linear in the concentration of defects. As a

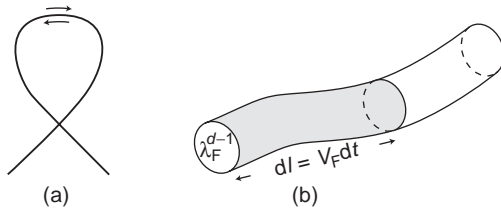


Fig. 13.4 (a) Time-reversed paths in a closed loop. (b) Volume element for a trajectory of a quantum mechanical particle. The cross-sectional area is λ_F^{d-1} , and the differential length is $d\ell = v_F dt$.

result, σ_0 has the simple Drude form

$$\sigma_0 = \frac{e^2 n_e}{m} \tau. \quad (13.14)$$

Between scattering events, the velocity of the particle is a constant; hence, $\ell = v_F \tau$. Because $v_F = \hbar k_F / m$, the zeroth-order conductivity is proportional to $k_F \ell$ or, equivalently, $\sigma_0 \propto \gamma^{-1}$.

To go beyond the Boltzmann limit, we need to consider the phase relationships that enter a scattering process. Quantum mechanically, when a particle makes an excursion from point A to point B, one must include a sum over all paths connecting these two points. Consider first the case in which A and B are spatially separated. The probability for an excursion from A to B,

$$P = \sum_i |A_i|^2 + \sum_{i,j} A_i A_j^*, \quad (13.15)$$

involves the sum of the square of each amplitude, A_i , as well as the interference terms between the paths, the second term in Eq. (13.15). When the end points are spatially separated, there is no special phase relationship between the paths. Consequently, the second term in Eq. (13.15) averages to zero. Hence, the Boltzmann treatment is adequate.

However, when A and B coincide, the result is quite different. Consider the loop shown in Fig. 13.4(a). Let A_1 represent the amplitude associated with the clockwise path around this loop and A_2 the amplitude for the time-reversed path. It is loops of this sort that are relevant in repeated scattering from the same impurity. We generate the time-reversed path from the direct path by the transformation $\mathbf{p} \rightarrow -\mathbf{p}$. Because phase coherence is maintained in the traversal of the closed loop, A_1 and A_2 interfere constructively, and as a result, we can set $A = A_1 = A_2$. Consequently, the quantum mechanical probability for traversing the closed loop is $P_{qm} = |A_1 + A_2|^2 = 4|A|^2$, while the classical result, $P_{cl} = |A_1|^2 + |A_2|^2 = 2|A|^2$, is a factor of 2 smaller, implying that backscattering effects are maximized in the

quantum mechanical case. Consequently, the return probability (or equivalently the likelihood of localization) in a quantum mechanical system always exceeds that in the corresponding classical problem. This state of affairs arises from the wave characteristics of an electron.

The contribution from closed-loop trajectories decreases the conductivity. Hence, $\delta\sigma$ enters with a minus sign. To estimate $\delta\sigma$, we must determine the probability that the diffusing particle traverses a closed loop without the loss of phase coherence. Consequently, the relevant time interval spans the minimum time for a single collision, τ , to the shortest time at which phase coherence is lost, τ_ϕ . Loss of phase coherence can arise from such disparate microscopic phenomena as phonon scattering (an explicitly inelastic process) and spin-flip scattering, which costs zero energy in the absence of a magnetic field. We focus on calculating the probability that an electron traverses the closed tube shown in Fig. 13.4(b). In this tube, the electron has a constant wavelength, $\lambda_F = \hbar/(v_F m)$. The volume of this tube is evolving in time through $d\ell = v_F dt$; hence, $dV = v_F \lambda_F^{d-1} dt$. If the particle were allowed to wander over all space, its mean-square displacement would increase as $D_0 t$, with D_0 the zeroth-order diffusion constant, which is proportional to σ_0 and hence scales as $1/\gamma$. The maximum “volume” element the particle would span scales as $V_{\max} \approx (D_0 t)^{d/2}$. The maximum value of this “volume” element is determined by the dephasing length, $L_\phi = \sqrt{D_0 \tau_\phi}$. The probability of finding the particle in the tube shown in Fig. 13.4(b),

$$P_{wl} = \int_{\tau}^{\tau_\phi} \frac{dV}{V_{\max}} = v_F \lambda_F^{d-1} \int_{\tau}^{\tau_\phi} \frac{dt}{(D_0 t)^{d/2}}, \quad (13.16)$$

is given by the ratio of dV to V_{\max} integrated over the time interval $[\tau, \tau_\phi]$. The probability P_{wl} is proportional to $\delta\sigma/\sigma_0$. Performing the time integral, we observe that the weak-localization correction

$$\frac{\delta\sigma}{\sigma_0} \approx -\gamma_d \begin{cases} \left(\frac{\tau_\phi}{\tau}\right)^{1/2}, & d = 1, \\ \hbar \ln\left(\frac{\tau_\phi}{\tau}\right), & d = 2, \\ \hbar^2 \left(\frac{\tau_\phi}{\tau}\right)^{-1/2}, & d = 3, \end{cases} \quad (13.17)$$

has a strong dimensional dependence, where $\gamma_d = \gamma v_F D_0^{-d/2} / (v_F m)^{d-1}$. The absence of \hbar implies that 1d weak localization is not quantum mechanical in origin, as far as the interference effects are concerned. Of course, factors of \hbar can be present in the inelastic relaxation time. Such quantum effects are different in kind from coherent backscattering. In $d = 1$, all paths are closed as there can only be forward and back scattering. Hence, there is no difference between the classical and quantum results in $d = 1$ as far as coherent backscattering is concerned. Second, to lowest order, the weak-localization correction is linear in γ .

If τ_ϕ is determined by phonon scattering or electron-electron interactions, then from Eqs. (11.96) and (12.67), $1/\tau_\phi \propto T^\eta$, where $\eta > 0$. For acoustic phonons, $\eta = 5$ (see Eq. (11.96)), whereas for electron-electron scattering in a Fermi liquid, $\eta = 2$ (see Eq. (12.67) and subsequent discussion). Substitution of this algebraic form for τ_ϕ leads to

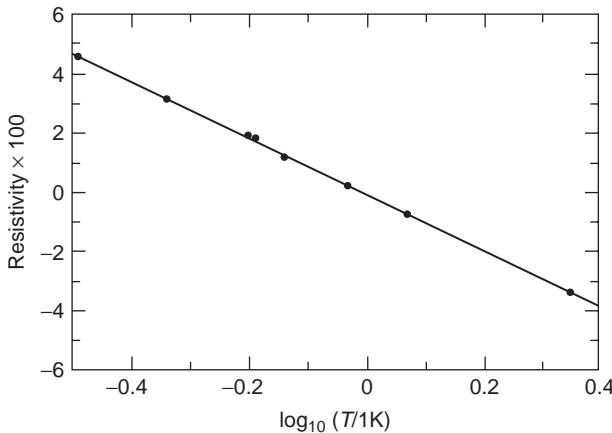


Fig. 13.5 Resistivity measurements of Dolan and Osheroff (DO1979) on weakly disordered thin films of palladium.

the temperature dependence

$$\frac{\delta\sigma}{\sigma_0} \approx -\gamma_d \begin{cases} T^{-\eta/2}, & d = 1, \\ \frac{\eta\hbar}{2} \ln(\frac{\hbar\tau}{k_B T}), & d = 2, \\ \hbar^2 T^{\eta/2}, & d = 3 \end{cases} \quad (13.18)$$

of the weak-localization correction. For $d \leq 2$, the temperature dependence is divergent as $T \rightarrow 0$. However, the expression we have derived here for $\delta\sigma/\sigma_0$ cannot exceed unity, in accordance with the initial assumption that $|\delta\sigma| \ll \sigma_0$. Hence, there is a lower limit to the temperature at which Eq. (13.18) can be used for $d \leq 2$. The resistivity measurements shown in Fig. 13.5 on weakly disordered palladium films have confirmed the logarithmic temperature dependence of weak localization (DO1979). In 3d, the weak-localization correction vanishes as $T \rightarrow 0$. This is a reflection of the relatively small probability an electron has of returning to the origin in a 3d weakly disordered system.

Our analysis of weak localization has shown that coherent backscattering plays a significant role in the localization problem. In fact, Vollhardt and Wölfle (VW1980) succeeded in developing a theory of the Anderson localization transition by including self-consistently the weak-localization terms to all orders, thereby reinforcing the fact that time-reversed trajectories are essential to localization. As such, it stands to reason that any external perturbation in a disordered system that disrupts time-reversal symmetry should destroy localization and, as a consequence, enhance the conductivity. Consider, for example, turning on a magnetic field. A magnetic field explicitly breaks the symmetry between \mathbf{p} and $-\mathbf{p}$. The momentum is now replaced by $\mathbf{p} - e\mathbf{A}/c$, where \mathbf{A} is the vector potential. The amplitudes along the direct and time-reversed paths are $A_1 \rightarrow Ae^{i\phi}$ and $A_2 \rightarrow Ae^{-i\phi}$, respectively, where

$$\phi = 2\pi \frac{\Phi}{hc/e}. \quad (13.19)$$

The magnetic flux is $\Phi = HR$, where R is the area of the region enclosed by the closed tube in Fig. 13.4(b). For diffusive motion, R is proportional to the mean-square displacement which scales as $D_0 t$. As a consequence, the return probability in the presence of a magnetic field

$$P_H = 4|A|^2 \cos^2 \left(\frac{eHD_0 t}{\hbar c} \right) \quad (13.20)$$

is an oscillatory function of time. It is left as a homework problem (13.2) to evaluate the corresponding magnetic field correction to the conductivity, $\Delta\sigma(H) = \delta\sigma(H) - \delta\sigma(0)$. This correction is always positive and proportional to $H^2 \tau_{\text{in}}^2$ at large fields and, at weak fields, grows logarithmically as $\ln(H \tau_{\text{in}})$. The critical field determining the crossover from the power law to $\ln H$ is found by setting $2eHD_0 \tau_{\text{in}}/\hbar c = 1$. Hence, the crossover field depends on the temperature. Experimentally, the crossover field is typically of the order of 100 G or, equivalently, 10 mT. The sensitivity of localization to such small magnetic fields reiterates that time-reversed scattering is the key physical origin of the localization transition.

A similar effect we are also equipped to treat is the breaking of phase coherence by spin-flip scattering. Spin-flip scattering weakens the localization effect, as it provides an effective oscillating magnetic field. To quantify this effect, we rely on the derivation of the spin-flip scattering time in Chapter 8. From Eq. (8.42), we have that

$$1/\tau_s = 1/\tau_s^0 \left(1 - 2J_0 N(0) \ln \frac{T_F}{T} + \dots \right). \quad (13.21)$$

Substitution of this result into Eq. (13.17) yields the contribution of spin-flip scattering to the conductivity,

$$\delta\sigma \approx \gamma\sigma_0 \left(\ln \frac{\tau_s^0}{\tau} - N(0)J_0 \ln \frac{T_F}{T} \right) \quad (13.22)$$

for a $d = 2$ sample.

Because $J_0 < 0$, the Kondo logarithmic term reduces the magnitude of the weak-localization correction. The reduction of the weak-localization correction by spin-flip scattering will ultimately lead to a disorder-induced suppression of the Kondo effect in thin films, as shown by Martin, Wan, and Phillips (MWP1997). This effect arises because the standard Kondo logarithm comes in with the opposite sign relative to the second term in Eq. (13.21). Consequently, if weak-localization physics dominates, disorder suppresses the Kondo resistivity, as is observed experimentally in thin-film metal alloys of Au(Fe) and Ag(Fe) (BG1995). Because spin-flip scattering counters weak localization, it is often invoked to explain deviations from the standard localization scenario. Consider, for example, the dephasing time, τ_ϕ . In an electronic system, phase coherence is lost by coupling to the environment. As in the case of phonon and electron-electron scattering, all standard dephasing mechanisms (A1980) turn off at low temperatures; consequently, τ_ϕ should diverge at low temperatures. In the late 1980s, several experiments (LG1987) reported that τ_ϕ

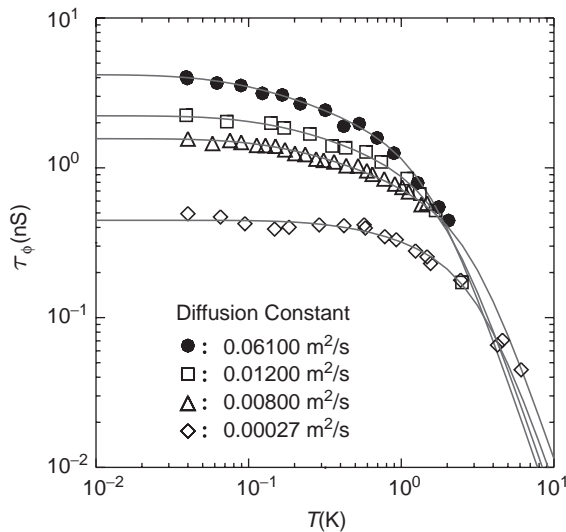


Fig. 13.6 Saturation of the electron dephasing time τ_ϕ observed in quasi-one-dimensional gold (Au) wires. The degree of disorder in these samples is denoted by the classical diffusion constant D_0 . The saturation time is typically longer and the saturation temperature is lower as the disorder decreases. The data are reprinted from P. Mohanty, E. M. Q. Jariwala, and R. A. Webb, *Phys. Rev. Lett.* **78**, 3366 (1997).

saturates at low temperatures. The possible role of magnetic impurities cast serious doubts on this result. However, recently more controlled experiments (MJW1997) have been performed and, as shown in Fig. 13.6, the saturation persists for a wide range of systems and down to temperatures $O(10 \text{ mK})$. The apparent saturation of τ_ϕ is one of the true surprises in the physics of metals. In fact, should the saturation of τ_ϕ as $T \rightarrow 0$ prove to be an intrinsic effect, as the current experiments seem to indicate, then this will place serious limitations on the degree to which quantum coherence can be controlled in conductors. As of this writing, there is no agreed-upon explanation for the saturation of τ_ϕ .

13.4 Scaling theory

The strong dimensional dependence of the weak-localization correction suggests that the localization transition should be highly dependent on the dimensionality of space. Even in the simpler problem of a single defect in an otherwise ordered system, dimensionality enters. As you will show in Problem 13.1, a single defect placed in an otherwise ordered lattice produces a bound state for $d \leq 2$, regardless of the strength of the defect. For $d > 2$, the defect strength must exceed a critical value for a bound state to form. Although the single defect results *cannot* be applied straightforwardly to the case of an infinite system containing a finite fraction of disordered sites, the strong dimensional dependence does suggest that the localization transition should somehow reflect this behavior. To this end,

we focus on the scaling theory of localization (A1979). The key assumption in this account is that, regardless of the dimensionality, a single parameter, the dimensionless conductance defined as

$$g(L) = \frac{2\hbar}{e^2} G(L), \quad (13.23)$$

is a universal function of the sample size, and it completely characterizes the localization transition. The conductance is $G(L)$, and L is the linear dimension of the sample. For a more complicated Hamiltonian containing random V s along with energy disorder, one-parameter scaling is not as immediately transparent as it is for the simple model in Eq. (13.1) with a single matrix element V and diagonal disorder of width W . Nonetheless, it describes this case as well.

Two other key ideas anchor the scaling theory of localization: (1) Fermi liquid theory completely describes the clean system, and (2) the logarithmic derivative of the conductance with respect to the system size is a monotonic function of the conductance, g . As we will see, these three postulates lead necessarily to an absence of current-carrying states for $d \leq 2$ and an absence of a minimum-metallic conductivity.

To develop the scaling account, we consider a hypercubic lattice with edge length L and increase the size of a unit cell of the lattice by a factor p . The new lattice constant is $L_1 = Lp$, where the new unit cell contains p^d old lattice sites. By our initial assumption, the localization properties in the new unit cell are determined entirely by $g(L_1)$. After m transformations, the new linear dimension is $L_m = Lp^m$. In such a sample, $g(L_m)$ characterizes the localization transition. A further consequence of the scaling assumption is that all of the $g(L_i)$ s must be related as a result of their universal length dependence. That is, we maintain that

$$g(pL) = f(p, g(L)). \quad (13.24)$$

Our goal is now to construct the universal function f . If the conductances are related when the sample size is increased, so are the eigenstates. Moreover, the new eigenstates in the scaled system must be constructible by knowing a single parameter, the dimensionless conductance. However, when the sample size is increased, there is a shift in both the energy level spacing, ΔW , and the energy of each eigenstate, ΔE . Consequently, when linear combinations of the eigenstates for the sample of length L_1 are taken to construct those of the sample of length L_2 , the crucial quantity of interest is $\Delta E/\Delta W$ (T1977). If a state is well localized within the initial sample size, changing the edge length from L to L_1 will not induce an energy shift, ΔE . Consequently, ΔE is generally computed by determining how sensitive the eigenstates are to a change in boundary conditions. A common boundary effect used in the computation of ΔE is a change from periodic to antiperiodic boundary conditions. As ΔE is largest for an extended state, and ΔW is determined by the density of states, the ratio $\Delta E/\Delta W$ should be a measure of the dimensionless conductance. This physical argument further supports the conclusion from one-parameter scaling that the dimensionless conductance must be given by the ratio $\Delta E/\Delta W$.

The mean spacing between the energy levels is simply given by the inverse of the number of particles in the system: $\Delta W = (n_e L^d)^{-1}$. Consequently, $g(L) = n_e L^d \Delta E$. What about ΔE ? From dimensional considerations, we can write $\Delta E = \hbar/\tau$, where τ represents some physical time associated with transport in our sample. Let us take τ to be the time it takes the particle to diffuse from the center to the edge of the sample (LT1975). That is, $\tau = (L/2)^2/D_0$, with D_0 the diffusion constant. Consequently, $\Delta E = 2\hbar\sigma/(e^2 n_e L^2)$, where we have used the Einstein relationship, $\sigma = 2e^2 n_e D_0$. Combining these relationships, we obtain

$$g(L) = \frac{2\hbar}{e^2} \sigma L^{d-2} = \frac{2\hbar}{e^2} G(L) \quad (13.25)$$

as the length dependence of our single parameter for the localization problem. In Eq. (13.25), $G(L) = \sigma L^{d-2}$ is the dc conductance. Note that the form given here for the conductance is simply Ohm's law for a metal. The crucial assumption, then, in one-parameter scaling theory is that the dimensionless conductance g relates the eigenstates in a sample of edge length $2L$ to those in an original sample of linear dimension L (A1979).

We define (A1979)

$$\beta = \frac{d \ln g(L)}{d \ln L} \quad (13.26)$$

as the logarithmic derivative of $g(L)$. As we mentioned in the context of the Kondo problem, $\beta(g)$ is referred to as the beta-function. The central physics of the localization problem is contained in $\beta(g)$. If in the limit that $L \rightarrow \infty$, $\beta(g) > 0$, then $g(L)$ must diverge. The divergence of the conductance is the signature of extended states. By contrast, if $\beta(g) < 0$ as $L \rightarrow \infty$, then $g(L)$ must monotonically tend to zero in this limit. Localization obtains in this case. It is evident, then, that the sign of $\beta(g)$ can be used to distinguish between localized and extended states. Invoking the assumption that $\beta(g)$ is a monotonic function of g or $\ln g$ leads necessarily to an absence of metallic behavior for $d > 2$. We proceed as follows. In the weak disorder limit, the conductance satisfies Ohm's law; that is, $G = \sigma L^{d-2}$. As a result, $\beta(g) = d - 2$ in the large conductance limit. In the limit of strong disorder, the localization length is much less than the sample size, $\xi \ll L$, and the conductance decays exponentially with L . This implies that $\beta(g) = \ln g$ is the form for the scaling function in the limit of strong disorder, $g \ll 1$. Our assumption of monotonicity guarantees that the strong disorder form for the conductance interpolates smoothly to the asymptotic value of $d - 2$ at weak disorder. Perturbative expansions in the weak-disorder regime (LN1966) in powers of $1/g$, as well as in the strongly localized regime in powers of g , confirm the assumption of monotonicity and continuous evolution between these two regimes. Consequently, $\beta(g) \leq 0$ for $d = 1, 2$, and all states are localized. A plot of the β -function illustrating this behavior is shown in Fig. 13.7. As is evident, $d = 2$ is the marginal dimension in which $\beta(g) = 0$ in the limit of large conductance. In $d = 3$, $\beta(g)$ crosses the $\ln g$ axis and asymptotically

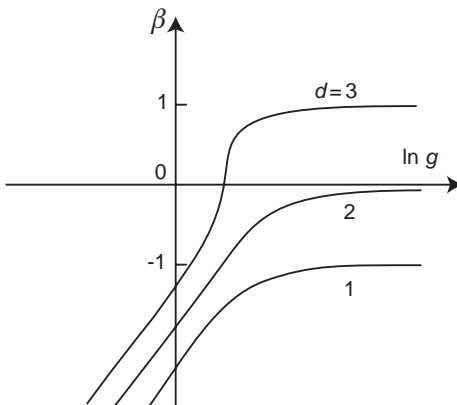


Fig. 13.7 Dimensional dependence of the scaling function $\beta(g) = d \ln(g)/d \ln L$ as a function of the conductance, g . For dimensions $d = 1, 2$, $\beta(g)$ is strictly negative and tends asymptotically to zero for large g in $d = 2$. This indicates the absence of a metal transition in $d = 1, 2$. In $d = 3$, $\beta(g)$ crosses the $\beta(g) = 0$ axis and asymptotically assumes the value of $d - 2$, therefore signaling the transition to a metallic state.

approaches unity, signaling an onset of metallic behavior. Note that the β -function is continuous in the vicinity of the $d = 3$ transition, hence the absence of a minimum metallic conductivity.

We extract the functional form of the conductance in the vicinity of the Anderson transition by considering the slope of the β -function near $\beta(g_c) = 0$. The zero of the β -function at g_c defines the critical or fixed point. In the vicinity of the critical point, g_c , we linearize the β -function such that

$$\beta(g) = \frac{g - g_c}{\nu g_c} = \frac{\delta g}{\nu}, \quad (13.27)$$

with ν a positive number determined by the slope. Near the transition point, the conductance is slowly varying. Consequently, we approximate the logarithmic derivative of the conductance by $(1/g_c)dg/d \ln L$. Combining this result with Eq. (13.27) yields

$$\frac{\delta g}{\nu} = \frac{1}{g_c} \frac{dg}{d \ln L}, \quad (13.28)$$

which we integrate in the interval $[L_0, L]$ to obtain

$$\frac{L}{L_0} = \left(\frac{g - g_c}{g_0 - g_c} \right)^\nu, \quad (13.29)$$

where $g_0 = g(L_0)$. The utility of Eq. (13.29) is made evident by first considering the localized regime in which $g_0 < g_c$. Introducing the length scale

$$\xi = L_0 \left(\frac{g_c}{g_0 - g_c} \right)^\nu = L_0 |\epsilon|^{-\nu} \quad (13.30)$$

allows us to conclude that, in the localized regime, the conductance

$$g = g_c \left(1 - \left(\frac{L}{\xi} \right)^{\frac{1}{v}} \right) \quad (13.31)$$

decreases algebraically with the length of the sample. The length scale ξ diverges at the transition point, g_c . As the localization length must diverge as the fixed point is approached from the insulating side, ξ is identified as the localization length (a key hypothesis of the gang of four, the colloquial name for the originators of the scaling theory), and v is its critical exponent. For sufficiently large samples, the conductivity obeys Ohm's law on the metallic side. However, at the critical point, the dc conductivity vanishes as $|\epsilon|^s$ with $s = (d - 2)v$. We prove the latter assertion by noting that the scaling hypothesis guarantees that the conductance is a universal function of L/ξ on all length scales. The behavior for $L \ll \xi$ is given by Eq. (13.29). At long length scales where Ohm's law is presumed to apply, the conductance must vary as $(L/\xi)^{d-2}$. Since the conductivity is defined as $\sigma(0) = g/L^{d-2}$, we have that

$$\sigma(0) \propto \xi^{2-d} \propto |\epsilon|^{(d-2)v}, \quad (13.32)$$

as advertised, and the conductivity vanishes continuously at the critical point, as opposed to the discontinuous drop predicted by Mott. Consequently, the localization length and conductivity exponents are related: $s = (d - 2)v$ (W1976). From the scaling analysis, $s = 1$ (see Problem 13.5). However, experimentally (T1982), s appears to vary between 1/2 and 1, depending on the degree of compensation. This evolution is shown in Fig. 13.8. For materials such as Nb_xSi_{1-x} or compensated Ge:Sb, $s = 1$; whereas for Si:P or uncompensated Ge:Sb, $s = 1/2$. In Si:P, each phosphorous atom gives up an electron. The random potential is due to the charged P-ions. Hence, there is a charge for each scattering center. In compensated Ge:Sb, equal amounts of Sb and B are added, which then exchange an electron. Hence, the number of scatterers exceeds the number of charge carriers in the compensated samples. Consequently, disorder plays a larger role in compensated than in uncompensated systems and hence the improved agreement with scaling theory. In the uncompensated materials, additional interactions, such as spin-orbit or electron-electron repulsion, are operative. Inclusion of such effects leads to a conductivity exponent of $s = 1/2$ (LR1985).

The logarithmic behavior of the weak-localization correction can also be seen by considering the asymptotic form for the β -function in two dimensions. Figure 13.7 illustrates that in $d = 2$, the β -function is always negative and goes to zero asymptotically as roughly $-1/g$, a result confirmed also from perturbative analyses. Integration of this asymptotic form in the interval $[L_0, L]$ leads to the familiar

$$g_{d=2}(L) = g(L_0) - \ln \frac{L}{L_0} \quad (13.33)$$

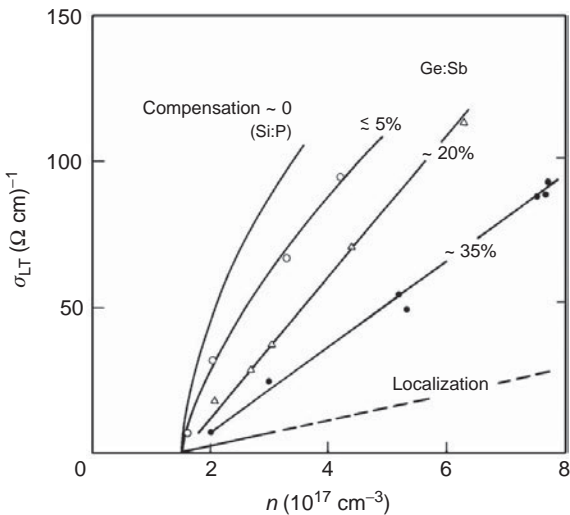


Fig. 13.8 Evolution of the conductivity exponent from $s = 1/2$ in the uncompensated semiconductor, Si:P, towards the value of $s = 1$ predicted from scaling theory (dashed line) as the compensation is increased in Ge:Sb: $s = 0.55$ at 0%, $s = 0.7 \pm 0.2$ at 5%, $s \approx 1$ at 20%, and $s \approx 1$ for 35% compensation. σ_{LT} is the low-temperature conductivity. Compensation increases the disorder and hence the increased validity of the disorder model of Anderson for which scaling theory predicts that $s = 1$. The data are taken from G. A. Thomas *et al.*, *Phys. Rev. B* **25**, 4288 (1982).

logarithmic decrease of the conductance as the system size increases. As with weak localization, this result is only valid as long as the second term remains smaller than the first. Consequently, there is a length cut-off beyond which perturbation theory fails.

The breakdown of perturbation theory at low temperatures or as $L \rightarrow \infty$ signifies an onset of the strong-localization regime. It turns out that the weak-localization argument presented above can be modified to tackle qualitatively the strong-localization problem. In the spirit of the argument presented above, we formulate the probability that a particle does not return to the origin during the time interval, $[\tau, \tau_\phi]$. The conductivity is directly proportional to this quantity. The probability that the particle does not return to the origin is equal to the product of the probabilities

$$P_{\text{no return}} = \prod_{i=1}^N \left(1 - \frac{\lambda_F^{d-1} v_F \Delta t_i}{(D_0 t_i)^{d/2}} \right) = \exp \left(- \sum_i \frac{\lambda_F^{d-1} v_F \Delta t_i}{(D_0 t_i)^{d/2}} \right) \quad (13.34)$$

that the particle does not return during any differential time element Δt_i . The conversion of the sum to an integral is left as an exercise (Problem 13.4). The result is analogous to the standard weak-localization result. However, the difference now is that the integral is in the exponent. For a 2d sample, we obtain that the conductivity

$$\sigma_{d=2} \approx \frac{e^2}{\hbar} \left(\frac{\ell}{L_\phi} \right)^{1/k_F \ell a} \quad (13.35)$$

scales algebraically with the dephasing length, but for a thin 1d wire, the conductivity

$$\sigma_{d=1} \approx \frac{e^2}{\hbar} L_\phi \exp\left(-\frac{1}{(k_F a)^2} \frac{L_\phi}{2\ell}\right) \quad (13.36)$$

decays exponentially with the phase coherence length. Exponential decay of the conductivity in 1d is the standard signature of the localizing effect of disorder. However, for 2d, the analysis presented here is insufficient to describe coherent backscattering effects that lead to exponential localization of the eigenstates.

While the scaling theory of localization has been highly successful, it does not constitute a mathematical proof that the return probability remains finite in $d = 1, 2$. Currently, there is no rigorous mathematical proof on the fate of the return probability for quantum transport in a d -dimensional random system. Nonetheless, the scaling analysis of the localization problem has received much support from more rigorous theories and numerical simulations, as well as from experiments (as seen in the preceding paragraph). As mentioned in the previous sections, the Green function calculations of Sokoulis and Economou (SE1984) confirmed an absence of extended states in a $d = 2$ disordered square lattice. Further support for the scaling theory of localization can be found in the work of Vollhardt and Wölfle (VW1980), who have shown that the dimensional predictions of scaling theory can be reproduced by a self-consistent diagrammatic expansion of the density response function for a system of independent particles moving in a random potential. A further key result of this work is that much of the physics of the localization problem can be obtained by analyzing the maximally crossed diagrams. Such diagrams contain the contribution from coherent backscattering. It is these diagrams that we will focus on in the next section, as they contain the essence of weak-localization physics. Other, more recent analytical work that has verified the scaling predictions is the random matrix theory approach of Muttalib (M1990). Based on earlier work by Imry (I1986), Muttalib has shown how the most probable value of the conductance can be calculated from the distribution of eigenvalues for the transfer matrices. One-parameter scaling theory follows immediately (M1990) once it is assumed that the distribution of eigenvalues of the transfer matrices is described by a single parameter. Although this assumption does not appear to hold for strong disorder, it is supported by numerical simulations in the presence of weak disorder (M1990). Only the weak disorder limit is of interest here, because it is in this regime that the one-parameter scaling function predicts an absence of a metal transition for $d = 1, 2$.

13.5 Exceptions to localization

The absence of current-carrying states in $d = 1, 2$ is one of the truly surprising results in disordered systems. As mentioned in the previous section, when time-reversal symmetry is broken, current-carrying states can survive in low dimensions. However, even when time-reversal symmetry is intact, three important exceptions exist to the localization principle: (1)

the random dimer model in which the disorder is correlated, (2) insulator–superconductor transitions in thin films, and (3) the newly-discovered conducting state in dilute 2d electron gases. In this section, we will review all three. However, our discussion of the latter two will be brief.

13.5.1 Random dimer model

In the models discussed thus far, the site energies or matrix elements were strictly statistically independent entities assigned from a single random distribution. In any real physical system, however, the site energies and matrix elements are correlated. Until the mid 1980s, there were strikingly few studies (JK1986) on the role of statistical correlations on the localization transition, partly because of the suspicion that correlations naturally present in real systems cannot be determined with any sort of certainty. Hence, the physical significance of proposed models would not be clear. For example, consider the eigenvalue equation

$$Ec_n = \epsilon_n c_n + V_{n,n+1} c_{n+1} + V_{n,n-1} c_{n-1} \quad (13.37)$$

for the site amplitudes in a nearest-neighbor tight-binding Hamiltonian for a linear chain. In the event that $-\epsilon_n = V_{n,n+1} + V_{n,n-1}$, the eigenvalue equation reduces to

$$Ec_n = V_{n,n+1}(c_{n+1} - c_n) + V_{n,n-1}(c_{n-1} - c_n), \quad (13.38)$$

which is identical in form to a diffusion equation for the probabilities with random nearest-neighbor hopping rates. This equation is well known to have a diffusion pole at $E = 0$; that is, the state with $E = 0$ is extended (A1981). Hence, the simple model used here for the correlated disorder has a diffusive mode. Except in the context of structural disorder, the correlation leading to Eq. (13.38) is, at best, artificial at the electronic level. Flores (F1989) has explored additional algebraic correlations between the site energies and matrix elements and found that an infinitesimal fraction of the electronic states possessed zero reflection coefficients and, hence, are extended in one dimension. This result is indeed surprising in light of the scaling arguments presented earlier, which prohibit extended states in one dimension.

To understand what minimal physical condition must be satisfied for 1d systems to possess extended states, we consider the model introduced by Dunlap, Wu, and Phillips (DWP1990) called the random dimer model (RDM). To put the RDM in context, consider the random binary alloy. In the tight-binding model of a random binary alloy, site energies ϵ_a and ϵ_b are assigned at random to the lattice sites with probability p and $1 - p$, respectively. A constant nearest-neighbor matrix element, V , mediates transport among the lattice sites. All states in this model are localized. A typical wavefunction in a random binary alloy is shown in Fig. 13.2. The RDM can be obtained from the binary alloy by replacing all clusters containing an odd number of ϵ_b s with clusters containing the same number of ϵ_a s. The result is a random lattice in which the b -defects occur randomly but in pairs. The RDM refers to any lattice in which at least one of the site energies is assigned at random to pairs of lattice sites. A typical dimer in the RDM is shown in Fig. 13.9. The surprising feature

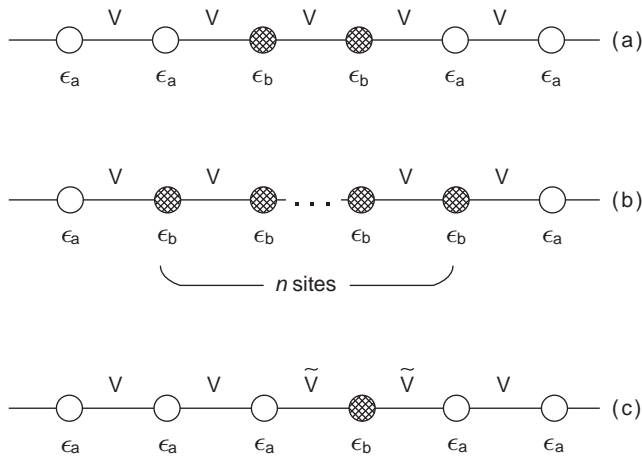


Fig. 13.9 (a) Dimer defect in the RDM, (b) n -site defect possessing the dimer symmetry, and (c) defect in the repulsive binary alloy.

of the RDM is that \sqrt{N} of the electronic states remain extended over the entire sample, provided that $-1 \leq W \leq 1$, with

$$W = \frac{\epsilon_a - \epsilon_b}{2V}. \quad (13.39)$$

An additional feature of the RDM is that the mean-square displacement of an initially localized particle grows superdiffusively as $t^{3/2}$, provided that $-1 < W < 1$. Diffusion obtains only when the disorder is increased, such that $W = \pm 1$. In all other cases, the particle remains localized at long times. The presence of at least diffusive transport is the key feature that ensures that the RDM does represent a counter-example to the scaling argument prohibiting long-range transport in 1d.

The simplest way to understand the RDM is to calculate the reflection coefficient through a dimer placed in an otherwise ordered lattice with unit lattice constant. Let us place the dimer on sites 0 and 1 with energy ϵ_b . We assign the energy ϵ_a to all other lattice sites. To compute the reflection (R) and transmission (T) amplitudes, we write the site amplitudes as

$$c_n = \begin{cases} e^{ikn} + Re^{-ikn}, & n \leq -1, \\ Te^{ikn}, & n \geq 1 \end{cases} \quad (13.40)$$

where k is the dimensionless wavevector. The site amplitude at the origin is determined by substituting Eq. (13.40) into the eigenvalue equation, Eq. (13.37), for sites 1 and -1 . The result is that $c_0 = 1 + R = T(\epsilon_- e^{-ik} + V)/V$ with $\epsilon_- = \epsilon_a - \epsilon_b$. Substituting this result into the eigenvalue equation for site 0 yields the closed-form expression

$$|R|^2 = \frac{(W + \cos k)^2}{(W + \cos k)^2 + \sin^2 k} \quad (13.41)$$

for the reflection probability. We see then that the reflection coefficient vanishes when $W = -\cos k$, which will occur for some value of k as long as $-1 \leq W \leq 1$. The location in the parent ordered band of the perfectly transmitted electronic state corresponds to the wavevector $k_o = \cos^{-1} W$. At k_o , there is no difference between the ordered and disordered bands; the densities of states coincide at this point. The vanishing of the reflection coefficient through a single dimer at a particular energy can be understood as a resonance effect. That is, the dimers are acting as resonance cavities. At a particular wavevector, $k_o = \cos^{-1} W$, the reflection from the second site in the dimer is 180° out of phase from the reflection from the first. At this energy, unit transmission obtains.

Consider the disordered case. Because the transmission coefficient through a single dimer is unity, the particular distribution of random dimers should not affect the perfectly transmitted states. Indeed, this is true, as can be seen from the following argument. Transport across an arbitrary segment of the RDM can be represented by $\dots T_a^{n_1} T_b^{2n_2} T_a^{n_3} T_b^{2n_4} \dots$ where the n_i s are random variables and T_n is the transfer matrix. Notice that the b -transfer matrices all occur an even number of times. This is the dimer constraint. From the eigenvalue equation for the site amplitudes, Eq. (13.37), the transfer matrix is given by

$$\begin{pmatrix} c_{n+1} \\ c_n \end{pmatrix} = \begin{bmatrix} \frac{E-\epsilon_b}{V} & -1 \\ 1 & 0 \end{bmatrix} \begin{pmatrix} c_n \\ c_{n-1} \end{pmatrix} = T_n \begin{pmatrix} c_n \\ c_{n-1} \end{pmatrix}. \quad (13.42)$$

The resonant condition $W = -\cos k$ is equivalent to $E = \epsilon_b$, because E is the energy of the ordered band. At this energy, the transfer matrix across a b -defect reduces to

$$T_b = \begin{bmatrix} 0 & -1 \\ 1 & 0 \end{bmatrix}. \quad (13.43)$$

The square of this matrix (which corresponds to the transfer matrix across a b -dimer) is the negative of the unit matrix. At resonance, then, the product of the transfer matrices in the RDM commutes and the b -dimers can simply be erased at the expense of a sign change. Consequently, the phase shift through a dimer defect is $\Omega = -2k + \pi$. The unscattered state corresponds to a Bloch state in which the dimer sites have been effectively decimated at the cost of a phase shift at the dimer sites. Hence, once an electron passes through a single dimer defect, it will not scatter from any other dimer defects, as all dimers possess the identical resonance condition regardless of their placement. If dimers are placed at sites 0, 1 and 2, 3, the unscattered state is

$$\dots, e^{-2ik}, e^{-ik}, 1, -e^{-ik}, -1, e^{-ik}, 1, e^{2ik}, \dots \quad (13.44)$$

An example of such an unscattered state is plotted in Fig. 13.10.

Of course, no transport would obtain if only a single electronic state remained unscattered. To determine the total number of states that extend over the entire sample, we expand R around k_o . To lowest order, we find that in the vicinity of k_o , $|R|^2 \propto (\Delta k)^2$, where $\Delta k = k - k_o$. The time between scattering events, τ , is inversely proportional to the reflection probability. As a result, the mean-free path $\ell = v_F \tau \propto 1/(\Delta k)^2$ in the vicinity of k_o . Upon equating the mean-free path to the length of the system N , we find that the total number (ΔN) of states whose mean-free path is equal to the system size scales as $\Delta N = \sqrt{N}$. Because the mean-free path and the localization length are equal in one

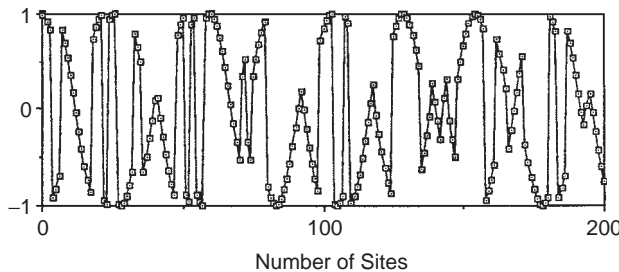


Fig. 13.10 The real part of a typical extended state in the random dimer model.

dimension, we find that the total number of states whose localization lengths diverge is \sqrt{N} . The single-dimer argument presented here has been shown to hold for a random system by Bovier (B1992). Bovier's argument is particularly elegant and establishes rigorously that the Lyapunov exponent (inverse localization length) vanishes quadratically (as a function of Δk_0) in the vicinity of the resonance, $k_0 = \cos^{-1} W$. Consequently, in the RDM, \sqrt{N} of the electronic states remain extended over the total length of the sample.

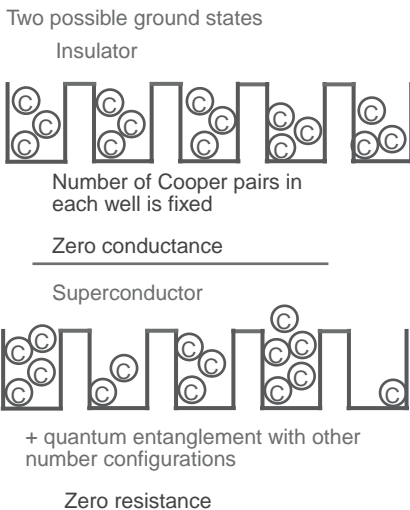
These states ultimately contribute to the transport properties. Because the mean-free path of the extended states in the RDM is at least the system size, such states move through the crystal ballistically with a constant group velocity [$v(k)$], except when they are located at the bottom or top of the band where the velocity vanishes. Because all the other electronic states are localized, we determine the diffusion constant by integrating $v(k)\ell(k)$ over the width of states that participate in the transport. The upper limit of the integration is then proportional to the total fraction of unscattered states, or $\ell(k)/\sqrt{N}$ and $\ell(k) \approx N$. When the velocity is a non-zero constant, we obtain that the $D \approx \sqrt{N}$. Because the states that contribute to transport traverse the length of the system with a constant velocity, the distance that they cover scales as a linear function of time. Hence, $N \propto t$ and $D \approx t^{1/2}$. Hence, the mean-square displacement grows as $t^{3/2}$. At the bottom or top of the band where the group velocity vanishes, $v(k) \propto k$ and $D \propto O(l)$. This illustrates that the narrow band of extended states in the RDM is sufficient to give rise to delocalization of an initially localized particle. It is certainly a curious feature of the RDM that so few states do so much.

Nonetheless, the RDM is completely compatible with the localization criterion based on the imaginary part of the self-energy. On this account, if as E approaches the real axis, $\text{Im } S(E) \rightarrow 0$, then the eigenstates are localized. $\text{Im } S(E)$ will be non-zero only if $G(E)$ has an imaginary part or equivalently has a branch point singularity. An infinitesimal number of extended states is not sufficient in the thermodynamic limit to give rise to a branch cut of non-vanishing width. Consequently, $\text{Im } S(E)$ will vanish for all energies in the RDM. The self-energy localization criterion is insensitive to a set of extended states of zero measure. What is surprising is that these states are sufficiently numerous to give rise to long-range transport. Pendry (P1987) has shown that in standard disordered models, isolated states at particular energies remain extended over \sqrt{N} of the lattice sites. However, the number of states that behave in this fashion is exponentially small and hence, of no consequence.

The essence of the RDM is that at an energy in the band, the defect transfer matrices reduce to the negative of the unit matrix (WGP1992). Consequently, at the dimer resonance, perfect transmission occurs from one side of the sample to the other. Local dimer correlations create this macroscopic quantum effect. It is straightforward to show that this result holds only if the site energies of the dimer are equal; that is, the dimer is symmetric. A plane of symmetry is a necessary and sufficient condition for a defect to possess a resonant state. The general statement that can be made is as follows. *The standard tendency of disorder to localize electronic states is suppressed at certain energies in the band whenever the defects contain a plane of symmetry.* This is the minimal requirement for extended states to exist in 1d. The RDM is just the simplest model in which the defects possess a plane of symmetry. Any random n -mer will suffice, as shown in Fig. 13.9(b). In addition, the single defect model shown in Fig. 13.9(c) is the off-diagonal dual of the RDM. Similar delocalization occurs in this model as well (P1993). Such simple correlated disorder models continue to be an active field of study. In fact, experiments in GaAs/AlGaAs heterostructures (B1999) in which RDM correlations were engineered have confirmed the existence of the extended states in the random dimer model.

13.5.2 Insulator–superconductor transitions

In the second class of exceptions, localization is thwarted by strong electron interactions. In the first case, we consider the transition from an insulator to a superconductor in thin films. While single electrons are localized by disorder, electrons forming Cooper pairs can become delocalized in 2d. Experimentally, a direct transition from a superconductor to an insulator in 2d has been observed by two distinct mechanisms. The first is simply to decrease the thickness of the sample (J1989; GM1998). This effectively changes the scattering length and hence is equivalent to changing the amount of disorder. As a result, Cooper pairs remain intact throughout the transition. However, in the insulator they are localized, whereas in the superconductor they form a coherent state. To understand how Cooper pairs can be tuned between the insulating and superconducting extremes, consider Fig. 13.11. As illustrated in Fig. 13.11, formation of Cooper pairs is not a sufficient condition for superconductivity. If one envisions dividing a thin film into partitions, as illustrated in Fig. 13.11, insulating behavior obtains if each partition at each snapshot in time has the same number of Cooper pairs. That is, the state is static. However, if the number of pairs fluctuates between partitions, transport of Cooper pairs is possible and superconductivity obtains. As shown in Chapter 12, phase and particle number are conjugate variables in a superconductor. If the phase is sharp, then the particle number is completely indeterminate. Likewise, complete determination of the particle number leads to infinite uncertainty in the phase. However, destruction of phase coherence suppresses superconductivity. Hence, a transition from an insulating state of Cooper pairs to a superconducting one obtains when an external parameter is tuned so that global phase coherence is instated. Film thickness or disorder is one such parameter. At criticality, the resistivity will be independent of temperature. Hence, Cooper pairs on the brink of losing their global phase coherence acquire a finite resistivity at zero temperature, as in a metal. This is a particularly important point because it illustrates that there are three

**Fig. 13.11**

Insulating and superconducting ground states of Cooper (C) pairs illustrating the conjugacy between phase and number fluctuations of the Cooper pairs. In the insulator, Cooper pair number fluctuations cease, leading to infinite uncertainty in the phase. In contrast, in a superconductor, phase coherence obtains, leading thereby to infinite uncertainty in the Cooper pair particle number.

options ([J1989](#); [GM1998](#); [F1990](#)) for Cooper pairs when they are confined to a plane: (1) an insulator with infinite resistivity, (2) a superconductor with vanishing resistivity, and (3) a metal with finite resistivity at zero temperature. Only the first is possible for single electrons. For Cooper pairs, phase coherence is maintained at sufficiently weak disorder, but above a critical value of the disorder, phase coherence is lost and insulating behavior with a divergent resistivity obtains. Regardless of the mechanism that drives an insulator–superconductor transition, it is the uncertainty relationship between the phase and particle number that ultimately leads to an evolution between the zero-resistance and divergent-resistance state.

The second means by which a superconducting state can be transformed to an insulator in 2d is by applying a perpendicular magnetic field ([YK1995](#); [MK1999](#); [HP1990](#)) on the superconducting side. Shown in Fig. 13.12 is the resistivity as a function of temperature for a magnetic field-tuned insulator–superconductor transition. Above a critical value of the magnetic field, the Cooper pairs are destroyed and insulating behavior obtains by means of single-particle localization. Once again, the resistivity is independent of temperature at the separatrix between these two phases. However, the surprise with this data is the presence of an apparent flattening (see inset in Fig. 13.12) of the resistivity at low temperatures on the “superconducting” side. That is, rather than continuing to drop to zero as is expected for a superconductor, the resistivity saturates ([YK1995](#); [E1996](#)). Identical behavior has been observed in the thickness-tuned transitions as well. The non-vanishing of the resistivity is indicative of a lack of phase coherence. Phase fluctuations are particularly strong in $d = 2$ and are well known to widen the temperature regime over which the resistivity

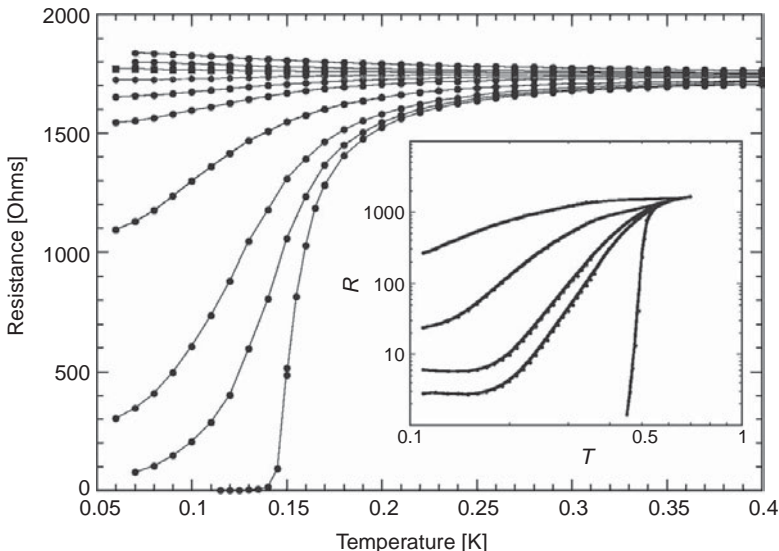


Fig. 13.12 Electrical resistance of MoGe thin film plotted vs temperature at $B = 0, 0.5, 1.0, 2.0, 3.0, 4.0, 4.4, 4.5, 5.5, 6$ kG. The sample becomes a superconductor at 0.15 K in zero field, but for fields larger than about 4.4 kG the sample becomes insulating. At fields lower than this but other than zero, the resistance saturates. The saturation behavior is better shown in the inset for another sample with a higher transition temperature. The inset shows data for $B = 0, 1.5, 2, 4$, and 7 kOe. At higher field, this sample is an insulator. The data is taken from A. Yazdani and A. Kapitulnik, *Phys. Rev. Lett.* **74**, 3037 (1995).

drops to zero. In addition, a perpendicular magnetic field creates resistive excitations called vortices (the dual of Cooper pairs) which frustrate the onset of global phase coherence. Nonetheless, no theoretical account has been able to explain adequately the apparent non-vanishing of the resistivity on the “superconducting” side as the temperature tends to zero. In fact, at this writing, the possible existence of an intervening metallic phase ([MK1999](#)) on the superconducting side is the outstanding problem in the insulator–superconductor field.

13.5.3 Conducting state in dilute electron gas

The final exception to localization is yet another surprise from electrons moving in a plane. In the experiments revealing the possible existence of a new conducting phase, the tuning parameter is the concentration of charge carriers ([K1996; PFW1997; S1998; H1998](#)). Electrons (or holes) were confined to move laterally at the interface between two semiconductors as in a Si metal-oxide-semiconductor-field-effect transistor (MOSFET) or in a quantum well, as in the case of GaAs. In both systems, the electron density is controlled by adjusting the bias voltage at the gate. For electrons (holes), the more positive (negative) the bias, the higher the electron density. Devices of this sort are identical to those used in the study of the quantum Hall effect (see Chapter 15). As illustrated in Fig. 13.13, when

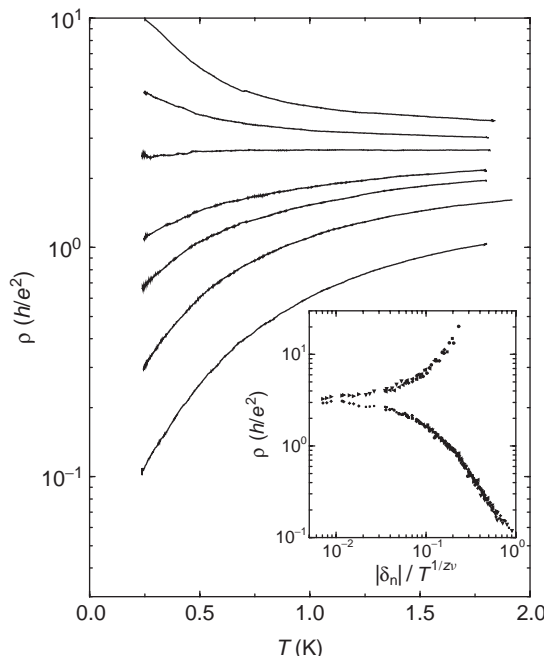


Fig. 13.13 Resistivity (ρ) vs temperature for two-dimensional electrons in silicon in zero magnetic field and at different electron densities (n) (from top to bottom: $0.86, 0.88, 0.90, 0.93, 0.95, 0.99$, and 1.10×10^{11} per cm^2). Collapse of the data onto two distinct scaling curves above and below the critical transition density (n_c) is shown in the inset. Here $\delta = (n - n_c)/n_c$, $z = 0.8$ and $\nu = 1.5$.

the electron density is slowly increased beyond $\approx 10^{11}/\text{cm}^2$, the resistivity changes from increasing (insulating behavior) to decreasing as the temperature decreases, the signature of conducting behavior. At the transition between these two limits, the resistivity is virtually independent of temperature. While it is still unclear ultimately what value the resistivity will acquire at zero temperature, the marked decrease in the resistivity above a certain density is totally unexpected and, more importantly, not predicted by any theory. Whether we can correctly conclude that a zero-temperature transition exists between two distinct phases of matter is still not settled, however. Nonetheless, the data do possess a feature common to quantum phase transitions such as insulator–superconductor transitions (S1999), namely scale invariance. In this context, scale invariance simply implies that the data above the flat region in Fig. 13.13 all look alike. This also holds for the data below the flat region in Fig. 13.13. As a consequence, the upper and lower family of resistivity curves at various densities can all be made to collapse onto just two distinct curves by scaling each curve with the same density-dependent scale factor. The resultant curves have slopes of opposite sign, as shown in the inset of Fig. 13.13. The product of exponents that arises in this case is the correlation length (or localization length) exponent, as well as the dynamical exponent, z . In quantum phase transitions, an energy scale vanishes at the critical point as $\Omega \propto \xi^{-z}$. It is difficult to reconcile such scaling behavior unless the two phases are electrically distinct at zero temperature.

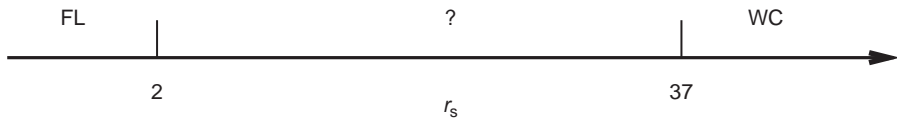


Fig. 13.14

Density regimes and what is known definitively about them for a 2d electron gas. At low density, a Wigner crystal (WC) forms, while at high density, a Fermi liquid (FL) arises. Both of these phases are localized by disorder. The Wigner crystal melting boundary has been determined by B. Tanatar and D. Ceperley, *Phys. Rev. B* **39**, 5005 (1989). The new conducting phase lies between these two regimes. It is unclear what state of matter forms in this regime.

Key experimental features (SK1999) that characterize the transition are as follows: (1) the existence of a critical electron or hole density, n_c , above which the conducting phase appears, (2) a characteristic temperature, typically of the order of half the Fermi temperature, T_F , below which the resistivity on the conducting side decreases roughly as $\rho_1 + \rho_0(T)$, where $\rho_0(T) \approx \rho_0 \exp(-T_0/T)$, (3) critical scaling, indicative of a quantum critical point, in the vicinity of the insulator–conducting phase transition, (4) non-linear current–voltage (I–V) curves, (5) suppression of the conducting phase by an in-plane magnetic field and magnetic impurities, and (6) a continuous evolution of the new conducting phase into some quantum Hall state once a perpendicular magnetic field is applied.

There is currently no agreed-upon explanation for these phenomena. In fact, some have proposed that there is ultimately no transition, and the resistivity downturn is really a refrigeration problem. Perhaps physics pertaining to the details of silicon (PF2005), rather than from non-perturbative effects arising from the electron interactions, are relevant. Regardless of what the ultimate answer is to this problem, these experiments have helped focus attention on the ground state of a dilute electron gas. We know definitively that at high and ultra-low densities, a 2d electron gas is localized by disorder. These regimes are distinguished by the magnitude of the Coulomb interaction between the electrons relative to their kinetic energy. As discussed in Chapter 6, because the Coulomb interaction decays as $1/r$ (with r the separation between the electrons) whereas the kinetic energy decays as $1/r^2$, Coulomb interactions dominate at low density. Consequently, in the high density regime, electrons are essentially non-interacting and insulating behavior obtains, as dictated by the Anderson localization principle. In the ultra-low density regime where the kinetic energy is almost zero, the Coulomb interaction drives the physics. In this limit, the electrons minimize the Coulomb interaction by being as far away from one another as possible, resulting in a crystalline array or Wigner crystal which is pinned by any amount of disorder, and hence, is an insulator. It is precisely between the Wigner limit and the non-interacting regime that the new conducting phase resides. As illustrated in Fig. 13.14, this density regime represents one of the yet-unconquered frontiers in solid state physics, as nothing definitive is known about the ground state that obtains when a Wigner-type crystal is destroyed upon increasing the carrier concentration. We placed the termination of the Fermi liquid regime at the value of r_s at which the compressibility changes sign and becomes negative (see Problem 9.6). Experimentally, the transition to the conducting state is accompanied by a sign change in the compressibility (DJ2000; I2000). A negative compressibility is a common instability in a dilute electron system, signifying an instability to a uniform density

state. If the compensating charge background is rigid, however, the ions cannot move to mediate a non-uniform electron state. Hence, the charge instability is not realized. Prior to the Si MOSFET and GaAs experiments, there was some anticipation that if a metallic phase could exist in 2d, it would obtain in the perturbative regime ($r_s \ll 1$) (LR1985). However, this does not appear to be the case. The new conducting phase occurs precisely in the non-perturbative regime where Fermi liquid theory cannot be assumed to be valid *a priori*.

Wigner crystals share a class resemblance to their correlated cousin, Mott insulators. The original argument (M1949) for a Mott insulating state was based on a lattice of one-electron atoms. Single occupancy of each site produces a half-filled band which typically permits free conduction of the electrons. However, Mott proposed that, as the lattice separation increases, the overlap can decrease so drastically that the electronic band reduces to the localized atomic states. In this limit, each atom is neutral, and hence no transport of charge is possible. Nonetheless, the band remains half filled. Consequently, like the Wigner crystal, the Mott insulating state obtains in the dilute regime where the Coulomb effects dominate.

Dilute electron systems, such as Mott insulators, are susceptible to numerous instabilities, the most notable of which is superconductivity. For example, the entire family of organic conductors (M1997) and the copper oxide high-temperature superconductors (A1992) are Mott insulators in the undoped state. Upon doping, both classes of materials become superconducting. In fact, it appears to be an experimental fact that doped Mott insulators composed from layered materials exhibit superconductivity in the vicinity of a charge or spin-ordered state. Why this state of affairs obtains continues to be one of the lasting puzzles in solid state physics. By analogy, some have proposed (P1998; BK1998) that a 2d electron gas in the vicinity of the Wigner crystal melting boundary should behave no differently. But this proposal is likely irrelevant to the experiments as there is no sign that the charge carriers are $2e$ rather than e in the new conducting phase. Clearly, further experiments are needed to settle the ultimate cause of the metallic state in a dilute 2d electron gas.

Summary

Localization obtains from phase-coherent backscattering. Such processes lead to a non-vanishing of the electron return probability and the subsequent absence of a metallic state for $d \leq 2$. Application of a magnetic field or the introduction of nearest-neighbor correlations of the dimer type can counteract the natural tendency of disorder to localize electronic states. These seemingly unrelated effects share a common origin, however. In the context of a magnetic field, the breaking of the discrete symmetry of time reversal diminishes the contribution of electron backscattering to the conductivity. In the random dimer model, a transmission resonance in the presence of defects that possess a plane of symmetry leads to a vanishing of the reflected or backscattered wave. It is the complete absence of backscattering that gives rise to long-range transport in models of the RDM

type. The other exceptions to localization occur in two dimensions and involve the electron interaction. Both problems are currently not settled, neither experimentally nor theoretically.

Problems

- 13.1 Consider a linear chain with a single defect placed at the m th site. Let the site amplitude be c_n and W the strength of the defect in a linear chain described by the following evolution equation:

$$Ec_n = \epsilon c_n + V(c_{n+1} + c_{n-1}) + W\delta_{nm}c_m. \quad (13.45)$$

Use the method of defects to show that a single bound state forms outside the continuous band for $W \neq 0$. To implement this method, use the following procedure.

(1) Multiply the eigenvalue equation by e^{ikn} and sum over n . (2) Then multiply the resultant equation by e^{-ikm} and integrate to obtain as a condition for the location of the bound state

$$1 = W\langle G(E) \rangle, \quad (13.46)$$

where

$$\langle G(E) \rangle = \frac{1}{2\pi} \int_{-\pi}^{\pi} \frac{dk}{E - \epsilon(k)} \quad (13.47)$$

with $\epsilon(k) = \epsilon + 2V \cos k$. Show that if $W > 0$, the bound state lies above the band, that is, at an energy $E > \epsilon + 2V$, whereas for $W < 0$, the bound state lies below the band. Repeat the same calculation for $d = 2$.

- 13.2 In the presence of a magnetic field, the total change of the conductivity, $\delta(H) - \delta(H = 0)$, depends on the difference between P_H and $P_{H=0}$. Use Eq. (13.20) to calculate this difference and integrate the result using Eq. (13.16). Define $x = 2HD_0\tau_{in}/c$ as a measure of the field strength. Show that when $x \ll 1$, $\Delta(H) \propto H^2\tau_{in}^2$. In the opposite limit $x \gg 1$, show that $\Delta(H) \propto \ln(H\tau_{in})$.
- 13.3 Show that the extended state in the off-diagonal dual of the RDM, see Fig. 13.9(c), differs from a perfect Bloch state by only a multiplicative factor V/\tilde{V} at the site of each defect.
- 13.4 Convert the sum to an integral in Eq. (13.34) and evaluate the conductivity for a thin film ($d = 2$) and for a wire ($d = 1$). You should obtain Eqs. (13.35) and (13.36), respectively.
- 13.5 Assume that in the Ohmic regime, the general form for the β -function is

$$\beta = d - 2 - \frac{A_d}{g}. \quad (13.48)$$

Integrate this quantity in the interval $[L_0, L]$ and obtain the explicit length dependence for the conductance for $d = 1$ and $d = 3$, respectively. Show that $s = 1$, provided that $\epsilon = d - 2 \ll 1$.

References

- [AAT1973] R. Abou-chakra, P. W. Anderson, and D. J. Thouless, *J. Phys. C* **6**, 1734 (1973).
- [A1979] E. Abrahams, P. W. Abrahams, D. C. Licciardello, and T. V. Ramakrishnan, *Phys. Rev. Lett.* **42**, 673 (1979).
- [A1981] S. Alexander, J. Bernasconi, W. R. Schneider, and R. Orbach, *Rev. Mod. Phys.* **53**, 175 (1981).
- [A1980] B. L. Altshuler, A. G. Aronov, D. E. Khmel'nitskii, and A. I. Larkin, in *Quantum Theory of Solids*, ed. I. M. Lifshits (MIR Publishers, Moscow, 1980).
- [A1958] P. W. Anderson, *Phys. Rev.* **109**, 1492 (1958).
- [A1992] P. W. Anderson, *Science* **256**, 1526 (1992).
- [BK1998] D. Belitz and T. R. Kirkpatrick, *Phys. Rev. B* **58**, 8214 (1998).
- [B1999] V. Bellani, E. Diez, R. Hey, *et al.*, *Phys. Rev. Lett.* **82**, 2159 (1999).
- [B1982] G. Bergmann, *Phys. Rev. B* **25**, 2937 (1982).
- [BG1995] M. A. Blachly and N. Giordano, *Phys. Rev. B* **51**, 12537 (1995).
- [B1963] R. E. Borland, *Proc. R. Soc. London Ser. A* **274**, 529 (1963).
- [B1992] A. Bovier, *J. Phys. A* **25**, 1021 (1992).
- [DO1979] G. J. Dolan and D. D. Osheroff, *Phys. Rev. Lett.* **43**, 721 (1979).
- [DJ2000] S. C. Dultz and H. W. Jiang, *Phys. Rev. Lett.* **84**, 4689 (2000).
- [DWP1990] D. H. Dunlap, H.-L. Wu, and P. Phillips, *Phys. Rev. Lett.* **65**, 88 (1990).
- [EC1970] E. N. Economou and M. H. Cohen, *Phys. Rev. Lett.* **24**, 1445 (1970).
- [E1996] D. E. Ephron, A. Yazdani, A. Kapitulnik, and M. Beasley, *Phys. Rev. Lett.* **76**, 529 (1996).
- [FFG1955] G. Feher, R. C. Fletcher, and E. A. Gere, *Phys. Rev.* **100**, 1784 (1955).
- [F1990] M. P. A. Fisher, G. Grinstein, and S. Girvin, *Phys. Rev. Lett.* **64**, 587 (1990).
- [F1989] J. C. Flores, *J. Phys. Condens. Matt.* **1**, 8471 (1989).
- [GM1998] A. M. Goldman and N. Markovic, *Physics Today* **51**, 39 (1998).
- [H1998] Y. Hanien, U. Meirav, D. Shahar, *et al.*, *Phys. Rev. Lett.* **80**, 1288 (1998).
- [HP1990] A. F. Hebard and M. A. Paalanen, *Phys. Rev. Lett.* **65**, 927 (1990).
- [I2000] S. Ilani, A. Yacoby, D. Mahalu, and H. Shtrikman, *Phys. Rev. Lett.* **84**, 3133 (2000).
- [I1986] Y. Imry, *Europhys. Lett.* **1**, 249 (1986).
- [J1989] H. M. Jaeger, D. B. Haviland, B. G. Orr, and A. M. Goldman, *Phys. Rev. B* **40**, 182 (1989).
- [JK1986] R. Johnston and B. Kramer, *Z. Phys. B* **63**, 273 (1986).
- [K1996] S. V. Kravchenko, D. Simonian, M. P. Sarachik, W. Mason, and J. E. Furneaux, *Phys. Rev. Lett.* **77**, 4938 (1996).
- [LN1966] J. S. Langer and T. Neal, *Phys. Rev. Lett.* **16**, 984 (1966).
- [LR1985] P. A. Lee and T. V. Ramakrishnan, *Rev. Mod. Phys.* **57**, 287 (1985).
- [LT1975] D. C. Licciardello and D. J. Thouless, *J. Phys. C* **8**, 4157 (1975).
- [LG1987] J. J. Lin and N. Giordano, *Phys. Rev. B* **35**, 1071 (1987).
- [MWP1997] I. Martin, Y. Wan, and P. Phillips, *Phys. Rev. Lett.* **78**, 114 (1997).
- [MK1999] N. Mason and A. Kapitulnik, *Phys. Rev. Lett.* **82**, 5341 (1999).

- [M1997] R. H. McKenzie, *Science* **278**, 820 (1997).
- [MJW1997] P. Mohanty, E. M. Q. Jariwala, and R. A. Webb, *Phys. Rev. Lett.* **78**, 3366 (1997).
- [M1949] N. F. Mott, *Proc. Phys. Soc. London Sect. A* **62**, 416 (1949).
- [M1972] N. F. Mott, *Phil. Mag.* **26**, 1015 (1972).
- [MT1961] N. F. Mott and W. D. Twose, *Adv. Phys.* **10**, 107 (1961).
- [M1990] K. A. Muttalib, *Phys. Rev. Lett.* **65**, 745 (1990).
- [P1987] J. B. Pendry, *J. Phys. C* **20**, 733 (1987).
- [P1993] P. Phillips, *Ann. Rev. Phys. Chem.* **44**, 115 (1993).
- [P1998] P. Phillips, Y. Wan, I. Martin, S. Knysh, and D. Dalidovich, *Nature* **395**, 253 (1998).
- [PF2005] A. Punnoose and A. M. Finkel'stein, *Science* **310**, 289 (2005).
- [PFW1997] D. Popovic, A. B. Fowler, and S. Washburn, *Phys. Rev. Lett.* **79**, 1543 (1997).
- [S1999] S. Sachdev, *Quantum Phase Transitions* (Cambridge University Press, Cambridge, 1999).
- [SK1999] M. P. Sarachik and S. V. Kravchenko, *Proc. Natl. Acad. Sci.* **96**, 5900 (1999).
- [S1998] M. Y. Simmons, A. R. Hamilton, M. Peppe, *et al.*, *Phys. Rev. Lett.* **80**, 1292 (1998).
- [SE1984] C. M. Soukoulis and E. N. Economou, *Phys. Rev. Lett.* **52**, 565 (1984).
- [T1982] G. A. Thomas, Y. Ootuka, S. Katsumoto, S. Kobayashi, and W. Sasaki, *Phys. Rev. B* **25**, 4288 (1982).
- [T1977] D. J. Thouless, *Phys. Rev. Lett.* **39**, 1167 (1977).
- [VW1980] D. Vollhardt and P. Wölfle, *Phys. Rev. Lett.* **45**, 482 (1980).
- [W1976] F. Wegner, *Z. Phys. B* **25**, 327 (1976).
- [WGP1992] H.-L. Wu, W. E. Goff, and P. Phillips, *Phys. Rev. B* **45**, 1623 (1992).
- [YK1995] A. Yazdani and A. Kapitulnik, *Phys. Rev. Lett.* **74**, 3037 (1995).

In the previous chapter, we discussed both the insulator–superconductor and the insulator–metal transitions. As such transitions are disorder or magnetic-field tuned, thermal fluctuations play no role. Phase transitions of the insulator–superconductor or insulator–metal type are called quantum phase transitions. Such phase transitions are not controlled by changing the temperature, as in the melting of ice or the λ -point of liquid helium, but rather by changing some system parameter, such as the number of defects or the concentration of charge carriers. In all such instances, the tuning parameter transforms the system between quantum mechanical states that either look different topologically (as in the transition between localized and extended electronic states) or have distinctly different magnetic properties. As quantum mechanics underlies such phase transitions, all quantum phase transitions obtain at the absolute zero of temperature and thus are governed by a $T = 0$ quantum critical point. While initially surprising, this state of affairs is expected, because quantum mechanics is explicitly a zero-temperature theory of matter. Of course, this is of no surprise to chemists who have known for quite some time that numerous materials can exhibit vastly distinct properties simply by changing the chemical composition and, most importantly, that such transformations persist down to zero temperature. Common examples include turning insulators such as the layered cuprates into superconductors simply by chemical doping or semiconductors into metals once again by doping, or ferromagnets such as $\text{Li}(\text{Ho}, \text{Tb})_x\text{Y}_{1-x}\text{F}_4$ into a spin glass ([AR1998](#)) by altering x . Certainly, the technological relevance of doped semiconductors, the backbone of the electronics industry, is well established.

Given the ubiquity and importance of quantum phase transitions, it would seem that a theory of such phenomena would be well developed. However, such is not the case. The problem in constructing a theory of quantum phase transitions (QPTs) lies in the fact that they occur at zero temperature. All phase transitions are driven by some type of fluctuation. As thermal fluctuations desist at zero temperature, QPTs must be driven by a distinctly different entity. The only fluctuations that survive at zero temperature are quantum mechanical in origin. Hence, the uncertainty principle lies at the heart of all QPTs. Consequently, present in a microscopic Hamiltonian that admits a quantum phase transition must be two non-commuting operators that describe two competing ordering tendencies. In all quantum phase transitions, the magnitude of the coupling constant describes the *essential tension* between the states that compete.

A clear example of this *essential tension* is found in the Hamiltonian for the Ising model in a transverse magnetic field ([P1979](#)). Consider a linear chain of spins, each spin is in an eigenstate of S^z , the z -component of the spin. Nearest-neighbor spins interact ferromagnetically with a strength $-J$. Also present is a field which tends to align individual

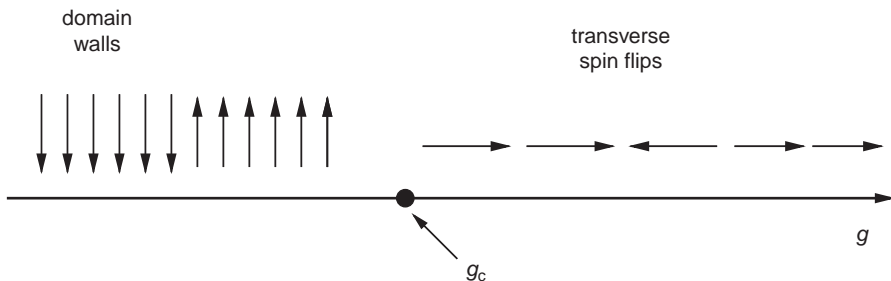


Fig. 14.1 Local excitations that occur on either side of the quantum phase transition in the transverse Ising model. As the coupling constant g increases, the magnitude of the transverse field increases with a critical point at $g_c = 1$.

spins along the x -direction. A spin along the $\pm x$ -axis is formed from the linear combination $|{\text{up}}\rangle \pm |{\text{down}}\rangle$. The Hamiltonian describing this system,

$$H_{\text{spin}} = -J \sum_j \left(g \hat{\sigma}_j^x + \hat{\sigma}_j^z \hat{\sigma}_{j+1}^z \right), \quad (14.1)$$

contains the Pauli matrices for the transverse as well as the z -component of the spins, $\hat{\sigma}_j^x$ and $\hat{\sigma}_j^z$, respectively. These are the two non-commuting operators that compete and ultimately determine the existence of the quantum critical point. While this Hamiltonian is simple, it is of immense utility as it can be generalized (S1999) to describe the magnetic system $\text{Li}(\text{Ho}, \text{Tb})_x \text{Y}_{1-x} \text{F}_4$. When $g = 0$, neighboring spins lower their energy by pointing parallel to one another. The overall system is thus in an eigenstate of the total S^z operator. The term proportional to g in Eq. (14.1) favors a transverse orientation of the spins. When $g = \infty$, all the spins point along the $+x$ or $-x$ direction, and hence the system is an eigenstate of S^x . Consequently, both the $g = 0$ and $g = \infty$ limits represent stationary states of the system in which $\langle \hat{\sigma}^z \rangle$ and $\langle \hat{\sigma}^x \rangle$ have well-defined values, respectively. In between these two limits, the system is not in a stationary state as local excitations exist that tend to destroy the perfect $g = 0$ or $g = \infty$ order. Figure 14.1 illustrates that close to $g = 0$, local excitations consist of a region or a domain wall of spins which all point in a direction opposite to the dominant order in the $g = 0$ ground state. Likewise, for $g \gg 1$, the excitations all resemble local transverse spin-flips, also shown in Fig. 14.1. Given that the ground states at $g = 0$ and $g = \infty$ are magnetically distinct, as are their quasi-particle excitations, it stands to reason that there should be a critical point at some finite value of g that signals the termination of the $g = 0$ ordered state. In fact, such a critical point does exist at $g = g_c = 1$, as shown by Pfeuty (P1979) in his exact solution of this model in 1d. For $g < 1$, the ground state is qualitatively similar to the $g = 0$ ferromagnet, while for $g > 1$, the ground state resembles the $g = \infty$ state with all spins aligned along the transverse direction. The coupling constant g represents the *essential tension* between the two ordering tendencies, with $g = g_c = 1$ defining the quantum critical point. In the $g \ll 1$ limit, $\hat{\sigma}^x$ has no well-defined value,

whereas in the opposite extreme, the uncertainty in the value of $\hat{\sigma}^z$ is essentially infinite. Consequently, the product of the uncertainty in the x and z components of the spin remains constant as g is varied, as dictated by the Heisenberg uncertainty principle. We see, then, that quantum uncertainty drives the phase transition as g is tuned.

At g_c , the ground state is not particularly straightforward. What we know about the ground state at g_c is that it exhibits scale invariance. That is, the correlations between spins are sufficiently long-range that if we increase the length scale over which we observe two spins, nothing changes. As a consequence, the ground state wavefunction tells us nothing about how far apart two spins are. This picture is expected to change at finite temperature, however, as finite temperature relaxation of the quasi-particles affects the purely quantum mechanical nature of the problem. The natural timescale that enters is $\hbar/k_B T$. Hence, while quantum phase transitions occur at $T = 0$, remnants of what is quantum mechanical about the phase transition can be seen at finite temperature, provided the time scale of observation satisfies certain constraints. A diverging length scale governing physical correlations and a time scale for quasi-particle relaxation are the key features characterizing continuous quantum phase transitions. In fact, it is the emergence of the time scale $\hbar/k_B T$ that compounds theoretical analyses of QPTs.

In this chapter, we will explore the intertwining of spatial and time dimensions as they determine the behavior of a quantum critical point. Rather than analyse the spin model, we will explore the phase-only model for insulator–superconductor transitions. In this model, the quantum phase transition is governed by fluctuations of the quantum mechanical phase of the order parameter. While we just as easily could have focused on a model in which the pair amplitude fluctuates, the phase-only model is particularly instructive because of its direct applicability to Josephson junction arrays and, further, it serves to illustrate beautifully the central role played by the uncertainty principle. Our analysis will be generally heuristic, except where a calculation must be performed. Emphasis will be placed on the essential tension embodied in the coupling constant that drives the underlying quantum critical point.

14.1 Quantum rotor model

The simplest way of introducing the phase-only model for an insulator–superconductor transition is to consider an array of superconducting islands placed on a 2d square lattice. All electrons on the grains are locked into Cooper pairs and are characterized by the same phase. Consequently, an essential ingredient of the phase-only model is that the pair amplitude remains frozen for all time. Hence, we associate with the j th grain a pair amplitude, Δ , a unique phase θ_j , and a complex wavefunction or order parameter, $\psi_j = \Delta e^{i\theta_j}$. Further, for simplicity, we will treat the Cooper pairs as bosons. There are two contributions to the energy of such a system: (1) the net energy of each superconducting grain and (2) the transport energy between two grains. Consider a grain of radius R and with a capacitance C relative to its surroundings. The energy required to remove a Cooper pair with charge $2e$ from such a grain and place it at infinity is $E_C = (2e)^2/2C$, the capacitance charging energy. There are two important features of E_C . First, E_C scales as the square of the charge

and hence must be proportional to N^2 , where N is the total number of Cooper pairs on the grain. Second, E_C is inversely proportional to the capacitance. Hence, the capacitance term dominates as the grain size decreases. Transport of Cooper pairs between grains i and j requires a term of the form $b_i^\dagger b_j$, where b_j is the annihilation operator for a Cooper pair on grain j . Consequently, our Hamiltonian is of the form

$$H = E_C \sum_i (\hat{n}_i - n_0)^2 - t \sum_{\langle ij \rangle} (b_i^\dagger b_j + b_j^\dagger b_i), \quad (14.2)$$

where $\hat{n}_i = b_i^\dagger b_i$ is the number operator for the i th grain, n_0 sets the average density on each grain, and $-t$ is the hopping matrix element between nearest-neighbor grains. The summation, $\langle ij \rangle$, is restricted to nearest-neighbor sites only. Known as the Bose–Hubbard model, Eq. (14.2) is closely related to its fermion analog discussed in Chapter 16. That Eq. (14.2) possesses two distinct limits can be seen by first setting the kinetic term to zero. In this limit, all Cooper pairs are frozen on their respective grains. In the opposite regime, $E_C = 0$, free transport of charge is permitted.

To see that the free transport and frozen charge regimes correspond to superconducting and “insulating” states, we make a transformation to phase-angle variables which is technically only valid at large boson occupancy per site. To this end, we set n_0 to be an integer. In this case, the translation $n_j \rightarrow n_j + n_0$ is permitted. Second, we note that, in a superconducting condensate, a conjugacy relationship exists between the phase and the particle number. This conjugacy allows us to equate the particle number for a pair on each grain with the phase momentum for a pair: $\hat{n}_j = \partial/\partial\theta_j$. Third, we set $b_j^\dagger = e^{i\theta_j}$. Combining these transformations results in the phase-only model,

$$H = E_C \sum_j \left(\frac{1}{i} \frac{\partial}{\partial \theta_j} \right)^2 - J \sum_{\langle ij \rangle} \cos(\theta_i - \theta_j) = H_0 + H_1, \quad (14.3)$$

also known as the quantum rotor model, which is strictly a large-filling reduction of the Bose–Hubbard model. We set $t = J$ because the second term in Eq. (14.3) is of the Josephson-tunneling form. The physics of this model is now immediately transparent. From the first term in Eq. (14.3), we see that the charging effects lead to fluctuations in the phase, whereas from the second term, phase coherence maximizes transport of Cooper pairs between grains. Consequently, we define the coupling constant, $g = E_C/J$, which embodies the *essential tension* between superconductivity and the loss of phase coherence. In the limit in which $g = 0$, there is no cost to charge a grain, and Cooper pairs transport freely via Josephson tunneling. Such a system has no phase fluctuations and hence is a superconductor. In the superconductor, $\langle \psi_j \rangle \neq 0$. In the opposite regime, $g = \infty$, charging effects dominate and the phase is randomized, thereby destroying superconductivity. In this limit, the system is in a ground state of kinetic energy and there is an almost equal probability of observing all possible phase angles. As charges are not permitted to transport freely in this regime, it is natural to expect an insulator in this limit. However, as we will see, this is not exactly so. We will show (DP2001) that while this phase is gapped, it still

admits a non-zero dc conductivity as $T \rightarrow 0$. What is clear at present, however, is that the phase-disordered regime is certainly not a superconductor. Consequently, the phase-only model displays a superconductor to non-superconductor transition somewhere between the limits $g = 0$ and $g = \infty$. The physical states demarcated by the quantum critical point, g_c , are depicted in Fig. 13.11. The superconductor to non-superconductor transition occurs when Cooper pairs no longer move freely between the grains. In this limit, the certainty that results in the particle number within each grain is counterbalanced by the complete loss of phase coherence. In a superconductor, phase certainty gives rise to infinite uncertainty in the particle number. Consequently, the product of the number uncertainty times the uncertainty in phase is the same on either side of the transition, as dictated by the Heisenberg uncertainty principle. Once again, we see that it is ultimately quantum uncertainty that drives the phase transition in the quantum rotor model. This model is relevant to Josephson junction arrays in which superconductivity is destroyed once E_C/J exceeds a critical value, as argued first by Anderson (A1964).

14.2 Scaling

Near a quantum critical point, we anticipate that we can express all physical quantities in terms of the deviation from criticality, $\delta = (g - g_c)$. In the context of the scaling theory of localization, we established that the localization length diverges at the transition as $\xi \approx |\delta|^{-\nu}$, where ν is the correlation length exponent. Divergence of the correlation length at criticality signifies that spatial fluctuations in two distant regions in the sample are related. However, because quantum critical points are driven by quantum rather than thermal fluctuations, an additional correlation “length” must enter the problem. Quantum fluctuations occur in time rather than in space. Consequently, the new correlation “length” represents the time scale over which the system fluctuates coherently. The correlation time is related to the correlation length,

$$\xi_\tau \approx \xi^z, \quad (14.4)$$

through the dynamical exponent, z . Because the exponent z is not necessarily unity, the dynamical exponent is a measure of the asymmetry between spatial and temporal fluctuations.

To explore further the significance of the dynamical exponent, we consider the partition function

$$Z = \text{Tr} [\exp(-\beta H_{\text{model}})] \quad (14.5)$$

for the model Hamiltonian,

$$H_{\text{model}} = \frac{p^2}{2m} + V(x) = T + V, \quad (14.6)$$

describing a single particle moving in an arbitrary 1d potential, $V(x)$. The trace is performed over all single-particle momentum eigenstates. We evaluate the partition function for this Hamiltonian,

$$\begin{aligned} Z &= \lim_{M \rightarrow \infty} \text{Tr} [\exp(-\beta(T + V)/M)]^M \\ &\approx \lim_{M \rightarrow \infty} \text{Tr} [\exp(-\Delta\tau T) \exp(-\Delta\tau V)]^M, \end{aligned} \quad (14.7)$$

by breaking up the imaginary time interval, $0 \leq \tau \leq \beta$, into discrete time segments,

$$\Delta\tau = \hbar\beta/M, \quad (14.8)$$

and inserting $M - 1$ complete sets of momentum eigenstates. The correct quantum mechanical problem is recovered in the limit in which the time slice $\Delta\tau \rightarrow 0$. The subsequent integrations over the intermediate momentum states are standard and can be found on pages 42 and 43 of Feynman and Hibbs (FH1965). In the limit that $\Delta\tau \rightarrow 0$, the final partition function is expressed as an integral over all paths, $x(t)$, with the associated action,

$$S_{\text{model}} = \int_0^\beta d\tau \left(\frac{m}{2} \dot{x}^2(\tau) + V(x(\tau)) \right). \quad (14.9)$$

The continuous integration in the action over imaginary time results explicitly from taking the $\Delta\tau \rightarrow 0$ limit. The analogous treatment can be performed for the quantum rotor model once we make the identification that

$$p_\theta = \frac{1}{i} \frac{\partial}{\partial \theta}. \quad (14.10)$$

Consequently, the quantum rotor Hamiltonian is recast as

$$H = E_C \sum_i p_{\theta_i}^2 - J \sum_{\langle ij \rangle} V(\theta_i - \theta_j) \quad (14.11)$$

with its associated action

$$S = \int_0^\beta d\tau \left(\frac{1}{4E_C} \sum_i (\partial_\tau \theta_i)^2 - J \sum_{\langle ij \rangle} \cos(\theta_i - \theta_j) \right), \quad (14.12)$$

obtained by discretizing the partition function and performing the trace over the momentum quantum rotor eigenstates.

The time integration in the action of the quantum rotor model has two consequences. First, the effective dimensionality of the problem has increased. In addition to the spatial dimensions, we must contend with system evolution along the imaginary time axis. Consequently, the effective dimensionality of the 2d quantum rotor model is $(2 + 1)$. Hence, this quantum mechanical problem in 2d spatial dimensions has the complication of a 3d classical problem. A second consequence is that time in quantum mechanics is imaginary and associated with inverse temperature. As a result, divergence of the correlation time at criticality is associated with a vanishing energy scale. This can be seen immediately from a

scaling analysis of the kinetic energy. The kinetic energy is proportional to τ^{-2} and hence in the vicinity of the critical point scales as $\xi_\tau^{-2} \approx \xi^{-2z}$, thereby vanishing at criticality. This is an important result. In Newtonian mechanics, the kinetic energy is generally associated with a second gradient with respect to position, $\nabla^2\theta$, thereby scaling as ξ^{-2} . The asymmetry between space and time is immediately apparent as a result of the ξ^{-2z} scaling of the kinetic energy in the imaginary-time Euclidean formalism. However, there is no asymmetry (H1976) between space and time if the number of time derivatives equals the number of spatial derivatives in the Euclidean and Newtonian representations, respectively, of the kinetic energy. In such cases, $z = 1$, as is the case with the isotropic quantum rotor model (also known as the (2+1)-dimensional XY model). Note, the result that $z = 1$ in the quantum rotor model holds only when n_0 is an integer (see Problem 14.1). Only the $z = 1$ case will be treated here.

Experiments are always performed at finite temperature, however. At finite temperature, the correlation time ξ_τ is finite. The finite temperature behavior is still controlled by the quantum critical point provided that the time scale for observation, τ , satisfies the constraint $\tau < \hbar/k_B T$, as advertised in the introduction. Experimental data obtained with this constraint in mind should exhibit universal behavior in terms of ξ_τ and ξ . To see how this works, consider first the case of zero temperature where the standard Widom (W1965) correlation length scaling applies. Consider an observable O which depends explicitly on the variable X . We assume $X \approx \xi^{d_X}$ and consequently, $\tilde{X} \approx \xi^{-d_X} X$ is scale invariant. Near the critical point,

$$O(X, \delta) = \xi^{d_O} \tilde{O}(\tilde{X}), \quad (14.13)$$

where d_O is the scaling dimension of the observable, O . This equation has profound experimental consequences. It implies that the family of curves $O(\delta, X)$ all collapse onto a single curve \tilde{O} when $\xi^{-d_O} O(X, \delta)$ is plotted as a function of \tilde{X} as opposed to X . Further, because the quantity \tilde{X} is scale invariant, so is any function of \tilde{X} . Hence, \tilde{O} does not depend on the distance from the critical point and consequently, neither does $\xi^{-d_O} O(X, \delta)$. This guarantees that critical exponents can be extracted accurately. At finite temperature, this procedure must be altered because the system is finite in the time dimension. All variables must be rescaled using Eq. (14.4) and noting that $\xi_\tau < 1/T$. For example, as a result of the finite size, the new scale-invariant quantity is $\tilde{X}_T \approx \xi_\tau^{-d_X/z} X \approx T^{d_X/z} X$. Consequently, the finite temperature form for any observable is

$$O(\delta, T, X) = T^{-d_O/z} \tilde{O}(\xi_\tau T, \tilde{X}_T). \quad (14.14)$$

In the case when X is the electric field, E , the scaling dimension is $d_E = -(z + 1)$. This result follows because the electric field is proportional to an energy divided by a length. Near the critical point, all energies scale as ξ_τ^{-1} , and lengths are proportional to ξ . Consequently, $E \approx \xi^{-(z+1)}$ and we anticipate data collapse for the conductivity with an exponent of

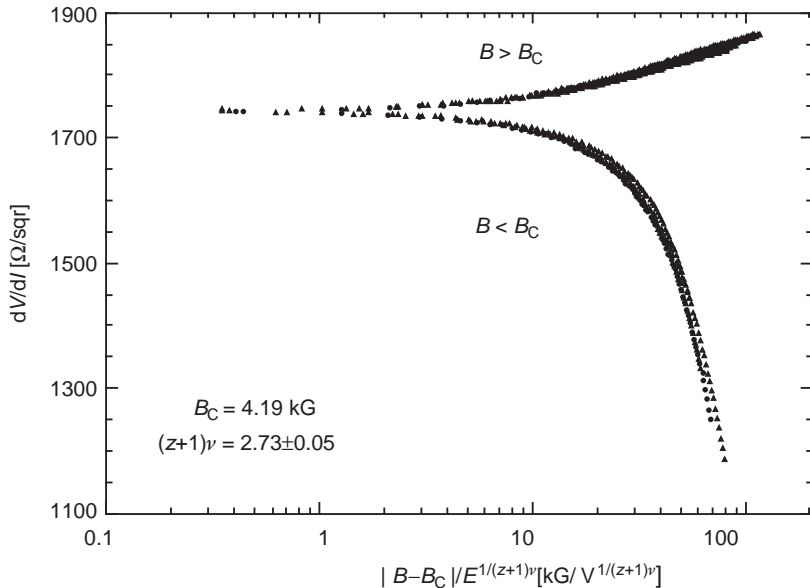


Fig. 14.2 Data collapse of the resistivity per square (dV/dl) for the insulator–superconductor transition in MoGe thin films as a function of an applied electric field. The tuning parameter is the magnetic field, B , with a critical value of $B_c = 4.19 \text{ kG}$. From the temperature scaling, $z\nu = 1.36$, whereas $(z + 1)\nu = 2.73 \pm 0.05$ collapses the electric field dependence. The data are taken from A. Yazdani and A. Kapitulnik, *Phys. Rev. Lett.* **74**, 3037 (1995).

$-\nu(z + 1)$ for electric field scaling in the vicinity of a quantum critical point, as illustrated in Fig. 14.2 for the nominal insulator–superconductor transition in MoGe thin films. In these films, the tuning parameter between the insulating and superconducting states is the magnetic field. As is evident, universal curves are obtained for both temperature and electric field scaling with $z = 1$ and $\nu = 1.36$.

14.3 Mean-field solution

The Hamiltonian for the phase-only model contains a non-linear term in the phase angle difference. As a result of this non-linearity, this model is intractable in 2d. However, we can obtain a mean-field solution that has the correct qualitative features by minimizing the free energy appearing in the partition function. Rather than write the partition function in terms of the action, we adopt a form which is amenable to perturbation theory. The partition function,

$$Z = \text{Tr} \exp [-\beta(H_0 + H_1)] = \text{Tr} [\rho], \quad (14.15)$$

is a trace of the density matrix for the total system. Let us define $\rho_0 = \exp(-\beta H_0)$ and its associated partition function, $Z_0 = \text{Tr} \rho_0$, with H_0 the kinetic energy term of the quantum rotor Hamiltonian. Following Feynman (F1972), we vary $e^{\beta H_0} \rho$ to obtain

$$\frac{\partial}{\partial \beta} (e^{\beta H_0} \rho) = -e^{H_0 \beta} H_1 \rho. \quad (14.16)$$

The formal solution to this equation is

$$\rho = \rho_0 T \exp \left[- \int_0^\beta d\tau \hat{H}_1(\tau) \right], \quad (14.17)$$

where T represents the time-ordered product. Consequently, the partition function is transformed to

$$Z = Z_0 \left\langle T \exp \left(- \int_0^\beta d\tau \hat{H}_1(\tau) \right) \right\rangle, \quad (14.18)$$

with $\langle \dots \rangle \equiv \langle \rho_0 \dots \rangle / Z_0$ and $\hat{H}_1(\tau)$ the interaction representation of the operator H_1 . The partition function is now in a form in which a perturbation series in powers of the interaction can be obtained. Our derivation here will closely mirror the original treatment by Doniach (D1981). To this end, we define a two-component vector, $\mathbf{S}_i = (\cos \theta_i, \sin \theta_i)$ and its Fourier components,

$$\mathbf{S}_{\mathbf{k}} = \frac{1}{\sqrt{N}} \sum_i \mathbf{S}_i e^{i\mathbf{k} \cdot \mathbf{R}_i}. \quad (14.19)$$

Our working form for the partition function is then

$$Z = Z_0 \left\langle T \exp \left(\int_0^\beta d\tau \sum_{\mathbf{k}} J_{\mathbf{k}} \mathbf{S}_{\mathbf{k}}(\tau) \cdot \mathbf{S}_{\mathbf{k}}^*(\tau) \right) \right\rangle, \quad (14.20)$$

where

$$J_{\mathbf{k}} = \frac{J}{N} \sum_{\langle ij \rangle} e^{i\mathbf{k} \cdot \mathbf{R}_{ij}} = J_0 (\cos k_x + \cos k_y), \quad (14.21)$$

$J_0 = J\alpha$, and α is the number of nearest neighbors.

Still, an intermediate step is needed. In terms of the discrete Matsubara frequencies, $\omega_l = 2\pi l/T$, $l = 0, \pm 1, \pm 2, \dots$, we recast the spin vectors as

$$\mathbf{S}_{\mathbf{k}}(\tau) = \frac{1}{\sqrt{\beta}} \sum_l e^{i\omega_l \tau} \mathbf{S}_{\mathbf{k}\omega_l}, \quad 0 \leq \tau \leq \beta, \quad (14.22)$$

which are normalized over the imaginary time interval $0 \leq \tau \leq \beta$. This allows us to simplify the exponential appearing in the partition function,

$$\exp \left[\int_0^\beta d\tau \sum_{\mathbf{k}} J_{\mathbf{k}} \mathbf{S}_{\mathbf{k}}(\tau) \cdot \mathbf{S}_{\mathbf{k}}^*(\tau) \right] = \prod_{\mathbf{k}, l} \exp [J_{\mathbf{k}} |\mathbf{S}_{\mathbf{k}, l}|^2], \quad (14.23)$$

to a product. We decouple the quadratic spin interaction in Eq. (14.23) by using the complex form of the Hubbard–Stratanovich transformation (H1959; S1958),

$$e^{-\lambda|a|^2} = \int \int \frac{d(\text{Re } \psi)(\text{Im } \psi)}{\pi} e^{-[|\psi|^2 + \sqrt{\lambda}(a\psi^* + a^*\psi)]}, \quad (14.24)$$

a common trick in many-particle physics used to simplify interaction terms appearing in the partition function. Resulting from this transformation is an added integration over an auxiliary field which can generally be performed by steepest-descent methods. Upon using this transformation in Eq. (14.20), we arrive at a simplified partition function,

$$Z = \frac{Z_0}{D} \int \prod \mathcal{D}\psi_{\mathbf{k}}(\tau) e^{-\mathcal{F}[\psi]}, \quad (14.25)$$

where \mathcal{F} is the free energy,

$$\begin{aligned} \mathcal{F}[\psi_{\mathbf{k}}(\tau)] &= \sum_{\mathbf{k}} \int_0^\beta d\tau \frac{\psi_{\mathbf{k}}^*(\tau) \cdot \psi_{\mathbf{k}}(\tau)}{J_{\mathbf{k}}} \\ &\quad - \ln \left[\left\langle T \exp \left[-2 \int_0^\beta d\tau \sum_{\mathbf{k}} \psi_{\mathbf{k}}(\tau) \cdot \mathbf{S}_{-\mathbf{k}}(\tau) \right] \right\rangle \right], \end{aligned} \quad (14.26)$$

and $D = \pi \prod_{\mathbf{k}} J_{\mathbf{k}}$. In obtaining this form for the free energy, we rescaled the auxiliary field $\psi_{\mathbf{k}} \rightarrow \psi_{\mathbf{k}}/\sqrt{J_{\mathbf{k}}}$.

In the mean-field approximation, we assume that ψ is constant. Further, we are free to choose any orientation of ψ . For convenience, we orient ψ along the x -axis, and consequently $\psi_{\mathbf{k}} = \sqrt{N} \delta_{\mathbf{k},0} \psi_x$. Substitution of this form for the auxiliary field into Eq. (14.26) results in the mean-field expression

$$\mathcal{F}[\psi_{\mathbf{k}}]_{\text{MF}} = \frac{\beta N \psi_x^2}{J_0} - \ln \left[\left\langle T \exp \left[-2 \int_0^\beta \psi_x \sum_i S_i^x(\tau) d\tau \right] \right\rangle \right] \quad (14.27)$$

for the free energy. Assuming that ψ is a small parameter, we are free to expand the exponential:

$$\begin{aligned} \left\langle T \exp \left[-2 \int_0^\beta \psi_x \sum_i S_i^x(\tau) d\tau \right] \right\rangle &= 1 - 2\psi_x \left\langle \int_0^\beta \sum_i S_i^x(\tau) d\tau \right\rangle \\ &\quad + 2\psi_x^2 \left\langle T \int_0^\beta \int_0^\beta d\tau d\tau' \sum_{ij} S_i^x(\tau) S_j^x(\tau') \right\rangle + \dots \end{aligned} \quad (14.28)$$

Physically, the terms in this expansion represent phase fluctuations of the order parameter. If such terms lead to a sign change in the free energy, a phase transition occurs. To evaluate

the averages, we expand in the free rotor eigenstates

$$\langle m | \theta \rangle = \frac{1}{2\pi} e^{im\theta}. \quad (14.29)$$

In this basis,

$$H_0 \langle m_i | \theta_i \rangle = m_i^2 E_C \langle m_i | \theta_i \rangle, \quad (14.30)$$

leading immediately to a compact form

$$Z_0 = \text{Tr } e^{-\beta H_0} = \sum_{\{m_i\}} e^{-\beta E_C \sum_i m_i^2} \quad (14.31)$$

for the zeroth-order partition function. An additional consequence of this choice of basis is that averages linear in S_i^x vanish identically:

$$\langle m_i | \cos \theta_i | m_i \rangle = \int_0^{2\pi} \frac{d\theta_i}{2\pi} e^{-im_i \theta_i} \cos \theta_i e^{im_i \theta_i} = 0. \quad (14.32)$$

Consequently, to lowest order in ψ , only the diagonal elements ($i = j$) in the second-order term in Eq. (14.28) yield a non-zero result. Upon substituting Eq. (14.28) into Eq. (14.27) and differentiating with respect to ψ , we obtain

$$\begin{aligned} \frac{\beta}{J_0} &= 2 \left\langle T \int_0^\beta \int_0^\beta d\tau d\tau' S_i^x(\tau) S_i^x(\tau') \right\rangle \\ &= 2 \int_0^\beta d\tau d\tau' C_0(\tau - \tau') \end{aligned} \quad (14.33)$$

as the saddle-point equation to lowest order, with

$$C_0(\tau - \tau') = \frac{1}{Z_0} \sum_{\{m_i\}} e^{-\beta E_C \sum_i m_i^2} \langle \{m_i\} | T \hat{S}_i^x(\tau) \hat{S}_i^x(\tau') | \{m_i\} \rangle \quad (14.34)$$

the phase fluctuation correlation function. This is the key quantity that enters the mean-field theory of the phase transition in the quantum rotor model.

The only matrix elements of S_i^x that are non-zero are of the form

$$\langle m_i | \cos \theta_i | m_i \pm 1 \rangle = \frac{1}{2}, \quad (14.35)$$

and the correlation function is given by

$$\langle \{m_i\} | T \hat{S}_i^x(\tau) \hat{S}_i^x(\tau') | \{m_i\} \rangle = \frac{1}{2} e^{-E_C |\tau - \tau'|} \cosh(2m_i E_C (\tau - \tau')). \quad (14.36)$$

There are two important limits of this expression. At low temperatures such that $E_C\beta \gg 1$, all the rotors can be treated as being in their ground states; that is, $m_i = 0$. In this case, the correlation function reduces to an exponential

$$C_0(\tau - \tau') = \frac{1}{2}e^{-E_C|\tau - \tau'|}, \quad \beta E_C \gg 1, \quad (14.37)$$

and the mean-field stability condition

$$1 = \frac{2J_0}{E_C} \left[1 - \frac{1 - e^{-\beta E_C}}{\beta E_C} \right], \quad \beta E_C \gg 1 \quad (14.38)$$

follows once the time integrations in Eq. (14.33) are performed. To leading order in $1/\beta$, we find that the stability condition for the coupling constant, $g = E_C/J_0$, is given by

$$g = 2 \left(1 - \frac{T}{E_C} \right) + O(T^2/J). \quad (14.39)$$

Hence, the critical value of the coupling constant at $T = 0$ is $g_c = 2$. For $g > g_c$, quantum fluctuations dominate, and the system is in the phase-disordered regime.

At high temperature, the full expression for the correlation function, Eq. (14.36), must be retained in performing the time integration in Eq. (14.33):

$$\begin{aligned} & \frac{1}{2} \int_0^\beta d\tau \int_0^\beta d\tau' e^{-E_C|\tau - \tau'|} \cosh 2m_i E_C |\tau - \tau'| \\ &= \frac{1}{2} \sum_\sigma \left[\frac{\beta}{E_C(1 + 2\sigma m_i)} - \frac{1 - e^{-\beta E_C(1 + 2\sigma m_i)}}{E_C^2(1 + 2\sigma m_i)^2} \right], \end{aligned} \quad (14.40)$$

with $\sigma = \pm 1$. The main contribution from the resultant sum over m_i arises from $m_i < 1/\beta E_C$. However, because $\beta E_C \ll 1$, we expand Eq. (14.40), keeping only the terms independent of m_i . Consequently, the sum over m_i in Eq. (14.34) is canceled by the factor of Z_0 in the denominator, resulting immediately in the stability condition

$$k_B T = J_0 - \frac{E_C}{3} + O((E_C/J)^2) \quad (14.41)$$

at high temperatures. The critical temperature is then $T_c = J_0/k_B$. The mean-field phase boundary connecting high- and low-temperature regimes as a function of the coupling constant g is shown in Fig. 14.3. While this is a mean-field phase diagram, it captures the correct qualitative features of the phase-fluctuation-induced destruction of superconductivity in 2d systems. The more exact description of the finite temperature line in Fig. 14.3 is due to Berezinskii (B1971) and Kosterlitz and Thouless (KT1973). The essence of the Berezinskii–Kosterlitz–Thouless (BKT) transition is that the ordered phase is characterized by bound vortex–antivortex pairs. Unbinding of vortices at criticality leads to dissipation and the onset of a resistive state. The phase-only model can be understood in terms of the

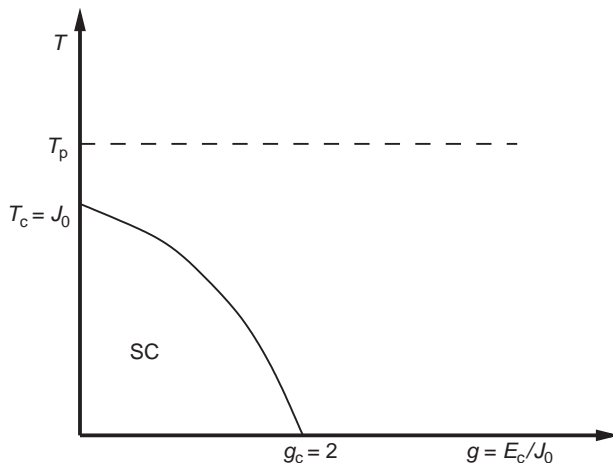


Fig. 14.3 Mean-field phase diagram from the quantum rotor model. The solid line represents a continuous line of second-order critical points. The mean-field values for transition temperature and the quantum critical point are $T_c/J_0 = 1$ and $g_c = 2$, respectively. Beyond the solid curve, phase coherence is lost, signaling an absence of the superconducting state. T_p indicates the temperature scale for the onset of the pairing amplitude.

vortex–antivortex unbinding transition as a result of the inherent duality (F1990) between charges and vortices within this model. This duality dictates that on the superconducting side of the transition, vortices are bound, whereas Cooper pairs are condensed in a state with a rigid phase. On the disordered side, it is the vortices that condense and the Cooper pairs that remain localized. In the context of a charged superfluid in 2d, the condition for vortex unbinding,

$$k_B T_{\text{BKT}} = \frac{\pi \hbar^2 n_s(T)}{2m^*}, \quad (14.42)$$

depends only on the superfluid density, $n_s(T)$, and the effective mass, m^* , of the charge carriers. Note that the mean-field condition, $T_c = J_0$, is quite similar to T_{BKT} , since the Josephson coupling, J_0 , is proportional to the superfluid density. Because disorder depletes the superfluid density, the T_{BKT} line should be inversely proportional to the normal state sheet resistance (BMO1979; HN1979). Above a critical value of the disorder, the superfluid density vanishes and the phase-ordered state ceases. Hence, disorder can tune the vortex unbinding transition. In fact, the system parameters for the quantum rotor model can be rewritten in terms of the normal state sheet resistance, R_N . The Josephson coupling, J_0 , is directly proportional to the zero temperature gap and inversely proportional to disorder, scaling roughly as R_N^{-1} . When the disorder increases, the size of the Josephson grains decreases and hence, the charging energy increases. As a result, E_C increases with R_N . Following Simanek (S1980), we make the approximation $E_C \propto R_N$. Consequently, $g \propto R_N^2$, and the phase-only model possesses a critical point when the normal sheet resistance exceeds

a critical value, consistent with experimental observations (HP1990; J1989). While it is most natural to envision disorder as the mechanism by which R_N increases, other external perturbations, such as an applied magnetic field, suffice as well. The magnetic-field-tuned destruction of the superconducting state in MoGe thin films is illustrated in Fig. 14.2.

Because pairs are assumed at the outset, T_{BKT} or the mean-field T_c shown in Fig. 14.3 are certainly below the temperature at which the pair amplitude first becomes non-zero. The temperature scale for pair formation is indicated by T_p in Fig. 14.3. Above T_c and g_c , the system is phase disordered. This is a crucial point. In 2d, the energy scales for pair formation and phase coherence are decoupled. This state of affairs arises from the severity of phase fluctuations in 2d. Also, in the vicinity of g_c , the temperature drops continuously to zero, indicating that the phase transition is second order. Once the temperature is raised at g_c , classical fluctuations obtain. Directly above g_c , the dynamics are controlled by the temperature. This regime is referred to generally as “quantum critical” as the system is torn between the ordered and disordered phases. Understanding this competition requires a computation of the correlation length as a function of g . To facilitate this, we resort to an effective Landau description of the quantum rotor model.

14.4 Landau–Ginsburg theory

The final step in our presentation of the quantum rotor model is to recast the corresponding free energy functional in terms of a Landau theory. To this end, we consider the form for the free energy in Eq. (14.26). To start, we write the auxiliary field as a sum over the discrete Matsubara frequencies,

$$\psi_{\mathbf{k}}(\tau) = \frac{1}{\sqrt{\beta}} \sum_l e^{i\omega_l \tau} \psi_{\mathbf{k}, \omega_l}, \quad (14.43)$$

where the Fourier-transformed field is given by

$$\psi_{\mathbf{k}, \omega_l} = \frac{1}{\sqrt{\beta}} \int_0^\beta \psi_{\mathbf{k}}(\tau) e^{-i\omega_l \tau}. \quad (14.44)$$

Next, we expand the logarithm in Eq. (14.27), keeping in mind that the odd powers of ψ vanish as a result of Eq. (14.32). As a result, the free energy

$$\mathcal{F}[\psi] = \sum_{\mathbf{k}, l, l'} \psi_{\mathbf{k}, l}^* \psi_{\mathbf{k}, l'} [J_{\mathbf{k}}^{-1} \delta_{l, l'} - 2C_0(\omega_l, \omega_{l'})] + O(\psi^4) + \dots \quad (14.45)$$

contains only even powers in ψ . The frequency-dependent spin-correlation function

$$\begin{aligned} C_0(\omega_l, \omega_{l'}) &= \frac{1}{\beta} \int_0^\beta \int_0^\beta d\tau d\tau' C_0(\tau, \tau') e^{i\omega_l \tau} e^{-i\omega_{l'} \tau} \\ &= \delta_{ll'} \frac{E_C}{E_C^2 + \omega_l^2} \approx \delta_{ll'} \frac{1}{E_C} \left(1 - \frac{\omega_l^2}{E_C^2} \right) \end{aligned} \quad (14.46)$$

has a simple form at low temperatures, where $C_0(\tau, \tau') \propto \exp -E_C |\tau - \tau'|$. The analogous correlation function can also be evaluated for the fourth-order term. However, its exact coefficient, which we represent heuristically as U is not particularly important in this context. As our focus is the long-wavelength physics, we expand $J_{\mathbf{k}}$, retaining only the quadratic terms, $J_{\mathbf{k}} \approx J_0(1 - (ka)^2/2)$, with a the lattice constant. Combining these results with those of Eqs. (14.45) and (14.46), we see immediately that the free energy

$$\begin{aligned} \mathcal{F}[\psi] &= \sum_{\mathbf{k}, l} \psi_{\mathbf{k}, l}^* \psi_{\mathbf{k}, l} \left[\left(\frac{1}{J_0} - \frac{2}{E_C} \right) + \frac{(ka)^2}{2J_0} + 2 \frac{\omega_l^2}{E_C^3} \right] \\ &\quad + \frac{U}{2\beta} \sum_{\substack{\omega_1, \dots, \omega_4 \\ \mathbf{k}_1, \dots, \mathbf{k}_4}} \delta_{\omega_1 + \dots + \omega_4, 0} \delta_{\mathbf{k}_1 + \dots + \mathbf{k}_4, 0} \psi_{\omega_1, \mathbf{k}_1}^* \psi_{\omega_2, \mathbf{k}_2}^* \psi_{\omega_3, \mathbf{k}_3} \psi_{\omega_4, \mathbf{k}_4} \end{aligned} \quad (14.47)$$

is of the Landau–Ginzburg form. Note that the mean-field solution for the zero-temperature quantum critical point is $J_0^{-1} = 2/E_C$ or, equivalently, $(1/J_0 - 2/E_C) = (g - g_c)/E_C$, implying that the constant coefficient of the quadratic term is proportional to the inverse correlation length. This term plays the role of $a(T)$ in Eq. (12.14) in Chapter 12. In addition, the quadratic frequency dependence arises from the two derivatives with respect to θ in Eq. (14.30). In the time domain, the quadratic frequency dependence translates into a second derivative with respect to time, as shown in Eq. (14.12). Consequently, in real space, the free energy density

$$\mathcal{F}[\psi] = \int d^2r \int d\tau \left[|\nabla \psi(\mathbf{r}, \tau)|^2 + |\partial_\tau \psi(\mathbf{r}, \tau)|^2 + \delta |\psi(\mathbf{r}, \tau)|^2 + \frac{U}{2} |\psi(\mathbf{r}, \tau)|^4 \right] \quad (14.48)$$

takes the familiar Landau–Ginzburg form upon appropriate rescalings of the coupling constants, the Matsubara frequencies, and the ψ fields. We have defined $\delta = g - g_c$ and set $\hbar = c = 1$. Absent from the earlier formulation of Landau–Ginzburg theory presented in Chapter 12, Eq. (12.14), but present in Eq. (14.48) is the explicit integration over imaginary time and the quantum fluctuation term proportional to ∂_τ^2 . Symmetry between space and time is guaranteed, as there are an equal number of time and spatial derivatives in the free energy. Consequently, we identify

$$\epsilon_k = \pm \sqrt{k^2 + \delta} \quad (14.49)$$

as the dispersion relationship for the single-particle spectrum. In the superconducting phase, $\delta = 0$, and we recover a linear dispersion relationship on momentum, as is

expected for bosons. However, the dispersion relationship is gapped, $\delta > 0$, when quantum fluctuations dominate. The critical point demarcates the transition between gapped ($g > g_c$) and free ($g < g_c$) quasi-particle excitations. On both sides of the phase transition, Cooper pairs are intact. Consequently, the phase transition inherent in the Landau–Ginzburg theory is not of the pair-breaking type but rather is driven by phase fluctuations of the order parameter, $\psi(\omega, \mathbf{k})$.

The role of the fourth-order term is to introduce quasi-particle scattering into the correlation length. The simplest way to quantify this effect is to use Hartree–Fock theory. In this context, we can implement this procedure by performing an expansion in the number components, N , of the field, ψ_μ , with μ the index for each component. For the rotor problem, ψ_μ is a two-component field. The Hartree–Fock procedure amounts to taking the $N \rightarrow \infty$ limit. Should the corrections in powers of $1/N$ prove to be small, then the large- N expansion offers a simple way of treating quartic terms in the free energy once we replace U by U/N . As we will see, the $1/N$ expansion cannot reproduce the finite temperature transition. However, it is instructive in delineating the distinct regimes that encompass the quantum critical point.

To obtain the correlation length, we exponentiate the free energy and use a slightly modified form of the Hubbard–Stratanovich (H1959; S1958) transformation,

$$\begin{aligned} & \exp \left\{ \frac{UT}{2N} \sum'_{\substack{\omega_1, \dots, \omega_4 \\ \mathbf{k}_1, \dots, \mathbf{k}_4}} \psi_\mu^*(\omega_1, \mathbf{k}_1) \psi_\mu^*(\omega_2, \mathbf{k}_2) \psi_\nu(\omega_3, \mathbf{k}_3) \psi_\nu(\omega_4, \mathbf{k}_4) \right\} \\ &= \int \mathcal{D}\lambda \exp \left\{ -\frac{N}{2U} \sum_{\mathbf{k}, \omega} |\lambda(\omega, \mathbf{k})|^2 \right. \\ & \quad \left. + \frac{1}{\sqrt{\beta}} \sum_{\mathbf{k}_1, \mathbf{k}_2, \omega_1, \omega_2} \lambda(\omega_1 - \omega_2, \mathbf{k}_1 - \mathbf{k}_2) \psi_\mu(\omega_1, \mathbf{k}_1) \psi_\mu(-\omega_2, -\mathbf{k}_2) + \text{hc} \right\}, \end{aligned} \quad (14.50)$$

to decouple the quartic term, where the prime represents the constraints, $\delta_{\omega_1+\dots+\omega_4,0}$ and $\delta_{\mathbf{k}_1+\dots+\mathbf{k}_4,0}$. In the saddle-point approximation, the auxiliary field is a constant: $\lambda(\omega, \mathbf{k}) = \sqrt{\beta} \lambda \delta_{\omega,0} \delta_{\mathbf{k},0}$. Substitution of this expression into the partition function and minimization with respect to λ results in the saddle-point equation

$$\lambda = \frac{U}{\beta} \sum_{\omega_m} \int \frac{d^2 k}{(2\pi)^2} \frac{1}{\delta + k^2 + \omega^2 + \lambda} \quad (14.51)$$

for λ in the large- N limit. Let $m^2 = \delta + \lambda$ be the square of the inverse correlation length. The critical point is now determined by $m = 0$. Once the integral over momentum is performed in Eq. (14.51), Poisson summation techniques can be used to evaluate (see Problem 14.4) the sum over the Matsubara frequencies. The resultant self-consistent condition

$$m^2 = \delta + \frac{UT}{2\pi} \ln \left(\frac{\sinh \sqrt{\Lambda^2 + m^2}/2T}{\sinh m/2T} \right) \quad (14.52)$$

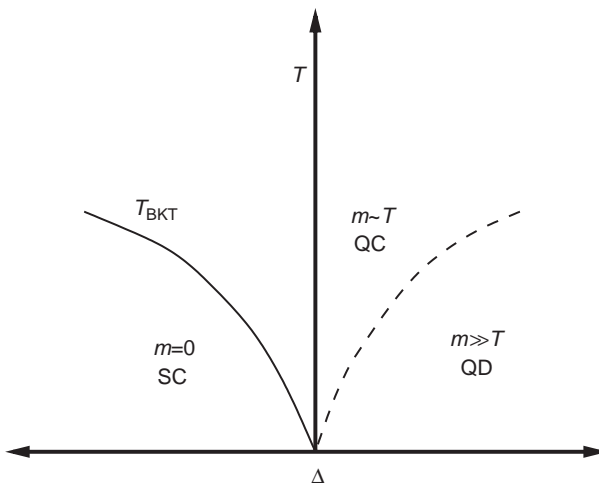


Fig. 14.4

Finite temperature phase diagram for the quantum rotor model as a function of temperature and the distance from the quantum critical point, $\Delta = g - g_c = 0$. The solid line, T_{BKT} , represents the line of second-order critical points determined by Berezinskii–Thouless–Kosterlitz. Below the solid line, the inverse correlation length, m , vanishes and phase coherence obtains. The dashed line represents a crossover from the quantum critical (QC) region in which the dynamics are determined by temperature, $m \propto T$, to the phase-disordered (QD) regime, where quantum fluctuations dominate, $m \gg T$. The behavior of the inverse correlation length in each of these regimes is given by Eq. (14.53).

admits the solution $m = 0$ provided that $T = 0$ and the renormalized tuning parameter, $\Delta = \delta + U\Lambda/4\pi$, vanishes. Here, Λ is the momentum cut-off. Hence, mean-field theory fails to recover the correct finite-temperature transition (of the BKT type) for the vanishing of the inverse correlation length. Nonetheless, as a function of temperature, three distinct regimes emerge:

$$m = \begin{cases} T \exp \left\{ -\frac{2\pi|\Delta|}{UT} \right\}, & \Delta < 0, \quad \text{ordered phase,} \\ 2 \ln \frac{\sqrt{5}+1}{2} T, & |\Delta| \ll T, \quad \text{quantum critical,} \\ \frac{4\pi\Delta}{U}, & \Delta > 0, \quad \text{quantum disordered,} \end{cases} \quad (14.53)$$

which characterize all quantum phase transitions. The phase diagram illustrating each of these regimes is shown in Fig. 14.4. The ordered phase occurs to the left ($\Delta < 0$) of the critical point, $\Delta = 0$, and is characterized by a vanishing of the inverse correlation length below some temperature. The solid line in Fig. 14.4 represents the T_{BKT} line of second-order critical points. For $N = 2$, the ordered state is a superconductor. The ordered state for $N = 1$ corresponds to a ferromagnet and hence is in the universality class of the 2d Ising model. For $N \geq 3$, the finite-temperature transition line is suppressed to $T = 0$, thereby indicating the absence of an ordered state at finite temperature. The failure of the $1/N$ expansion to yield a finite-temperature transition is immediately evident from Eq. (14.53), as m vanishes only at $T = 0$ for $\Delta < 0$. Directly above $\Delta = 0$, the system crosses over

to an intermediate regime in which thermal rather than quantum fluctuations determine the dynamics. In this regime, the inverse correlation length scales linearly with temperature with a coefficient that is universal. This regime is referred to as quantum critical because the system is trying to decide which of the two ground states is preferable. A fundamental characteristic of all systems in such an indeterminate state is the linear scaling of all energy scales or, equivalently, relaxation rates with temperature. Hence, in the quantum-critical regime, quasi-particle excitations are not well-defined, as discussed in the introduction. As Δ is increased, the system crosses over from the quantum-critical to the quantum-disordered regime. In this limit, temperature is subdominant, and quantum fluctuations of the order parameter determine the physics. Consequently, $\langle \psi^*(\mathbf{r})\psi(\mathbf{r}) \rangle \propto \exp(-r/\xi) \propto \exp(-mr)$. The energy excitations in this regime are gapped and given by $\epsilon_k = \sqrt{k^2 + m^2}$.

14.5 Transport properties

The conductivity is a function of both the frequency and the temperature. The distance from the critical point also determines the conductivity. Hence, $\sigma = \Sigma(\hbar\omega, T, \Delta)$. Consider the simple case of $\Delta = 0$. How should the zero-temperature transport properties be determined? Because the quantum critical point occurs at $T = 0$, it seems reasonable to assume that the correct $T = 0$ limit is obtained from $\Sigma(\hbar\omega, T = 0, 0)$ and the dc conductivity by taking the limit of zero frequency. This of course assumes that the frequency and temperature dependence are decoupled. If in fact they are decoupled, then the two limits, $\omega \rightarrow 0, T = 0$ and $\omega = 0, T \rightarrow 0$ commute.

In a pioneering paper, Damle and Sachdev (DS1997) showed that in the vicinity of a quantum critical point, these two limits do not commute after all. Their argument is based on the observation that in the vicinity of a quantum critical point, the conductivity is a universal function of $\hbar\omega/k_B T$. This signifies that there are two distinctly different $T \rightarrow 0$ limits of $\Sigma(\hbar\omega/k_B T)$. The limit $\Sigma(\hbar\omega \rightarrow 0, T = 0) = \Sigma(\infty)$, while $\Sigma(\omega = 0, T \rightarrow 0) = \Sigma(0)$. The essential point of Damle and Sachdev is that Σ is a monotonic function, and hence, $\Sigma(0) \neq \Sigma(\infty)$. Experimentally, all measurements of the dc transport properties are performed in the limit $\hbar\omega \ll k_B T$. Hence, it is the limit $\Sigma(0)$ that is relevant to experiments. All of the early theoretical work (C1991; WZ1990; KZ1993; W1994) on insulator–superconductor transitions was based on the limiting form $\Sigma(\infty)$. This limit corresponds to the coherent regime or high-frequency limit in which relaxation from the externally applied electric field determines the transport properties. The opposite regime is different in kind, however. In the limiting form $\Sigma(0)$, collisions between thermally excited quasi-particles dominate all relaxation processes. To describe this regime, one must formulate a quantum kinetic equation for the quasi-particle scattering directly analogous to the Boltzmann approach formulated for phonon-dominated transport in a metal. The key surprise here is that the transport properties of a $T = 0$ quantum critical point cannot be understood without an analysis of the finite temperature relaxation processes.

To illustrate how the non-commutativity of the frequency and temperature tending to zero limits drastically affects the conductivity, consider the quantum-disordered regime. In this regime, $m \gg T$, and thermally excited quasi-particles exist above the gap. However, from naive considerations, the presence of a gap indicates that the dc conductivity should vanish. But this is not so. The constraint $m \gg T$ in the quantum-disordered regime signifies that the relevant momenta satisfy the constraint $k < \sqrt{mT} < m$. Consequently, the dispersion relation can be written as

$$\epsilon_{\mathbf{k}} \approx m + \frac{k^2}{2m} \approx m, \quad m \gg T, \quad (14.54)$$

and the quasi-particle statistics becomes Boltzmannian in the quantum-disordered regime. Hence, the population of quasi-particles is exponentially small. However, this exponential smallness of the population of quasi-particles also gives rise to an exponentially small probability of scattering. The exact calculation (DP2001) reveals that, in the quantum-disordered regime, the scattering rate

$$\frac{1}{\tau} = \pi T e^{-m/T} \quad (14.55)$$

is independent of momentum and governed by the same exponential that attenuates the population of quasi-particles. From the Einstein relation, the conductivity is a product of the density of quasi-particles and the scattering time. The product of exponentials cancels (DP2001), giving rise to a conductivity

$$\sigma_{\text{qd}} = \frac{2}{\pi} \frac{4e^2}{h} \quad (14.56)$$

that is finite for $m \ll 1$. Further away from the critical point, the coefficient is modified by the form of the interactions. However, the dc conductivity remains finite, nonetheless. In addition, all logarithmic contributions to the scattering rate (DP2001) vanish at low temperatures and hence do not affect the finite dc conductivity at $T = 0$. The key to this argument is that once the quasi-particles obey Boltzmann statistics, scattering events are rare. Hence, quasi-particles roam considerable distances without scattering. Consequently, the generic phase diagram for the phase-only model, Fig. 14.5, contains an ordered phase which is a superconductor and a phase-disordered regime which is “metallic”. The “insulator” is a metal with a finite dc conductivity. This is one of the key surprises that has come out of the non-commutativity of the frequency and temperature tending to zero limits. Green and Sondhi (GS2005) have also shown the gapped or quantum-disordered phase is in fact metallic from the cancellation argument discussed above. We refer to this phase as a Bose metal because the fundamental excitations are bosons. At finite frequency, $\Sigma(\omega, T)$ has a Lorentzian-type peak at $\omega = 0$, with a width of order $1/\tau$. Consequently, the constraint on the experimental observation of the Bose metal is that $\omega \ll 1/\tau$. For a temperature of

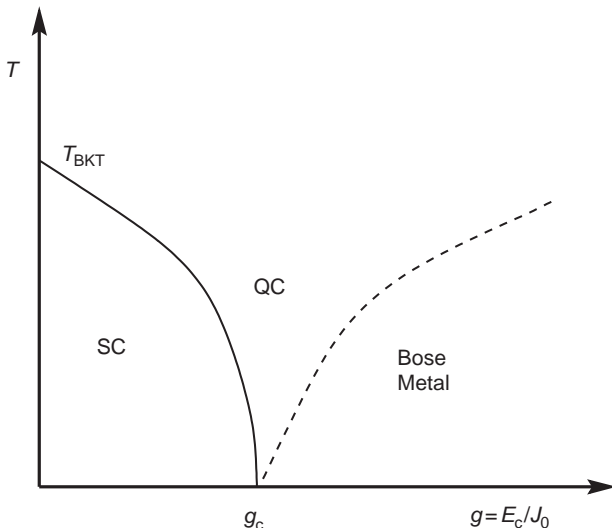


Fig. 14.5 Phase diagram for the destruction of phase coherence in an array of Josephson junctions. For this system, g is given by the ratio of the charging energy, E_c , to the Josephson coupling, J_0 . T_{BKT} is the Berezinskii–Kosterlitz–Thouless temperature below which phase coherence obtains and g_c defines the critical value of the phase disorder needed to destroy the superconducting phase. QC refers to the quantum critical regime in which the inverse correlation length is linear in the temperature. Once phase coherence is destroyed, a metallic state ensues. The metallic state arises entirely from the lack of commutativity between the frequency and temperature tending to zero limits of the conductivity.

0.1 K, the relaxation time is $10^{10} \exp(-m/T) \text{ s}^{-1}$, where $m \gg T$. Typical experimental frequencies under which the dc conductivity is measured are of the order of 2–27 Hz. Hence, the Bose metal can be observed provided that $T > 0.05m$. Typically, $T > 0.1m$. Consequently, there does not appear to be any experimental constraint regarding the frequency that prohibits the observation of the Bose metal phase. However, the Bose metal described here is fragile as all other scattering mechanisms, for example disorder, will destroy the perfect cancellation leading to Eq. (14.56). Consequently, one of the open problems with the insulator–superconductor transition is the origin of the intervening metallic phase at low temperatures.

14.6 Experiments

The applicability of the phase-only model to insulator–superconductor transitions (IST) in thin films hinges on the existence of Cooper pairs on both sides of the transition. Consequently, tunneling experiments which directly measure the single-particle spectrum are ideally suited for testing the key prediction of the phase-only model. Such experiments (B1994) on granular films reveal that the single-particle energy gap remains finite and unattenuated from the bulk superconducting value on the insulating side of the transition. Consequently, the phase-only model offers an accurate description of the experimentally observed IST in granular thin films.

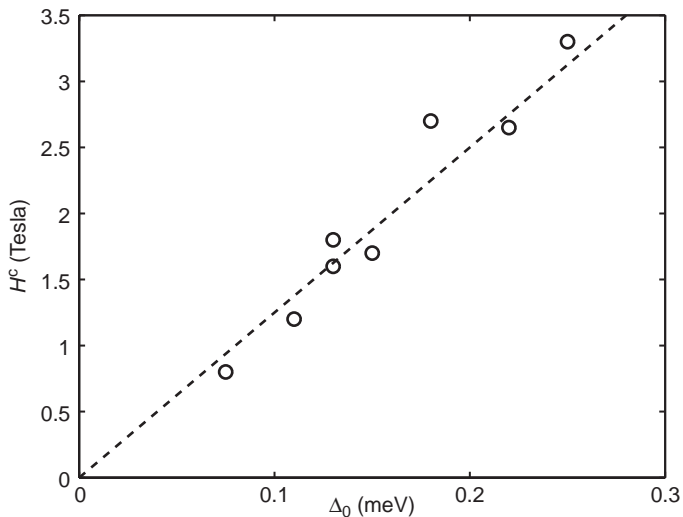


Fig. 14.6 Critical magnetic field H_c versus the energy gap Δ_0 for PbBi/Ge films. Redrawn from S.-Y. Hsu's thesis ([H1995](#)).

What about homogeneously disordered thin films? Here the situation is quite different. Shown in Fig. 14.6 is the critical magnetic field needed to destroy the superconducting state in PbBi/Ge as a function of the single-particle energy gap. As is evident, H_c scales as a linear function of the gap. Such a correspondence is expected within BCS theory (see Eq. (12.207)), provided that H_c corresponds to H_{c2} , the Cooper pair-breaking field. In fact, Valles and co-workers ([HCV1995](#)) have determined that at H_c , the density of states at the Fermi energy is 80 percent of its value in the normal state, as would be the case if $H_c \approx H_{c2}$. Consequently, a large fraction of the sample contains no Cooper pairs. This observation is also consistent with the series of experiments by Dynes and co-workers ([V1992](#)) in which the energy gap was observed to vanish at the nominal critical field, H_c . For MoGe, Yazdani and Kapitulnik ([YK1995](#)) also found that $H_c \approx H_{c2}$. Collectively, these observations imply that electron-like quasi-particles resulting from Cooper pair-breaking populate the insulating side of the transition in homogeneously disordered thin films. Consequently, physics beyond the phase-only model is necessary to describe these systems.

That this state of affairs obtains could also have been inferred from the experimental fact that in a vast array of homogeneously disordered thin films, the resistivity at criticality, R_c , is equal to the resistivity of the normal state, R_N . A typical plot of R_c versus R_N for Bi ([GM1998](#)) and MoGe ([YK1995](#)) is shown in Fig. 14.7. The normal state resistance, R_N , was extracted ([YK1995; GM1998](#)) from transport measurements at $T > T_p$ (see Fig. 14.3). Hence, only electron-like excitations abound in this temperature range. The critical resistance, R_c , is extracted much below T_p and represents the resistivity at the single crossing point of $R(T)$ vs tuning parameter and as $T \rightarrow 0$. In both the Bi and MoGe films, a magnetic field induces the IST. As is evident from the data shown for both Bi and MoGe, $R_c \approx R_N$. Unless a transition to the normal ground state occurs at R_c , there is no reason for the correspondence $R_c \approx R_N$. Because R_N is associated with high-temperature

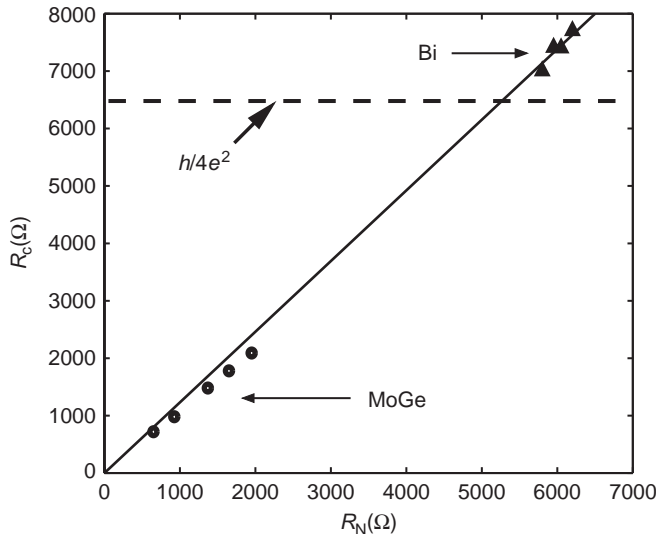


Fig. 14.7 Critical resistance, R_c , as a function of the normal state resistance, R_N , for Bi (GM1998) and MoGe (YK1995) samples. The lack of a universal value at the transition and the correlation of R_c with R_N are indications that the transition to the insulating state has electron-like quasi-particles, indicative of the high-temperature normal state.

physics in which no Cooper pairs exist, the fact that $R_c \approx R_N$ signifies that the insulating state must have electron-like quasi-particles in these homogeneously disordered thin films. Further, in all cases, R_c slightly exceeds R_N and ranges between 900Ω and 8000Ω . These values certainly differ significantly from the boson quantum of resistance, $h/4e^2 = 6500 \Omega$, predicted from the phase-only models, further indicating that physics beyond the phase-only model is at work.

To conclude, phase-only physics seems to be adequate to describe granular films. However, for most homogeneously disordered films, the experiments point to an insulating state populated with electron-like quasi-particles. Consequently, pair-breaking seems to be the dominant mechanism that drives the IST. Consequently, the 3d XY model is no longer adequate to describe the IST in homogeneously disordered films as gapless electronic excitations exist in the insulator. In this case, the critical resistance need not be defined by the quantum of resistance for $2e$ bosons, $R_Q = h/4e^2$, as is observed experimentally. Progress in including normal electrons into the IST could be made along the lines pursued recently by Feigelman and Larkin (FL1998).

14.7 Scaling and T-linear resistivity

Quantum phase transitions are governed by a $T = 0$ quantum critical point. Further, as temperature plays a crucial role, the corresponding field theory for quantum phase transitions is $(d + z)$ -dimensional. The quantum rotor model is the simplest model that

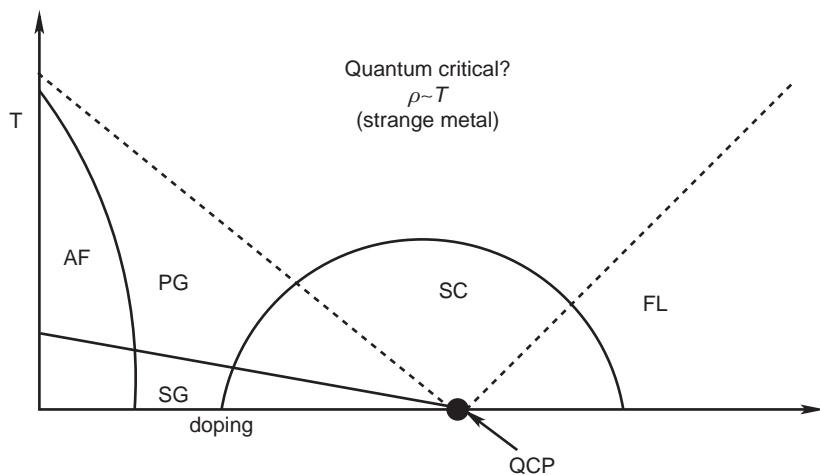


Fig. 14.8

Heuristic phase diagram of the high-temperature copper oxide superconductors as a function of temperature and hole concentration (doping). The phases are as follows: AF represents antiferromagnet, SG the spin glass, and SC the superconductor with $d_{x^2-y^2}$ symmetry. The spin-glass phase terminates at a critical doping level (quantum critical point, QCP) inside the dome. The dashed lines indicate crossovers, not critical behavior. In this context PG and FL represent the pseudo-gap and Fermi liquid phases in which respectively the single-particle spectrum develops a dip and the transport properties become more conventional. The strange-metal behavior, T -linear resistivity, in the funnel-shaped regime has been attributed to quantum critical behavior. A scaling analysis of the conductivity at the quantum critical point rules out this scenario, however.

captures the essential tension between the competing ground states near the superconductor to non-superconductor quantum critical point. This model can be recast as a Landau–Ginzburg theory. A key surprise with $T = 0$ quantum critical points is that the transport properties must be determined by collisions between thermally excited quasi-particles. In the context of the quantum rotor model, inclusion of quasi-particle scattering results in a metallic phase in the quantum disordered regime. The Bose metal phase is stable to weak disorder as long as the disorder is non-pair breaking.

Directly above the quantum critical point, the dynamics are determined by temperature. Hence, it is tempting to associate resistivities that are linear in temperature with the possible existence of a quantum critical point, as in the case of the copper-oxide superconductors (or cuprates) (BTKW1993). T -linear resistivity in the cuprates stands as the key challenge in the physics of the normal state. Early in the theory of the cuprates, explanations (T1999; V1989) based on some type of quantum criticality were invoked to explain T -linear resistivity. One can ask the simple question, does quantum criticality place any restriction on the form of the resultant resistivity? Indeed it does, as can be seen from the following scaling analysis.

The argument (PC2005) is based on three general assumptions: (1) the critical degrees of freedom carry the current, (2) only a single length scale is relevant near the critical point, and (3) charge is conserved. Granted true, these assumptions rule out quantum criticality as the cause of the T -linear resistivity.

Consider a general action S whose microscopic details are unimportant as long as the current is critical. An externally applied electromagnetic vector potential A^μ , $\mu = 0, 1, \dots, d$, couples to the electrical current, j_μ , such that

$$S \rightarrow S + \int d\tau d^d x A^\mu j_\mu. \quad (14.57)$$

The key point here is that the vector potential couples linearly to the current and hence has a scaling dimension of unity. This fact will be crucial later in the proof. Under the one-parameter scaling hypothesis for quantum systems, the spatial correlations in a volume smaller than the correlation volume, ξ^d , and temporal correlations on a time scale shorter than $\xi_t \propto \xi^z$ are small, and space-time regions of size $\xi^d \xi_t$ behave as independent blocks. Using this hypothesis, we write the scaling form for the singular part of the logarithm of the partition function by counting the number of correlated volumes in the whole system:

$$\ln Z = \frac{L^d \beta}{\xi^d \xi_t} F(\delta \xi^{d_\delta}, \{A_\lambda^i \xi^{d_A}\}). \quad (14.58)$$

In this expression, L is the system size, δ the distance from the critical point, and d_δ and d_A the scaling dimensions of the critical coupling and vector potential, respectively. The variables $A_\lambda^i = A^i(\omega = \lambda \xi_t^{-1})$ correspond to the (uniform, $k = 0$) electromagnetic vector potential at the scaled frequency $\lambda = \omega \xi_t$, and $i = 1, \dots, d$ labels the spatial components. Two derivatives of the logarithm of the partition function with respect to the electromagnetic gauge $A^i(\omega)$,

$$\begin{aligned} \sigma_{ij}(\omega, T) &= \frac{1}{L^d \beta} \frac{1}{\omega} \frac{\delta^2 \ln Z}{\delta A^i(-\omega) \delta A^j(\omega)} \\ &= \xi^{-d} \frac{\xi_t^{-1}}{\omega} \xi^{2d_A} \frac{\delta^2}{\delta A_{-\bar{\lambda}}^i \delta A_{\bar{\lambda}}^j} F(\delta = 0) \Big|_{\substack{\bar{\lambda} = \omega \xi_t \\ \{A_\lambda^i = 0\}}} \\ &= \frac{Q^2}{\hbar} \xi^{2d_A - d} \Sigma_{ij}(\omega \xi_t), \end{aligned} \quad (14.59)$$

determine the conductivity for carriers with charge Q . We have explicitly set $\delta = 0$ as our focus is the quantum critical regime. At finite temperature, the time correlation length is cut off by the temperature as $\xi_t \propto 1/T$, and $\xi_t \propto \xi^z$. The engineering dimension of the electromagnetic gauge is unity ($d_A = 1$), as remarked earlier. This result follows entirely from charge conservation (W1992). We then arrive at the general scaling form

$$\sigma(\omega, T) = \frac{Q^2}{\hbar} T^{(d-2)/z} \Sigma \left(\frac{\hbar \omega}{k_B T} \right) \quad (14.60)$$

for the conductivity, where Σ is an explicit function only of the ratio ω/T . (The ij tensor indices have been dropped for simplicity.) This scaling form generalizes the $T = 0$ frequency dependent critical conductivity derived by Wen (W1992) to non-zero temperature. The generic scaling form, Eq. (14.60), is also in agreement with that proposed by Damle and Sachdev (DS1997) in their extensive study of collision-dominated transport near a

quantum critical point (see also the scaling analysis in (SS2000)). What the current derivation lays plain is that, regardless of the underlying statistics or microscopic details of the Hamiltonian, be it bosonic (as in the work of Damle and Sachdev (DS1997)) or otherwise, be it disordered or not, the general scaling form of the conductivity is unchanged. The conductivity (see Eq. (13.25)) for the Anderson metal–insulator transition in $d = 2 + \epsilon$, which can be thought of as a quantum phase transition where the dimensionless disorder strength is the control parameter (W1979; AALR1979), obeys the scaling function derived here for the conductivity.

At zero frequency, the dc limit, we obtain

$$\sigma(\omega = 0) = \frac{Q^2}{\hbar} \Sigma(0) \left(\frac{k_B T}{\hbar c} \right)^{(d-2)/z}. \quad (14.61)$$

In general $\Sigma(0) \neq 0$. Otherwise, the conductivity is determined entirely by the non-singular and hence non-critical part of the free energy. The cuprates are anisotropic three-dimensional systems. Hence, the relevant dimension for the critical modes is $d = 3$ not $d = 2$. In the latter case, the temperature prefactor is constant. For $d = 3$, we find that T -linear resistivity obtains only if $z = -1$. Such a negative value of z is unphysical in standard commutative field theories as it implies that energy scales diverge for long-wavelength fluctuations at the critical point.

While it is certainly reasonable to assume that $\Sigma(0)$ is finite at zero temperature, it is certainly a possibility that $\Sigma(0)$ might in fact diverge. A possible scenario of how this state of affairs might obtain is that a dangerously irrelevant operator could govern the conductivity. In this case, $\Sigma(0) \sim 1/T^p$, and T -linear behavior obtains if $p = (d - 2)/z + 1$. This can only occur above the upper critical dimension. In this regime, all criticality is mean-field-like. Hence, a possibility that cannot be eliminated at this time is that all criticality in the cuprates is inherently mean-field and dangerously irrelevant operators control the conductivity. For strongly correlated systems, however, it is unlikely that criticality is inherently mean-field.

This proof suggests one of three possibilities might be relevant: (1) quantum criticality has nothing to do with the problem, (2) the current is carried by non-critical degrees of freedom, or (3) new quantum critical scenarios in which additional length scales describe the physics. In a scenario involving non-critical degrees of freedom, fermionic charge carriers in the normal state of the cuprates could couple to a critical bosonic mode. Such an account is similar to that in magnetic systems (H1976) in which fermions scatter off massless bosonic density or spin fluctuations and lead to an array of algebraic forms for the resistivity (K1996; R1999) ranging from $T^{4/3}$ to $T^{3/2}$ in antiferromagnetic and ferromagnetic systems, respectively. While disorder can alter the exponent (R1999), T -linear resistivity results only in a restricted parameter space. The robustness of T -linear resistivity in the cuprates makes this type of scenario unlikely. The scenario we have advocated is one in which additional length scales enter the problem. The extra degree of freedom arises from dynamical spectral weight transfer across the Mott gap. This is described in the final chapter.

Problems

14.1 In the quantum rotor model

$$H = E_C \sum_i (\hat{n}_i - n_0)^2 - t \sum_{\langle ij \rangle} (b_i^\dagger b_j + b_j^\dagger b_i), \quad (14.62)$$

show that when n_0 is not an integer, the corresponding action is of the form

$$S \propto \int_0^\beta d\tau \theta \partial_\tau \theta - \sum_{\langle ij \rangle} V(\cos \theta_i - \theta_j). \quad (14.63)$$

This version of the quantum rotor model is known as the incommensurate Bose–Hubbard model. What consequences does this have on the value of the dynamical exponent?

- 14.2 Using Eq. (14.35), prove the result in Eq. (14.36).
- 14.3 Use the low-temperature form of $C_0(\tau, \tau')$, Eq. (14.37), to establish the final equality in Eq. (14.46).
- 14.4 Perform the integral in Eq. (14.51) and then use the Poisson summation formula to arrive at Eq. (14.52).

References

- [AALR1979] E. Abrahams, P. W. Anderson, D. C. Licciardello, and T. V. Ramakrishnan, *Phys. Rev. Lett.* **42**, 673 (1979).
- [AR1998] G. Aeppli and T. F. Rosenbaum, in *Dynamical Properties of Unconventional Magnetic Systems*, eds. A. T. Skjeltorp and D. Sherrington (Kluwer Academic Publishers, Netherlands, 1998), p. 107.
- [A1964] P. W. Anderson, in *Lectures on the Many Body Problem*, ed. E. R. Caianiello (Academic, New York, 1964), Vol. 2, p. 127.
- [B1994] R. P. Barber, Jr., L. M. Merchant, A. La Porta, and R. C. Dynes, *Phys. Rev. B* **49**, 3409 (1994).
- [BTKW1993] For a review, see B. Batlogg, H. Takagi, H. L. Kao, and J. Kwo, *Electronic Properties of High- T_c Superconductors*, eds. H. Kuzmany, *et al.* (Springer-Verlag, Berlin, 1993), p. 5.
- [B1971] V. L. Berezinskii, *Zh. Eksp. Teor. Fiz.* **61**, 1144 (1971) [*Sov. Phys.-JETP* **34**, 610 (1971)].
- [BMO1979] M. R. Beasley, J. E. Mooij, and T. P. Orlando, *Phys. Rev. Lett.* **42**, 1165 (1979).
- [C1991] M. C. Cha, M. P. A. Fisher, S. M. Girvin, M. Wallin, and A. P. Young, *Phys. Rev. B* **44**, 6883 (1991).
- [DP2001] D. Dalidovich and P. Phillips, *Phys. Rev. B* **64**, 052507 (2001).

- [DS1997] K. Damle and S. Sachdev, *Phys. Rev. B* **56**, 8714 (1997).
- [D1981] S. Doniach, *Phys. Rev. B* **24**, 55063 (1981).
- [FL1998] M. V. Feigelman and A. I. Larkin, *Chem. Phys.* **235**, 107 (1998).
- [F1972] R. P. Feynman, *Statistical Mechanics* (W. A. Benjamin, Reading, Mass., 1972), p. 66.
- [FH1965] R. P. Feynman and A. R. Hibbs, *Quantum Mechanics and Path Integrals* (McGraw-Hill, New York, 1965), p. 42.
- [F1990] M. P. A. Fisher, *Phys. Rev. Lett.* **65**, 923 (1990).
- [GM1998] For a review, see A. M. Goldman and N. Markovic, *Physics Today* **51** (11) 39 (1998).
- [GS2005] A. G. Green and S. L. Sondhi, *Phys. Rev. Lett.* **95**, 267001 (2005).
- [HN1979] B. I. Halperin and D. R. Nelson, *J. Low Temp. Phys.* **36**, 5999 (1979).
- [HP1990] A. F. Hebard and M. A. Paalanen, *Phys. Rev. Lett.* **65**, 927 (1990).
- [H1976] J. A. Hertz, *Phys. Rev. B* **14**, 1165 (1976).
- [H1995] S.-Y. Hsu, Ph.D. Thesis, Brown University, 1995.
- [HCV1995] S.-Y. Hsu, J. A. Chervenak, and J. M. Valles, Jr., *Phys. Rev. Lett.* **75**, 132 (1995).
- [H1959] J. Hubbard, *Phys. Rev. Lett.* **3**, 77 (1959).
- [J1989] H. M. Jaeger, D. B. Haviland, B. G. Orr, and A. M. Goldman, *Phys. Rev. B* **40**, 182 (1989).
- [K1996] S. Kambe, S. Raimond, L.-P. Regnault, *et al.*, *J. Phys. Soc. Jpn.* **65**, 3294 (1996).
- [KZ1993] A. P. Kampf and G. T. Zimanyi, *Phys. B* **47**, 279 (1993).
- [KT1973] J. M. Kosterlitz and D. J. Thouless, *J. Phys. C* **6**, 1181 (1973).
- [P1979] P. Pfeuty, *Phys. Lett. A* **72**, 245 (1979).
- [PC2005] P. Phillips and C. Chamon, *Phys. Rev. Lett.* **95**, 107002 (2005).
- [R1999] A. Rosch, *Phys. Rev. Lett.* **82**, 4280 (1999).
- [S1999] S. Sachdev, *Quantum Phase Transitions* (Cambridge University Press, Cambridge, 1999).
- [SS2000] T. Schneider and J. M. Singer, *Phase Transition Approach to High Temperature Superconductivity: Universal Properties of Cuprate Superconductors* (Imperial College Press, London, 2000), p. 238.
- [S1980] E. Simanek, *Phys. Rev. Lett.* **45**, 1442 (1980).
- [S1958] R. L. Stratanovich, *Sov. Phys. Dokl.* **2**, 416 (1958).
- [T1999] J. T. Tallon, J. W. Loram, G. V. M. Williams, *et al.*, *Phys. Stat. Sol. (b)* **215**, 531 (1999).
- [V1992] J. M. Valles, Jr., R. C. Dynes, and J. P. Garno, *Phys. Rev. Lett.* **69**, 3567 (1992).
- [V1989] C. M. Varma, P. B. Littlewood, S. Schmitt-Rink, and A. E. Ruckenstein, *Phys. Rev. Lett.* **63**, 1996 (1989).
- [W1994] M. Wallin, E. S. Sorensen, S. M. Girvin, and A. P. Young, *Phys. Rev. B* **49**, 12115 (1994).
- [W1979] F. J. Wegner, *Z. Phys. B* **35**, 207 (1979).

- [W1992] X.-G. Wen, *Phys. Rev. B* **46**, 2655 (1992).
- [WZ1990] X. G. Wen and A. Zee, *Intl. J. Mod. Phys. B* **4**, 437 (1990).
- [W1965] B. Widom, *J. Chem. Phys.* **43**, 3892 (1965).
- [YK1995] A. Yazdani and A. Kapitulnik, *Phys. Rev. Lett.* **74**, 3037 (1995).

When an electron gas is confined to move at the interface between two semiconductors and a magnetic field is applied perpendicular to the plane, a new state of matter ([TSG1982](#)) arises at sufficiently low temperatures. This state of matter is unique in condensed matter physics in that it has a gap to all excitations and exhibits fractional statistics. It is generally referred to as an incompressible quantum liquid or as a Laughlin liquid ([L1983](#)), in reference to the architect of this state. While the Laughlin state is mediated by the mutual repulsions among the electrons, it is the presence of the large perpendicular magnetic field that leads to the incompressible nature of this new many-body state. The precursor to this state is the integer quantum Hall state. In this state, disorder and the magnetic field conspire to limit the relevant charge transport to a narrow strip around the rim of the sample. The novel feature of this rim or edge current is that it is quantized in integer multiples of e^2/h ([KDP1980](#)). The equivalent current in the Laughlin state is still quantized but rather in fractional multiples of e^2/h . We present in this chapter the phenomenology and the mathematical description needed to understand the essential physics of both of these effects.

As we will see, topology is an integral part of the quantum Hall effect. Regardless of the geometry or smooth changes in the Hamiltonian, the quantization of the conductance depends solely on the existence of edge states which have a well-defined chirality. While edge states are easy to rationalize in the existence of a magnetic field, such a time-reversal breaking field is not necessary. It is the realization that edge states can exist in the presence of time-reversal symmetry that has led to the new field of topological insulators ([KM2005a; KM2005b; TFK2008; HK2010; BHZ2006; R2009; MB2007; X2009; Z2009; QHZ2008; QZ2010; K2007; BZ2006](#)). The key difference from quantum Hall systems is that the edge states are necessarily doubly degenerate, one for each spin, as opposed to a single current-carrying state in the quantum Hall effect. A simple model will be presented which captures the essence of such topologically protected states in an otherwise insulating sample.

15.1 What is the quantum Hall effect?

To understand what is quantum about the Hall effect, we must first define the concept of the Hall voltage ([H1879](#)). To this end, we consider a conducting metal slab in which a current, I , is directed along the x -direction. The current produces a voltage drop and an electric field, E_x , and current density, j_x , along the x -axis, as illustrated in Fig. 15.1(a). We will assume that the current density and the electric field are linearly related (Ohm's law),

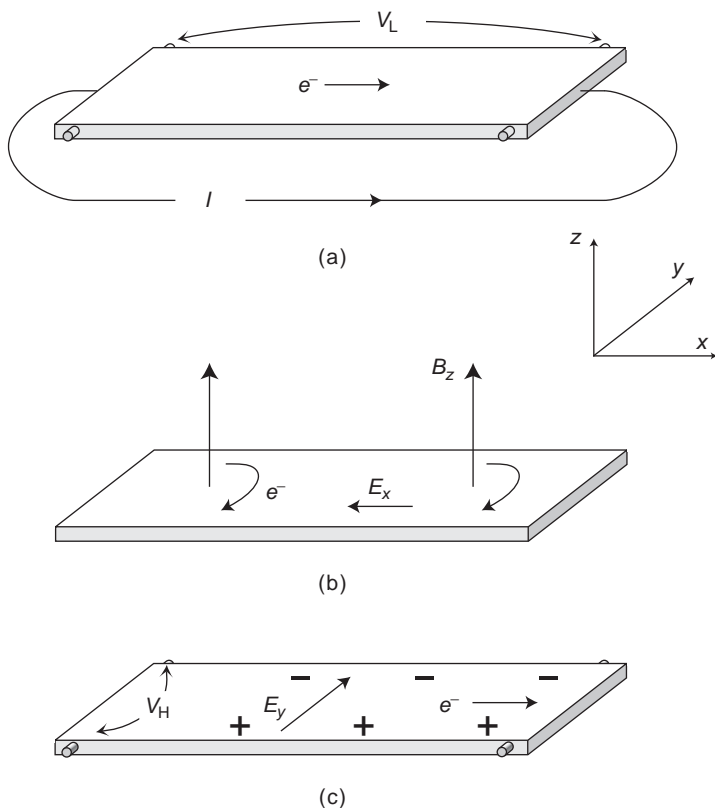


Fig. 15.1

(a) Standard geometry for the Hall effect. A current, I , is passed through a thin sample in the x -direction, leading to a voltage drop and an electric field E_x along the x -axis. The sample is pierced in the positive z -direction by a uniform magnetic field B_z . (b) The resultant sideways motion in the y -direction of the electrons in response to the magnetic field. Electrons accumulate on one face of the material, creating a transverse electric field E_y . (c) A positive ion excess is established until the Hall field, E_y , cancels the Lorentz force .

$j_x = \sigma_0 E_x$, and the constant of proportionality is given by the Drude conductivity derived in Chapter 10. In the presence of a magnetic field oriented upwards along the z -axis, the electrons will be deflected sideways in the negative y -direction (Fig. 15.1(b)) by the Lorentz force. If the sample is infinite in the y -direction, the current will no longer be directed solely along the x -axis. Rather, the electrons will move at some angle relative to the x -axis. This angle defines the Hall angle. However, if the sample is constrained in the y -direction, electrons deflected by the magnetic field will ultimately run into the edges of the sample. As they accumulate there, they will produce an electric field, E_y , which will point in the positive y -direction. Further accumulation of electrons at the edges of the sample ceases when the electric field E_y is sufficiently large to cancel the Lorentz force. Cancellation of the Lorentz force in equilibrium (Fig. 15.1(c)) signifies that electrons will transport purely along the x -axis. The additional electric field, E_y , which facilitates the cancellation can be

thought of simply as an induction field which arises from the magnetic flux of the charges at the boundaries. It is the field E_y that is referred to as the Hall field. In a uniform system at equilibrium, the Hall field is perpendicular to the current. For a strictly 2d sample of width W , the Hall voltage V_H is related to the Hall field through $E_y = V_H/W$. The total current is given by $I = W j_x$.

To understand the functional dependence of E_y as a function of the magnetic field, we develop a semiclassical or high-temperature theory. In this regime, we can determine the magnitude of the Hall field by applying Newton's second law

$$F = -e \left(\mathbf{E} + \frac{1}{c} \mathbf{v} \times \mathbf{B} \right) \quad (15.1)$$

to our constrained metal slab, where \mathbf{v} and \mathbf{B} are the electron velocity and the magnetic field, respectively. Cancellation of the forces in the y -direction requires that

$$E_y = \frac{v_x B_z}{c}. \quad (15.2)$$

As in Chapter 10, we invoke the relaxation time approximation for the electron velocity, $v_x = -e E_x \tau / m$, where τ is the collision time. The other fundamental time scale in this problem is set by the cyclotron frequency,

$$\omega_c \equiv \frac{e B_z}{mc}. \quad (15.3)$$

With the relaxation time approximation, we can rewrite the Hall field

$$E_y = -\omega_c \tau E_x \quad (15.4)$$

in terms of the cyclotron frequency. Because the current density,

$$j_x = \frac{e^2 \tau \rho E_x}{m}, \quad (15.5)$$

is proportional to τE_x , the transverse resistivity defined as

$$\rho_H = \frac{E_y}{I} = \frac{E_y}{W j_x} \quad (15.6)$$

is independent of the relaxation time. In Hall experiments, however, the measured quantities are the transverse voltage, V_H , and the longitudinal voltage, $V_L = E_x L$, where L is the longitudinal distance across which the voltage changes by V_L . Hence, rather than working with resistivities, it is more convenient in the Hall effect to consider the resistance. The

Hall resistance,

$$R_H = \frac{V_H}{I} = \frac{WE_y}{W j_x} = -\frac{B_z}{ec\rho}, \quad (15.7)$$

is linearly related to the applied magnetic field, while the longitudinal resistance,

$$R_L = \frac{V_L}{I} = \frac{LE_x}{W j_x} = \frac{L}{W} \frac{1}{\sigma_0}, \quad (15.8)$$

is independent of the magnetic field. Experimentally, these relationships agree well with Hall's measurements in 1879 ([H1879](#)). Note that R_H as we have calculated it here is independent of the details of the electron scattering processes. In general there is a weak dependence on such processes.

In 1980 von Klitzing and collaborators ([KDP1980](#)) noticed striking deviations from the resistances given by Eqs. (15.7) and (15.8) at sufficiently high magnetic fields and ultra-low temperatures. They performed their remarkable experiments on a 2d electron gas confined at the interface between SiO_2 and Si in an Si MOSFET. They found that the Hall voltage as the magnetic field increased exhibited distinct flat or plateau regions that were highly reproducible from sample to sample, as shown in Fig. 15.2. From the value of the Hall voltage at the plateau regions, they deduced that the Hall conductance (the inverse of the resistance) must be quantized in units of e^2/h . The quantization of the conductance in the form

$$\sigma_H = -\frac{ne^2}{h}, \quad (15.9)$$

where n is an integer, was found to hold for one part in 10^7 . Equally surprising was the behavior of the longitudinal resistance. They found that the longitudinal resistance vanished exactly at the Hall plateaus, indicating the onset of dissipationless transport. The presence of both quantization and perfect conduction indicates that something quite fundamental is at the heart of these experiments. At much higher magnetic fields and lower temperatures, Tsui, Störmer, and Gossard ([TSG1982](#)) found that the plateau regions in the Hall voltage were more plentiful than had been thought possible. They found that the plateau regions can occur when the conductance is a fractional multiple of e^2/h , indicating the presence of fractionally charged excitations. We will show that the integer Hall effect can be understood simply as a quantization of the edge current, whereas the fractional effect arises from a fundamentally new correlated many-body state, the Laughlin state ([L1983](#)).

15.2 Landau levels

To start, we solve for the wavefunctions describing an electron moving in a plane pierced by a perpendicular magnetic field. Following Landau's original treatment, we orient the

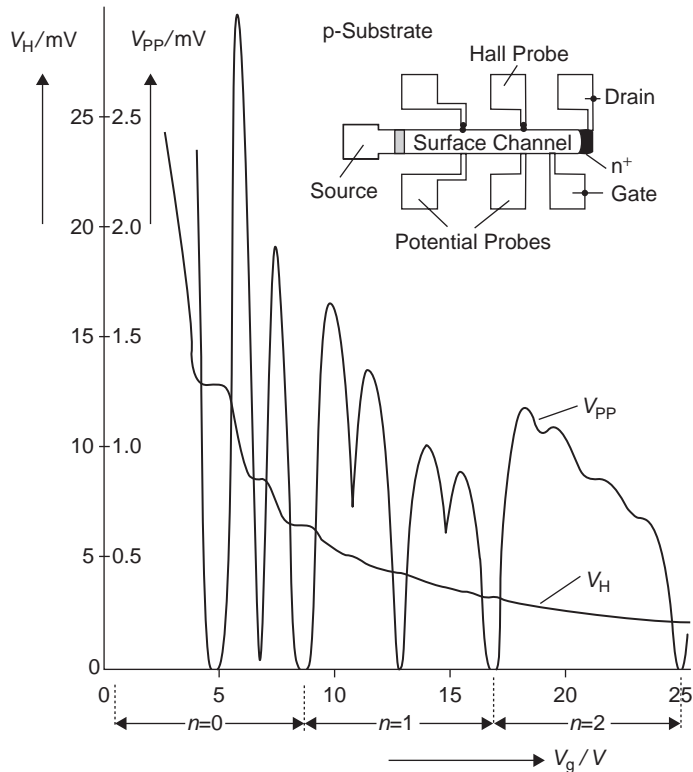


Fig. 15.2 Hall voltage, V_H , and the potential drop between the potential probes, V_{PP} , as a function of gate voltage V_g at $T = 1.5$ K. The magnetic field was held fixed at 18 T and the source drain current at $1 \mu\text{A}$. Shown in the inset is a top view of the device with a length of $L = 400 \mu\text{m}$, a width of $W = 50 \mu\text{m}$, and a distance between the potential probes of $L_{pp} = 130 \mu\text{m}$. The Hall plateaus occur at integer values of the filling in each Landau level indicated with the index, n . At the plateaus in the Hall voltage, the longitudinal voltage goes to zero, indicating the presence of dissipationless transport.

vector potential

$$A_y = Bx, \quad A_x = 0, \quad (15.10)$$

along the y -direction and the single-particle Schrödinger equation takes the form

$$-\frac{\hbar^2}{2m} \left(\partial_x^2 + (\partial_y - ieBx/\hbar c)^2 \right) \psi(x, y) = E\psi(x, y). \quad (15.11)$$

This choice of gauge is most convenient to describe transport in the integer quantum Hall effect. In the context of the fractional quantum Hall effect, however, we will find it expedient to work in the symmetric gauge in which

$$\mathbf{A} = \frac{B}{2}(\hat{y}\hat{x} - \hat{x}\hat{y}). \quad (15.12)$$

In the symmetric gauge, applying a magnetic field in the z -direction leads to a harmonic oscillator problem along both the x - and y -axes. Hence, this problem can easily be solved once the solution to the simpler problem described by Eq. (15.10) is obtained.

Translational invariance in the y -direction suggests that we write the wavefunction as

$$\psi_{n,k}(x, y) = e^{iky} f_n(x). \quad (15.13)$$

Substitution of $\psi_{n,k}(x, y)$ into Eq. (15.11) reveals that $f_n(x)$ is a solution to a harmonic oscillator equation

$$\frac{\hbar\omega_c}{2} (-\ell^2 \partial_x^2 + (x/\ell - \ell k)^2) f_n(x) = \epsilon_n f_n(x), \quad (15.14)$$

where, unlike the cyclotron frequency, the length scale

$$\ell \equiv \sqrt{\frac{\hbar c}{eB}} = \frac{250\text{\AA}}{\sqrt{B}} \quad (15.15)$$

is independent of the effective mass and is changed entirely by varying the magnetic field. Known as the magnetic length, ℓ is roughly 250 Å for a field of $B = 1$ T. From the harmonic oscillator ground state, we generate a Gaussian family of wavefunctions

$$\psi_{n,k}(x, y) = e^{iky} H_n(x/\ell - \ell k) e^{-\frac{(x-x_k)^2}{2\ell^2}} \quad (15.16)$$

which are extended in the y -direction but localized in x and centered at $x_k = \ell^2 k$. In Eq. (15.16), H_n is a Hermite polynomial. Each state indexed by n is known as a Landau level. The energy of each Landau level is

$$\epsilon_n = \hbar\omega_c \left(n + \frac{1}{2} \right) \quad (15.17)$$

and hence is independent of k . As a result, several iso-energetic states compose each Landau level. For a field of $B = 1$ T, the zero-point energy is on the order of 10^{-4} eV, or 1.34 K. We will see the effects of quantization in the discrete Landau levels if the temperature is lower than that determined by the zero-point energy. Our estimate of 1.34 K is a bit in error as we have not used the semiconductor effective mass. For GaAs, $m^* = 0.06m$; hence, the zero-point energy increases by a factor of 16 as does the temperature at which quantization effects in Landau levels are experimentally observable.

As a result of the degeneracy, each Landau level can hold many electrons. The degeneracy is determined by the distinct number of k values that generate a state within the same Landau level. We note that the states comprising each Landau level are centered at $x_k = \ell^2 k$, where

k can take on a range of values consistent with the confinement of the system in the y -direction. Let L and W be the spatial extents of the sample in the x - and y -directions, respectively. If we write the wavevector k as

$$k_m = \frac{2\pi m}{W}, \quad (15.18)$$

with m an integer, the maximum number of states allowable in each Landau level is obtained by solving the condition $L = \ell^2 k_{N_{\max}}$ or, equivalently,

$$N_{\max} = \frac{LW}{2\pi\ell^2} = \frac{eBLW}{hc}. \quad (15.19)$$

The right-hand side of this expression has a simple physical interpretation. The total magnetic flux in each Landau level is a product of the magnetic field and the area of the sample, BLW . This quantity must be equal to the number of electrons in each level times the flux quantum, hc/e . We see then that N_{\max} is also the number of electrons in each Landau level. Consequently, we associate with each Landau level

$$n_B = \frac{1}{2\pi\ell^2} = \frac{eB}{hc} \quad (15.20)$$

as the number of states per unit area. Physically, $1/n_B$ is the irreducible area each state occupies in a Landau level. For $B = 1$ T, the irreducible area corresponds to a square with sides of about 0.6×10^{-9} m, roughly ten times the Bohr radius. Note the area $1/n_B$ is invariant from one Landau level to the next. As a result, the total number of filled Landau levels is given by

$$\nu = \frac{\rho}{n_B} \quad (15.21)$$

where ρ is the number of electrons per unit area. In the integer quantum Hall effect, ν is an integer.

It should now be clear that if the number of electrons in the system is an integral multiple of n_B , then the conductance is quantized. Under such conditions, the electron density $\rho = nn_B$, where n is an integer. As the reciprocal of the Hall resistance, the Hall conductance is given by $\sigma_H = -ec\rho/B = ecnn_B/B = -ne^2/h$.

We can formulate a more penetrating argument for the quantization by appealing to the vanishing of the Lorentz force. If the system is translationally invariant, then the vanishing of the Lorentz force signifies that we can switch to a reference frame which moves at a velocity \mathbf{v} relative to the laboratory frame such that $\mathbf{v} \times \mathbf{B} = -c\mathbf{E}$. In this reference frame, the velocity is given by $v_i = cE_j/B_k\epsilon_{ijk}$ where ϵ_{ijk} is the totally antisymmetric unit tensor defined by

$$\begin{aligned} \epsilon_{123} &= \epsilon_{231} = \epsilon_{312} = 1, & \text{even permutation,} \\ \epsilon_{321} &= \epsilon_{213} = \epsilon_{132} = -1, & \text{odd permutation.} \end{aligned} \quad (15.22)$$

The total current along the i -axis is given by Qev_i , where Q is the total charge in the system. If n Landau levels are occupied with N_{\max} electrons in each, then $Q = nN_{\max}$. Hence, the current density is given by

$$j_i = \frac{eQv_i}{LW} = \frac{ecQE_j}{BLW} \epsilon_{ij} = \sigma_{ij}E_j, \quad (15.23)$$

where σ_{ij} , the coefficient of E_j , is the transverse current. This current is antisymmetric with respect to permutation of the indices x and y . Recall that the total magnetic flux $BLW = N_{\max}hc/e$. As a consequence,

$$\sigma_{xy} = \frac{ecQ}{BLW} = \frac{ecnN_{\max}}{N_{\max}hc/e} = \frac{ne^2}{h}. \quad (15.24)$$

Because the transverse current is antisymmetric, $\sigma_{xy} = -\sigma_{yx}$. In the moving reference frame, the diagonal conductance, $\sigma_{xx} = 0$ as a result of the vanishing of the longitudinal electric field. There is a fundamental physical reason for the vanishing of σ_{xx} , however. Because the Fermi level lies in the gap between the highest-occupied and the lowest-unoccupied Landau levels, σ_{xx} vanishes. Alternatively, the allowable phase space for scattering states vanishes when the Fermi level lies in a gap; hence $\rho_{xx} = 0$ as well. We see then that the conductance in the quantum Hall regime is a purely off-diagonal tensor with elements

$$\sigma = \begin{bmatrix} 0 & \frac{ne^2}{h} \\ -\frac{ne^2}{h} & 0 \end{bmatrix}. \quad (15.25)$$

Whether σ_{xy} or σ_{yx} are identified as the proper Hall conductance simply depends on the axis system used to orient the electric and magnetic fields.

15.3 The role of disorder

While the preceding argument is simple, it does not apply to dirty systems in which translational invariance is broken. Further, it cannot explain the origin of fractional values of the conductance. In fact, it is easy to see that, without disorder, we cannot account for the plateau nature of the quantum Hall effect. In a translationally invariant system, all the electronic states are extended. If an integral number of Landau levels are occupied, then the Fermi level lies in the gap between the highest-occupied and lowest-unoccupied Landau levels. As the magnetic field decreases, the Fermi level remains constant until the next Landau level is filled, at which point it jumps discontinuously. This would suggest that the Hall conductance should decrease monotonically as a function of magnetic field as in the classical case. From whence then do the plateaus come?

It turns out that disorder saves us. As we showed in Chapter 13, disorder changes both the spatial extent and the energy of electronic states. Hence, the degenerate band of states comprising each Landau level can be thought of as being broadened into a band of states that we describe approximately as having a Lorentzian lineshape centered at the unperturbed

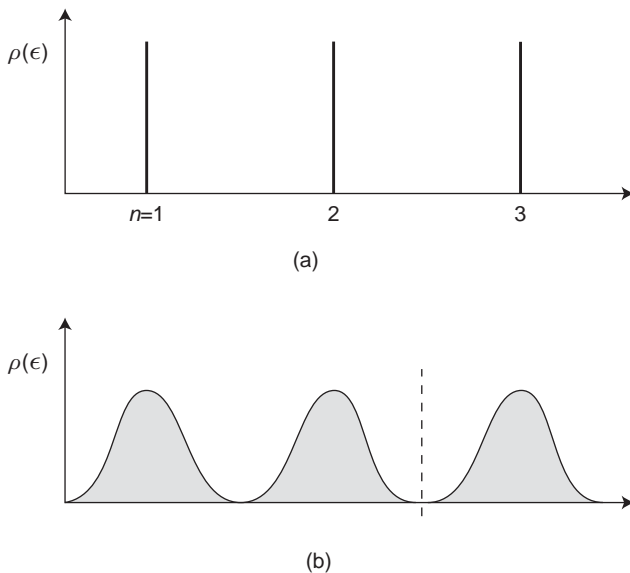


Fig. 15.3 (a) Density of states of Landau levels in a magnetic field. (b) Broadening of the Landau levels as a result of disorder. The dashed line shows the position of the Fermi level.

energy of each Landau level. This is illustrated in Fig. 15.3. Intuitively, the further an electronic state moves away from the unperturbed energy of each Landau level, the more affected it is by the disorder and hence the more it has a tendency to be localized. This can be seen by treating the disorder perturbatively. Hence, we arrive at the simple picture that the states close to the center of the Landau level are less localized than those at the edge of the Lorentzian distribution. We showed in Chapter 13, however, that current-carrying states do not survive for even an infinitesimal amount of disorder in $d = 2$. If this state of affairs persists in the presence of a magnetic field, we arrive at the conclusion that the conductance should vanish in quantum Hall systems as well. However, a magnetic field is present. As we showed in Chapter 12, magnetic fields break time-reversal symmetry and hence disrupt the phase coherence needed to localize electronic states. In $d = 2$, field theoretic (P1984) as well as numerical studies (AA1981; P1981; T1983) show that the scaling theory of localization does in fact break down and current-carrying states obtain. As expected, they remain clustered at the unperturbed energy of each Landau level. All other states are localized. A sharp mobility edge demarcates the separation in energy between the extended and localized states.

From the simple picture that extended states form only at the center of each Landau level and all the other states are localized, we can explain the origin of the quantum Hall plateaus. Because the current is carried only by the states at the center of each Landau level, the current should jump discontinuously as the Fermi level is tuned through the center of each Landau level. Further, the current should remain constant if the occupation of the extended states remains unchanged. That is, although increasing the magnetic field causes the chemical potential to move away from the magical place where the extended states are

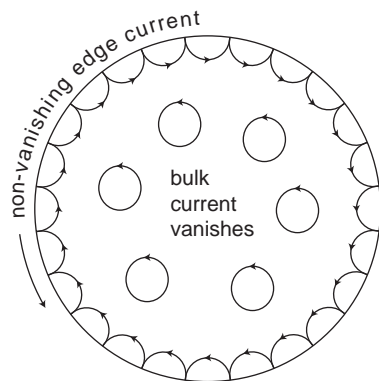
located, the conductance does not change because the chemical potential now resides in a region where the states are localized. The plateaus correspond to the range of magnetic fields for which the population in the extended states is fixed. The presence of precisely flat steps in the Hall voltage attests to the extreme localization of all states in a Landau level except for the narrow region of extended states located at the center. It is for this reason that the quantum Hall effect is fundamentally rooted in disorder. Paradoxically, disorder does not affect the value of the Hall conductance. Specifically, Aoki and Ando ([AA1981](#)) and Prange ([P1981; P1987](#)) showed to the lowest order in the drift velocity, $v_x = cE_x/B_z$, that although an isolated δ -function impurity binds an electron state, the extended states carry just enough extra current to compensate for the loss.

15.4 Currents at the edge

Thus far, we have argued that disorder localizes all electronic states except for those in a narrow window around the unperturbed energy of each Landau level. Once the chemical potential moves into this region, increasing the field further has no effect on the conductance because all other states are localized. Quantum Hall plateaus originate then from the separation in energy between extended and localized states. The only possible deviations from perfectly flat plateaus might originate from thermally activated transport from a localized state to an extended state at the center of a Landau level. At low temperatures, such processes contribute negligibly to the transport.

We have yet to explain, however, why the quantization of the conductance in integral multiples of e^2/h is so precise. As noted by Laughlin ([L1980](#)), the precise quantization of the conductance suggests that the quantum Hall effect must be due to a fundamental principle devoid of any material parameters, such as geometry. To this end, Laughlin formulated a gauge principle to explain the quantization of the Hall conductance.

To understand the essence of this argument, we first make a general observation regarding the current in 2d systems in a magnetic field. As stated earlier, electrons in a magnetic field move in circular orbits as a result of the Lorentz force. As illustrated in Fig. 15.4, in the bulk of a sample, clockwise and counter-clockwise pieces of neighboring cyclotron orbits overlap, leading to a vanishing of the current in the bulk. The situation is quite different at the edges of the sample, however. At the edge, the orbits are truncated in response to the confining potential created by the boundary. Once an electron is reflected by the boundary, it still attempts to move in a circular orbit. This induces a skipping-type motion of an electron at the boundary of the sample, as shown in Fig. 15.4. Such motion generates an edge current that flows in the clockwise direction for a magnetic field oriented along the positive z -direction. The chirality of the edge current is determined then by the direction of the magnetic field. While the above argument is valid strictly when the magnetic length much exceeds the wavelength of the electron, $\ell \gg \hbar/p_F$, the chirality of the edge current can be established quite generally from the presence of an induction field at the boundary ([W1990](#)). That the current arises from states at the edge is a truly novel feature of quantum Hall systems. The chirality of the current at the edge is also at the heart of why the edge states remain extended. As we learned in Chapter 12, backscattering is essential

**Fig. 15.4**

Cyclotron orbits in a quantum Hall system. The circular orbits are caused by the Lorentz force. In the bulk of the sample, clockwise and counter-clockwise pieces of cyclotron orbits overlap and cancel, leading to a vanishing of the current in the bulk. At the edges, the orbits are truncated and give rise to an edge current.

for localization to obtain. There can be no backscattering for a chiral edge state. Hence, they resist localization by a random potential.

Since the current is carried entirely by the edges, the geometry of our system cannot matter. This simple realization already implies that the current in the quantum Hall effect is a topological invariant. We consider then a quantum Hall disk with a hole punched into the center, as depicted in Fig. 15.5. This geometry is equivalent to the one used by Halperin (H1982) in his reformulation of the original Laughlin argument. The disk is pierced with a uniform magnetic field in the positive z -direction. Truncation of the cyclotron orbits at the outer rim of the disk leads to an edge current that flows in the clockwise direction. However, at the inner radius, confinement leads to a current in the opposite direction. Clearly then, if the outer and inner edges of our annulus are at the same chemical potential, no net current will flow in the system. Let's assume that the Fermi levels of the inner and outer edges differ by an amount eE_0 . This difference might be due to asymmetries in the confinement potentials at the inner and outer edges as well as to any electro-chemical potentials that might be present. If n Landau levels are occupied, then the total potential drop is neE_0 . The identical argument leading to Eq. (15.23) can now be invoked and we obtain immediately that the net current between the inner and outer edges is quantized in units of e^2/h .

However, with a little more effort, we can extract the same result from a different way. We consider now the second geometry shown in Fig. 15.5(b). In formulating the gauge argument, we will find it easier to work with this geometry as the Landau gauge used previously is directly applicable. Our coordinate system is chosen so that the y -coordinate runs around the ribbon. As before, the current is carried by the edge states only. These states encircle the ribbon preserving phase coherence as they return to the origin. For the wavefunctions characterizing the edge states to be single-valued, the flux enclosed upon one trek around the disk must be an integral multiple of 2π . Hence, whatever change we make in the vector potential should satisfy the condition that

$$A = \frac{nhc}{eL}, \quad (15.26)$$

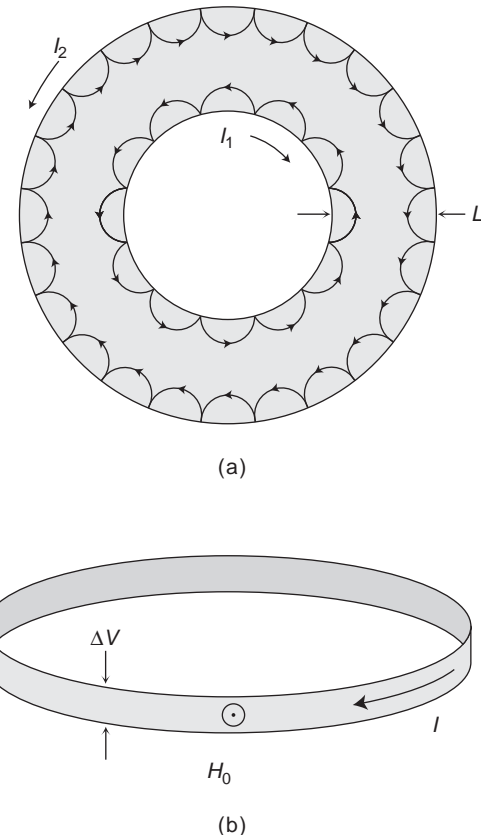


Fig. 15.5 (a) A quantum Hall disk pierced by a magnetic field pointing out of the page. The arrows indicate the direction of the edge currents. (b) A quantum Hall ribbon in which the magnetic field is everywhere perpendicular to the surface. This geometry is mathematically equivalent to a rectangle with periodic boundary conditions in one direction. The circumference of the ribbon is L and its width is W . The Hall voltage is $\Delta V = E_0 W$.

where L is the circumference of the ribbon. For small changes in the vector potential, the current in our system is gauge invariant. Consider now the energy

$$\epsilon_\alpha = \langle \Psi_\alpha | H | \Psi_\alpha \rangle \quad (15.27)$$

of a particular single-particle state, Ψ_α , where H is given by the left-hand side of Eq. (15.11). For short-hand notation, we have defined $\alpha = (n, k)$. We are interested in the derivative of the ϵ_α with respect to A . To simplify this derivative, we use the Hellman–Feynman (H1937) theorem

$$\frac{\partial E(\lambda)}{\partial \lambda} = \langle \Psi_\alpha | \frac{\partial H(\lambda)}{\partial \lambda} | \Psi_\alpha \rangle, \quad (15.28)$$

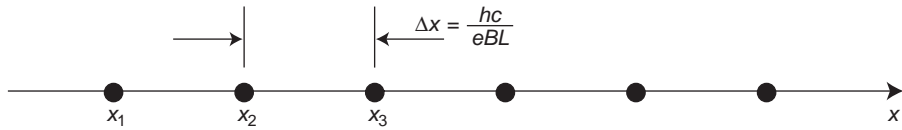


Fig. 15.6

The location of the centers for the electron states that comprise each Landau level. All states are assumed to be degenerate, with their centers given by $\ell^2 k_m = 2\pi \hbar c m / eBL$. The difference between two centers is hc/eBL . Threading the sample with one flux quantum transforms the m th state into the $(m - 1)$ st. This results in the transfer of charge from one edge of the sample to the other.

where λ is simply some variable in the Hamiltonian. Varying the single-particle energy with respect to A ,

$$\begin{aligned} \frac{\partial \epsilon_\alpha}{\partial A} &= \frac{-e}{mc} \langle \Psi_\alpha | \mathbf{p} - \frac{eA}{c} | \Psi_\alpha \rangle \\ &= L \frac{I_\alpha}{c}, \end{aligned} \quad (15.29)$$

defines the current density carried by the state α as it traverses the disk. To evaluate the derivative, we note that in the presence of an electric field, the single-particle energies scale linearly with $eE_0 x_k$, where x_k locates the center of the states comprising each Landau level. If we modify the gauge term in the Hamiltonian such that $\mathbf{A} = Bx\hat{y} \rightarrow Bx\hat{y} + \Delta A\hat{y}$, then the location of each center is shifted by $x_k \rightarrow x_k - \Delta A/B$. Consequently, the single-particle energies are translated to $\epsilon_{n,k} \rightarrow \epsilon_{n,k} - eE_0 \Delta A/B$, and

$$\frac{\partial \epsilon_\alpha}{\partial A} = -\frac{eE_0}{B} \quad (15.30)$$

is independent of the state index. As illustrated in Fig. 15.6, Laughlin's gauge principle (L1980) follows from the fact that the difference between the location of the centers of two neighboring states in the same Landau level,

$$\begin{aligned} \Delta x_k &= x_k^{m+1} - x_k^m = \ell^2 (k_{m+1} - k_m) = \frac{2\pi \ell^2}{L} \\ &= \frac{hc}{eBL} = \frac{\Delta A}{B}, \end{aligned} \quad (15.31)$$

is directly related to the change in the vector potential. Consequently, if A is changed by a single flux quantum, the location of the m th center,

$$x_k^m \rightarrow x_k^m - \frac{\Delta A}{B} = x_k^m - \frac{hc}{eBL} = x_k^{m-1}, \quad (15.32)$$

is now coincident with the location of the $(m - 1)$ st center. Hence, when one flux quantum is threaded through the ribbon, the states in a Landau level all shift over by one, leading

to the net transfer of a single electron (per Landau level) from one edge of the sample to the other. Quantization of the gauge leads to quantization in the charge transfer! This is the Laughlin gauge principle. It illustrates beautifully the topological (T1982) nature of charge transport in the quantum Hall effect. To calculate the current, we substitute Eq. (15.30) into Eq. (15.29) and sum over all occupied Landau levels. We obtain immediately that the net current between the edges,

$$\begin{aligned} I &= \sum_{n,k} I_{n,k} \\ &= -\frac{ecN_e E_0}{LB} = -\frac{ecnn_B V_H}{B} = -\frac{ne^2 V_H}{h}, \end{aligned} \quad (15.33)$$

is an integer multiple of e^2/h with $V_H = E_0 W$, the Hall voltage and $N_e = nn_B LW$. The negative sign in the current corresponds to counter-clockwise motion on the ribbon. The Laughlin argument lays plain that the quantization of the Hall current or Hall conductance arises primarily from the restriction that the extended states must be single-valued as they traverse the edge of the sample. For a system in a magnetic field, the single-valuedness of the eigenstates manifests itself as a condition on allowable gauge transformations. It is this condition coupled with the integer filling of Landau levels that leads to the quantization. It is also paramount that the gauge transformation be carried adiabatically, so that the system remains in its ground state as the flux penetrating the system is changed.

As the plateau transitions are driven by changing the magnetic field or the filling, they constitute a genuine quantum phase transition of the kind studied in the previous chapter. In fact, because disorder is central to the story of the integer quantum Hall effect, the underlying plateau transitions represent one of the clearest examples of quantum critical phenomena in a disordered system. Progress in understanding the underlying field-theoretical description of the plateau transitions is based largely on the Chalker–Coddington tunneling network model (CC1988; MT1999; Z1999). Numerical simulations of this model (LWK1993; LC1994) have yielded a correlation length exponent of $\nu = 2.3$ which is consistent with experimental observations. However, this exponent is yet to be predicted by a rigorous theoretical account.

15.5 Topological insulators

In the quantum Hall effect, the current is carried by the edge. That it must be an integer multiple of e^2/h is determined entirely by the fact that when the electromagnetic gauge is changed by a single flux quantum, a single charge is transported across the sample. Since the edge states must be single-valued and their single-valuedness places a constraint on the possible changes in the electromagnetic gauge, the current in the quantum Hall system is robust. The topology of the sample is the only determining factor since σ_{xy} is entirely an edge effect. While the edge of the sample conducts, the bulk is entirely insulating. Hence, quantum Hall samples are topological insulators. Because time-reversal symmetry is broken, the backward- and forward-moving edge states are spatially separated. Hence, if

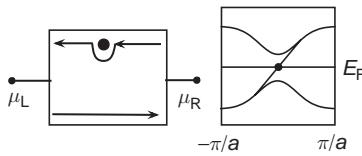


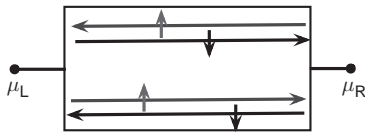
Fig. 15.7 (a) A quantum Hall bar with chiral edge states. (b) Corresponding schematic band structure for a quantum Hall system with a single edge state crossing the band gap. In the absence of time-reversal symmetry breaking, the edge states of a particular chirality cross the Fermi level once.

we plot the band structure of a quantum Hall system near an edge, it would look something like Fig. 15.7. Shown here is the band gap between two Landau levels and a single edge state traversing the gap. The key observation in quantum Hall systems is that $2 = 1 + 1$. That is, there are two edge states but only one at each edge as a result of the breaking of time-reversal symmetry. As pointed out previously, elastic scattering arising from impurities at each edge will not result in backscattering since the states at each edge propagate in only a single direction. There is a possibility that elastic scattering from one edge could give rise to a counter-propagating state. But this would require an electron jumping across the sample to the other edge. The probability for such an event is exponentially small, however. Hence, the only option for an electron encountering an elastic impurity is simply to go around it and continue moving in the same direction.

Consider now turning off the magnetic field. Is it still possible to have edge states that are impervious to backscattering? It turns out the answer is yes. It is this simple realization that spawned the field of topological insulators (KM2005a; KM2005b; TFK2008; HK2010; BHZ2006; R2009; MB2007; X2009; Z2009; QHZ2008; QZ2010; K2007; BZ2006). The key point here is that $4 = 2 + 2$ (QZ2010). That is, when time-reversal symmetry is preserved, there must be two propagating states at each edge. Time-reversal symmetry at each edge ensures that the forward and backward propagating states have opposite spin. Of course an electron can move in the opposite direction if it scatters to the opposite side of the sample. Here again, this is an exponentially small process. Hence, as long as the impurities are featureless in that the interactions arising from them cannot mix spin, there is no way to backscatter an electron. However, this argument, as formulated, fails if spin-orbit scattering is present. To our rescue comes a remarkable property of time-reversal for spin-1/2 particles. In quantum mechanics, the time-reversal operator for spin-1/2 particles is governed by the anti-unitary operator,

$$T = e^{i\frac{\pi}{2}\sigma_y} K, \quad (15.34)$$

where σ_y is the y -Pauli matrix defined in Chapter 7 and K performs complex conjugation. Using the fact that $\sigma_y^2 = 1$, one can expand the exponential in the time-reversal operator

**Fig. 15.8**

A quantum spin Hall system with two propagating states per edge. Kramers' theorem implies that such states must be doubly degenerate. The up and down arrows indicate the spin.

and establish that for an arbitrary angle α ,

$$e^{i\alpha/2\sigma_y} = i\alpha\sigma_y \sin \alpha/2 + \cos \alpha/2. \quad (15.35)$$

Consequently, rotating a spin-1/2 particle by 2π does not return the particle to its original state but to its negative and $T^2 = -1$. This is the origin of the Kramers doubling. Namely, all eigenstates of a time-reversal invariant (TRI) Hamiltonian must be doubly degenerate. Hence, the edge states have to come in pairs, one for each spin, as depicted in Fig. 15.8.

That $T^2 = -1$ protects the surface states from opening a gap in the presence of spin-orbit scattering can be illustrated in one of two ways. Consider the consequences of elastic scattering. In a semiclassical picture, a forward-moving electron encountering an impurity which can have spin-orbit scattering can be reflected backwards. However, since the only channel for backward motion at the edge in question has the opposite spin, the electron must flip its spin. In this process, the spin picks up a phase of π . Running this process backward in time, TRI implies that there is an equivalent process in which a forward-moving electron is scattered backward, but picks up a phase change of $-\pi$. (The two processes can be thought of as anticlockwise and clockwise rotations of spin.) The magnitudes of these amplitudes are identical as long as TRI is present. However, the phase change between these two paths is 2π and hence the wavefunction changes by -1 . Both paths add to yield a vanishing scattering amplitude from an impurity; that is, there is perfect destructive interference. Consequently, as long as TRI is present, there is no way to backscatter off an impurity, and the surface states must cross the gap, thereby giving rise to a net longitudinal current. Alternatively, we can establish the robustness of the surface states from a band argument. TRI implies that the surface states must come in pairs with equal and opposite momenta. Which momentum is assigned spin up or spin down is irrelevant. Further, the edge states must have the same energy at the TRI points in the Brillouin zone which for one-dimensional edge states are $k = 0$ and $k = \pi/a$. Note, the $k = -\pi/a$ point is identical to π/a by TRI. Away from the TRI points, the spin-orbit interaction can lift the degeneracy between the edge states. The question is how is the degeneracy lifted. If the pair of edge states joins the degenerate points as in Fig. 15.9(a), then the surface states are not robust. Figure 15.9(a) is topologically identical to Fig. 15.9(b) as the chemical potential can be moved up and down in the gap. Note, it is irrelevant that the edges states cross the Fermi energy twice. As long as they cross an even number of times, the analog of Fig. 15.9(b) can always be constructed. Consequently, the edge states acquire a mass. However, this is

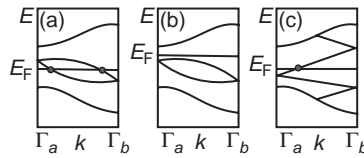


Fig. 15.9

Electronic dispersion between two Kramers degenerate (or time-reversal-invariance) points Γ_a and Γ_b . For a 2d sample, the degenerate points are at $\Gamma_a = 0$ and $\Gamma_b = \pi/a$. (a) Evolution of the surface states between the two Kramers points when the number of Fermi crossing points is even. (b) A distortion of (a) which gaps the surface states. Such a deformation of (a) is always possible if the edge states cross the chemical potential an even number of times. Consequently (a) and (b) are topologically indistinguishable. In (c), there is only a single crossing point in which case any deformation of the sample maintains the integrity of the edge states.

not the only option. The degeneracy can be lifted such that there is only a single crossing away from the TRI points, as illustrated in Fig. 15.9(c). In this case, the sample cannot be deformed (cut, for example) in any way to get rid of the single crossing point. That is, such states are protected by topology. We can distinguish these two cases by defining the index (TFK2008; KM2005a; KM2005b)

$$N_K = m \bmod 2, \quad (15.36)$$

where N_K is the number of Kramers pairs of edge states that cross the Fermi energy. For clarity, by $m \bmod 2$ we simply mean $m + 2p$, where p is any integer. If N_K is even, then $m = 0$, whereas $m = 1$ corresponds to N_K odd. Since there are only two possible values for m , we can think of m as being a Z_2 invariant. Z_2 is the group with two elements, namely 1 and 0, and hence is the simplest non-trivial group.

There is something subtle going on here which can be laid plain by considering spinful free electrons in two dimensions. If time-reversal symmetry is present, the simplest Hamiltonian that can be written for electrons propagating on the edge of a $(2+1)$ -dimensional system is

$$H = p\sigma^z. \quad (15.37)$$

We ask a simple question: how can such edge states be gapped? The simplest augmentation is to add a term of the form $m_y\sigma^y + m_z\sigma^z$. However, since the mass remains invariant under $t \rightarrow -t$, this kind of coupling breaks TRI and hence is not allowed. To open a gap, we need to consider more than a single pair of edge states. Consider two copies of the system

$$H^{(2)} = p\mathbf{I} \otimes \sigma^z = \begin{pmatrix} p\sigma^z & 0 \\ 0 & p\sigma^z \end{pmatrix}.$$

In this expanded space, we can generate a gap (in the presence of TRI) by adding a term of the form $m\tau^y \otimes \sigma^x$ such that

$$H^{(2)} \rightarrow p\mathbf{I} \otimes \sigma^z + m\tau^y \otimes \sigma^x \quad (15.38)$$

with

$$\tau^y = \begin{pmatrix} 0 & -i \\ i & 0 \end{pmatrix}.$$

The eigenvalues of this matrix,

$$\lambda_{\pm} = \pm\sqrt{p^2 + m^2}, \quad (15.39)$$

are doubly degenerate and possess a gap. Hence, unless there is a single Dirac cone (or an odd number of Dirac cones), the edge states are susceptible to the opening of a gap.

While this physics can be generalized to the edge of a three-dimensional sample, there is a more familiar playground for such physics in four spatial dimensions, namely chiral fermions. Such fermions describe the propagating modes at the boundary of a $(4+1)$ -dimensional system. The boundary states are described by two Weyl (not Dirac) equations,

$$\left(\sigma \cdot \nabla - i\frac{\partial}{\partial x_0}\right)\phi^{(L)} = 0, \quad \left(-\sigma \cdot \nabla - i\frac{\partial}{\partial x_0}\right)\phi^{(R)} = 0, \quad (15.40)$$

where $x_0 = t$. In these equations we have set $\hbar = c = 1$ for simplicity. However, this is not the most general description of two chiral fermions. For example there is no mass term. Let us define the two-component spinor

$$\psi = \begin{pmatrix} \phi^{(R)} \\ \phi^{(L)} \end{pmatrix}. \quad (15.41)$$

The massive generalization of the decoupled Weyl equations,

$$(i\gamma_\mu \partial_\mu - m)\psi = 0, \quad (15.42)$$

is the Dirac equation with γ_μ the Dirac matrices. Let us define $\sigma^\mu = (I, \sigma)$. That is, $\sigma^0 = I$. From the form of the components of this matrix equation of motion,

$$\begin{pmatrix} i\sigma^\mu \cdot \partial_\mu & -m \\ -m & i\sigma^\mu \partial_\mu \end{pmatrix} \begin{pmatrix} \phi^{(R)} \\ \phi^{(L)} \end{pmatrix} = 0, \quad (15.43)$$

it is clear that the mass term couples left and right movers. Consequently, only if the left- and right-moving pairs both cross the chemical potential as in Fig. 15.9(b) can they be coupled to generate a mass. More precisely, each of the Weyl equations for the left and right movers has its own SU(2) symmetry. Hence, the overall symmetry is $SU(2) \times SU(2)$. A non-zero mass means that the individual left and right components of the wavefunction

cannot be rotated independently. That is, the symmetry has been lowered to a global $SU(2)$.

What kind of Hamiltonians give rise to topological insulation? Typically they involve the spin-orbit interaction. Consider a simple model (BHZ2006),

$$H = \sum_{m,n} \frac{1}{2} \left[\Psi_{m+1,n}^\dagger (i\Gamma^x - \Gamma^0) \Psi_{m,n} + \Psi_{m,n}^\dagger (-i\Gamma^x - \Gamma^0) \Psi_{m+1,n} + \Psi_{m,n+1}^\dagger (i\Gamma^y - \Gamma^0) \Psi_{m,n} \right. \\ \left. + \Psi_{m,n}^\dagger (-i\Gamma^y - \Gamma^0) \Psi_{m,n+1} \right] + (2 - M) \Psi_{m,n}^\dagger \Gamma^0 \Psi_{m,n} \quad (15.44)$$

with two orbitals per site and nearest-neighbor hopping. Here

$$\Psi_{m,n} = (c_{\uparrow A}, c_{\uparrow B}, c_{\downarrow A}, c_{\downarrow B})_{m,n}^T \quad (15.45)$$

is a two-component spinor corresponding to the two-orbital basis, and $\Gamma^x = \sigma^z \otimes \tau^x$, $\Gamma^y = \mathbf{I} \otimes \tau^y$, and $\Gamma^0 = \mathbf{I} \otimes \tau^z$. Here, τ^a is a Pauli matrix in the orbital basis and σ^a is one in the spin basis. This Hamiltonian is brought into diagonal form,

$$H = \sum_{\mathbf{k}} H(\mathbf{k}) \Psi^\dagger(\mathbf{k}) \Psi(\mathbf{k}), \quad (15.46)$$

by Fourier transformation,

$$\Psi(\mathbf{k}) = \frac{1}{\sqrt{N}} \sum_{m,n} e^{i(k_x m + k_y n)} \Psi_{m,n}. \quad (15.47)$$

The 4×4 Bloch Hamiltonian is

$$H(\mathbf{k}) = \Gamma^x \sin k_x + \Gamma^y \sin k_y + \Gamma^0 (2 - M - \cos k_x - \cos k_y). \quad (15.48)$$

For this 4×4 Hamiltonian,

$$T = i\sigma^y \otimes \mathbf{I} K \quad (15.49)$$

is the time-reversal operator. The matrices Γ^x and Γ^y are both odd under time-reversal but Γ^0 is even. Since the former is coupled to $\sin k_i$ and the latter to $\cos k_i$, the Hamiltonian is TRI. Although this Hamiltonian is 4×4 , it is composed of 2×2 (spin) blocks each of the form

$$H_{LD} = d_a(\mathbf{p}) \tau^a, \quad (15.50)$$

where $d_a(\mathbf{p})$ is a three-component vector in which the third entry is the mass term. Written in this form, it is clear that the mass term in each spin sector determines the direction of the arrow of time as it is odd under time reversal. Quite generally, all models for topological insulators can be reduced to something of this form. Upon diagonalization, we find the

eigenvalues of our Hamiltonian to be

$$E_{\pm} = \pm \sqrt{\sin^2 k_x + \sin^2 k_y + M^2(\mathbf{k})}, \quad (15.51)$$

where $M(k) = 2 - M - \cos k_x - \cos k_y$. This dispersion corresponds to two copies of the massive Weyl equation, one for each spin with M the mass. In the long-wavelength limit, $E_{\pm}(\mathbf{k} \rightarrow 0) \rightarrow \pm \sqrt{k_x^2 + k_y^2 + M^2}$. The mass vanishes at special values of M . For example at $M = 0, 2, 4$, the spectrum is gapless at (1) $(0, 0)$, (2) $(\pi, 0)$ and $(0, \pi)$, and (3) (π, π) , respectively. Since these are the only points in the Brillouin zone that determine the low-energy physics, we expand the Hamiltonian around each of these momenta,

$$H_{\uparrow}(k_x = 0, k_y = 0) = k_x \tau^x + k_y \tau^y - M \tau^z, \quad (15.52)$$

$$H_{\uparrow}(k_x = \pi, k_y = 0) = -k_x \tau^x + k_y \tau^y + (2 - M) \tau^z, \quad (15.53)$$

$$H_{\uparrow}(k_x = 0, k_y = \pi) = k_x \tau^x - k_y \tau^y + (2 - M) \tau^z, \quad (15.54)$$

$$H_{\uparrow}(k_x = \pi, k_y = \pi) = -k_x \tau^x - k_y \tau^y + (4 - M) \tau^z, \quad (15.55)$$

for a given spin, say \uparrow . The equations for the \downarrow -spin sector are constructed from the lower diagonal block in $H(\mathbf{k})$, which simply switches the sign of the k_x terms.

We wish to determine the contribution each of these edge states makes to the Hall conductivity. Each 2×2 block of our Hamiltonian describes a single Dirac cone, so we need to calculate the Hall conductivity of a single Dirac cone. This can be done using the following symmetry argument. Consider a domain wall which separates opposite signs of the mass in a Hamiltonian with a single Dirac cone, as depicted in Fig. 15.10. There is a single edge mode localized at the domain wall where $m = 0$. Therefore, according to our previous discussion, the conductivity carried by the edge state is e^2/h . By symmetry each side of the system must contribute equally to the edge current. Hence, the conductivity of each Dirac cone must be half the quantum of conductance. Moreover, the sign of the conductance is determined by the sign of the mass term in the Dirac equation. This can be understood from Fig. 15.10 by noting that the edge mode is to the right of the negative-mass region, but to the left of the positive-mass region. Therefore, the direction of the current induced by each region depends on the sign of the mass in that region. In the general case, this sign is determined by how the orbital “spin” (τ^x, τ^y, τ^z) , which is shown by the arrows in Fig. 15.10, is arranged around the Dirac cone. So, the signs of the momenta in Eq. (15.50) also contribute to the sign of the Hall conductivity. This can also be seen in the following way. In 2d, the parity operator

$$P(x, y) \rightarrow (-x, y) \quad \text{or} \quad (x, -y) \quad (15.56)$$

acts on only one of the coordinates. Hence, sending $k_x \rightarrow -k_x$ flips the sign of the Hall conductivity.

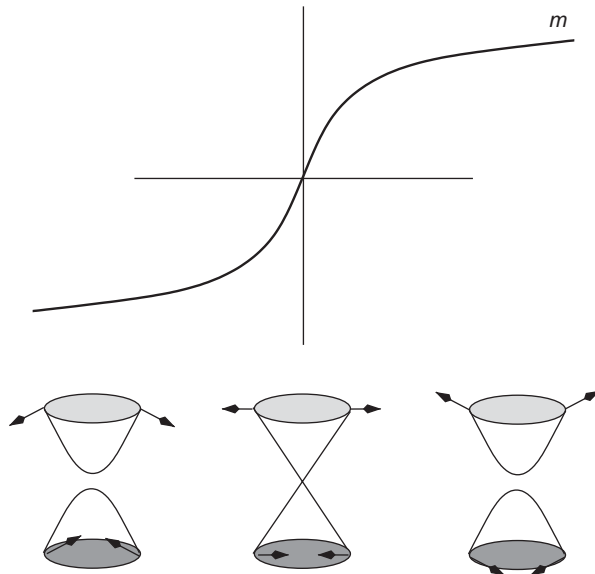


Fig. 15.10 A domain wall in the mass of the Dirac Hamiltonian. The spectrum of the states at each value of the mass is shown schematically. The arrows show the expectation value of the orbital “spin” (τ^x, τ^y, τ^z) at the given \mathbf{k} . Since the conductance at the edge is e^2/h and it arises only from the Dirac cones, the conductance of each cone is $e^2/2h$.

To determine the actual value of the conductivity at each Dirac point, we use the convention that if the corresponding Hamiltonian is of the form $k_x\sigma^x + k_y\sigma^y + M\sigma^z$, then the conductivity is $(e^2/2h) \operatorname{sgn}(M)$. Consider the Hamiltonian at the $(0, 0)$ point for $M < 0$. It is precisely of the form to result in a conductivity of $e^2/2h$. Now consider the $(\pi, 0)$ point. Compared to the $(0, 0)$ point, we need to send $k_x \rightarrow -k_x$, resulting in a contribution of $-e^2/2h$ from the $(\pi, 0)$ point. At the $(\pi, 0)$ point, we must send $k_y \rightarrow -k_y$ to recover our desired form and hence $-e^2/2h$ results for the conductivity. Two sign changes are necessary at the (π, π) point and hence $e^2/2h$. The sum of all of these is zero. Consequently, for $M < 0$, there is no net conduction on the surface for either spin- \uparrow or spin- \downarrow , and a trivial insulator obtains. The same analysis can be performed for $0 < M < 2$, $2 < M < 4$, and $M > 4$. The results are shown in Table 15.1.

Since k_x switches sign for spin- \downarrow , the Hall conductance for each node switches sign for opposite spin blocks. Therefore, the net Hall conductance is always zero, as dictated by TRI. But if we now define a spin Hall conductance (BZ2006; KM2005a) as

$$\sigma_{xy}^s = \sum_{s=\uparrow,\downarrow} \operatorname{sgn}(s) \sigma_{xy,s} \quad (15.57)$$

we find that for $0 < M < 2$, $\sigma_{xy}^s = -2e^2/h$, and for $2 < M < 4$ it is $2e^2/h$. For all other values, it vanishes and a trivial insulator obtains.

Table 15.1 Hall conductance for each of the Dirac cones that contribute to the edge transport in the model defined by Eq. (15.40). The Hall conductance is in units of e^2/h and M is the mass. The total Hall conductance for each spin, $\sigma_{xy,s}$, the net Hall conductance, σ_{xy} , and the spin Hall conductance, σ_{xy}^s , are also shown.

\mathbf{k}	$M < 0$	$0 < M < 2$	$2 < M < 4$	$M > 4$
(0, 0)	1/2	-1/2	-1/2	-1/2
(π , 0)	-1/2	-1/2	1/2	1/2
(0, π)	-1/2	-1/2	1/2	1/2
(π , π)	1/2	1/2	1/2	-1/2
$\sigma_{xy,\uparrow}$	0	-1	1	0
$\sigma_{xy,\downarrow}$	0	+1	-1	0
σ_{xy}	0	0	0	0
σ_{xy}^s	0	-2	+2	0

In quantum well systems such as HgTe/HgCdTe, the value of M is adjusted simply by changing the thickness of the quantum well. In particular, the *sign* of M can be changed when the thickness of the quantum well exceeds a critical value. This was first predicted by Bernevig, Hughes, and Zhang (BHZ2006). State-of-the-art experiments have been performed on HgTe/HgCdTe quantum wells to confirm the existence of a topological insulator (K2007). In the geometry of Fig. 15.8, the current from left (L) to right (R) is carried by two conducting edge modes, one of each spin for the top and bottom edge. So, based on the edge picture, the conductance in the topological state must be $G_{LR} = 2e^2/h$. This has been clearly observed in the experiment, as shown in Fig. 15.11. We must note that while the conductance for each of the spin channels add, this is not necessarily a robust feature of topological insulators. Such additivity is true only if the spin channels do not mix as in Eq. (15.48).

A powerful method to see the surface modes in three-dimensional systems is provided by angle-resolved photo-emission scattering (ARPES), which can probe the surface electronic band structure with fine momentum and energy resolution. Candidate materials were identified in BiSb alloys as well as Bi_2Se_3 and Bi_2Te_3 crystals (TFK2008; Z2009; X2009). ARPES measurements confirmed the existence of an odd number of Kramers-paired surface modes (H2008; X2009; H2009). Figure 15.12 shows the ARPES data on Bi_2Se_3 which has exactly one such pair forming a single Dirac cone at the surface.

15.5.1 General formulation

Our current formulation of topological insulators is based entirely on single-particle physics and is quite specific to two spatial dimensions. Nonetheless, the physics holds even in the many-particle regime and in three spatial dimensions. While it is possible to carry the

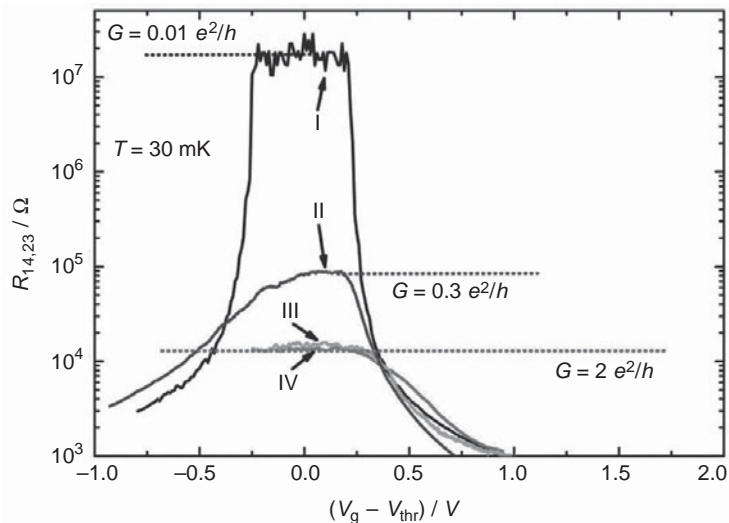


Fig. 15.11 The longitudinal resistance of various quantum well systems with thickness below (I) and above (II, III, IV) the critical value. The size of the systems I and II (III and IV) is larger (smaller) than the inelastic mean-free path. The conductance of system II does not reach the predicted value due to inelastic backscattering processes at the edge. Figure taken from (K2007).

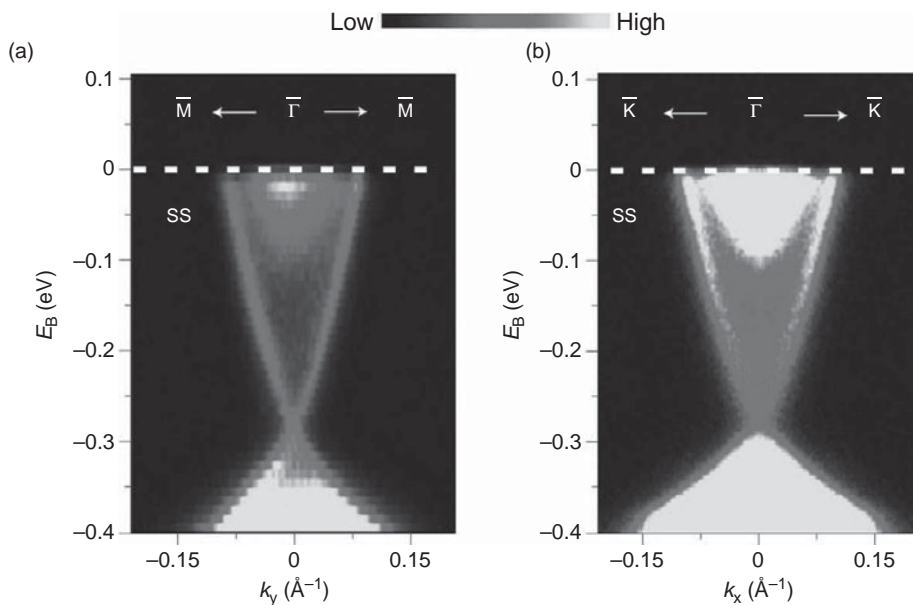


Fig. 15.12 ARPES data on Bi_2Se_3 shows a single Kramers pair in the surface band structure in addition to the states in the bulk (lighter gray) within the bulk energy gap. Panels a and b show different cuts in the momentum space. Figure taken from (X2009).

single-particle picture forward to $d = 3$ (MB2007; R2009; HK2010), we pursue another approach (QHZ2008; QZ2010) here which applies equally to many-particle systems. Interacting electrons in a solid have well-defined responses to external electric and magnetic fields. Consequently, we write the general action, $S = S_0 + S_\theta$, for an insulator in terms of a total energy term,

$$S_0 = \frac{1}{8\pi} \int d^3x dt \left(\epsilon \mathbf{E}^2 - \frac{1}{\mu} \mathbf{B}^2 \right), \quad (15.58)$$

with ϵ and μ the dielectric constants and magnetic permitivities plus an additional term,

$$S_\theta = \left(\frac{\theta}{\pi c^2} \right) \left(\frac{e^2}{2h} \right) \int d^3x dt \mathbf{E} \cdot \mathbf{B}, \quad (15.59)$$

which is typically ignored because it patently breaks time-reversal symmetry. The latter term accounts for the magneto-electric effect. However, as we will see, when periodic boundary conditions are present, this term is allowed. Before we evaluate this term explicitly, we first show that it reduces entirely to a boundary contribution and hence is inherently topological. To simplify the S_θ term, we recall that the electromagnetic field strength, $F_{\mu\nu}$, is related to the vector potential through

$$F_{\mu\nu} \equiv \partial_\mu A_\nu - \partial_\nu A_\mu, \quad (15.60)$$

where

$$A_\mu = (-\Phi, A^1, A^2, A^3) \quad (15.61)$$

with Φ the scalar potential. Since $F_{\mu\nu}$ is purely antisymmetric, $F_{\mu\mu} = 0$ for all μ . Defining i to be a spatial index which can take on values 1, 2, or 3, it follows that

$$F_{0i} = \frac{1}{c} \frac{\partial A^i}{\partial t} + \frac{\partial \Phi}{\partial x^i} = -E_i. \quad (15.62)$$

Likewise, the z -component of the \mathbf{B} -field is defined through

$$F_{12} = \partial_1 A_2 - \partial_2 A_1 = \partial_x A_y - \partial_y A_x \equiv B_z, \quad (15.63)$$

which of course is equivalent to the z -component of $\mathbf{B} = \nabla \times \mathbf{A}$. Consequently, the electromagnetic field strength has the components

$$F_{\mu\nu} = \begin{pmatrix} 0 & E_x & E_y & E_z \\ -E_x & 0 & B_z & -B_y \\ -E_y & -B_z & 0 & B_x \\ -E_z & B_y & -B_x & 0 \end{pmatrix}. \quad (15.64)$$

The dot product of \mathbf{E} and \mathbf{B} then reduces to

$$\mathbf{E} \cdot \mathbf{B} = F_{0i} F_{jk} \epsilon^{0ijk}, \quad (15.65)$$

with ϵ^{0ijk} the completely antisymmetric tensor. We use the convention that

$$\epsilon^{0xyz} = 1. \quad (15.66)$$

To obtain our final result that S_θ is actually a topological term, we introduce some simplifying notation. Let

$$F = \frac{1}{2} F_{\mu\nu} dx^\mu \wedge dx^\nu, \quad (15.67)$$

where

$$dx^\mu \wedge dx^\nu = dx^\mu \otimes dx^\nu - dx^\nu \otimes dx^\mu. \quad (15.68)$$

In general for any one-form (a linear operator on a vector) $v \wedge w = -w \wedge v$, hence the factor of 2 in the denominator in the definition of F . In general, for the antisymmetrization of an n -form, $n!$ enters the denominator. As a consequence,

$$\begin{aligned} F \wedge F &= \frac{1}{4} F_{\mu\nu} F_{\rho\lambda} dx^\mu \wedge dx^\nu \wedge dx^\rho \wedge dx^\lambda \\ &= \frac{1}{4} \epsilon^{\mu\nu\rho\lambda} F_{\mu\nu} F_{\rho\lambda} dx \wedge dy \wedge dz \wedge dt, \end{aligned} \quad (15.69)$$

where $dt \wedge dx \wedge dy \wedge dz \equiv d^4x$ is the four-dimensional volume element. With these definitions and Eq. (15.65), the extra term in the action simplifies to

$$S_\theta = \left(\frac{\theta}{\pi c^2} \right) \left(\frac{e^2}{2h} \right) \int d^3x dt \mathbf{E} \cdot \mathbf{B} = \left(\frac{\theta}{2\pi c^2} \right) \left(\frac{e^2}{2h} \right) \int F \wedge F. \quad (15.70)$$

In terms of the components of the one-form, $\mathbf{A} = A_\mu dx^\mu$,

$$\begin{aligned} F &\equiv dA = \partial_\mu A_\nu dx^\mu \wedge dx^\nu \\ &= \frac{1}{2} (\partial_\mu A_\nu - \partial_\nu A_\mu) dx^\mu \wedge dx^\nu \end{aligned} \quad (15.71)$$

because F is entirely antisymmetric. Note F is a 2-form as it contains two differentials. This allows us to simplify $F \wedge F = dA \wedge dA$. This notation is not just an exercise. If we integrate by parts,

$$\int dA \wedge dA = \int d(A \wedge dA) + A \wedge d^2A, \quad (15.72)$$

we generate a boundary term which contains the operator d^2A . In obtaining this result, we have applied the rule

$$d(A \wedge B) = dA \wedge B + (-1)^r A \wedge dB, \quad (15.73)$$

where r is the order of the form. Equation (15.72) follows because \mathbf{A} is a one-form. From our rule for dA (Eq. (15.71)), we can immediately write down what is meant by d^2A ,

$$d^2A = \partial_\lambda \partial_\mu A_\nu dx^\lambda \wedge dx^\mu \wedge dx^\nu, \quad (15.74)$$

by simply applying it twice. The two derivatives in front are symmetric. However, the basis $dx^\lambda \wedge dx^\mu$ is antisymmetric. Hence, $d^2A = 0$. Upon integrating by parts and noting that $d^2A = 0$, we reduce the topological term in the action to

$$S_\theta = \left(\frac{\theta}{\pi c^2} \right) \left(\frac{e^2}{2h} \right) \int d(A \wedge dA), \quad (15.75)$$

which reduces to a boundary integral

$$S_\theta = \left(\frac{\theta}{\pi c^2} \right) \left(\frac{e^2}{2h} \right) \int_{\partial M} A \wedge dA, \quad (15.76)$$

as a result of Stokes' theorem. Hence, the extra term in the action is entirely a boundary term determined solely by the topology. As a boundary term, it cannot change the equations of motion. In actuality, S_θ is the second Chern number.

To get a handle on what is contained in S_θ , we simplify to a particular choice for the gauge and evaluate Eq. (15.59) directly. For simplicity, we set $A_0 = 0$ and choose $\mathbf{B} = B_z \hat{z}$ which results in $\mathbf{E} = E_z \hat{z}$. Our normalization of S_θ will now become clear. Substituting this choice for the gauge into Eq. (15.59) leads to

$$S_\theta = \left(\frac{\theta}{\pi c^2} \right) \left(\frac{e^2}{2h} \right) \int d\mathbf{a} \cdot \nabla \times \mathbf{A} \int dt dz \partial_t A^z. \quad (15.77)$$

Assuming all the dimensions are periodic on a torus, we can evaluate this integral immediately,

$$S_\theta = \left(\frac{\theta}{\pi c^2} \right) \left(\frac{e^2}{2h} \right) n \left(\frac{hc}{e} \right)^2 = \theta n \hbar, \quad (15.78)$$

noting that each of the integrals is just related to the flux hc/e . This quantity appears in a path integral giving a statistical weight of

$$e^{i \frac{S_\theta}{\hbar}} = e^{\frac{i n \theta \hbar}{\hbar}}. \quad (15.79)$$

We choose θ such that the integral remains invariant under time reversal. Since $\mathbf{B} \rightarrow -\mathbf{B}$ under time reversal, we must have that

$$e^{i n \theta} = e^{-i n \theta}. \quad (15.80)$$

There are only two distinct solutions to this equation, $\theta = 0$ and $\theta = \pi$. The former corresponds to the standard band insulator and the latter to the topological insulator. We can express this simply as

$$\theta = \pi (m \bmod 2) \quad (15.81)$$

and hence θ is the key Z_2 invariant that allows us to distinguish traditional insulators from band insulators. What does this mean physically? Applying a field produces a flux which in turn gives rise to a Hall conductance. The normalization we have chosen such that θ is the Z_2 invariant tells us immediately that the Hall conductance for a single Dirac cone is

$$\sigma_{xy} = \frac{1}{2} \frac{e^2}{h}. \quad (15.82)$$

In effect, $\theta = \pi$ implies that there is only a single Dirac cone on the surface of a topological insulator and hence such states are distinct from a single layer of carbon, graphene, which has an even number. Although this formulation has a drawback in that it assumes a gap exists, it does serve to illustrate clearly that the Z_2 invariance of the magneto-electric term in the action underlies the physics of topological insulators.

15.6 Laughlin liquid

In the original experiments of Tsui, Störmer, and Gossard (TSG1982), the Hall conductance exhibited a sharp plateau at the value of $e^2/3h$. In later experiments, fractional quantization of the Hall conductance was also observed for values of $4/3$, $5/3$, $7/3$, $1/5$, $2/5$, $3/5$, $7/5$, $8/5$, etc. The common ingredient in these sequences is the presence of the odd denominator. The original challenge in explaining these experiments, however, lay not so much in accounting for the fractional value of the Hall conductance but rather in explaining the nature of the electronic state that exhibited the fractional quantization. For example, a non-interacting model in which the lowest Landau level is fractionally occupied at a filling of v will exhibit a conductance ve^2/h . However, when a Landau level is fractionally occupied, electrons can scatter into the empty states and hence longitudinal transport will not be dissipationless; as a consequence, $\sigma_{xx} \neq 0$. In addition, the persistence of a plateau at fractional filling indicates that somehow an appropriately partially occupied Landau level is stable to even the lowest-lying excitations. That is, an energy gap separates the ground state from all excited states. In the absence of electron interactions, the energy cost to add an additional electron to a partially filled Landau level is essentially zero. This would suggest that as the field is changed, sharp plateaus in the conductance should desist in the non-interacting model for a partially filled Landau level.

Consequently, the fractional quantum Hall state cannot be understood without including the role of electron interactions. However, at the outset, it is not clear what this state should look like. Thus far, we have introduced two electronic states that arise fundamentally from electron–electron interactions: the Wigner crystal and the superconducting state. While the vanishing of the longitudinal resistance suggests that the fractional quantum Hall state bears some resemblance to a superconducting state, it is not clear how such a state would survive a large perpendicular magnetic field. What about the Wigner crystal? As mentioned in Chapter 5, because a magnetic field freezes the electron zero-point motion, Wigner crystallization is stabilized. In fact, in the limit in which the interparticle separation is large relative to the cyclotron radius (magnetic length), electron correlations dominate and the conditions for Wigner crystallization become favorable. However, a Wigner crystal does not exhibit dissipationless transport as a threshold voltage must be applied before transport obtains. We suspect then that the resolution of the fractional quantum Hall state lies elsewhere.

Indeed it does. After Laughlin (L1983; L1987), we consider an interacting electron gas in the presence of a perpendicular magnetic field

$$H = \sum_i \left[\frac{1}{2m} \left(\mathbf{p}_i - \frac{e}{c} \mathbf{A}_i \right)^2 + V(\mathbf{r}_i) \right] + \frac{1}{2} \sum_{\substack{i,j \\ i \neq j}} \frac{e^2}{|\mathbf{r}_i - \mathbf{r}_j|}, \quad (15.83)$$

where $V(\mathbf{r})$ is the compensating neutralizing potential from the ions and the sums over i and j are over the electrons. Fractional quantization of the Hall conductance is observed at a field of 15 T. At this field, the cyclotron energy is roughly three times the Coulomb energy, e^2/ℓ . Hence, it should be a fairly good approximation to use the non-interacting eigenstates of the lowest Landau level as a starting basis for constructing the true many-body wavefunction. In general, the non-interacting eigenstates are products of a polynomial in the electron coordinate and a Gaussian. For an interacting system, we expect that the true many-body state will involve differences of the electron coordinates. Let us define the complex electron coordinate, $z = x + iy$. We consider the ansatz,

$$\Psi_N(\mathbf{r}_1, \dots, \mathbf{r}_N) = \prod_{1 \leq j < k \leq N} f(z_j - z_k) \exp \left(- \sum_{j=1}^N \frac{|z_j|^2}{4\ell^2} \right), \quad (15.84)$$

where $f(z_j - z_k)$ is a polynomial in the electron coordinates. After studying the two-electron problem described by Eq. (15.83), Laughlin found that $f(z_1 - z_2) = (z_1 - z_2)^{2p+1}$, where p is an integer. Because the exponent $2p + 1$ is odd, the wavefunction is antisymmetric with respect to interchange of two electrons. Analogous results were also obtained for the equivalent three-electron problem (L1983). Hence, Laughlin proposed that

$$\Psi_m(\mathbf{r}_1, \dots, \mathbf{r}_N) = \prod_{1 \leq j < k \leq N} (z_j - z_k)^m \exp \left(- \sum_{j=1}^N \frac{|z_j|^2}{4\ell^2} \right) \quad (15.85)$$

must accurately describe the ground state of a fractional quantum Hall system. While this wavefunction was originally argued to be a variational state (where m must be determined), the overlap of this wavefunction with the exact eigenstate for small clusters of electrons is typically greater than 99 percent for interaction potentials of the form $u(r) = 1/r$, $-\ln r$, and $\exp(-r^2/2)$. This would suggest that the variational character of Ψ_m is minimal, and m must be determined from a fundamental principle. It turns out that Ψ_m is an eigenstate of the total angular momentum operator with eigenvalue

$$M = \frac{N(N-1)m}{2}. \quad (15.86)$$

That M is the total angular momentum of the operator L_z follows from expanding the product over $z_j - z_k$ in Eq. (15.84) and realizing that there are at most $N(N-1)m/2$ factors of z_i in each term. If the differential form of the L_z operator is applied to such a product, the eigenvalue M results. As a consequence, we can think of the Laughlin state as being a superposition of states within the lowest Landau level with the same angular momentum. This removes completely the variational character of the Laughlin state.

To understand precisely what physics the Laughlin state describes, we write the square of this state

$$|\Psi_m|^2 = \exp[-\beta\Phi] \quad (15.87)$$

in terms of a Boltzmann weight, where Φ is the interaction energy,

$$\Phi(z_1, \dots, z_N) = -2 \sum_{1 \leq j < k \leq N} \ln |z_j - z_k| + \frac{1}{2m\ell^2} \sum_{j=1}^N |z_j|^2 \quad (15.88)$$

and $\beta = m$ plays the role of the inverse temperature. Equation (15.88) is exactly the interaction energy for a one-component plasma (such as an electron gas) consisting of N identical charges with charge $\sqrt{2}$. The second term in Eq. (15.88) represents the interaction energy with the neutralizing background, $U_b(z_i) = |z_i|^2/(2m\ell^2)$. To see this clearly, we note that the potential for the compensating background should satisfy a Poisson equation, $\nabla^2 U_b(z_i) = 4\pi\rho$, where ρ is given by $v n_B = v/(2\pi\ell^2)$ (see Eq. (15.21)). Performing the differentiation in the Poisson equation reveals that the compensating charge density per unit area,

$$\rho = \frac{1}{2\pi\ell^2 m} \equiv \frac{v}{2\pi\ell^2}, \quad (15.89)$$

is exactly the uniform electron charge density in the lowest Landau level if we identify the Landau filling factor v with $1/m$. The Laughlin state accurately describes the ground state of an N -electron system for density and magnetic field strengths such that the filling in the lowest Landau level is given by $v = 1/m$. As a system with a uniform electron density, the Laughlin state is distinct from an electron crystal state, such as a Wigner crystal. In fact, electrons condensing into the Laughlin state do so without breaking any symmetries. Hence, a Landau-type description presented in the previous chapter, which necessarily

involves the symmetry breaking of some order parameter, is not possible for the formation of fractional quantum Hall states. The importance of the Laughlin state in the development of the fractional quantum Hall effect cannot be overestimated.

We are now poised to explore the excitations of the Laughlin liquid. For filling fractions ν different from $1/m$, excitations emerge. Consider changing the filling by piercing the sample at z_0 with an infinitely thin magnetic solenoid. Although ν is now slightly less than $1/m$, the electrons will attempt to stay in the state Ψ_m . However, they cannot do this without diminishing the charge density at the insertion point of the magnetic solenoid. We can simulate such a depletion by excluding the electrons from z_0 . Consequently, we anticipate that

$$\begin{aligned}\Psi_m^+(z_0; z_1, \dots, z_N) &= \prod_{j=1}^N (z_j - z_0) \Psi_m(z_1, \dots, z_N) \\ &= A_{z_0}^+ \Psi_m(z_1, \dots, z_N)\end{aligned}\quad (15.90)$$

might describe the wavefunction for the new many-body state with a “quasi-hole” at z_0 . Indeed it does, as shown by Laughlin (L1983). A more quantitative argument for the quasi-particle wavefunction in Eq. (15.90) stems from noting that if the solenoid carries flux ϕ , each single-particle state is changed accordingly,

$$z^n e^{-\frac{|z|^2}{4\ell^2}} \rightarrow z^{n+\alpha} e^{-\frac{|z|^2}{4\ell^2}}, \quad (15.91)$$

to accommodate the additional flux. Here $\alpha = \phi/\phi_0$, with $\phi_0 = hc/e$ the flux quantum. If the solenoid carries one quantum of flux, then the prefactor of the Gaussian is z^{n+1} . That each single-particle state is now multiplied by an extra factor of z supports the ansatz for the quasi-particle wavefunction, Eq. (15.90). To utilize the plasma analogy, we square the quasi-particle wavefunction to find that, aside from a background normalization factor of $|z_0|^2$, the energy of the many-body state with a “quasi-hole”,

$$\Phi_{qp}(z_0; z_1, \dots, z_N) = \Phi(z_1, \dots, z_N) - \frac{2}{m} \sum_{j=1}^N \ln |z_j - z_0|, \quad (15.92)$$

is that of a one-component plasma interacting with a charge fixed at z_0 . The magnitude of the charge is $1/m$ or, in electron units, e/m . Likewise, if the solenoid were to extract a single flux quantum, a “quasi-electron” would be created with charge $-e/m$. Numerically, the energy to create or destroy quasi-particles in a three-electron fractional quantum Hall state is roughly 4 K at a field of 15 T (L1983). Improved estimates of the gap in the fractional quantum Hall state were obtained by Girvin, MacDonald, and Platzman (GMP1985). In fact, their work was pivotal in establishing that all collective excitations from the Laughlin state have a finite energy gap. Hence, the Laughlin state does satisfy the criterion of having a gap to all excitations. The excitation energy can be thought of as the Coulomb energy required to place a particle of charge $\pm e/m$ in the quantum liquid. The distance over which the charge acts is proportional to the magnetic length, $\propto \ell$. Hence, the excitation energy

should scale as $e^2/\ell \propto \sqrt{B}$ and thus vanishes in the absence of an applied magnetic field. It is the presence of the energy gap in the excitation spectrum that makes the Laughlin state incompressible and ultimately leads to dissipationless transport.

Nonetheless, some experiments have revealed the existence of gapless excitations (ASH1983; MDF1985) in 2d quantum Hall systems. These excitations are believed to live on the edge of quantum Hall systems as they are explicitly excluded from the bulk by Laughlin's gauge argument. For integer quantum Hall states, the edge excitations are well described by Fermi liquid theory as electron interactions are relatively unimportant in the integer effect. However, in the fractional quantum Hall effect, the situation is entirely different, as we have seen. Quantum mechanical states confined to move at the edge of a fractional quantum Hall system are essentially 1d strongly correlated electron systems. We have shown in Chapter 10 that electron interactions in a 1d system give rise to Luttinger rather than Fermi liquid behavior. As a result of the chirality of the edge current, edge states in the fractional quantum Hall effect are chiral Luttinger liquids (W1990). They exhibit all the properties indicative of Luttinger liquids discussed in Chapter 9, including an excitation spectrum that vanishes algebraically in the vicinity of the Fermi energy. Figure 10.6 confirms the algebraic dependence of the excitation spectrum in the edge of the $\nu = 1/3$ quantum Hall state, thereby putting the chiral Luttinger liquid model for the edge states in the fractional quantum Hall effect on firm experimental footing.

Consider for the moment the problem of the statistics associated with interchanging (A1985; F1992) two quasi-holes or two quasi-electrons in a fractional quantum Hall state. The wavefunction describing such pair excitations, which we will locate at $z = z'$ and $z = z''$, is analogous to Eq. (15.90) except the product $A_{z'}^\pm A_{z''}^\pm$ now multiplies the Laughlin state Ψ_m . The problem we address is, under interchange of two quasi-particles such that

$$A_{z'}^\pm A_{z''}^\pm \Psi_m(z_1, \dots, z_N) = e^{i\phi} A_{z''}^\pm A_{z'}^\pm \Psi_m(z_1, \dots, z_N), \quad (15.93)$$

what phase, ϕ , does the wavefunction incur? For interchange of electrons, $\phi = \pi$ and for bosons, $\phi = 2\pi$ or, equivalently, 0. We will show now that the phase change for the interchange of two quasi-particles in the Laughlin state is $1/m$ and hence fractional.

Quite generally, the wavefunction of a particle traversing a closed loop in the presence of a vector potential will acquire the phase

$$i\gamma = i \frac{q}{\hbar c} \oint d\ell \cdot \mathbf{A}. \quad (15.94)$$

We will take the vector potential to be the generator of the magnetic field B felt by the particle. Consequently, the line integral that determines the phase is simply equal to the field times the surface area enclosed by the path. Let R be the radius of the loop. As a result, the phase change is $\gamma = q\pi R^2 B / \hbar c$. Recalling that the magnetic field is related to the electron density through $\rho = veB/\hbar c$, and the quasi-particle charge is ev , we find that the total phase encountered is $\gamma = 2\pi N$, where N is the number of electrons in the system. This is a key result as the phase is proportional to the number of electrons enclosed in the loop. Now let us redo the argument assuming that amidst the sea of electrons lies a quasi-hole of charge

e/m . In this case, we must take into consideration the depletion in the density as a result of the quasi-hole. For a quasi-hole, the depletion is given by the filling ν or $1/m$. Hence, the phase is now given by $2\pi(N - 1/m)$. Let us assume that $|z'| < |z''|$. As a consequence, when the quasi-hole at z'' is moved in a loop that encircles the quasi-hole at z' , the phase change is $2\pi(N - 1/m)$. The $2\pi N$ factor does not change the sign of the wavefunction. As a consequence, the extra phase that is gained is $2\pi/m$. However, to interchange two quasi-particles, we need only traverse a half circle and then translate the particles. As the translations do not result in any phase change, the net phase change under the interchange of two quasi-particles is π/m . For $m = 1$, we recover the result for electrons. However, for any fractional filling, the phase change is a fraction. Hence, quasi-particles in the Laughlin liquid exhibit both fractional charge and fractional statistics. Particles obeying fractional statistics (W1982) are termed *anyons* because they can acquire *any* phase change upon interchange.

In closing this section, we introduce a seemingly innocent rewriting (J1989)

$$\Psi_m(\mathbf{r}_1, \dots, \mathbf{r}_N) = \prod_{1 \leq j < k \leq N} (z_j - z_k)^{m-1} \Psi_1(\mathbf{r}_1, \dots, \mathbf{r}_N) \quad (15.95)$$

of the Laughlin state. Here $\Psi_1(\mathbf{r}_1, \dots, \mathbf{r}_N)$ is simply the Laughlin state with $m = 1$ and hence corresponds to the wavefunction for a completely filled Landau level. The prefactor in this expression resembles the flux attachment prefactor in the “quasi-hole” wavefunction. The Laughlin state can be thought of as a completely filled Landau level in which each electron has physically attached to it $m - 1$ flux quanta. While in no real sense can electrons bind flux in the manner that pages are bound in a book, the flux attachment scheme offers a pictorial way of thinking about the fractional quantum Hall effect. Further, it has the advantage that the fractional quantum Hall effect can be viewed as a variant of the integer quantum Hall effect with fictitious particles bearing electric charge e and $m - 1$ units of magnetic flux. As a computational tool, the flux attachment scheme or composite particle picture is of extreme utility in generating the hierarchy of fractional states in the lowest Landau level and as a consequence forms the basis for current field theoretical approaches to the quantum Hall problem (F1991; LF1991; HLR1993; KLZ1992). In fact, in the context of the even denominator states, the composite fermion approach has played a central role. The even denominator state at $\nu = 1/2$ is particularly odd (W1993) in that it does not appear to be a true fractional state with a vanishing longitudinal resistance. The flux attachment scheme at $\nu = 1/2$ leads to a composite fermion liquid in which the average magnetic field felt by the composite fermions vanishes. In such a system, a Fermi surface should emerge as a result of the apparent vanishing of the field. Recent work (R1998; SM1997) on this problem suggests that the $\nu = 1/2$ state is a compressible state composed of fermionic excitations that possess a dipole moment.

An additional problem of current interest is the low magnetic field limit of the quantum Hall effect. When the perpendicular magnetic field is sufficiently low such that the filling fraction exceeds $\nu > 7/2$, the longitudinal resistivity in the vicinity of the half-integer states is observed (D1999; L1999) to depend on the direction of the current, that is, $\rho_{xx} \neq \rho_{yy}$. Anisotropic transport is inconsistent with a uniform electron state. In principle, the ground state of a 2d electron gas is expected to be non-uniform when the magnetic

field is sufficiently low so that no fractional quantum Hall states are accessible but not so low that disorder destroys the gap established by the cyclotron frequency, ω_c . In this intermediate range of magnetic fields, the ground state is governed by the competition between the short-range exchange and long-range direct Coulomb interaction. Because these interactions are of opposite sign, the electron gas breaks into domains (FPA1979; FKS1996; MC1996; RHY1999; J1999; SMP2000). Current theoretical work is directed at formulating effective low-energy theories (FK1999; MF2000; BF2001; B2001; L2001) and the transport properties in the presence of a charge modulation in the low-field limit.

Summary

We presented here the essential physics behind the quantum Hall effect. The integer effect arises from the boundary condition that the current-carrying states or edge states be single valued when an integer number of Landau levels are filled. In the fractional quantum Hall effect, electrons partially occupying the lowest Landau level condense into a strongly correlated state (the Laughlin state) whose energy is lower than the corresponding Wigner crystal. This state is incompressible in that it has a gap to all excitations and exhibits fractionally charged excitations with charge $\pm e/m$. The excitation energy for such charged excitations scales as $1/\ell$ and hence vanishes in zero field. It is for this reason that while the Laughlin state is mediated by strong electron correlations, the incompressibility stems from the large perpendicular magnetic field. Quantum Hall problems of current interest include the apparently Fermi liquid-like state at $\nu = 1/2$ as well as the onset of an anisotropic state at sufficiently low magnetic fields so that the filling exceeds $\nu = 7/2$.

Problems

15.1 Consider the two-dimensional Hamiltonian

$$p_x\sigma^x + p_y\sigma^y + m(x)\sigma^z, \quad (15.96)$$

where

$$m(x) = \begin{cases} m, & x > 0, \\ -m, & x < 0, \end{cases}$$

(a) Show that a wavefunction of the form

$$\psi(x, y) = e^{ip_y y} \phi(x) \quad (15.97)$$

with

$$\phi(x) = \exp \left[- \int_0^x m(x') dx' \right] \phi_0, \quad (15.98)$$

where ϕ_0 is a two-component spinor, describes zero-energy states localized at the boundary, $x = 0$. That is, find ϕ_0 explicitly. (b) Show also that the same state describes a dispersing state bound at $x = 0$. What is the energy of this state? Why is there only one such state?

- 15.2 (a) A single particle confined to move solely in the x - y plane is described by the single-particle wavefunction

$$\Psi_m(z) = z^m \exp\left(\frac{-|z|^2}{4\ell^2}\right), \quad (15.99)$$

where $z = x + iy$. Show that this wavefunction is an eigenstate of L_z . (b) Now consider the generalization

$$\Psi_m(r_1, \dots, r_N) = \prod_{j < k} (z_j - z_k)^m \exp\left(-\sum_{j=1}^N \frac{|z_j|^2}{4\ell^2}\right) \quad (15.100)$$

to N particles confined to move in the x - y plane, where $z_j = x_j + iy_j$. For what values of m is this wavefunction antisymmetric with respect to particle interchange? (c) Show that this wavefunction is an eigenstate of the total L_z operator with eigenvalue

$$M = \frac{N(N-1)m}{2}. \quad (15.101)$$

For N particles, the total L_z operator is simply the sum of L_z for each particle.

- 15.3 Prove that Eq. (15.29) is the time-reversal operator for Eq. (15.48).
 15.4 From the fact that $T^2 = -1$, T the time-reversal operator, prove the Kramers doubling theorem.

References

- [ASH1983] S. J. Allen, Jr., H. L. Störmer, and J. C. M. Hwang, *Phys. Rev. B* **28**, 4875 (1983).
- [AMY1975] T. Ando, Y. Matsumoto, and Y. Uemura, *J. Phys. Soc. Jpn.* **39**, 279 (1975).
- [AA1981] H. Aoki and T. Ando, *Solid St. Comm.* **38**, 1079 (1981).
- [A1985] D. P. Arovas, in *Geometric Phases in Physics*, eds. A. Shapere and F. Wilczek (World Scientific, Singapore, 1985), p. 284.
- [BF2001] D. G. Barci and E. Fradkin, cond-mat/0106171.
- [B2001] D. G. Barci, E. Fradkin, S. A. Kivelson, and V. Oganesyan, cond-mat/0105448.
- [BHZ2006] B. A. Bernevig, T. L. Hughes, and S.-C. Zhang, *Science* **314**, 1757 (2006).
- [BZ2006] B. A. Bernevig and S.-C. Zhang, *Phys. Rev. Lett.* **96**, 106802 (2006).
- [CC1988] J. T. Chalker and P. D. Coddington, *J. Phys. C* **21**, 2665 (1988).
- [D1999] R. R. Du, D. C. Tsui, H. L. Störmer, L. N. Pfeiffer, K. W. Baldwin, and K. W. West, *Solid St. Commun.* **109**, 389 (1999).
- [FKS1996] M. M. Fogler, A. A. Koulakov, and B. I. Shklovskii, *Phys. Rev. B* **54**, 1853 (1996).
- [F1992] S. Forte, *Rev. Mod. Phys.* **64**, 193 (1992).

- [F1991] E. Fradkin, *Field Theories of Condensed Matter Systems*, (Addison-Wesley, Redwood City, USA, 1991).
- [FK1999] E. Fradkin and S. Kivelson, *Phys. Rev. B* **59**, 8065 (1999).
- [FPA1979] H. Fukuyama, P. Platzman, and P. W. Anderson, *Phys. Rev. B* **19**, 5211 (1979).
- [GMP1985] S. M. Girvin, A. H. MacDonald, and P. M. Platzman, *Phys. Rev. Lett.* **54**, 581 (1985).
- [H1879] E. H. Hall, *Am. J. Math.* **2**, 287 (1879).
- [H1982] B. I. Halperin, *Phys. Rev. B* **25**, 2185 (1982).
- [HLR1993] B. I. Halperin, P. A. Lee, and N. Read, *Phys. Rev. B* **47**, 7312 (1993).
- [HK2010] M. Z. Hasan and C. L. Kane, *Rev. Mod. Phys.* **82**, 3045 (2010).
- [H1937] H. Hellmann, *Einführung in die Quantenchemie* (Franz Denticke, Leipzig, Germany, 1937) p. 285; see also R. P. Feynman, *Phys. Rev.* **56**, 340 (1939).
- [H2008] D. Hsieh, D. Qian, L. Wray, Y. Xia, Y. S. Hor, R. J. Cava, and M. Z. Hasan, *Nature* **452**, 970 (2008).
- [H2009] D. Hsieh, Y. Xia, D. Qian, et al., *Nature* **460**, 1101 (2009).
- [J1989] J. Jain, *Phys. Rev. B* **40**, 8079 (1989).
- [J1999] T. Jungwirth, A. H. MacDonald, L. Smrcka, and S. M. Girvin, *Phys. Rev.* **60**, 15574 (1999).
- [KM2005a] C. L. Kane and E. J. Mele, *Phys. Rev. Lett.* **95**, 226801 (2005).
- [KM2005b] C. L. Kane and E. J. Mele, *Phys. Rev. Lett.* **95**, 146802 (2005).
- [KLZ1992] S. Kivelson, D.-H. Lee, and S.-C. Zhang, *Phys. Rev. B* **46**, 2223 (1992).
- [KDP1980] K. von Klitzing, G. Dorda, and M. Pepper, *Phys. Rev. Lett.* **45**, 494 (1980).
- [K2007] M. König, S. Wiedmann, C. Brüne, et al., *Science* **318**, 766 (2007).
- [L1980] R. B. Laughlin, *Phys. Rev. B* **23**, 5632 (1980).
- [L1983] R. B. Laughlin, *Phys. Rev. B* **27**, 3383 (1983); *Phys. Rev. Lett.* **50**, 873 (1983).
- [L1987] R. B. Laughlin, in *The Quantum Hall Effect*, eds. E. Prange and S. M. Girvin (Springer, Berlin, 1987) p. 233.
- [LWK1993] D.-H. Lee, Z. Wang, and S. A. Kivelson, *Phys. Rev. Lett.* **70**, 4130 (1993).
- [LC1994] D. K. K. Lee and J. T. Chalker, *Phys. Rev. Lett.* **72**, 1510 (1994).
- [L1999] M. P. Lilly, K. B. Cooper, J. P. Eisenstein, L. N. Pfeiffer, and K. W. West, *Phys. Rev. Lett.* **82**, 394 (1999).
- [L2001] A. Lopatnikova, S. H. Simon, B. I. Halperin, and X.-G. Wen, cond-mat/0105079.
- [LF1991] A. Lopez and E. Fradkin, *Phys. Rev. B* **44**, 5246 (1991).
- [MF2000] A. H. MacDonald and M. P. A. Fisher, *Phys. Rev. B* **61**, 5724 (2000).
- [MT1999] J. B. Marston and S.-W. Tsai, *Phys. Rev. Lett.* **82**, 4906 (1999).
- [MDF1985] D. B. Mast, A. J. Dahm, and A. L. Fetter, *Phys. Rev. Lett.* **54**, 1706 (1985).
- [MC1996] R. Moessner and J. T. Chalker, *Phys. Rev. B* **54**, 5006 (1996).
- [MB2007] J. E. Moore and L. Balents, *Phys. Rev. B* **75**, 121306 (R) (2007).
- [P1981] R. E. Prange, *Phys. B* **23**, 4802 (1981).
- [P1987] R. E. Prange, in *The Quantum Hall Effect*, eds. R. E. Prange and S. M. Girvin (Springer, Berlin, 1987) p. 1.
- [P1984] A. Pruisken, *Nucl. Phys. B* **235** (FS11), 277 (1984).
- [QHZ2008] X.-L. Qi, T. L. Hughes, and S.-C. Zhang, *Phys. Rev. B* **78**, 195424 (2008).
- [QZ2010] X.-L. Qi and S.-C. Zhang, *Phys. Today* **63**, 33 (2010).
- [R1998] N. Read, *Phys. Rev. B* **58**, 16262 (1998).

- [RHY1999] E. H. Rezayi, F. D. M. Haldane, and K. Yang, *Phys. Rev. Lett.* **83**, 1219 (1999).
- [R2009] R. Roy, *Phys. Rev. B* **79**, 195321 (2009).
- [SM1997] R. Shankar and G. Murthy, *Phys. Rev. Lett.* **79**, 4437 (1997).
- [SMP2000] T. D. Stanescu, I. Martin, and P. Phillips, *Phys. Rev. Lett.* **84**, 1288 (2000).
- [TFK2008] J. C. Y. Teo, L. Fu, and C. L. Kane, *Phys. Rev. B* **78**, 045426 (2008).
- [T1982] D. Thouless, M. Kohmoto, M. denNijs, and M. Nightingale, *Phys. Rev. Lett.* **49**, 405 (1982).
- [T1983] S. A. Trugman, *Phys. Rev. B* **27**, 7539 (1983).
- [TSG1982] D. C. Tsui, H. L. Störmer, and A. C. Gossard, *Phys. Rev. Lett.* **48**, 1599 (1982).
- [W1990] X. G. Wen, *Phys. Rev. B* **41**, 12838 (1990).
- [W1982] F. Wilczek, *Phys. Rev. Lett.* **49**, 957 (1982).
- [W1993] R. L. Willett, R. R. Ruel, M. A. Paalanen, K. W. West, and L. N. Pfeiffer, *Phys. Rev. B* **47**, 7344 (1993).
- [X2009] Y. Xia, D. Qian, D. Hsieh, *et al.*, *Nature Physics* **5**, 398 (2009).
- [Z2009] H. Zhang, C.-X. Liu, X.-L. Qi, X. Dai, Z. Fang, and S.-C. Zhang, *Nature Physics* **5**, 438 (2009).
- [Z1999] M. R. Zirnbauer, hep-th/9905054.

Prior to 1986, research on strongly interacting electron systems was a fringe subject in solid state physics. The discovery of high-temperature superconductivity in the copper-oxide ceramics changed this perception radically. The reason is simple. Undoped, the copper-oxide materials contain a partially filled d -band of electrons ([A1987](#)). Band theory tells us that partially filled bands conduct. However, the undoped cuprates are extremely good insulators. Although they become conducting after they are doped, they exhibit spectral weight redistributions over large energy scales that cannot be understood within the traditional theory of metals. It is this failure of band theory to predict insulating states in certain half-filled bands that Mott addressed in 1949 ([M1949](#)). Mott's analysis grew out of his study of NiO which contains two unpaired d electrons per unit cell but insulates nonetheless. Similar insulating states are found in most transition metal oxides, most notably VO_2 and V_2O_3 . Since band theory failed, Mott zeroed in on the electron correlations as the root cause of the insulating state in NiO. This line of inquiry has yielded some of the most subtle results and enigmatic problems in solid state physics. It is the physics of the Mott state and how it plays out in the cuprates and other systems that we describe in this chapter.

Any problem in solid state physics can be said to be solved once one has isolated the propagating degrees of freedom. These are the excitations that make the Lagrangian quadratic and give rise to pole-like singularities in the single-particle Green function. The Mott problem persists today because of the inherent problem in bringing an interacting Lagrangian into quadratic form without at the same time introducing operators which have non-canonical commutation relations. To some extent, we have seen such a problem before in the context of Fermi liquid theory presented in Chapter 12. However, because all repulsive short-range interactions renormalize towards the Fermi surface, their presence does not destroy the underlying free-particle picture of a Fermi liquid. That is, the interactions can be integrated out, leaving behind renormalized electron or quasi-particle states. Hence, in a Fermi liquid there is a simple principle that can be invoked to lay plain that free electrons are the propagating degrees of freedom. Without the assumption of a Fermi surface, no principle exists that allows us to smooth away the interactions. We refer to such problems as being strongly correlated, namely those in which no obvious principle, such as that delineated for Fermi liquids, exists that governs the renormalization of the electron-electron interactions. In approaching such strongly coupled systems, one can define a charge current. However, giving the charge current a particle interpretation can only be done once the propagating degrees of freedom are identified. A typical characteristic of the propagating degrees of freedom at strong coupling is that they tend to be composite excitations or bound states made out of the basic building blocks. Celebrated examples are quantum chromodynamics in which free quarks at high energy form bound entities at low energies and vulcanized

rubber in which individual polymer strands lose their integrity and become enmeshed in a cross-linked network. Isolating such collective phenomena is the central problem of strong coupling physics. The Mott problem is no exception, as we will demonstrate.

16.1 Band insulator

To understand what sets the Mott problem apart, let us start with a band insulator. We model such a system by allowing electrons to hop on a linear chain,

$$H_{\text{BI}} = -t \sum_{j,\sigma} \left(c_{j\sigma}^\dagger c_{(j+1)\sigma} + c_{(j+1)\sigma}^\dagger c_{j\sigma} \right) + V \sum_{j,\sigma} (-1)^j c_{j\sigma}^\dagger c_{j\sigma} = H_t + H_V, \quad (16.1)$$

of N sites in the presence of a periodic potential (S2010) with strength V . Although $[H_t, H_V] \neq 0$, both terms can be brought into diagonal form simultaneously because the Hamiltonian is quadratic. As a result of the hopping term, the eigenstates are linear combinations of the local states. Consequently, we define

$$c_{n\sigma} = \frac{1}{\sqrt{N}} \sum_{k\sigma} e^{ikna} c_{k\sigma} \quad (16.2)$$

in terms of the Fourier amplitude, $c_{k\sigma}$. Substituting Eq. (16.2) into the hopping term,

$$H_t = -\frac{t}{N} \sum_{n,k,k',\sigma} \left(e^{-ikna} e^{ik'(n+1)a} c_{k\sigma}^\dagger c_{k'\sigma} + e^{ikna} e^{-ik'(n+1)a} c_{k'\sigma}^\dagger c_{k\sigma} \right), \quad (16.3)$$

in conjunction with

$$\frac{1}{N} \sum_n e^{ikna} e^{-ik'na} = \delta_{k-k'}, \quad (16.4)$$

yields

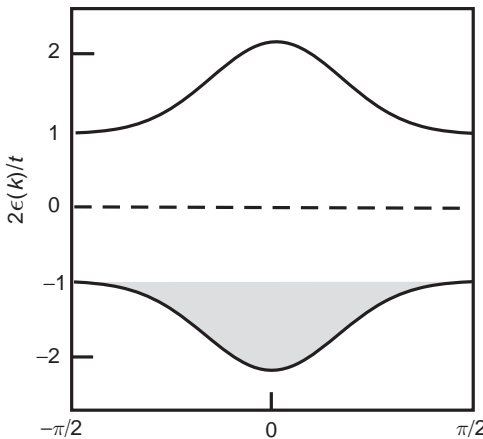
$$H_t = \sum_{k\sigma} \epsilon(k) c_{k\sigma}^\dagger c_{k\sigma} = \sum'_{k\sigma} \epsilon(k) c_{k\sigma}^\dagger c_{k\sigma} - \epsilon(k) c_{(k-\pi/a)\sigma}^\dagger c_{(k-\pi/a)\sigma}, \quad (16.5)$$

where $\epsilon(k) = -2t \cos ka$ and the prime on the summation refers to restraining the k s to $[-\pi/2a, \pi/2a]$. Similarly, the periodic potential term becomes

$$H_V = \frac{V}{N} \sum_{n,k,k'\sigma} e^{in(ka-k'a+\pi)} c_{k'\sigma}^\dagger c_{k\sigma} = \sum'_{k\sigma} \left(c_{k\sigma}^\dagger c_{(k-\pi/a)\sigma} + \text{h.c.} \right). \quad (16.6)$$

Upon symmetrizing the hopping term, we write the full Hamiltonian

$$H_{\text{BI}} = H_t + H_V = \sum'_{k\sigma} \Psi_{k\sigma}^\dagger \begin{pmatrix} \epsilon(k) & V \\ V & -\epsilon(k) \end{pmatrix} \Psi_{k\sigma} \quad (16.7)$$

**Fig. 16.1**

Band structure for a band insulator in units of the hopping integral t and a periodic potential, of strength $V = t$. The valence band (shaded region) is full while the upper band (conduction band) is empty.

in matrix form with

$$\Psi_\sigma = \begin{pmatrix} c_{k\sigma} \\ c_{(k-\pi/a)\sigma} \end{pmatrix}. \quad (16.8)$$

The Hamiltonian matrix can be diagonalized immediately. Its eigenvalues are

$$\varepsilon(k) = \pm \sqrt{V^2 + \epsilon(k)^2}. \quad (16.9)$$

Consequently, two bands emerge, as shown in Fig. 16.1, the bottom shaded one being the filled valence band and the upper one being the empty conduction band, which correspond to the bonding and antibonding combinations of $c_{k\sigma}$ and $c_{(k-\pi/a)\sigma}$, respectively. As long as the valence band is full, there is a gap equal to $2V$ for placing an additional electron into the system.

Consequently, the valence and conduction bands have simple interpretations in terms of the orthogonal eigenstates of the non-interacting Hamiltonian. Of course electrons in any material interact. Is there a correspondingly simple interpretation of the conduction and valence bands in the presence of interactions? This is a subtle question. Answering it is easiest if a fixed point exists which protects the gap. Establishing any such fixed point requires taking the continuum limit of our lattice model. The difficulties in such a limit are immediate. In terms of the lattice constant, the length of our lattice is

$$L = Na. \quad (16.10)$$

The continuum limit corresponds to $N \rightarrow \infty$ and $a \rightarrow 0$ such that L stays fixed. The subtlety arises in the number of particles. If we keep the particle number fixed, then the particle filling, N_p/N , actually vanishes in the continuum limit. That is, a continuum limit of a lattice model is valid strictly in the low-density limit such that only the bottom of the

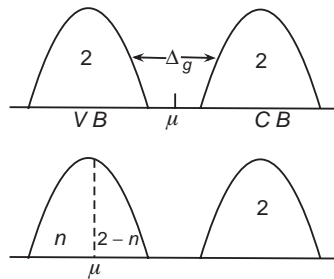


Fig. 16.2 Evolution of the single-particle density of states in a band insulator as a function of the electron filling, n . VB and CB correspond to valence and conduction bands, respectively. The total weight of the valence band is a constant 2, that is, 2 states per site. Doping simply pushes one state above the chemical potential. The integral of the density of states below the chemical potential is always the filling, n .

band or equivalently the low-momentum states are occupied. Formally, we arrive at the same conclusion by rewriting Eq. (16.2),

$$\frac{c_{n\sigma}}{\sqrt{a}} = \frac{1}{\sqrt{L}} \sum_{k\sigma} e^{ikx} c_{k\sigma}, \quad (16.11)$$

in terms of its explicit dependence on L with $x = na$. From this expression it is clear that the right-hand side depends only on x since it is summed over all k . As a result, the left-hand side must also depend only on the continuous variable x . Consequently, we make the association

$$\psi_\sigma(x) = \lim_{a \rightarrow 0} \frac{c_{n\sigma}}{\sqrt{a}} \Big|_x \quad (16.12)$$

between the continuum field, $\psi_\sigma(x)$, which annihilates a particle at x and its lattice counterpart. Equation (16.11) only has meaning if there is a finite number of creation operators on the right-hand side, otherwise the result is infinite. That is, the continuum limit corresponds to creating a finite number of particles on an infinite number of lattice sites. Consequently, the density must vanish. The states at the bottom of the band have a wavelength large relative to the lattice constant. The states at the top of a band, which are the ones relevant for describing the gap, have a large momentum. As a result, continuum limits are of no use in settling this question. An exception, of course, is if the gap opens at a Dirac point, in which case a continuum limit about the bottom of the band is relevant.

What really sets the band insulator problem apart from the Mott insulator is that the bands are rigid in the former but not in the latter. In the absence of interactions, band insulators consist of bands which are strictly eigenstates of single-particle (or single-electron) operators. Hence, changing the particle number in the valence band affects nothing about the conduction band, as illustrated in Fig. 16.2. In the undoped system, the total

number of states per site in each band is two (Fig. 16.2). Any system in which the density of states evolves according to Fig. 16.2 is identical to a band insulator, for example a semiconductor. As we will see, in the Mott problem even in the limit where the gap can be solved for exactly regardless of dimension, the bands that emerge are not rigid. No picture like Fig. 16.2 is valid in any limit of a doped Mott insulator. In fact, even the total spectral weight carried by each band depends on the electron filling. That is, what is meant by the high-energy band depends on the occupancy in the lower band. As a consequence, there is no single-electron interpretation of the Mott gap. In fact, there is no interpretation possible in terms of particles that have canonical commutation relations. Hence, the Mott problem is fundamentally about composite objects. Since it is the non-rigidity of the Mott bands that is the intrinsic feature of the Mott problem, we have introduced the term Mottness to refer to all the experimentally relevant properties that are coincident on such non-rigidity.

16.2 Mott's problem

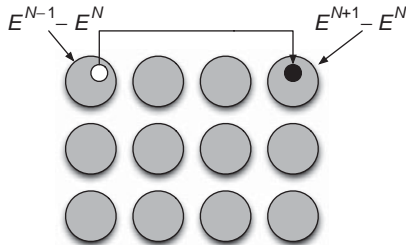
Mott's 1949 paper ([M1949](#)) consists of two parts. In the first part, he offered a simple explanation for the insulating state of NiO based entirely on potential energy considerations. In the second half of his paper, he discussed extensively why the simple picture cannot actually work. Simply, it ignores quantum mechanics! What seems to have followed in the subsequent literature is an unfortunate amnesia in which simplicity has prevailed over accuracy.

NiO contains an even number of unpaired electrons in a unit cell but insulates, nonetheless. To see this, consider the orbital configuration for NiO. Ni is $4s^2 3d^8$, and O is $2s^2 2p^4$. The two $4s$ electrons of Ni are donated to oxygen, thereby filling the $2p$ shell and leaving Ni in a +2 valence state. Consequently, the outer d -shell in NiO has two unpaired electrons. As a result, it is expected in a band picture to conduct electricity. However, it has a charge gap. To explain the gap, Mott appealed to the interactions between the electrons. In Mott's construction, the relevant interaction that dominates for narrow d -bands is the energy cost,

$$U = E^{N+1} + E^{N-1} - 2E^N, \quad (16.13)$$

for placing two electrons on the same Ni atom. Here E^N is the ground state energy for an atom with N valence electrons. Excluding the filled levels, $N = 2$ for Ni. At zero temperature, Mott reasoned that there is no Ni atom with $N \pm 1$ electrons if U exceeds a critical value, typically on the order of the bandwidth. That is, all Ni atoms have valence of +2, and no conduction obtains, as illustrated in Fig. 16.3. On this account, the resultant charge gap is the energy cost for doubly occupying the same site with spin-up and spin-down electrons. As a result, the simple Hamiltonian,

$$H_{\text{Hubb}} = -t \sum_{i,j,\sigma} g_{ij} c_{i\sigma}^\dagger c_{j\sigma} + U \sum_{i,\sigma} n_{i\uparrow} n_{i\downarrow} - \mu \sum_{i,\sigma} n_{i\sigma}, \quad (16.14)$$



$$U = E^{N+1} + E^{N-1} - 2E^N$$

Fig. 16.3 A half-filled band as envisioned by Mott. Each circle represents a neutral atom with N electrons and ground-state energy E^N . The energy differences for electron removal and addition are explicitly shown. Mott reasoned that no doubly occupied sites exist because at zero temperature, $U = E^{N+1} + E^{N-1} - 2E^N \gg 0$. This is, of course, not true. As a consequence the Mott gap must be thought of dynamically rather than statically.

first introduced by Hubbard (H1963), in which electrons hop among a set of lattice sites with matrix element t , but pay an energy cost U whenever they doubly occupy the same site, is sufficient to describe the transition to the state envisioned by Mott. In this model, i, j label lattice sites, g_{ij} is equal to one iff i, j are nearest neighbors, $c_{i\sigma}$ annihilates an electron with spin σ on lattice site i , and t is the nearest-neighbor hopping matrix element. In light of Eq. (16.14), the simple Mott picture in which no Ni^{+++} nor Ni^+ ions exist in the ground state only works when the hopping vanishes. This is the atomic limit and the argument presented in the first part of Mott's paper.

We can make Mott's first argument more precise. The Hubbard model consists of two terms which do not commute. Unlike H_{BI} , the Hubbard model is not quadratic in the electron operators, and as a result, the non-commutativity of the potential and kinetic terms poses a distinct problem. Nonetheless, the Hubbard model can be brought into quadratic form by writing the electron annihilation operator,

$$c_{i\sigma} = c_{i\sigma}(1 - n_{i\bar{\sigma}}) + c_{i\sigma}n_{i\bar{\sigma}} = \xi_{i\sigma} + \eta_{i\sigma}, \quad (16.15)$$

as a sum of two operators, each of which acts on two kinds of site. The operator $\xi_{i\sigma}$ annihilates an electron from sites which are singly occupied and $\eta_{i\sigma}$ annihilates one from sites which are doubly occupied. Noting that $n_{i\sigma}^2 = 1$ for fermions, it follows that $n_{i\uparrow}n_{i\downarrow} = n_{i\uparrow}n_{i\downarrow}^2 = \eta_{i\uparrow}^\dagger\eta_{i\uparrow}$, implying that the interaction term,

$$H_U = U \sum_i n_{i\uparrow}n_{i\downarrow} = \frac{U}{2} \sum_{i\sigma} \eta_{i\sigma}^\dagger \eta_{i\sigma}, \quad (16.16)$$

can be written in a quadratic form entirely in terms of $\eta_{i\sigma}$. We can do the same for the kinetic term by simply substituting Eq. (16.15), thereby recasting the Hubbard model,

$$H_{\text{Hubb}} = -t \sum_{i,j,\sigma} \left(\eta_{i\sigma}^\dagger \eta_{j\sigma} + \xi_{i\sigma}^\dagger \xi_{j\sigma} + \eta_{i\sigma}^\dagger \xi_{j\sigma} + \xi_{i\sigma}^\dagger \eta_{i\sigma} \right) + \frac{U}{2} \sum_{i,\sigma} \eta_{i\sigma}^\dagger \eta_{i\sigma}, \quad (16.17)$$

entirely in quadratic form. It turns out that this sort of transformation can always be done in any interacting problem. The complication is that the $\xi_{i\sigma}$ and $\eta_{j\sigma}$ operators obey non-canonical commutation relations,

$$\begin{aligned}\{\eta_{i\alpha}, \xi_{j\beta}\} &= \delta_{ij} c_{i\beta} c_{j\alpha}, \\ \{\eta_{i\alpha}, \eta_{j\beta}^\dagger\} &= \delta_{ij} (n_{i\bar{\alpha}} \delta_{\alpha\beta} - c_{i\beta}^\dagger c_{i\alpha} \delta_{\alpha\bar{\beta}}), \\ \{\xi_{i\alpha}, \xi_{j\beta}^\dagger\} &= \delta_{ij} ((1 - n_{i\bar{\alpha}}) \delta_{\alpha\beta} + c_{i\beta}^\dagger c_{i\alpha} \delta_{\alpha\bar{\beta}}), \\ \{\eta_{i\alpha}, \eta_{j\beta}\} &= \{\xi_{i\alpha}, \xi_{j\beta}\} = \{\xi_{i\alpha}, \eta_{j\beta}^\dagger\} = 0.\end{aligned}\quad (16.18)$$

While the interaction term is diagonal in this new basis, the hopping term is not. It explicitly mixes the doubly and singly occupied sectors. Consequently, the $\eta_{i\sigma}$ and $\xi_{i\sigma}$ operators form the basis for a strong-coupling expansion for the Hubbard model. Since these operators diagonalize the interaction, it is incorrect to think of them in terms of a single-particle Fock space. That is, there is no sense in which a Wick theorem can be defined in this new basis.

Consider the atomic limit. Since all the eigenstates are eigenstates of local particle occupation, they can be ordered by how many doubly occupied sites they contain. At half-filling, the ground state has one electron per site. The first excited state has one double occupancy, and so forth. The gap to the first excited state is precisely U . This is Mott's picture. Each atom is neutral in the ground state, and the gap represents the energy difference to the first state that has double occupancy.

However inceptive the $t = 0$ picture is, it still contains Mottness in its simplest form. Namely, the bands that arise from $\eta_{i\sigma}$ and $\xi_{i\sigma}$ are not static in that the total spectral weight they carry depends on the filling. That is, the bands defined by $\eta_{i\sigma}$ and $\xi_{i\sigma}$ are not bands in the traditional band insulator picture. We will illustrate this two ways. First, as shown in Eq. (7.100) in the section on Green functions, the total spectral intensity of a band is given by the anticommutation relationship of the operators that create particles in that band. The spectral weight in the lower band (the $\xi_{i\sigma}$ band) is determined entirely by

$$m_{\text{LHB}}^0 = \frac{1}{N} \sum_{i,\sigma} \langle \{\xi_{i\sigma}, \xi_{i\sigma}^\dagger\} \rangle = 2 - n = 1 + x, \quad (16.19)$$

where we have used Eq. (16.18) and x is the number of holes introduced into the lower band. The number of holes is defined relative to half-filling and hence $n \equiv \langle (n_{i\downarrow} + n_{i\uparrow}) \rangle = 1 - x$. Since the total weight must be 2 between the upper and lower bands, the weight in the upper band must be

$$m_{\text{UHB}}^0 = \frac{1}{N} \sum_{i,\sigma} \langle \{\eta_{i\sigma}, \eta_{i\sigma}^\dagger\} \rangle = n = 1 - x \quad (16.20)$$

in the atomic limit. These weights would be inverted if we were interested in electron doping. The first point that is clear is that at half-filling, $x = 0$, the lower and upper bands

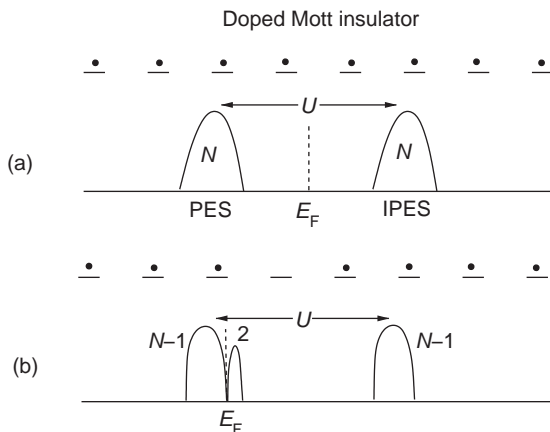


Fig. 16.4 (a) Half-filled band in the limit of large $U \gg t$ results in a gap in the single-particle spectrum. The bands shown represent the upper and lower Hubbard bands. In an N -site system, the total number of single-particle states in each band at half-filling is N . The electron-removal or photoemission (PES) band and electron-addition, inverse-photoemission (IPES) band correspond to an electron moving on empty and singly-occupied sites, respectively. In the atomic limit the splitting between the bands is U . (b) Evolution of the single-particle density of states from half-filling to the one-hole limit in a doped Mott insulator in the atomic limit of the Hubbard model. Removal of an electron results in two empty states at low energy as opposed to one in the band-insulator limit. The key difference with the Fermi liquid is that the total spectral weight carried by the lower Hubbard band (analog of the valence band in a Fermi liquid) is not a constant but a function of the filling.

carry the same spectral weight. In stark contrast stands the band insulator in which only the valence band has any spectral weight in the insulating state. Moreover, at any finite doping, the spectral weight depends on the doping level, also in contrast to a band insulator in which it is strictly a constant. This difference arises entirely because the gap in the Mott problem even at $t = 0$ is not defined in terms of single-electron operators. That is, there is no single-electron picture behind the Mott gap in any limit, unlike Eq. (16.1). Nonetheless, a simple physical picture underlies the doping dependence of the spectral weights in the upper and lower bands in the atomic limit. Consider Fig. 16.4. At half-filling in the atomic limit, there are exactly N ways to add and remove an electron in an N -site system. Consequently, the photoemission and inverse photoemission bands have N states each. A hole in a band insulator creates a single empty state in the valence band and leaves the conduction band untouched. Such is not the case in a Mott insulator even at half-filling. Consider creating a hole. There are now $N - 1$ ways to remove an electron and also $N - 1$ ways to create double occupancy. However, we have to conserve states. The two mysterious states we have yet to account for correspond to the two ways of occupying the empty site with either a spin-up or a spin-down electron. Hence, the total spectral weight for each empty site is two. Since it costs no energy to put an electron in either of these states, these states must lie immediately above the chemical potential and form the empty part of the lower band, as depicted in Fig. 16.4. When n_h holes are introduced such that $x = n_h/N$, the total weight in the lower band is $1 + x$. The weight below the chemical potential is $1 - x$ and $2x$ states lie above. Note the weight below the chemical potential is identical to that in the upper band since the weight

in the upper band exists only if a site is already singly occupied. Hence, in the atomic limit, the weight in the upper and in the lower band below the chemical potential must mirror one another. The sense in which such mirroring persists away from the atomic limit is one of the true subtleties of the Mott problem.

16.2.1 Green function: atomic limit

The second way to demonstrate that the weight of each band in the Hubbard model depends on the filling is through a direct calculation of the single-particle Green function. Following Chapter 7, we define the relevant retarded Green function as

$$G_{i\sigma}^R(t, 0) = -i\theta(t)\langle\{c_{i\sigma}(t), c_{i\sigma}^\dagger(0)\}\rangle, \quad (16.21)$$

which is purely diagonal in site space. In general this is not the case, as we will see in our more complete treatment of the full Hubbard model. In the atomic limit, the Green function can be derived in closed form using the equations of motion technique. Differentiating both sides, we obtain

$$\partial_t G_{i\sigma}^R(t, 0) = -i\delta(t) - i\theta(t)\langle\{\dot{c}_{i\sigma}, c_{i\sigma}^\dagger\}\rangle, \quad (16.22)$$

where the first term arises from differentiating the Heaviside step function. From the Heisenberg equations of motion,

$$i\dot{c}_{i\sigma} = \frac{U}{\hbar}c_{i\sigma}n_{i\bar{\sigma}} - \frac{\mu}{\hbar}c_{i\sigma}, \quad (16.23)$$

it makes sense to introduce an additional Green function,

$$\tilde{G}_{i\sigma}^R(t, 0) = -i\theta(t)\langle\{c_{i\sigma}(t)n_{i\bar{\sigma}}(t), c_{i\sigma}^\dagger(0)\}\rangle. \quad (16.24)$$

Substituting Eq. (16.23) into Eq. (16.22),

$$\partial_t G_{i\sigma}^R(t, 0) = -i\delta(t) - i\frac{U}{\hbar}\tilde{G}_{i\sigma}^R(t, 0) + i\frac{\mu}{\hbar}G_{i\sigma}^R(t, 0), \quad (16.25)$$

reveals the inherent problem with the equations of motion approach, namely the telescoping dependence on a series of other Green functions. Luckily, in the atomic limit, the equations can be closed because the derivative of $\tilde{G}_{i\sigma}^R(t, 0)$,

$$\partial_t \tilde{G}_{i\sigma}^R(t, 0) = -i\delta(t)\langle\{c_{i\sigma}n_{i\bar{\sigma}}, c_{i\sigma}^\dagger\}\rangle - i\theta(t)\langle\{\dot{c}_{i\sigma}(t)n_{i\bar{\sigma}}(t), c_{i\sigma}^\dagger\}\rangle, \quad (16.26)$$

reduces to a simple function,

$$\partial_t \tilde{G}_{i\sigma}^R(t, 0) = -i\delta(t)\langle n_{i\bar{\sigma}} \rangle - i\frac{U}{\hbar}\tilde{G}_{i\sigma}^R(t, 0) + i\frac{\mu}{\hbar}\tilde{G}_{i\sigma}^R(t, 0). \quad (16.27)$$

In simplifying this equation, we used the equations of motion, Eq. (16.23), and the facts that $\dot{n}_{i\sigma} = 0$ and $n_{i\sigma}^2 = n_{i\sigma}$. The rest is now simple. Introducing the Fourier transform,

$$f(\omega) = \int_{-\infty}^{\infty} e^{i\omega t/\hbar} f(t) dt, \quad (16.28)$$

we find that

$$\tilde{G}_{i\sigma}^R(\omega) = \frac{\hbar n_{i\bar{\sigma}}}{\omega - U + \mu} \quad (16.29)$$

and as a result

$$G_{i\sigma}^R(\omega) = \hbar \left(\frac{1}{\omega + \mu} + \frac{U \langle n_{i\bar{\sigma}} \rangle}{(\omega + \mu)(\omega + \mu - U)} \right), \quad (16.30)$$

where it is understood that ω has a positive imaginary part. The physical import of this equation is more immediate if it is decomposed in terms of partial fractions,

$$G_i^R(\omega) = \frac{1}{\hbar} \sum_{\sigma} G_{i\sigma}^R(\omega) = \frac{2-n}{\omega + \mu} + \frac{n}{\omega + \mu - U}, \quad (16.31)$$

which expose the underlying two-pole structure. We obtain a more symmetrized expression,

$$G_i^R(\omega) = \frac{1+x}{\omega + \mu + \frac{U}{2}} + \frac{1-x}{\omega + \mu - \frac{U}{2}}, \quad (16.32)$$

by making the shift $\mu \rightarrow \mu + \frac{U}{2}$ and setting $n = 1 - x$ for a hole-doped system. The two poles, split by U , carry spectral weights of $1+x$ and $1-x$ respectively. Each hole subtracts a single state from the high-energy sector, thereby leading to the $1-x$ residue. The empty state reappears at low energies as part of the addition spectrum at low energies. The fact that the empty part of the spectrum grows as $2x$ as opposed to x in a band insulator reflects this static transfer of spectral weight. The term static here signifies that the spectral weight can be accounted for by simply counting electron states. As we will see, there is an additional dynamical effect which cannot be enumerated by such state counting. The reader should keep in mind that the usage of the term band to refer to the location of the turn-on of the spectral weight above and below the chemical potential in Mott systems carries with it a fundamentally different set of notions than in the standard rigid-band picture of a band insulator, in particular spectral weight transfer.

In thinking about the atomic limit, it is helpful to introduce Haldane's ([H1991](#)) generalization of the Pauli principle. Here, Haldane pointed out that we can think about statistics,

$$\Delta d_{\alpha} = - \sum_{\beta} g_{\alpha\beta} \Delta N_{\beta}, \quad (16.33)$$

entirely in terms of how the number of states for adding particles of kind α changes, Δd_{α} , when the number of particles of type β is incremented, ΔN_{β} . Here $g_{\alpha\beta}$ is the statistical matrix that determines how the Hilbert spaces for the particles of type α and β are affected. Consider the simple case of up or down spins. For non-interacting electrons, $g_{\alpha\beta} = \delta_{\alpha\beta}$. That is, the phase space for adding up electrons is independent of the number of down-spin electrons. In the atomic limit of the Hubbard model for $U = \infty$, there can be only one electron per site. Consequently, the Hilbert spaces for up and down electrons are connected and the g -matrix,

$$g = \begin{pmatrix} 1 & 1 \\ 1 & 1 \end{pmatrix}, \quad (16.34)$$

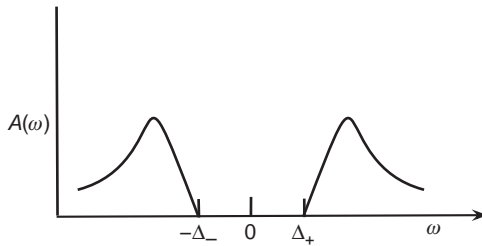


Fig. 16.5 Spectral function as a function of frequency in a half-filled system. $\pm\Delta_{\pm}$ represent the lower (−sign) and upper (+ sign) edges of the Mott gap.

has off-diagonal elements. Since each particle excludes others from occupying the same site, the particles which obey Eq. (16.34) are sometimes called *exclusions*. What Eq. (16.34) lays plain is that interactions between electrons can, in some cases, be recast as a new statistical principle. Away from the $U = \infty$ limit, this is not true.

16.3 Much ado about zeros: Luttinger surface

There is an additional difference between band and Mott insulators that can be illustrated with the atomic limit of the Hubbard model. To illustrate this, we calculate the spectral function,

$$\begin{aligned} A(\omega) &= -\frac{1}{\pi} \text{Im } G_i^R(\omega + i\Gamma) \\ &= ((1+x)\delta(\omega - \mu + U/2) + (1-x)\delta(\omega - \mu - U/2)), \end{aligned} \quad (16.35)$$

in the atomic limit. In a band insulator, there is no spectral weight in the band above the chemical potential. Not so in a Mott insulator. This has a profound consequence. From the Kramers–Kronig relations, the real part of the retarded Green function,

$$R(\omega) \equiv \text{Re } G_i^R(\omega) = \int_{-\infty}^{\infty} d\omega' \frac{A(\omega')}{\omega - \omega'}, \quad (16.36)$$

is directly related to the spectral function. We are interested in the behavior of this integral at zero frequency in the half-filled system. Since the spectral function vanishes within the Mott gap, this integral simplifies at zero frequency (the location of the chemical potential for the particle-hole symmetric case), to

$$R(0) = - \int_{-\infty}^{-\Delta_-} \frac{A(\omega')}{\omega'} d\omega' - \int_{\Delta_+}^{\infty} \frac{A(\omega')}{\omega'} d\omega', \quad (16.37)$$

where Δ_- and Δ_+ are the lower and upper edges of the Mott gap, as depicted in Fig. 16.5. This integral carries no particular significance for a band insulator. However, in a Mott system even beyond the atomic limit, this integral has the possibility (D2003) of

vanishing simply because the spectral function is always positive and non-zero above and below the chemical potential. The integral of the first term is negative, whereas the second is positive. Hence, $R(0)$ can be zero. In the atomic limit for $x = 0$, this calculation can be performed explicitly,

$$R(0) = - \int_{-\infty}^{-\Delta_-} \frac{\delta(\omega' - \mu + U/2)}{\omega'} d\omega' - \int_{\Delta_+}^{\infty} \frac{\delta(\omega' - \mu - U/2)}{\omega'} d\omega', \quad (16.38)$$

which vanishes for $\mu = 0$ for all momenta. The condition that $R(0) = 0$ for all momenta is only true in the atomic limit. Away from this limit, the zero-condition will depend on momentum as a result of the explicit momentum dependence of the spectral function. The technical definition of a Mott insulator is: *any partially filled band for which the corresponding retarded Green function in the paramagnetic state has a vanishing real part at some value of the chemical potential along a connected surface in momentum space*. Such a surface defines what is called the Luttinger surface and arises entirely because Mott insulators have non-vanishing spectral functions both above and below the chemical potential. No such surface exists for a band insulator. The significance of the zero surface in a Mott insulator is that it is the surface along which the electron propagator vanishes. As expected, the electrons are not the propagating degrees of freedom. The caveat that the surface of zeros exists for some value of the chemical potential is essential because it is clear from Eq. (16.38) that only at the particle-hole symmetric point does $R(0) = 0$. There is an arbitrariness (R2007) associated with the placement of the chemical potential in an incompressible state since any location in the gap preserves the insulating nature of the Mott state.

Away from the atomic limit, we can establish (SPC2007) the exact location of the surface of zeros without any explicit calculation of the spectral function, but only when the Hamiltonian has particle-hole symmetry. From Eq. (16.37), we simply need to establish for which momenta the spectral function is even with respect to frequency. To proceed, we consider a general particle-hole transformation,

$$c_{i\sigma} \rightarrow e^{i\mathbf{Q}\cdot\mathbf{r}} c_{i\sigma}^\dagger, \quad (16.39)$$

of the electron annihilation operator. That the Hamiltonian remains invariant under this transformation places constraints on both \mathbf{Q} and the chemical potential. The Hubbard model with nearest-neighbor hopping remains invariant under Eq. (16.39) for $\mathbf{Q} = (\pi, \pi)$ and $\mu = U/2$. The latter is the value of the chemical potential at half-filling, the Mott state. Recall, in deriving Eq. (16.32), we symmetrized about $U/2$ through the transformation $\mu \rightarrow \mu + U/2$. Transforming the operators in the Green function,

$$G_{ij\sigma}^R(t, 0) = -i\theta(t)\langle\{c_{i\sigma}(t), c_{j\sigma}^\dagger(0)\}\rangle, \quad (16.40)$$

according to Eq. (16.39), using Eqs. (7.95) and (7.97), and keeping the chemical potential fixed at $\mu = U/2$, leads to the identity

$$A_\sigma(\omega, \mathbf{k}) = A_\sigma(-\omega, -\mathbf{k} - \mathbf{Q} + 2n\pi). \quad (16.41)$$

Hence, the spectral function is an even function of frequency for $\mathbf{k} = \mathbf{Q}/2 + n\pi$. At such momenta, the integral in Eq. (16.37) vanishes. Consider one dimension and nearest-neighbor hopping. In this case, the symmetry points are $\pm\pi/2$, the Fermi points for the

half-filled non-interacting band. In two dimensions, this proof is sufficient to establish the existence of only two points, not a surface of zeros. To determine the surface, we take advantage of an added symmetry in higher dimensions. For example, in two dimensions, we can interchange the canonical (x, y) axes leaving the Hamiltonian unchanged only if the hopping is isotropic. This invariance allows us to interchange k_x and k_y on the left-hand side of Eq. (16.41), resulting in the conditions

$$k_y = -k_x - q + 2n\pi \quad (16.42)$$

and by reflection symmetry

$$-k_y = -k_x - q + 2n\pi, \quad (16.43)$$

where $\mathbf{Q} = (q, q)$. For nearest-neighbor hopping, the resultant condition, $k_x \pm k_y = -\pi + 2n\pi$, is the solution to $\cos k_x + \cos k_y = 0$, which defines the Fermi surface for the non-interacting system. If only next-nearest-neighbor hopping is present, the value of the wavevector that leaves the kinetic energy term unchanged after a particle–hole transformation is $\mathbf{Q} = (\pi, 0)$ or $(0, \pi)$. Coupled with Eq. (16.41) and reflection symmetry we also obtain the Fermi surface of the non-interacting system. The interactions need not be the local on-site repulsion in the Hubbard model for the surface of zeros to persist. Nearest-neighbor interactions of strength V depend only on the particle density and hence are independent of Q under a particle–hole transformation. Such interactions renormalize the chemical potential from $U/2$ (on-site interactions) to $(U + 2V)/2$ at the particle–hole symmetric point (see Problem 16.1).

A shortcoming of this proof is that it does not apply to a band structure that has unequal hoppings along the (x, y) axes, for example. In the presence of such an anisotropy, we cannot interchange k_x and k_y . Nonetheless, our result can be generalized. To prove this, we consider the moments

$$M_n^\sigma(\mathbf{k}) \equiv \int d\omega \omega^n A_\sigma(\omega, \mathbf{k}) \quad (16.44)$$

of the spectral function. Our goal is to establish under which conditions all the odd moments vanish, thereby rendering $A_\sigma(\omega, \mathbf{k})$ an even function of frequency. Recall from Eq. (7.97) that the spectral function can be written entirely in terms of two correlation functions

$$A_\sigma(\omega, \mathbf{k}) = \frac{i}{2\pi} (G_\sigma^>(\omega, \mathbf{k}) - G_\sigma^<(\omega, \mathbf{k})). \quad (16.45)$$

Hence, the moments of the spectral function in real space,

$$\int d\omega \omega^n A_{\sigma,ij}(\omega) = \int d\omega \omega^n \int dt e^{i\omega t/\hbar} (\langle c_i(t)c_j(0)^\dagger \rangle + \langle c_j(0)^\dagger c_i(t) \rangle), \quad (16.46)$$

can be simplified by writing

$$\omega^n e^{i\omega t/\hbar} = (-i\hbar)^n \partial_t^n e^{i\omega t/\hbar}. \quad (16.47)$$

Integrating by parts puts all of the derivatives on $c_{i\sigma}(t)$ which can be simplified using the Heisenberg equations of motion. The integration over the frequency yields $2\pi\delta(t)$. Consequently, we obtain that

$$\int \frac{d\omega}{2\pi} \omega^n A_{\sigma,ij}(\omega) = M_n^\sigma(i,j), \quad (16.48)$$

where

$$\begin{aligned} M_n^\sigma(i,j) &= \frac{1}{2} \left[\langle \{ [H_{\text{Hubb}}, [H_{\text{Hubb}} \dots [H_{\text{Hubb}}, c_{i\sigma}] \dots]_n \text{ times}, c_{j\sigma}^\dagger \} \right. \\ &\quad \left. + \langle \{ c_{i\sigma}, [\dots [c_{j\sigma}^\dagger, H_{\text{Hubb}}] \dots H_{\text{Hubb}}], H_{\text{Hubb}} \}_n \text{ times} \} \rangle \right] \end{aligned} \quad (16.49)$$

is a symmetrized string of commutators of the electron creation or annihilation operators with the Hubbard Hamiltonian. To evaluate the string of commutators, it suffices to focus on the properties of

$$K_{i\sigma}^{(n)} = [\dots [c_{i\sigma}, H_{\text{Hubb}}], \dots H_{\text{Hubb}}]_n \text{ times}, \quad (16.50)$$

where by construction, $K_{i\sigma}^{(0)} = c_{i\sigma}$. We write the Hubbard Hamiltonian as $H_{\text{Hubb}} = H_t + H_U$, where H_U includes the interaction as well as the chemical potential terms and H_t , the hopping term. The form of the first commutator,

$$K_{i\sigma}^{(1)} = \sum_j t_{ij} c_{j\sigma} + U c_{i\sigma} n_{i-\sigma} - \mu c_{i\sigma}, \quad (16.51)$$

suggests that we seek a solution of the form

$$K_{i\sigma}^{(n)} = \sum_j t_{ij} \Lambda_{j\sigma}^{(n)} + Q_{i\sigma}^{(n)}, \quad (16.52)$$

where $Q_{i\sigma}^{(n)} = [\dots [c_{i\sigma}, H_U], \dots H_U]_n$ involves a string containing H_U n times and in $\Lambda_{j\sigma}$, H_t **appears at least once**. Our proof hinges on the form of $Q_{i\sigma}^{(n)}$ which we write in general as $Q_{i\sigma}^{(n)} = \alpha_n c_{i\sigma} n_{i-\sigma} + \beta_n c_{i\sigma}$. The solution for the coefficients,

$$\begin{aligned} \alpha_{n+1} &= (U - \mu)\alpha_n + U(-\mu)^n, \\ \beta_n &= (-\mu)^n, \end{aligned} \quad (16.53)$$

is determined from the recursion relationship $Q_{i\sigma}^{(n+1)} = [Q_{i\sigma}^{(n)}, H_U]$. In the moments, the quantity which appears is

$$\langle \{Q_{i\sigma}^{(n)}, c_{j\sigma}^\dagger\} \rangle = \delta_{ij} [\alpha_n \langle n_{i-\sigma} \rangle + \beta_n] \equiv \delta_{ij} \gamma_n. \quad (16.54)$$

Consequently, the moments simplify to

$$M_n^\sigma(i, j) = \delta_{ij}\gamma_n + \frac{1}{2} \sum_l t_{il} \left(\langle \{\Lambda_{l\sigma}^{(n)}, c_{j\sigma}^\dagger\} \rangle + \text{h.c.} \right). \quad (16.55)$$

The criterion for the zeros of the Green function now reduces to a condition on the parity of the right-hand side of Eq. (16.55). Consider the case of half-filling, particle-hole symmetry and nearest-neighbor hopping. Under these conditions, $\langle n_{i\sigma} \rangle = 1/2$ and by particle-hole symmetry, $\mu = U/2$. The expressions for α_n and β_n lay plain that the resultant coefficients

$$\gamma_n = \left(\frac{U}{2}\right)^n \frac{1 + (-1)^n}{2} \quad (16.56)$$

vanish for n odd. Consequently, $G_\sigma(\mathbf{k}, \omega)$ is an even function if the second term in Eq. (16.55) vanishes. In Fourier space, the second term is proportional to the non-interacting band structure $t(k)$. The momenta at which $t(\mathbf{k}) = 0$ define the Fermi surface of the non-interacting system. Note that the condition $t(\mathbf{k}) = 0$, which defines the surface of zeros, is independent of the anisotropy of the hopping. We conclude that when particle-hole symmetry is present, $G(0, \mathbf{k} = \mathbf{k}_F) = 0$ for a Mott insulator, where \mathbf{k}_F is the Fermi surface for the non-interacting system. In this case, the volume of the surface of zeros is identically equal to the particle density. Hence, even for a Mott insulator (provided particle-hole symmetry is present), the Luttinger theorem applies. This constitutes one of the few exact results for Mott insulators that is independent of spatial dimension, or at least as long as $d \neq \infty$. As mentioned previously, if $d = \infty$, there is no Luttinger surface as Σ diverges as $1/\omega$ for all momenta (GKKR1996; J1992). Finally, the only condition for the applicability of our proof is that the form of the spectral function leads to the continuity of $R_\sigma(\omega, \mathbf{k})$ at $\omega = 0$. Hence, the minimal condition is that the spectral function be continuous at $\omega = 0$. Therefore, if there is a gapless quasi-particle excitation, for example, $A_\sigma(\epsilon, \mathbf{k}) = \delta(\omega)$, our proof becomes invalid.

Before we leave this section, a word on the significance of the zeros of the Green function is in order. Let us write the single-particle retarded Green function at half-filling in the atomic limit,

$$G_{i\sigma}^R(\omega) = \frac{1}{\omega + \mu + U/2 - \Sigma_{\text{loc}}(\omega)}, \quad (16.57)$$

in terms of the corresponding self-energy,

$$\Sigma_{\text{loc}}(\omega) = \frac{U}{2} + \left(\frac{U}{2}\right)^2 \frac{1}{\omega + \mu}. \quad (16.58)$$

A vanishing of the single-particle Green function clearly corresponds to a divergence of the self-energy. In this case, anytime $\omega = -\mu$, the self-energy diverges. Recall, at the chemical potential, the self-energy in a Fermi liquid vanishes. Here, this is not the case. This stark difference further amplifies the fact that in a Mott insulator, electrons are not sharp excitations.

While the volume of this zero surface is not directly tied to the particle density except in the case of particle-hole symmetry (R2007; SPC2007), in direct contrast to the surface enclosed by the divergence of the Green function in a Fermi liquid, all is not lost. The surface of zeros tells us that electrons are not the propagating degrees of freedom. A correct identification of the propagating modes would result in a pole in the associated single-particle Green function. An analogy to QCD is in order here. At IR energy scales, the quark propagator vanishes, at least in $1 + 1$ dimensions where QCD can be solved exactly (H1974). However, the meson or bound quark propagator has a pole. The Mott problem amounts to finding the particle whose pole in the single-particle propagator leads to the band structure of a Mott insulator depicted in Fig. 16.5.

16.4 Beyond the atomic limit: Heisenberg versus Slater

The essence of Mott's problem, namely the presence of non-rigid bands and hence the invalidity of the single-electron picture, can be illustrated entirely from the atomic limit. However, additional problems arise away from the atomic limit. As Eq. (16.17) makes clear, away from the atomic limit, $\xi_{i\sigma}$ and $\eta_{i\sigma}$ do not propagate independently. Consequently, we cannot attribute the Mott gap entirely to the gap between $\xi_{i\sigma}$ and $\eta_{i\sigma}$. That is, the Mott gap is not due to the gap to the first excited state that has doubly occupied character. Note: this problem is distinct from the fact that the non-interacting bands in a band insulator are strictly no longer orthogonal in the presence of interactions. Interactions in a band insulator do not destroy the underlying single-electron nature of the bands. The Mott problem is the other extreme in which expanding in the eigenstates of the interaction term already forces us out of range of validity of a single-particle picture. When the hopping is turned on, several competing tendencies arise, which obfuscates the Mott problem.

16.4.1 Slater: Hartree–Fock account of Néel ordering

Slater was one of the first to point out that half-filled bands are highly susceptible to antiferromagnetic order. We illustrate this by performing a Hartree–Fock analysis of the Hubbard model. As we saw in our treatment of local moments, Hartree–Fock is inherently a non-interacting picture in which some sort of mean-field decoupling is invoked on the interaction term. For the Hubbard model, this can be accomplished by writing the density operator as $n_{\mathbf{r}\sigma} = O_{\mathbf{r}\sigma} + \delta O_{\mathbf{r}\sigma}$ such that

$$n_{\mathbf{r}\uparrow} n_{\mathbf{r}\downarrow} \rightarrow n_{\mathbf{r}\uparrow} (O_{\mathbf{r}\downarrow} + \delta O_{\mathbf{r}\downarrow}) + n_{\mathbf{r}\downarrow} (O_{\mathbf{r}\uparrow} + \delta O_{\mathbf{r}\uparrow}) - (O_{\mathbf{r}\uparrow} + \delta O_{\mathbf{r}\uparrow})(O_{\mathbf{r}\downarrow} + \delta O_{\mathbf{r}\downarrow}). \quad (16.59)$$

The last term is necessary to make the mean field value $\langle n_{\mathbf{r}\uparrow} n_{\mathbf{r}\downarrow} \rangle$ equal to $\langle O_{\mathbf{r}\uparrow} O_{\mathbf{r}\downarrow} \rangle$. Recall in mean-field, all fluctuation terms are dropped. Since this decoupling has gotten rid of the interaction term, reducing the problem to an effective single-particle one, the magnitude of U has no real meaning. That is, although U/t is allowed to be large, this regime cannot truthfully represent strong coupling physics. However, there is something to be learned from this procedure. We can eliminate the explicit dependence on $O_{\mathbf{r}\sigma}$ by defining the effective spin along the z -axis,

$$\Omega_{\mathbf{r}}^z = \frac{1}{2}(O_{\mathbf{r}\uparrow} - O_{\mathbf{r}\downarrow}), \quad (16.60)$$

and net charge density,

$$\bar{n}_{\mathbf{r}} = \frac{1}{2}(O_{\mathbf{r}\uparrow} + O_{\mathbf{r}\downarrow}). \quad (16.61)$$

Our effective Hartree–Fock Hamiltonian becomes

$$H_{\text{HF}} = -t \sum_{\mathbf{r}, \delta, \sigma} c_{\mathbf{r}, \sigma}^\dagger c_{\mathbf{r}+\delta, \sigma} + U \sum_{\mathbf{r}} (\bar{n}_{\mathbf{r}}(n_{\mathbf{r}\uparrow} + n_{\mathbf{r}\downarrow}) - \Omega_{\mathbf{r}}^z(n_{\mathbf{r}\uparrow} - n_{\mathbf{r}\downarrow}) - \bar{n}_{\mathbf{r}}^2 + (\Omega_{\mathbf{r}}^z)^2), \quad (16.62)$$

where we have dropped the second-order fluctuation term $\delta O_{\mathbf{r}\uparrow} \delta O_{\mathbf{r}\downarrow}$. This classical approximation should be valid as long as the order parameter acquires a non-zero value. While the deviations from this classical theory can be treated perturbatively, this is not our concern here.

We now specialize to a half-filled bipartite lattice. The ground state is indeed a Néel antiferromagnet with a uniform charge density. In such a state, the value of $\Omega_{\mathbf{r}}^z$ alternates in sign from site to site. It is convenient then to define two sublattices A and B such that $\bar{n}_{\mathbf{r}} \equiv \bar{n}$ for all sites, $\Omega_{\mathbf{r}} = (0, 0, \Omega)$ for $\mathbf{r} \in A$, and $\Omega_{\mathbf{r}} = (0, 0, -\Omega)$ for $\mathbf{r} \in B$. It is helpful, then, to define, $\Omega_{\uparrow} = -\Omega_{\downarrow} = \Omega$. Our Hamiltonian for the Néel state,

$$H_{\text{N\'eel}}^{\text{HF}} = -t \sum_{\mathbf{r}\delta\sigma} (c_{\mathbf{r}A\sigma}^\dagger c_{\mathbf{r}+\delta,B\sigma} + c_{\mathbf{r}B\sigma}^\dagger c_{\mathbf{r}+\delta,A\sigma}) + U \sum_{\mathbf{r}\sigma} [(\bar{n} + \Omega_{\sigma})n_{\mathbf{r}A\sigma} + (\bar{n} - \Omega_{\sigma})n_{\mathbf{r}B\sigma}] + E_0, \quad (16.63)$$

now involves electron operators that carry the index of the sublattice. Here, the constant term, $E_0 = U(-\bar{n}^2 + \Omega^2)$, and the site index \mathbf{r} refers to a new unit cell that includes each neighboring A and B site. In this picture, a unit vector between two neighboring unit cells connects two neighboring A (or B) sites. In other words, δ can take only $\pm \mathbf{e}_x \pm \mathbf{e}_y$, which can be obtained by the $\pi/4$ rotation and subsequent elongation by $\sqrt{2}$ from the original unit vectors, \mathbf{e}_x and \mathbf{e}_y . As a result, the shape of the new or reduced Brillouin zone (rBZ) is

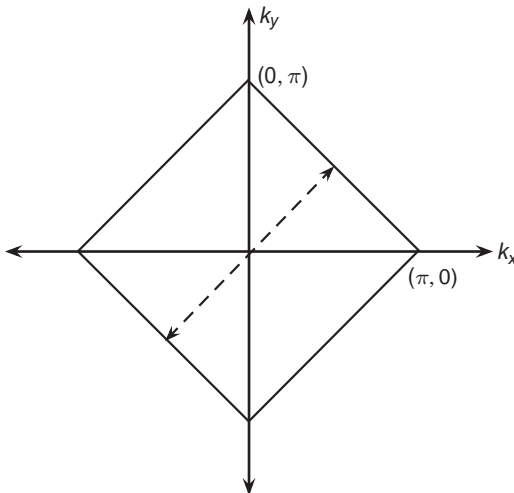


Fig. 16.6

Fermi surface of a half-filled band on a square lattice. The dashed line is the nesting vector, (π, π) .

the square diamond that fills exactly half of the original BZ, such that $\sum_{\mathbf{k} \in rBZ} = \frac{1}{2} \sum_{\mathbf{k} \in BZ}$ where rBZ stands for the reduced Brillouin zone, which arises as a result of ordering. We diagonalize this Hamiltonian by switching to momentum space,

$$\begin{aligned} H_{\text{Neel}}^{\text{HF}} &= E_0 + \sum_{\mathbf{k} \in rBZ, \sigma} \epsilon_{\mathbf{k}} (c_{\mathbf{k}A\sigma}^\dagger c_{\mathbf{k}B\sigma} + c_{\mathbf{k}B\sigma}^\dagger c_{\mathbf{k}A\sigma}) \\ &\quad + U \sum_{\mathbf{k} \in rBZ, \sigma} [(\bar{n} + \Omega_\sigma) c_{\mathbf{k}A\sigma}^\dagger c_{\mathbf{k}A\sigma} + (\bar{n} - \Omega_\sigma) c_{\mathbf{k}B\sigma}^\dagger c_{\mathbf{k}B\sigma}] \\ &= E_0 + \sum_{\mathbf{k} \in rBZ, \sigma} (c_{\mathbf{k}A\sigma}^\dagger \quad c_{\mathbf{k}B\sigma}^\dagger) \begin{pmatrix} U(\bar{n} + \Omega_\sigma) & \epsilon_{\mathbf{k}} \\ \epsilon_{\mathbf{k}} & U(\bar{n} - \Omega_\sigma) \end{pmatrix} \begin{pmatrix} c_{\mathbf{k}A\sigma} \\ c_{\mathbf{k}B\sigma} \end{pmatrix}, \end{aligned} \quad (16.64)$$

where $\epsilon_{\mathbf{k}} = -2t(\cos k_x + \cos k_y)$. For this simple band structure, $\epsilon_{\mathbf{k}} = -\epsilon_{\mathbf{k}+\pi}$. Consequently, (π, π) is the nesting vector. Upon diagonalization, we find two doubly spin-degenerate bands with dispersion

$$\omega_{\mathbf{k}}^\pm(\bar{n}, \Omega) = U\bar{n} \pm \sqrt{U^2\Omega^2 + \epsilon_{\mathbf{k}}^2}. \quad (16.65)$$

That is, there is a gap in the system and it arises entirely from ordering. As we will see, this kind of insulator is identical to a band insulator and has nothing in common with an insulator of the Mott type. Note that $\epsilon_{\mathbf{k}} = 0$ along the edge of the reduced BZ, $|k_x| + |k_y| = \pi$. Hence, excitations are gapless along the zone edges only if $\Omega = 0$. Each parallel edge is connected by a single momentum (π, π) or $(\pi, -\pi)$, as is expected for perfect nesting on a square lattice and depicted in Fig. 16.6. Since the upper and the lower bands are symmetric with respect to the energy level $U\bar{n}$, the lower band should be completely filled at half-filling.

The consequent classical energy density is

$$E(\bar{n}, \Omega) = U(-\bar{n}^2 + \Omega^2) + \frac{2}{N} \sum_{\mathbf{k} \in \text{BZ}} \omega_{\mathbf{k}}^-(\bar{n}, \Omega), \quad (16.66)$$

where the first term is E_0 and the factor of 2 in front of the second term arises from the sum over spin. The self-consistent condition for this mean-field calculation is determined by minimizing the energy

$$\frac{\partial}{\partial \bar{n}} E = 0, \quad \frac{\partial}{\partial \Omega} E = 0, \quad (16.67)$$

with respect to the two variational parameters, \bar{n} and Ω . Because $\partial \omega_{\mathbf{k}}^- / \partial \bar{n} = U$ and $\partial E_0 / \partial \bar{n} = -2\bar{n}U$, $\bar{n} = 1/2$. From the second condition, we obtain

$$\Omega = \frac{1}{N} \sum_{\mathbf{k} \in \text{BZ}} \frac{1}{\sqrt{1 + (\epsilon_{\mathbf{k}}/U\Omega)^2}}. \quad (16.68)$$

In evaluating the sum in Eq. (16.68), we will find it expedient to use the rule

$$\frac{1}{N} \sum_{\mathbf{k} \in \text{BZ}} \rightarrow \frac{1}{V_{\text{BZ}}} \int_{\text{BZ}} d^d \mathbf{k} \quad (16.69)$$

for converting the sum to an integral with V_{BZ} the volume of the Brillouin zone. Realizing that our sum is only over the reduced Brillouin zone, we convert Ω to

$$\Omega = \frac{1}{(2\pi)^2} \int_{|k_x|+|k_y| \leq \pi} \frac{dk_x dk_y}{\sqrt{1 + \left[\frac{2t}{U\Omega} (\cos k_x + \cos k_y) \right]^2}}. \quad (16.70)$$

With the change of variables, $h_x = (k_x + k_y)/2$ and $h_y = (k_y - k_x)/2$, which both rotates and scales the domain of integration, we arrive at

$$\begin{aligned} \Omega &= \frac{1}{4\pi^2} \int_{-\pi/2}^{\pi/2} dh_x \int_{-\pi/2}^{\pi/2} dh_y \frac{|\partial(k_x, k_y)/\partial(h_x, h_y)|}{\sqrt{1 + \left(\frac{2t}{U\Omega} (\cos(h_x + h_y) + \cos(h_y - h_x)) \right)^2}} \\ &= \frac{2}{\pi^2} \int_0^{\pi/2} dh_x \int_0^{\pi/2} dh_y \frac{1}{\sqrt{1 + \left(\frac{4t}{U\Omega} \cos h_x \cos h_y \right)^2}}. \end{aligned} \quad (16.71)$$

In the limit $t/U \ll 1$, we approximate the integrand,

$$\frac{1}{\sqrt{1 + (\epsilon_{\mathbf{k}}/(U\Omega))^2}} = 1 - \frac{1}{2} \left(\frac{4t}{U\Omega} \right)^2 \cos^2 h_x \cos^2 h_y + O(t/U)^4, \quad (16.72)$$

by expanding in powers of $t/(U\Omega)$. An internal assumption in this expansion is that $t/U\Omega \ll 1$ rather than just simply $t/U \ll 1$. Integrating the expansion up to first order, one finds

$$\Omega = \frac{1}{2} \left(1 - 2 \left(\frac{t}{U} \right)^2 \frac{1}{\Omega^2} + O(t/U)^4 \right), \quad (16.73)$$

thereby implying that quantum fluctuations decrease the tendency to order.

To find the leading correction, we set $\Omega = \frac{1}{2} - \epsilon$, which yields

$$\epsilon = \frac{4(t/U)^2}{1 - 16(t/U)^2} \simeq 4 \left(\frac{t}{U} \right)^2. \quad (16.74)$$

It is noteworthy that this result satisfies the previous internal assumption $t/U \ll \Omega$. For the energy density, the small t/U expansion yields

$$\begin{aligned} E(\bar{n} = \frac{1}{2}, \Omega) &= U \left(\Omega^2 - \frac{1}{4} \right) + \frac{2U\Omega}{\pi^2} \int_0^{\pi/2} dh_x dh_y \left(\frac{1}{2\Omega} - \sqrt{1 + \left(\frac{4t}{U\Omega} \cos h_x \cos h_y \right)^2} \right) \\ &= U \left(\Omega^2 - \frac{1}{4} \right) \\ &\quad + \frac{2U\Omega}{\pi^2} \int dh_x dh_y \left[\frac{1}{2\Omega} - 1 - \frac{1}{2} \left(\frac{4t}{U\Omega} \right)^2 \cos^2 h_x \cos^2 h_y + O(t/U\Omega)^4 \right] \\ &= U \left[\left(\Omega^2 - \frac{1}{4} \right) + \Omega \left(\frac{1}{4\Omega} - \frac{1}{2} - \frac{t^2}{U^2\Omega^2} \right) \right]. \end{aligned} \quad (16.75)$$

Inserting the result for the order parameter, $\Omega = \frac{1}{2} - 4 \left(\frac{t}{U} \right)^2$, we find that the ground-state energy is $E = -4 \frac{t^2}{U}$. A perturbative t/U expansion of the Hubbard model also yields the same result for the spin sector for the half-filled Hubbard band. However, since there are strictly no interactions in the Hartree–Fock approximation, the correspondence of either the large t/U or small t/U limits with strong and weak coupling is entirely heuristic.

Consider now the opposite regime, $t/U \gg 1$. In this limit, we approximate the integral by linearizing $\cos h_x$ around the upper limit of the integral and replacing $\cos h_y$ with $\langle \cos h_y \rangle = 1/2$. Consequently, we obtain

$$\Omega = \frac{1}{\pi} \int_0^{\pi/2} \frac{dh_x}{\sqrt{1 + \frac{8}{U^2\Omega^2} h_x^2}} = \frac{1}{\alpha\pi} \sinh^{-1} \frac{\alpha\pi}{2}, \quad (16.76)$$

where $\alpha = \frac{4\sqrt{2}t}{U\Omega}$. Solving for Ω , we arrive at the exponentially suppressed solution

$$\Omega = \frac{2\sqrt{2}\pi \frac{t}{U}}{\sinh(4\sqrt{2}\pi \frac{t}{U})} \sim 4\sqrt{2}\pi \frac{t}{U} e^{-4\sqrt{2}\pi \frac{t}{U}} \ll 1. \quad (16.77)$$

Hence, we find that, regardless of the magnitude of t/U , antiferromagnetic order opens a gap in the single-particle spectrum. However, in either case, a non-interacting Hamiltonian emerges. Consequently, although the corresponding single-particle Green function depends on the electron filling, the weight of each band does not. It remains a constant, as it does in the band insulator problem. The message is clear from this analysis. If the experimental systems show spectral weight transfer on the scale of the gap, then Hartree–Fock antiferromagnetism

is insufficient to explain the physics. The explanatory residue that remains is what we call Mottness.

16.4.2 Heisenberg: t/U perturbation theory

Ultimately the goal of mean-field theory is to model an interacting system by replacing it with a simpler one described by a quadratic Hamiltonian. This can only be done by decoupling in some way the four-fermion interaction. The natural question that arises is when is it legitimate to decouple a four-fermion term and replace it with some type of ordering tendency? Since the ordering is only possible when the interaction is present, mean-field theory is not directly linked to weak coupling. It is simply a statement that the interactions, regardless of their magnitude, lead to ordering. However, in the Hubbard model, there are two distinct mechanisms that give rise to antiferromagnetic ordering. Aside from the mean-field mechanism based on Fermi surface nesting, a strong-coupling analog also exists in which local physics leads to a staggered ordering of the electron spins. These mechanisms are distinct. To establish the latter, it is sufficient to derive an effective Hamiltonian in the strong-coupling regime $t/U \ll 1$ by expanding around the atomic limit. In this limit, an effective Hamiltonian can be developed perturbatively that can be shown to favor antiferromagnetism. There are several ways to implement such a calculation. The primary goal of a strong-coupling expansion is to bring the Hubbard model into block diagonal form with respect to the large-energy scale in the atomic limit, U . Consequently, the low-energy model will correspond to the Hamiltonian that operates in the no-double-occupancy sector. However, such a transformation to eliminate double occupancy mixes the original atomic states regardless of their occupancy.

Hubbard dimer

A t/U expansion in the Hubbard model is an exercise in degenerate perturbation theory. Any eigenstate in the Hubbard model can be written as a sum of terms,

$$|\psi\rangle = a_0|\psi_0\rangle + a_1|\psi_1\rangle + \dots = \sum_m a_m|\psi_m\rangle \quad (16.78)$$

each with a fixed number of doubly occupied sites, $|\psi_m\rangle$. The $|\psi_m\rangle$ s are the eigenstates in the atomic limit ($t = 0$). In this limit, there are many arrangements of the local site occupations that keep m invariant, hence the large degeneracy. What is clear from Eq. (16.78) is that no eigenstate of the Hubbard model has a fixed number of doubly occupied sites. Consider the two-site system with two electrons, one with spin up and the other with spin down. Naively, the ground state of this system is expected to be a singlet:

$$|\psi_S\rangle = \frac{1}{\sqrt{2}} (|\uparrow, \downarrow\rangle - |\downarrow, \uparrow\rangle). \quad (16.79)$$

However, $|\psi_S\rangle$ is not an eigenstate of the Hubbard model. The true normalized ground state,

$$|\psi_{\text{2-site}}\rangle = \frac{\alpha}{\sqrt{2(\alpha^2 + 1)}} (|\uparrow, \downarrow\rangle - |\downarrow, \uparrow\rangle + \alpha^{-1}|0, 2\rangle - \alpha^{-1}|2, 0\rangle), \quad (16.80)$$

contains an admixture with the doubly-occupied sector ($|0, 2\rangle \equiv |0, \uparrow\downarrow\rangle$) with a mixing coefficient of $\alpha = 4t/(-U + \sqrt{16t^2 + U^2}) \approx 2U/t$, and hence α^{-1} vanishes at $U = \infty$. As a result, for any finite U , the admixture with the doubly occupied sector is present even in the ground state. This feature is apparent regardless of the filling and the size of the system.

Similarity transformation

The Hubbard dimer example illustrates that the true low-energy ground state contains non-zero mixing with all the atomic states regardless of their energy. In this sense, it is a misconception to envision that a low-energy theory is obtained by removing double occupancy of the bare electron states. There is a sense, however, in which this is precisely what perturbation theory does. When the Hubbard Hamiltonian is brought into block diagonal form, the operators which make this possible correspond to admixtures of multi-particle electron states. It is with respect to these operators that the blocks in the Hubbard model preserve the number of doubly occupied sites. Let us define (E1994; C2004) $f_{i\sigma}$ to represent the transformed fermions in which the Hubbard model is block diagonal. That is, $f_{i\sigma}$ preserves the number of doubly occupied sites. For any operator O , we define \tilde{O} such that

$$O \equiv \mathbf{O}(c), \quad \tilde{O} \equiv \mathbf{O}(f), \quad (16.81)$$

simply by replacing the Fermi operators $c_{i\sigma}$ with the transformed fermions $f_{i\sigma}$. For example,

$$\tilde{V} = U \sum_i \tilde{n}_{i\uparrow} \tilde{n}_{i\downarrow} = U \sum_i f_{i\uparrow}^\dagger f_{i\uparrow} f_{i\downarrow}^\dagger f_{i\downarrow}. \quad (16.82)$$

As we will see explicitly, O and \tilde{O} are only equivalent at $U = \infty$.

The procedure which makes the Hubbard model block diagonal is now well known (E1994; C2004). One constructs a similarity transformation S which connects sectors that differ by at most one “fictive” doubly occupied site such that the original Hubbard model,

$$H = e^S \tilde{H} e^{-S}, \quad (16.83)$$

obeys the commutation relation

$$[H, \tilde{V}] = 0, \quad (16.84)$$

implying that double occupation of the transformed fermions is a good quantum number, and all of the eigenstates can be indexed as such. In the ground state, $\tilde{V} = 0$ and

$$f_{i\uparrow} f_{i\downarrow} |GS\rangle = 0. \quad (16.85)$$

This will help us organize the perturbation theory. Note that the transformed Hamiltonian does not satisfy $[\tilde{H}, V] = 0$. To organize the perturbation theory, we introduce the operators \tilde{T}_m for each of the contributions to the kinetic term in Eq. (16.17). \tilde{T}_m increases the number of doubly occupied sites by m . From Eq. (16.17), we have that

$$\begin{aligned}\tilde{T}_0 &= -t \sum_{\langle ij \rangle} \left(\tilde{\eta}_{i\sigma}^\dagger \tilde{\eta}_{j\sigma} + \tilde{\xi}_{i\sigma}^\dagger \tilde{\xi}_{j\sigma} \right), \\ \tilde{T}_1 &= -t \sum_{\langle ij \rangle} \tilde{\eta}_{i\sigma}^\dagger \tilde{\xi}_{j\sigma},\end{aligned} \quad (16.86)$$

with $\tilde{T}_{-1} = \tilde{T}_1^\dagger$. Because each \tilde{T}_m increments the number of doubly occupied sites by m sites, a simple commutation relation,

$$[\tilde{V}, \tilde{T}_m] = mU\tilde{T}_m, \quad (16.87)$$

governs the various contributions of the kinetic energy and the potential terms. The Hamiltonian \tilde{H} contains the transformed kinetic energy term, $\tilde{T}_0 + \tilde{T}_{-1} + \tilde{T}_1$. The latter two terms must be eliminated as they do not conserve the number of doubly occupied sites. We can find an S that satisfies Eq. (16.84) order by order in perturbation theory. By expanding Eq. (16.83), we find that the lowest-order term satisfies

$$H = \tilde{V} + \tilde{T}_0 + \tilde{T}_{-1} + \tilde{T}_1 + [S^{(1)}, \tilde{V} + \tilde{T}_0 + \tilde{T}_{-1} + \tilde{T}_1]. \quad (16.88)$$

We define $S^{(1)}$ as the solution to

$$\tilde{T}_1 + \tilde{T}_{-1} + [S^{(1)}, \tilde{V}] = 0. \quad (16.89)$$

Using Eq. (16.87), we find that

$$S^{(1)} = \frac{1}{U} (\tilde{T}_1 - \tilde{T}_{-1}). \quad (16.90)$$

Consequently, our transformed Hamiltonian becomes

$$H = \tilde{V} + \tilde{T}_0 + [\tilde{T}_1, \tilde{T}_{-1}] \frac{1}{U} + [\tilde{T}_1 - \tilde{T}_{-1}, \tilde{T}_0] \frac{1}{U} + \dots \quad (16.91)$$

The last term involving the commutator with \tilde{T}_0 does not preserve the number of doubly occupied sites. It can be eliminated by the similarity transformation

$$S^{(2)} = [\tilde{T}_1 + \tilde{T}_{-1}, \tilde{T}_0] \frac{1}{U^2}, \quad (16.92)$$

to second order. For the purpose of our discussion, we will retain only the terms in the effective Hamiltonian to second order in t/U . Consequently, our Hamiltonian to $O(t^2/U)$,

$$H = \tilde{V} + \tilde{T}_0 + [\tilde{T}_1, \tilde{T}_{-1}] \frac{1}{U}, \quad (16.93)$$

contains only terms in which the sum of the indices on the \tilde{T}_m terms is zero. The commutator appearing in this Hamiltonian vanishes unless \tilde{T}_1 and \tilde{T}_{-1} contain a common index. Our Hamiltonian describes transport in any of the blocks of the Hamiltonian in which \tilde{V} has a definite value. Recall, part of \tilde{T}_0 moves charges around strictly in the UHB. If we wish to describe only the lowest-energy sector, we eliminate all terms which require that $\tilde{V} \neq 0$. This can be done by projecting our Hamiltonian onto the no-double-occupancy sector,

$$P_0 H P_0 = -t \sum_{\langle i,j \rangle} \tilde{\xi}_{i\sigma}^\dagger \tilde{\xi}_{j\sigma} - \frac{1}{U} \tilde{T}_{-1} \tilde{T}_1, \quad (16.94)$$

where it is implicit that the \tilde{T}_m operators share a common index. We simplify further by noting that there are two distinct types of interactions in the second term, namely two-site and three-site terms. Consider the two-site term which contains neighboring sites only. Direct substitution of Eq. (16.86) reveals that the only non-zero nearest-neighbor term in $\tilde{T}_{-1} \tilde{T}_1$ is of the form

$$(\tilde{T}_{-1} \tilde{T}_1)_{\text{2-site}} = t^2 \sum_{i,j,\sigma} \tilde{\xi}_{i\sigma}^\dagger \tilde{\eta}_{i+j\sigma} \tilde{\eta}_{i+j\sigma'}^\dagger \tilde{\xi}_{i\sigma'}. \quad (16.95)$$

This term either converts an up spin to a down spin on neighboring sites or it preserves the spin configuration. Hence, schematically it is of the form

$$\begin{aligned} \sum_{\sigma,\sigma'} \tilde{\xi}_{i\sigma}^\dagger \tilde{\eta}_{j\sigma} \tilde{\eta}_{j\sigma'}^\dagger \tilde{\xi}_{i\sigma'} &= \sum_{\sigma} |\sigma_i, \bar{\sigma}_j\rangle \langle \sigma_i, \bar{\sigma}_j| + |\sigma_i, \bar{\sigma}_j\rangle \langle \bar{\sigma}_i, \sigma_j| \\ &= \sum_{\sigma} (1 - \tilde{n}_{i\bar{\sigma}}) \tilde{n}_{i\sigma} \tilde{n}_{j\bar{\sigma}} (1 - \tilde{n}_{j\sigma}) - \tilde{c}_{i\sigma}^\dagger \tilde{c}_{i\bar{\sigma}} \tilde{c}_{j\bar{\sigma}}^\dagger \tilde{c}_{j\sigma}. \end{aligned} \quad (16.96)$$

On the other hand, the spin–spin interaction term $\mathbf{S}_i \cdot \mathbf{S}_j$ can be written as

$$\mathbf{S}_i \cdot \mathbf{S}_j = \sum_{\sigma} \frac{1}{2} \tilde{c}_{i\sigma}^\dagger \tilde{c}_{i\bar{\sigma}} \tilde{c}_{j\bar{\sigma}}^\dagger \tilde{c}_{j\sigma} + \frac{1}{4} (\tilde{n}_{i\sigma} \tilde{n}_{j\sigma} - \tilde{n}_{i\sigma} \tilde{n}_{j\bar{\sigma}}). \quad (16.97)$$

The first term represents $S_i^+ S_j^- + S_i^- S_j^+$, while the second denotes the $S_i^z S_j^z$. Substituting the latter into Eq (16.96), we obtain

$$-\frac{t^2}{U} \sum_{\sigma,\sigma',\langle ij \rangle} \tilde{\xi}_{i\sigma}^\dagger \tilde{\eta}_{j\sigma} \tilde{\eta}_{j\sigma'}^\dagger \tilde{\xi}_{i\sigma'} = \frac{2t^2}{U} \sum_{\langle ij \rangle} \mathbf{S}_i \cdot \mathbf{S}_j - H_2 \quad (16.98)$$

as our working expression for the interaction term involving nearest-neighbor sites in which

$$H_2 = \frac{t^2}{U} \sum_{\langle ij \rangle \sigma} \left[\frac{1}{2} (\tilde{n}_{i\sigma} \tilde{n}_{j\sigma} + \tilde{n}_{i\sigma} \tilde{n}_{j\bar{\sigma}}) + (1 - \tilde{n}_{i\bar{\sigma}}) \tilde{n}_{i\sigma} \tilde{n}_{j\bar{\sigma}} (1 - \tilde{n}_{j\sigma}) \right]. \quad (16.99)$$

The three-site hopping term arises from $\tilde{\xi}_{i+\delta\sigma}^\dagger \tilde{n}_{i\sigma} \tilde{n}_{j\sigma}^\dagger \tilde{\xi}_{i+\delta'\sigma'}$ and reduces to

$$H_3 \equiv -t^2/U \sum_{\sigma, \sigma', i, \delta, \delta'} \left[(1 - \tilde{n}_{i+\delta, \bar{\sigma}}) f_{i+\delta, \sigma}^\dagger \tilde{n}_{i\bar{\sigma}} (1 - \tilde{n}_{i\sigma}) f_{i+\delta', \sigma} (1 - \tilde{n}_{i+\delta', \bar{\sigma}}) - (1 - \tilde{n}_{i+\delta, \sigma}) f_{i+\delta, \bar{\sigma}}^\dagger f_{i, \sigma}^\dagger f_{i\bar{\sigma}} f_{i+\delta', \sigma} (1 - \tilde{n}_{i+\delta', \bar{\sigma}}) \right]. \quad (16.100)$$

Consequently, the Hamiltonian in the lowest energy sector is

$$H_{\text{LHB}} = P_0 H P_0 = H_{t-J} - H_2 + H_3 \quad (16.101)$$

where

$$H_{t-J} = -t \sum_{\langle ij \rangle} \tilde{\xi}_{i\sigma}^\dagger \tilde{\xi}_{j\sigma} + 2 \frac{t^2}{U} \sum_{\langle ij \rangle} \mathbf{S}_i \cdot \mathbf{S}_j \quad (16.102)$$

is the $t-J$ limit commonly used in the study of the hole-doped Hubbard model. The terms H_2 and H_3 make it clear that the $t-J$ model is not the true low-energy limit of the Hubbard model. In fact, at half-filling asserting that the $t-J$ model is the low-energy theory of the Hubbard model poses a problem. Because the spin operators can be written in terms of

$$\Psi = \begin{pmatrix} f_\uparrow & f_\downarrow \\ f_\downarrow^\dagger & -f_\uparrow^\dagger \end{pmatrix}, \quad (16.103)$$

as $\mathbf{S} = \frac{1}{2} \text{Tr } \Psi^\dagger \Psi \sigma^T$, the $t-J$ model has an added symmetry at half-filling. At half-filling (one electron per site), the kinetic energy term vanishes. As a result, the $t-J$ model reduces entirely to a spin–spin model, namely the Heisenberg model in which the ground-state energy is precisely the $-4t^2/U$ we computed from our Hartree–Fock ansatz. However, the Heisenberg model has a higher symmetry than does the Hubbard model (DFM1988; AZ1988). Specifically, if we let $\Psi \rightarrow h\Psi$, where h is an $SU(2)$ matrix of the form

$$h = \begin{pmatrix} a_1 & b_1 \\ -b_1^* & a_1^* \end{pmatrix} \quad (16.104)$$

with $|a_1|^2 + |b_1|^2 = 1$, each spin operator, S , remains unchanged because

$$\Psi^\dagger \Psi \rightarrow \Psi^\dagger h^\dagger h \Psi = \Psi^\dagger \Psi. \quad (16.105)$$

Hence, each spin can be rotated independently of the others. In the full Hubbard model, all spins must be rotated in an identical fashion for the Hamiltonian to remain invariant, that

is, a global $SU(2)$ symmetry: $\Psi \rightarrow \Psi g$, where g is an $SU(2)$ matrix. While H_3 is explicitly zero at half-filling in the transformed basis of no double occupancy with respect to the $f_{i\sigma}$ fermions, H_2 is not. The second term in H_2 breaks the local $SU(2)$ symmetry of the $t - J$ limit at half-filling, giving rise to just the global $SU(2)$ symmetry of the Hubbard model.

It is helpful at this point to re-express our reduced Hamiltonian in terms of the original electron operators. In so doing, we will see more clearly in terms of the electron operators why the the local $SU(2)$ symmetry of the $t - J$ model at half-filling is reduced to a global $SU(2)$ symmetry. To this end, we need to transform the electron operators. From the general transformation of an operator O ,

$$O = e^S \tilde{O} e^{-S} = \tilde{O} + [S, \tilde{O}] + \frac{1}{2!} [S, [S, \tilde{O}]] + \dots, \quad (16.106)$$

we obtain an expression valid through $O(t/U)$,

$$O = \tilde{O} + \frac{1}{U} [\tilde{T}_1 - \tilde{T}_{-1}, \tilde{O}] + \dots, \quad (16.107)$$

by substituting Eq. (16.90). Because S connects sectors that differ by one doubly occupied site, the operator O lives in the full Hilbert space of the Hubbard model. Nonetheless, we can obtain an expansion for any operator entirely in the lowest-energy sector because the \tilde{O} operators can be decomposed into parts creating or annihilating a particular number of doubly occupied sites. That is, we decompose the transformed operators as

$$\tilde{O} = \sum_{n \in \mathbb{Z}} \tilde{O}_{nU}. \quad (16.108)$$

As a simple example, consider the transformed electron annihilation operator

$$f_{i\sigma} = f_{i\sigma;0} + f_{i\sigma;-U}, \quad (16.109)$$

where $f_{i\sigma;0} = \tilde{\xi}_{i\sigma}$ and $f_{i\sigma;-U} = \tilde{\eta}_{i\sigma}$. Note, a similar rewriting does not work for the bare fermion operators; that is, $c_{i\sigma;0} \neq \tilde{\xi}_{i\sigma}$, because these operators respect the full Hilbert space of the Hubbard model. Nonetheless, we can formulate an expansion for $c_{i\sigma;0}$ using Eq. (16.107) by utilizing the decomposition property of the $f_{i\sigma}$ operators. We simply have to make sure that the indices in all of the commutators sum to zero, as illustrated in Problem 16.4. Consequently, we obtain that

$$c_{i\sigma;0} = \tilde{\xi}_{i\sigma} + \frac{1}{U} [\tilde{T}_1, \tilde{\eta}_{i\sigma}] + \dots = \tilde{\xi}_{i\sigma} - \frac{1}{U} \eta_{i\sigma} \tilde{T}_1 + \dots. \quad (16.110)$$

The simplification in the last line follows because for hole-doping there is no double occupancy of the transformed fermions. This type of expression will be used in a later section to derive the spectral weight of the lower Hubbard band. But it is clear from this expression that the spectral weight has t/U components and hence is not given exactly by $1+x$. This will be highlighted when we discuss dynamical spectral weight transfer.

Our goal at present, however, is to re-express our t/U expansion for the Hamiltonian in terms of the bare electron operators that live in the full Hilbert space of the Hubbard model. This can be done by simply applying the canonical transformation to the electron operators directly and retaining all the terms rather than the terms that preserve the energy of a particular block in the Hubbard model as in Eq. (16.110). Using Eq. (16.107), we find that

$$\xi_{i\sigma} = \tilde{\xi}_{i\sigma} + \frac{1}{U} [\tilde{T}_1 - \tilde{T}_{-1}, \tilde{\xi}_{i\sigma}] + O(t/U)^2. \quad (16.111)$$

Each of the commutators can be simplified using

$$[AB, C] = A\{B, C\} - \{A, C\}B \quad (16.112)$$

and the anticommutation relations in Eq. (16.90). As expected, the result,

$$\xi_{i\sigma} = \tilde{\xi}_{i\sigma} - \frac{t}{U} \sum_j g_{ij} [(1 - \tilde{n}_{i\bar{\sigma}}) \tilde{n}_{j\bar{\sigma}} f_{j\sigma} + f_{i\bar{\sigma}}^\dagger f_{i\sigma} \tilde{n}_{j\sigma} f_{j\bar{\sigma}} - (1 - \tilde{n}_{j\sigma}) f_{j\bar{\sigma}}^\dagger f_{j\sigma} f_{i\bar{\sigma}}] + O(t/U)^2, \quad (16.113)$$

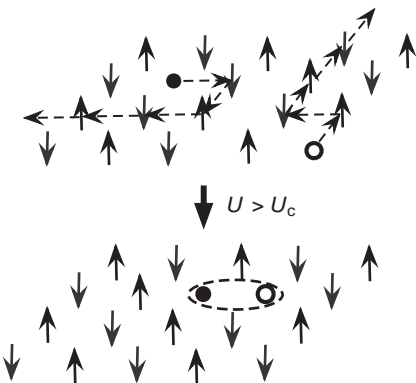
is a linear combination of multiparticle states in the rotated space. The key difference between $\xi_{i\sigma}$ and Eq. (16.110) is that the former picks out all singly occupied sites whereas the latter counts only the singly occupied sites in the lowest band. The expression for $\xi_{i\sigma}$ can be inverted so that $\tilde{\xi}_{i\sigma}$,

$$\tilde{\xi}_{i\sigma} = \xi_{i\sigma} + \frac{t}{U} \sum_j g_{ij} [(1 - n_{i\bar{\sigma}}) n_{j\bar{\sigma}} c_{j\sigma} + c_{i\bar{\sigma}}^\dagger c_{i\sigma} n_{j\sigma} c_{j\bar{\sigma}} - (1 - n_{j\sigma}) c_{j\bar{\sigma}}^\dagger c_{i\sigma} c_{i\bar{\sigma}}] + O(t/U)^2, \quad (16.114)$$

is expressed in terms of the bare electron operators. All of the terms proportional to t/U involve double occupancy explicitly. Hence, only when $U = \infty$ does $\tilde{\xi}_{i\sigma} = \xi_{i\sigma}$. It is the t/U corrections that restore the symmetry to just the global $SU(2)$ symmetry of the Hubbard model. To see this, we simply substitute Eq. (16.114) into H_2 and H_3 . Note, because there are t/U corrections to $\tilde{\xi}_{i\sigma}$, new interactions will arise from the kinetic term that are proportional to t^2/U . Such terms will have nothing to do with spin physics but will involve double occupancy explicitly, as can be seen as follows:

$$\begin{aligned} H_{\text{LHB}} &= e^{-S} P_0 e^S H e^{-S} P_0 e^S \\ &= -t \sum_{\langle i,j \rangle} \tilde{\xi}_{i\sigma}^\dagger \tilde{\xi}_{j\sigma} - \frac{t^2}{U} \sum_i b_i^{(\xi)}{}^\dagger b_i^{(\xi)} \\ &\quad - \frac{t^2}{U} \sum_{\langle i,j \rangle, \langle i,k \rangle, \sigma} \{ \tilde{\xi}_{k\sigma}^\dagger [(1 - n_{i\bar{\sigma}}) \eta_{j\sigma} + \tilde{\xi}_{j\bar{\sigma}}^\dagger \tilde{\xi}_{i\bar{\sigma}} \eta_{i\sigma} + \tilde{\xi}_{i\bar{\sigma}}^\dagger \tilde{\xi}_{i\sigma} \eta_{j\bar{\sigma}}] + \text{h.c.} \}. \end{aligned} \quad (16.115)$$

The first term in the last line of Eq. (16.115) represents the three-site hopping process. The remainder in the last line arise from H_2 and are present even at half-filling. All such terms

**Fig. 16.7**

The mechanism for the insulating state in the parent material, a half-filled band, as proposed by Mott. Up (down) arrows indicate spin up (down) electrons. Below a critical value of the on-site interaction U , doubly occupied (solid circles) sites and holes (empty circles) are free to transport. Above a critical value of U , they are bound in localized pairs, thereby preventing conduction.

are typically dropped. However, as we see, if one transforms the operators, they appear naturally and contribute to the same order of t^2/U as does the spin-exchange term. Hence, there is no systematic rationale for their exclusion.

16.5 Dynamical spectral weight transfer

What the perturbative analysis lays plain is that Mott insulating states are not as easy to understand as the atomic limit picture would have us believe. The problem is that double occupancy appears explicitly in the ground state. As a consequence, the Mott gap cannot be thought of simply as the gap to the first state that contains double occupancy. Nonetheless, the criterion for the charge gap can still be formulated sharply. Double occupancy leaves behind an empty site, as depicted in Fig. 16.7. The empty site may be free to move around without any further excursion to the upper band. If it does, then the half-filled band is actually a conductor. Mott (M1949) noted this in his classic paper and argued that there must be some kind of binding (see Fig. 16.7) between the empty and doubly occupied site for the half-filled band to insulate. In fact, several researchers since then, for example, Kohn (K1964), Fulde (KHF1982), and Castellani and colleagues (C1979), have noted that the Mott insulator can be thought of as a state in which double occupancy is localized but delocalized in the conducting state. Hence, the Mott transition to a localized state involves degrees of freedom that are not explicitly in the starting high-energy ultraviolet (UV) complete model. That is, the Mott gap is dynamically generated and any single-electron description of a Mott system is moot. While ordering can be understood directly from a weak or strong coupling (t/U) analysis of the Hubbard model, bound-state formation cannot as it arises fundamentally from a reorganization of the elemental fields.

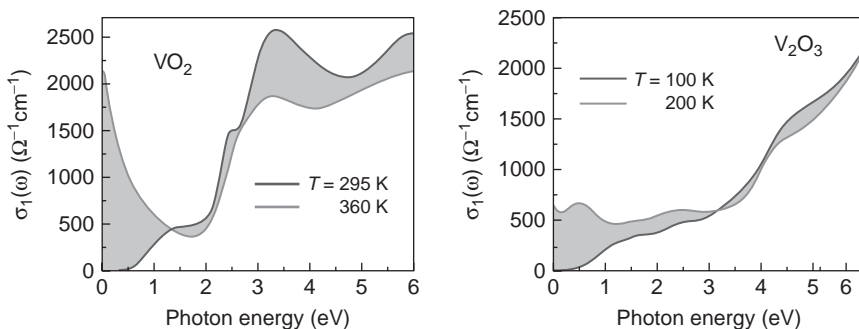


Fig. 16.8 Real part of the optical conductivity above and below the temperature for the onset of the Mott insulating state for VO_2 and V_2O_3 . In both VO_2 and V_2O_3 , the transition to the insulating state is accompanied by a transfer of spectral weight from the vicinity of the chemical potential to states as far as 6 eV away. This massive reshuffling of the spectral weight upon the transition to the Mott state is a ubiquity of the Mott transition. Data reprinted from Qazilbash *et al.*, *Phys. Rev. B* **77**, 115121 (2008).

It signals a breakdown of perturbation theory, as we have seen in the Kondo problem in which the degrees of freedom at low temperatures were bound states not in the starting Hamiltonian.

As we have seen in the previous section, Mott insulators are characterized by a vanishing of the single-particle electron Green function along a connected surface in momentum space. A prerequisite for the real part of the Green function to vanish is that the spectral function must be non-zero both above and below the chemical potential. In the metal, spectral weight lies near the chemical potential. The question arises: where does this spectral weight which was at the chemical potential go once the gap opens? Is it pushed to states just above the gap as it is in mean-field theory or does it reappear at energies that vastly exceed the gap? The answer to this question gets at the heart of the Mott problem. Consider the classic Mott system VO_2 , which undergoes a transition to an insulating state below 340 K. In this system, each vanadium ion has a valence of +4 giving rise to a half-filled d^1 configuration. What is peculiar about VO_2 is that it does not order magnetically down to the lowest temperatures. However, there is an accompanying structural rearrangement which has clouded the role of the strong correlations. Across the transition as the temperature is lowered, the structure changes from being the highly symmetric tetragonal rutile one to a monoclinic one in which the vanadium atoms dimerize and tilt relative to the c -axis. In addition, the charge carrier density (G1971) decreases from 10^{23} cm^{-3} at high temperatures to 10^{18} cm^{-3} at low temperatures. As a result, the same question has arisen in VO_2 as in most half-filled bands: does the insulating state arise from broken symmetry or entirely from the strong correlations in the manner denoted in Fig. 16.7, for example? This question persisted even though Mott (ZM1975; RLP1994) pointed out that a gap of 0.6 eV, the charge gap in VO_2 , is beyond any energy scale entailed by dimerization of the vanadium ions. The optical response of this system probed by ellipsometry is particularly useful here in settling this question. The key feature shown in Fig. 16.8 is that lowering the temperature to 295 K (Q2008), an energy scale considerably less than 0.6 eV, leads to transfer of spectral weight from states in the vicinity of the chemical potential (lighter line) to those at considerably

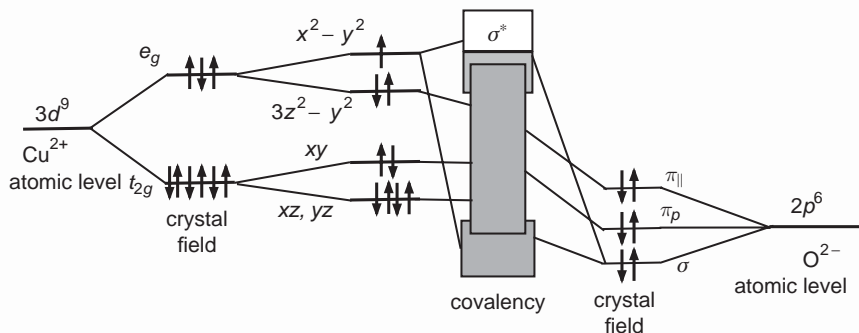
higher energies (darker line), roughly 6 eV away and beyond. Such energy scales over which the spectral weight is redistributed vastly exceed those relevant to dimerization. They are, however, consistent with correlation physics on the U scale. This is Mottness and it persists, as we will see, even upon a transition to the superconducting state. In fact, this state of affairs obtains even in half-filled bands, for example, V_2O_3 , which are known (Q2008) to order antiferromagnetically in the insulating state. The second panel in Fig. 16.8 shows the analogous optical conductivity across the metal-to-insulator transition in V_2O_3 . As in the case of VO_2 , the transition to the insulating state also involves transfer of spectral weight from the chemical potential to states at least 6 eV away. This mixing of high and low energy scales is a ubiquity in Mott systems. Hence, central to the charge gap are propagating degrees of freedom that entail the U scale, not simply the smaller energy scale associated with whatever ordering phenomenon might obtain. Also peculiar in VO_2 is the fact that the temperature at which the gap opens is much smaller than the gap. In fact, $\Delta/T_{\text{MI}} \approx 20$ for VO_2 , which exceeds the corresponding ratio in BCS theory by a factor of at least 10.

16.5.1 Doped Mott insulator: copper-oxide plane

The high-temperature copper-oxide superconductors represent another class of Mott systems which display the same type of UV–IR mixing typified by VO_2 . The electronic structure of the cuprates, layered perovskites in which the active layer is the copper-oxide plane, is shown in Fig. 16.9(a). In the tetrahedral crystal field relevant for the cuprates, a single unpaired electron resides on the $d_{x^2-y^2}$ orbital. Consequently, it might be natural to consider only a one-band model of the Hubbard type. However, the undoped cuprates are actually charge-transfer insulators as in Fig. 16.9(b). In such systems, more than one atom resides in each unit cell, in this case an oxygen atom. The $d_{x^2-y^2}$ orbital hybridizes with the p_x and p_y oxygen orbitals, and hence a three-band model is natural. However, as long as the on-site U repulsion energy is the largest energy scale and the hybridization between the atoms in the unit cell is sizeable (ZR1988; MES1993), a reduction to a one-band Hubbard model is warranted. Such is the case with the cuprates. As a consequence, the secret to superconductivity in the cuprates resides in the solution of at least the $2d$ Hubbard model. Shown in Fig. 16.10 is the optical conductivity (C1990; L2005) for $\text{YBa}_2\text{Cu}_3\text{O}_y$ along the CuO_2 plane for oxygen doping levels of $y = 6.1$ and $y = 6.6$. To a good facsimile, $y = 6.1$ represents the parent material and a noticeable suppression of the optical absorption is present for frequencies less than 1.2 eV, the optical gap in the cuprates. This is consistent with a Mott gap in the parent insulating material. However, in the doped system, $y = 6.6$, the strong suppression of the optical conductivity below ≈ 1.2 eV vanishes and is accompanied by a decrease in the spectral intensity in the high-energy sector, roughly 3 eV away from the chemical potential. This behavior is analogous to the inversion of the spectral weights above 340 K in the VO_2 upon a transition to the metallic state. In fact, the energy scales in the doping-induced metallic state are identical to those in the temperature-induced transition in these two systems. Such rearrangements on energy scales on the $O(U)$ can only arise from the strong electron correlations.

The probe in the optical conductivity is the current and hence it should provide a direct indication of the total number of charge carriers. As we saw at the beginning of this chapter,

(a) Electronic structure



(b) Band filling

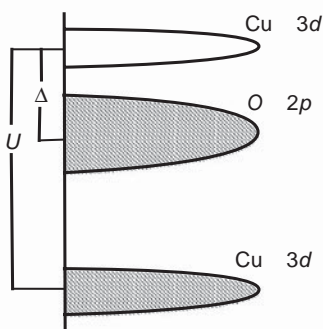


Fig. 16.9 Electronic structure of the copper-oxygen plane in the copper-oxygen superconductors. (a) Orbital occupancy and energy-level splitting for the atoms in the copper-oxygen plane. The upper d -level is singly occupied but the material is an insulator rendering the correlations as the central player in the electronic properties. (b) Heuristic depiction of the band filling of the parent material. U is the on-site repulsion energy when two electrons occupy the $d_{x^2-y^2}$ energy level. Δ is the gap between the oxygen p band and the empty d -levels. In the limit that $U \gg \Delta$ and the hybridization is sufficiently large, charge transfer insulators are reducible to a one-band Hubbard model and hence are equivalent to Mott insulators.

each hole introduced into a band insulator or a semiconductor results in a single quasi-particle above the chemical potential. What happens in a doped Mott insulator? We suspect that the number of quasi-particles must exceed the bare doping level because of the transfer of spectral weight from the high-energy part of the spectrum. Indeed, this is so. We can use the optical conductivity to compute the effective number of carriers, or more precisely the normalized carrier density, by integrating the optical conductivity,

$$N_{\text{eff}}(\Omega) = \frac{2mV_{\text{cell}}}{\pi e^2} \int_0^\Omega \sigma(\omega) d\omega, \quad (16.116)$$

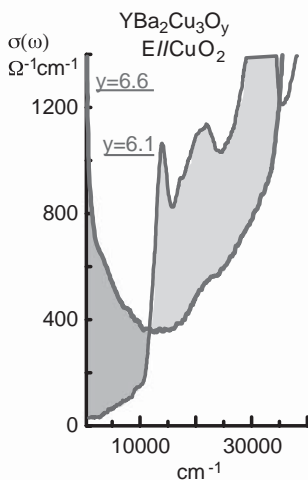


Fig. 16.10 Evolution of the in-plane optical conductivity in $\text{YBa}_2\text{Cu}_3\text{O}_y$ (YBCO) for two doping levels. To a good facsimile, $y = 6.1$ represents the parent material and $y = 6.6$ an overdoped sample. The key feature is the transfer of spectral weight above 1.2 eV in the “parent” material to states in the vicinity of the chemical potential upon doping. Reprinted from Cooper *et al.*, *Phys. Rev. B* **47**, 8233 (1993).

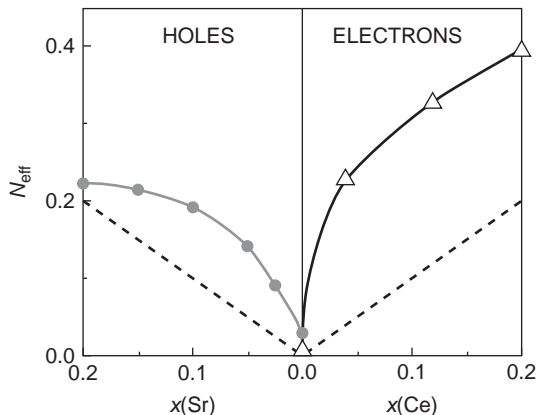


Fig. 16.11 Integrated optical conductivity for a hole-doped (YBCO) and an electron-doped ($\text{Nd}_{2-x}\text{Ce}_2\text{CuO}_4$ (NCCO)) cuprate reflecting the normalized carrier density. The dashed line indicates what is expected for a doping a semiconductor. Within the Hubbard model, the charge density in excess of the nominal doping level is generated by dynamical spectral weight transfer. Reprinted from Cooper *et al.*, *Phys. Rev. B* **41**, 11605 (1990).

up to the optical gap $\Omega \approx 1.2$ eV. This is a form of the f-sum rule in Eq. (9.143). Here $\sigma(\omega)$ is the optical conductivity, V_{cell} the unit-cell volume per formula unit, m the free electron mass, and e the electron charge. In the absence of doping where a metallic state does not ensue, $N_{\text{eff}} = 0$. As is evident from Fig. 16.11, the normalized carrier density exceeds the carrier density that would obtain in a doped semiconductor model (the dashed line). The deviation from $N_{\text{eff}} = x$ is significant at all doping levels. Hence, any model that only considers the nominal doping level is insufficient to describe the complete low-energy charge dynamics in the cuprates. This result is highly significant because it tells us

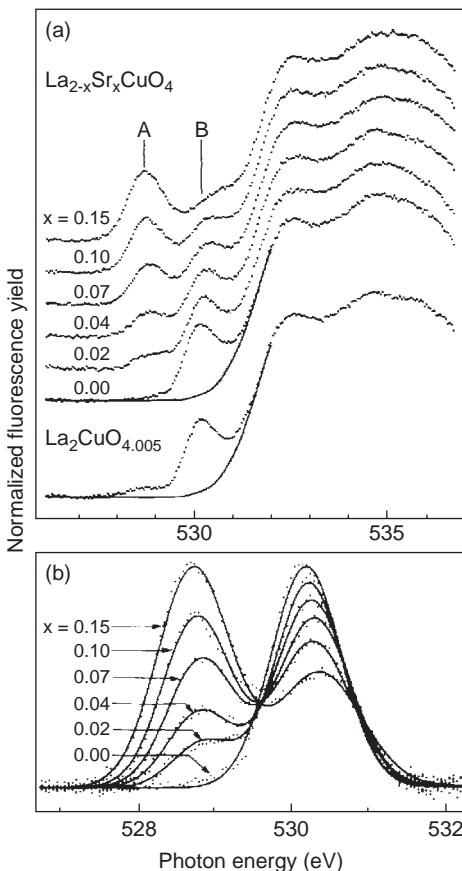


Fig. 16.12 Normalized fluorescence (C1991) yield at the oxygen K edge of $\text{La}_{2-x}\text{Sr}_x\text{CuO}_{4+\delta}$. (a) In the undoped sample, the only absorption occurs at 530 eV, indicated by B. Upon doping the intensity at B is transferred to the feature at A, located at 528 eV. (b) Gaussian fits to the absorption features at A and B with the background subtracted. Reprinted from Chen *et al.*, *Phys. Rev. Lett.* **66**, 104 (1991).

that the number of low-energy charge degrees of freedom exceeds the bare doping level. Hence, in the context of strong correlation, it is best to consider a renormalized doping level $x' \equiv x + \alpha$. A purpose of this chapter is to propose a prescription for determining α . In essence, something other than bare electrons are in the band in which the chemical potential resides. While this might seem a bizarre result, it is in fact true and part of the ubiquity of strong correlations and the mixing that ensues between the high- and low-energy parts of the spectrum. Subtract spectral weight transfer and the dashed (semiconductor) line obtains. However, removing spectral weight transfer also means subtracting the strong correlations. A final feature which deserves mention is the non-zero intercept of N_{eff} at $x = 0$. This suggests that, even at half-filling, a remnant of the excitations that fill in the spectral density below the Mott gap is present. This gives us a hint as to the origin of the charge count exceeding the dashed line in Fig. 16.11.

Although the optical conductivity can be used to extract the effective charge carrier number, it is ultimately a two-particle probe. Hence, if the charge carrier density really exceeds

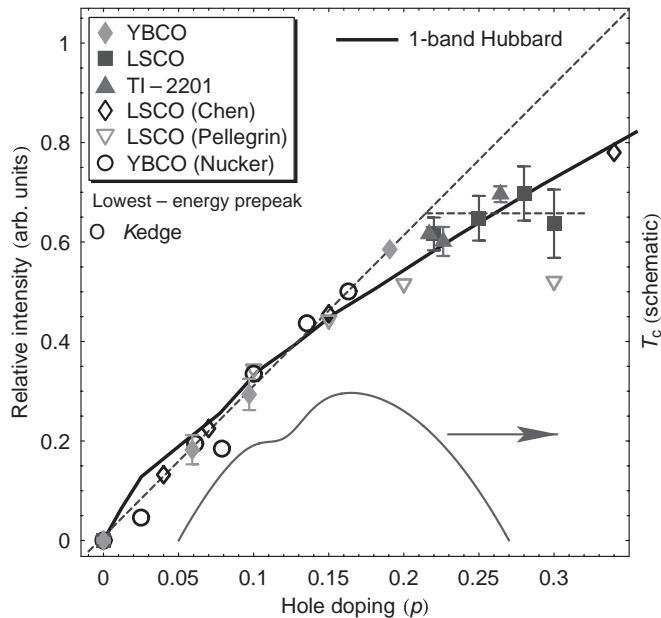
x in the cuprates, it would be more convincing to see this directly from a single-particle probe. Indeed, this can be done. To this end, we analyze the oxygen 1s x-ray absorption experiments (C1991) on $\text{La}_{2-x}\text{Sr}_x\text{CuO}_4$ (LSCO) shown in Fig. 16.12. In such experiments, an electron is promoted from the core 1s to an unoccupied level. The experimental observable is the fluorescence yield as a function of energy as electrons relax back to the valence states. The experiments, Fig. 16.12, show that at $x = 0$, all the available states lie at 530 eV. As a function of doping, the intensity in the high-energy peak decreases and is transferred to states at 528 eV. In fact, experimentally (C1991), the lower peak grows faster than $2x$ while the upper peak decreases faster than $1 - x$, x being the number of holes. In $\text{La}_{2-x}\text{Sr}_x\text{CuO}_4$, the doping level x can be unambiguously determined because each Sr atom produces one hole. The separation between these two peaks is the optical gap in the parent insulating material.

The redistribution of the spectral weight seen in the experiments can be explained within the Hubbard model. Since the experiments are probing the fluorescence yield into the available low-energy states, the relevant theoretical quantity is the number of single-particle addition states per site at low energy,

$$L = \int_{\mu}^{\Lambda} N(\omega) d\omega, \quad (16.117)$$

defined as the integral of the single-particle density of states ($N(\omega)$) from the chemical potential, μ , to a cut-off energy scale, Λ , demarcating the division between the IR and UV scales. In a Fermi liquid, Λ can be extended to infinity as there is no upper band, whereas in a semiconductor, Λ should extend only to the top of the valence band to count the states available upon the addition of holes. To calibrate this quantity, we compare it with the number of ways electrons can be added to the empty states created by the dopants. Let this quantity be n_h . Consider first the case of a Fermi liquid or non-interacting system. As illustrated in Fig. 16.2, the total weight of the valence band is 2; that is, there are two states per site. The integrated weight of the valence band up to the chemical potential determines the filling. Consequently, the unoccupied part of the spectrum, which determines L , is given by $L = 2 - n$. The number of ways electrons can be added to the empty sites is also $n_h = 2 - n$ (see Fig. 13.2). Consequently, the number of low-energy states per electron per spin is identically unity. The key fact on which this result hinges is that the total weight of the valence band is a constant independent of the electron density.

Consider now a Mott insulator. In the atomic limit, we have established already (see, for example, Eq. (16.32)) that the weight of the lower band is $1 + x$. Since there are exactly $1 - x$ filled states, $L = 2x$ is exact in the atomic limit. That is, each hole leaves behind an empty site that can be occupied by a spin-up or spin-down electron, as illustrated in Fig. 16.4. Hence, based on the atomic limit of the Hubbard model, we do expect a growth of the fluorescence yield proportional to x at 528 eV in LSCO with an equivalent decrease at 530 eV, the position of the upper Hubbard band. However, the fluorescence yield increases faster than $2x$, as is clear from Fig. 16.13. The Hubbard model at finite t/U reproduces

**Fig. 16.13**

Compilation of the doping dependence of the lowest-energy oxygen K-edge pre-peak for various cuprates. The solid straight line is the low-energy spectrum in the Hubbard model computed by A. Liebsch ([L2010](#)). A constant scale factor was used to collapse the points of Liebsch onto the experimental data since the units of experimental data are arbitrary. The superconducting dome is indicated for reference. Reprinted from Phillips and Jarrell, *Phys. Rev. Lett.* **105**, 199701 (2010).

this result. The quantity of interest, L , can be extracted from the total weight of the lower band,

$$m_{\text{LHB}} = \frac{1}{N} \sum_i \langle \{c_{i\sigma;0}, c_{i\sigma;0}^\dagger\} \rangle, \quad (16.118)$$

by simply subtracting the nominally occupied weight, $1 - x$. The use of nominal here refers to the doping level established from the static degrees of freedom, not those that enter as a result of dynamical (t/U) effects. Such mixing implies that the doping level itself is modified, as in Fig. 16.11. From the equation for the electron operator projected onto the lowest energy sector, Eq. (16.110), we simplify our expression for the moment to

$$m_{\text{LHB}}^0 = \frac{1}{N} \sum_i (\langle \{\tilde{\xi}_{i\sigma}, \tilde{\xi}_{i\sigma}^\dagger\} \rangle + \langle \frac{1}{U} (\{\tilde{\xi}_{i\sigma}^\dagger, [\tilde{T}_1, \tilde{\eta}_{i\sigma}]\} + \text{h.c.}) \rangle + \dots). \quad (16.119)$$

Using the identity

$$\tilde{\xi}_{i\sigma} \tilde{\eta}_{i\sigma} = \tilde{\xi}_{i\sigma} \tilde{\eta}_{i\sigma}^\dagger = 0 \quad (16.120)$$

and the ground state property $\tilde{\eta}_{i\sigma}|G\rangle = 0$, we have that

$$\langle \{\tilde{\xi}_{i\sigma}^\dagger, [\tilde{T}_1, \tilde{\eta}_{i\sigma}]\} \rangle = -\langle \tilde{\eta}_{i\sigma} \tilde{T}_1 \tilde{\xi}_{i\sigma}^\dagger \rangle. \quad (16.121)$$

Repeated use of the commutator,

$$[\tilde{n}_{i\bar{\sigma}}, f_{j\sigma'}^\dagger] = \delta_{ij} \delta_{\bar{\sigma}\sigma'} f_{j\sigma'}^\dagger, \quad (16.122)$$

allows us to reduce the moment,

$$\begin{aligned} -\langle \tilde{\eta}_{i\sigma} \tilde{T}_1 \tilde{\xi}_{i\sigma}^\dagger \rangle &= t \sum_{j,\delta,\sigma'} \langle f_{i\sigma}^\dagger \tilde{n}_{i\bar{\sigma}} \tilde{n}_{j\bar{\sigma}'} f_{j\sigma'}^\dagger f_{j+\delta\sigma'} (1 - \tilde{n}_{j+\delta\bar{\sigma}'}) (1 - \tilde{n}_{i\bar{\sigma}}) f_{i\sigma}^\dagger \rangle \\ &= t \sum_{j,\delta,\sigma'} \delta_{ij} \delta_{\bar{\sigma}\sigma'} \langle f_{i\sigma}^\dagger \tilde{n}_{j\bar{\sigma}'} f_{j\sigma'}^\dagger f_{j+\delta\sigma'} (1 - \tilde{n}_{j+\delta\bar{\sigma}'}) (1 - \tilde{n}_{i\bar{\sigma}}) f_{i\sigma}^\dagger \rangle \\ &\quad + t \sum_{j,\delta,\sigma'} \langle f_{i\sigma}^\dagger \tilde{n}_{j\bar{\sigma}'} f_{j\sigma'}^\dagger \tilde{n}_{i\bar{\sigma}} f_{j+\delta\sigma'} (1 - \tilde{n}_{j+\delta\bar{\sigma}'}) (1 - \tilde{n}_{i\bar{\sigma}}) f_{i\sigma}^\dagger \rangle \\ &= t \sum_{\delta} \langle f_{i\sigma} \tilde{n}_{i\sigma} f_{i\bar{\sigma}}^\dagger f_{i+\delta\bar{\sigma}} (1 - \tilde{n}_{i+\delta\sigma}) (1 - \tilde{n}_{i\bar{\sigma}}) f_{i\sigma}^\dagger \rangle \\ &\quad + t \sum_{j,\delta,\sigma'} \langle f_{i\sigma}^\dagger \tilde{n}_{j\bar{\sigma}'} f_{j\sigma'}^\dagger \tilde{n}_{i\bar{\sigma}} f_{j+\delta\sigma'} (1 - \tilde{n}_{j+\delta\bar{\sigma}'}) (1 - \tilde{n}_{i\bar{\sigma}}) f_{i\sigma}^\dagger \rangle, \end{aligned} \quad (16.123)$$

to a sum of two terms. Similar use of the commutator in Eq. (16.122) and the relations

$$(1 - \tilde{n}_{i\sigma})(1 - \tilde{n}_{i\bar{\sigma}}) f_{i\sigma}^\dagger = (1 - \tilde{n}_{i\bar{\sigma}})(1 - \tilde{n}_{i\sigma}) f_{i\sigma}^\dagger = 0 \quad (16.124)$$

and

$$\tilde{n}_{i\bar{\sigma}} (1 - \tilde{n}_{j+\delta\bar{\sigma}'}) (1 - \tilde{n}_{i\bar{\sigma}}) = (1 - \tilde{n}_{j+\delta\bar{\sigma}'}) \tilde{n}_{i\bar{\sigma}} (1 - \tilde{n}_{i\bar{\sigma}}) = 0 \quad (16.125)$$

allows us to show that the second term in Eq. (16.123),

$$\begin{aligned} &\sum_{j,\delta,\sigma'} \langle f_{i\sigma}^\dagger \tilde{n}_{j\bar{\sigma}'} f_{j\sigma'}^\dagger \tilde{n}_{i\bar{\sigma}} f_{j+\delta\sigma'} (1 - \tilde{n}_{j+\delta\bar{\sigma}'}) (1 - \tilde{n}_{i\bar{\sigma}}) f_{i\sigma}^\dagger \rangle \\ &= -t \sum_{j,\delta,\sigma'} \delta_{i,j+\delta} \delta_{\bar{\sigma}\sigma'} \langle f_{i\sigma}^\dagger \tilde{n}_{j\bar{\sigma}'} f_{j\sigma'}^\dagger f_{j+\delta\sigma'} (1 - \tilde{n}_{j+\delta\bar{\sigma}'}) (1 - \tilde{n}_{i\bar{\sigma}}) f_{i\sigma}^\dagger \rangle \\ &\quad + t \sum_{j,\delta,\sigma'} \langle f_{i\sigma}^\dagger \tilde{n}_{j\bar{\sigma}'} f_{j\sigma'}^\dagger f_{j+\delta\sigma'} \tilde{n}_{i\bar{\sigma}} (1 - \tilde{n}_{j+\delta\bar{\sigma}'}) (1 - \tilde{n}_{i\bar{\sigma}}) f_{i\sigma}^\dagger \rangle \\ &= -t \sum_{\delta} \langle f_{i\sigma}^\dagger \tilde{n}_{i-\delta\sigma} f_{i-\delta\bar{\sigma}}^\dagger f_{i\bar{\sigma}} (1 - \tilde{n}_{i\sigma}) (1 - \tilde{n}_{i\bar{\sigma}}) f_{i\sigma}^\dagger \rangle \\ &\quad + t \sum_{j,\delta,\sigma'} \langle f_{i\sigma}^\dagger \tilde{n}_{j\bar{\sigma}'} f_{j\sigma'}^\dagger f_{j+\delta\sigma'} \tilde{n}_{i\bar{\sigma}} (1 - \tilde{n}_{j+\delta\bar{\sigma}'}) (1 - \tilde{n}_{i\bar{\sigma}}) f_{i\sigma}^\dagger \rangle = 0 \end{aligned} \quad (16.126)$$

is identically zero. We are almost done. There are several factors in the remaining term that can be simplified upon using the identities

$$\begin{aligned} f_{i\sigma} \tilde{n}_{i\sigma} &= f_{i\sigma}, \\ f_{i\bar{\sigma}}^\dagger (1 - \tilde{n}_{i\bar{\sigma}}) &= f_{i\bar{\sigma}}^\dagger. \end{aligned} \quad (16.127)$$

Consequently,

$$\begin{aligned}
 -\langle \tilde{\eta}_{i\sigma} \tilde{T}_1 \tilde{\xi}_{i\sigma}^\dagger \rangle &= t \sum_{\delta} \langle f_{i\sigma} \tilde{n}_{i\sigma} f_{i\bar{\sigma}}^\dagger f_{i+\delta\bar{\sigma}} (1 - \tilde{n}_{i+\delta\sigma}) (1 - \tilde{n}_{i\bar{\sigma}}) f_{i\sigma}^\dagger \rangle \\
 &= t \sum_{\delta} \langle f_{i\sigma} \tilde{n}_{i\sigma} f_{i\bar{\sigma}}^\dagger f_{i\bar{\sigma}}^\dagger (1 - \tilde{n}_{i\bar{\sigma}}) f_{i+\delta\bar{\sigma}} (1 - \tilde{n}_{i+\delta\sigma}) \rangle \\
 &= t \sum_{\delta} \langle f_{i\sigma} f_{i\bar{\sigma}}^\dagger f_{i\bar{\sigma}}^\dagger f_{i+\delta\bar{\sigma}} (1 - \tilde{n}_{i+\delta\sigma}) \rangle \\
 &= t \sum_{\delta} \langle (1 - \tilde{n}_{i\sigma}) f_{i\bar{\sigma}}^\dagger f_{i+\delta\bar{\sigma}} (1 - \tilde{n}_{i+\delta\sigma}) \rangle. \tag{16.128}
 \end{aligned}$$

Because the average is with respect to a ground state which has no double occupancy of the $f_{i\sigma}$ fermions, the terms with density factors, $\tilde{n}_{i\sigma}$, all vanish and the total weight of the lower band,

$$m_{\text{LHB}} = 1 + x + \frac{2t}{U} \frac{1}{N} \sum_{i\delta\sigma} \langle f_{i\bar{\sigma}}^\dagger f_{i+\delta\bar{\sigma}} \rangle + \dots = 1 + x + \alpha(t/U, x) > 1 + x, \tag{16.129}$$

has explicit t/U corrections, the first term of which is proportional to the kinetic energy of the empty site created in the lower band as a result of the dynamical generation of double occupancy. We denote all t/U corrections by α , a measure of the dynamical transfer of the spectral weight. A version of this formula was first derived by Harris and Lange (HL1967) in 1967 and rederived with the correct operators in (E1994). It is important to note that the operators appearing in this expression are the transformed fermions not the bare ones. One can express the spectral weight of the lower band in terms of the bare fermions, but the expression is quite unwieldy (E1994). It is also important to note that regardless of the order in perturbation theory, α is entirely positive (HL1967; E1994; MES1993). The reason is simple. Dynamics in the lower band can only occur at the expense of creating doubly occupied sites. This necessarily decreases the intensity of the upper band (see Fig. 16.14) as there are now fewer ways to create double occupancy. To conserve spectral weight, the intensity of the lower band must increase by an equivalent amount. In essence, dynamical spectral weight transfer exists because the operators $\xi_{i\sigma}$ and $\eta_{i\sigma}$ do not propagate independently on any energy scale. If the occupied part of the spectrum in the lower band is assigned the weight of the conserved charge $1 - x$, then the empty part of the spectrum in the lower band carries a weight of $2x + \alpha > 2x$. There is no reason to insist in this assignment of the spectrum, however, because once the weight of a band exceeds the total number of electron states in the band, that is, $1 + x + \alpha > 1 + x$, what the electrons are doing is irrelevant. We know from Fig. 16.11 that the effective doping level exceeds x . The assignment (CHP2010) of the spectral weight in Fig. 16.14(b) reflects the dynamical generation of the charge carriers. With this assignment of the spectral weight, the empty part of the spectrum per spin in the LHB is precisely the effective doping level, x' . That is, this assignment of the spectrum reinstates the semi-rigid band picture of the atomic limit, as in Fig. 16.4. Shown in Fig. 16.13

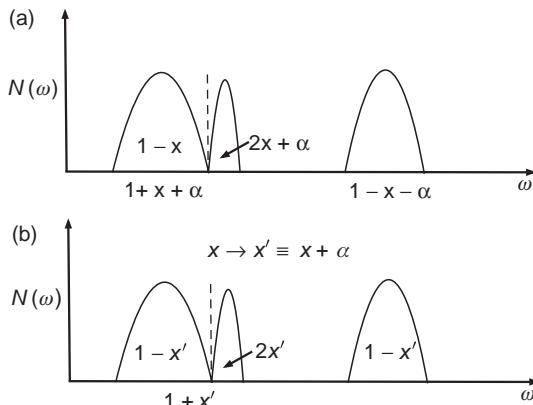
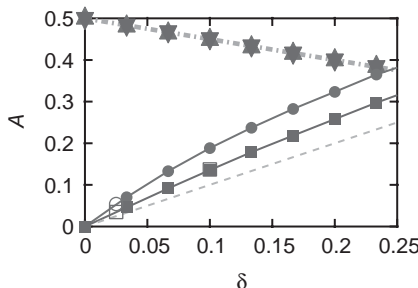


Fig. 16.14 Single-particle density of states in the Hubbard model as a function of hole doping, x . α denotes the dynamical or t/U corrections to the spectral weight delineated in Eq. (16.129). (a) Traditional separation of the spectral weight in the lower band in which the filled part of the lower band is simply the conserved charge. (b) Separation of the spectral weight that takes into consideration the renormalization of the doping level seen in Fig. 16.11.

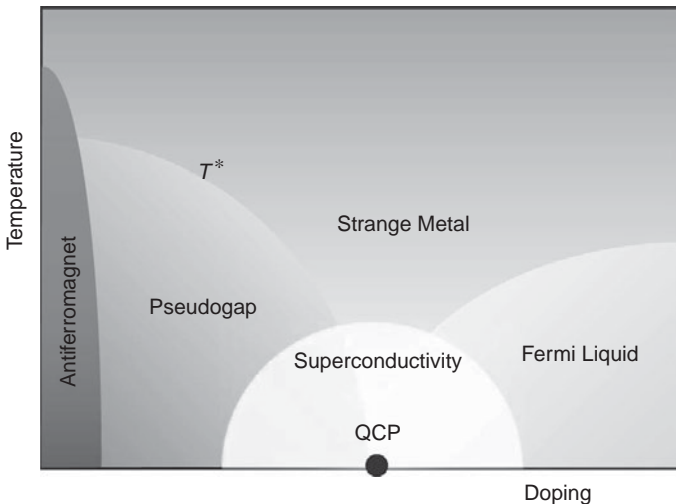
is a comparison of the experimental values for L with those obtained from state-of-the art calculations (solid line) on the Hubbard model. A word of caution on interpreting the experimental values is in order. Because arbitrary units are used to express the intensity, the y -axis does not really correspond to the actual spectral density of the empty part of the band. Note the dashed line has a slope of 3. Consequently, the straight dashed line should not be construed as a measure of $2x$ growth of the oxygen K-edge spectrum. To make a comparison between the results of the Hubbard model and the experiments, the Hubbard data were scaled appropriately. What is striking is the close quantitative agreement between the solid line and the experimental values in the range of doping studied. Around a hole doping level of $p \approx 0.18$, there is considerable deviation from the dashed line (which commenced at the origin). The Hubbard model also reproduces this deviation and it signals that beyond a critical doping value, the dynamical correction is strongly diminished. The reason for this is simple. The dynamical correction must vanish by $x = 1$. Hence, it cannot increase monotonically.

The Hubbard model in $d = 1$ serves as a benchmark for computing α . In this case, α can be determined essentially exactly using Bethe ansatz (LW1968) methods coupled with the dynamical matrix renormalization group (K2010) to evaluate the dynamical correlation functions that enter the spectral function. Figure 16.15 shows the results for the integrated weights of the spectral density below (squares) and above the chemical potential in the lower Hubbard band. The stars in Fig. 16.15 represent the occupied part of the spectrum, $1-x$. The remainder of the spectral weight per spin (circles, $U = 4t$, and squares, $U = 8t$) provides a measure of L (computed according to Fig. 16.14(a)). As is evident, both exceed the dashed line, as is expected from the perturbative expansion in Eq. (16.129) and in agreement with the 2d calculation shown in Fig. 16.13. In general, for any finite-dimensional lattice, dynamical spectral weight transfer is unavoidable.

**Fig. 16.15**

Integrated spectral weight per spin of the lower band in the $d = 1$ Hubbard model. The stars represent the occupied part of the lower band. The solid squares and circles correspond to the particle-addition part (immediately above the chemical potential) for $U = 8t$ and $U = 4t$ respectively. The dashed line has a slope of unity. Reprinted from Kohno, *Phys. Rev. Lett.* **105**, 106402 (2010).

Dynamical spectral weight transfer is important because it produces a fundamentally new qualitative effect. It is an example of “more” being totally different (A1972). In a Fermi liquid, the intensity of a band is equal to the number of electrons the band can hold. In the presence of dynamical spectral weight transfer, the intensities of both the lower band and the empty part of the band exceed the number of electrons those states can hold at low energy, in sharp contrast to a Fermi liquid. The number of electrons that can fit into the lower band is determined solely by the number of lattice sites and not on system parameters such as t and U . Hence, it remains fixed at $1 + x$. Likewise, the empty part of the spectrum in the lower band can be occupied by electrons in only $2x$ ways. However, there are at least $2x + \alpha$ states available for particle addition. As a result, any description of the physics in the lower band cannot be exhausted by counting electrons alone. In essence, if the total spectral weight of a band exceeds the electron count, in this case $1 + x + \alpha > 1 + x$, then what the electrons are doing is irrelevant. This underscores the key ingredient in strong coupling that the propagating degrees of freedom bear no resemblance to the basic building blocks in the original UV-complete theory. Consider, for example, L . L measures the total spectral density for adding a particle to the lower band. If this exceeds x per spin, then the total number of ways of adding a particle exceeds the number of ways of adding an *electron* to the lower band. As a consequence, $L/2 > x$ implies that some particle addition states in the lower band are gapped to the addition of an electron. That is, some of the states in the lower band are orthogonal to the addition of an electron. The states that give rise to this orthogonality are those that are admixed with the upper band. Hence, it is the sheer existence of the upper band that produces this gapped spectrum in the lower band. Since the upper band arises entirely from the strong correlations, the extra states that mix into the lower band have no counterpart in a weakly interacting system and Fermi liquid theory fails. Hence, dynamical spectral weight transfer offers a concrete mechanism for the breakdown of an effective Fermi liquid description in the lower band. While Anderson postulated previously (A1997) that the upper Hubbard band gives rise to an orthogonality for electron addition at low energies, no specific mention was made of dynamical spectral weight transfer as the specific mechanism for the orthogonality. In fact, his recent work

**Fig. 16.16**

Heuristic phase diagram as a function of holes doped into the copper-oxide plane. The pseudo-gap and strange metal are characterized by a depletion of the density of states and a T -linear resistivity, respectively. The pseudo-gap terminates at a zero-temperature critical point or quantum critical point (QCP). To the right is a Fermi liquid where weak-coupling accounts become valid.

(A2006) has focused on extracting such an orthogonality strictly from the $U = \infty$ limit where the dynamical correction vanishes.

Orthogonality to electron addition is the central problem in the normal state of the cuprates. Figure 16.16 represents a heuristic phase diagram of the cuprates in which the key players that emerge upon the doping of a Mott insulator are highlighted. The pseudo-gap and the strange metal are the two phases of interest in the normal state. In the pseudo-gap region, a gap exists but superconductivity is absent. In contrast to a Fermi liquid, the strange metal exhibits a T -linear resistivity. Indeed, as the phase diagram suggests, the strange metal and the pseudo-gap are intimately connected. Experimentally, the T^* line is identified from transport as the lowest temperature at which T -linear resistivity obtains (KLR2001; AKS2004). Since the superconducting state has $d_{x^2-y^2}$ symmetry (H1995), the zone diagonal represents the nodal direction. Plotted in Fig. 16.17 is a high-precision measurement of the strength of the pole

$$G(\omega, \mathbf{q}) = \frac{Z}{\omega - \epsilon_F} \quad (16.130)$$

in the electron Green propagator along the zone-diagonal in the cuprates. A word on interpreting Eq. (16.130) is in order. Even if the electron propagator possesses a self-energy as in Eq. (16.58), an expression such as Eq. (16.130) is still valid. Simply expand the self-energy,

$$\Sigma(\omega, \mathbf{k}) = \Sigma_0 + (\omega - \epsilon_F) \frac{\partial \Sigma^R(\omega, \mathbf{k})}{\partial \omega} \Big|_{\omega=\epsilon_F} + \dots, \quad (16.131)$$

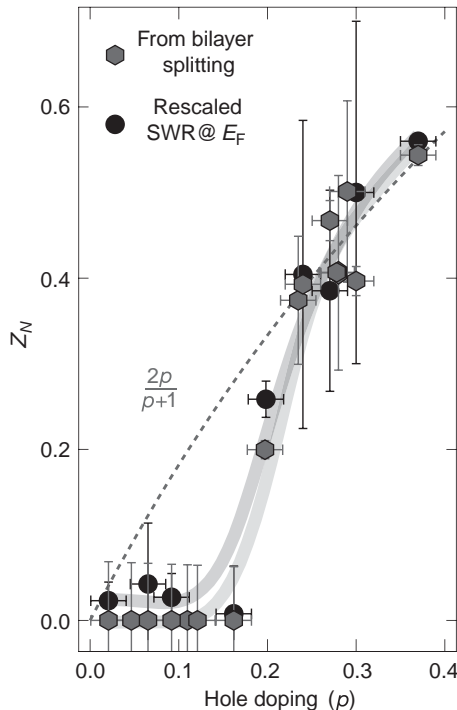


Fig. 16.17 Quasi-particle weight as measured from angle-resolved photoemission in YBCO. The vanishing of the quasi-particle weight indicates that the normal state of the cuprates is a non-Fermi liquid. Reprinted from Fournier *et al.*, *Nat. Phys.* **6**, 905 (2010).

around the Fermi energy. Retaining only the first derivative term, we express the quasi-particle weight as

$$Z = (1 - \partial \Sigma^R / \partial \omega)^{-1}. \quad (16.132)$$

In a Fermi liquid, each dopant creates a quasi-particle excitation above the chemical potential. As a consequence, the quasi-particle weight is expected to scale as x . Such is not the case in the cuprates. What is remarkable is that the quasi-particle weight (F2010) vanishes around a doping level of 0.15, indicating that the underlying state from which superconductivity emerges is a non-Fermi liquid in which the electrons are *not* the propagating degrees of freedom. Precisely what the propagating modes are is the central problem in the cuprates. The theory (A2004) to which Fig. 16.17 compares the quasi-particle weight is one in which the $Z \propto 2x/(1+x)$. This expression should vanish only at $x = 0$. This formula originates by simply applying the Fermi liquid form for the quasi-particle weight to the static part, that is the part that follows strictly from state counting of the spectral weight in the lower band. According to Fermi liquid theory, the quasi-particle weight should scale as the empty part of the spectrum weighted by the total intensity of the band. Since there are $2x$ particle addition states and the total weight of the band is $1+x$, the result $Z = 2x/(1+x)$ is natural. However, the data (see Fig. 16.17) show that this formula fails.

As discussed above, dynamical spectral weight transfer offers a natural mechanism for the breakdown of Fermi liquid theory and hence the vanishing of Z . Ultimately, if dynamical spectral weight transfer is the mechanism for the breakdown of Fermi liquid theory, then this physics should still be present in the superconducting state as it is impervious to ordering. Indeed it is. To guide this discussion, we focus on the f-sum rule,

$$A = \frac{\pi n_e e^2}{m} = \int_0^\infty \sigma(\omega) d\omega. \quad (16.133)$$

In understanding the spectral changes in a high- T_c superconductor, it is helpful to separate A into a low-energy component,

$$A_l = \int_{0^+}^\Omega \sigma(\omega) d\omega, \quad (16.134)$$

and a high-energy part,

$$A_h = \int_\Omega^\infty \sigma(\omega) d\omega. \quad (16.135)$$

The cut-off Ω is chosen so that A_h contains strictly the spectral weight associated with interband transitions. Typically, $\Omega/(2\pi c) = 10\,000\,\text{cm}^{-1}$ is sufficient to demarcate the minimum of $\sigma(\omega)$ which marks the boundary between the intra-band and inter-band transitions, essentially the cut-off between the lower and upper Hubbard bands. Recall from Eq. (9.136) that the electrical conductivity has an imaginary part of the form

$$\text{Im } \sigma(\omega) = \frac{n_e e^2 / m}{\omega}. \quad (16.136)$$

Only in a superconductor is this contribution non-zero. From the Kramers–Kronig relationship,

$$\text{Im } \sigma(\omega) = \frac{1}{\pi} P \int_{-\infty}^\infty \frac{d\omega' \text{Re } \sigma(\omega')}{\omega' - \omega}, \quad (16.137)$$

the real part of the conductivity that is compatible with Eq. (16.136) is $\text{Re } \sigma(\omega) = A\delta(\omega)$. In a superconductor, the spectral weight removed for $\hbar\omega < 2\Delta$, Δ the superconducting gap, is transferred to a δ -function at zero frequency. The weight in the δ -function must be the spectral weight removed upon condensation to the superconducting state. This effect is captured by the Ferrell–Glover–Tinkham (T2004) sum rule,

$$D = A_l^n - A_l^s + A_h^n - A_h^s, \quad (16.138)$$

where the superscripts n and s refer to the normal and superconducting states, respectively. In BCS superconductors which are characterized by a clear demarcation between the high and low energy scales, there is no contribution to D from A_h . Typically, D is recovered simply by integrating up to no more than 10Δ . However, in high- T_c superconductors, ellipsometry experiments (RG2001) in which changes in the dielectric function obtain for 100Δ upon a transition to the superconducting state suggest otherwise for the cuprates.

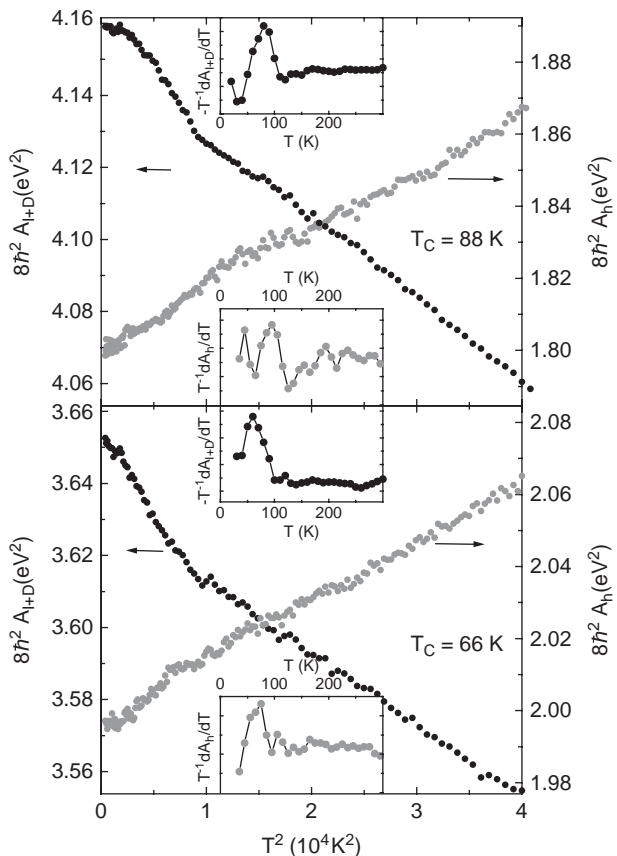


Fig. 16.18 Temperature dependence of the low-frequency spectral weight $A_{I+D}(T)$ and the high-frequency spectral weight $A_h(T)$ for optimally doped (top) and underdoped (bottom) $\text{Bi}_2\text{Sr}_2\text{Ca}\text{Cu}_2\text{O}_{8-\delta}$. The insets show the derivatives of these quantities multiplied by T^{-1} . Reprinted from Molegraaf *et al.*, *Science* **295**, 5563 (2002).

For BSCO (M2002) both optimally and underdoped, A_h exhibits an accelerated decrease as the temperature is lowered below T_c with a compensating increase in A_I , as depicted in Fig. 16.18. This indicates that it is the loss of spectral weight in the high-energy sector that drives the superconducting state. These data are also consistent with other optical measurements which indicate that the full weight of the δ -function in the superconducting state is recovered by integrating the optical conductivity out to 2 eV (SL2003) and with numerical calculations (MPS2008) which show that the frequency-dependent pairing interaction in the Hubbard model involves a non-retarded part that arises entirely from the upper Hubbard band. This color change from the visible to the infrared implies that superconductivity in the cuprates is fundamentally different from that in metals. That is, in the cuprates, superconductivity is not simply about low-energy physics on a Fermi surface. The correct theory should explain precisely how loss of spectral weight at high energies (2 eV away from the chemical potential) leads to a growth of the superfluid density.

16.6 Epilogue: $1 = 2 - 1$

As we have seen, the cuprates embody a breakdown of the three pillars of solid state physics: (1) band theory of metals, (2) Fermi liquid theory, and (3) the BCS theory of superconductivity. At the center of this notional triumvirate is the absence of the rigid band concept. As noted at the outset of the chapter, the UHB and LHB are not bands in the traditional sense. Nonetheless, we can partition the spectrum based on the intuition gained in the atomic limit following the perturbative procedure outlined above. Equation (16.129) implies that the total intensity of the lower band exceeds $1 + x$, the total number of electron states in the lower band. The dynamical correction, α , is experimentally observable directly in x-ray K-edge experiments (C1991) as well as in optical measurements (C1990) which show that the effective doping level exceeds the bare hole count, x . How can the intensity of a band exceed the number of electron states in the band? There clearly must be something else in the band and it must have charge e since the intensity counts the number of charge e excitations. What are these extra charge e excitations? We have two choices. Either split the electron spin and charge apart or opt for a composite excitation. Splitting the spin and charge apart does not solve the extra intensity problem because this could not result in an intensity larger than $1 + x$. The only option is a composite excitation. The equation at the beginning of this section provides the answer: $1 = 2 - 1$. A charge $2e$ entity binding to a hole, charge $-e$, fits the bill. The result is a charge e composite excitation. There are more complicated scenarios that are imaginable. However, $1 = 2 - 1$ is the simplest. Further, this makes physical sense. Dynamical spectral weight transfer involves the precise kinds of excitations that Mott (M1949) and others (KHF1982; K1964; C1979) argued must bind together to mediate the Mott gap (see Fig. 16.7). At finite doping, such excitations still exist. They represent bound states between a doubly occupied site and a hole on an empty site, thereby providing a physical route to $1 = 2 - 1$. In essence, double occupancy at low energies represents a collective excitation arising from the lack of rigidity of the lower and upper bands. Such an excitation can be made concrete in a field theory (LPC2007; P2010) by introducing a constraint on the upper band such that, when it is maintained, the upper band is rigid. When the constraint is relaxed, a charge $2e$ bosonic field will emerge as the collective excitation at low energies, much the way that plasmons emerged in the electron gas problem once the constraint on the extended Hilbert space was relaxed. In fact, the technique used to integrate out the upper Hubbard band exactly (LPC2007; P2010) (which is beyond the scope of this book) is identical to the collective field theory method introduced in Chapter 9 in the context of plasmons. The emergence of a charge $2e$ collective field (clearly bosonic and distinct from anything like a Cooper pair. Cooper pairs are made out of the elemental excitations. The charge $2e$ boson arises from the dynamics and hence is not) at low energies, which binds to a hole, typifies the physics of strong coupling. Specifically, new excitations (typically composites) emerge as the propagating degrees of freedom at low energy that have no counterpart in the UV-complete theory. Such excitations also solve the orthogonality problem in Fig. 16.17. Since they have internal degrees of freedom, they are orthogonal to a bare electron and hence offer a resolution of the $Z \rightarrow 0$ problem in Fig. 16.17. As a result, the simple equation

$1 = 2 - 1$ contains the essence of dynamical spectral weight transfer. The experiments in Fig. 16.18 indicate that such excitations responsible for dynamical spectral weight transfer play a crucial though unknown role in the superconductivity problem in the cuprates.

Problems

16.1 The Hubbard model with nearest-neighbor interactions takes on the form

$$H_{\text{Hubb}} = -t \sum_{i,j,\sigma} (\eta_{i\sigma}^\dagger \eta_{j\sigma} + \xi_{i\sigma}^\dagger \xi_{j\sigma} + \eta_{i\sigma}^\dagger \xi_{j\sigma}) + \frac{U}{2} \sum_{i,\sigma} \eta_{i\sigma}^\dagger \eta_{i,\sigma} + V \sum_{i,j} n_i n_j, \quad (16.139)$$

where $n_i = n_{i\uparrow} + n_{i\downarrow}$. Prove that the value of the chemical potential that leaves this model invariant under Eq. (16.39) is $\mu = (U + 2V)/2$.

16.2 Show explicitly that the coefficients are

$$\begin{aligned} \alpha_{n+1} &= (U - \mu)\alpha_n + U(-\mu)^n, \\ \beta_n &= (-\mu)^n, \end{aligned} \quad (16.140)$$

by using the recursion relationship

$$Q_{i\sigma}^{(n+1)} = [Q_{i\sigma}^{(n)}, H_U]. \quad (16.141)$$

16.3 Derive all the eigenstates and eigenvalues for the half-filled Hubbard dimer. By half-filling, I mean two electrons on two sites, one with spin up and the other with spin down. For the ground state, you should obtain Eq. (16.80).

16.4 Consider an operator O . In general

$$O = \sum_{n \in \mathbb{Z}} O_{nU}. \quad (16.142)$$

You are to derive an explicit expression for O_{nU} in terms of the transformed operators \tilde{O} . From the general expression

$$O = e^S \tilde{O} e^{-S} \quad (16.143)$$

show that

$$\begin{aligned} O_{nU} &= \tilde{O}_{nU} + \frac{1}{U} [\tilde{T}_1, \tilde{O}_{(n-1)U}] - \frac{1}{U} [\tilde{T}_{-1}, \tilde{O}_{(n+1)U}] \\ &\quad + \frac{1}{U^2} ([[\tilde{T}_1, \tilde{T}_0], \tilde{O}_{(n-1)U}] + [[\tilde{T}_{-1}, \tilde{T}_0], \tilde{O}_{(n+1)U}]) \\ &\quad + \frac{1}{2} [\tilde{T}_1, [\tilde{T}_1, \tilde{O}_{(n-2)U}]] + \frac{1}{2} [\tilde{T}_{-1}, [\tilde{T}_{-1}, \tilde{O}_{(n+2)U}]] \\ &\quad - \frac{1}{2} [\tilde{T}_1, [\tilde{T}_{-1}, \tilde{O}_{nU}]] - \frac{1}{2} [\tilde{T}_{-1}, [\tilde{T}_1, \tilde{O}_{nU}]]. \end{aligned} \quad (16.144)$$

References

- [AZ1988] I. Affleck, Z. Zou, T. Hsu, and P. W. Anderson, *Phys. Rev. B* **38**, 745 (1988).
- [A1972] This is a rephrasing of the essay title “More is Different” by P. W. Anderson, *Science* **177**, 393 (1972).
- [A1987] P. W. Anderson, *Science* **235**, 1196 (1987).
- [A1997] P. W. Anderson, *The Theory of Superconductivity in the High- T_c Cuprates* (Princeton Series in Physics, Princeton University Press, 1997).
- [A2006] P. W. Anderson, *Nat. Phys.* **2**, 626 (2006).
- [A2004] P. W. Anderson, P. A. Lee, M. Randeria, T. M. Rice, N. Trivedi, and F. C. Zhang, *J. Phys.: Cond. Matt.* **16**, R755 (2004).
- [AKS2004] Y. Ando, S. Komiya, K. Segawa, S. Ono, and Y. Kurita, *Phys. Rev. Lett.* **93**, 267001 (2004).
- [C1979] C. Castellani, C. Di Castro, D. Feinberg, and J. Ranninger, *Phys. Rev. Lett.* **43**, 1957 (1979).
- [CHP2010] S. Chakraborty, S. Hong, and P. Phillips, *Phys. Rev. B* **81**, 235135 (2010).
- [C1991] C. T. Chen, F. Sette, Y. Ma, *et al.*, *Phys. Rev. Lett.* **66**, 104 (1991).
- [C2004] A. L. Chernyshev, D. Galanakis, P. Phillips, A. V. Rozhkov, and A.-M. S. Tremblay, *Phys. Rev. B* **70**, 235111 (2004).
- [C1990] S. L. Cooper, G. A. Thomas, J. Ornstein, *et al.*, *Phys. Rev. B* **41**, 11605 (1990).
- [C1993] S. L. Cooper, D. Reznik, A. Kotz, *et al.*, *Phys. Rev. B* **47**, 8233 (1993).
- [DFM1988] E. Dagotto, E. Fradkin, and A. Moreo, *Phys. Rev. B* **38**, 2926 (1988).
- [D2003] I. Dzyaloshinskii, *Phys. Rev. B* **68**, 085113 (2003).
- [E1994] H. Eskes, A. M. Oleś, M. B. J. Meinders, and W. Stephan, *Phys. Rev. B* **50**, 17980 (1994).
- [F2010] D. Fournier, G. Levy, Y. Pennec, *et al.*, *Nat. Phys.* **6**, 905 (2010).
- [GKKR1996] A. Georges, G. Kotliar, W. Krauth, and M. J. Rozenberg, *Rev. Mod. Phys.* **68**, 13 (1996).
- [G1971] J. B. Goodenough, *J. Solid State Chem.* **3**, 490 (1971).
- [H1991] F. D. M. Haldane, *Phys. Rev. Lett.* **67**, 937 (1991).
- [H1995] D. J. van Harlingen, *Rev. Mod. Phys.* **67**, 515 (1995).
- [HL1967] A. B. Harris and R. V. Lange, *Phys. Rev.* **157**, 295 (1967).
- [H1974] G. ’t Hooft, *N. Phys. B* **75**, 461 (1974).
- [H1963] J. Hubbard, *Proc. Roy. Soc. London, Ser. A*, **276**, 238 (1963).
- [J1992] M. Jarrell, *Phys. Rev. Lett.* **69**, 168 (1992).
- [KHF1982] T. A. Kaplan, P. Horsch, and P. Fulde, *Phys. Rev. Lett.* **49**, 889 (1982).
- [K1964] W. Kohn, *Phys. Rev.* **133**, A171 (1964).
- [K2010] M. Kohno, *Phys. Rev. Lett.* **105**, 106402 (2010).
- [KLR2001] Z. Konstantinovic, Z. Z. Li, and H. Raffy, *Physica C* **351**, 1653 (2001).
- [L2005] Y. S. Lee, K. Segawa, Z. Q. Li, *et al.*, *Phys. Rev. B* **72**, 054529 (2005).
- [LPC2007] R. G. Leigh, P. Phillips, and T.-P. Choy, *Phys. Rev. Lett.* **99**, 046404 (2007).
- [LW1968] E. H. Lieb and F. Y. Wu, *Phys. Rev. Lett.* **20**, 1445 (1968).

- [L2010] A. Liebsch, *Phys. Rev. B* **81**, 235133 (2010).
- [MPS2008] T. A. Maier, D. Poilblanc, and D. J. Scalapino, *Phys. Rev. Lett.* **100**, 237001 (2008).
- [MES1993] M. B. J. Meinders, H. Eskes, and G. A. Sawatzky, *Phys. Rev. B* **48**, 3916 (1993).
- [M2002] H. J. A. Molegraaf, C. Presura, D. van der Marel, P. H. Kes, and M. Li, *Science* **295**, 2239 (2002).
- [M1949] N. F. Mott, *Proc. Phys. Soc. A* **62**, 416 (1949).
- [P2010] P. Phillips, *Rev. Mod. Phys.* **82**, 1719 (2010).
- [Q2008] M. M. Qazilbash, A. A. Schafgans, K. S. Burch, *et al.*, *Phys. Rev. B* **77**, 115121 (2008).
- [RLP1994] T. M. Rice, H. Launois, and J. P. Pouget, *Phys. Rev. Lett.* **73**, 3042 (1994).
- [R2007] A. Rosch, *Eur. Phys. J. B* **59**, 495 (2007).
- [RG2001] M. Rübhausen, A. Gozar, M. V. Klein, P. Guptasarma, and D. G. Hinks, *Phys. Rev. B* **63**, 224514 (2001).
- [SL2003] A. F. Santander-Syro, R. P. S. M. Lobo, N. Bontemps, Z. Konstantinovic, Z. Z. Li, and H. Raffy, *Eur. Phys. Lett.* **62**, 568 (2003).
- [SPC2007] T. D. Stanescu, P. Phillips, and T.-P. Choy, *Phys. Rev. B* **75**, 104503 (2007).
- [S2010] I thank M. Sobol for suggesting presenting the Mott problem starting from this model.
- [T2004] M. Tinkham, *Introduction to Superconductivity* (Dover, 2004), 2nd edition.
- [ZR1988] F. C. Zhang and T. M. Rice, *Phys. Rev. B* **37**, 3759 (1988).
- [ZM1975] A. Zylbersztejn and N. F. Mott, *Phys. Rev. B* **11**, 4383 (1975).

Index

- acoustic phonons, 170–172, 266
Adler’s theorem, 173
advanced Green function, 62, 67, 77
Anderson localization, 261, 264, 267, 284
antiferromagnetic interaction, 82, 83, 99, 101
antiferromagnetism, 372, 373
antiferromagnets, 170
antisymmetry, 27
anyons, 348
atomic limit, 358–364, 367, 368, 373, 380, 386
backscattering, 155, 156, 266, 275, 285, 326, 327, 339
Baker–Hausdorff identity, 155, 163, 167
Barkhaussen, 4
BCS ground state, 221–226, 233, 235
Berezinskii–Kosterlitz–Thouless, 300, 308
 β -function, 271, 272
Bethe ansatz, 108, 390
binary alloy, 262, 263, 276, 277
Bohr radius, 11, 323
Boltzmann equation, 93, 179–184, 187, 264
Born–Oppenheimer approximation, 16–18
bosonization, 146, 148, 151–155, 157, 159
bound state, 7, 8, 97, 101, 102, 113, 203, 218, 269, 286
Brueckner, 46, 47, 49, 132
BSCO, 395
canonical transformation, 120, 149
cesium, 11
charge neutrality, 38, 97, 98, 115
charge transfer insulators, 383
charge- $2e$ boson, 396
chemical potential, 10–12, 14, 15, 69, 99, 116, 212, 226, 253, 325–327, 332–334
chiral fermions, 334
coherence factors, 229, 233, 239, 241, 243, 247, 251
coherent states, 207, 209, 210
cohesive energy, 42, 44, 48
collective excitations, 3, 117, 118, 167, 346
collective phenomena, 118, 120, 121
compensating background, 49
composite fermions, 348
composite particle, 348
compressibility, 144, 200, 284, 349
condensation energy, 229
conductance, 165, 270–275, 286, 317, 320, 323–326, 330, 336–339, 343, 344
conductivity exponent, 273, 274
contour integrals, 77
Cooper pair, 101, 189, 193, 204, 205, 216, 254, 256, 281, 291, 292, 309
correlation energy, 46, 47
correlation length, 283, 293, 295, 302–306, 308, 330
critical magnetic field, 229, 309
critical point, 272, 273, 283, 289–291, 293, 295, 296, 301, 303–307, 310, 311
cuprates, 255, 289, 311, 353, 382, 384, 386, 387, 392–397
cyclotron frequency, 319, 349
Debye temperature, 185
density of states, 13, 40, 54, 55, 57–59, 70, 71, 74, 86–88, 98, 101, 132, 162, 164–167, 203, 219, 232, 251, 252, 263, 270, 309, 325
dephasing length, 266, 275
dephasing time, 268, 269
detailed balance, 130, 182
dielectric response, 127, 135, 136
diffusion constant, 266, 269, 279
dilute electron systems, 144, 285
Dirac cone, 334, 336, 338, 343
Dirac equation, 334
Dirac sea, 147, 149–153
direct Coulomb interaction, 33, 46, 349
disorder, 1, 186, 187, 258–260, 263, 264, 268–271, 273–277, 280, 281, 284, 285, 289, 301, 302, 305, 308, 311, 317, 324–326, 330, 349
domain wall, 4, 336, 337
Drude formula, 178, 182, 186
dynamical exponent, 283, 293, 314
dynamical spectral weight transfer, 313, 380, 384, 389–391, 394, 396
edge states, 104, 166, 317, 326, 327, 330–334, 336, 347, 349
electromagnetic absorption, 241, 244, 245
electron–phonon interaction, 6, 172–174, 197, 199
energy gap, 160, 189, 194, 195, 221, 227, 231, 308, 339, 343, 346
entropy, 12–15, 194, 195, 237, 239
exchange hole, 144
exchange interaction, 34, 36, 41, 48, 49, 81, 83, 85, 87, 103, 104, 106, 108, 109, 111, 215

- excitation spectrum, 8, 40, 49, 162, 165, 194, 232, 347
 exclusons, 363
 extended states, 259, 263, 264, 271, 275, 276, 279, 280, 325, 326, 330
- f-sum rule, 139
 Fermi liquid theory, 8, 160, 205, 207, 347
 Fermi liquids, 162
 Fermi's golden rule, 53, 140, 176
 Fermi–Dirac distribution, 12, 116, 179, 181, 183, 187, 215, 216, 237, 239
 fermions, 1, 24–26, 30, 61, 75, 114, 146, 154, 160, 334
 Ferrell–Glover–Tinkham, 394
 ferromagnet, 4, 6, 34, 46, 49, 74, 80, 83, 101, 106–108, 113, 170, 289, 290, 305
 fluctuation–dissipation theorem, 124, 177
 fractional quantum Hall, 1, 10, 166, 321, 344–348
 fractional statistics, 317, 348
 free energy, 193, 195, 237–240, 255, 296, 298, 302–304
 Friedel, 51, 79, 145
 Friedel oscillation, 137
 Friedel's sum rule, 70, 71, 97
- gauge principle, 326, 329
 Gell-Mann, 46, 47, 49, 108, 114, 132
 Goldstone's theorem, 3
 granular films, 308, 310
 graphene, 22, 23, 343
 Green functions, 57, 60, 62, 63, 68, 75, 76, 79
- Haldane, 168, 351
 Hall plateau, 320, 325, 326
 Hall voltage, 317, 319–321, 326, 330
 harmonic modes, 172
 Hartree–Fock, 31–42, 44, 45, 48, 49, 55, 56, 59, 71, 74, 79, 86, 98, 128, 132, 304, 368, 369, 372, 377
 heat capacity, 13, 15, 37, 40, 41, 194, 195, 237, 240–242
 Hebel–Slichter, 196
 Heisenberg equations of motion, 152, 171, 261, 361, 366
 Heisenberg model, 377
 holon, 160–162, 166
 Hubbard approximation, 144
 Hubbard model, 52, 119, 148, 292, 314, 358–361, 363–365, 368, 372–374, 377–380, 382–384, 386, 387, 390, 391, 395, 396
 Hubbard–Stratanovich, 298, 304
 hybridization, 52–55, 59, 73, 74, 83, 382, 383
 hysteresis, 4, 5
- imaginary time, 75, 209, 294, 297, 303
 insulator–superconductor transitions, 258, 276, 280, 291, 306
 irrelevant operator, 211
- Jordan–Wigner, 152
 Josephson effect, 224, 253
- Kondo effect, 101, 106, 268
 Kondo problem, 8, 10, 71, 80–83, 96, 99, 102, 103, 108, 109, 113–115, 213, 215, 259, 271, 381
 Kondo temperature, 80, 86, 99, 101, 107–109
 Kramers' doubling theorem, 332
 Kramers pairs, 333
 Kramers–Kronig relationships, 136
 Kubo formula, 137
- Landau gauge, 327
 Landau levels, 320, 322–325, 327, 330, 331, 349
 Landau–Ginzburg, 6, 303, 304, 311
 Laughlin liquid, 343
 Lehman representation, 65
 Lieb, 149–152, 168, 398
 Lindhard, 126, 136, 145
 linear response theory, 122, 124, 125
 linearized Hamiltonian, 149
 local magnetic moment, 51, 80, 82
 localization length, 262, 273, 278, 279, 283, 293
 localized states, 53, 260, 263, 325, 326
 Lorentz force, 318, 323, 326, 327
 LSCO, 386
 Luttinger liquid, 8, 108, 146, 148, 161, 162, 164–166, 347
 Luttinger surface, 363, 364, 367
 Luttinger's theorem, 75, 78
- magnetic length, 322, 326, 344, 346
 marginal operator, 211
 Matsubara frequencies, 75, 302–304
 Matsubara Green function, 75–77
 mean-field theory, 80, 299, 305, 373, 381
 mean-square displacement, 266, 268, 277, 279
 Meissner effect, 189–192, 194
 mesons, 7, 368
 minimum-metallic conductivity, 260, 270
 mobility edge, 260, 325
 Mott insulators, 9, 10, 69, 119, 255, 285, 363, 364, 367, 381, 383
 Mottness, 353, 357, 359, 373, 382
- Nambu–Goldstone bosons, 2–4
 nickel oxide, 357
 normal ordering, 150, 152, 155, 157, 158
 nuclear-spin lattice relaxation, 251
- Ohm's law, 271, 273, 317
 optical conductivity, 381–385, 395
 optical phonons, 173
- pair amplitude, 216–221, 225, 256, 291
 pair-binding, 161, 201, 204
 parameter differentiation, 131

- partition function, 168, 209, 210, 293, 294, 296–299, 304
 path integral, 208, 210, 342
 penetration depth, 190, 191, 193
 permutation group, 1
 phase coherence, 253, 266, 268, 275, 280–282, 292, 293, 301, 302, 305, 308, 325, 327
 phase shift, 71, 97, 278
 plasma oscillations, 117, 119, 136, 142, 143, 146
 plasmons, 115, 117, 119–121, 142–144, 396
 Poisson summation, 304, 314
 Poor Man's scaling, 102
 quantum critical point, 392
 quantum fluctuations, 293, 300, 305, 306
 quantum Hall, 50, 166, 282, 284, 317, 321, 323–328, 330, 331, 347–349, 351
 quantum phase transitions, 283, 288, 289, 291, 305, 310, 315
 quantum rotor model, 291–295, 299, 301, 302, 305, 310, 311, 314
 quarks, 7, 353, 368
 quasi-electron, 346, 347
 quasi-particles, 8, 160, 164, 205, 206, 215, 216, 234, 237, 238, 242, 246, 250, 253, 291, 306, 307, 309–311, 346–348, 383
 random dimer model, 258, 276, 279, 280, 285
 random phase approximation, 119, 128, 146, 187
 relaxation-time approximation, 181, 183, 187
 relevant operator, 211
 renormalization, 8, 56, 82, 103, 105, 108, 112, 162, 215, 353, 390
 resistivity minimum, 80, 82, 86, 87
 retarded Green function, 61, 62, 66, 68, 77, 78
 return probability, 261, 263, 266, 268, 275
 scaling dimension, 210, 211, 295
 scaling theory, 258–260, 269–271, 273–275, 293, 325
 scattering amplitudes, 87, 94–96
 Schrieffer–Wolff, 109, 110, 114
 Schrieffer–Wolff Transformation, 109
 Schwinger, 151, 168
 screening, 41, 48, 97, 102, 115–117, 121, 122, 126, 127, 129, 132, 135–137, 140, 141, 143, 144, 185, 199, 200, 206
 second quantization, 24, 27, 28
 self-energy, 63, 78, 262–264, 279
 Si MOSFET, 285, 320
 Slater, 27, 30, 88, 368
 Sommerfeld expansion, 15
 spectral function, 62, 68, 69, 363–365, 367, 381
 spin–charge separation, 146, 234, 237
 spin-flip scattering, 71, 81, 84, 98, 268
 spinon, 160–162
 Stoner criterion, 74
 stopping power, 140, 142, 144
 strong coupling, 8, 106, 215, 232, 353, 354, 369, 380, 391, 396
 structure function, 129, 130, 132, 134, 135, 141, 142, 176–178, 184, 207
 SU(2), 334, 335 377–379
 superconducting instability, 137, 160
 superconductivity, 3, 10, 101, 160, 169, 173, 176, 186, 189–194, 197, 199, 207, 212, 215, 225, 230, 255, 257, 280, 285, 292, 293, 300, 353, 382, 392, 393, 395–397, 399
 symmetric gauge, 321
 symmetry, 1–8, 26, 97, 130, 182, 194, 201, 226, 243, 258, 267, 277, 280, 285, 293, 295, 303, 325, 331, 333–336, 340, 346
 $t-J$, 377, 378, 380
 T -linear resistivity, 310, 311, 313
 tight-binding model, 147, 254, 259, 276
 time-reversal symmetry, 267, 275, 317, 330, 331
 time-reversal invariance, 333
 Tomonaga model, 149
 topological insulators, 330, 331, 335, 338, 343
 transfer matrix, 278
 tunneling, 165–167, 194, 253–255, 292, 308, 330
 ultrasonic attenuation, 176, 196, 241, 244, 246, 248, 251
 Umklapp, 155, 166, 174
 uniform electron gas, 38, 47, 49
 vacuum state, 25, 29
 vortex unbinding, 301
 vortices, 282, 300, 301
 vulcanization, 7, 354
 weak localization, 258, 261, 264, 267, 268, 274, 275
 Wick, 33, 36
 Wick's theorem, 46, 359
 Wigner crystal, 11, 45, 46, 48, 50, 284, 285, 344, 345, 349
 XY model, 295, 310
 YBCO, 393
 zeros, 63